Engineering Aerodynamics

Diehl

AD-A188 344

①

DTIC FILE COPY

[illegible] dynamics

By

[illegible]

DTIC
ELECTE
NOV 1 9 1987
S D
H

87 11 [illegible] 008

DISCLAIMER NOTICE

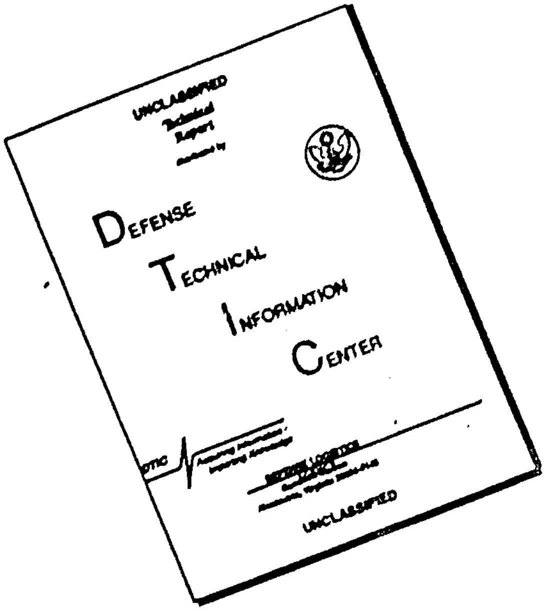

UNCLASSIFIED

Technical Report

DEFENSE TECHNICAL INFORMATION CENTER

UNCLASSIFIED

THIS DOCUMENT IS BEST QUALITY AVAILABLE. THE COPY FURNISHED TO DTIC CONTAINED A SIGNIFICANT NUMBER OF PAGES WHICH DO NOT REPRODUCE LEGIBLY.

①

ENGINEERING AERODYNAMICS

By

WALTER STUART DIEHL
Captain, United States Navy, Engineering Division, Bureau of Aeronautics, Navy Department. Fellow, Institute of the Aeronautical Sciences. Member, Aerodynamics Committee and Seaplane Sub-Committee, National Advisory Committee for Aeronautics.

DTIC
ELECTE
NOV 1 9 1987
S D
H

REVISED EDITION
(Reprint, 1986)

DISTRIBUTION STATEMENT A
Approved for public release;
Distribution Unlimited

DAVID W. TAYLOR NAVAL SHIP
RESEARCH AND DEVELOPMENT CENTER
BETHESDA, MARYLAND

Copyright, 1928, by
The Ronald Press Company

Copyright, 1936, by
The Ronald Press Company

Reprint, 1986
This publication is reprinted by permission of
Walter Colburn Diehl, Washington, D.C.

All Rights Reserved
The text of this publication or any part thereof may *not be reproduced* in any manner whatsoever without permission in writing from the heirs of the author.

PRINTED IN THE UNITED STATES OF AMERICA

FOREWORD

The United States Navy has been a major contributor to the development of aviation. In the beginning, a handful of highly dedicated, visionary naval officers led the way to building a strong aviation program that had its roots in aerodynamics research and development. In a time when few people would have dreamed of the incredible achievements 75 years of naval aviation would bring, Captain Walter Stuart Diehl was among those outstanding pioneers whose active dedication led to a coherent, effective aerodynamics research and development program.

The Navy's first wind tunnel was constructed at the Washington Navy Yard in 1914. In 1918 Captain Diehl was placed in charge of the Navy's work in aerodynamics and hydrodynamics, a responsibility he maintained until his retirement in 1951. When the Bureau of Aeronautics was established in 1921, Captain Diehl became a charter member assuming the responsibility for the funding, programs, and facilities of the Aerodynamics Laboratory at the Washington Navy Yard. His strong influence on advancing aerodynamics and hydrodynamics technology and aircraft design was highlighted by specific contributions in such technical areas as airplane performance and stability, reduction of flight test and towing basin data, seaplane design, and quantification of the standard atmosphere. As aviation progressed, Captain Diehl played a major role in influencing the direction of research and experimental investigations at transonic and high speeds, and was instrumental in the development of the Skystreak and Skyrocket high-speed, high-altitude research aircraft.

Captain Diehl was an active participant in the National Advisory Committee for Aeronautics (NACA), and he was the author of 46 NACA reports. However, it was through his book, "Engineering Aerodynamics"—for many years known as the aeronautical engineers' "bible"—that he was able to share his vast knowledge and experience with the technical community. As a fitting tribute to Captain Diehl's significant presence and contributions, the David W. Taylor Naval Ship Research and Development Center is publishing this commemorative edition upon the celebration of the 75th Anniversary of Naval Aviation.

☑
☐
☐

Availability Codes

Dist	Avail and/or Special
A-1	

DTIC COPY INSPECTED 6

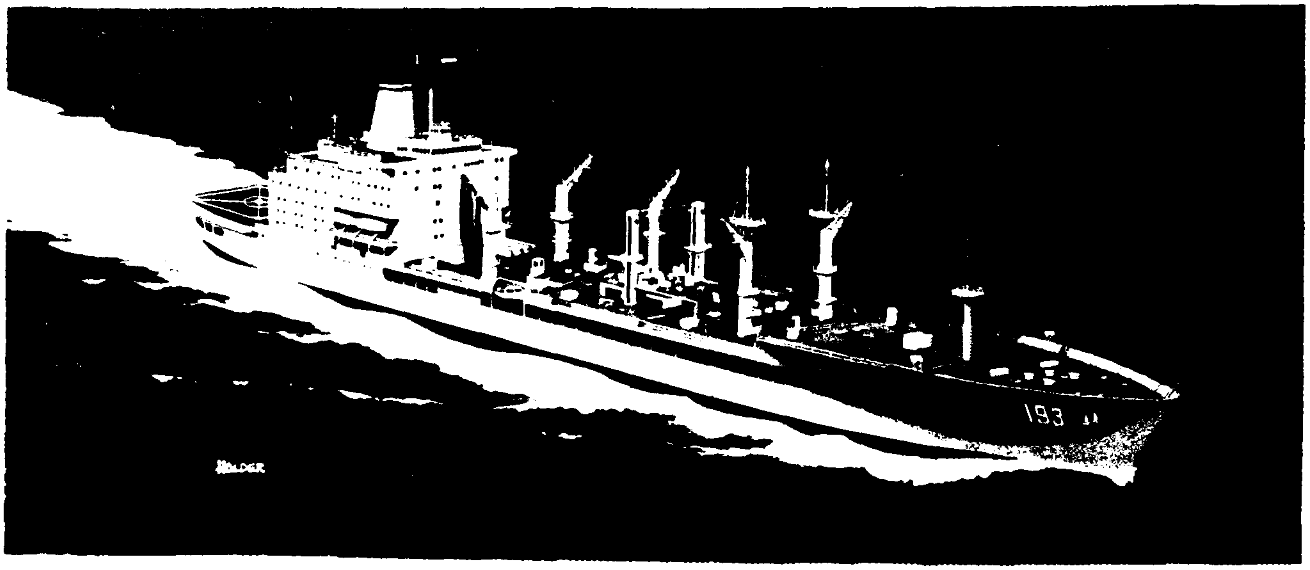

USNS Walter S. Diehl (1987)

TAO-193 is a 40,700-ton Fleet Oiler providing logistics support to the U.S. Navy. Owned and operated by the Military Sealift Command, she was named to honor Captain Diehl's lifetime of dedicated service to the Navy.

Walter Stuart Diehl, Captain, USN

Outstanding Pioneer in Naval Aviation

PREFACE

ENGINEERING AERODYNAMICS in its present form is essentially a new book, the greater part of which is now available for the first time.

Intensive aerodynamic research on the part of various laboratories and active experimental construction on the part of the airplane manufacturers have made available so much new material that the original edition, published in 1928, is obviously out of date. The preparation of this second edition has incorporated the new material, and afforded the opportunity for a complete revision.

ENGINEERING AERODYNAMICS has been written to supply the designer and the advanced aeronautical student with concise, practical information on the dynamics of airplane design. It is not a mere compilation of material from various sources nor does it contain undigested test data. It is a carefully planned original development of practical design methods based on theory and experiment.

In preparing this volume the author has analyzed a vast amount of test data and endeavored to present the essential conclusions in the form of equations or charts from which desired factors may be obtained directly. Tabular data and numerical examples are given where required. Derivations are given for many equations, but an effort has been made to avoid including unnecessary material. For this reason the conventional treatment of elementary aerodynamic problems is omitted. Descriptions of procedure and details of tests are either given briefly or omitted entirely, but numerous references are cited for the benefit of those desiring to consult the original sources.

The author is deeply indebted to Mr. F. A. Louden of the Bureau of Aeronautics, U. S. Navy, for assistance in proofreading and for helpful criticism; to Mr. C. H. Zimmerman of the N.A.C.A. Staff for criticisms, suggestions, and checking the chapter on Dynamic Stability; to Mr. C. H. Helms of the N.A.C.A. for checking manuscript; to Mr. W. D. Clark, Mr. R. E. McCally, Mr. C. T. Newman, Mr. W. S. Simpson, Mr. R. L. Creel, Mr. L. J. Friedman and Mr. J. P. Fersinger of the Bureau of Aeronautics, U. S. Navy, for assistance in preparing the charts, and to Miss Frances A. McLean for typing the entire text.

In accordance with the provisions of Article 113 of U. S. Navy Regulations, the author assumes full personal responsibility for the contents of this volume. No statement contained herein is to be construed as official or as reflecting the views of the Navy Department, the Bureau of Aeronautics, or the National Advisory Committee for Aeronautics.

WALTER S. DIEHL

Bureau of Aeronautics,
Navy Department,
Washington, D. C.

CONTENTS

CHAPTER 1

PAGE

INTRODUCTION: DEFINITIONS AND SYMBOLS 3

Design compromise – Definition of aerodynamics – Fundamental statics – Fundamental dynamics. FUNDAMENTAL UNITS. DERIVED UNITS. REFERENCE AXES: Air forces and moments – Dynamic pressure – Coefficients. SYMBOLS: Abbreviations.

CHAPTER 2

ELEMENTS OF THEORETICAL FLUID DYNAMICS 19

Literature on theoretical aerodynamics – Hydrodynamical definitions – Fluid flow – Superposed flows – Two-dimensional flow – Three-dimensional flow – *Stream function* – Streamline – Circulation – Rotation – Bernoulli's theorem – Velocity potential – Sources and sinks – Vortex motion—vortices.

CHAPTER 3

APPLIED WING THEORY 31

Induced drag – Induced angle of attack – Munk's span factor – Prandtl's interference factors – Induced drag of biplanes – Proportions of the most efficient biplane – Induced drag of triplanes – Induced drag of tandem wings – Low aspect ratio – Slope of lift curve – Correction for rectangular wing tips – Slope of biplane lift curve – Wing with a fore-and-aft slot – Downwash – Ground effect – Aspect ratio and span loading – Moment coefficient – Aerodynamic center – Center of pressure – Zero lift: zero moment – Moment coefficient about any point – Relative loading on biplane wings – Moment coefficient for a biplane.

CHAPTER 4

WIND-TUNNEL TESTS 73

The wind tunnel – Types of wind tunnels – Wind-tunnel balances – Reliability of data – Test conditions – General drag equation – Reynolds Number – Effect of Reynolds Number – Determination of Reynolds Number – Wall interference – Correction for static-pressure gradient – Turbulence – Airfoil tests – Airplane model tests – Lift and drag curves – Pitching moments – Longitudinal balance – Rolling moments – Yawing moments – Calculation of performance from model tests.

CHAPTER 5

PAGE
AIRFOIL DATA 109

Airfoil sections – Interpretation of airfoil data – The N.A.C.A. related airfoils – Maximum lift coefficient: C_L maximum – Profile drag coefficients – Minimum profile drag coefficient C_{D_0} minimum – Scale effect – Ratio $C_{L\,max}/C_{D_0\,min}$ – Angle of attack for zero lift – Moment coefficient at zero lift: C_{M_0} – Aerodynamic center – Optimum lift coefficient – Maximum negative lift coefficient – Slope of lift curve – Selection of a wing section – Corrections for aspect ratio – Airfoil ordinates – Airfoil section equivalents – C_L maximum for biplanes – Tapered airfoils – Cut-outs – Surface effects – Protuberances – Wing-fuselage interference – Compressibility.

CHAPTER 6

FLAPS AND HIGH-LIFT DEVICES 141

General – Types – Flap theory and test data – The plain flap – Effect of leakage between wing and flap – Slotted flaps – Split flaps – Split flaps on tapered wings – Partial-span split flaps – Zap flap – Variable area – The slotted wing – The external-airfoil flap – Rotor wings – Boundary layer control – Effect of flaps on performance – Additional comment on flaps.

CHAPTER 7

STATIC STABILITY AND CONTROL 171

Stability – Control surface design – Center-of-gravity location – Effect of c. g. location on moment curves – Moment coefficient about any point – Mean chord of a biplane – Virtual mean chord – Locus of c. g. for constant stability – Horizontal tail area – Longitudinal stability coefficient K – Tail efficiency factor η_T – Downwash factor F_2 – Relative effect of variables – Turbulent wake – Stabilizer setting for trim – Servo-controlled elevators: tabs – Plan-form of horizontal tail surfaces – Tail surface sections – Effect of flaps on horizontal tail area – Vertical tail area – Rudder area – Effects of dihedral – Dihedral required – Ailerons – Aileron area required – Aileron types – Balanced controls – Types of balanced controls – Calculation for simple balances – Leakage at hinge joints – Effect of balance emergence – Static balance – Flutter - Flutter prevention – Apparent instability.

CHAPTER 8

DYNAMIC STABILITY 236

Dynamic stability – Stability equation: general considerations – "Wind" axes – Non-dimensional stability derivatives – Longitudinal stability: force derivatives; moment derivatives – Estimating radii of gyration – Notes on longitudinal stability – Longitudinal stability: power on – Lateral stability – Discussion of lateral stability – Calculation of lateral stability derivatives – Collected lateral stability formulas.

CHAPTER 9

PAGE
PARASITE DRAG DATA 260

Drag Coefficients - Square flat plates - Rectangular flat plates normal to wind - Circular discs - Spheres - Spheroids and ellipsoids - Hemispheres; parachutes - Cylinder with axis normal to wind - Cylinder with axis parallel to wind - Skin friction - Wing profile drag - Wing surface finish - Rivets - Protuberances on wing - Corrugated metal wings - Gas tank on wing - Tail surfaces - Struts - Streamline bodies - Aircraft cable - Streamline wire - Fuselage drag: model data - Effect of pitch on fuselage drag - Fuselage drag: full scale - Floats - Wing-tip floats - Flying boat hulls - Air-cooled engines: uncowled - Air-cooled engines: cowled - Nacelles on monoplane wings - Nacelles on biplane wings - Pusher nacelles - Tandem nacelles - Landing gear - Fittings - Cellular radiators - Landing lamps - Wire mesh - Machine guns - Bombs and Torpedoes - Radio antenna - Interference.

CHAPTER 10

ENGINE AND PROPELLER CONSIDERATIONS 312

Engine and propeller - General power curves: sea-level engines; supercharged engines - Variation of bhp with altitude: supercharged engine - Specific fuel consumption - Propeller coefficients - Propulsive efficiency - Propeller pitch - Propeller design characteristics - Tip-speed - Velocity of sound in air - Cut-off tips - Approximate diameter formula - Maximum efficiency - General efficiency curves - Controllable-pitch propellers - Static thrust - Propeller thrust at any speed - Calculated thrust power - Zero thrust: zero torque - Negative thrust and torque - Drag of a locked propeller - General power coefficient curves - Variation of bhp with V - General thrust horsepower curves - Variation of thp with altitude: fixed-pitch propeller; controllable-pitch propeller - Propeller rpm in throttled flight.

CHAPTER 11

PERFORMANCE CALCULATION—POWER CURVES 362

Performance calculation - Power required for horizontal flight - Wing drag—induced - Parasite drag P_t: variation with angle of attack - Example of calculation of power required - Maximum thrust power available at sea-level - Rate of climb - Absolute ceiling - Service ceiling - Time of climb - Calculation of power required at altitude - Calculation of power available at altitude - Performance at altitude - Performance with supercharged engines and controllable-pitch propeller - Effect of slipstream and miscellaneous corrections.

CHAPTER 12

PERFORMANCE ESTIMATION 383

Performance estimation - Estimating parasite drag - Stalling speed - Maximum speed - Variation in V_{max} with altitude - Effect of gross weight on V_M - General power and drag relations - Maximum

PAGE

L/D - Virtual aspect ratio - Determination of airplane efficiency - Initial rate of climb - Absolute ceiling: fixed-pitch propeller; controllable-pitch propeller - Service ceiling - Time of climb.

CHAPTER 13

RANGE AND ENDURANCE 414

Maximum range - Calculation of maximum endurance - General thp curves - Range and endurance: constant angle of attack - Range at constant air speed - Bombing range - Effect of wind on range - Estimating range and endurance.

CHAPTER 14

SPECIAL PERFORMANCE PROBLEMS 435

Take-off run - Take-off run with controllable-pitch propeller - Effect of wind on take-off run - Effect of gross weight on ground run - Effect of change in take-off speed - Effect of altitude on take-off run - Path angle of climb - Take-off over an obstacle - Gliding Angle - Landing over an obstacle - Landing run - Sinking speed - Terminal velocity - Terminal velocity of an airplane - The terminal velocity dive - Effect of dive angle on terminal velocity.

CHAPTER 15

SPECIAL FLIGHT PROBLEMS 459

Gliding flight without power - Gliding flight with power - Circling flight - Spiral gliding flight - Effect of a diving start on speed over a measured course - The zoom.

CHAPTER 16

FUNDAMENTAL DESIGN CONSIDERATIONS 468

Fundamental design considerations - Some general effects of aspect ratio and parasite drag - Wing area and stalling speed - Limiting performance.

CHAPTER 17

SEAPLANES AND FLYING BOATS 491

Seaplanes and flying boats - Definitions - Metacentric height - Metacentric height required - Transverse metacentric height of twin floats - Longitudinal metacentric height - Transverse stability: single-float seaplanes and flying boats - Vertical location of side floats - Float performance - Corresponding speeds: Froude's Law - Model test methods - Non-dimensional coefficients - Calculation for take-off - Effect of wind on take-off - Maximum load that can be taken off - Notes on float and hull lines - Length - Beam - Depth - Dead rise - The step - Keel-angle at step - Spray strips.

CHAPTER 18

PAGE

FLIGHT TESTING AND PERFORMANCE REDUCTION 510

Calibration of air-speed indicators – Maximum speed – Importance of correct air speed in climb – Variation of best climbing air speed with pressure and temperature – Determination of best climbing air speeds – Climbing tests – Variation of rate of climb with altitude – Reduction of observed performance to standard conditions – The reduction of climb to standard – The reduction of maximum speed to standard conditions – Example of climb reduction to standard.

APPENDIX I

STANDARD ATMOSPHERE 527

Approximate equations for the standard atmosphere – Standard atmospheric relations used in performance reduction.

APPENDIX II

GENERAL CONVERSION FACTORS 536

Fundamental conversion factors.

APPENDIX III

USEFUL FORMULAS 542

Powers and roots – Logarithms – Derivatives – Integrals.

INDEX 545

ILLUSTRATIONS

FIGURE PAGE

1. Positive Directions for Wind Axes 11
2. Fluid Flow Components 22
3. Effect of Rotation on the Motion of a Fluid Particle 25
4. Munk's Interference Factor for Induced Angle of Attack 36
5. Prandtl's Drag Interference Factor for Biplanes, in Terms of Average Span 37
6. Prandtl's Drag Interference Factor for Biplanes in Terms of Maximum Span 38
7. Munk's Span Factor *k* for $G/b_1 = 0.05$ 40
8. Munk's Span Factor *k* for $G/b_1 = 0.10$ 41
9. Munk's Span Factor *k* for $G/b_1 = 0.15$ 42
10. Munk's Span Factor *k* for $G/b_1 = 0.20$ 43
11. Munk's Span Factor *k* for $G/b_1 = 0.25$ 44
12. Munk's Span Factor *k* for Biplanes with Wings of Equal Chords 45
13. Munk's Span Factor *k* for Biplanes with Wings of Equal Aspect Ratio 46
14. Proportions of the Most Efficient Biplane 47
15. Munk's Span Factor *k* for Triplanes 49
16. Munk's Span Factor *k* for Tandem Wings 50
17. Tau and Sigma Correction Factors 53
18. Comparison of Theoretical and Observed Slopes of Biplane Lift Curves 54
19. Munk's Span Factor for Wing with Fore-and-Aft Slot 56
20. Observed Increase in Drag Due to Fore-and-Aft Slot 56
21. Downwash Factor F_2 57
22. Ground Interference Effect on Drag and Power 59
23. Ground Interference Effect on Slope of Lift Curve 60
24. Munk's Methods for Finding Zero Lift and Zero Moment Lines 64
25. Moment Coefficient About Any Point 65
26. Effect of Gap and Wing Thickness on K_1 67
27. Effect of Stagger on K_1 67
28. Effect of Decalage on K_1 68
29. Effect of Overhang on K_1 69
30. Effect of G/c and Aspect Ratio on K_2 70
31. Effect of Overhang on K_2 71
32. Moment Coefficient for a Biplane 71
33. Variation of $C_{L\,max}$ with Reynolds Number 80
34. Reynolds Number Coefficient 82
35. Wall Interference Correction Factors 84
36. Effect of Turbulence and Reynolds Number on the Drag Coefficient of a Sphere 87
37. Effect of Turbulence on Sphere Drag 88

FIGURE PAGE

38. Tabulation of Drag Correction for Airplane Model Test 94
39. Effect of Interference on the Lift Curve 96
40. Effect of Interference on the Drag Curve 97
41. Effect of Angle of Attack and c.g. Location on Stabilizer Angle for Trim 100
42. Effect of Stalling Speed on Yawing Moment Coefficient 104
43. DH-4B Power Curves from Wind-Tunnel Tests 108
44. Effect of Thickness and Mean Camber Line on Maximum Lift Coefficient 113
45. Effect of Thickness and Mean Camber Line on Minimum Profile Drag Coefficient 116
46. Variation of C_L Maximum with Effective Reynolds Number . . 117
47. Variation of Minimum Profile Drag Coefficient with Reynolds Number 118
48. $C_{L\,max}/C_{Do\,min}$ vs. Thickness/Chord for Three Mean Camber Lines 119
49. $C_{L\,max}/C_{Do\,min}$ as a Function of Maximum Mean Camber, $t/c = 0.12$ 120
50. Angle of Attack for Zero Lift as a Function of Maximum Mean Camber 121
51. Moment Coefficient at Zero Lift as a Function of Maximum Mean Camber 122
52. Aerodynamic Center as a Function of Maximum Thickness . . . 123
53. Optimum Lift Coefficient as a Function of Maximum Mean Camber and Thickness 124
54. Effect of Maximum Mean Camber and Thickness on Maximum Negative Lift Coefficient 125
55. Slope of Lift Curve as a Function of Thickness and Aspect Ratio 127
56. Effect of Stagger and Gap/Chord Ratio on Maximum Lift of a Biplane 132
57. Increase in Profile Drag Coefficient Due to Wing-Fuselage Interference 138
58. Compressibility Effect on Lift and Drag Coefficients 139
59. Types of Flaps 143
60. Theoretical Flap Relations 145
61. Observed Increase in C_L Due to Plain Flaps 145
62. Comparison of Theoretical and Observed Flap Relations 146
63. Increase in Moment Coefficient Due to Flaps 147
64. Hinge Moment Coefficients for Flaps—from Test Data 149
65. Observed Flap Hinge Moment Coefficients 149
66. Increase in Profile Drag Coefficient Due to Flaps 150
67. Observed Increase in C_L Maximum Due to Plain Flaps 152
68. Effect of Leakage at Flap Hinge Axis 152
69. Increase in C_L Maximum Due to Full-Span Split-Flaps 154
70. Increase in Profile Drag Coefficient Due to Full-Span Split-Flaps 155
71. Partial Span Split-Flaps 157
72. Increase in C_L Maximum Due to Full-Span Zap Flaps 158
73. Effect of Full-Span Zap Flaps on Wing Moment Coefficient . . . 159
74. Maximum Lift Coefficient Obtained with Fowler Variable-Area Wing 161

FIGURE PAGE

75. Effect of Slots and Flap on Lift Coefficient . . . 163
76. Aerodynamic Characteristics of a Clark Y Wing with Multiple Fixed Slots . . . 164
77. Aerodynamic Characteristics of a Clark Y Wing with Multiple Fixed Slots and a Slotted Flap Down 45° . . . 165
78. Effect of Flaps on Take-off and Climb over an Obstacle . . . 168
79. Coordinates for Center of Gravity . . . 173
80. Moment Curves for c.g. Below Wing Chord . . . 174
81. Moment Curves for c.g. on Wing Chord . . . 175
82. Moment Curves for c.g. Above Wing Chord . . . 176
83. Vertical Location of Virtual Mean Chord with Respect to Geometrical Mean Chord . . . 180
84. Horizontal Location of Virtual Mean Chord with Respect to Geometrical Mean Chord . . . 181
85. Slope of Lift Curve F_1 and F_4 for Tail Surface Equations . . . 185
86. Downwash Correction Factor for Horizontal Tail Surface Equations . . . 188
87. Effect of Wing Aspect Ratio on Horizontal Tail Area Required for Constant Static Stability . . . 189
88. Effect of Tail Aspect Ratio on Tail Area Required for Constant Static Stability . . . 190
89. Effect of Tail Length on Tail Area Required for Constant Static Stability . . . 191
90. Effect of c.g. Location on Tail Area Required for Constant Static Stability . . . 192
91. Contours of Equal Resultant Velocity Around a Wing, Showing Turbulent Wake . . . 194–195
92. Effect of c.g. Location on Stabilizer Adjustment Required . . . 196
93. Effect of Elevator Area on Elevator Angle Equivalent to Given Stabilizer Angle . . . 199
94. Tail Surface Plan-Forms . . . 200
95. Stabilizing Area Coefficients for Fuselages . . . 204
96. Stabilizing Area Coefficients for Seaplane Floats . . . 205
97. Effect of Fineness Ratio on Yawing Moment Coefficient . . . 207
98. Stabilizing Area Coefficient . . . 207
99. Slope of Lift Curve for Vertical Tail Surfaces . . . 209
100. Ratio of Rudder Area to Total Vertical Fin Area . . . 211
101. Effect of Dihedral in a Side Slip . . . 212
102. Aileron Proportions. Relative Span and Chord . . . 218
103. Aileron Proportions. Relative Area and Chord . . . 219
104. Aileron Coefficient K_a . . . 220
105. Aileron Types . . . 221
106. Balanced Controls . . . 223
107. Balanced Controls . . . 224
108. Illustrating Calculation for Rudder Balance . . . 226
109. Loss of Control Effectiveness Due to Emergence of Leading Edge of Balanced Portion . . . 228
110. Mass Balance of an Aileron . . . 230
111. Effect of Area on Drag Coefficient for Square Flat Plates . 261

FIGURE PAGE
112. Drag Coefficients for Rectangles and Annular Discs 262
113. Variation of C_D with Reynolds Number – Cylinders and Spheres 263
114. Drag Coefficients for Spheroids and Ellipsoids 264
115. Drag Coefficients for Cylinders Parallel to the Wind 265
116. Skin Friction Drag Coefficient C_{DF} 266
117. Airfoil Drag as a Function of Thickness Ratio 268
118. Tail Surface Drag as a Function of Thickness Ratio 271
119. Drag Coefficients for Struts 273
120. Drag per Foot at 100 mph. Navy Struts 274
121. Variation of Drag Coefficient with Fineness Ratio for Struts and Streamline Bodies 274
122. Effect of Fineness Ratio on K and n in Equation for Drag of C-Class Airship 276
123. Variation of C_D with Reynolds Number for Wires 277
124. Drag per Foot at 100 mph for Cables with Turnbuckles and Eyes 277
125. Effect of Fore-and-Aft Spacing on the Drag of a Pair of Wires . 279
126. Effect of Inclination on the Drag of Wire and Cable 279
127. Lift and Drag Coefficients for Round Wire and Cable 280
128. Drag of Streamline Wire and Standard Terminals 281
129. Drag per Foot at 100 mph for Streamline Wire with Standard Terminals 282
130. Effect of Yaw on Drag of Streamline Wire 282
131. Fuselage Models 285–288
132. Fuselage Drag as a Function of Cross-Section Area 288
133. Float Models 292–296
134. Drag Due to Cowled Air-Cooled Engine 299
135. Relative Drag Contours of a Cowled Tractor Nacelle at 0° . . . 300
136. Relative Drag of a Cowled Tractor Nacelle on a Biplane 301
137. General bhp Curves 313
138. Effect of Supercharging on Power Drop Factor 314
139. Variation of bhp with Altitude 316
140. Effect of Supercharging on Power-Altitude Curve 317
141. Variation of bhp with Altitude for Supercharged Engines . . . 318
142. Average Specific Fuel Consumption at Part Throttle 319
143. Variation of Specific Fuel Consumption with Compression Ratio and Mixture Control 320
144. Variation of Specific Fuel Consumption with Altitude 321
145. Difference Between Blade Angle at 0.75 R and at 42-in. Radius . 324
146. Propeller Design Chart Based on Speed-Power Coefficient C_s . . 326
147. Fifth Roots for Calculating C_s 327
148. Propeller Design Chart Based on Speed-Power Coefficient K_s . . 329
149. Characteristic Curves Showing Loss of Efficiency Due to Excessive Tip Speed 330
150. Relation Between Actual Tip Speed and Rotational Tip Speed . . 331
151. Maximum Efficiency as a Function of V/nD 333
152. Effect of Body Interference on Propulsive Efficiency 334
153. General Efficiency Curves as a Function of V/nD and θ 335
154. General Efficiency and thp Curve for Controllable-Pitch Propellers 337
155. Static Thrust Coefficients for Adjustable-Blade Metal Propellers . 338

FIGURE PAGE
156. Propeller Performance Chart for Calculating Thrust 339
157. Effective Power Coefficient and V/nD as Functions of θ and $K_{Q\theta}$ 341
158. V/nD for Zero Thrust and Zero Torque 342
159. Negative Thrust and Torque Coefficients with a Nacelle 343
160. Variation of Negative Thrust Coefficient with Blade Angle for a Locked Propeller 344
161. General Power Coefficient Curve 345
162. General Curves of bhp, V and N 346
163. Variation of bhp with V—Fixed-Pitch Propeller 347
164. Variation of rpm with V—Fixed-Pitch Propeller 348
165. Variation of thp with V—Fixed-Pitch Propeller. PDF=0.72 . 350
166. Variation of thp with V—Fixed-Pitch Propeller. PDF=0.76 . 351
167. Variation of thp with V—Fixed-Pitch Propeller. PDF=0.80 . 352
168. Variation of thp with V—Fixed-Pitch Propeller. PDF=0.84 . 353
169. Variation of thp with V—Fixed-Pitch Propeller. PDF=0.88 . 354
170. Effect of rpm on Propeller and Engine bhp 355
171. Variation of thp with Altitude Fixed-Pitch Propeller 356
172. Variation of thp with Altitude Controllable-Pitch Propeller . . . 359
173. Effect of Altitude on Propeller Blade Angle (at 0.75 R) for Constant rpm 360
174. Factor F_v for Finding Value of Variable Parasite Drag P_1 at Any Speed 366
175. Curves of Power Available and Power Required, Illustrating Graphical Solution for Absolute Ceiling 372
176. Absolute Ceiling Chart. Variation of thp and V with Altitude . 374
177. Curves of Power Available and Power Required at Various Altitudes 378
178. Variation of Rate of Climb with Altitude 379
179. Variation of Maximum Speed and Best Climbing Speed with Altitude 381
180. Variation of C_L Maximum with Reynolds Number 384
181. Effect of Induced Drag on Maximum Speed 387
182. Effect of Induced Drag on Maximum Speed 388
183. Effect of Induced Drag on Maximum Speed 389
184. Effect of Induced Drag on Maximum Speed 390
185. Effect of Altitude on V_P and R 392
186. Effect of Altitude on Maximum Speed (Sea-Level Engine) . . 393
187. L/D, Power Required, and Speed for Minimum Drag 395
188. Minimum Power and Speed for Minimum Power 396
189. Maximum L/D as a Function of Aspect Ratio and Parasite Drag Coefficient 398
190. Airplane Efficiency as a Function of Aspect Ratio and Parasite Drag Coefficient 400
191. Effect of Aspect Ratio and Parasite on Air Speed for Best Climb at Sea-Level 402
192. Absolute Ceiling Chart—Fixed-Pitch Propeller 404
193. Difference Between Service Ceilings for Linear and Non-Linear Rate-of-Climb Curves 407
194. General Rate-of-Climb Curve 408

FIGURE PAGE
195. Relation Between the Times to Climb to a Given Altitude with Linear and Non-Linear Rate-of-Climb Curves 409
196. Time to Climb to a Given Altitude. T_s for Linear, T_e for Non-Linear Rate-of-Climb Curves 410
197. Climb in 10 Minutes, from Absolute Ceiling and Initial Rate of Climb (linear). Values of h_{10}/H are Above and Values of C_0/H are Below Base Lines 411
198. Climb in 10 Minutes from Absolute Ceiling and Initial Rate of Climb (Linear) 411
199. Climb in 10 Minutes from Service Ceiling and Initial Rate of Climb (Linear) 413
200. General thp Curves in Terms of V/V_M and R_M. $R_M = (D_t$ at $V_M)/(D_P$ at $V_M)$ 418
201. Range and Endurance Coefficients as a Function of Fuel-Load Ratio 421
202. Initial Specific Fuel Consumption at Most Economical Speed . . 422
203. Graphical Solution for Bombing Range 424
204. Effect of Wind on Most Economical Speed 426
205. Effect of Wind on Fuel Consumption for a Typical Flying Boat . 427
206. Effect of Wind on Most Economical Speed for a Typical Flying Boat 427
207. Reduction of Range in a Steady Wind 428
208. Endurance Factor F_E as a Function of V/V_M and R_M 430
209. Range Factor F_R as a Function of V/V_M and R_M 431
210. Endurance Factor F_E as a Function of R_M and V/V_M 432
211. Range Factor F_R as a Function of R_M and V/V_M 433
212. Effect of R_M on the Values of F_R and F_E for Maximum Range . . 434
213. Take-off Coefficient K_s 436
214. thp/thp$_m$ Curves for Use in Calculating Take-off Run. Fixed-Pitch Propeller 437
215. thp/thp$_m$ Curve for Use in Calculating Take-off Run. Controllable-Pitch Propeller 439
216. General Curve of Effect of Wind on Take-off Run 440
217. Change in Take-off Run Due to Change in Gross Weight . . . 441
218. Effect of Altitude on Take-off Run 442
219. Graphical Solution of Maximum Path Angle of Climb 444
220. Ground Effect on L/D at Speed for Minimum Power 446
221. Relation Between Landing Run, Landing Speed, Coefficient of Friction and L/D 448
222. Graphical Solution for Terminal Velocity 451
223. Relation Between True Velocity and Altitude for Terminal Velocity Dives Starting at 20,000 Feet 453
224. Relation Between Indicated Velocity and Altitude for Terminal Velocity Dives Starting at 20,000 Feet 454
225. Altitude-Loss Required to Attain Terminal Velocity in a Vertical Dive 455
226. Altitude-Loss Required to Attain Indicated Terminal Velocity in a Vertical Dive 456

FIGURE PAGE
227. Determination of Approximate Terminal Velocity from a Short Vertical Dive 457
228. Equilibrium in a Glide Without Power 459
229. Air Speed in a Dive with Power On. Thrust Zero at $V = 2\ V_M$. 461
230. Air Speed in a Dive with Power On. $T = T_o/2$ at $V = 2\ V_M$ . . 462
231. Graphical Solution for Speed in a Turn 463
232. Full-Scale Polar for VE-7 Airplane 468
233. Curves of Power Required at Sea-Level for Various Aspect Ratios with Normal Parasite 469
234. Curves of Power Required at Sea-Level for Various Aspect Ratios with Low Parasite 470
235. Curves of Power Required at Sea-Level for Various Aspect Ratios with High Parasite 471
236. Comparative Effect of Aspect Ratio and Parasite on High Speed at Sea-Level 472
237. Comparative Effect of Aspect Ratio and Parasite on Initial Rate of Climb 473
238. Comparative Effect of Aspect Ratio and Parasite on Absolute Ceiling 474
239. Effect of Wing Area on Speeds at Altitude 475
240. Effect of Wing Area on Rate of Climb at Altitude 476
241. Effect of Wing Area on Minimum Radius of Turn at Various Altitudes 477
242. Variation of Minimum Radius of Turn with Altitude 478
243. Effect of Stalling Speed and Altitude on Maneuverability Factor 479
244. General Curve of Maneuverability Factor Against Altitude . . . 480
245. Effect of Stalling Speed and Altitude on Time for a 360° Turn . 481
246. Effect of Aspect Ratio and Parasite on Maximum Possible Power Loading Corresponding to Zero Rate of Climb 482
247. Effect of Aspect Ratio and Parasite on Maximum Practicable Power Loading Corresponding to 300 fpm Rate of Climb . . . 483
248. Effect of Stalling Speed on Maximum Power Loading 484
249. Effect of Stalling Speed, Aspect Ratio and Parasite on the Product $V_S \cdot w_p$ for Zero Rate of Climb 485
250. Effect of Stalling Speed, Aspect Ratio and Parasite on the Product $V_S \cdot w_p$ for 300 fpm Rate of Climb 486
251. Effect of Stalling Speed on Maximum Value of $V_S \cdot w_p$ 487
252. Effect of Aspect Ratio and Parasite on the Value of $w_s + w_p$ for Zero Rate of Climb 488
253. Effect of Aspect Ratio and Parasite on the Value of $w_s + w_p$ for 300 fpm Rate of Climb 489
254. Variation of Moments with Angle of Heel for Seaplanes 496
255. Effect of Wind on Time Required for Seaplane Take-off 503
256. Variation of Load Coefficient with Speed Coefficient at Get-away Speed 505
257. Effect of Step Ventilation at Hump Speed 508
258. Variation of Climb with Air Speed and Altitude, Showing Necessity for Making Climb at Correct Air Speeds 512

FIGURE PAGE
259. Effect of Aspect Ratio and Parasite on Air Speed for Best Climb at Altitudes 513
260. Variation of Rate of Climb with Altitude 517
261. Graphical Solution for *a* and *b* 519
262. Comparison of Reduced Performance from Two Climbs by Different Pilots 524
263. Density Ratio p/p_0 at Any Altitude in Standard Atmosphere . . 532
264. Pressure Ratio p/p_0 at Any Altitude in Standard Atmosphere . . 533
265. Pressure in mm. Hg. at Any Altitude in Standard Atmosphere . . 534
266. $\sqrt{\rho_0/\rho}$ at Any Altitude in Standard Atmosphere 535

TABLES

TABLE PAGE
1. Equivalent Monoplane Span Factors 49
2. Wind-Tunnel Test Data on DH-4B Airplane Model Scale Ratio 1/16 107
3. Calculation for thp Required in Horizontal Flight at Sea-Level. DH-4B Airplane 107
4. Profile Drag Coefficients from Variable-Density Wind Tunnel . . 115
5. Airfoil Ordinates 131
6. N. A. C. A. Symbolic Equivalents for Common Airfoil Sections . 131
7. Theoretical Flap Relations 151
8. Example of Calculation for Biplane C_M 177
9. Lateral Stability Approximation Formulas 259
10. Offsets for Navy Strut and C-Class Airship 272
11. Data on Aircraft Cable 278
12. Streamline Wire Data 283
13. Data on Airplane Fuselage Models Shown in Figure 131 284
14. Data on Seaplane Float Models Shown in Figure 133 291
15. Variation of Thrust Power with Altitude: Fixed-Pitch Propeller . 357
16. Variation of Thrust Power with Altitude: Controllable-Pitch Propeller 360
17. Example of Calculation for Thrust Power Required at Sea-Level . 369
18. Example of Calculation of Thrust Power Available at Various Speeds 370
19. Calculation of Maximum Thrust Horsepower Available Using General Curves 371
20. Thrust Power Required at Altitude 376
21. Maximum Thrust Horsepower Available at Altitudes 377
22. General Speed, Drag and Power Relations 397
23. Power Available in a Climb at Constant Angle of Attack 405
24. Time of Climb Factors 412
25. Calculations for Air Speed in a Turn 465
26. Effect of Stalling Speed on Performance 480
27. Reduction of Climb to Standard, Climb No. 1 525
28. Reduction of Climb to Standard, Climb No. 2 525
29. Standard Atmosphere 528
Conversion Factors 537-541

ENGINEERING AERODYNAMICS

CHAPTER 1

INTRODUCTION; DEFINITIONS AND SYMBOLS

Design Compromise. The designer of an airplane is confronted with an endless series of compromises. At each stage in the design he must decide just how far a loss in one characteristic is justified by a gain in some other characteristic. The degree of success finally attained depends largely on the soundness of the judgment exercised in the designer's decisions.

The ability to exercise sound engineering judgment may be a natural talent, but it is more often the result of training and experience. Given all of the data on a problem, the solution is usually obvious. It is, therefore, essential that the aeronautical engineer have immediately available as much information as he can obtain on the problems confronting him. Many of these problems involve detailed knowledge of aerodynamics. In the succeeding chapters an attempt has been made to supply information on applied aerodynamics in the form best adapted for direct application to design problems. The proper understanding of these data requires a thorough knowledge of the fundamental laws of mechanics. The remainder of Chapter I is concerned chiefly with fundamentals.

Definition of Aerodynamics. Before attempting to give a definition of aerodynamics, it is desirable to trace its relationship to kindred branches of mechanical science, all coming under the classification of physics.

According to the Century Dictionary, physics is defined as "The science of the principles operative in organic nature; the science of forces or forms of energy." We are now concerned with the division of physics known as mechanics and usually defined as "the science of motion." While that definition is correct, it is probably better to say that mechanics is that branch of physics which is concerned with forces, motion, and energy.

Mechanics is divided into four general branches; kinematics, kinetics, statics, and dynamics.

Kinematics is sometimes called the geometry of motion. The Euclidian geometry is concerned only with space; kinematics is concerned with both space and time, but not with forces.

Kinetics is the science that treats of the mutual relations between moving bodies. It is concerned with forces and the resultant motions.

Statics is concerned with the equilibrium conditions for forces acting on a body at rest.

Dynamics is concerned with forces and motion, and in particular with the forces due to motion. Hydrodynamics is that branch of dynamics that is concerned with forces and motions in an incompressible fluid. Aerodynamics is that branch of dynamics that is concerned with forces and motions in a compressible fluid or gas. The definition of aerodynamics in N.A.C.A. Nomenclature for Aeronautics (Technical Report No. 474) is "The branch of dynamics that treats of the motion of air and other gaseous fluids and of the forces acting on solids in motion relative to such fluids."

There is considerable overlapping in all branches of mechanics. The definition of aerodynamics given above is scientifically correct, but there is a definite tendency to include under the heading of aerodynamics all of the applied dynamics and kinetics used in aircraft design. To the aeronautical engineer, most of the problems involving forces and motions are "aerodynamic" problems, and he is not greatly concerned over the fact that the theoretical solution to the problems of fluid motion are usually obtained by the methods of hydrodynamics. For this reason *Engineering Aerodynamics* will treat many problems not strictly within the science of aerodynamics.

Fundamental Statics. The condition of equilibrium for any rigid body requires that, in any reference plane:

1. The algebraic sum of all horizontal force components equals zero.
2. The algebraic sum of all vertical force components equals zero.
3. The algebraic sum of the moments of all the force components, taken about any point in the plane, must equal zero.

If these conditions are not met, there must be motion in accordance with the laws of dynamics. This motion may be either translation or rotation alone, or it may be any combination of the two.

A couple is two equal, oppositely directed, parallel forces not acting in the same straight line. The force components of a couple are zero, but the moment has the same value for every origin in the plane of the couple. This moment is equal to the product of one of the two forces by the perpendicular distance between the lines of action. Any system of forces acting on a rigid body may be reduced to a force and a couple. The moment coefficient for an airfoil at zero lift is a couple.

Fundamental Dynamics. Newton's laws of motion are:

1. Every body continues in its state of rest or its state of uniform motion in a straight line, unless it is compelled by external forces to change that state.
2. Change in momentum is proportional to impressed force, and takes place in the direction in which the force acts.
3. Action and reaction are equal and opposite.

Newton's second law is sometimes amplified, or a fourth law set up by the statement, "The effect of a force on a body is the same, whether it acts alone or in conjunction with other forces."

The law of conservation of energy is, "The total energy of any material system is a quantity which can neither be increased or diminished by any action between the parts of the system, although the form of the energy may be changed."

The foregoing laws enter into the solution of practically all problems involving forces and motions.

Fundamental Units

Nearly all of the physical quantities used in mechanics may be expressed in terms of three independent fundamental units. A fundamental unit should have the following properties:

1. It should be a quantity for which very accurate comparisons are possible with other quantities of the same kind.
2. The comparison should be simple and direct.
3. The comparison should be possible at any time or place. That is, the quantity should be such that a suitable standard value can be established and copies made.

The three quantities best adapted for use as fundamental units are length, mass, and time. All other units are derived in terms of these. The fact that any value may be assigned to the fundamental standards has led to considerable confusion in standard length and standard mass. The mean solar second, defined as 1/86,400 of a mean solar day is the universal standard unit of time.

There are two important systems of fundamental units in wide use. These are the metric centimeter-gram-second or cgs system and the English or foot-pound-second system.

The centimeter is defined as 1/100 part of a meter. The standard meter is the length between two marks on a platinum alloy rod prepared by Borda in 1795, and originally intended to be 1/10,000,000 part of the distance between the equator and the pole measured along the meridian through Paris. The fact that it is not exactly the intended length has little bearing on its value as a standard. The gram is defined as 1/1,000 part of the standard kilogram. The standard kilogram is the mass of a block of platinum also prepared by Borda in 1795, and intended to equal the mass of 1,000 cubic centimeters of distilled water at 4° Centigrade. Subsequent measurements show that while the two masses are very nearly equal, there is enough difference to require that we consider the standard of mass as Borda's block and not as 1,000 cc of distilled water. These discrepancies have no bearing on the usefulness of the metric system. It is the decimal divisions rather than the actual units that have led to the almost universal use of the metric system in scientific work.

The English system of units is used in Great Britain and the United States, but owing to slight differences in the legal definitions, the actual standards in the two countries are not the same. The legal standard of length in Great Britain is the yard, now having a legal equivalent of 0.9143992 meters. By Act of Congress July 28, 1866, the standard yard in the United States was established as 3,600/3,937 = 0.91440183 meters. The difference is about 1 part in 360,000. A slight discrepancy also exists in the standard of mass. The legal equivalent of the British pound mass is 453.59245 grams. The legal equivalent of the United States pound mass is 453.5924277 grams. The British standard mass is, therefore, heavier than the United States standard mass by about one part in 20,000,000. These discrepancies are obviously of no practical importance in engineering calculations. They are pointed out at this time to emphasize the arbitrary nature of the fundamental standards and to indicate the main reason why scientists recommend the universal adoption of the metric system.

Derived Units

Two systems of units, the absolute and the gravitational, may be derived from the fundamental standards. The fundamental equation $F = ma$ may be written

$$\text{Unit Force} = \text{Unit Mass} \times \text{Unit Acceleration}$$

In the English system the unit of mass is the standard pound weight. The unit of acceleration is one foot per second per second. Since the acceleration due to gravity is about 32 feet per second per second for the force of a pound weight acting on a pound mass, it is obvious that the unit of force must be $1/g$ or about $1/32$ of the force due to gravity on the pound weight. This unit, called the poundal, is approximately equivalent to the force exerted by gravity on a half-ounce weight. It is an absolute force, independent of the value of gravity.

The poundal is inconveniently small as unit force in engineering work. The engineer, therefore, adopts what are known as gravitational units and takes for the unit force the weight of the standard pound. This force is g times the poundal, so the unit of mass must be g times the standard pound weight. This unit of mass is usually called the "slug" or the "gee pound."

The fundamental equation $F = ma$ may be written in three ways:

$$p = ma \tag{1a}$$

where p is the force in poundals, and m is the mass in pounds,

$$gF = ma \tag{1b}$$

where F is the force in pounds, and m is the mass in pounds, or

$$F = \frac{W}{g} a \tag{1c}$$

where F is the force in pounds and W is weight in pounds.

If local g is used, there is no difference in these equations. However, the inconvenience of varying g is greater than the effect of varying F, and the engineer adopts as standard a value of g that is about the average for 45° latitude. This standard value is 980.665 cm/sec/sec or 32.1740 ft/sec/sec. Actual values of g vary from this standard by a maximum of about one-third of one per cent. The errors involved are negligible, but it is highly important that the engineer understand just what assumptions have been made in order that confusion may be avoided.

In the cgs system, the same conditions exist. The absolute unit of force is the dyne, about 1/981 of the weight of one gram. The metric-gravitational system uses as the unit of force the weight of one kilogram and the unit of acceleration is one meter/sec/sec. Hence, the "metric slug" is Kg weight divided by g in meters/sec/sec or

$$\text{Force in Kg} = \frac{\text{weight Kg}}{9.80665} \text{ (meters/sec/sec)}$$

Reference Axes

Forces and moments acting on an airplane are conveniently referred to a definite set of three mutually perpendicular axes having specified directions for positive forces and positive moments. A positive moment is always assumed to act in the direction of rotation between positive directions of the axes in cyclic alphabetical order:

$$X \longrightarrow Y \qquad Y \longrightarrow Z \text{ and } Z \longrightarrow X$$

Three types of axes are used in aeronautical computations. Each type has its special applications and there should be no confusion regarding the conventions in any given case. The three types are:

1. *Axes fixed in space.* These are the "gravity axes" used in following the motion of the center of gravity in certain performance problems. The X axis is horizontal with the positive direction in the general line of flight which, in accordance with the usual convention, is plotted with the positive direction from left to right. The Y axis is also horizontal with its positive direction away from the observer on the ground. The Z axis is vertical with the positive direction upwards. These axes are used chiefly for motion in a vertical plane, involving only X and Z.
2. *Axes fixed in the airplane.* These are the "airplane axes" or "body axes," and the chief use is in stability calculations. The origin is taken at the c.g. of the airplane. The X or longitudinal axis is directed forward and made parallel to the thrust line or to the wing chord, although any definite reference line may be used, such as the keel line of a flying boat hull. The Y or lateral axis is normal to the plane of symmetry and its positive direction is towards the right wing tip. The Z or normal axis is in the plane of symmetry and directed downwards.
3. *Axes moving with the airplane.* These are called "wind axes," or "wind-tunnel axes." Unless otherwise specified, these axes are understood to be used in all general aeronautical work. The X or drag axis is directed to the rear, in line with the direction of the relative wind. The Y or cross-wind axis is perpendicular to the plane of symmetry and if the convention as to direction of positive moments is to be consistent, its positive direction must be from right to left. The Z or lift axis lies in the plane of symmetry with positive direction upward.

It will be noted that the wind axes are directed exactly opposite to the body axes. The body axes are known as right-hand because in looking along the positive direction of any one of the axes, the positive moment acts clockwise or in the direction of motion of a right-hand screw. With the same convention, the wind axes would be left-hand, since the direction of rotation for positive moment is counter clockwise. However, wind axes are seldom used in this sense. They are used almost entirely under conditions which place the observer outside of the airplane so that the direction of positive moments becomes right-hand, if from any point on the positive branch of an axis the observer looks toward the origin. Since the wind axes, as defined above, are the natural axes to use, it makes little difference whether they are right-hand or left-hand with regard to an unused convention.

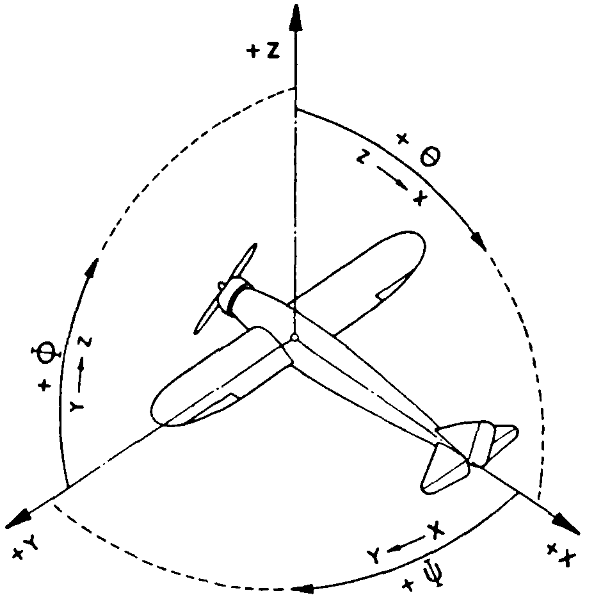

WIND AXES

Figure 1. Positive Directions for Wind Axes

The extensive use of wind axes makes it imperative that the engineer visualize clearly the relations involved in the positive reference angles. Figure 1 may be of some assistance in this respect.

Air Forces and Moments. Unless otherwise specified, it will be understood that the air forces acting on an airplane are referred to the wind axes previously described.

Forces or force components along the three axes X, Y, and Z in this system are known as drag, cross-wind force, and lift, respectively.

Angular displacements about the three axes X, Y, and Z in this system are known as roll (or bank), pitch, and yaw. Moments have the same designation as angular displacements, for example, a pitching moment tends to cause rotation about the transverse or Y axis.

Dynamic Pressure. The dynamic pressure $q = \rho V^2/2$ is the pressure developed in bringing a moving perfect fluid to rest. Since the standard density is $\rho_0 = 0.002378$ slugs per cu ft

$$q_0 = 0.001189\ V^2 \tag{2}$$

where q_0 is in lb/sq ft and V is in fps, or

$$q_0 = 0.002558\ V^2 \tag{2a}$$

where q_0 is in lb/sq ft and V is in mph.

The value of q at any air density other than the standard is obviously

$$q = q_0 \frac{\rho}{\rho_0} \tag{3}$$

The relation between velocity in standard air and a given dynamic pressure in lb/sq ft is

$$V = 29.00 \sqrt{q_0}\ \text{fps} \tag{4}$$

or

$$V = 19.77 \sqrt{q_0}\ \text{mph} \tag{4a}$$

In the metric system for q in Kg/sq m and V in m/sec

$$q_0 = 0.0625\ V^2 \tag{5}$$

and

$$V = 4\sqrt{q_0} \tag{5a}$$

Coefficients. Forces and moments are usually given, as a matter of convenience, in the form of coefficients. Practically all of the early work in this country made use of coefficients having the dimensions of (lb/sq ft)/(mph)^2, and used the symbols K_y for lift and K_x for drag. These coefficients were based on air of standard density and defined by the relations

$$\text{Lift} = L = K_y\,(\rho/\rho_0)\,SV^2 \tag{6}$$

$$\text{Drag} = D = K_x\,(\rho/\rho_0)\,SV^2 \tag{7}$$

Where S is the area in sq ft and V the relative air speed in miles per hour. This form of coefficient is numerically equal to the force acting on one square foot of surface at a speed of one mile per hour in standard air.

About 1919 the National Advisory Committee for Aeronautics recommended the adoption of "Absolute Coefficients" having the same value in any consistent system of units. The coefficients tentatively adopted were defined by the relations

$$L = L_c\,\rho\,S\,V^2 \tag{8}$$

$$D = D_c\,\rho\,S\,V^2 \tag{9}$$

The coefficients L_c and D_c are the same as K_L and K_D used by the British.

With the improvement in theoretical aerodynamics it became evident that there were many advantages in the use of the particular form of absolute coefficients employed by Prandtl. Therefore, in 1921, the National Advisory Committee for Aeronautics decided to recommend the general use of these coefficients C_L and C_D, defined by the relations

$$L = C_L \, q \, S \tag{10}$$

$$D = C_D \, q \, S \tag{11}$$

where q is the dynamic pressure $\frac{1}{2}\rho V^2$. This form of coefficient is now used almost exclusively.

The relations between the three types of coefficients are

$$C_L = 2L_c = 391 \, K_y \qquad K_y = 0.002558 \, C_L = 0.005116 \, L_c$$

$$C_D = 2D_c = 391 \, K_x \qquad K_x = 0.002558 \, C_D = 0.005116 \, D_c$$

Absolute coefficients used for moments are similar in form to C_L and C_D. Since these must include a characteristic length in addition to the area S, the span b is used for rolling and yawing moments and the chord c for pitching moments as follows:

$$\text{Rolling Moment, } L = C_l \, q \, b \, S$$

$$\text{Pitching Moment, } M = C_m \, q \, c \, S$$

$$\text{Yawing Moment, } N = C_n \, q \, b \, S$$

Symbols

Where there is no confusion regarding the intended meaning, the use of symbols for various physical quantities leads to conciseness and clarity. However, if there is any ambiguity of meaning, the symbol loses its value entirely and becomes an unqualified nuisance. In order to avoid this situation, the author prefers to use only those symbols for which there can be no confusion regarding the intended meaning and to insure clarity by repeated definition in the text.

The following list of symbols in general use is included for reference:

Aerodynamic center (in terms of chord)	a
Acceleration due to gravity	g
Air speed (general)	V
Indicated	V_i

Maximum	V_M
Stalling	V_S
Altitude	h
Angle of:	
Attack (measured from chord line)	α
Attack, absolute (measured from zero lift)	α_a
Attack, induced	α_i
Pitch	θ
Roll or bank	φ
Trim (seaplane)	τ
Yaw	ψ
Control-surface deflection:	
Elevator	δ_e
Rudder	δ_r
Aileron	δ_a
Flap	δ_F
Tab	δ_t
Downwash	ϵ
Wing setting or incidence	i_w
Stabilizer setting or incidence	i_t
Angular velocity	ω
Area general	S
Wing (upper S_U, lower S_L)	S_W
Tail	S_T
Area ratio (reciprocal of aspect ratio)	λ
Aspect ratio (b^2/S)	n
Ceiling, absolute	H
Ceiling, service	h_s
Center of gravity	c.g.
Center of pressure	c.p.
Center of pressure coefficient	C_p
Chord, mean aerodynamic (M.A.C.)	c
Upper wing	c_U
Lower wing	c_L
Cross-wind force	C

Density, air mass per unit volume	ρ
Standard	ρ_0
Relative	$\rho/\rho_0 = \sigma$
Displacement, axial:	
Longitudinal	x
Lateral	y
Normal	z
Displacement, angular:	
In roll	φ
In pitch	θ
In yaw	ψ
Displacement, lb (seaplane hulls and floats)	Δ
Distance from c.g. to elevator hinge axis	l
Drag, in general	D
Induced	D_i
Parasite	D_p
Profile	D_o
Drag coefficient, absolute	C_D
Drag coefficient, minimum	$C_{D\,min}$
Drag coefficient, induced	C_{Di}
Drag coefficient, parasite	C_{Dp}
Drag coefficient, profile	C_{Do}
Dynamic pressure $\rho V^2/2$	q
Efficiency	η
Force, cross-wind	C
Force, coefficient of cross-wind	C_C
Force, general	F
Force, parallel to body axes:	
Longitudinal	X
Lateral	Y
Normal	Z
Gap	G
Kinematic viscosity	ν
Lift	L
Lift coefficient, absolute	C_L

Lift coefficient, maximum	$C_{L\,max}$
Lift/Drag ratio	L/D
Loading, power lb/bhp	w_p
Loading, wing lb/sq ft	w_s
Mass (= w/g)	m
Moments:	
Rolling	L
Pitching	M
Yawing	N
Moment coefficients, absolute (for wind axes):	
Rolling	C'_l
Pitching	C_m
Pitching at zero lift	C_{m0}
Yawing	C'_n
Moment of inertia [= $(W/g) \times k^2$]	I
Moments of inertia (about axes):	
Longitudinal (in roll)	A
Lateral (in pitch)	B
Normal (in yaw)	C
Normal force coefficient	C_N
Pitching moment coefficient at zero lift	C_{M0}
Pitch ratio, effective	V/nD or J
Power	P
Brake horsepower	bhp
Thrust horsepower	thp
Power coefficient (= $P/\rho\, n^3\, D^5$)	C_P
Pressure	p
Propeller diameter	D or Diam.
Propeller pitch, geometric	p
Propeller rate of rotation: Revolutions per second	n
Radius of gyration	k
Resultant force	R
Reynolds Number (= $\rho VL/\mu$)	RN
Slope of lift curve (= $dC_L/d\alpha$)	a
Span	b

Span factor, Munk's equivalent monoplane	k
Thrust	T
Thrust coefficient (= $T/\rho n^2 D^4$)	C_T
Torque	Q
Torque coefficient (= $Q/\rho n^2 D^5$)	C_Q
Velocity	V
Velocity, angular component in:	
Roll (about longitudinal axis)	p
Pitch (about lateral axis)	q
Yaw (about normal axis)	r
Velocity, linear component along:	
Longitudinal axis	u
Lateral axis	v
Normal axis	w
Velocity of sound	a
Velocity, terminal	V_T
Viscosity, coefficient of	μ
Viscosity, kinematic	ν
Weight	W

Abbreviations. Throughout this volume it will be necessary to make frequent reference to the publications of the National Advisory Committee for Aeronautics, hereafter referred to as N.A.C.A., and to the publications of the British Aeronautical Research Committee, hereafter referred to as the Br.A.R.C.

The N.A.C.A. publications are classified in three groups, as Technical Reports, Technical Notes, and Technical Memorandums which will be designated as T.R., T.N., and T. M., respectively, followed by the serial number of the publication.

The publications of the Br.A.R.C. are entitled "Reports and Memoranda." These will be designated as R. & M. followed by the proper serial number.

CHAPTER 2

ELEMENTS OF THEORETICAL FLUID DYNAMICS

Literature on Theoretical Aerodynamics. There are now available in English a considerable number of works on theoretical Hydrodynamics and Aerodynamics. No one volume among these can be selected as filling all possible requirements. The following list does cover the field, however:

Lamb, H., "Hydrodynamics," Cambridge University Press (1916).
Wilson, E. B., "Aeronautics," John Wiley & Sons, Inc. (1920).
Glauert, H., "The Elements of Airfoil and Airscrew Theory," Cambridge University Press (1926).
Munk, Max M., "Fundamentals of Fluid Dynamics for Aircraft Designers," The Ronald Press Co. (1929).
Reid, E. G., "Applied Wing Theory," McGraw-Hill Book Co., Inc. (1932).
Munk, Max M., "The Principles of Aerodynamics," Munk (1933).
Durand, W. F., and Munk, M. M., "Aerodynamic Theory," Vol. I, Part I and Part II, Julius Springer, Berlin (1934).

Each of the volumes listed above contains much of value to the student. Wilson, Glauert, Reid, and Munk are recommended as elementary and fundamental treatments suitable for the beginner. Lamb's "Hydrodynamics" is the classical general treatment of the subject. It is complete, but perhaps rather difficult for the student to follow unless he has a fair knowledge of the fundamentals. "Aerodynamic Theory," edited by Dr. Durand, is the first volume of a proposed six-volume "General Review of Progress under a Grant of the Guggenheim Fund for the Promotion of Aeronautics." It contains an excellent presentation of all of the fundamental theory, well arranged and illustrated in a manner that is of great assistance to the student in grasping the physical significance of the fundamental relations employed.

A number of excellent works on hydrodynamics are also available in French and German. Those best known to the engineers in this country are:

Joukowski, N., "Aerodynamique," Pub. Gauthier-Villars et Cie., Paris (1916).

Fuchs, R., and Hopf, L., "Aerodynamik," Pub. R. C. Schmidt & Co., Berlin (1922).

Eberhardt, C., "Einfuhrung in die Theoretische Aerodynamik," Pub. R. Oldenbourg, München (1927).

Hydrodynamical Definitions. Before giving an outline of some of the important applications of theoretical aerodynamics to the problems of airplane design, it is desirable to define the terms most frequently employed. These definitions necessarily involve the mathematical relations employed in the original derivations, but the inclusion of the complete derivations is beyond the scope of this volume. The highly abridged definitions that follow are intended to give the engineer a reasonably clear conception of the meaning of the terms most frequently used. The student is referred to any of the works listed in the preceding paragraphs for the complete derivations.

Fluid Flow. The first step in the mathematical investigation of fluid flow is usually made with the assumption of a continuous perfect fluid, incompressible and without viscosity. Although air is compressible and viscous, these factors are normally of secondary importance in the types of flows that are of greatest interest.

The second step is the selection of a set of rectangular axes to which the motion may be referred. If the flow around an object is being considered, these axes may most conveniently be fixed relative to the body which may be considered stationary in the moving fluid. The fluid velocity at any point is defined by its axial components u, v, and w, along the axes X, Y and Z, respectively. The chief problem in the mathematical investigation of fluid flow is to determine the velocity at a given point. The method actually used depends on the conditions of the problem. If the flow is of a simple type, it may be possible to obtain a simple expression for the velocity field. If the flow is complex, it may be necessary to resolve it into simple components before a mathematical relation can be found. In most cases the solution follows from the application of the simple fundamental laws of motion to a particle in the fluid. Three types of fluid motion are involved: (1) translation, (2) rotation, and (3) deformation.

Superposed Flows. In many of the problems in hydrodynamics, it is desirable to consider that a given flow is produced by two or more component flows. The usual case superposes a local circulation or a system of flow in closed curves upon a general flow in which the particles move in parallel straight lines. If the variation of velocity in the field of the circulatory flow can be expressed in terms of the distance from the origin, then the vector resultant of the circulatory and translatory velocities at any point may be obtained by calculation. The flow around an airfoil may be obtained in this manner.

Two-Dimensional Flow. A flow which is two-dimensional in the plane of X-Y will be exactly similar in any parallel plane. An example of such a flow is that around the center of a very long cylinder or strut. Two-dimensional flows can be completely investigated by considering the flow in a single plane.

The mathematical conditions for two-dimensional flow are: (1) no velocity component along the Z axis, and (2) no X or Y velocity gradients along the Z axis. That is,

$$w = 0$$

$$\frac{\partial u}{\partial z} = \frac{\partial v}{\partial z} = 0$$

Three-Dimensional Flow. The general motion of a fluid is three-dimensional with acceleration and velocity components along all three axes. An elementary example of three-dimensional flow is that about a solid of revolution or a streamline body.

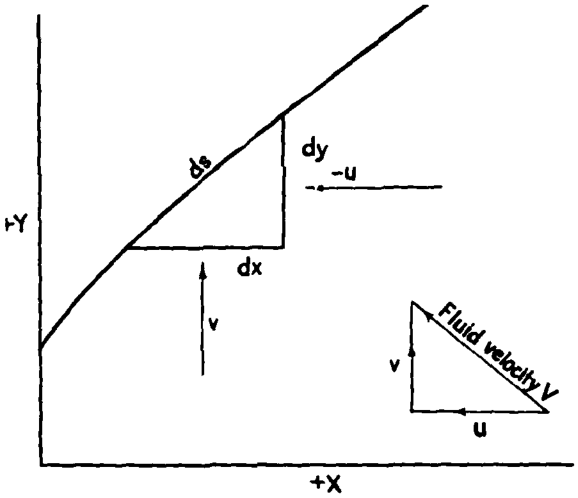

Figure 2. Fluid Flow Components

Stream Function. Consider the two-dimensional flow of a continuous and incompressible fluid across an element ds of any curve in the plane of the flow, as shown on Figure 2. The general fluid velocity is V having axial components u and v. The flow across ds must be equal to the algebraic sum of the flows across dx and dy, since otherwise the density within the triangle formed by ds, dx and dy would not remain constant. The flow across dx is $v\,dx$, and the flow across dy is $-u\,dy$. Hence, the flow across ds from right to left is

$$v\,dx - u\,dy = d\psi \tag{12}$$

and the flow across any curve joining the points (x_0, y_0) and (x, y) is

$$\psi = \int_{x_0, y_0}^{x, y} (v\,dx - u\,dy) = \psi(x, y) - \psi(x_0, y_0) \tag{13}$$

ψ is called the "Stream Function" because it determines the amount of fluid streaming across any curve connecting two points in the fluid. When ψ is known, the velocity components are determined by

$$u = -\frac{\partial\psi}{\partial y} \qquad v = \frac{\partial\psi}{\partial x}$$

Streamline. The instantaneous path of a fluid particle is called a streamline. Mathematically, a streamline is defined by ψ = constant or $d\psi = 0$, since for this condition no fluid can stream across the curve so defined. In steady flow, the streamlines are the actual paths of particles in the fluid.

Circulation. The circulation of a fluid is determined by the flow *along* a boundary as contrasted with the flow *across* a boundary used in defining stream function. The flow along an element ds of any curve in the fluid is the product of ds by the component of the velocity along ds. The component of the velocity along ds is $(V_r \cdot \cos\theta)$, where V_r is the resultant velocity making an angle θ with the element ds. The circulation is determined by the line integral of the tangential velocity $V_r \cos\theta$ taken around any closed circuit or

$$\Gamma = \int V_r \cos\theta\, ds \tag{14}$$

Resolving the tangential velocity into its axial components gives

$$V_r \cos\theta = u\frac{dx}{ds} + v\frac{dy}{ds}$$

hence
$$\Gamma = \int (u\,dx + v\,dy) \tag{15}$$

As an example of the use of circulation, the lift on an element of unit length in a wing of infinite span varies directly with the circulation around it. That is,

$$L = \rho\Gamma V \tag{16}$$

where ρ is the density and V the relative velocity measured at a great distance from the element. This is the well-known Kutta-Joukowski equation. Owing to its frequent use, many engineers instinctively associate circulation with lift. It should be understood that circulation, in general, is a type of fluid motion and that in any particular case it has the value given by the line integral, equation (15).

For a wing of finite span, the lift, and from it the induced drag, can be calculated only when the distribution of circulation along the span is known. If the circulation is constant along the span, then $d\Gamma/db$ is zero except at the tips where it equals Γ. This would correspond to a constant lift along the span, and there would be a vortex at each tip only. Actually, there is a vortex at each tip and a gradient of Γ along the span giving a maximum value of Γ at the center and zero at the tips. The vortices which peel off of the trailing edge vary in strength with $d\Gamma/db$. Hence, the variation in vorticity along the span is from a maximum positive value at one tip to an equal negative value at the other tip, passing through zero at the center.

Rotation. Rotation in a two-dimensional flow is defined as the ratio of the circulation around the boundary of a closed curve to the area enclosed by the curve. In three-dimensional flow, the component of rotation about one of the reference axes is determined by the component of circulation in the plane of the other two axes.

Circulation and rotation are thus related, although they differ in that circulation refers to a definite area or mass of the fluid while rotation refers to the constituent particles that combine to produce circulation. Rotation and vorticity are identical.

Rotation in a fluid does not mean the same thing as circulatory motion. It may be shown that the motion of a fluid in concentric streamlines is irrotational if the velocity varies inversely as the radius. It may also be shown that a particle of fluid rotating like a solid body has a rotation of twice its mean angular velocity.

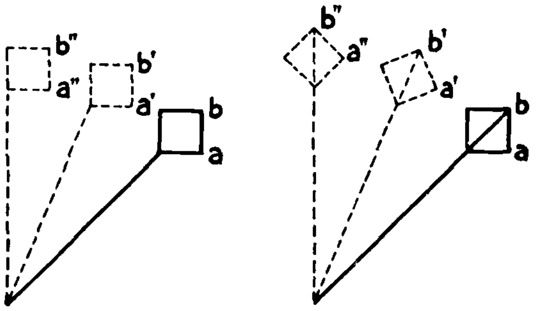

IRROTATIONAL **ROTATIONAL**

Figure 3. Effect of Rotation on the Motion of a Fluid Particle

The sketch, Figure 3, shows the difference in the behavior of a fluid particle in the two types of motions.

Bernoulli's Theorem. Bernoulli's theorem states that the total energy of a fluid particle is constant at all points on its path in a steady flow. In equation form,

$$\frac{P}{w} + \frac{V^2}{2g} + Z = H \qquad (17)$$

where P/w is the "pressure head," $V^2/2g$ the "velocity head," Z the potential head, and H a constant. w is the specific weight of the fluid. It will be noted that this equation is essentially an application of the law of conservation of energy to a fluid particle.

The equation is due to Daniel Bernoulli and dates from 1737. In the original form and as given, it applies only to steady flow of an incompressible fluid, but many of the more common problems of hydrodynamics are solved by its use, with the following restrictions:

> For a general fluid in general motion, H is never constant.
> For an incompressible fluid in general motion, H is constant for a given particle.
> For an incompressible fluid in steady motion, H is constant for all particles along a streamline.
> For an incompressible fluid in steady irrotational motion, H is constant for all particles throughout the fluid.

In most of the flows considered in aerodynamics, the potential or elevation head Z does not change and Bernoulli's equation takes the form

$$p + \tfrac{1}{2}\rho V^2 = \text{a constant} \tag{18}$$

or

static pressure + dynamic pressure = total pressure.

Velocity Potential. If the fluid flow is such that the circulation about every closed curve vanishes, it may be shown that $u\,dx + v\,dy$ is an exact differential which may be written

$$u\,dx + v\,dy = -\,d\Phi \tag{19}$$

from which

$$u = -\,\partial\Phi/\partial x \qquad v = -\,\partial\Phi/\partial y$$

In a flow of this type, the velocities are negative derivatives of the function $\Phi\,(x, y)$ which is known as velocity potential. The flows of this type are designated potential flows and exist only where the motion is irrotational

There is a definite physical significance in the velocity potential. It is a velocity gradient that may be produced by an impulsive pressure acting on a fluid boundary. Velocity potential and stream function are analogous to the lines of force and magnetic flux in a magnetic field. Constant values of the velocity potential Φ give equipotential contours or lines of force. Constant values of the stream function ψ give the streamlines or instantaneous directions of flow. Lines of constant Φ and constant ψ always intersect at right angles.

The lines of constant ψ and constant Φ may be visible in certain cases. For example, an observer on a boat can see the streamlines made visible by foam or floating objects. The lines of constant Φ are visible on the surface of calm water, while a boat is being accelerated from rest. This effect requires proper lighting and surface conditions such as are found, for example, in a model basin.

Φ and ψ are connected by the mathematical relation

$$d\psi = v\,dx - u\,dy = -\frac{\partial \Phi}{\partial y}dx + \frac{\partial \Phi}{\partial x}dy \qquad (20)$$

To recapitulate, a velocity potential Φ can exist only when the motion is irrotational. If the motion is irrotational, Φ can exist in either a compressible or an incompressible fluid. A stream function ψ can exist only in an incompressible fluid, but it is independent of rotation. For irrotational motion in an incompressible fluid, either a velocity potential or a stream function, or both, may exist.

Sources and Sinks. Many flow conditions are readily duplicated by the assumption that fluid is generated at certain points called "sources" and absorbed at other points called "sinks." Sources and sinks are not necessarily confined to points. They may be given any desired distribution along a line or over a surface. The only requirement is that if the boundary curve between the fluid in the general flow and the fluid produced by the sources is to be closed, then the total fluid absorbed by the sinks must be equal to the fluid produced by the sources.

The flows produced by sources and sinks are easily calculated and visualized. Hence, they are very useful for illustrating some of the fundamental methods in the mathematical analysis of fluid flow.

Consider the two-dimensional flow due to a line source generating fluid per unit length at the rate of Q units per second. Assuming that the fluid is continuous and incompressible, the flow must be outward in radial lines along which the velocity decreases inversely as the distance from the center. The flow across a circle of radius r with its center at the origin is

$$V = Q/2\pi r$$

This is a form of potential flow. Since $V = -\partial\Phi/\partial r$, the velocity potential for a source is

$$\Phi = -\frac{Q}{2\pi}\int\frac{dr}{r} = -\frac{Q}{2\pi}\log r \tag{21}$$

The flow for a sink is obtained by reversing the sign of Q.

The combined effect at any point produced by a system of sources and sinks is obtained by adding the individual velocity potentials.

Vortex Motion—Vortices. Vortex motion is a common natural phenomenon appearing in different outward forms and covering a tremendous range in scale extending from a tiny whirlpool or eddy that is barely visible to the naked eye to a tropical hurricane or a cyclonic air movement that affects an entire continent. The vortex in nature, considered as a fluid motion, may or may not be irrotational. It is irrotational if the tangential velocity varies inversely as the distance from the center. It is rotational to the extent that the velocities vary from the inverse law. In all probability some rotation is always present in a natural vortex.

The mathematical vortex used in hydrodynamics is simply an irrotational motion in which the velocity varies inversely as the distance from the center. It is a concept that has been found very helpful in the solution of many problems connected with a lifting wing. The important point for the engineer to grasp is that by the superposition of a vortex field on a simple potential flow, it is possible to duplicate very closely the actual flow around a wing. This does not mean that there is an actual physical vortex surrounding the wing. It means that the distribution of circulation velocity corresponds closely to that required for a vortex. As a matter of fact, identical results can be obtained in many cases as Munk[1] has shown by the use of fundamental energy relations instead of vortices.

In order to avoid the infinite velocities otherwise required at the origin, it is assumed that vortex motion takes place about a very small core within which the motion is rotational. Vortex motion may be distributed along a line of any desired shape. Such a line is known as a vortex line or vortex filament. The core enclosing such a line is known as a vortex tube.

A vortex is stable motion, persisting indefinitely in a perfect fluid. Its strength is constant with time and constant over the entire filament length. A vortex filament cannot begin or end at a point within the fluid.

In the application of vortices to the lifting wing, these requirements are met by considering the vortex motion distributed along three sides of an open rectangle, one side of which is the span of the "lifting line" that replaces the wing, and the other two are lines extending (theoretically to an infinite distance) backward from the wing tip. The circulation around this "horseshoe" or U-shaped vortex tube may be visualized as being similar to the flow in a section of a smoke-ring; that is, the direction of rotation does not change in going around the ring. Looking downstream from the wing, the circulation in the left-hand branch is clockwise and that in the right-hand branch is counter clockwise, so that their motion, like two gears in mesh, is such as to produce a downwash along the center-line.

---

[1] Max M. Munk, "Elements of the Wing Section Theory and of the Wing Theory," N.A.C.A. Technical Report No. 191.

CHAPTER 3

APPLIED WING THEORY

The application of theoretical hydrodynamics to the problems of air flow around a lifting wing has yielded results that are exceedingly valuable to the airplane designer. By the aid of these theoretical relations, it is now possible to predict accurately the effects that changes in wing arrangement will have on the aerodynamic characteristics of a given airplane design.

In the original form, as reported by the scientists and mathematicians responsible for the theoretical investigations, many of these important solutions are unsuited for design application. It is the purpose of this chapter to present applied wing theory in the form of design data. Very few derivations will be given, but in each case reference is given to the original source of the theoretical derivation.

The contents of this chapter are concerned almost entirely with the application of theory to wing design, but this does not include all of the applied wing theory. An attempt has been made to place some very important theoretical relations in other chapters where they logically belong.

Induced Drag. In 1911, Dr. Prandtl and his assistants at Göttingen derived a relation between the circulation Γ and the vertical or downwash velocity component w, due to a lifting wing. At the same time it was proved that half of the final downwash velocity was acquired forward of the center of pressure, or in other words, a downward acceleration was imparted to the air at some distance forward of a lifting wing which, therefore, operated in a downwardly inclined air stream. The average downwash velocity at the center of pressure was found to be greater, the greater the lift, and the nearer to the center of the wing the main production of vortices.

As a result of the virtual inclination of the air stream through the angle $\varphi = \tan^{-1}(w/v)$, the wing "goes up a hill" having the slope φ. Consequently, the lift, which is vertical to the relative wind, now has a rearward or drag component. Without going into the details of the derivation[1] it was shown that the inclination of the lift vector, and hence the drag, was a minimum when the downwash was constant along the span, and that this condition corresponded to a lift distribution proportional to the ordinates of an ellipse having the span as a diameter.[2] The constant value of the downwash velocity resulting from the elliptical lift distribution was shown to be

$$w = \Gamma_0/2b$$

where Γ_0 is the circulation at the center of the span b. It may be shown that the value of Γ_0 is

$$\Gamma_0 = 4L/\pi\rho Vb$$

where L is the lift and ρ the density. Hence, the downwash velocity is

$$w = 2L/\pi\rho\, Vb^2$$

Since the downwash is constant along the span, the drag D is

$$D = L(w/V) = 2L^2/\pi\rho V^2b^2 = L^2/\pi qb^2 \qquad (22)$$

---

[1] See L. Prandtl, "Applications of Modern Hydrodynamics to Aeronautics," N.A.C.A Technical Report No. 116 (1921).

[2] The mathematical proof was first given by Munk in his Göttingen Dissertation which was subsequently translated and published as N.A.C.A. Technical Report No. 121 "The Minimum Induced Drag of Aerofoils."

It was found in 1913 that the actual measured drags were greater than this theoretical minimum but the wing sections investigated were very poor. Two years later, investigations on much better wing sections showed close agreement between the theoretical and the measured drag. The investigation was then continued on wings of various aspect ratio and a very important discovery made. At the same lift coefficient with the same wing section, the difference between the theoretical and measured drag coefficients was always the same, within the experimental error, of course, for any aspect ratio. The part of the total drag which does not change with aspect ratio is due to the shape of the wing section and hence it was given the designation "Profile Drag" or "Section Drag." The theoretical drag, varying only with lift and span, was given the designation "Induced Drag" from the analogy to electrical induction phenomena. This constituted one of the most important advances ever made in theoretical aerodynamics and opened an immense field of practical application.

Substituting $C_L qS$ for L and $C_D qS$ for D in equation (22) gives the coefficient of induced drag

$$C_{D_i} = \frac{C_L^2 S}{\pi b^2} \tag{23}$$

The section drag is $C_{D_0} = C_D - C_{D_i}$ and this is constant for any given section and lift coefficient. Hence, at a constant value of C_L the relation between the drags for two aspect ratios is

$$C_{D_1} - \frac{C_L^2 S_1}{\pi b_1^2} = C_{D_2} - \frac{C_L^2 S_2}{\pi b_2^2}$$

or

$$C_{D_2} = C_{D_1} + \frac{C_L^2}{\pi}\left[\frac{S_2}{b_2^2} - \frac{S_1}{b_1^2}\right] \tag{24}$$

which enables the drag to be calculated for any aspect ratio when the drag is known for one aspect ratio.

Induced Angle of Attack. Since the wing is operating in a vertical downwash velocity of

$$w = \frac{2L}{\pi \rho V b^2}$$

and a horizontal velocity of V, the relative wind direction is inclined downward to the rear of the wing by the angle having the value

$$\varphi = \alpha_i = \tan^{-1}\left(\frac{w}{V}\right) = \tan^{-1}\left(\frac{2L}{\pi \rho V^2 b^2}\right)$$

φ is always small so that $\tan \varphi = \varphi$, hence

$$\varphi = \alpha_i = \frac{2L}{\pi \rho V^2 b^2} \qquad (25)$$

α_i is the "induced angle of attack." It increases as the aspect ratio decreases. The physical significance is that as the aspect ratio is decreased, the downwash increases and the wing must be turned up to a higher apparent or geometrical angle of attack in order to obtain a given lift coefficient.

Munk's Span Factor. Equation (23) was completed by Munk, who showed that in order to apply to biplanes (or multiplanes) the maximum span b must be replaced by kb, which is the span of the monoplane having the same area and induced drag as the biplane (or multiplane). For a monoplane $k = 1.00$, but for a biplane k varies with the ratio of gap to span, the ratio of the spans, and the proportional area in the two wings as will be shown later.

The introduction of the span factor was of great practical importance. With this factor, equation (23) becomes

$$C_{Di} = \frac{C_L^2 S}{\pi (kb)^2} \tag{23a}$$

and equation (24) becomes

$$C_{D_2} = C_{D_1} + \frac{C_L^2}{\pi}\left[\frac{S_2}{(k_2b_2)^2} - \frac{S_1}{(k_1b_1)^2}\right] \tag{24a}$$

In a similar manner, the induced angle of attack in radians is

$$\alpha_i = \frac{C_L S}{\pi (kb)^2} \tag{25a}$$

and in degrees the total angle of attack is

$$\alpha_2 = \alpha_1 + \frac{57.3 C_L}{\pi}\left[\frac{S_2}{(k_2b_2)^2} - \frac{S_1}{(k_1b_1)^2}\right] \tag{26}$$

Equation (26) is only approximately correct. Munk completed it later[3] by dividing into three parts the angle of attack necessary to produce a given lift coefficient. These parts are as follows: (a) the intrinsic angle of attack for the given wing section and lift coefficient, (b) the additional induced angle of attack, and (c) the additional interference angle of attack. With this modification, equation (26) becomes

$$\alpha_2 = \alpha_1 + \frac{57.3 C_L}{\pi}\left[\left(\frac{S_2}{(k_2b_2)^2} + I_2\right) - \left(\frac{S_1}{(k_1b_1)^2} + I_1\right)\right] \tag{26a}$$

where I is the interference factor. I varies slightly with stagger and with wing section, and is less for a lift produced by curvature than for lift produced by angle of attack. However, I is approximately a function of gap-chord ratio only, with the following average values according to Munk:

---

[3] Max M. Munk. "General Biplane Theory," N.A.C.A. Technical Report No. 151 (1922).

$\frac{\text{Gap}}{\text{Chord}}$	∞	2.87	2.02	1.46	1.11	.98	.79	.64
I	0	.012	.024	.030	.055	.060	.082	.104

These values are plotted in Figure 4.

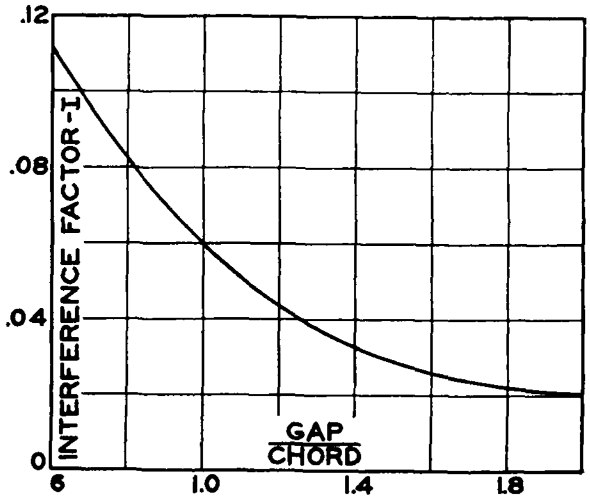

Figure 4. Munk's Interference Factor for Induced Angle of Attack

Prandtl's Interference Factors. Prandtl has shown[4] that the drag of one wing of a biplane in the presence of the other may be expressed in the form

$$D_{12} = \sigma \frac{L_1 L_2}{\pi q b_1 b_2} \tag{27}$$

---

[4] "Technische Berichte," Vol. II, No. 6 (N.A.C.A. Technical Note No. 182) and N.A.C.A. Technical Report No. 116.

where D_{12} is the drag of wing 1 (having lift L_1 and span b_1) in the presence of wing 2 (having lift L_2 and span b_2) and σ is an "interference factor" which varies with the ratios of gap to span and shorter span to longer span.

Prandtl gives values of σ in terms of $\frac{b_2}{b_1}$ and $\frac{\text{gap}}{\text{average span}}$ or $\left(\frac{2G}{b_1 + b_2}\right)$ as shown in Figure 5. These data have been converted and replotted in Figure 6, using the ratio of gap to maximum span, instead of the ratio gap to average span.

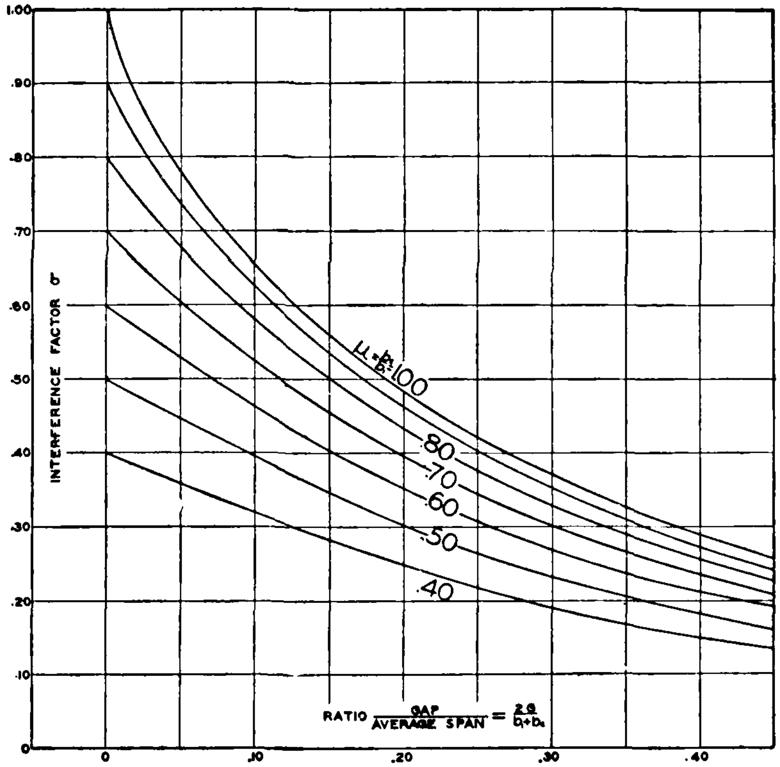

Figure 5. Prandtl's Drag Interference Factor for Biplanes, in Terms of Average Span

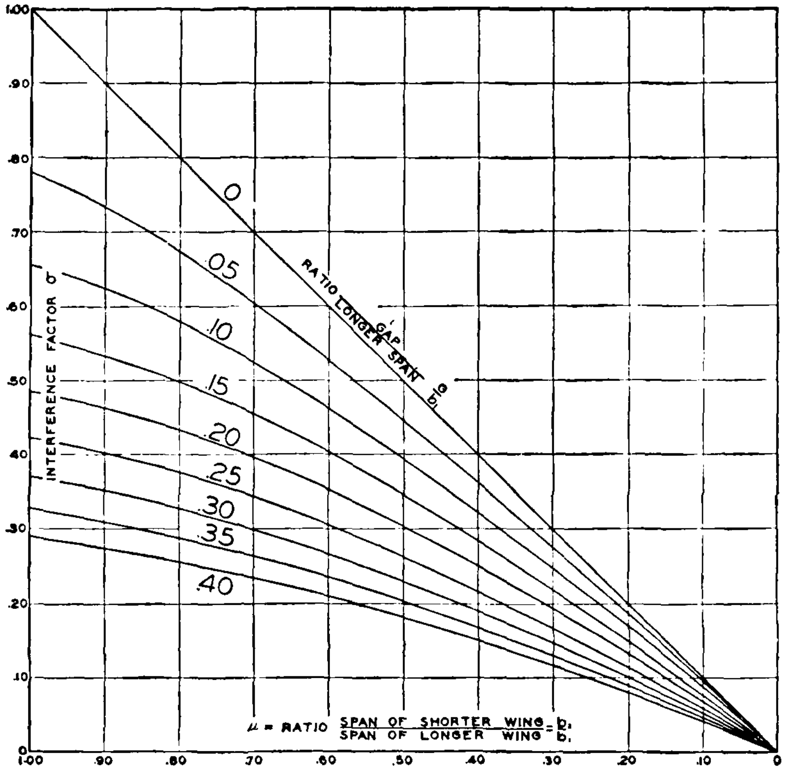

Figure 6. Prandtl's Drag Interference Factor for Biplanes in Terms of Maximum Span

Induced Drag of Biplanes. The interference factor σ may be used to calculate the value of the span factor k for any biplane, as shown by Prandtl. The method is as follows:

Let b_1 = span of longer wing
b_2 = span of shorter wing
$\mu = \frac{b_2}{b_1}$ = ratio shorter span to longer
L_1 = lift on longer wing
L_2 = lift on shorter wing
$L = L_1 + L_2$ = total lift

Prandtl's equation for total induced drag is

$$D_i = \frac{1}{\pi q}\left[\frac{L_1^2}{b_1^2} + 2\sigma\frac{L_1L_2}{b_1b_2} + \frac{L_2^2}{b_2^2}\right] \tag{28}$$

This is a minimum when

$$L_2/L_1 = (\mu - \sigma)/[(1/\mu) - \sigma]$$

and has the value

$$\text{Minimum } D_i = \frac{L^2}{\pi q b_1^2}\left[\frac{1 - \sigma^2}{1 - 2\sigma\mu + \mu^2}\right] \tag{29}$$

Assuming the lift proportional to the area and setting $S_1 = rS$, it follows that $S_2 = (1 - r)S$, $L_1 = rL$ and $L_2 = (1 - r)L$. The factor r is obviously the ratio of area (or lift) of the longer wing to the total area (or lift). Substituting these relations into equation (28) gives

$$D_i = \frac{L^2}{\pi q b_1^2}\left[r^2 + \frac{2\sigma}{\mu}r(1 - r) + \left(\frac{1 - r}{\mu}\right)^2\right] \tag{28a}$$

from which the span factor is seen to be

$$k = \left[\frac{\mu^2}{r^2(\mu^2 - 2\mu\sigma + 1) + 2r(\mu\sigma - 1) + 1}\right]^{\frac{1}{2}} \tag{30}$$

Figures 7, 8, 9, 10, and 11 give the values of k against μ and r for G/b_1 = .05, .10, .15, .20, and .25. This covers the extreme range ordinarily used. The variation of k is substantially linear with G/b_1 between any two adjacent values of G/b_1 and hence k may be obtained by interpolation. However, a great majority of biplane designs have wings which approximate either equal chords or equal aspect ratio. Figures 12 and 13 have been prepared to give the value of k directly in terms of b_2/b_1 and G/b_1.

Proportions of the Most Efficient Biplane. Figure 14 gives the proportions of the most efficient biplane as determined from Figures 7 to 11. From this diagram the best value of any one variable, c_2/c_1, G/b_1 or b_2/b_1 is determined when the other two are assumed or known.

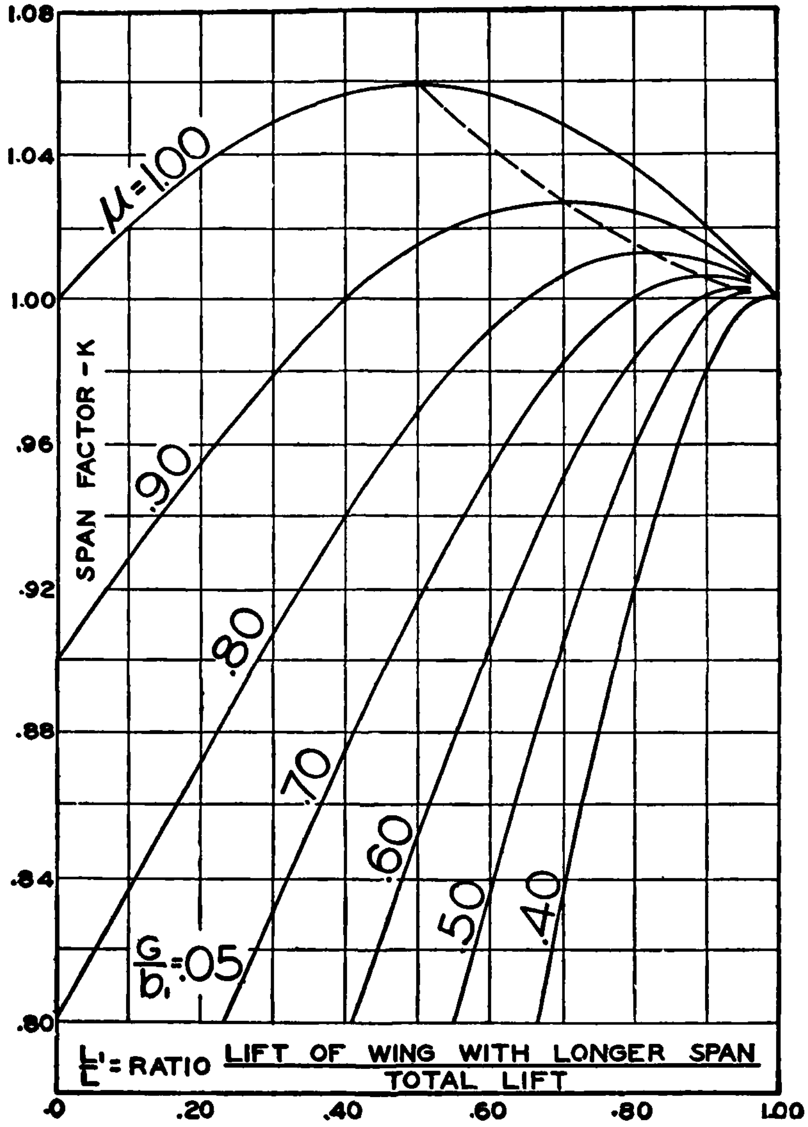

Figure 7. Munk's Span Factor k for $\frac{G}{b_1} = .05$

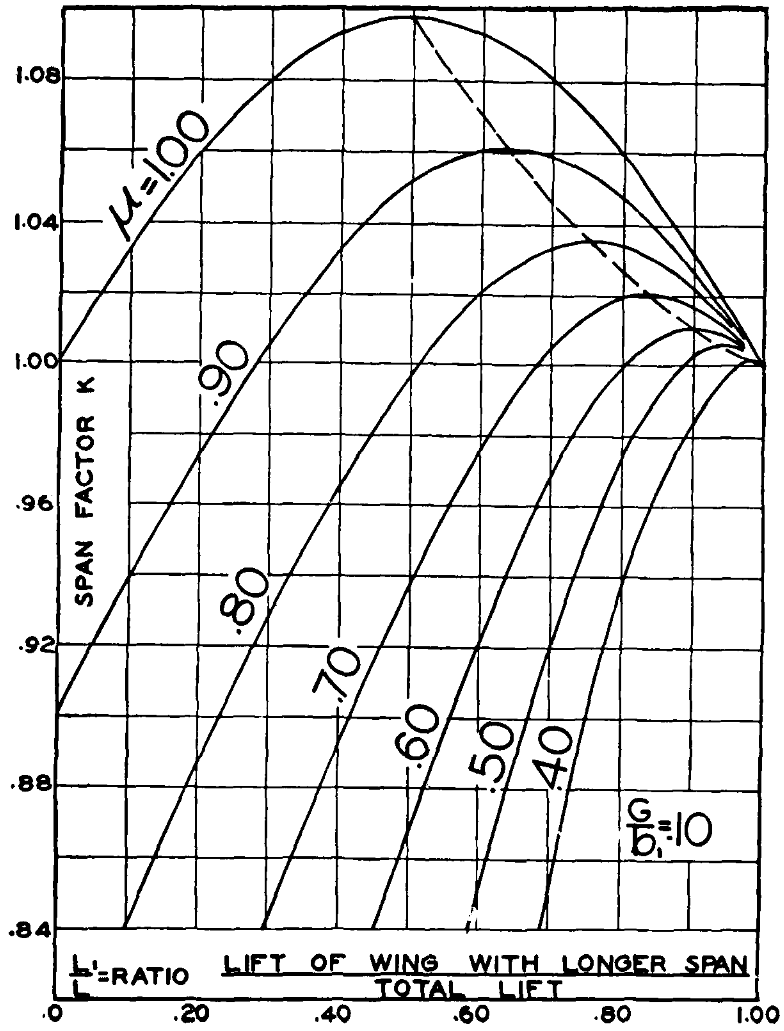

Figure 8. Munk's Span Factor k for $\frac{G}{b_1} = 0.10$

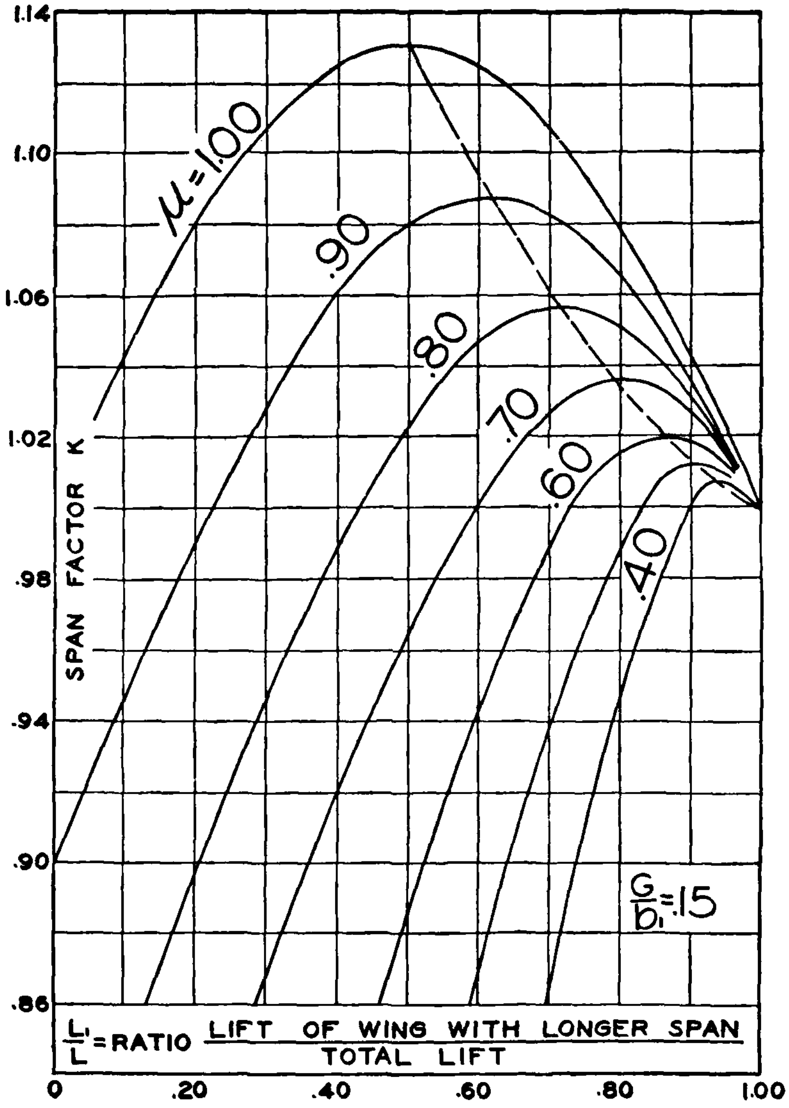

Figure 9. Munk's Span Factor k for $\frac{G}{b_1} = 0.15$

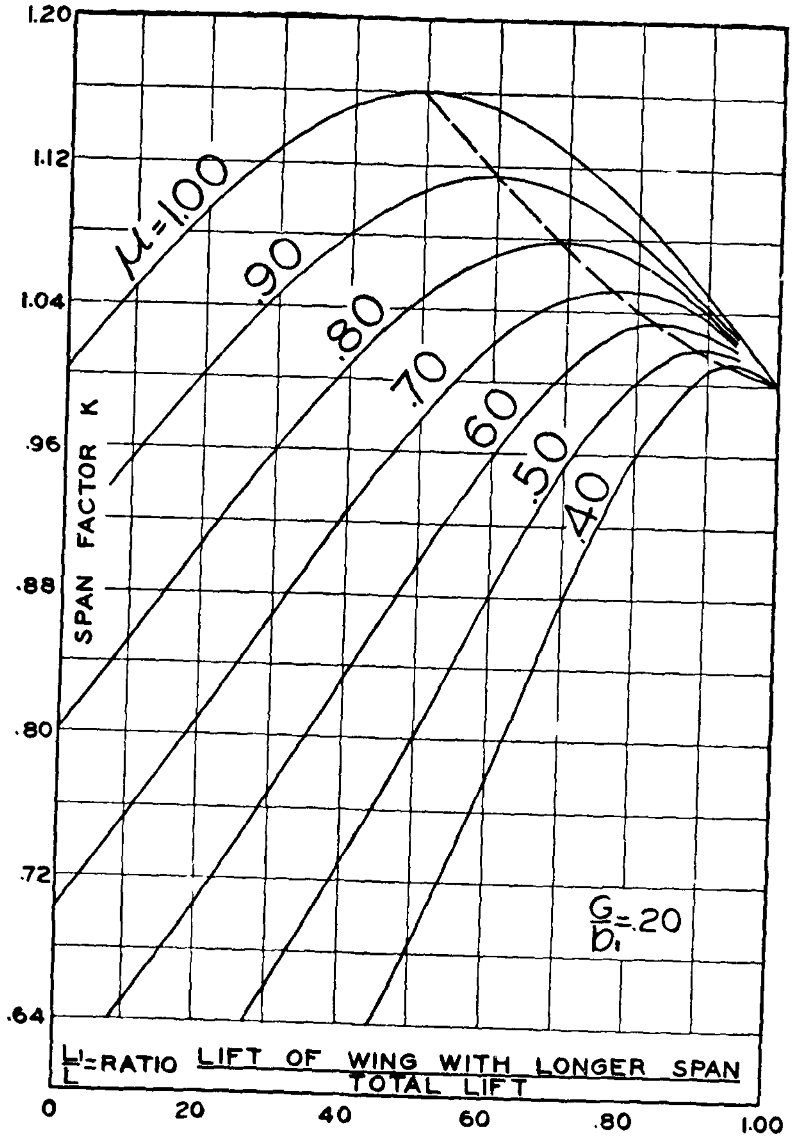

Figure 10. Munk's Span Factor k for $\frac{G}{b_1} = 0.20$

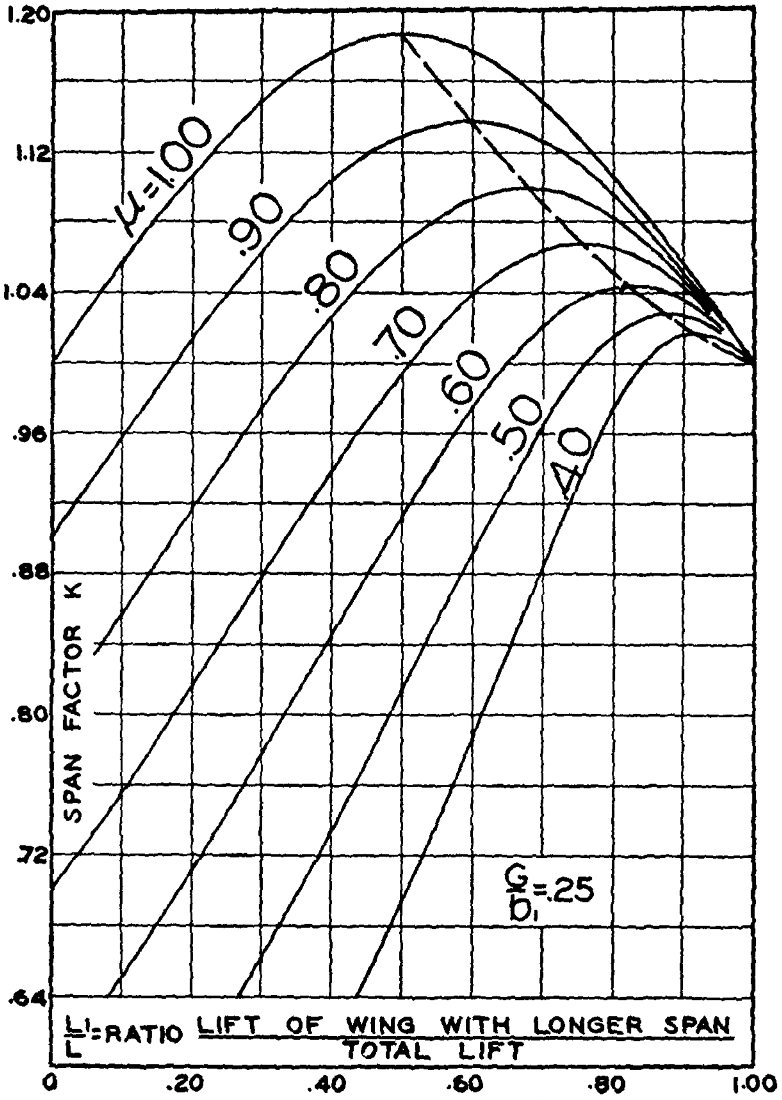

Figure 11. Munk's Span Factor k for $\frac{G}{b_1} = 0.25$

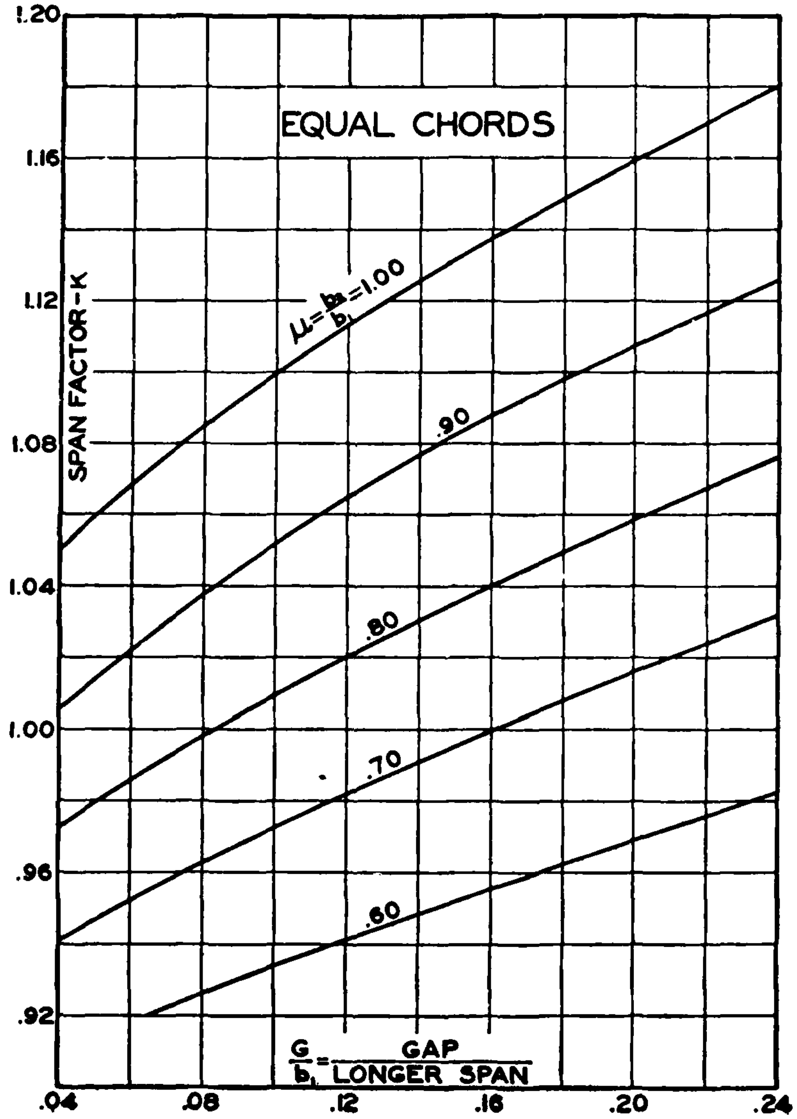

Figure 12. Munk's Span Factor k for Biplanes with Wings of Equal Chords

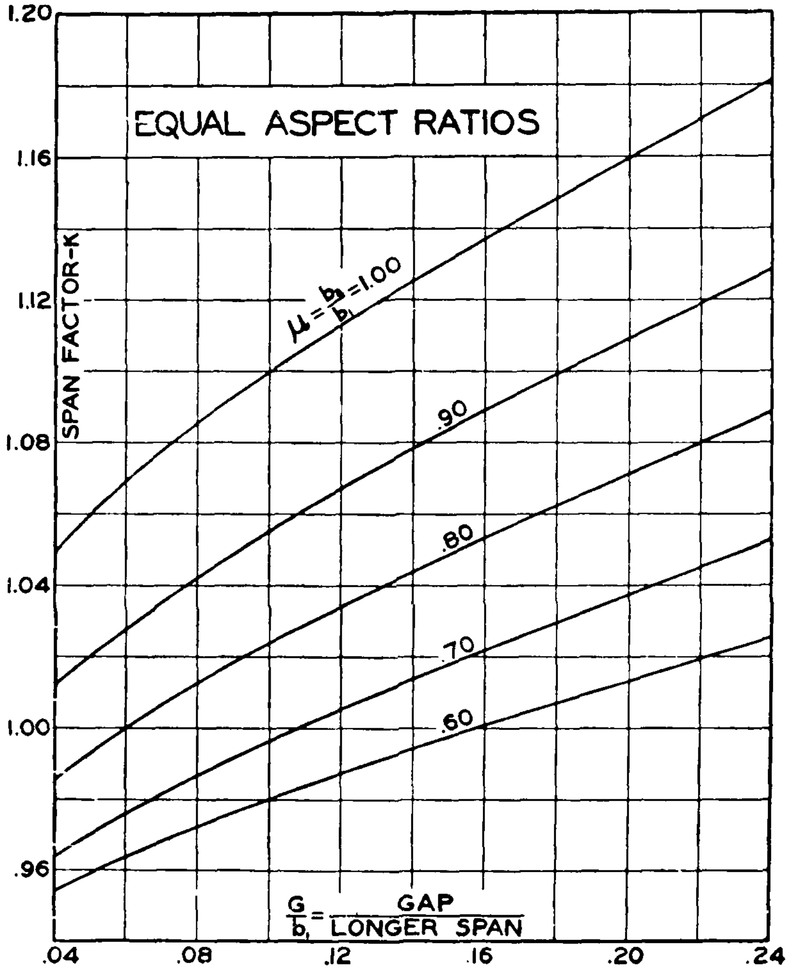

Figure 13. Munk's Span Factor *k* for Biplanes with Wings of Equal Aspect Ratio

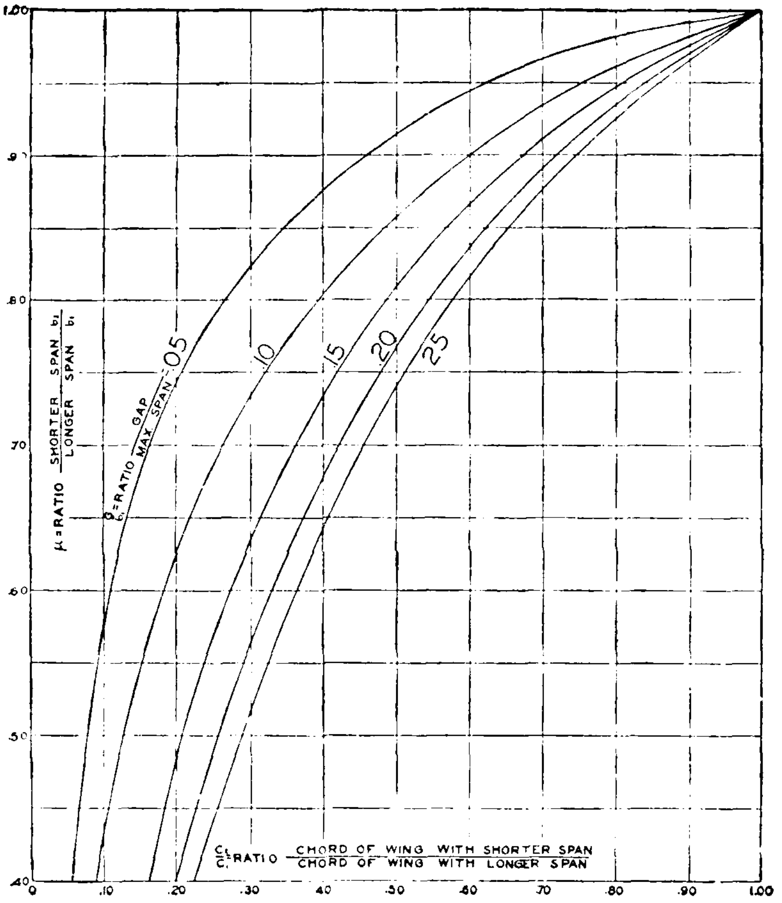

Figure 14. Proportions of the Most Efficient Biplane

Induced Drag of Triplanes. Prandtl[5] has given a solution for the induced drag of a triplane using the same notation previously used for the biplane. It is assumed that the three wings have the same span and that the middle wing is equidistant from the upper and the lower wing. From the results of the biplane theory, it appears that the lift of the upper and lower wings should be equal for minimum induced drag. Setting the lift of the middle wing $L_2 = xL$, then $L_1 + L_3 = L - xL = L(1 - x)$ or $L_1 = L_3 = L(1 - x)/2$.

The adjacent wings have a mutual interference factor σ_1 based on gap $G/2$. The upper and lower wings have a corresponding factor σ_2 based on a gap G. The individual induced drags are given by

$$\pi q b^2 D_1 = (L_1^2 + \sigma_1 L_1 L_2 + \sigma_2 L_1 L_3) \tag{31a}$$

$$\pi q b^2 D_2 = [L_2^2 + \sigma_1 (L_1 L_2 + L_2 L_3)] \tag{31b}$$

$$\pi q b^2 D_3 = (L_3^2 + \sigma_1 L_2 L_3 + \sigma_2 L_1 L_3) \tag{31c}$$

The total drag in terms of L and x is

$$D = \frac{L^2}{2\pi q b^2}\left[1 + \sigma_2 - 2x(1 + \sigma_2 - 2\sigma_1) + x^2(3 + \sigma_2 - 4\sigma_1)\right] \tag{32}$$

which is a minimum when

$$x = \frac{1 + \sigma_2 - 2\sigma_1}{3 + \sigma_2 - 4\sigma_1} \tag{33}$$

Values of the equivalent monoplane span factors are given in Table 1, and the triplane span factors are plotted against G/b in Figure 15.

Induced Drag of Tandem Wings. The arrangement of wings in tandem is of limited practical interest and the

---

[5] L. Prandtl, "Der induzierte Widerstand von Mehrdeckern," Technische Berichte Vol. III, No. 7, Pa. 309. (Translated and published as N.A.C.A. Technical Note No. 182.)

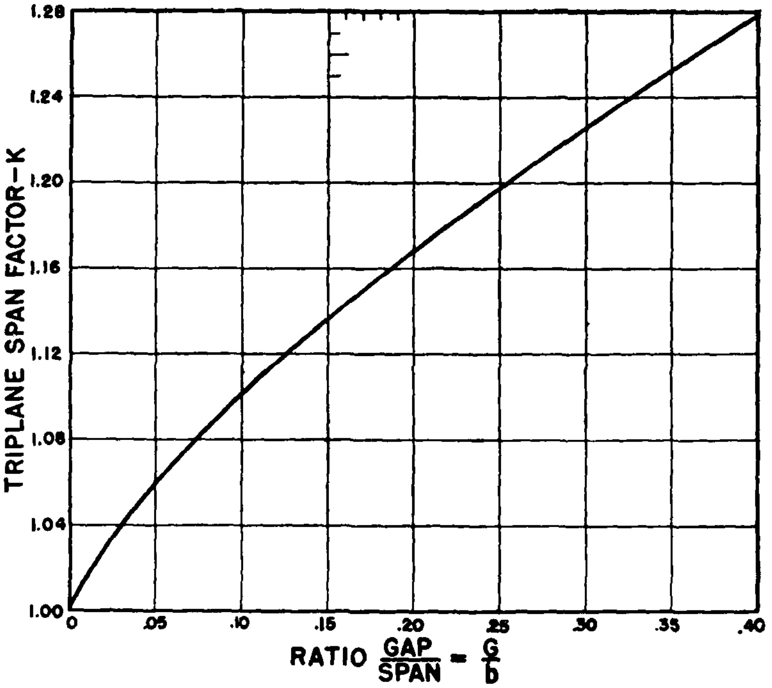

Figure 15. Munk's Span Factor k for Triplanes

TABLE 1. EQUIVALENT MONOPLANE SPAN FACTORS

Gap/Span $\frac{G}{b}$	Biplane k	Triplane $x = 0.33$ k	Best Triplane k	Value of x for Best Triplane x	Best Wing System k
0	1.000	1.000	1.000	0	1.000
.05	1.060	1.060	1.062	.161	1.075
.10	1.100	1.102	1.105	.177	1.127
.15	1.133	1.136	1.142	.190	1.172
.20	1.161	1.168	1.175	.202	1.214
.25	1.187	1.199	1.207	.212	1.252
.30	1.207	1.227	1.235	.222	1.289
.35	1.229	1.252	1.260	.231	1.321
.40	1.245	1.278	1.283	.238	1.355
.45	1.260	1.300	1.307	.244	1.385
.50	1.275	1.323	1.330	.251	1.414

aerodynamic characteristics have not been as thoroughly investigated as other types. Glauert[6] gives a solution based on the mutual induced angles of attack. This results in a moderate drag reduction for the leading wing and marked drag increase for the following wing. The net result is a rather large induced drag for the combination.

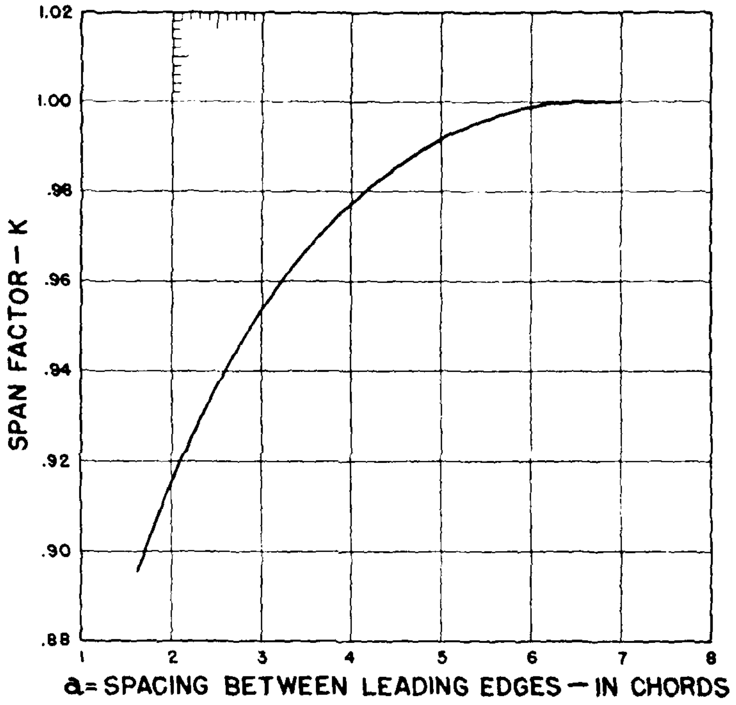

Figure 16. Munk's Span Factor *k* for Tandem Wings

Munk's tests reported in Volume II of the Technische Berichte have been analyzed to determine the equivalent monoplane span; the resulting factors in terms of the spacing between the leading edges are given on Figure 16.

---

[6] H. Glauert, "The Performance of Tandem Systems," Br. A.R.C., R.&M. No. 949, 1925.

This curve is for tandem wings of equal span and area. The effective span of two wings in biplane arrangement is approximately 10% greater than in tandem arrangement.

Low Aspect Ratio. The theoretical effects of aspect ratio have been fully substantiated by test data at moderate and high values of aspect ratio. However, for values of aspect ratio below 2.0 the flow conditions are modified somewhat by the interference between the tip vortices. This interference has the effect of producing an increased virtual span so that the induced drag for an aspect ratio less than unity is appreciably less than the unmodified theoretical induced drag.

Zimmerman's[7] tests show that for values of n between 0.5 and 1.25 the relations between the actual and the effective spans are as follows:

Actual span	0.50	0.75	1.00	1.25
Effective span	0.63	0.88	1.11	1.34

This increase in effective span is not great, but it does have a very large effect on the induced drag, which is sometimes quoted as an argument in favor of low aspect ratio. The fallacy in the argument is obvious since the effect is merely to reduce by a slight amount the inherent aerodynamic inefficiency of the low aspect ratio arrangement.

Slope of Lift Curve. The theoretical slope of the lift curve for a wing of infinite aspect ratio is, for α in radians

$$\frac{dC_L}{d\alpha} = a_0 = 2\pi \tag{34}$$

or for α in degrees

$$a_0 = 0.1097 \tag{34a}$$

---

[7] C. H. Zimmerman, "Characteristics of Clark Y Airfoils of Small Aspect Ratios," N.A.C.A. Technical Report No. 431, 1932.

The variation of a with aspect ratio is readily calculated from the induced angle of attack. In passing from a higher to a lower aspect ratio, the induced angle of attack is increased and the slope is decreased. The new slope is

$$a_2 = \frac{\Delta C_L}{\Delta\alpha_1 + \Delta\alpha_i} = \frac{a_1}{1 + (\Delta\alpha_i/\Delta\alpha_1)} = \frac{a_1}{1 + a_1(\Delta\alpha_i/\Delta C_L)} \tag{35}$$

From equation (26) the value of $\Delta\alpha_i/\Delta C_L$ is

$$\Delta\alpha_i/\Delta C_L = 18.24\ [(1/n_2) - (1/n_1)]$$

hence

$$a_2 = \frac{a_1}{1 + 18.24\, a_1[(1/n_2) - (1/n_1)]} \tag{36}$$

If a_0 is the slope of the lift curve for infinite aspect ratio, the slope a for any finite aspect ratio n is

$$a = a_0/(1 + \frac{18.24}{n} a_0) \tag{37}$$

The slope for infinite aspect ratio is obtained from the slope for a finite aspect ratio by

$$a_0 = a/(1 - \frac{18.24}{n} a) \tag{38}$$

Equations (36), (37), and (38) are for elliptical lift distribution. For the modified distribution with square wing tips, the τ correction, Figure 17, must be used, and the equations become

$$a_2 = \frac{a_1}{1 + 18.24a_1\left[\frac{(1 + \tau_2)}{n_2} - \frac{(1 + \tau_1)}{n_1}\right]} \tag{36a}$$

$$a = \frac{a_0}{1 + \frac{18.24a_0}{n}(1 + \tau)} \tag{37a}$$

$$a_0 = \frac{a}{1 - \frac{18.24a}{n}(1 + \tau)} \tag{38a}$$

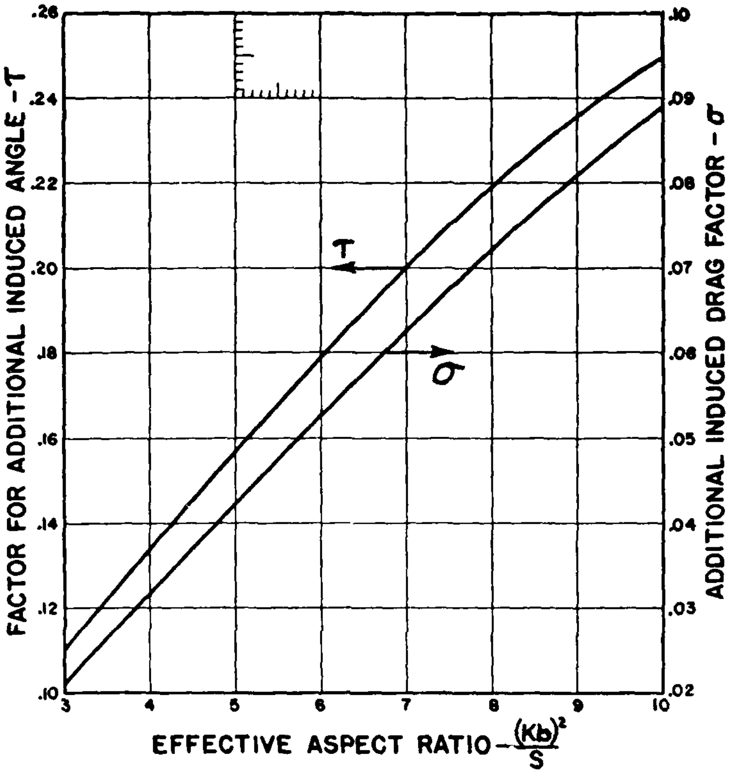

Figure 17. Tau and Sigma Correction Factors

Observed values of a average about 10% lower than the theoretical value of 2π. Experimental data on slope of the lift curve are given on page 126.

Correction for Rectangular Wing Tips. The induction theory is based on an assumed elliptical lift distribution corresponding to a moderately tapered wing with faired or rounded tips. A rectangular wing such as the conventional airfoil model requires correction factors for the induced angle of attack α_i and the induced drag coefficient

C_{D_i}. The corrections, due to Glauert, are usually given in the form

$$\alpha_i = \frac{C_L}{\pi n}(1 + \tau) \tag{39}$$

$$C_{D_i} = \frac{C_L^2}{\pi n}(1 + \sigma) \tag{40}$$

where τ and σ depend upon aspect ratio as shown on Figure 17.

Rectangular tips increase the induced angle of attack about 18% and the induced drag about 5%.

The factors τ and σ must always be used with square tips if accurate results are required.

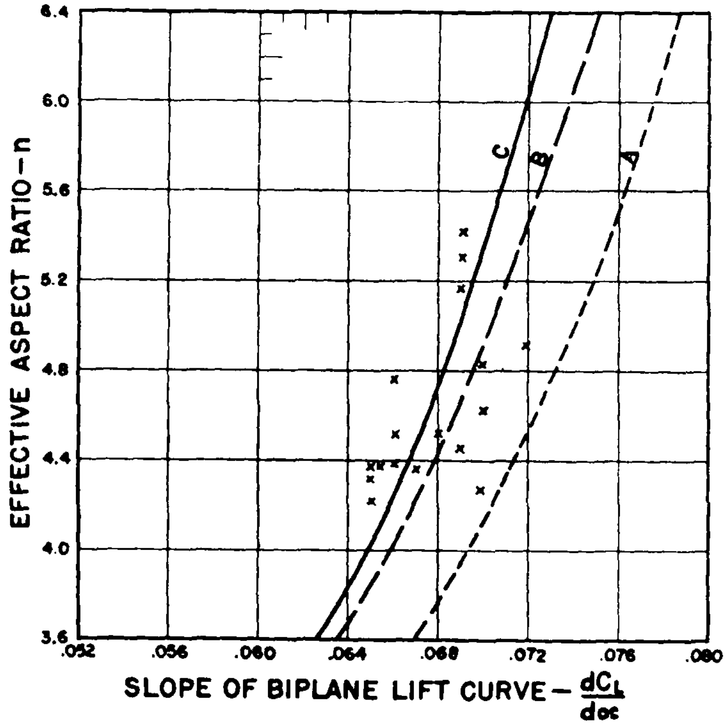

Figure 18. Comparison of Theoretical and Observed Slopes of Biplane Lift Curves

Slope of Biplane Lift Curve. The slope of the lift curve for a biplane does not differ appreciably from the theoretical value for the same effective aspect ratio. Figure 18 gives a comparison of theoretical and observed slopes. The curve marked **A** is the theoretical slope for elliptical lift distribution. Curve **B** is the theoretical slope with the τ correction for square tips. Curve **C** is the theoretical slope including Munk's interference factor, equation (26a).

From an inspection of these data, it appears that Munk's factor gives very close agreement, and that the "tau" correction, curve **B**, is also satisfactory.

Wing with a Fore-and-Aft Slot. Prandtl gives the theoretical solution[8] for the effect of a fore-and-aft slot in a wing, such as that existing at a panel joint. This solution is of great practical value in that it indicates the necessity for avoiding any kind of "leakage" joints in wing construction.

For a monoplane with a fore-and-aft slot, Munk's span factor k is no longer unity, but much less than unity, even for a quite narrow slot. The variation of k with the width of the slot is given on Figure 19. The curve marked **A** on this figure is an enlargement for small slot widths. A slot width of $0.001 \times$ span reduces k to 0.87, which is equivalent to a reduction of about 24% in aspect ratio. This effect has long been known from Munk and Cario's wind-tunnel tests.

The average increase in drag due to various slot widths, as found in these tests, is given in Figure 20. A slot width of 1% of the chord on a wing of aspect ratio 6 increases the drag about 6%.

A fore-and-aft slot is very objectionable in a horizontal surface, owing to the reduction in slope of the lift curve and attendant loss in stabilizing effect.

---

[8] Due to Grammel and Polhausen. See N.A.C.A. Technical Report No. 116.

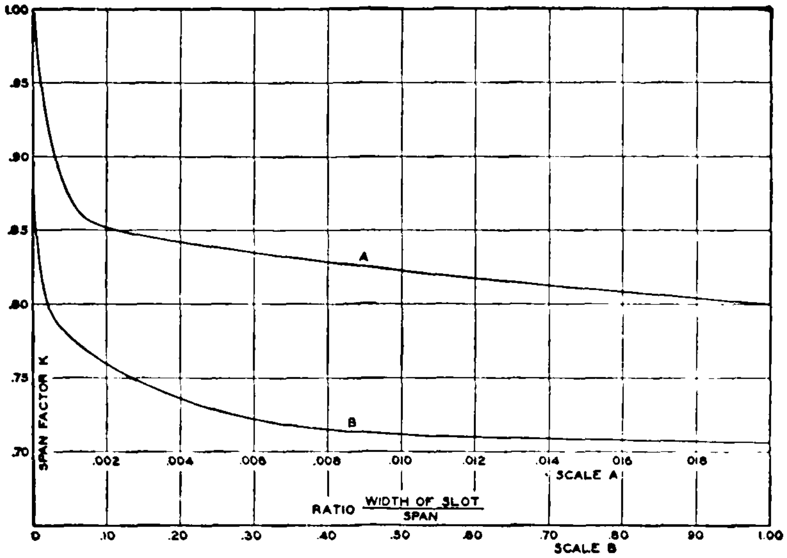

Figure 19. Munk's Span Factor for Wing with Fore-and-Aft Slot

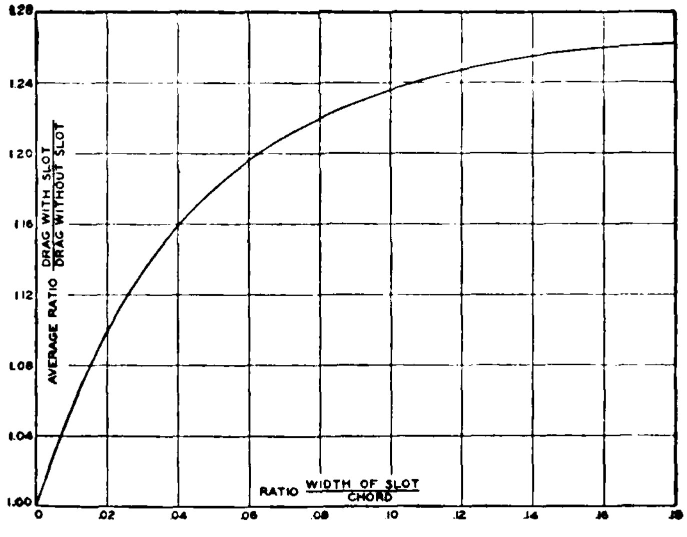

Figure 20. Observed Increase in Drag Due to Fore-and-Aft Slot

Downwash. The theoretical downwash angle at the trailing edge is

$$\epsilon = 2\alpha_i = \frac{2C_L}{\pi n} \text{ radians} \tag{41}$$

or in degrees

$$\epsilon = 36.5C_L/n \tag{41a}$$

where n is the effective aspect ratio.

Wind-tunnel explorations of the flow behind an airfoil indicate a narrow, highly turbulent wake extending down-

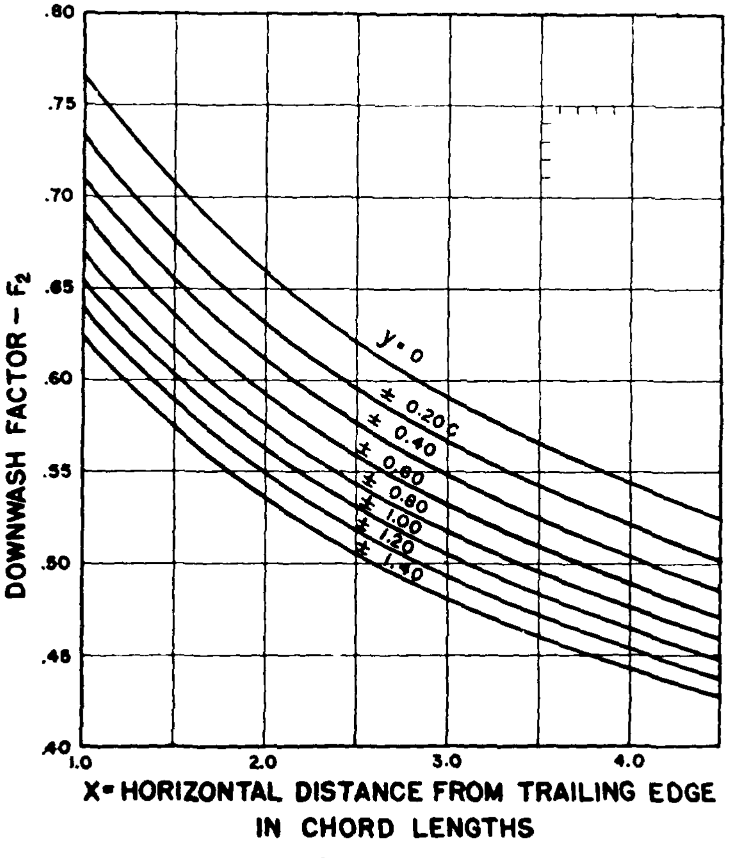

Figure 21. Downwash Factor F_2

stream from the trailing edge. The angle of downwash is a maximum in the wake and decreases with distance along, above, or below the wake. The observed angles of downwash are slightly less than the theoretical values given by equation (41).

Letting the distances measured in chord lengths be x downstream and y above or below the wake, the average downwash is found to be

$$\epsilon = \frac{52\, C_L}{n}(x + 1)^{-0.38}(y + 1)^{-0.23}$$

$$= 52 C_L F_2 / n \qquad \textbf{(41b)}$$

Values of F_2 are plotted against x and y on Figure 21.

Ground Effect. The lift of an airplane in steady horizontal flight is transferred to the ground in the form of an increase in static pressure. Prandtl[9] has shown that the integral of the increased ground pressure is exactly equal to the weight of the airplane. The increase in ground pressure at any point is given by

$$\Delta p = p - p_0 = \frac{Wh}{2\pi R^3} = \frac{Wh}{2\pi(h^2 + r^2)^{3/2}} \qquad \textbf{(42)}$$

where W is the gross weight, h is the height of the airplane above the ground, r is the horizontal distance of the reference point from the airplane, and $R^2 = h^2 + r^2$.

The influence of the ground in modifying the forces on the airplane may be calculated. Wieselsberger[10] shows that it is equivalent to an increase in the effective aspect ratio which reduces the induced drag and increases the slope of the lift curve. The maximum lift is unchanged, but it may occur at an appreciably lower angle of attack.

---

[9] L. Prandtl, "Applications of Modern Hydrodynamics to Aeronautics," N.A.C.A. T.R. No. 116 (1921).

[10] C. Wieselsberger, "Der Einfluss der Erdbodennähe auf den Flügelwiderstand," Ergebnisse der Aerodynamischen Versuchsanstalt zu Göttingen, Vol. II, R. Oldenbourg, München (1923).

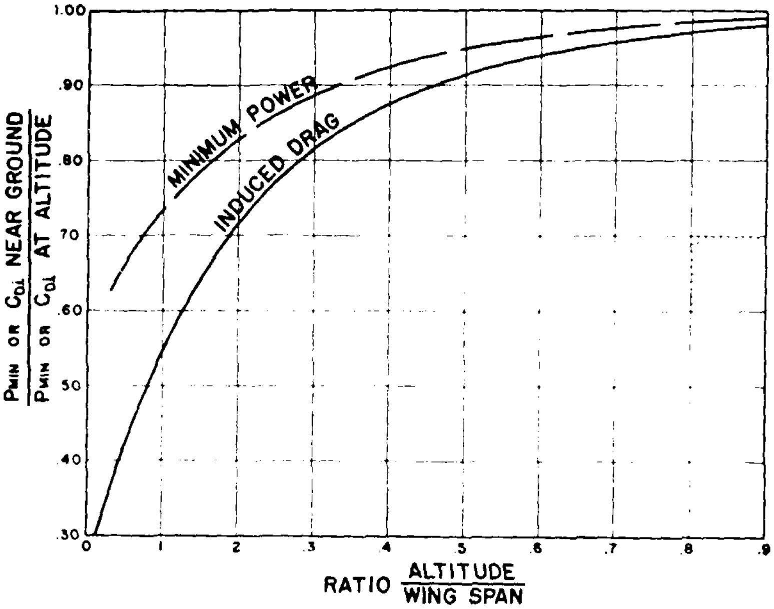

Figure 22 Ground Interference Effect on Drag and Power

Reported cases of marked increase in C_L maximum for low-wing monoplanes flying near the ground are probably based on the effects of increased slope of the lift curve and reduced drag. Numerous wind-tunnel and flight tests fail to show any change in the maximum lift coefficient.

The change in induced drag is given by

$$\Delta C_{Di} = -\sigma C_L^2/\pi n \tag{43}$$

where σ is the interference factor based on a reflection image of the wing symmetrically located with respect to the ground surface. That is, σ is the interference factor for a biplane having a gap twice the vertical distance of the wing from the ground. Values of σ are given on Figure 5. Equation (43) is equivalent to an aspect ratio change to

$$n_G = n/(1 - \sigma) \tag{44}$$

where n_G is the value near the ground. Figure 22 gives the effect of the ground on induced drag and minimum power. The effect on the slope of the lift varies with aspect ratio as shown on Figure 23. For a low-wing monoplane in the landing attitude, h/b may have a value of about 0.1, giving about 12% increase in $dC_L/d\alpha$. This would reduce by about 2° the angle of attack for maximum lift.

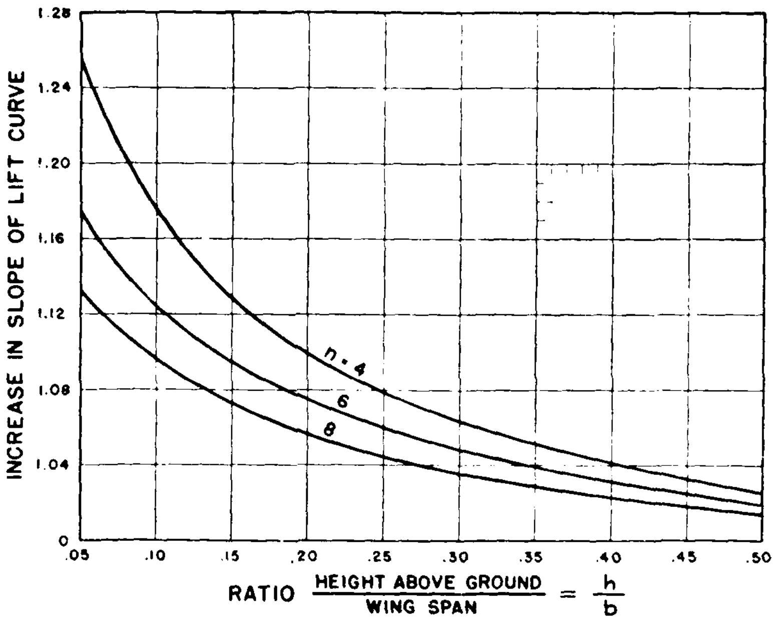

Figure 23. Ground Interference Effect on Slope of Lift Curve

Aspect Ratio and Span Loading. The induced drag coefficient is

$$C_{Di} = C_L^2/\pi n = C_L^2 S/\pi(kb)^2 \qquad (23a)$$

Introducing Munk's span factor in equation (22), the induced drag is

$$D_i = L^2/\pi q(kb)^2 = (1/\pi q)(W/kb)^2 \qquad (22a)$$

Hence, at a given value of the dynamic pressure q, the induced drag is determined by the equivalent span loading W/kb and not by the aspect ratio. In other words, at any given lift coefficient the induced drag coefficient depends upon the effective aspect ratio, but the actual induced drag at any given speed depends on the span loading. It is highly important that the engineer distinguish clearly between the two conditions:

> Induced drag depends on span loading.
> Induced drag coefficient depends on effective aspect ratio.

Moment Coefficient. If the term "moment coefficient" is used without qualification in discussing wing section data, it may always be assumed to refer to the pitching moment coefficient taken about the quarter-chord point. At zero lift there is an aerodynamic couple acting on an airfoil. The moment of a couple is the same about any point in the plane of couple, hence the moment coefficient at zero-lift is independent of the axis about which it is taken. The moment coefficient at zero lift C_{M_0} is a fundamental characteristic of an airfoil section.

Aerodynamic Center. Munk has shown in a notable paper[11] that the classical treatment of wing theory by means of vortices may be replaced by energy considerations. In this paper he shows that the lift due to the curvature of a wing acts at 50% of the chord while the lift due to angle of attack acts at 25% of the chord. Consequently, the moment coefficient taken about the quarter-chord point should be substantially constant for a given airfoil section. This relation has been amply verified by wind-tunnel tests and the quarter-chord point is now used almost exclusively as the reference axis for moments.

---

[11] Max M. Munk, "Elements of the Wing Section Theory and of the Wing Theory," N.A.C.A. T.R. No. 191 (1924).

The moment coefficients taken about the quarter-chord point are almost but not quite constant. Investigations made in the N.A.C.A. variable-density wind tunnel have indicated that for each airfoil section there is a point, the ***aerodynamic center***, about which the moments are constant over a wide range in C_L. Two points, one for positive values of C_L and one for negative values of C_L, serve as exact aerodynamic centers for all practical purposes.

Center of Pressure. The center of pressure is defined as the point on the wing chord through which the resultant force acts. In many design problems it is desirable to use the center of pressure rather than the moment coefficient. The center of pressure is readily found from the moment coefficient about the quarter chord by the relation

$$C_p = 0.25 - \frac{C_{M\,c/4}}{C_N} \tag{45}$$

where C_N is the normal force coefficient $(C_N = C_L \cos \alpha + C_D \sin \alpha)$. For all but very small lift coefficients and very large angle of attack, it is sufficiently accurate to take $C_N = C_L$.

If the moment coefficient is given about the aerodynamic center a expressed as a decimal fraction of the chord

$$C_p = a - \frac{C_{M\,ac}}{C_N} \tag{46}$$

Zero Lift: Zero Moment. Munk has shown[12] that the angle of attack for zero lift is given approximately by the line drawn through the trailing edge and a point located on the mean camber at 50% of the chord. The exact angle of zero lift is determined as follows: pass a straight line **AB** through the trailing edge **A** and a point on the mean camber 11% of the chord aft of the leading edge, pass a second straight line **AC** through the trailing edge and a point on the mean camber 89% of the chord aft of the leading edge. The line **AD** bisecting the angle **BAC** is the direction of zero lift. These constructions are shown on Figure 24.

---

[12] Max M. Munk, "The Determination of the Angles of Attack of Zero Lift and Zero Moment, Based on Munk's Integrals," N.A.C.A. T.N. 122 (1923).

The angle for zero moment about the leading edge is found by passing a straight line through two points on the mean camber. The first point is $4\frac{1}{4}\%$ of the chord and the second is at $95\frac{3}{4}\%$ of the chord measured from the leading edge. This construction is also shown on Figure 24.

If the wing section has a large leading edge radius *r*, the mean-camber curve should pass through the center of this arc and be prolonged to a point **P**, which is one-half *r* distant from the center. The chord length should then be measured from the point **P** instead of the actual leading edge.

Moment Coefficient about Any Point. The moment coefficient about the aerodynamic center is constant. The moment coefficient about any point on the zero lift line drawn through the aerodynamic center of the wing is given by

$$C_{M_G} = C_{M_0} - (a - x)\,C_L \tag{47}$$

where a is the aerodynamic center and x is the center of moments, both in terms of the chord.

The effect of a displacement normal to the zero lift line may be calculated as follows. This effect is due to the *inclination of the vector*, as shown on Figure 25, giving a moment arm d varying with the normal displacement h. When d and h are in terms of the chord, this increment is

$$\Delta C_{M_G} = +\,C_L \cdot d = +\,C_L \cdot h \sin\theta$$

The angle of attack α is equivalent to

$$\alpha = C_L/(dC_L/d\alpha)$$

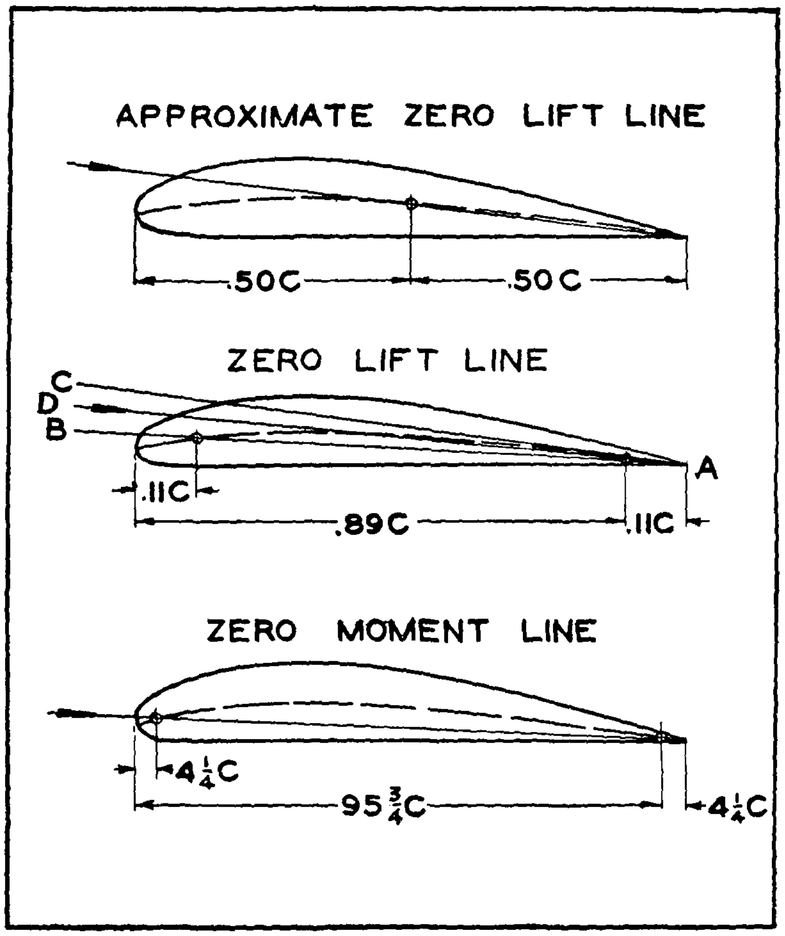
APPROXIMATE ZERO LIFT LINE
.50C
.50C
ZERO LIFT LINE
C
D
B
A
.11C
.89C
.11C
ZERO MOMENT LINE
4¼C
95¾C
4¼C

Figure 24. Munk's Methods for Finding Zero Lift and Zero Moment Lines

The angle between the lift and the resultant force vectors is

$$\gamma = \tan^{-1}(C_D/C_L) = C_D/C_L = C_L/\pi n$$

The angle of inclination of the resultant force vector to the normal is

$$\theta = \alpha - \gamma = C_L\left[\frac{d\alpha}{dC_L} - \frac{1}{\pi n}\right]$$

The term in the brackets is practically constant. It is independent of aspect ratio, although it varies slightly with the basic lift-curve slope. The average theoretical value is about 0.175, but a long series of comparative calculations indicate that better agreement is obtained with observed data for a value of 0.15. Hence, the moment increment due to vector inclination is

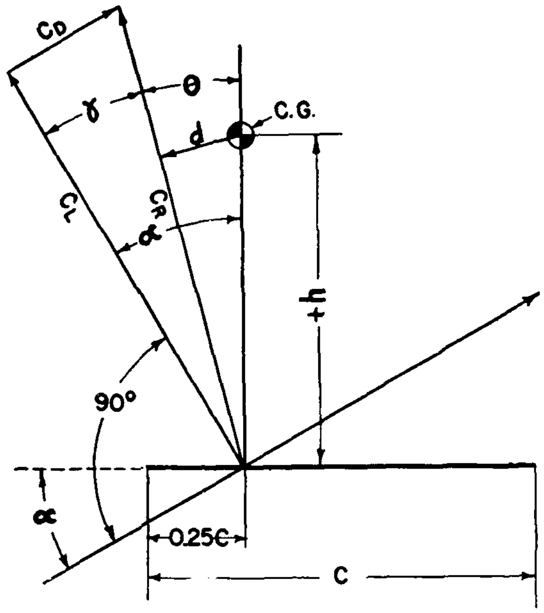

Figure 25. Moment Coefficient About Any Point

$$\Delta C_{MG} = 0.15h\,C_L^2 \tag{48}$$

Adding this term to equation (47) gives

$$C_{MG} = C_{M_0} - (a - x)C_L + 0.15h\,C_L^2 \tag{49}$$

which may be used to obtain the wing pitching moment about any desired c.g. location.

Relative Loading on Biplane Wings. The distribution of lift between the upper and lower wings of a biplane[13] may be determined by equations of the form

$$C_{LU} = C_L \pm \Delta C_{LU}$$

and

$$C_{LL} = C_L \pm \Delta C_{LL}$$

where C_L is the biplane lift coefficient, C_{LU} and C_{LL} the lift coefficients for the upper and lower wings and ΔC_{LU} and ΔC_{LL} the lift coefficient increments for the upper and lower wings, respectively. The lift increments are connected by the relation

$$\Delta C_{LL} = -\Delta C_{LU}(S_U/S_L) \tag{50}$$

where S_U and S_L are the areas of the upper and lower wings.

ΔC_{LU} is given by the equation

$$\Delta C_{LU} = K_1 + K_2 C_L \tag{51}$$

where K_1 and K_2 are functions of gap, chord, chord ratio, wing thickness, stagger, decalage, and overhang.

For any given biplane, K_1 may be written

$$K_1 = [K_{10} + K_{11} + K_{12} + K_{13}] \times \left(\frac{c_L}{c_U}\right) \tag{52}$$

where K_{10} is the value of K_1 for no stagger, decalage, or overhang. K_{10} depends on wing thickness and the gap as shown on Figure 26. K_{11} is the ΔK_1 due to stagger as shown on Figure 27. K_{12} is the value of ΔK_1 due to decalage given by Figure 28, and K_{13} is the value of ΔK_1 due to overhang given by Figure 29. Figures 26 to 29 are based on biplanes with wings of equal chords. For unequal chords the values must be multiplied by the ratio of the average chord of the lower wing to the average chord of the upper wing (c_L/c_U) as indicated in equation (52).

---

[13] W. S. Diehl, "Relative Loading of Biplane Wings," N.A.C.A. T.R. No. 458 ([illegible]) and "Relative Loading on Biplane Wings of Unequal Chords," N.A.C.A. T.R. No. 501 (1934).

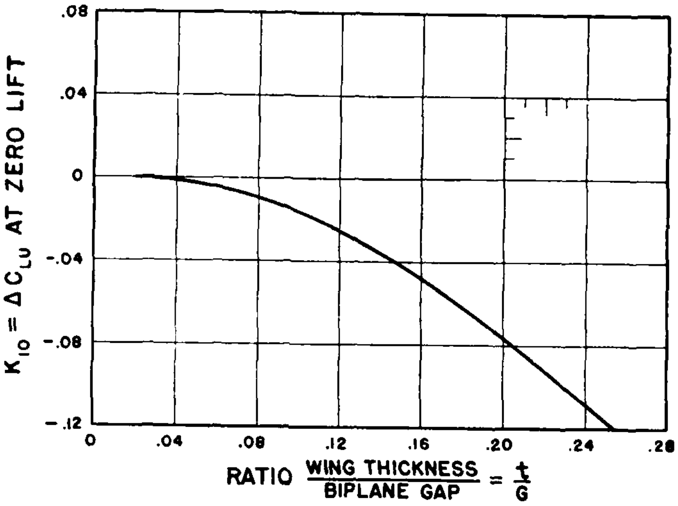

Figure 26. Effect of Gap and Wing Thickness on K_1

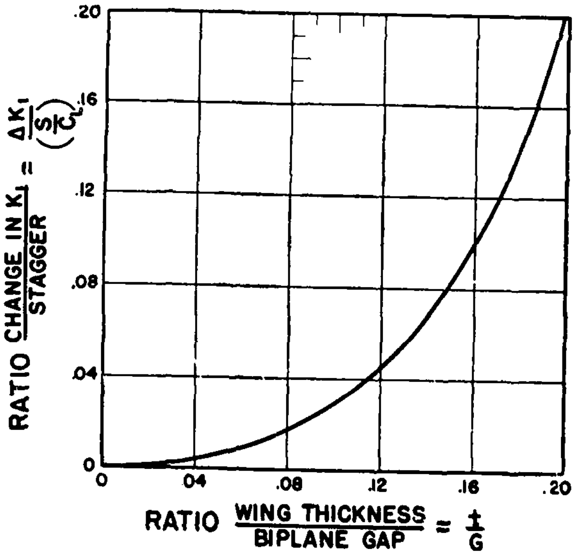

Figure 27. Effect of Stagger on K_1

K_2 is given by

$$K_2 = [(F_2 \times K_{20}) + K_{21} + K_{22}] \times \left(\frac{c_L}{c_U}\right) \tag{53}$$

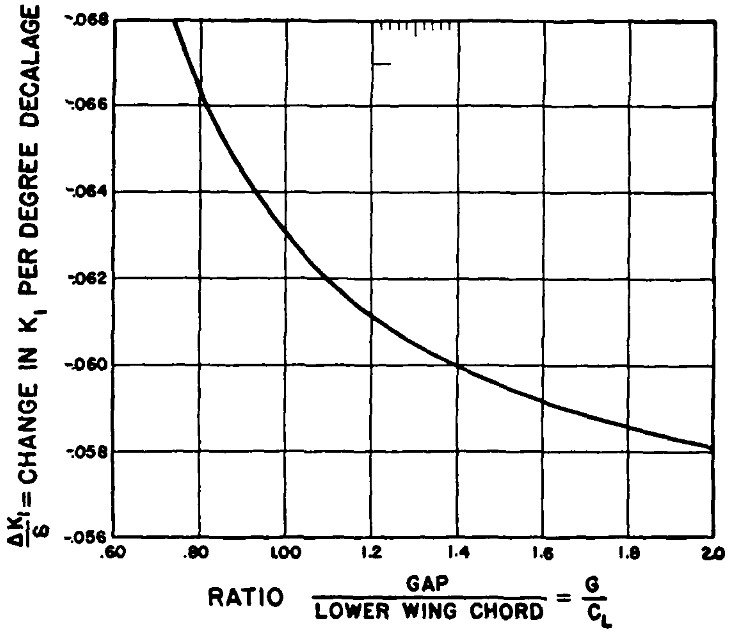

Figure 28. Effect on Decalage on K_1

where K_{20} is the basic value of K_2 for a biplane with individual wings aspect ratio 6, equal chords, zero decalage, and no overhang. K_{20} is given by

$$K_{20} = \left[0.050 + 0.17\left(\frac{s}{c_L}\right)\right] \tag{54}$$

where s is the stagger and c_L the average chord of the lower wing. The effect of stagger on K_2 varies with aspect ratio of the individual wings and with gap-chord ratio, as shown on Figure 30, which gives the factor F_2.

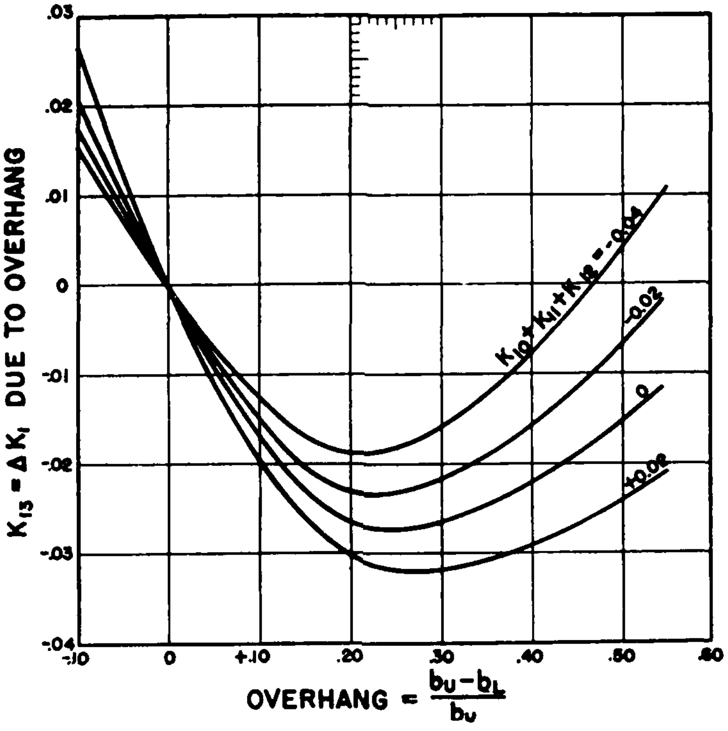

Figure 29. Effect of Overhang on K_1

K_{21} is the effect of decalage on K_2 and is given by the following:

$$K_{21} = +0.0186\,\delta^\circ \tag{55}$$

where δ is the angle between the zero-lift lines of the two wings, considered positive when these intersect forward of the leading edge.

K_{22}, the effect of overhang on K_2, is given by Figure 31 on page 71.

Stagger should be measured between the $\frac{1}{3}$ chord points at the zero-lift attitude.

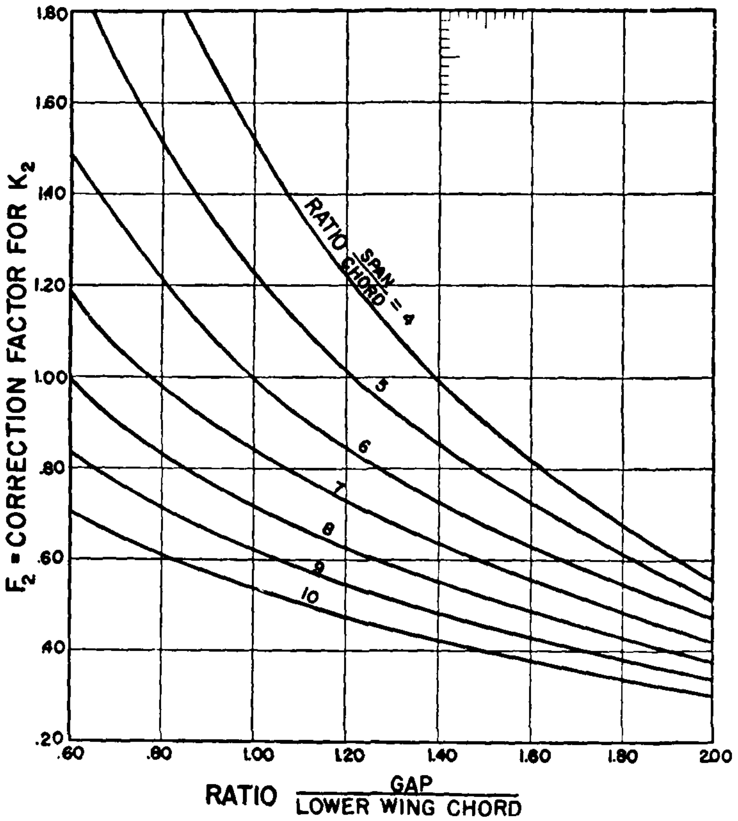

Figure 30. Effect of G/c and Aspect Ratio on K_2

Moment Coefficient for a Biplane. When the load distribution is known, the moment coefficient for a biplane may be obtained for any desired axis such as a given center of gravity location, by calculating the contribution of each wing. Let the arrangement be as shown on Figure 32, with the upper wing area = S_U and lower area = S_L. Then from equation (49),

$$C_{MU} = C_{M_0} - (a - x_U)\, C_{LU} + 0.15\, h_U\, C_{LU}^2 \tag{56}$$

$$C_{ML} = C_{M_0} - (a - x_L)\, C_{LL} + 0.15\, h_L\, C_{LL}^2 \tag{57}$$

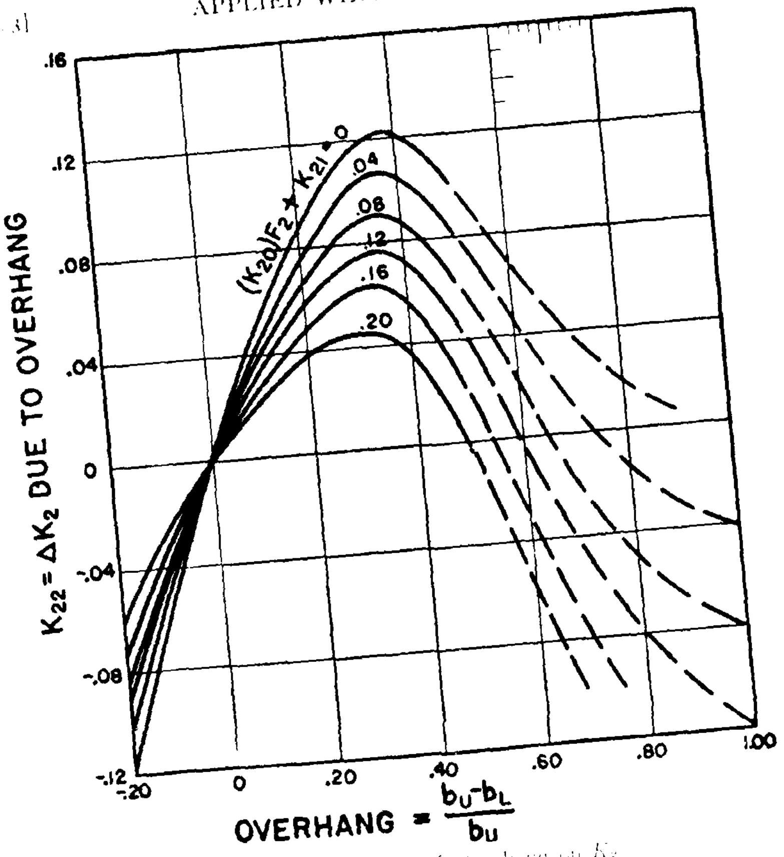

Figure 31 Effect of Overhang on K_2

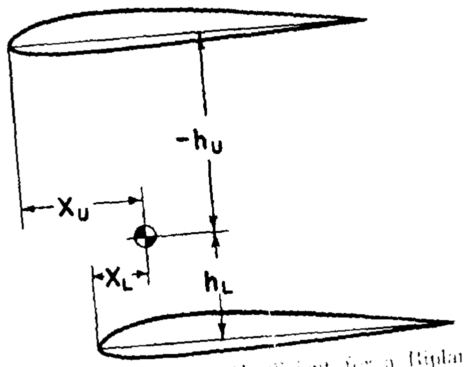

Figure 32. Moment Coefficient for a Biplane

The moment equations are:

$$M_U = C_{MU}\, q\, S_U\, c_U$$
$$M_L = C_{ML}\, q\, S_L\, c_L$$
$$M = C_M\, q\, S\, c$$

Since $M = M_U + M_L$, it follows that

$$C_M = C_{MU} \frac{S_U}{S} \frac{c_U}{c} + C_{ML} \frac{S_L}{S} \frac{c_L}{c} \qquad (58)$$

Where the upper and lower chords are equal, $c_U = c_L = c$. When they are unequal, the mean chord c must either be assumed as the geometrical mean chord or calculated as the aerodynamic mean chord in accordance with the method given on page 178.

CHAPTER 4

WIND-TUNNEL TESTS

The Wind Tunnel. While it is possible to calculate the induced drag under various conditions, as indicated in Chapter 3, it is impracticable, if not actually impossible, to calculate the total drag or the resultant air force. Fortunately for the aeronautical engineer, the wind tunnel offers a direct solution to the problem.

The wind tunnel is essentially a confined air stream that is kept in motion by a blower or propeller. At some point in the circuit a "test section" is provided with a reasonably steady and uniform flow by the use of devices such as guide vanes or "entrance cones." An accurate balance, designed to measure forces and moments, supports the object in the test section. Suitable manometers and speed controlling devices enable the operator to secure and maintain constant the air speed desired while reading the forces and moments indicated on the balance. These readings are then available for comparison with similar readings or for design calculations as will be shown later. The proper interpretation of the readings requires a thorough understanding of the characteristics and the limitations of the wind tunnel. This understanding is a joint responsibility of the operator who conducts the test and of the engineer who interprets the data.

Types of Wind Tunnels. Wind tunnels may be broadly classified as atmospheric and variable-density types.

The atmospheric tunnel operates at substantially atmospheric pressure. It may be either open-circuit type or closed-circuit type. The closed-circuit types may be either open throat with the test section in an exposed free jet, or closed throat with the test section located within an unbroken passage. The open-circuit type is very simple. It consists essentially of a long tube, fitted at one end with an intake cone and at the other end with an exit cone or a "diffuser." The return passage is the entire room surrounding the tunnel. The usual construction in the direction of flow is the intake cone, the straightening device or honeycomb, the test section, the expanding cone, the propeller, and the diffuser. The diffuser is a device, such as a latticed passage, to iron out irregularities in air flow due to the propeller. The open-circuit type was at one time in extensive use, but the closed-circuit types are now preferred.

In the closed-circuit type the moving air is confined and guided around the entire circuit. The power losses are comparatively low so that high test speeds may be obtained with reasonable power input. Where visual observations of air flow over the model are required, the open-jet wind tunnel is used

The variable-density tunnel is enclosed within a huge steel tank designed to withstand pressures up to 20 atmospheres or more. By changing the air density within the tank, the Reynolds Number may be varied over a wide range so that full-scale coefficients can be obtained from a small model.

Wind-Tunnel Balances. The accurate measurement of the three forces and the three moments for a given set of reference axes requires a special balance. The design of such a balance for use in a wind tunnel is complicated by numerous conflicting requirements; for example, a high degree of accuracy is required on minimum drag yet the balance must be able to measure forces several hundred times greater; readings must be easily obtained yet the balance must not be too sluggish; the attachments to the model should not cause large interference drag or tare values, but the deflections under load must be small. While no one type of balance can possibly meet all of the requirements, any type that is carefully designed and properly operated will give satisfactory results.

The first wind-tunnel balances were of the beam type and measured forces as moments so that it was necessary either to assume a line of action of the air force or to calculate its location from two or more readings. These have been superseded by types that measure forces directly, either with a parallel motion linkage or a system of wires. Owing to low first cost, the wire balance is now used extensively.

Descriptions of wind tunnels and wind-tunnel balances may be found in the following reports:

Warner, E. P., and Norton, F. H., "Wind Tunnel Balances," N.A.C.A. T.R. No. 72 (1919).
Zahm, A. F., "The Six-Component Wind Balance," N.A.C.A. T.R. No. 146 (1922).
Reid, E. G., "Standardization Tests of N.A.C.A. No. 1 Wind Tunnel," N.A.C.A. T.R. No. 195 (1924).
Weick, F. E., and Wood, D. H., "The Twenty-Foot Propeller Research Tunnel of the National Advisory Committee for Aeronautics," N.A.C.A. T.R. No. 300 (1928).
Harris, T. A., "The 7 by 10-Foot Wind Tunnel of the National Advisory Committee for Aeronautics," N.A.C.A. T.R. No. 412 (1931).
Jacobs, E. N., and Abbott, I. H., "The N.A.C.A. Variable-Density Wind Tunnel," N.A.C.A. T.R. No. 416 (1932).
DeFrance, S. J., "The N.A.C.A. Full-Scale Wind Tunnel," N.A.C.A. T.R. No. 459 (1933).

Reliability of Data. Wind tunnels are occasionally criticized as unreliable. Such criticism is thoughtless and unjust. It is true that some unreliable wind-tunnel data have been published in the past, but the wind tunnels should not be held responsible for the errors made by careless engineers. Without the exercise of patience and skill, it is almost impossible to secure consistent wind-tunnel results. The accuracy obtained in the testing is largely a matter of the intelligence, experience, patience, and good judgment of the operator. An efficient person can obtain better data with crude equipment than a careless one with the finest equipment. Some of the most brilliant experimental results ever obtained from a wind tunnel were obtained, as the engineer in charge expressed it, "Because the air flow and the balance were so bad we could take nothing for granted."

Wind-tunnel tests carefully made and properly interpreted are reliable. The actual testing should be a continuous series of checks and rechecks, modified in accordance with skill and experience. The wind speed must be checked, the alignment of the balance checked, the zero readings checked, the setting of the model checked, and so on. Unless all of these are done and done intelligently, the accuracy will suffer.

Assuming that the wind-tunnel tests have been properly made, there remains the interpretation of the data. This is also a matter of skill and experience. The remainder of this chapter is intended chiefly for the man who must interpret the test data.

Test Conditions. The proper interpretation of a wind-tunnel test requires a knowledge of the modifying influence of three important "effects" or conditions of test. These are: the scale effect or Reynolds Number, the wall effect or wall interference, and the turbulence in the air stream. A test is made at a definite Reynolds Number with a definite wall effect, but the effects of turbulence in the air stream are somewhat indefinite. The problem in general is to make the correct allowance for these conditions in passing from model to full scale. In many cases this allowance must be qualitative rather than quantitative. This will be clear from a consideration of the complexity of the general drag equation.

General Drag Equation. The chief variables that affect the air force on any aerodynamic object, such as a wing, are: (1) angle of attack α, (2) relative wind velocity V, (3) scale of the object L, (4) density of the fluid ρ, (5) compressibility of the fluid, (6) gravity g, (7) surface roughness, and (8) texture of the air flow. From the theory of dimensions, it may be shown that the general drag equation, for example, is

$$D = \rho V^2 L^2 \cdot \varphi \left[\alpha, \frac{\rho V L}{\mu}, \frac{V}{a}, \frac{V^2}{gL}, \frac{l}{L}, \frac{v}{V} \right] \tag{59}$$

We are accustomed to the use of a drag coefficient C_D instead of the function in the brackets, but in so doing, sight must not be lost of the fact that C_D may and does vary with a number of non-dimensional terms, and that this variation must, in general, be determined experimentally. The purpose of the ordinary wind-tunnel test is to determine $\varphi_1(\alpha)$ or the variation of C_D with angle of attack. The purpose of testing at various speeds is to determine $\varphi_2(\rho VL/\mu)$ over a part of its range. Propeller designers understand the effect of $\varphi_3(V/a)$ on propeller characteristics in general, if not in particular, when they try to hold the tip speeds well below the velocity of sound. Model tank experiments are usually made on the basis of V^2/gL because this term brings in the gravity effects associated with wave-making. If tests on two models do not agree, the surface roughness l/L may not bear the same relation in the two cases, and this is often observed in skin-friction tests. Finally, if two wind tunnels do not agree in tests on the same model, it may be due to a difference in turbulence represented by the ratio of the average lateral turbulence velocity to the measured axial velocity.

These terms do not have the same weight. In aeronautical engineering, angle of attack is considerably more important than turbulence or surface effect. Next to angle of attack in importance is either the Reynolds Number $\rho VL/\mu$ or the compressibility effect V/a. As long as the relative speed is low, the compressibility effects are negligible; but as the speed increases, they become increasingly more important. It is for this reason that wind-tunnel tests at very high speed do not agree with tests at the same Reynolds Number at a lower speed. Such tests may include both $\varphi_2(\rho VL/\mu)$ and $\varphi_3(V/a)$.

Reynolds Number. In a paper presented to the Royal Society in 1883, Professor Osborne Reynolds reported the results of his tests on flow through tubes. Among his findings it was shown that the type of flow through the tube was a function of DV/P, where D is the diameter, V the velocity of flow, and P is proportional to the coefficient of viscosity μ. Professor Reynolds showed that below a definite "lower critical value" of DV/μ, the flow was "smooth," or what is now known as laminar. Above a definite "higher critical value" of DV/μ, the flow was "sinuous," or what is now known as turbulent. The intermediate values constitute a transition régime in which the type of flow depends on the prior history of the particular flow.

The first application of these findings to aeronautical work is believed to be due to Lord J. W. S. Rayleigh who suggested the plotting of $P/\rho V^2$ against ν/VL, where P is the pressure and ν the kinematic viscosity, $\nu = \mu/\rho$. This suggestion was given in a short paper "Note as to the Application of the Principle of Dynamical Similarity," which was included as Part 2 of Br.A.C.A. R. & M. No. 15, published in 1909. Lord Rayleigh stated that this method had been used in 1899 to study the size of drops formed under various conditions.

The author has been unable to locate definitely the first use of the term "Reynolds Number" for VL/ν, but it is so designated by Joukowski in Chapter IX of "Aerodynamique," which indicates its usage prior to 1914.

Reynolds Number is of such fundamental importance in aerodynamics that a clear conception of its physical significance is essential. It is one of the most unusual numbers used in scientific work. Itself a pure number or ratio having no dimensions, it combines the effects of the four most important variables affecting air forces. Several derivations are possible, each introducing a different physical aspect, but the basic relation involved is the balance of forces. At a given Reynolds Number, regardless of the numerical values of the component terms, the ratio between the forces due to density and the forces due to viscosity is constant. The proof of this relation is readily obtained. Let

$$\frac{F_\rho}{F_\mu} = \frac{\text{Force due to density}}{\text{Force due to viscosity}} = \text{RN}$$

The force due to density is the main term of equation (59) $F_\rho = \rho V^2L^2$. The force due to viscosity on two parallel square plates of side L separated by distance L and moving with velocity V is $F_\mu/L^2 = \mu V/L$ or $F_\mu = \mu VL$. Hence,

$$\frac{F_\rho}{F_\mu} = \frac{\rho V^2L^2}{\mu VL} = \frac{\rho VL}{\mu} = \text{RN} \qquad (60)$$

The actual value of a Reynolds Number has no significance except in comparing a given series of geometrical similar forms. Since the type of flow varies with the geometrical form, the particular characteristic length L that is adopted for any given form is purely arbitrary. For a wing, the chord length is used. For a streamline body, the overall length or the cube root of the volume is taken as L.

Effect of Reynolds Number. In general, the principal effect of increasing Reynolds Number is a reduction of frictional drag as shown in Chapter 9. A series of tests at various speeds on a wing, a fuselage, or a complete airplane model usually shows the drag to vary with a velocity exponent less than 2. An average airplane model will show an exponent of about 1.90. Theoretically, the extrapolation of a curve of this type should give full-scale drag values, but the results are inclined to be highly erratic owing to the variable influence of model surface finish and wind-tunnel turbulence on frictional exponents and coefficients. In airplane model tests the correction or allowance for scale effect must be tempered by experience and due consideration given to the type of airplane, the details of the full-scale construction, the conditions of the test, and the susceptibility of the wing section character-

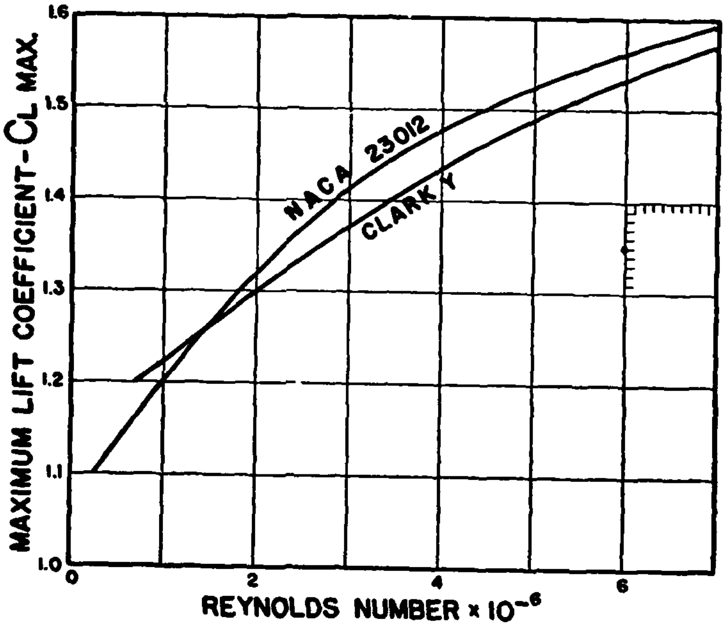

Figure 33. Variation of $C_{L\,max}$ with Reynolds Number

istics to the conditions of test. In general, the differences between wing sections become less as the Reynolds Number is increased. The scale effect on drag coefficient will be greater on a section having a comparatively high C_D at low RN, and the scale effect on maximum lift coefficient will be greater on a section having comparatively low C_L maximum at low RN.

Allowance for these effects may be made by use of data given in Chapter 5. The allowance for reduction in C_D is probably best made by calculating the model drag correction represented by the anticipated reduction in C_D minimum passing from model test to full-scale RN, but if this is done, an allowance must be made for drag increases due to rivets, seams, fittings, and other protuberances.

The allowance for increase in C_L maximum is less difficult to justify. For the type of section generally used, a model test will show a C_L maximum between 1.10 and 1.25. The full-scale C_L maximum will be between 1.40 and 1.60. Figure 33 gives the variation of C_L maximum with RN based on the full-scale wind-tunnel tests.

Determination of Reynolds Number. $(\rho VL/\mu)$ will have the same value in any consistent system of units. If the units for ρ, V, and L are respectively pounds mass per cubic foot $(\rho = w/g)$, ft/sec, and feet, then μ must have the dimensions of M/LT. In the cgs system, the value of μ is given for air by Holman's formula

$$10^7\mu = 1715.5\ (1 + 0.00275t - 0.00000034t^2) \tag{61}$$

In ft-lb-sec units, μ is

$$10^{10}\mu = 3582.9\ (1 + 0.00275t - 0.00000034t^2) \tag{61a}$$

t being in °C. The deviation of μ from a straight-line function of t is less than 1 part in 3,000 over the usual working range and one may write

$$10^{10}\mu = 3408 + 5.483t\ (°\text{F}) \tag{62}$$

$$= 3583 + 9.870t\ (°\text{C}) \tag{62a}$$

for use in determining the value of $\rho VL/\mu$. The value of μ at 15°C or 59°F by the approximate formula is 3731×10^{-10}, while Holman's formula gives 3730×10^{-10}. Figure 34 has been prepared for use in reading the value of ρ/μ directly, or for checking calculations. Reynolds Number is obtained by multiplying the value of ρ/μ from this figure by V in feet per second and L in feet. The value of the kinematic viscosity ν for air at standard temperature is

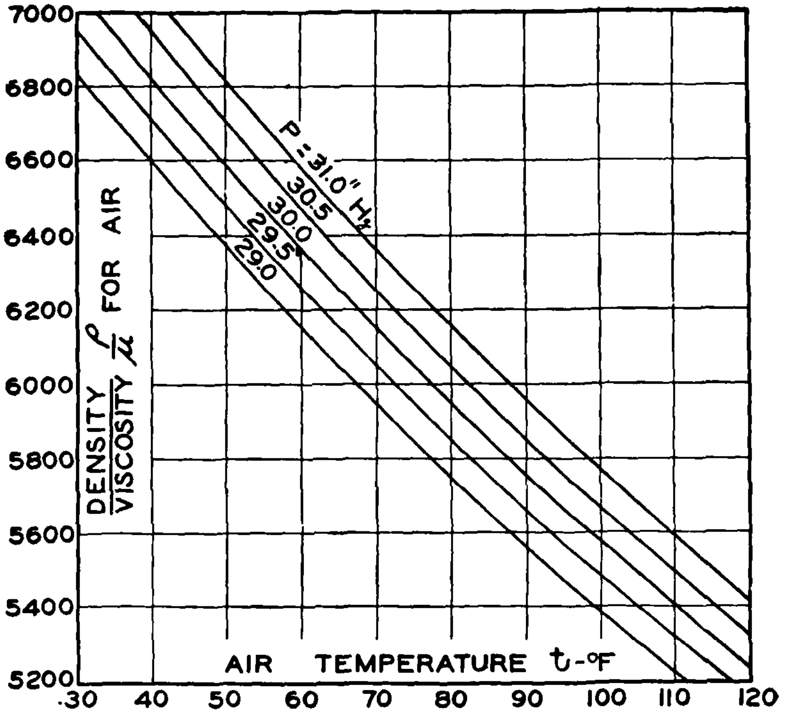

Figure 34. Reynolds Number Coefficient

$$\nu = \mu/\rho = 0.1457 \text{ cm}^2/\text{sec} = 1.568 \times 10^{-4} \text{ ft}^2/\text{sec}$$

hence in ft-sec units

$$1/\nu = 6378$$

It is convenient to remember that in standard air a wing of 1.0 feet chord at 100 mph gives a Reynolds Number of 935,400 or approximately one million.

The value of the kinematic viscosity for water at ordinary temperatures is about 1/13th of the value of air. Taken at the same temperature the relative values of ν for air and water are

Temp.°C	0	10	15	20	30
$\frac{\nu \text{ air}}{\nu \text{ water}}$	7.5	10.8	12.8	14.9	18.7

Wall Interference. Prandtl[1] has shown that the boundary of any finite wind stream, in either a closed or an open working-section wind tunnel, restricts the flow past an object under test. For a lifting airfoil, the boundary conditions of constant pressure for the free jet and zero normal velocity for the closed tube give an induced velocity at the model under test. This induced velocity is equivalent to a downwash for an open section or an upwash for a closed section. This causes the angle of attack and the drag as measured to be increased in a free jet and decreased in a closed tube by the amounts

$$(\Delta\alpha)^\circ = 57.3\,\delta\,\frac{C_L S}{C} \tag{63}$$

$$\Delta C_{Di} = \delta\,\frac{C_L^2 S}{C} \tag{64}$$

where S is the model wing area and C is the area of the jet cross-section. δ is a factor depending on the geometry of the jet. For a circular jet $\delta = \pm 0.125$. For a square jet $\delta = \pm 0.138$.

Theodorsen[2] has determined the variation of δ for five types of rectangular tunnels as follows:

---

[1] L. Prandtl, "Application of Modern Hydrodynamics to Aeronautics," N.A.C.A. T.R. No. 116 (1921).

[2] Theodore Theodorsen, "The Theory of Wind-Tunnel Wall Interference," N.A.C.A. T.R. No. 410 (1931).

I. Closed Rectangular Tunnel
II. Open Rectangular Jet
III. Rectangular Jet with Horizontal Boundaries
IV. Rectangular Jet with Vertical Boundaries
V. Rectangular Jet with One Horizontal Boundary.

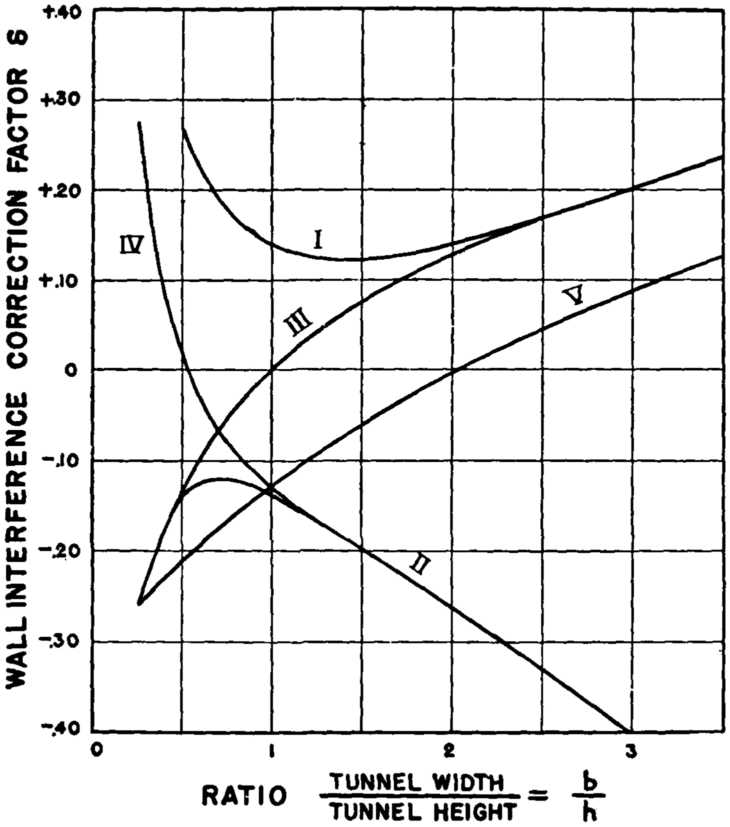

Figure 35. Wall Interference Correction Factors

Values of δ for these five cases are plotted against the ratio of tunnel width to tunnel height in Figure 35. The most striking feature of these curves is the indication of three types of wind tunnels having zero boundary correction.

Experimental determinations of δ are given in N.A.C.A. T.R. No. 478 and T.N. No. 506. Excellent agreement is obtained between theoretical and experimental values.

Tunnel wall interference also affects the indicated stability and balance of an airplane model, since the induced angle correction at the tail is not the same as that for the wings. Glauert has shown in R. & M. Nos. 947 and 1566 that the change in induced downwash at the tail is given by

$$\epsilon_2^\circ = 57{\cdot}3\,\delta' \frac{l}{d} \cdot \frac{S}{C} C_L \tag{65}$$

where l is the distance from the wings to the tail surface (l may be taken as distance from c.g. to elevator hinge axis), d is the tunnel diameter, C is the cross-sectional area of the jet, S is the model wing area and δ' is an interference factor, analogous to δ in equation (63). For a closed square or circular jet $\delta' = 0.24$. For an open circular jet $\delta' = -0.20$.

In a closed tunnel, the effect of wall interference is to reduce, by the angle ϵ_2, the downwash at the tail and also the stabilizer setting required for trim. The reduced downwash gives a greater negative slope to the pitching moment curve. In an open tunnel the downwash at the tail and the stabilizer is increased by wall interference. This decreases the slope of the pitching moment curve. These corrections are negligible for a conventional model with a span less than half of the tunnel diameter, but the tendency is clearly apparent in comparable tests even where the corrections are negligible. If the model area exceeds 10% of the tunnel area, the corrections should be applied.

Correction for Static-Pressure Gradient. The equivalent drag effect of an axial static pressure gradient in a wind tunnel appears to have been first noted by Pannell and Campbell.[3] A graphical solution for this correction was given by Pannell, Jones, and Pell in Br.A.R.C. R. & M. No. 564 in 1918.

---

[3] J. R. Pannell and N. R. Campbell, "The Variation of the Resistance of Rigid Airship Models with the Scale and Wind Speed," Br.A.R.C. R. & M. No. 302 (1916).

Dr. A. F. Zahm[4] showed that where the static-pressure gradient is linear along the axis, there is an additional drag that is exactly proportional to the volume of the model. The additional drag is, therefore, a "horizontal buoyancy." Since the normal static-pressure gradient is linear or approximately so, the correction is readily made. This correction is necessary if accurate results are to be obtained for objects having large volume and low drag, such as streamline shapes. It should also be applied to airfoils. For a typical streamline body, such as an airship hull, this correction may amount to as much as 20% of the measured drag. For an airfoil, the correction is normally about 2% of the minimum drag.

Turbulence. The air flow in a wind tunnel is comparatively smooth and steady only when the entire mass is considered. If the flow through a small portion of the cross-section is considered, it is found to contain numerous small vortex filaments that are generated at the propeller and flow-control vanes. With sufficient magnification, these eddy flows are found to change rapidly in strength and position. Dryden and Kuethe[5] define turbulence as the ratio of the square root of the mean square of the deviations of the speed from its mean value to the mean value of the speed. A turbulence of 1% is equivalent to a sine wave fluctuation in speed of ±1.4% from the mean speed. These changes in speed are so rapid that special instruments are required to detect and measure them. Any change that has a period long enough to show up on a pitot tube or similar device cannot be classed as turbulence.

---

[4] A. F. Zahm, "Horizontal Buoyancy in Wind Tunnels," N.A.C.A. T.N. No. 23 (1920).

[5] H. L. Dryden and A. M. Kuethe, "Effect of Turbulence in Wind Tunnel Measurements," N.A.C.A. T.R. No. 342 (1929).

Turbulence effects are greatest on cylinders, spheres, streamline bodies, and similar shapes for which there exist two régimes of flow separated by a transition range in Reynolds Number. The maximum lift of certain airfoils is also affected by turbulence.

The effect of turbulence on sphere drag coefficient is given on Figure 36, which is based on Dryden and Kuethe's data. They recommend that the Reynolds Number at which the sphere drag coefficient is 0.30 be taken as an index of the turbulence. Figure 37 is a plot of the turbulence against RN for $C_D = 0.30$, as given by Figure 36. These values should be considered as approximations, since subsequent data show some variation at a given turbulence depending on the mesh of the turbulence screen and the size of the sphere.

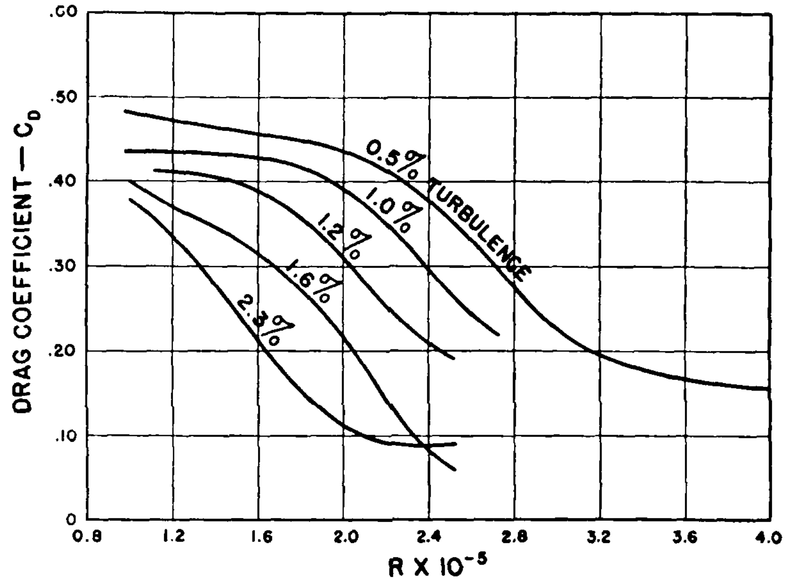

Figure 36. Effect of Turbulence and Reynolds Number on the Drag Coefficient of a Sphere

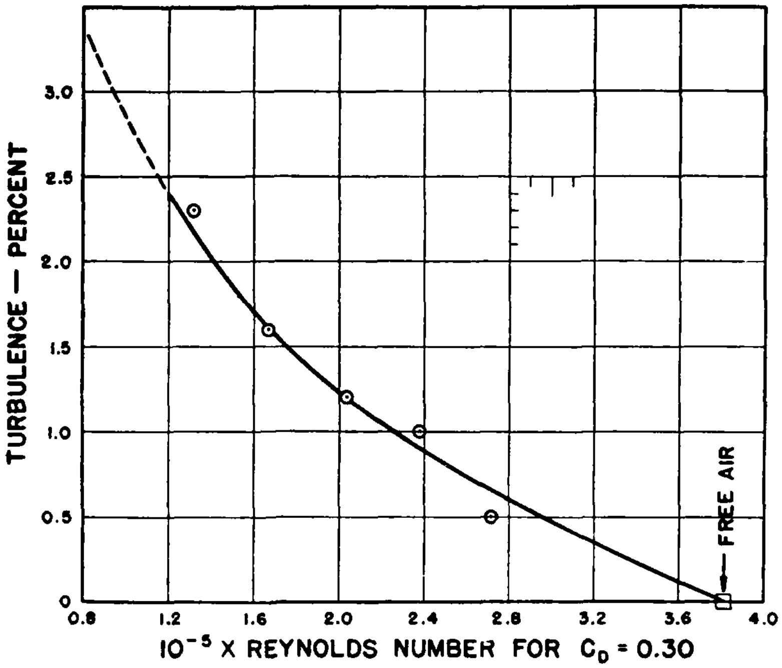

Figure 37. Effect of Turbulence on Sphere Drag

The theoretical frictional drag coefficient of a streamline body may be written

$$C_D = 1.327\,(\rho VL/\mu)^{-0.5} \tag{66}$$

for laminar flow or

$$C_D = 0.074\,(\rho VL/\mu)^{-0.2} \tag{67}$$

for turbulent flow. The effect of turbulence in the wind-tunnel air stream is to advance or retard the Reynolds Number at which the transition from laminar flow to turbulent flow occurs. Typical transition curves are given in N.A.C.A. T.R. No. 342.

The effect of turbulence on airfoils is mostly confined to maximum lift, and this effect is closely approximated by an apparent increase in Reynolds Number when turbulence is present.

Airfoil Tests. For many years some form of airfoil testing constituted the chief activity of all wind tunnels. This condition has been completely changed by the advance in wing theory combined with the mass of systematic experimental data obtained in France, Germany, Italy, and the United States. The systematically varied families of airfoils investigated at Göttingen University and at Langley Field have been of greatest importance. References to these tests are given in Chapter 5.

While the details of airfoil testing are perhaps of limited interest, it may be worthwhile to consider the main features of an airfoil test. The model is usually of rectangular plan-form and aspect ratio 6. In this country the dimensions are 5″ x 30″, 6″ x 36″, 8″ x 48″, or 10″ x 60″, depending on the size of the tunnel. In Europe the span is either 100 cm or 120 cm with a chord of 20 cm. There is at present a definite tendency to use rounded instead of square tips on airfoil models.

To obtain a high degree of accuracy in airfoil data requires great patience and skill on the part of the tunnel operator. The model construction must be very accurate, particularly on the forward part of the upper surface. The surface finish must have a high polish. Two items are of particular importance: the balance must be aligned with the air stream and the tare drag must be very accurately obtained. The mean direction of the air stream may be obtained from a test on a thin double-cambered section. The effect of slight misalignment can also be eliminated by testing the model first upright, then inverted and taking the average reading, or more accurately by use of the method outlined in the Appendix to N.A.C.A. T.R. No. 361. The accurate determination of the tare drag is highly important for two reasons. First, with the usual wire balance the tare drag may amount to 75% of the measured minimum drag. Second, the tare drag includes mutual interference effects between the clips and the model. It is, therefore, not the simple free-air drag of the attaching wires or clips.

The method of attachment as well as the point of attachment may have a large effect on the observed results. A clip, or clips, let into the upper surface may have a profound effect on the characteristics, particularly at maximum lift. Allowance should be made for the "horizontal buoyancy" due to local pressure gradient along the tunnel axis.

The wind-tunnel tests of an airfoil normally include measurement of lift, drag, and pitching moments over an angular range which should extend from an angle of attack well below the maximum negative lift to an angle of attack well above the maximum positive lift. The wind tunnel after converting the forces and moments to coefficients finds it convenient to present the original data plotted against angle of attack. Comparisons between sections, however, are best made with the plot of C_L against C_D — the Lilienthal diagram. When the same scale is used for both C_L and C_D, this is the "polar diagram." The diagrams were formerly given for aspect ratio 6, but there are several important advantages in the use of infinite ratio. The form of plotting now generally used is profile drag coefficient C_{D_0}, moment coefficient about the quarter chord point $C_{M_{c/4}}$ and angle of attack for infinite aspect ratio as ordinates against lift coefficients C_L as abscissas.

Airplane Model Tests. The purpose of a routine wind-tunnel test on an airplane model is to determine performance, stability, and control, with reasonable engineering accuracy, and the advantage of a wind-tunnel test over any other method lies chiefly in its quick and definite indications when reasonable deviations from mathematical exactitude are allowed. Routine testing of airplane models cannot well be justified on any other basis.

It is an easily demonstrated, but not a widely recognized fact, that any model test is a compromise. There are always some conditions of similitude which conflict or cannot be met, but these conditions do not all have the same weight in determining air forces. Since there is no known theoretical method of assigning the proper relative values to the various conditions, a practical solution based, for example, on experience or on trial and error, must serve instead. The principle of dimensional homogeneity leads to an equation for air force in the form

$$F = \rho V^2 L^2 \cdot \varphi\left[\alpha, \frac{\rho VL}{\mu}, \frac{V^2}{gL}, \frac{V}{a}, \frac{l}{L}, \frac{v}{V}, \frac{b}{c}\right] \tag{59a}$$

where α is the angle of attack, $\rho VL/\mu$ the well-known Reynolds Number, V^2/gL the "wave making" or gravitational term, V/a the ratio of the relative wind to the velocity of sound, l/L a measure of surface roughness, v/V a measure of turbulence in the air, and b/c the aspect ratio. These are by no means all of the dimensionless combinations which may be written, but they comprise what are usually considered the most important ones. It is desired to point out three facts: (1) theoretically no model test can completely represent a full-scale condition unless all of the dimensionless ratios are held constant; (2) it is impossible to hold all of these ratios constant at the full-scale value in a model test, for some of them are contradictory; and (3) the dimensionless ratios may not have equal weight, but theory does not show it. Experience tells us, however, that the angle of attack α is the most important of all the terms given, and that Reynolds Number probably comes second in importance. The "wave-making" term V^2/gL, which is so important in testing ship models, is negligible in air work. The term

V/a does not have any great importance at speeds less than about 300 fps, where compressibility effects begin to appear. The surface roughness has a very great effect under many conditions and cannot be neglected. Turbulence is known to have a fairly large influence, particularly on critical flow conditions. The large effect of aspect ratio is well known, and so on through the list of minor unconsidered terms.

The only major term which cannot be satisfactorily met is the Reynolds Number $\rho VL/\mu$. If the value of the function was the same for all airplanes, or even for all parts of an airplane, the problem would be capable of a satisfactory solution. Actually the effect of Reynolds Number is different on each item: wings, fuselage, struts, wires, etc. Furthermore, the effect is not the same on all wings or on all struts, but varies widely in each group.

As a concrete example, the drag coefficient on streamline struts may be four times greater on a 1/24-scale model than on the full-size airplane; streamline wire may show even greater scale effects. This is very much in excess of any scale effect on wings or fuselage. The conclusion is inevitable, that reasonable engineering accuracy is best secured by constructing a model airplane with no streamline struts, wires, fittings, or minor details, and correcting the measured model drag for the scaled-down calculated full-scale drag of the omitted parts. The wings of the simplified model can be held together and the landing gear attached by means of a simple system of round brass wire struts (about 3/32″ diameter), threaded right-hand on one end and left-hand on the other; the minimum length of wire necessary to insure rigidity being used. This method has three very important advantages.

The drag of the round wire struts is quite definite and can be determined very accurately from runs with an exact duplicate set of struts attached symmetrically and in such a manner as to avoid interference while duplicating each item. If ΔD is the drag of one set of struts, it is obvious that

$$D_0 = (D_0 + \Delta D) - [(D_0 + 2\Delta D) - (D_0 + \Delta D)] \qquad (68)$$

where D_0 is the drag of the model without struts, wires, fittings, or miscellaneous omitted parts. The full-scale drag of these parts can be calculated with reasonable accuracy. Assume that the value so calculated at a speed V, be d. Then assuming d to vary as $(VL)^2$

$$d_m = d\, S^2\, (V_m/V)^2 \qquad (69)$$

where S is the (fractional) model scale ratio (for example, 1/20), V the model test speed, and d_m the correction to be applied to the model test. The correct model drag will be

$$D = D_0 + d_m \qquad (70)$$

Lift and moment corrections are also obtained from the "duplicate strut" runs. An additional moment correction due to the omitted parts is obtained by calculating the line of action of d (and therefore d_m) so that the distance of this line of action from the moment axis is known. The table shown in Figure 38 is a very convenient form for calculating simultaneously the drag correction and its line of action. A typical lift wire calculation is given to illustrate the steps followed.

The other advantages of the method are that it allows very accurate alignment of the model, and reduces greatly the cost of model construction. The necessity for very accurate model alignment is not generally appreciated, but it has been shown at the Washington Navy Yard that any difficulty in checking test data after a lapse of time is almost entirely due to warping or change in alignment of the model. Of course, this difficulty is partially obviated when metal wings are used.

DRAG CORRECTION FOR WIND TUNNEL TEST:

TYPE ------------------------------ DATE ------------

MODEL SCALE ≈ ----------

DESIGNATION OR DESCRIPTION OF ITEM	NUMBER N	LENGTH EACH ℓ FT.	SIZE ℓ IN.	TOTAL LENGTH $L = N \times \ell$	D/L AT 100 M.P.H.	DRAG D LBS.	DISTANCE ABOVE BASE LINE ℓ FT.	MOMENT $D\ell$
LIFT WIRES	4	10.0	$\frac{1}{4}$	40.0	.075	3.00	8.00	24.0

DISTANCE FROM BASE LINE TO C.G. = ------------ FT.

DISTANCE FROM BASE LINE TO $\Sigma D = \Sigma D\ell / \Sigma D =$ ----------

ΣD IS ------ INCHES -------- C.G. ON MODEL

DRAG CORRECTION $= d_m =$ ------ LBS.

Figure 38. Tabulation of Drag Correction for Airplane Model Test

The simplified model cannot allow for scale effect on wings or fuselage, but in general it does confine the total scale effect to these two items. The full-scale values of profile drag for various wing sections are given in Chapters 5 and 9 and an estimate can be made of the scale effect on the wings if greater accuracy is required. Normally the scale effect on fuselage drag is not large.

To sum up briefly, it may be stated that in order to obtain good results in an airplane model test it is necessary to omit all minor parts which show excessive scale effects, such as struts, wires, fittings, small attachments, etc. A drag correction which includes the resistance of all omitted parts must be calculated and added to the basic model drag.

The objections to this method are usually based on the two arguments: (1) that the principle of dynamic similarity is violated, and (2) that interference effects are neglected. These objections cannot be maintained since it has been shown that the principle of dynamic similarity does not apply for an exact scale model and since the interference effects of a strut, for example, certainly cannot be more than a small fraction of the four-fold resistance which this method corrects. On the basis of results, the method is quite satisfactory. The high speed predicted by a careful wind-tunnel test on a simplified model normally differs less than 3% from that obtained in flight tests, and it is not unusual to obtain less than 1% difference.

For additional detail on model construction and test corrections see N.A.C.A. Technical Notes No. 82 "Notes on the Construction and Testing of Model Airplanes," W. S. Diehl (1922), and No. 254 "Method of Correcting Wind Tunnel Data for Omitted Parts of Airplane Models," R. H. Smith (1927).

Lift and Drag Curves. When plotted against angle of attack the lift curve should be smooth and regular with a substantially linear slope up to an angle of attack just below the stall. A sudden inflection in the lift curve indicates an interference burble, which may be due to strut attachment interference, poor fairings around nacelles or wing root, or to any object that is attached to the upper surface of the wing. Figure 39 shows the type of lift curve that is obtained with pronounced interference. In such cases the trouble is eliminated by proper fairings. When a wind-tunnel test gives an irregular lift curve, every effort should be made to locate and eliminate the cause of the interference.

The interference effect on drag may be even greater than that on lift. Figure 40 shows a typical drag curve in which obvious interference effects were eliminated by various fairings on the model.

Certain wing sections, notably the CYH, have a pronounced irregularity in the lift curve at low angles of attack. This is probably due to the reflexed trailing edge. This type of characteristic curve must not be confused with the interference burble that occurs at a higher angle of attack.

As airplane designs become more efficient, the necessity for avoiding bad interference effects becomes greater.

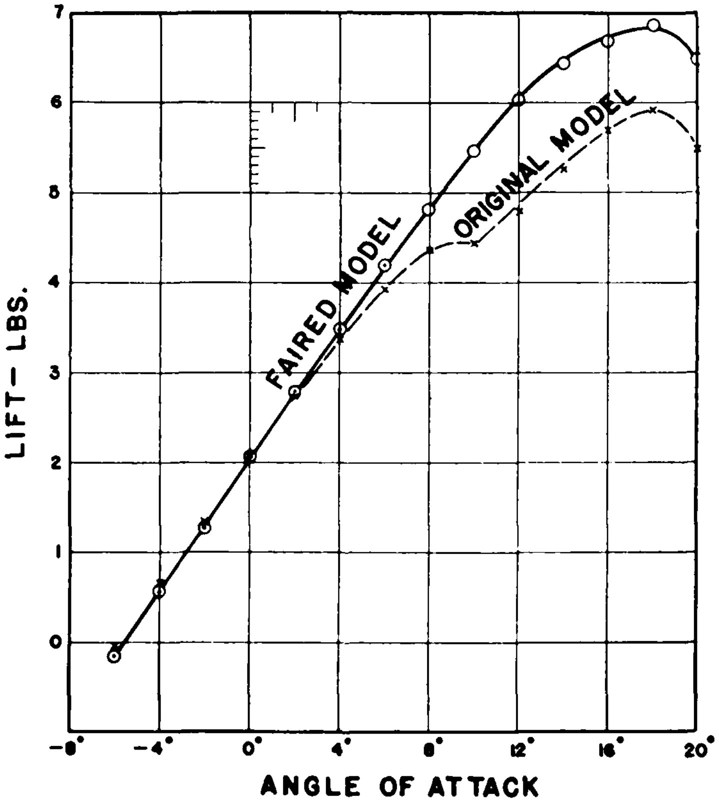

Figure 30. Effect of Interference on the Lift Curve

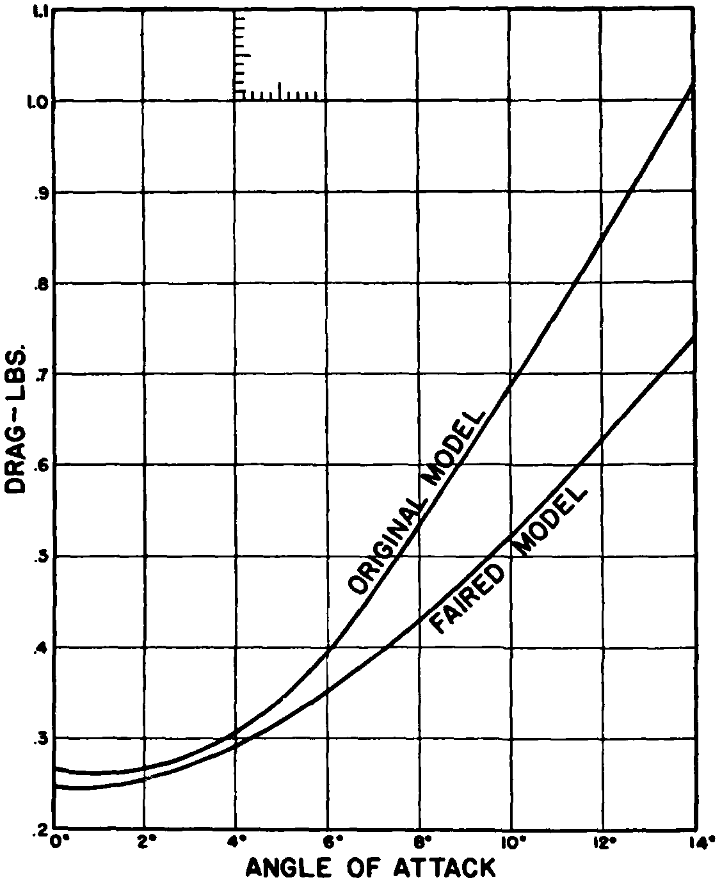

Figure 40. Effect of Interference on the Drag Curve

Until the knowledge of air-flow interference is perfected, the designer must depend on the wind tunnel for assurance that the model is free from gross defects.

Pitching Moments. Information concerning the longitudinal static stability and control is given by pitching moment curves for three or more elevator settings at a selected stabilizer setting. This part of the tests and the lift and drag data should be considered of equal importance.

In general, the pitching moments will be measured about an axis which is parallel to, but considerably displaced from, the gravity axis. Since the final moments must be referred to the c.g., either a graphical or an analytical method must be used in the conversion. The graphical method is simple, quick, and accurate if care is used in drawing the vector diagram. This diagram once drawn is always available for rapid calculations of the pitching moment about any new c.g. location. While an experienced engineer can obtain an excellent idea of stability characteristics directly from the vector diagram, the slope of the moment curve is the only reliable criterion on which to base definite conclusions regarding static stability.

All airplane model tests should include pitching moment curves about the center of gravity for at least two different stabilizer settings with elevators at 0°. The purpose of this being to determine the moment change due to a definite increment in stabilizer angle, so that settings required for balance, or moments for new conditions, may be accurately calculated from the test data. It is easily shown that changing the stabilizer setting or elevator angle does not appreciably affect the slope of the moment curve, and merely shifts it up or down by a definite increment.

The elevator angles usually investigated are 0°, ±5°, ±10°, −15°, −20°, and −30° where the + sign refers to "down" elevator. With the exception of the 0° and ±10° settings, it is unnecessary to cover a greater angular range than that required to give the zero moment, or balance, condition. In general, the moment curve is not satisfactory unless it has a negative slope over the entire range of flight angles. Slight waves in the curve giving zero or slight positive slopes are not actually dangerous, but they are indicative of some very undesirable condition.

The desirable slope of the moment curve varies with the type and purpose of the airplane. The slope of the full-scale moment curve should be either

$$dM/d\alpha = KqWc \tag{71}$$

or

$$dM/d\alpha = K_1qSc \tag{72}$$

where $dM/d\alpha$ is the slope (in lb-ft per degree), q the dynamic pressure $\rho V^2/2$, W the gross weight (lb), c the wing chord (ft), and S the total wing area (sq ft). The value of K should lie between -0.0006 and -0.0010 according to the stability desired. The corresponding values for K_1 are -0.006 and -0.010, but K_1 is not equal to $10K$, since

$$K = K_1/(W/S)$$

Some additional data on slope of the pitching moment curve may be found in Chapter 7.

Whether or not the elevators give adequate control is usually quite obvious from an inspection of the moment curves or vector diagrams. It is a common rule to assume that 20° up elevator should balance the airplane at the angle of attack where maximum lift is obtained, assuming that balance with neutral elevators is in the normal range between 0° to 6° angle of attack.

Longitudinal Balance. The wind-tunnel test on an airplane model usually determines the stabilizer setting required for a specified center-of-gravity location. If the airplane is normal, the relation between c.g. location and stabilizer setting is linear for each trim angle of attack. A few additional readings in the wind-tunnel test data enables the plotting of the balance diagram as in Figure 41. This diagram gives the stabilizer setting required to balance the airplane at any angle of attack with any center of gravity location.

The stabilizer adjustment should be capable of trimming the airplane at any speed above $1.2 V_S$. In preparing the balance diagram, five angles of attack should be used. These angles should be selected to give approximately equal spacing when plotted, but this is not essential. Since the spacing will be proportional to the lift coefficients, angles of attack giving about 0%, 20%, 40%, 60%, and 80% maximum model lift may be used.

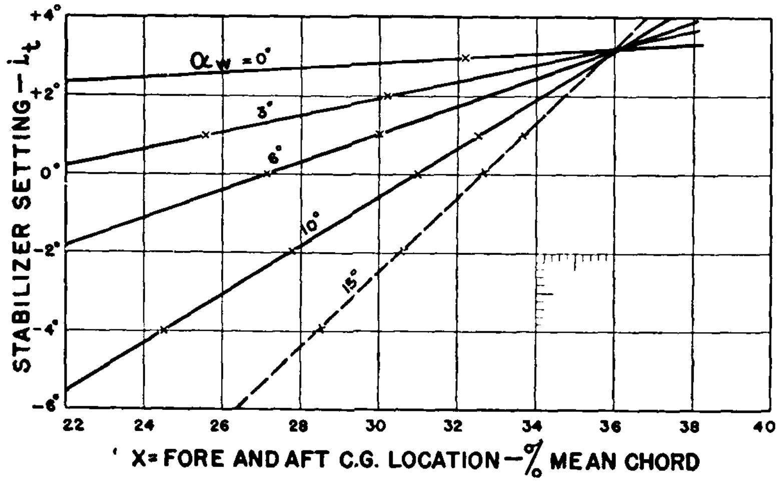

Figure 41. Effect of Angle of Attack and c.g. Location on Stabilizer Angle for Trim

Rolling Moments. There is little information of value to be obtained from rolling-moment tests on an airplane model under steady flow conditions. The National Advisory Committee for Aeronautics tests have shown very definitely that the dynamic effects of velocity in roll cannot be safely neglected.

Fortunately, the design data on ailerons and other lateral control devices are sufficiently complete to make rolling-moment tests unnecessary in most cases. When ailerons are included on an airplane model for test, both rolling and yawing moments should be determined for several aileron angles. Weick, Soulé, and Gough[6] conclude that a criterion for satisfactory rolling moments is

$$RC = C'_l/C_L \tag{73}$$

where C'_l is the rolling moment referred to wind axes and C_L is the lift coefficient. The original studies indicated that the desirable value of RC was 0.075 at 10° angle of attack. Subsequent data indicate satisfactory lateral control for values of RC as low as 0.030. Much depends on the other forces and moments. Low rolling moments may be satisfactory if the yawing moments and the damping in roll are also low.

The rolling moment criterion RC is numerically a lateral center of pressure. Substituting the values of C'_l and C_L,

$$\frac{C'_l}{C_L} = \frac{l'}{qSb} \times \frac{qS}{L} = \frac{l'}{Lb} \tag{73a}$$

Hence, from a model test the dynamic pressure and the wing area cancel out leaving only the ratio of the actual moment to the actual lift as a fraction of the span. This actual lift must be taken at the same angle of attack as the rolling moment.

It is important to note that reducing the span and the stalling speed increases the difficulty in securing adequate lateral control. The airplane is controlled by a rolling moment and not by a rolling-moment coefficient. Consequently, a lateral control device may be entirely satisfactory on a given airplane until the stalling speed is appreciably reduced by a light load or by the action of flaps. The rolling moment criterion must, therefore, be applied with some judgment, taking in consideration the relative span. If the span is relatively short, a high coefficient will be required. If the span is relatively long, a low coefficient may be satisfactory.

---

[6] F. E. Weick, H. A. Soulé, and M. N. Gough, "A Flight Investigation of the Lateral Control Characteristics of Short, Wide Ailerons and Various Spoilers with Different Amounts of Wing Dihedral," N.A.C.A. T.R. No. 494 (1934).

Additional data on lateral control may be found in Chapter 7.

Yawing Moments. The conventional tests to determine directional stability and control consist of three parts as follows:

1. Yawing moments measured with neutral rudder. Usually made at only one angle of attack, about 0° and with a range of ± 20° in yaw.
2. Yawing moments due to various rudder settings with body at 0° yaw and fixed pitch. Usual range of rudder angles 0° to 20°.
3. Angles of yaw held by various rudder settings up to 20°.

While it is desirable that these tests be made at two or more angles of attack, the time required is often an important factor. If the stability and control shown by the first tests are fully satisfactory, there may be little to be gained by tests at additional angles of attack unless the lateral stability is being investigated completely.

Satisfactory conditions in yaw are indicated by:

1. Definite negative slopes to the yawing moment curves. Absence of either irregularities in the curves or unsteadiness in test readings on the balance, particularly at small angles of yaw.
2. The slope of the curve of angle of static yaw held by the rudder, when plotted against rudder angle must be definite, and the curve must be free from marked irregularities. The ratio of static yaw angle to rudder angle should be greater than 0.6 and less than 1.0. A value less than 0.6 may indicate either too much directional (weathercock) stability or deficient rudder control. A value greater than 1.0 may indicate either too little directional stability or too much rudder control.

A yawing moment criterion may be written in the same form as the rolling moment criterion of equation (73). This gives

$$\frac{C'_n}{C_L} = \frac{N}{Wb} \tag{74}$$

where C'_n is the yawing moment coefficient for wind axes, C_L is the lift coefficient, N is the actual yawing moment ($N = C'_n\, q\, Sb$) and W is the gross weight. Since the observed value of N will vary with q, it follows that the desirable slope of the yawing moment curve should be of the form

$$dN/d\psi = KqWb \tag{75}$$

where $dN/d\psi$ is the full-scale slope determined from a test at the dynamic pressure q. Analysis of more than one hundred airplane model tests show that, in general, K should be between -4.0×10^{-5} and -8.0×10^{-5} for best results. The value is not very critical since some airplanes have been reported to have satisfactory directional stability with test values of K well outside of these limits. The most favorable results have been obtained, however, within the limits given, but this has been due partially to the rather narrow limits in stalling speed. For airplanes having either a very low or a very high stalling speed, it is desirable to insure a correct slope by allowing for the departure from normal. There are several ways in which this can be done, but the most practical method appears to require the use of the dynamic pressure at the stalling speed.

Equation (75) may be written

$$\begin{aligned} dN/d\psi &= K\,(q_s/q_0)\,q_M Wb \\ &= K' q_M Wb \end{aligned} \tag{76}$$

where q_s is the dynamic pressure at the stalling speed for the particular airplane and q_0 is the basic value corresponding to average stalling speed which may be taken as 60 mph. q_M is the model test dynamic pressure, W the gross weight of the airplane, and b the span.

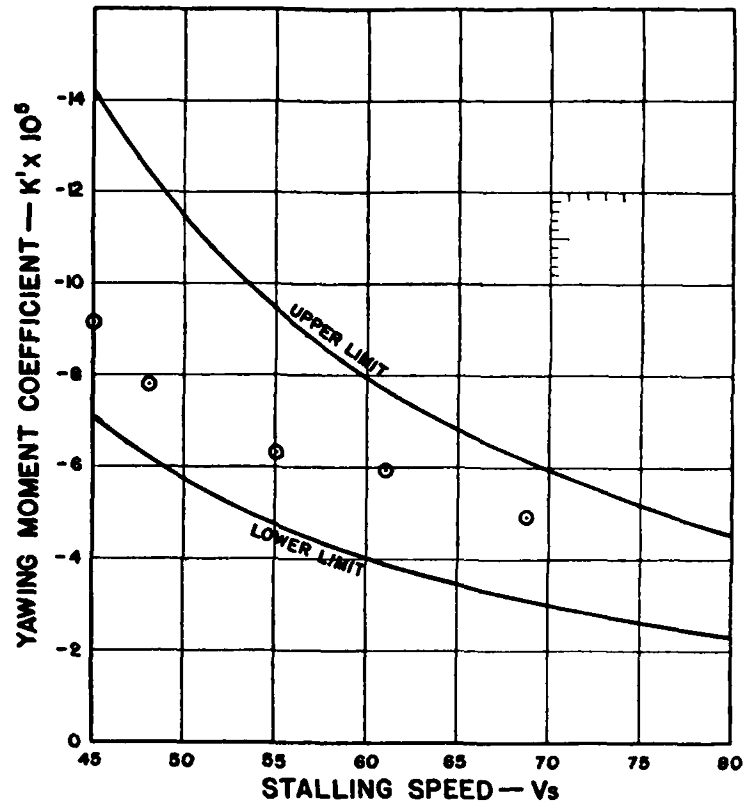

Figure 42. Effect of Stalling Speed on Yawing Moment Coefficient

K' may be plotted against stalling speed as in Figure 42. Five airplanes reported exceptionally satisfactory are spotted on this figure.

Calculation of Performance from Model Tests. Assuming that the air forces vary as $(Vl)^2$, the relations between model and full scale are readily obtained. Designating the model values by the subscript *m* and letting the scale ratio, Model to Full Scale $= l_m/l$, the drag relations at a given angle of attack are

$$\text{Model drag} \quad D_m = (C_D)_m \tfrac{1}{2}\rho\,(V_m\,l_m)^2 \tag{77}$$

$$\text{Full-scale drag} \quad D = C_D\,\tfrac{1}{2}\rho\,(Vl)^2 \tag{78}$$

Since the air forces are assumed to vary as $(Vl)^2$, the drag coefficients will be equal $C_D = (C_D)_m$. Hence

$$D/(Vl)^2 = D_m/(V_m\,l_m)^2$$

or

$$D = D_m\,(l/l_m)^2\,(V/V_m)^2 \tag{79}$$

Similarly

$$L = L_m\,(l/l_m)^2\,(V/V_m)^2 \tag{80}$$

In steady horizontal flight $L = W$. Hence

$$V = V_m\,(l_m/l)\,\sqrt{W/L_m} \tag{81}$$

The minimum or stalling speed is given by substituting the maximum model lift $L_{m\ max}$ in equation (81)

$$V_S = V_m\,(l_m/l)\,\sqrt{W/L_{m\ max}} \tag{82}$$

It is often more convenient to work with speed ratios, rather than to calculate each speed separately

$$V/V_S = \sqrt{L_{m\ max}/L} \ \text{ or } \ V = V_S\,\sqrt{L_{m\ max}/L} \tag{83}$$

but equation (81) can be simplified for any given model, to

$$V = \sqrt{K/L_m} \tag{84}$$

where $K = W(V_m)^2 \times (l_m/l)^2$. Equation (84) can be solved very rapidly on a slide rule by setting the runner to *K* on the *A* scale and moving the slide so that L_m on the *B* scale is in line with *K*. Then the index on the *C* scale will rest at the desired value of *V* on the *D* scale.

Full-scale drag values may be calculated by equation (79), but time can be saved by using the values of L/D from the model test. Where curves of power required are to be calculated for two or more weights, the values of L/D

can be plotted against V/V_S. This curve can then be used in conjunction with equation (83) since $D = \frac{W}{L/D}$ when $L = W$.

In order to secure accurate results, particularly at the lower speeds corresponding to large angles of attack, it is advisable to correct both lift and drag for the elevator angle necessary to maintain balance. If lift, drag, and pitching moments are measured for several elevator settings, this may be done with sufficient accuracy by simple interpolation. Elevator angles of +10° (down), 0° (neutral), −5° (up), −10°, −15°, and −20° are usually required, but the −5°, −15°, and −20° settings need be investigated over only a limited angular range at high angles.

The methods employed in a typical performance calculation will now be illustrated by an example. Table 2 contains the wind-tunnel data obtained in the Washington Navy Yard tests on a 1:16 scale model of the DH-4B, the lift and drag values, L and D, having been corrected for elevator setting.

The maximum lift is 7.571 lb (at 20°) at a speed of 40 mph. The gross weight is 3876 lb. Hence, according to equation (82), the stalling speed is

$$V_S = (40/16)\sqrt{3876/7.571} = 56.6 \text{ mph}$$

For any other weight, the stalling speed is

$$V_S = (40/16)\sqrt{W/7.571} = 0.91\sqrt{W}$$

also

$$V_{S_2} = V_{S_1}\sqrt{W_2/W_1}$$

The speed at any lift is

$$V = (40/16)\sqrt{W/L_m}$$

Table 3 contains the calculations for power required in horizontal flight at sea-level with two gross weights. The

TABLE 2. WIND-TUNNEL TEST DATA ON DH-4B AIRPLANE MODEL SCALE RATIO 1/16. TEST SPEED 40 MPH (standard air)

Angle of Attack α	Elevator Angle for Balance	Lift lb. L_m	Drag lb. D_m	$\frac{L}{D}$	$\frac{V}{V_S}$
1	+ .7	1.214	.392	3.10	2.500
2	+ .4	1.853	.404	4.58	2.020
3	0	2.475	.420	5.90	1.746
4	− .4	3.040	.458	6.63	1.576
6	− 1.2	4.053	.527	7.68	1.366
8	− 2.0	5.045	.623	8.10	1.223
10	− 3.2	5.858	.747	7.83	1.136
12	− 4.7	6.574	.903	7.27	1.073
16	−10.0	7.498	1.745	4.29	1.004
20	−18.5	7.571	2.641	3.10	1.000

TABLE 3. CALCULATION FOR THP REQUIRED IN HORIZONTAL FLIGHT AT SEA-LEVEL. DH-4B AIRPLANE.

(Based on Wind-Tunnel Data in Table 2)

Angle of Attack α	Wind-Tunnel Data		$W = 3876$			$W = 4300$		
	$\frac{L}{D}$	Speed Ratio $\frac{V}{V_S}$	Air Speed V mph	Drag D lb.	thp_r	Air Speed V mph	Drag D lb.	thp_r
1	3.10	2.500	141.4	1,250	472.0	149.0	1,385	550.0
2	4.58	2.020	114.3	847	258.0	120.3	938	301.0
3	5.90	1.746	98.8	657	173.3	104.0	728	202.0
4	6.63	1.576	89.2	585	139.0	93.8	648	162.2
6	7.68	1.366	77.2	505	104.0	81.3	560	121.3
8	8.10	1.223	69.2	478	88.2	72.8	530	103.0
10	7.83	1.136	64.2	495	85.0	67.7	548	98.8
12	7.27	1.073	60.7	533	86.3	64.0	591	100.7
16	4.29	1.004	56.8	903	136.8	59.8	1,002	160.0
20	3.10	1.000	56.6	1,250	189.0	59.6	1,385	220.0

$$\text{thp}_r = \frac{VD}{375}$$

corresponding powers required at any desired altitude may be obtained by multiplying each value of V and thp, by the value of $\sqrt{\rho_0/\rho}$ for the altitude under consideration, as explained in Chapter 11. Figure 43 is a plot of the thp available and thp required against air speed at sea-level. The performance indicated is in excellent agreement with the flight test results on this airplane in the condition represented by the model.

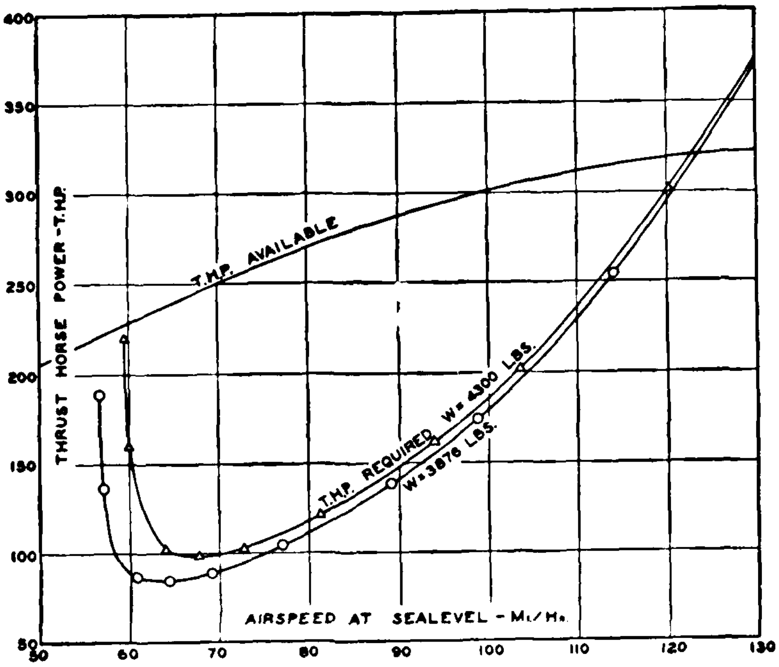

Figure 43. DH-4B Power Curves from Wind-Tunnel Tests

CHAPTER 5

AIRFOIL DATA

Airfoil Sections. Prior to 1912, an airplane wing was given any cross-section that the designer felt was sufficiently different from existing types. The appearance of data on various sections tested at the National Physical Laboratory in England, and at Eiffel's Laboratory in France led to the general adoption of a moderately thick and fully covered section of the RAF-6 or Eiffel-36 type. Between 1912 and 1920, numerous tests were made in various countries on sections incorporating slight modifications. The first tests on a really extensive series of related sections appears to have been made at Göttingen University during the war period on groups of sections of the Joukowsky type. These sections are derived from arbitrary theoretical flow conditions and are characterized by a blunt leading edge and a very thin trailing edge. They are now of academic interest only and it may be here noted that the only apparent advantages of mathematically derived sections lie in the accuracy of fairing and the ease with which a series of systematic changes may be made. There appears to be little or no aerodynamic merit attached to any exact mathematical curve or combination of curves.

The next extensive series of related airfoils appears to be Munk's "M" sections[1] which were tested in the variable-density tunnel in 1924. This series was based on the combination of a single profile shape in three thicknesses with nine systematically varied mean camber lines, including one designed to give zero moment. This series is noteworthy in several respects, although it gave only two outstanding sections, the M-6 and the M-12. It was the first extensive series of related sections to be tested at high Reynolds Number, it was the first serious study of zero-moment sections, and it indicated the lines for needed research.

---

[1] M. M. Munk and E. W. Miller, "Model Tests with a Systematic Series of 27 Wing Sections at Full Reynolds Number," N.A.C.A. T.R. No. 221 (1925).

In 1928, Schrenk[2] reported the results of tests at Göttingen on a series of 30 sections in which the camber and thickness were changed systematically. These tests were made at a Reynolds Number of about 500,000.

About 1928, arrangements were made for an extensive series of tests at full-scale Reynolds Number in the National Advisory Committee for Aeronautics variable-density wind tunnel at Langley Field. The major portion of this program was completed in 1932, and the results published in N.A.C.A. T.R. No. 460.[3] This report is by far the most valuable source of airfoil data now available. It has greatly simplified the designer's problem of selecting the best wing section.

Interpretation of Airfoil Data. Airfoil characteristics as measured in a wind tunnel are greatly influenced by the Reynolds Number of the test, by the surface finish of the model and by the turbulence in the wind tunnel. The method of supporting the model and the type of tunnel also affect the results, but to a negligible degree in a carefully made test. However, the combined effect of all of these factors makes it advisable to use extreme caution in comparing the results of tests from different wind tunnels, particularly with reference to selection of a wing section. The selection of a wing section at this time is best made on the basis of comparative results from the National Advisory Committee for Aeronautics variable-density wind tunnel.

---

[2] O. Schrenk, "Systematische Untersuchungen an Joukowsky Profilen", ZFM, May 29, 1928.

[3] E. N. Jacobs, K. E. Ward and R. M. Pinkerton, "The Characteristics of 78 Related Airfoil Sections from Tests in the Variable-Density Wind Tunnel" (1933).

The N.A.C.A. Related Airfoils. An airfoil section is completely defined by certain conditions as follows:

1. *Mean camber-line equation*—
   - (a) Value of maximum mean camber
   - (b) Location of maximum mean camber
2. *Profile thickness equation*—
   - (a) Maximum profile thickness
   - (b) Location of maximum profile thickness
   - (c) Leading edge radius
   - (d) Trailing edge radius

In the N.A.C.A. series of related airfoils, the adoption of equations for the mean camber line and the profile thickness also determined the location of the maximum profile thickness at 30% of the chord and the leading edge radius. Assuming that the trailing edge is simply rounded off to no particular radius (although a radius would be determined by the equation adopted) there remains only three factors necessary to define a particular section, namely, 1(a), 1(b), and 2(a). Consequently, a four-digit number may be used, the first digit being the maximum mean camber in per cent of the chord, the second digit being the location of the maximum mean camber in tenths of the chord, and the last two digits being the thickness in per cent of the chord. For example, 2412 designates a section 12% c in thickness, having 2% maximum mean camber located at 40% of the chord.

In this series the ordinates for any thickness are determined from the equation

$$\begin{aligned}\pm y = 5t\,(0.29690\sqrt{x} - 0.12600x - 0.35160\,x^2 \\ + 0.28430\,x^3 - 0.10150\,x^4)\end{aligned}$$

in which the constants were selected to fit closely the basic profile thickness curves of the Göttingen 398 and Clark Y sections. The leading edge radius is

$$r = 1.10\,t^2$$

The mean camber line is formed from two parabolic equations having vertices at the maximum mean camber.

On completion of the tests on the first series of sections, a supplemental series was prepared to study the effect of forward locations of the maximum mean camber. The positions selected were $0.05c$, $0.10c$, $0.15c$, $0.20c$, and $0.25c$, and the corresponding mean line shapes were designated 10, 20, 30, 40, and 50. Thus, the combination of the mean line 30 with 2% camber gives the family "230" and for 12% thickness the section "23012." This particular section appears to be of outstanding merit.

Test data on this series of related airfoils are given in N.A.C.A. T.R. Nos. 460 and 537, copies of which should be obtained by every aeronautical engineer. It is impracticable and undesirable to give in this chapter more than a summary of the results supplemented by detailed data on certain selected sections.

Maximum Lift Coefficient: C_L Maximum. The variation of C_L maximum with thickness ratio is given on Figure 44. Each curve on this figure represents a single mean camber line. The two digit identification numbers are the first two numbers in the airfoil designation number. The first digit is the per cent maximum mean camber, the second digit is the location of the maximum mean camber in tenths of the chord. Thus "24" would represent 2% maximum mean camber located at 40% of the chord and "45" would represent 4% maximum mean camber located at 50% of the chord. This system is followed in the remainder of the discussion of the series.

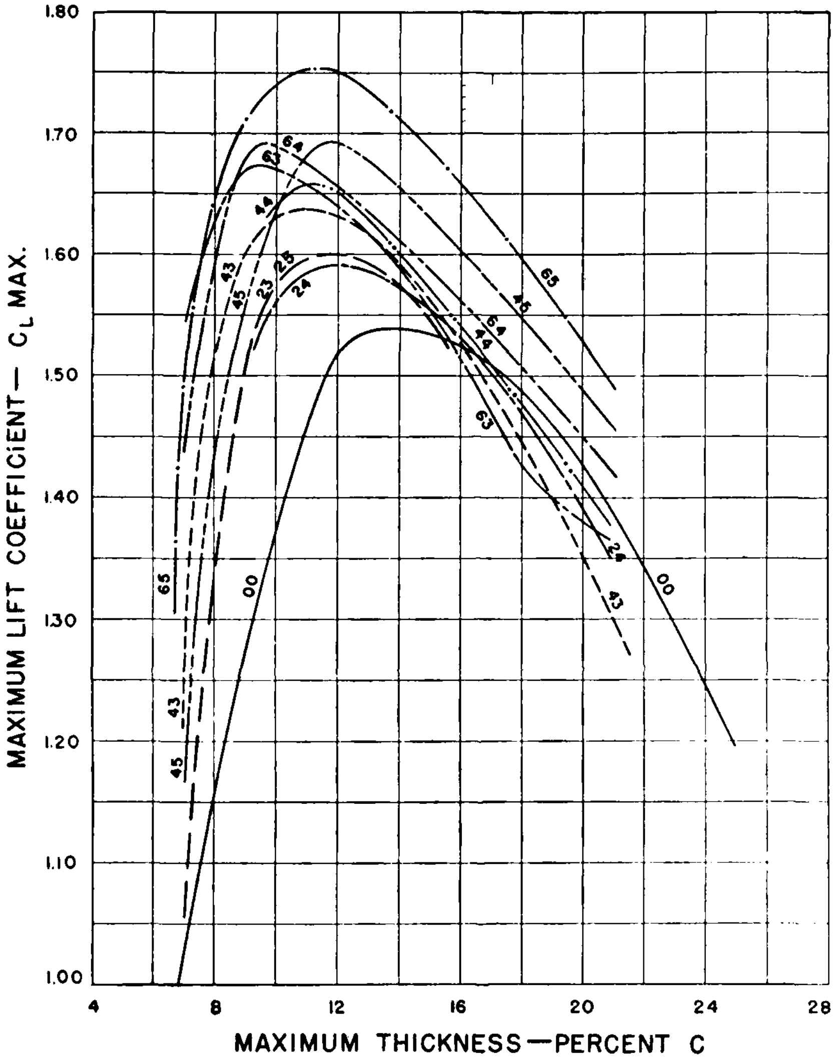

Figure 44. Effect of Thickness and Mean Camber Line on Maximum Lift Coefficient

Examination of Figure 44 leads to the following conclusions:

1. C_L maximum is more dependent on thickness than shape of the mean camber line.
2. For each mean camber line, there is an optimum thickness for C_L maximum. This optimum thickness decreases as the maximum mean camber is increased or moved forward.
3. The maximum lift for each series would be as follows:

Section	$C_{L\,max}$
0014	1.54
2312	1.60
2412	1.60
2512	1.60
4311	1.63
4411	1.66
4512	1.65
6310	1.67
6410	1.69
6511	1.75

4. The tests on supplementary airfoils (not plotted on Figure 44) show that C_L maximum is sensitive to leading edge radius. The best leading edge radius appears to be approximately

$$r = 0.2\,t$$

where t is the thickness.

5. The tests on airfoils with reflexed trailing edges show that the reduction in C_L maximum is almost directly proportional to the reduction in C_{M_0} and that

$$\Delta C_{L\,max} = -2.5\,\Delta C_{M_0}$$

Profile Drag Coefficients. The variation of profile drag with lift coefficient is the most important single characteristic of a wing section. The usual curves are plotted to such a scale that it is impossible to read C_{D_0} with reasonable accuracy. Table 4, giving values of C_{D_0} for the best sections now available, will be found more convenient than the conventional plotting.

The values in Table 4 have been taken from large-scale plots drawn up from the variable-density wind tunnel data. Interpretations or conclusions based on these data should not overlook the fact that there is an inherent experimental uncertainty of about ±0.0003 in the value of C_{D_0} at low values of C_L.

TABLE 4. PROFILE DRAG COEFFICIENTS FROM VARIABLE-DENSITY WIND TUNNEL

$C_{D_0} \times 10^4$

Section	C_L									Value of $C_{L\,max}$
	0	0.2	0.4	0.6	0.8	1.0	1.2	1.4	max	
0009	74	78	86	95	113	146	207	....	810	1.27
0012	83	85	90	101	116	142	183	262	420	1.53
0015	92	95	100	111	126	151	198	272	550	1.53
0018	108	109	112	121	135	160	204	292	550	1.49
2212	88	87	90	95	102	123	163	230	500	1.60
2312	89	89	91	98	111	132	172	235	540	1.61
2409	81	80	85	93	106	129	165	230	(450)	(1.54)
2412	87	85	90	97	112	133	169	235	600	1.61
2415	100	99	103	112	124	147	185	253	630	1.54
2418	112	112	117	126	141	168	224	410	590	1.43
2512	90	88	89	97	111	135	172	231	700	1.62
4412	97	92	92	97	105	124	161	227	650	1.65
23009	79	79	84	92	104	125	161	227	360	1.55
23012	87	86	92	102	114	130	161	223	350	1.63
23015	99	98	99	105	116	134	167	218	430	1.61
2R$_1$12	87	83	85	93	107	130	170	243	520	1.53
M-6	92	92	96	107	127	160	244	500	551	1.41
NACA-21	91	88	89	94	106	127	164	238	475	1.60
Clark Y	99	98	99	106	121	144	180	257	550	1.60
YH	92	91	95	104	119	144	190	279	550	1.47
G-398	112	106	109	117	131	155	195	273	638	1.57
N-22	103	99	101	109	119	143	178	247	470	1.60
N-80	85	83	84	92	107	126	156	212	540	1.63

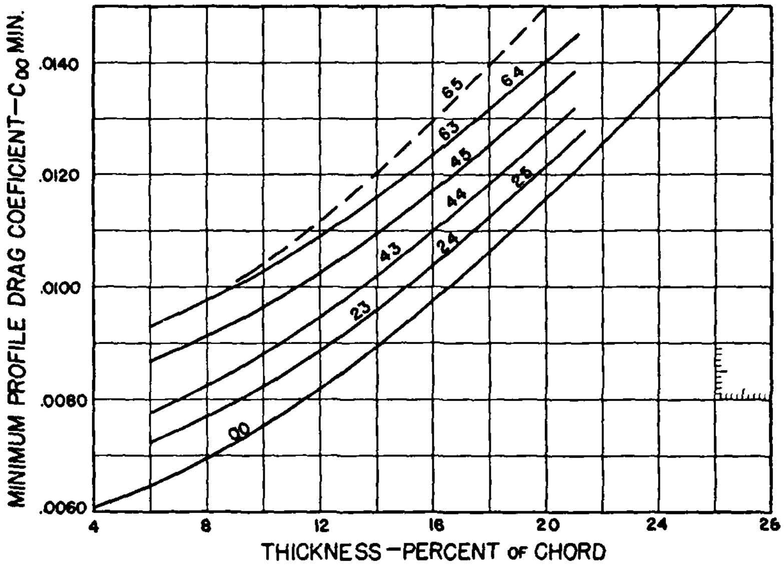

Figure 45. Effect of Thickness and Mean Camber Line on Minimum Profile Drag Coefficient

Minimum Profile Drag Coefficient C_{D_0} Minimum. Figure 45 gives the variation of the minimum profile drag coefficient with thickness for each mean camber line. The effect of thickness is seen to be practically independent of the mean camber line. The variation in C_{D_0} minimum is given approximately by the equation

$$C_{D_0\,min} = K + 0.0056 + 0.01t + 0.1\,t^2 \tag{85}$$

Values of K are as follows:

Mean camber line	K
00	0
23, 24, 25	.0007
43, 44	.0012
45	.0021
63, 64	.0027
65	.0028

The observed values of C_{D_0} minimum may also be represented closely by an equation of the form

$$C_{D_0\,min} = K_1 + K_2 t^{1.5} \qquad (85a)$$

These tests were made at an actual Reynolds Number of about 3×10^6 or an effective Reynolds Number of about 8×10^6. The variation of these values with Reynolds Number should be similar to the variation obtained on other sections.

Scale Effect. With the exception of C_L maximum and C_{D_0}, airfoil characteristics in general are not appreciably

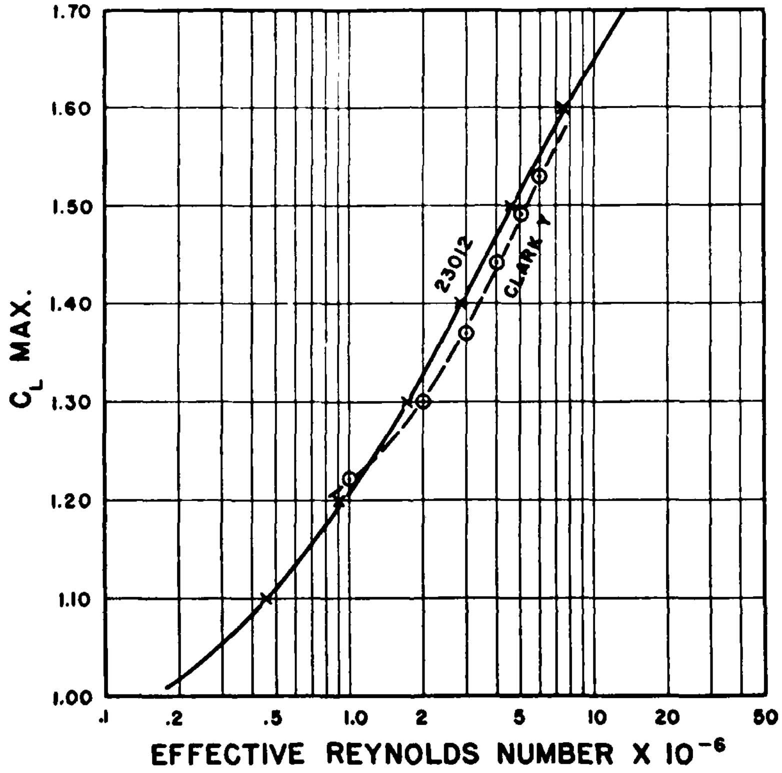

Figure 46. Variation of C_L Maximum with Effective Reynolds Number

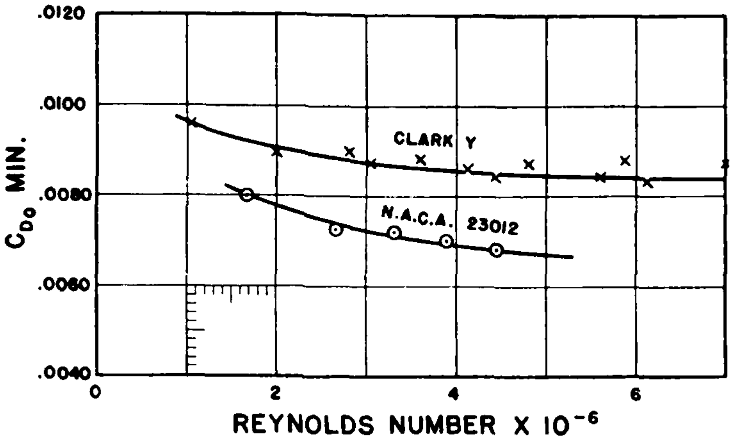

Figure 47. Variation of Minimum Profile Drag Coefficient with Reynolds Number

dependent on Reynolds Number. The effects of Reynolds Number on C_L maximum and C_{D_0} depend upon the turbulence in the air stream and the type of wing section. In comparing data from the variable-density and full-scale wind tunnels at Langley Field, it was found that a given C_L maximum required in the full-scale wind tunnel a Reynolds Number about 2.4 times that required in the variable-density tunnel.[4] This led to the conception of an effective Reynolds Number[5] to include the effect of turbulence, which was supported in a convincing manner by the same ratio of 2.4 between the Reynolds Numbers for a sphere drag coefficient of 0.30 in the two wind tunnels.

The effect of Reynolds Number on C_L maximum depends greatly on the type of wing section and especially on the mean camber. Sections with zero or small mean camber show a large increase in C_L maximum with R.

---

[4] A. Silverstein, "Scale Effect on Clark Y Airfoil Characteristics from N.A.C.A. Full-Scale Wind Tunnel Tests," N.A.C.A. T.R. No. 502 (1934).

[5] E. N. Jacobs, "Recent Progress Concerning the Aerodynamics of Wing Sections," A.S.M.E. Paper read at University of California, June 19, 1934.

Sections with a moderate camber show a moderate increase and very highly cambered sections such as the RAF-19 actually show a decrease in C_L maximum as R is increased. There is a tendency for all sections to give about the same C_L maximum at very high values of R. Considering only the highly efficient sections now used almost universally, the variation of C_L maximum with effective Reynolds Number will be substantially as shown on Figure 46.

The effect of Reynolds Number on C_{D_0} is largely due to the reduction in frictional coefficient. Typical curves are given on Figure 47.

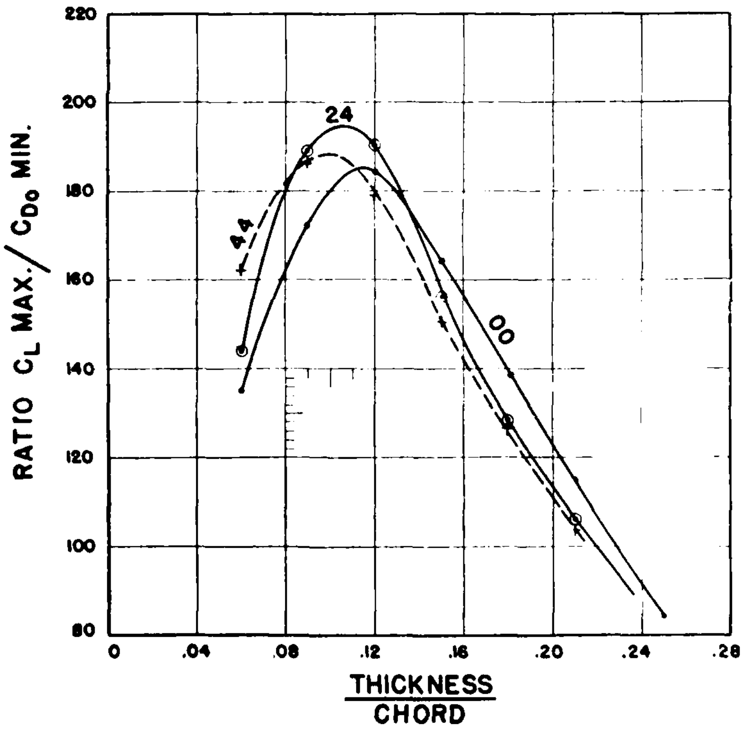

Figure 48. $C_{L\ max}/C_{D0\ min}$ vs. Thickness/Chord for Three Mean Camber Lines

Ratio $C_{L\,max}/C_{D0\,min}$. The ratio of maximum lift coefficient to minimum profile drag coefficient is probably the most reliable single criterion of airfoil efficiency. Unfortunately, it is difficult to obtain accurate values of the ratio for exact comparisons.

Figure 48 shows the variation of $C_{L\,max}/C_{D0\,min}$ with thickness for three mean camber lines. Figure 49 shows the variation with mean camber line for constant thickness 0.12 c. The maximum value of the ratio is obtained with a thickness of about 0.12 c. The thickness for maximum value of $C_{L\,max}/C_{D0\,min}$ decreases as the camber is increased. The variation of the ratio with location of maximum mean camber is irregular.

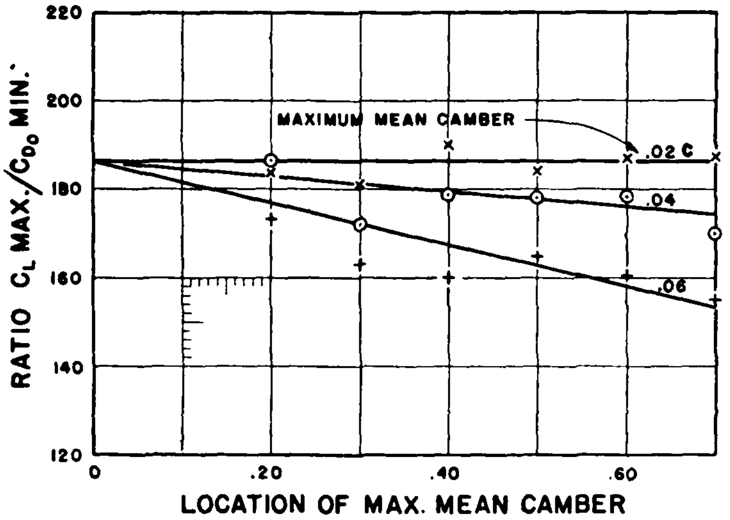

Figure 49. $C_{L\,max}/C_{D0\,min}$ as a Function of Maximum Mean Camber. $t/c = 0.12$

Angle of Attack for Zero Lift. Theoretically the angle of attack for zero lift is independent of the thickness and varies with the mean camber line only. For the conventional sections of moderate camber, there is excellent agreement between the theoretical and the observed values. However, for thickness in excess of 0.15 *c* with the 45, 63, 64, and 65 mean camber lines, the observed angle of attack for zero lift is appreciably less negative than required by theory. The deviation increases as the maximum mean camber is increased or moved aft.

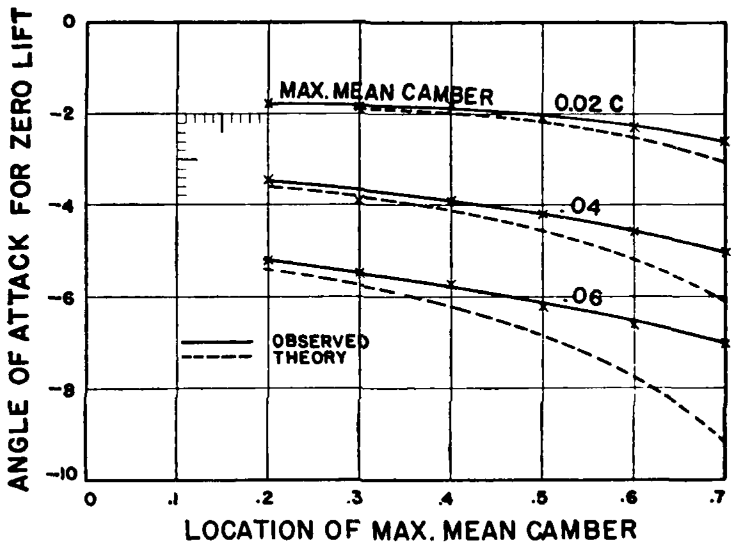

Figure 50. Angle of Attack for Zero Lift as a Function of Maximum Mean Camber

Figure 50 compares the observed and theoretical zero-lift angles for the 12% thickness group.

Moment Coefficient at Zero Lift: C_{M_0}. The observed moment coefficient at zero lift theoretically depends on the mean camber line only. A comparison of theoretical and observed values of C_{M_0} is given for various mean camber lines on Figure 51 which appears on the following page.

The observed values are appreciably less negative than the theory requires.

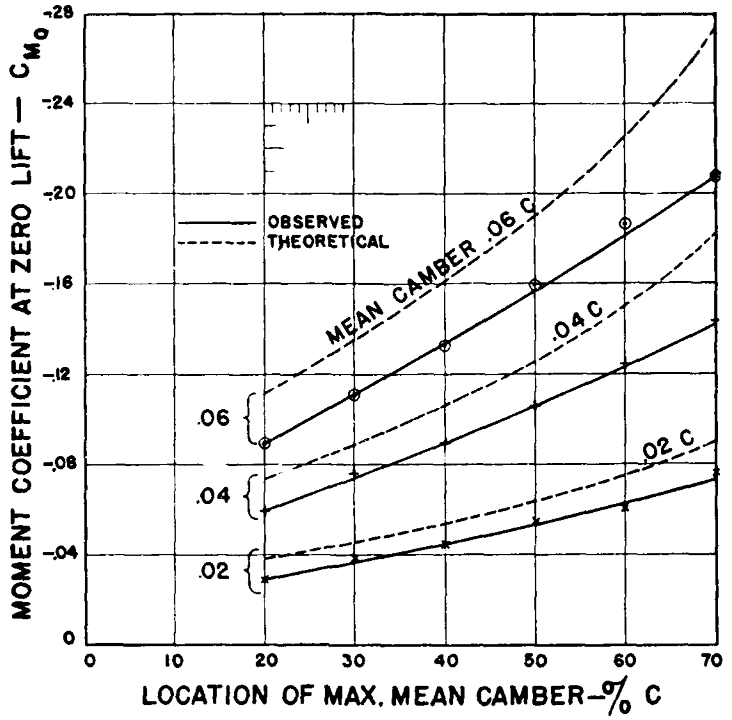

Figure 51. Moment Coefficient at Zero Lift as a Function of Maximum Mean Camber

The observed values in Figure 51 are for a thickness of 12% c. Tests on other sections show a definite decrease in C_{M_0} as the thickness is increased. The variation of the ratio of observed to theoretical values of C_{M_0} is as follows:

t/c	.06	.09	.12	.15	.18	.21
$(C_{M_0}$ Obs.$)/(C_{M_0}$ Theo.$)$	.83	.82	.80	.77	.73	.67

Aerodynamic Center. The moment coefficient about the quarter-chord point is not exactly constant as required by Munk's theory. However, the deviation is small and a point about which the moment coefficient is constant may be found. This point is the "aerodynamic center" and it is normally located at about 24% of the chord.

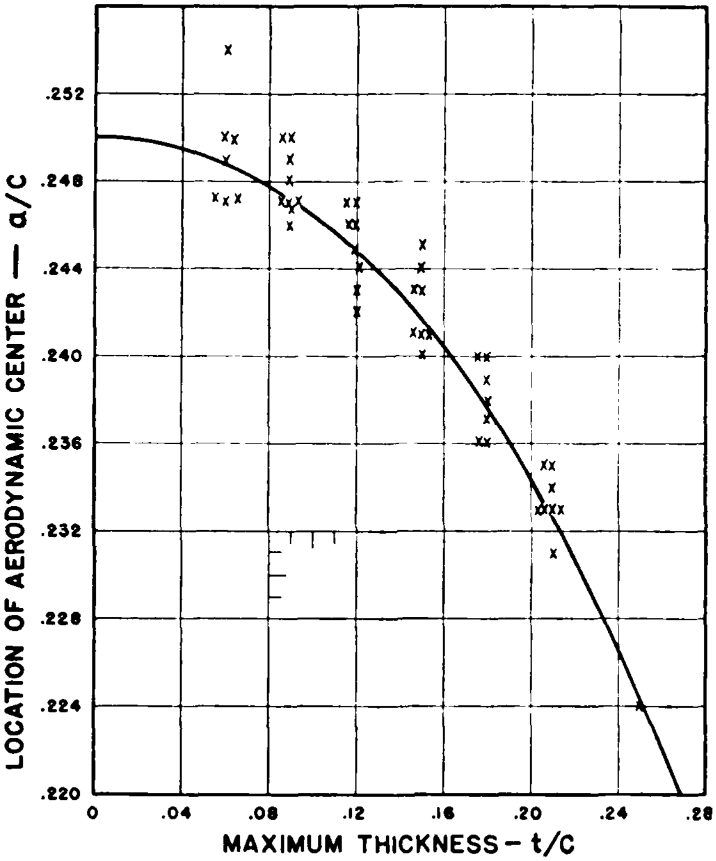

Figure 52. Aerodynamic Center as a Function of Maximum Thickness

Figure 52 gives a plot of the aerodynamic center as a function of the thickness. It is not greatly affected by changes in the mean camber line. Accurate calculations show that the aerodynamic center is not exactly on the mean camber line—it is slightly above or below.

Optimum Lift Coefficient. The optimum lift coefficient $C_{L\,opt.}$ may be defined as the value of C_L for minimum profile drag coefficient. It is a function of the maximum mean camber and the thickness as shown on Figure 53.

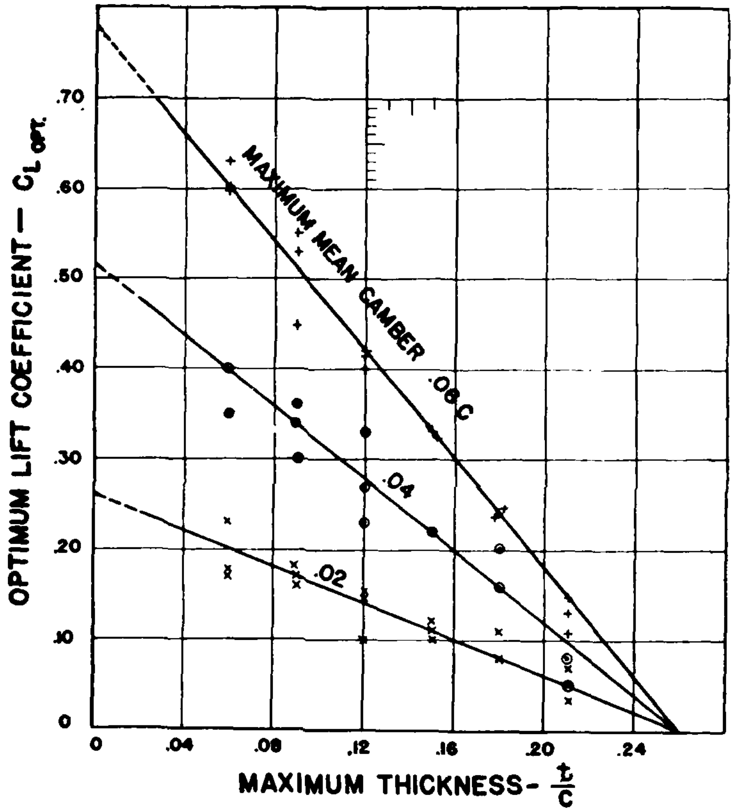

Figure 53. Optimum Lift Coefficient as a Function of Maximum Mean Camber and Thickness

It is independent of the location of the maximum mean camber. Figure 53 may be represented by the equation

$$C_{L\,opt.} = h\,(13 - 50\,t) \tag{86}$$

where h is the maximum mean camber and t is the thickness, both expressed as decimal fractions of the chord.

C_L optimum should be considered in design since the minimum profile drag should occur at the C_L for high speed. This is not the only criterion, however, since the actual value of the minimum profile drag coefficient is of greater importance than the value of C_L at which it occurs.

Maximum Negative Lift Coefficient. The maximum negative lift coefficient of an airfoil section depends on the maximum mean camber and thickness. It is apparently independent of the location of the maximum mean camber.

Analysis of the negative angle tests in the N.A.C.A. variable-density wind tunnel[6] indicates that the effects of

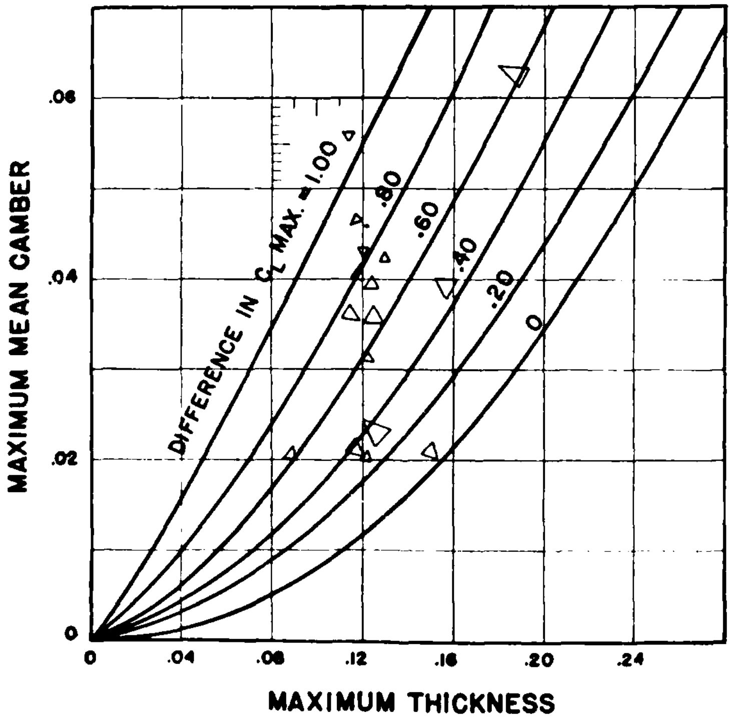

Figure 54. Effect of Maximum Mean Camber and Thickness on Maximum Negative Lift Coefficient

maximum mean camber and thickness are approximately as shown on Figure 54. In this figure the parameter is the difference between the numerical values of the maximum positive and negative lift coefficients or the algebraic sum of the maximum positive and negative values of C_L. Experimental values are indicated as triangles, one side of which is the observed value of ΔC_L maximum while the opposite apex represents the airfoil designation. It will be noted that the average deviation is small. To illustrate the use of this figure, take section 6321 for which the positive C_L maximum = 1.37. For 6% maximum mean camber and 21% thickness ΔC_L maximum = 0.40. Hence, the maximum negative C_L for 6321 is $-(1.37 - 0.40) = -0.97$.

---

[6] R. F. Anderson, "The Aerodynamic Characteristics of Airfoils at Negative Angles of Attack," N.A.C.A. T.N. No. 412 (1932).

Slope of Lift Curve. The theoretical slope of the lift curve is

$$\begin{aligned} dC_L/d\alpha &= 2\pi \text{ for } \alpha \text{ in radians} \\ &= 0.1097 \text{ for } \alpha \text{ in degrees} \qquad (34a) \end{aligned}$$

Slopes for all of the N.A.C.A. variable-density airfoil tests have been plotted against thickness ratio, as in Figure 95 of Technical Report No. 352. If allowance is made for the difficulty of obtaining a high degree of accuracy in the measured slope, it appears that the theoretical value should be obtained for a flat plate and that the slope for infinite aspect ratio decreases with thickness ratio (t/c) according to

$$dC_L/d\alpha = 0.1097 - 0.070\,(t/c) \qquad (87)$$

If the slope of the lift curve is known for one aspect ratio, the value for any other aspect ratio may be obtained from the equation

$$a_2 = \frac{a_1}{1 + 18.24\,a_1\,(\lambda_2 - \lambda_1)} \qquad (36)$$

where a_1 and a_2 are the slopes of the lift curves for the area ratios λ_1 and λ_2 respectively. The area ratio is the reciprocal of the aspect ratio or

$$\lambda = S/b^2 = 1/n$$

Equations (36) and (87) may be used to prepare a group of curves giving slope against aspect ratio for given thickness ratio as in Figure 55. These curves may be used when the actual slope for some given aspect ratio is unknown.

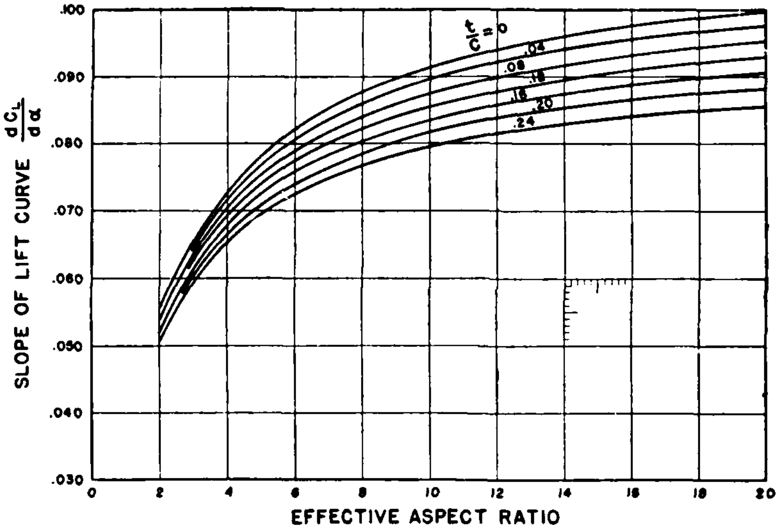

Figure 55. Slope of Lift Curve as a Function of Thickness and Aspect Ratio

For many purposes an approximate value of the slope is sufficient. The curve for $t/c = 0.12$ from Figure 55 is very closely represented by

$$\frac{dC_L}{d\alpha} = \frac{n}{10\,(n + 1.8)} \tag{88}$$

The foregoing slopes are based on the elliptical lift distribution which is attained for all practical purposes with well-rounded tips. With square tips, the slopes will be about 4% less than the values which are given on Figure 55.

Selection of a Wing Section. There are so many factors to be considered in determining the relative merit of a wing section, that a very precise analysis is unnecessary and may even be misleading. The designer usually works to a set of specifications that rule out, for example, all wing sections for which the moment coefficient is greater than some value, say −0.04, or for which the maximum lift coefficient is less than 1.50. Referring to tabulated airfoil characteristics, it is not difficult to select those sections meeting simple limits. From the list that is so selected, the final choice is normally made on the basis of structural characteristics, drag coefficient, or some special requirement. A word of caution is necessary regarding too great a dependence on test data in making the selection. The reports presenting airfoil characteristics list the limits of accuracy in the test data. These limits are normally within 2% when special care is taken. They may be much greater due to variations in model surface finish and airflow conditions in the wind tunnel. Furthermore, there is so little difference between the sections in a selected group that the final choice appears a matter of relatively minor importance. In making such a selection, it is highly important to use strictly comparable test data from the same wind tunnel, since otherwise actual differences might be masked by differences due to tunnel characteristics. At present the N.A.C.A. variable-density wind tunnel, usually referred to as the VDT, is the best source of comparable data.

The actual selection may be based on the relative value of a number of factors, those commonly used being the following:

1. Maximum lift coefficient, $C_{L\,max}$
2. Minimum drag coefficient, $C_{D\,min}$
3. Ratio $C_{L\,max}/C_{D\,min}$
4. Moment coefficient at zero lift, C_{M_0}
5. Maximum value of ratio L/D

In certain special cases, the comparison may be extended to include one or more of the following factors:

6. Value of C_L for maximum L/D
7. Value of C_L for minimum profile drag
8. L/D at $C_L = 0.70$ (for climb)
9. Maximum value of C_L^3/C_D^2 (for ceiling)
10. Type of lift curve peak

It is impossible to find any one factor or combination of factors that will completely and definitely assign a rating to an airfoil section. However, the designer may be able to find a grouping that will be of some assistance in any particular design problem. As an example of this type of analysis, one might take as a measure of the general aerodynamic efficiency

$$E = \frac{(C_{L\,max}/C_{D\,min})}{(\Delta C_M - C_{M_0})} \cdot \left(\frac{L}{D}\right)_{max} \tag{89}$$

where ΔC_M is assigned a value that properly allows for the effects of a low C_{M_0}. If increasing C_{M_0} from 0 to -0.10 is considered offset by a 10% increase in $(L/D)_{max}$, then $\Delta C_M = 1.00$. In applying any criterion, the group of sections to be considered is initially restricted to those meeting obvious requirements such as adequate thickness for efficient spars or control attachments. A brief inspection of the VDT data, previously discussed, will show certain sections of outstanding general merit. These are the sections of 12% thickness. A list limited to ten sections will include about all that are worth considering, except in very special cases. The ten sections selected on the basis of data now available are as follows:

Section	$C_{L\,max}$	$C_{D0\,min}$	Ratio $\frac{C_{L\,max}}{C_{D0\,min}}$	C_{M0}
0012	1.53	.0083	184	−.002
2212	1.60	.0087	184	−.029
2312	1.61	.0089	181	−.038
2412	1.61	.0085	189	−.044
4412	1.65	.0092	179	−.089
$2R_1 12$	1.53	.0083	184	−.020
NACA 21	1.60	.0088	182	−.038
N-80	1.63	.0083	196	−.045
CYH	1.47	.0086	172	−.027
23012	1.63	.0086	190	−.008

Corrections for Aspect Ratio. Basic airfoil data are usually given for infinite aspect ratio. To convert these data to any finite aspect ratio, the following formulas are used:

$$a = \frac{a_0}{1 + \frac{18.24}{n} a_0 (1 + \tau)} \tag{37a}$$

$$\alpha_n = \alpha_0 + \frac{18.24}{n} C_L (1 + \tau) \tag{39a}$$

$$C_{D_n} = C_{D_0} + \frac{C_L^2}{\pi n} (1 + \sigma) \tag{40a}$$

where τ and σ are the corrections for the shape of the span loading curve. For an elliptical wing, or for a well-rounded tip, both τ and σ are zero. For a wing with square tips they vary with aspect ratio as shown on Figure 17.

Airfoil Ordinates. Airfoil ordinates are readily available in the original publications and in various N.A.C.A. Technical Reports giving collected data, such as T.R. Nos. 93, 124, 182, 221, 233, 244, 286, 315, 331, 352, and 460. Table 5 lists for convenient reference the ordinates of a limited number of outstanding sections.

Airfoil Section Equivalents. It may be of interest to compare the present N.A.C.A. family of related sections with the sections most frequently used in the past. Table 6

TABLE 5. AIRFOIL ORDINATES

STA	0012		2212		2412		23012		CYH		N-80	
	U	L	U	L	U	L	U	L	U	L	U	L
0	0	0	–	0	–	0	–	0	3.50	+3.50	.33	0
1.25	1.894	−1.894	2.44	−1.46	2.15	−1.65	2.67	−1.23	5.45	+1.93	2.02	1.33
2.5	2.615	−2.615	3.35	−1.96	2.99	−2.27	3.61	−1.71	6.50	+1.47	2.84	1.83
5.0	3.555	−3.555	4.62	−2.55	4.13	−3.01	4.91	−2.26	7.90	+ .93	4.03	2.38
7.5	4.200	−4.200	5.55	−2.89	4.96	−3.46	5.80	−2.61	8.85	+ .63	4.94	2.73
10.0	4.683	−4.683	6.27	−3.11	5.63	−3.75	6.43	−2.92	9.60	+ .42	5.68	2.97
15.0	5.345	−5.345	7.25	−3.44	6.61	−4.10	7.14	−3.50	10.69	+ .15	6.78	3.24
20.0	5.738	−5.738	7.74	−3.74	7.26	−4.23	7.50	−3.97	11.36	.03	7.51	3.37
25.0	5.941	−5.941	7.93	−3.94	7.67	−4.22	7.60	−4.28	11.70	0	7.92	3.45
30.0	6.002	−6.002	7.97	−4.03	7.88	−4.12	7.55	−4.46	11.40	0	8.07	3.47
40 0	5.803	−5.803	7.68	−3.92	7.80	−3.80	7.14	−4.48	10.52	0	7.75	3.25
50.0	5.294	−5.294	7.02	−3.56	7.24	−3.34	6.41	−4.17	9.15	0	7.09	2.84
60.0	4.563	−4.563	6.07	−3.05	6.36	−2.76	5.47	−3.67	8.30	0	6.13	2.34
70.0	3.664	−3.664	4.80	−2.43	5.18	−2.14	4.36	−3.00	7.41	+ .06	4.89	1.78
80.0	2.623	−2.623	3.52	−1.74	3.75	−1.50	3.08	−2.10	5.62	+ .38	3.47	1.21
90.0	1.448	−1.448	1.93	− .97	2.08	− .82	1.68	−1.23	3.84	+1.02	1.82	.58
95.0	.807	− .807	1.05	− .56	1.14	− .48	.92	− .70	2.93	+1.40	–	–
100.0	0	−0	–	0	–	0	–	0	2.05	+1.85	0	0
L.E.R.	1.58		1.58		1.58		1.58		1.5			

TABLE 6. N.A.C.A. SYMBOLIC EQUIVALENTS FOR COMMON AIRFOIL SECTIONS

Section	Maximum Mean Camber		Thickness % c	Nearest N.A.C.A. Section
	% c	Location % c		
Clark Y	3.9	40	11.7	4412
Y-15	5.2	37	15.0	5415
Y-18	6.3	37	18.0	6418
YM-15	4.0	40	15.0	4415
YM-18	4.0	40	18.0	4418
CYH	3.1	31	11.7	3312
M-6	2.4	29	12.0	2312
M-12	2.0	30	12.0	2312
N-22	3.5	36	12.4	4412
G-398	3.5	36	13.1	4413
USA-27	5.6	34	11.0	6311
USA-35B	4.6	38	11.6	5412
C-72	4.0	46	11.7	4512
Boeing 103	4.2	36	12.7	4413
Boeing 106	3.5	36	13.1	4413

lists a few of the outstanding older sections with the nearest N.A.C.A. equivalent designation number.

C_L Maximum for Biplanes. The theoretical treatment of the biplane has been confined to that portion of the lift curve where $dC_L/d\alpha$ is constant. It should be possible to extend the existing theory and obtain an approximate solution for C_L maximum.

Experimental data[7] indicates that the effect on C_L maximum varies with wing section and cellule proportions. Certain sections, such as the USA-27 and the G-387, give consistently low C_L maximum in the biplane arrangement. Other sections, notably the G-398, give

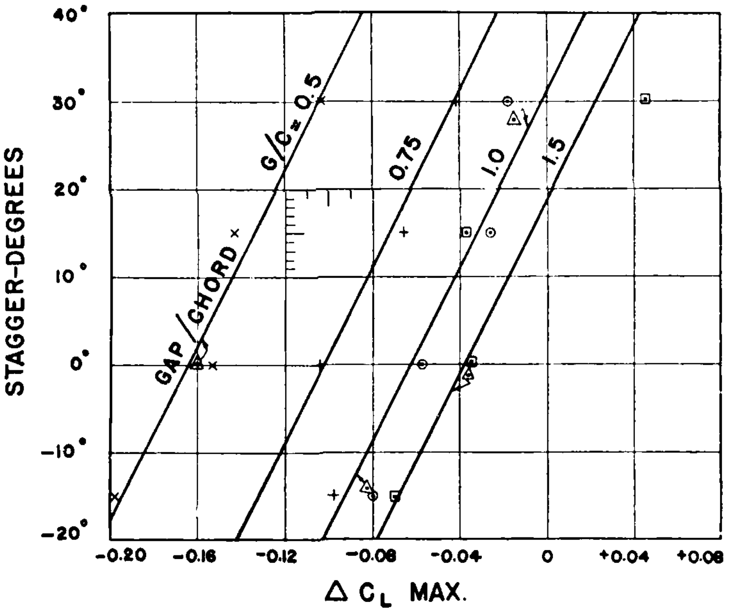

Figure 56. Effect of Stagger and Gap/Chord Ratio on Maximum Lift of a Biplane

consistently high C_L maximum in the biplane arrangement. Satisfactory test data are available for the RAF-15 section only, and these data do not include the effect of decalage.

---

[7] W. L. Cowley, A. G. Gadd, L. J. Jones and S. W. Skan, "Biplane Investigation with RAF 15 Section, Part III—Tests at Various Staggers and Gap/Chord Ratios," Br.A.R.C. R. & M. No. 872 (1923).

The effect of the biplane arrangement on C_L maximum may be plotted as in Figure 56. While this plot is based on RAF-15 data, the limited tests available on other normal sections show reasonable agreement. Four points for Clark Y biplanes taken from the data in N.A.C.A. T. R. No. 317 are plotted as triangles on Figure 56. These points show very close agreement with the RAF-15 data.

The value of ΔC_L maximum, as plotted on Figure 56, is given by

$$\Delta C_{L\,max} = \frac{-0.060}{(G/c)^{1.5}} + 0.002\,s^{\circ} \tag{90}$$

Where G is the gap, c is the mean chord and s is the stagger.

Tapered Airfoils. Test data on three tapered airfoils are given in N.A.C.A. T. N. No. 487.[8] The models had a 2:1 taper from the 18% root section at a point 0.635 chord lengths from the center line to a 9% section at the tip. The root section was 1.27 c and the basic tip section 0.635 c. All sections along the span were parallel with the 30% upper surface stations in a straight line across the span. The tips were rounded.

It may be shown that the average geometrical thickness of such a tapered wing is 14%. If allowance is made for variation in loading along the span, the average aerodynamic thickness is about 15%. The test data are as follows:

Section	$C_{L\,max}$	$C_{D_0\,min}$	Ratio $\frac{C_{L\,max}}{C_{D_0\,min}}$	C_{M_0}
NACA 2218-09	1.60	.0100	160	−.029
NACA M-6	1.49	.0095	157	−.006
Clark Y	1.67	.0102	164	−.071
NACA 2215	1.54	.0098	157	−.022

---

[8] R. F. Anderson, "Tests on Three Tapered Airfoils Based on the NACA-2200, the NACA M-6 and the Clark Y Sections," N.A.C.A. T.N. No. 487 (1934).

The estimated values for untapered 2215 are included for comparison. The agreement indicates that the characteristics of the mean section may be safely used for untested tapered wings. Consideration of lateral control and lateral stability must also enter into the selection of a tapered wing.

Comparing the three tapered wings, the Clark Y is slightly superior on maximum lift and $C_{L\,max}/C_{D_0\,min}$. The differences are so slight that choice would probably be made on the basis of moment coefficient.

Cut-outs. The center section cut-out cannot be avoided in many airplane designs. Properly made, the increase in profile drag need not be great. In a theoretical study of the wing cut-out given by Sherman,[9] it is shown that the adverse effects are due to induced interference, and that extension of the cut-out in a chord direction has a greater effect than extension along the span. The interference is greatly increased by mutilation or unfairness of the center sections at the leading edge, although unfairness in planform has little effect. Ackeret's[10] tests show that the trailing edge may be cut off normal to the chord without seriously affecting the characteristics. Based on the original area, the reduction in C_L maximum is almost linear from 1.40 with the original wing to 0.90 when 50% of the chord is removed. There is an increase in profile drag at all lift coefficients that is approximately 10% of the decrease in C_L maximum. For example, removal of 30% of the chord from the trailing edge decreases C_L maximum from 1.40 to 1.10 and increases C_{D_0} by an average of $0.30 \times 0.10 = 0.030$.

The angles of the chords of the center section may be increased to allow for the loss of lift due to a cut-out and almost perfect compensation can be obtained at one angle of attack. This refinement is probably of less importance than it appears. The main care of the designer should be to avoid distortion of the forward part of the wing at the center section.

---

[9] A. Sherman, "The Aerodynamic Effects of Wing Cut-outs," N.A.C.A. T.R. No. 480 (1934).

[10] J. Ackeret, "Messungen an Profilen Mit Abgeschnittener Hinterkante," Gottingen Ergebnisse II and III.

An opening through the wing at the center section gives a large increase in C_{D_0}. The effect is substantially the same as the reduction in aspect ratio due to a fore-and-aft slot.

Surface Effects. The surface finish of a wing may have a profound effect on its characteristics. The variable-density tunnel data are obtained on metal models buffed to a high polish. Special tests[11] that have been made with various surface finishes indicate that unless this highly polished surface is used, there is a reduction in maximum lift coefficient and an increase in profile drag coefficient. It is a matter of interest that in the VDT tests, a wooden model could not be given a sufficiently high polish to enable duplication of the metal model data. A very slight roughening of the surface of the metal model with emery cloth reduced the maximum lift about 20% and increased C_{D_0} about 20%.

In these tests the greatest effect was found when the model surface was sprinkled with No. 180 carborundum to represent the finish used on walkways. In this case C_L maximum was reduced about 50% and C_{D_0} was increased about 100%.

Tests on a wing in the full-scale wind tunnel indicated that a 10% reduction in C_{D_0} could be obtained with a waxed and polished surface as compared to a standard doped surface.

Lap-joints give a small but definite increase in C_{D_0}.

---

[11] R. W. Hooker, "The Aerodynamic Characteristics of Airfoils as Affected by Surface Roughness," N.A.C.A. T.N. No. 457 (1933).

The practical importance of these findings is obvious. It is necessary to insure a high degree of surface smoothness if the full advantage of the ultimate wing characteristics and freedom from any kind of disturbing projection is especially important near the leading edge and on the upper surface forward of the maximum thickness.

Protuberances. The effects of protuberances extending from the surface of an airfoil have been investigated in the variable-density tunnel.[12] The effect on drag varies with the size and location. On the forward upper surface the additional drag is about twice the drag of a flat plate having the same projected area. On the lower surface, the drag increase is about that of a flat plate having the same projected area.

Short protuberances such as fittings have an interference effect on induced drag that is out of all proportion to their relative size. This effect varies with the location along the span and is much greater near the center of the wing than at the tips. Hence, if the full possibilities of the wing section are to be realized in an airplane, it is essential that the upper surface be smooth and free from projections. Even small projections such as rivet heads are to be avoided. The tests reported in N.A.C.A. T.N. No. 461 show that a single row of $\frac{1}{8}$-inch brazier-head rivets spaced one inch apart along the span on the upper surface at 5% of the chord gave $\Delta C_{D_0} = 0.0012$ or about 13% increase in profile drag. Nine rows spaced along the chord on the upper and the lower surfaces gave $\Delta C_{D_0} = 0.0016$ at 120 mph on the 6′ x 36′ Clark Y wing used in the test. The slight increase due to the additional rows is explained by the effect of the disturbance in the boundary layer introduced by the first row. In this connection it should be noted that the ΔC_{D_0} values given have been taken at the highest test speed and are appreciably lower than the values at 55 mph used in the discussion in T.N. No. 461. Owing to the large scale effect shown, the 55 mph values are considered pessimistic.

---

[12] E. N. Jacbos, "Airfoil Section Characteristics as Affected by Protuberances," N.A.C.A. T.R. No. 446 (1932). E. N. Jacobs and A. Sherman, "Wing Characteristics as Affected by Protuberances of Short Span," N.A.C.A. T.R. No. 449 (1933).

Wing-Fuselage Interference. The basic airfoil characteristics may be considerably modified by the effects of wing-fuselage interference.[13] These effects depend on fuselage shape, wing section, wing location with respect to fuselage axis, and to a limited extent on the angle of incidence of the wing and its location along the fuselage axis. In the most unfavorable cases there may be as much as 30% reduction in C_L maximum and several hundred per cent increase in C_{D_0}. Most of the interference effects may be eliminated by adequate fillets and fairings.

In general, the low-wing arrangement is definitely handicapped by interference effects, although when adequate fillets are used, it can be made to approximate the efficiency of the more favorable locations. Efficient airfoils of small camber and moderate thickness are most susceptible to adverse interference effects. Airfoils of moderate camber located slightly above the center-line of the fuselage are least affected by interference.

Figure 57 gives the variation of the additional profile drag coefficient with wing location on a fuselage of circular cross-section, as determined in the N.A.C.A. tests. ΔC_{D_0} is given for $C_L = 0$ and $C_L = 1.0$. The general effects are quite similar for the two conditions except that the increase in ΔC_{D_0} is more marked for $C_L = 1.0$. It is of interest to note that for $C_L = 1.0$ and $h = -0.4\ c$, the value of ΔC_{D_0} is 0.0380 and that this is reduced to 0.0070 by the use of a large expanding fillet. This latter

---

[13] E. N. Jacobs and K. E. Ward, "Interference of Wing and Fuselage from Tests of 209 Combinations in the N.A.C.A. Variable-Density Tunnel," N.A.C.A. T.R. No. 540 (1935).

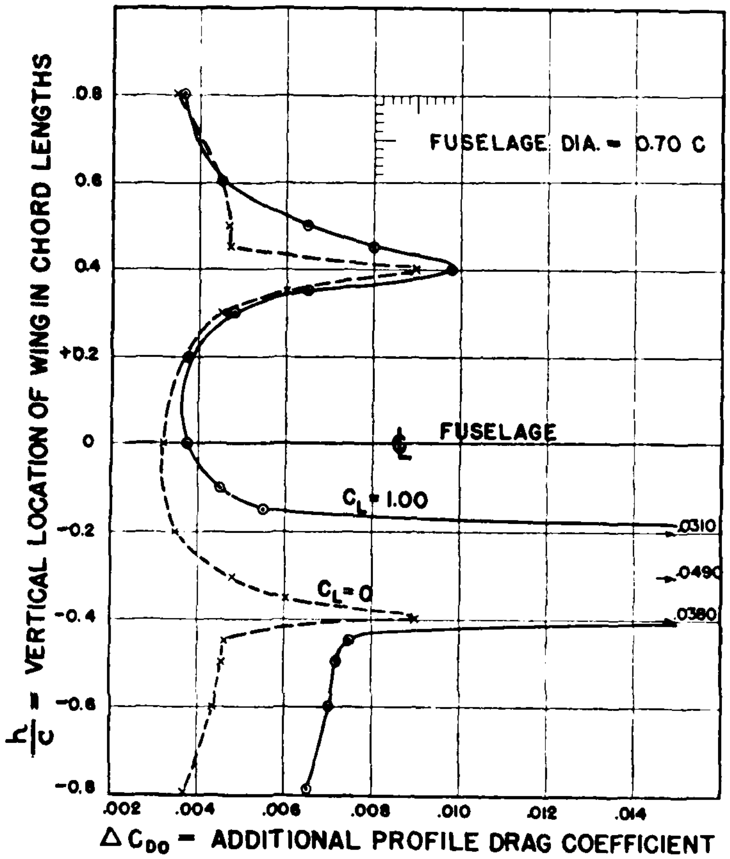

Figure 57. Increase in Profile Drag Coefficient Due to Wing-Fuselage Interference

value may be compared with $\Delta C_{D_0} = 0.0040$ obtained with the most favorable mid-wing and high-wing positions.

The critical conditions for these large changes in lift and drag make it necessary for the designer to apply the corrections indicated necessary for the arrangement used. Since it is impracticable to give here a satisfactory working abstract of the N.A.C.A. tests, reference is made to the original data for design use.

Compressibility. As pointed out in Chapter 3, practically all of the solutions in theoretical aerodynamics are obtained by assuming an incompressible fluid. The solutions obtained are valid only when there are negligible compression effects and as far as wing characteristics are concerned, the effects begin to be appreciable at about 30% of the velocity of sound. It is necessary to make some allowance for compressibility when the speeds are greater than about 300 mph.

Figure 58 shows the variation of C_L and C_{D_0} at constant angles of attack for a special wing section,[13] the

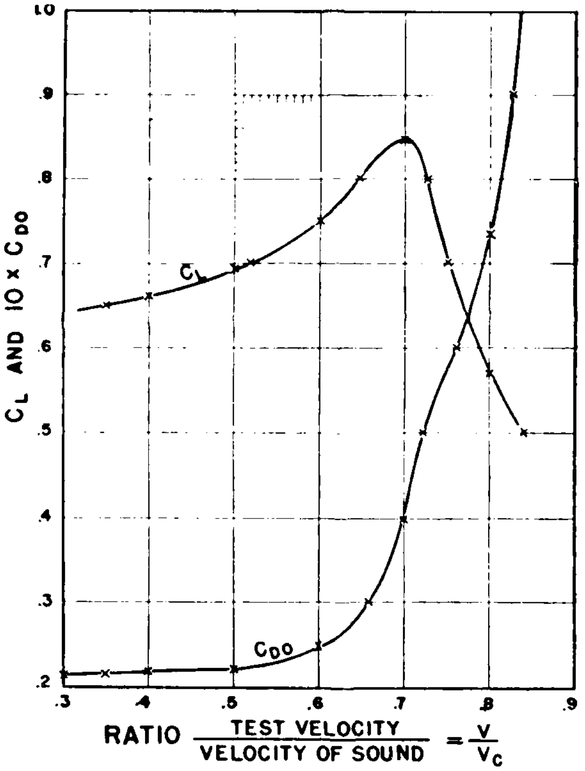

Figure 58. Compressibility Effect on Lift and Drag Coefficients

---

[13] J. Stack and A. E. von Doenhoff, "Tests of 16 Related Airfoils at High Speeds," N.A.C.A. T.R. No. 492 (1934).

NACA 2409-34. The variation shown includes the effect of increasing both Reynolds Number and the speed ratio. The point of particular interest is the "compressibility burble" that occurs at about 0.7 V_c. Increasing the speed above this point results in a marked decrease in C_L accompanied by a tremendous increase in C_{D_0}. This effect is similar for all sections so far tested, but there are enough differences to justify the expectation that new sections can be developed with greatly improved characteristics.

For thin sections, the compressibility burble occurs at higher values of V/V_c than for thick sections. Also, the higher the value of C_L, the lower the value of V/V_c for the compressibility burble. For minimum C_{D_0}, the burble for one airfoil with a 6% thickness was at $V/V_c = 0.88$, and for a 12% thickness it was at $V/V_c = 0.80$.

CHAPTER 6

FLAPS AND HIGH-LIFT DEVICES

General. The possibilities of obtaining a device for increasing the lift and decreasing the drag of an airplane wing have attracted many inventors. A large number of schemes have been proposed and many of them have been given wind-tunnel and flight tests. Some of the devices have definite practical value and are now in extensive use, but many of them merely serve to increase the weight and structural complication.

In evaluating any of these devices the airplane designer must consider a number of factors and either consciously or unconsciously assign a definite weight to each item of performance. An answer must be found to the question "Do the advantages outweigh the disadvantages?" Let it be emphasized that it is not a simple matter to answer this question correctly, even when a relative weight is assigned to each item of performance. The device that affects only one characteristic does not exist, and it is yet to be demonstrated that superior all-round performance cannot be obtained with plain wings.

Many designers consider that the chief purpose of flaps and related devices is to increase the maximum lift. A good wing section will give $C_{L\,max} = 1.60$, and this may be increased to something between 1.80 and 2.50, depending on the device and the design characteristics. The increase in lift may be used either to reduce the stalling speed or reduce the wing area required for a given stalling speed. In either case a number of factors must be considered. The effect of the flap is not confined to increasing $C_{L\,max}$.

Both drag coefficient and moment coefficient are greatly increased. Fortunately, the downwash on the tail is also increased so that longitudinal stability and balance may be maintained in spite of the marked increase in C_M. However, the increased down load on the tail opposes the wing lift so that the net $C_{L\,max}$ is appreciably reduced. This reduction in $C_{L\,max}$ is approximately

$$\Delta\, C_{L\,max} = C_M/(l/c) \tag{91}$$

where C_M is the wing moment coefficient at $C_{L\,max}$, l is the tail length and c is the mean chord. Some types of flaps give C_M values as high as -0.60 at $C_{L\,max}$. For $l/c = 3.0$, the corresponding $\Delta C_{L\,max}$ is -0.20 or a reduction of about 8%.

Under normal conditions the enormous increase in wing drag with fully extended flaps is of considerable value in landing. It is highly objectionable, however, in the take-off. The best take-off is usually obtained with a partial setting that varies, with the type, from 25% to 75% of the full throw. The best setting may be very critical. Under favorable conditions the best setting gives about 30% reduction in take-off run required with the device fully retracted. If the comparison is made with plain wing area increased to give the same stalling speed, the take-off run for the wing with flaps is found to be the longer. In other words, the true effect of a high lift device is not obtained from comparison of take-off runs at various settings. These data should be compared with the corresponding plain-wing area that gives the same stalling speed. This method of comparison applies to all performance characteristics.

Further discussion of the advantages and disadvantages of various types of high-lift devices will follow:

Types. There are at present eight distinct methods available for increasing lift coefficients. Six of these methods incorporating various forms of flaps are shown on Figure 59. The other two methods, Boundary Layer Control and the Magnus Effect (or Flettner Rotor), are in an entirely different status and will be discussed later in this chapter.

The six types of flaps shown on Figure 59 fall into three groups: the plain or aileron flap which may be used with or without the leading edge slot, the split or lower surface flap which may have either a fixed or a movable hinge axis, and the external airfoil flap which either may be movable about a fixed axis or secure substantially the same motion in a retracting-extending operation. Each

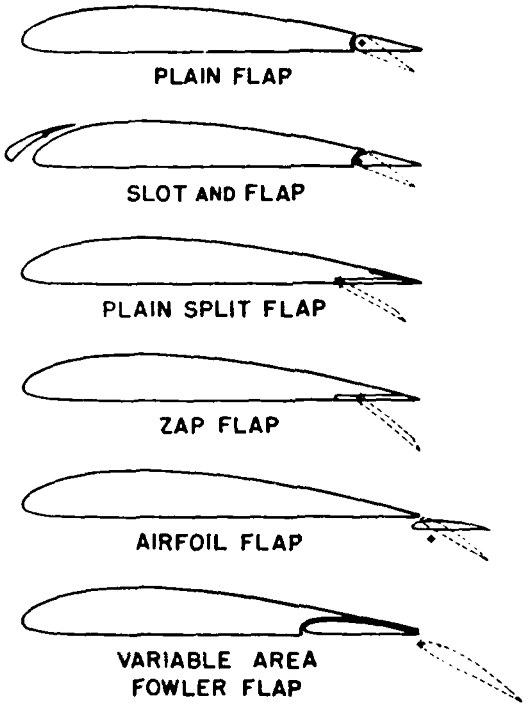
PLAIN FLAP
SLOT AND FLAP
PLAIN SPLIT FLAP
ZAP FLAP
AIRFOIL FLAP
VARIABLE AREA
FOWLER FLAP

Figure 59. Types of Flaps

of these types has certain advantages and disadvantages that determine its suitability for any particular set of design conditions. No one type is inherently superior in all possible applications.

Flap Theory and Test Data. Glauert and Munk have derived theoretical solutions for the effect of simple trailing edge flaps. Both solutions are similar but Glauert's[1] is more complete and better known. A brief summary will be given with comparative experimental data.

The effect on lift coefficient due to moving a flap through the angle δ_F to the main surface is given by

$$C_L = a_1\,\alpha_a + a_2\,\delta_F \qquad (92)$$

where $a_1 = \frac{dC_L}{d\alpha}$ is the slope of the wing lift, α_a is the absolute angle of attack and a_2 is the slope of the lift increase due to the flap angle or $a_2 = \frac{dC_L}{d\delta_F}$. The ratio (a_2/a_1) is independent of aspect ratio and the theoretical values are given in Table 7 on page 151, and in Figure 60 on the opposite page.

Equation (92) is equivalent to $C_L = C_{L_0} + \Delta C_L$. A study of experimental data, Figure 61, indicates that ΔC_L is not linear with δ_F as the theory would require and furthermore, at high values of C_L, the initial slope is about 60% of the theoretical value. A comparison of the theoretical and observed values of a_2/a_1 is given on Figure 62. The experimental data are closely represented by

$$\Delta C_L = \delta_F\,(a'_2 - K \cdot \delta_F) \qquad (93)$$

where a'_2 and K are functions of the ratio $E = \frac{\text{Flap chord}}{\text{Wing chord}}$ and have the values given on Figure 62. For $E = 0.20$, $a'_2/a_1 = 0.34$ and $K = 0.000185$ when δ_F is in degrees

---

[1] H. Glauert, "Theoretical Relationships for an Airfoil with Hinged Flap," Br.A.R.C. R. & M. No. 1095 (1927).

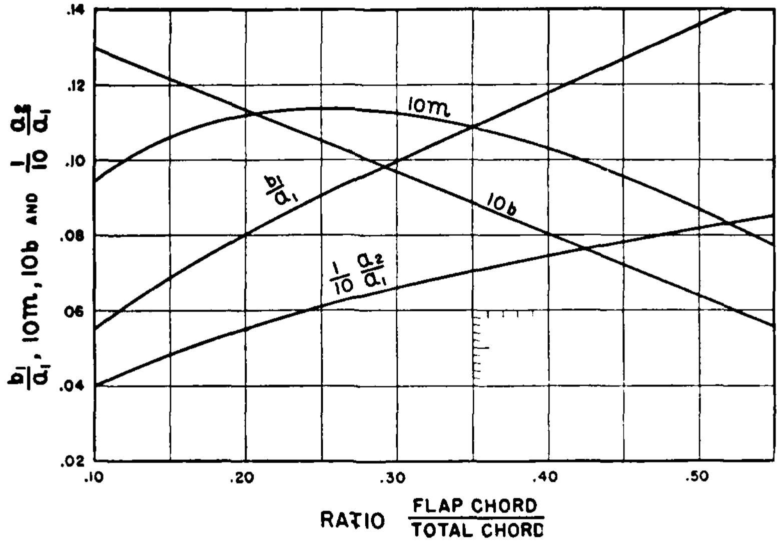

Figure 60. Theoretical Flap Relations

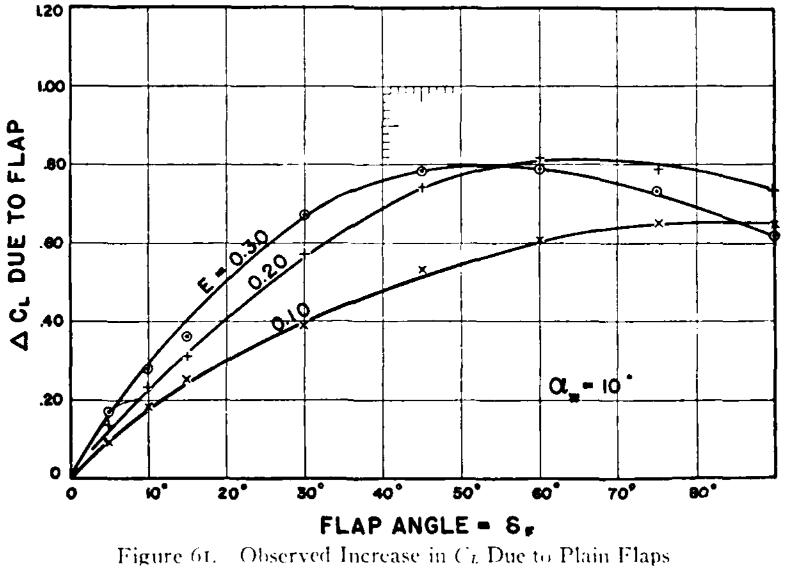

Figure 61. Observed Increase in C_L Due to Plain Flaps

taken positive when trailing edge is lowered. K appears to vary as $E^{0.75}$ so that

$$K = 0.00061\ E^{0.75} \tag{94}$$

The theoretical effect of the flap on moment coefficient measured about the leading edge of the airfoil is given by

$$C_M = C_{M_0} - 0.25\ C_L - m\delta_F \tag{95}$$

where m is a coefficient depending only on the ratio E. Values of m for δ_F measured in degrees are given in Table 7 and on Figure 60.

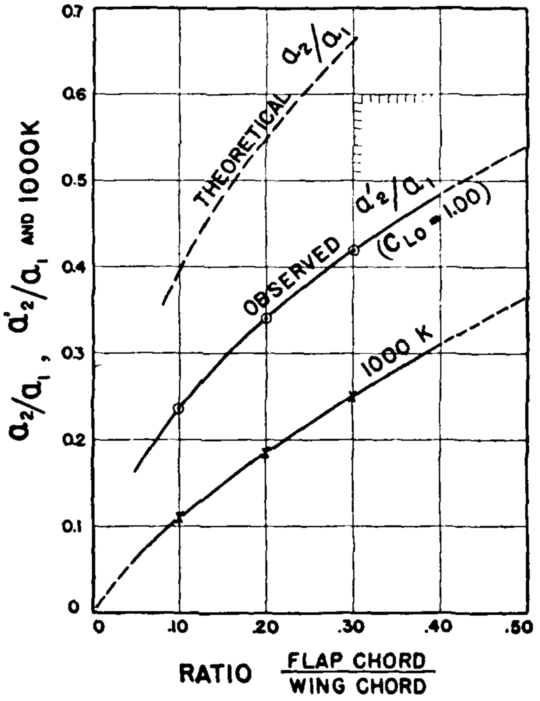

Figure 62. Comparison of Theoretical and Observed Flap Relations

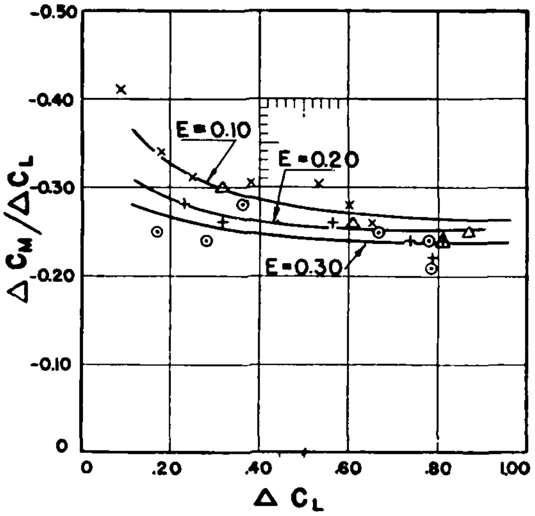

Figure 63. Increase in Moment Coefficient Due to Flaps

According to Jacobs and Pinkerton,[2] equation (95) gives reasonable agreement with test data for flap angles less than 10°, but in other attempts to obtain a comparison the agreement has not been satisfactory, particularly at high values of C_L.

According to Munk's theory, the resultant of the lift due to camber acts at 0.50 c and the resultant of the lift due to angle of attack acts at 0.25 c. Moving the flap from the neutral position has the effect of changing both camber and angle of attack, so that the increase in moment coefficient will be a complex function of E and δ_F. It appears, however, from analysis of test data, that ΔC_M is a fairly definite function of E and ΔC_L as shown on Figure 63. For all practical purposes it is sufficiently accurate to assume $\Delta C_M/\Delta C_L = -0.25$ where ΔC_M and ΔC_L are taken at any given angle of attack of the main surface.

---

[2] E. N. Jacobs and R. M. Pinkerton, "Pressure Distribution over a Symmetrical Airfoil Section with a Trailing Edge Flap," N.A.C.A. T.R. No. 360 (1930).

The hinge moment of a flap is defined by the equation

$$H = C_H \, q \, S_F \, c_F \tag{96}$$

where C_H is the hinge moment coefficient, S_F is the flap area, and c_F is the flap chord. According to Glauert the value of C_H is given by

$$C_H = C_{H_0} - \left(\frac{b_1}{a_1}\right) C_L - b\delta_F \tag{97}$$

The coefficient b and the ratio b_1/a_1 are independent of aspect ratio but they vary with the chord ratio E as indicated in Table 7 and on Figure 60.

Figure 64 is a plot of hinge moment coefficients[3] against flap angle for three values of E. The initial slope of C_H is in close agreement with the average theoretical value of b but there is only a slight decrease in the slope as E increases, the change being much less than the theoretical value. For all practical purposes a value of $b = 0.0110$ may be taken for all values of E less than 0.30.

The same test data are plotted in Figure 65, giving C_H as a function of C_L and δ_F. While there is some variation with C_L, it is not the linear effect required by equation (97).

The use of large values of δ_F at moderate angles of attack may give as much as a twenty-fold increase in total wing drag coefficient. This increase is due in part to the effect of induced drag and in part to the increase in profile drag. Figure 66 gives ΔC_{D_0} as a function of E and δ_F. At a given angle of attack, the relation between the total drag coefficient C_D for the wing with flap neutral and C_{DF} for the flap displaced through the angle δ_F is

$$C_{DF} = C_D + \frac{[(C_L + \Delta C_L)^2 - C_L^2]}{\pi n} + \Delta C_{D_0} \tag{98}$$

where C_L is the lift coefficient for the basic wing section at the given angle of attack, ΔC_L the increase due to the

---

[3] From N.A.C.A. Tests.

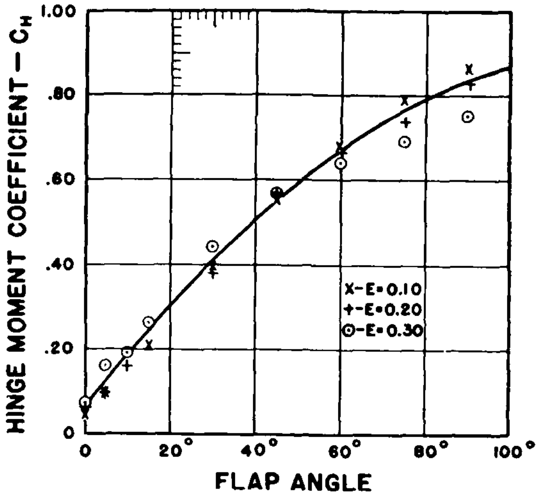

Figure 64. Hinge Moment Coefficients for Flaps—from Test Data

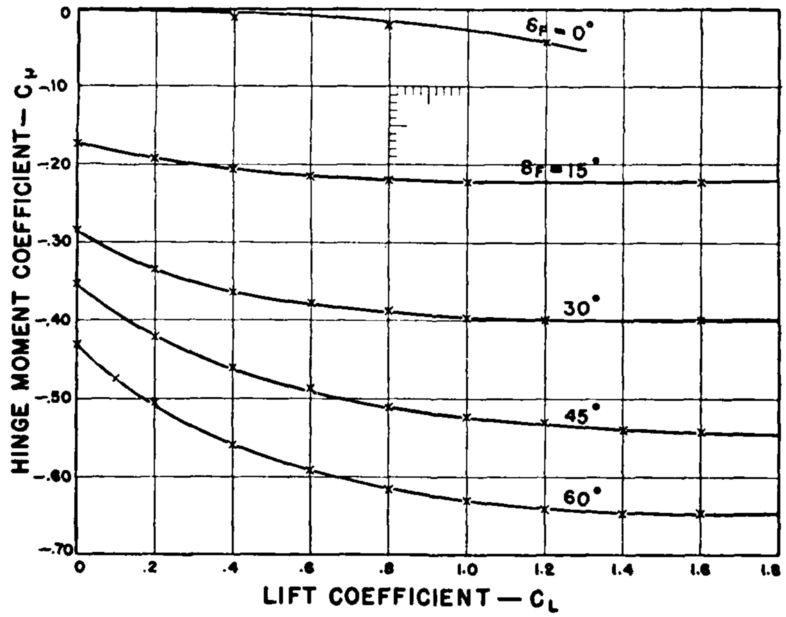

Figure 65. Observed Flap Hinge Moment Coefficients

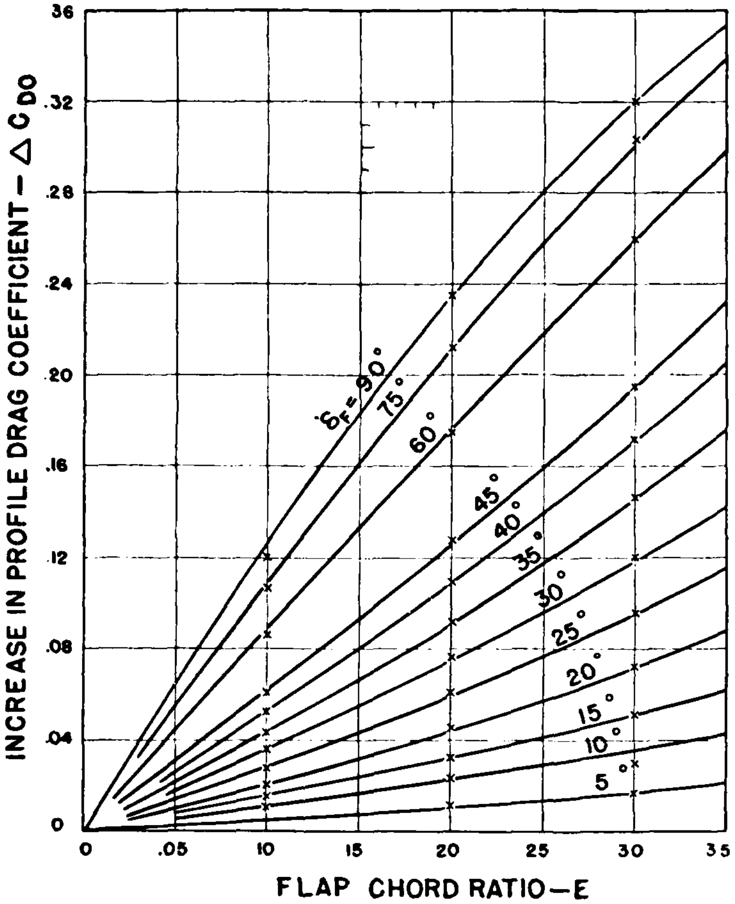

Figure 66. Increase in Profile Drag Coefficient Due to Flaps

flap, and ΔC_{D_0} is the increment obtained from Figure 66. n is the effective aspect ratio and in the case of partial span flaps some allowance should be made for the increased induced drag due to distorted span loading. For flap settings below $\delta_F = 60°$, the value of ΔC_{D_0} is given closely by

$$\Delta C_{D_0} = 0.0135\, E\, \delta_F \tag{99}$$

where δ_F is in degrees.

In the preceding discussion, the comparison between theoretical and experimental values has been taken at an angle of attack of about 10° or at a basic C_L of about 1.0. This corresponds to a mean value in gliding or landing. It should be emphasized that the initial agreement between theoretical and experimental values is much better for thin symmetrical sections used as control surfaces. Additional data on this point are given in Chapter 7.

TABLE 7. THEORETICAL FLAP RELATIONS

$\frac{\text{Flap chord}}{\text{Wing chord}}$ E	$\frac{a_2}{a_1}$	m for δ in Degrees	$\frac{b_1}{a_1}$	b
0	0	0	0	.0148
.05	.282	.0070	.038	.0139
.10	.396	.0094	.055	.0130
.15	.480	.0106	.068	.0121
.20	.550	.0112	.080	.0113
.25	.607	.0113	.090	.0105
.30	.660	.0112	.100	.0096
.35	.704	.0108	.109	.0089
.40	.746	.0103	.117	.0080
.45	.782	.0095	.127	.0072
.50	.818	.0087	.136	.0064
.60	.876	.0068	.155	.0048
.80	.960	.0028	.194	.0020
1.00	1.000	0	.250	0

The Plain Flap. The plain or aileron type of flap has no special aerodynamic advantages over other types, except when used with leading edge slots or when used in an arrangement that enables the flaps to be differentially operated for lateral control from a lowered position. In such an arrangement the flap chord should be small with a value of E less than 0.15. It appears possible to show excellent results with a carefully designed 10% simple flap. The lower C_L maximum with the small flap is offset by reduced loads. Values of $\Delta C_{L\ max}$ are given as a function of E and δ_F in Figure 67.

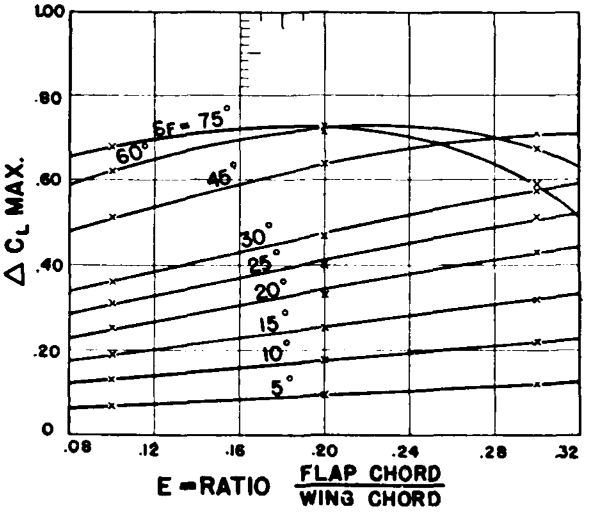

Figure 67. Observed Increase in C_L Maximum Due to Plain Flaps

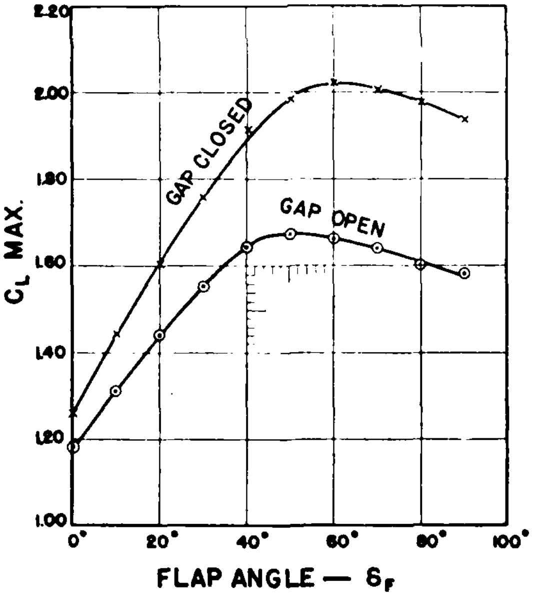

Figure 68. Effect of Leakage at Flap Hinge Axis

Effect of Leakage Between Wing and Flap. While claims have been made that a properly formed slot ahead of a flap increases the lift obtained, there is ample proof that leakage through a gap between the wing and flap is highly detrimental. N.A.C.A. tests show that for the average case, there is a loss of about 30% in $\Delta C_{L\,max}$ due to a gap measuring 0.0032 *c*, or about 3/16" on a 5-foot chord. The effect varies with flap angle as shown on Figure 68, which is based on tests with a 20% full-span plain flap on a Clark Y wing.

The loss in efficiency due to leakage may have a serious effect in reducing the effectiveness of flaps or controls. It may explain why many installations of plain flaps have failed to give expected increases in $C_{L\,max}$.

Slotted Flaps. An increase of about 0.20 in $\Delta C_{L\,max}$ has been claimed for a slot located just ahead of an aileron or a plain flap. This claim is not substantiated by existing data, which indicate erratic results with no consistent improvement.

N.A.C.A. tests[4] show that when the upper surface of the wing is given a rearward extension projecting over the flap, a value $C_{L\,max} = 1.98$ is obtained. Without this extension $C_{L\,max} = 1.77$. This difference is probably the basis of the claims for the slotted flap, but the same tests show that the plain unslotted flap gave $C_{L\,max} = 1.95$. Hence, any gain due to the use of a slotted flap appears to be a nullification of the adverse effects of leakage. In view of these adverse effects, a slotted flap should not be used without the rearward projection recommended in T.R. No. 427. This form is shown in Figure 77 which is a reproduction of Table III of that report.

Split Flaps. The Wright-Jacobs split flap is formed by splitting the trailing edge of the wing and hinging the lower portion to rotate about an axis within the wing. This axis forms the leading edge of the flap. The upper surface of the wing is intact, and when retracted, the flap is flush with the lower surface.

---

[4] F. E. Weick and J. A. Shortal, "The Effect of Multiple Fixed Slots and a Trailing Edge Flap on the Lift and Drag of a Clark Y Airfoil," N.A.C.A. T.R. No. 427 (1932).

The split flap has definite advantages and disadvantages. It is comparatively light and simple in construction. The maximum lifts obtained have been rather high, probably due in no small measure to the sealed gap construction inherent in the normal design. The increase in profile drag is high, giving very desirable gliding and landing characteristics. However, this increase in drag prevents the full use of the flap in take-off unless very low power-loadings are used. The greatest disadvantage of the split flap is in the large hinge moments that require either mechanical operation or an excessive number of turns on the crank of a manually operated gear. Considerable

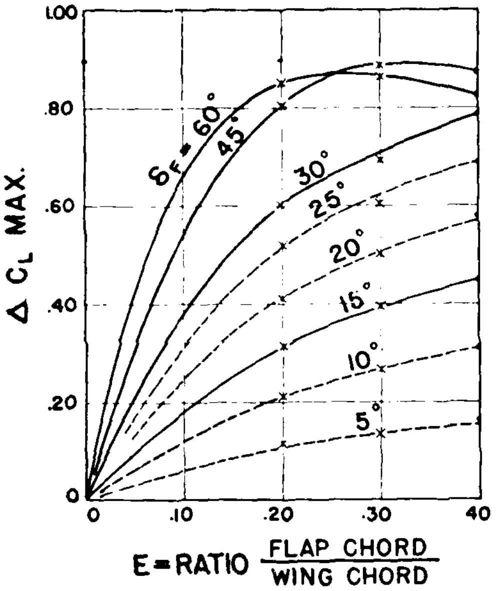

Figure 60. Increase in C_L Maximum Due to Full-Span Split Flaps

time and effort have been expended to develop an aerodynamic balance for this type of flap.

Values of $\Delta C_{L\,max}$ for full-span split flaps on rectangular wings are plotted against δ_F and E on Figure 69. For all practical purposes there is little gain from the use of flap angles greater than $\delta_F = 45°$, unless E is less than 0.15.

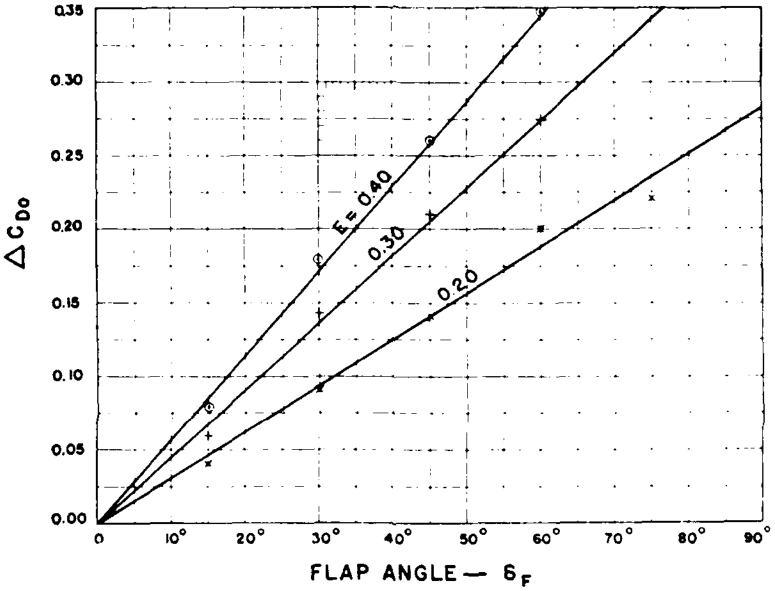

Figure 70. Increase in Profile Drag Coefficient Due to Full-Span Split Flaps

The increase in profile drag coefficient due to a full-span split flap is given on Figure 70. ΔC_{D_0} is closely approximated by the empirical equation

$$\Delta C_{D_0} = 0.015\, E\, \delta_F \tag{100}$$

where δ_F is in degrees. Comparing this value of ΔC_{D_0} with that for a plain flap, equation (99), it is seen that the increase in profile drag coefficient is about 10% greater for the split flap. The difference in corresponding total drag coefficients is, in general, somewhat less than 10%.

The hinge moments for a split flap are almost identical with the hinge moments for a plain flap and Figure 65 may be used for either type.

The ratio of $\Delta C_M/\Delta C_L$ for split flaps appears to vary with E and ΔC_L in a manner almost identical with that found for plain flaps, Figure 63, except that the values for the split flaps are more negative by an average value of about 10%. For all practical purposes, it is sufficiently accurate to assume $\Delta C_M/\Delta C_L = -0.28$.

Split Flaps on Tapered Wings. The effect of split flaps on tapered wings has been measured at Langley Field.[5] Four models having 5:1 taper were fitted with flaps thus:

1. Flap tapered with wing to give constant ratio $E = 0.15$
2. Flap tapered with wing to give constant ratio $E = 0.25$
3. Flap of constant chord to give $E = 0.15$ at mean chord
4. Flap of constant chord to give $E = 0.25$ at mean chord

The values of $\Delta C_{L\,max}$ for the tapered flaps agree closely with the corresponding values for the same E on rectangular wings, but the $\Delta C_{L\,max}$ values for the constant chord flaps are appreciably lower than the corresponding values on rectangular wings. The difference is due to the non-linear relation between $\Delta C_{L\,max}$ and E. The effect of a split flap on a tapered wing must be obtained as follows:

1. Divide the semi-span into fore-and-aft strips uniformly spaced.
2. Find mean value of E for each strip.
3. Find value of $\Delta C_{L\,max}$ for corresponding E on a rectangular wing.
4. Find area of each strip ΔS.
5. Take products $\Delta S \times \Delta C_{L\,max}$.
6. Find $\Sigma(\Delta S \cdot \Delta C_{L\,max})$ by trapezoidal rule or planimeter.
7. Divide $\Sigma(\Delta S \cdot \Delta C_{L\,max})$ by area of the semi-span to get $\Delta C_{L\,max}$.

---

[5] C. J. Wenzinger, "The Effect of Full-Span and Partial-Span Split Flaps on the Aerodynamic Characteristics of a Tapered Wing," N.A.C.A. T.N. No. 505 (1934).

For the 15% constant chord flap of T.N. No. 505, the value of $\Delta C_{L\,max}$ calculated by this method is 0.66 as compared with an observed value of 0.67. For comparison, the value for uniform $E = 0.15$ is 0.78 by Figure 69, while the observed value in Figure 2 of T.N. No. 505 is 0.80.

ΔC_{D_0} and ΔC_M may be found by the ΔC_L values weighted for area.

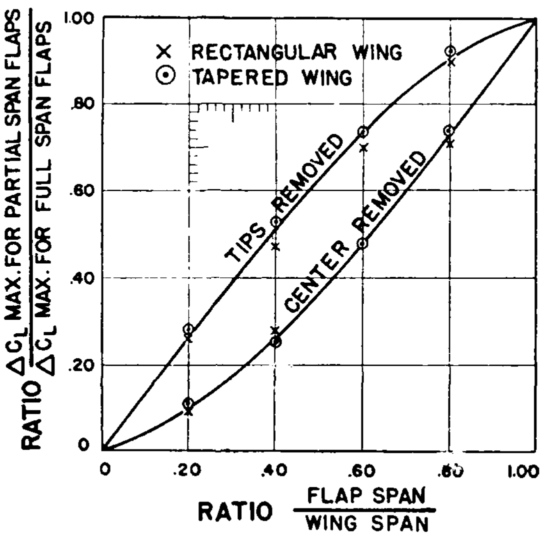

Figure 71. Partial Span Split-Flaps

Partial-Span Split Flaps. Partial-span flaps have been investigated at Langley Field.[6] The effect on $\Delta C_{L\,max}$ depends on the location of the flap as shown on Figure 71. It is of considerable interest to note that when data are plotted in a non-dimensional form, there is no appreciable difference between rectangular and tapered wings.

---

[6] C. J. Wenzinger, "The Effect of Partial-Span Split Flaps on the Aerodynamic Characteristics of a Clark Y Wing," N.A.C.A. T.N. No. 472 (1933). C. J. Wenzinger, "The Effects of Full-Span and Partial-Span Split Flaps on the Aerodynamic Characteristics of a Tapered Wing," N.A.C.A. T.N. No. 505 (1934).

The relations between C_{D_0}, C_M, and C_L will be the same for a partial-span flap as for a full-span flap if the data are weighted for area affected.

Zap Flap. The Zap flap is a form of the split flap in which the hinge axis moves aft along the chord as the flap is lowered. The trailing edge of the split flap describes an arc passing through the trailing edge of the wing.

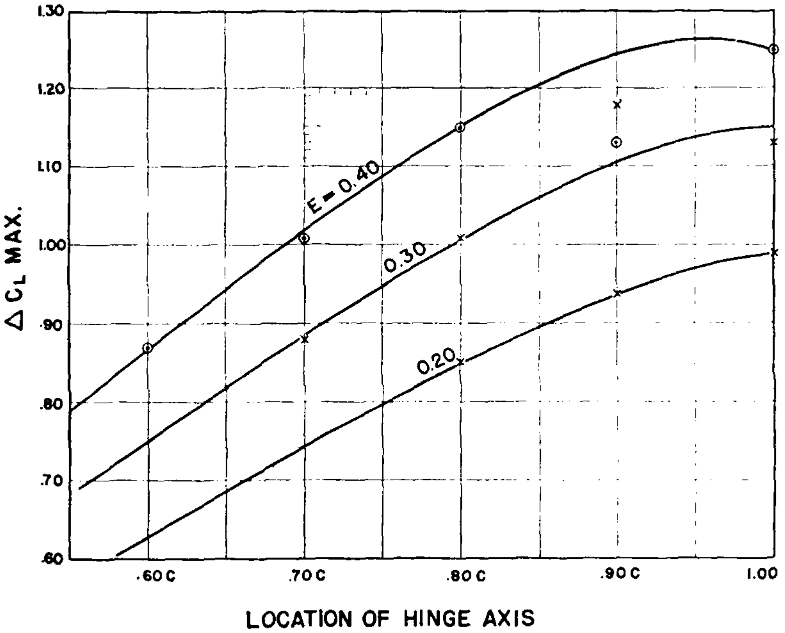

Figure 72. Increase in C_L Maximum Due to Full-Span Zap Flaps

The trailing edge of the Zap flap moves along a straight or substantially straight line passing through the trailing edge of the wing. The actual motion depends on the particular linkage used.

The advantages of the Zap flap over the split flap are reduced hinge moments and increased $C_{L_{max}}$. These are offset somewhat by the structural complication.

The N.A.C.A. tests[7] cover all practicable motions of the hinge axis. Measurements were made with the hinge axis at 10% intervals along the chord. Figure 72 gives $\Delta C_{L\ max}$ in terms of E and hinge axis location.

The effect of a 45° flap setting on C_M is approximated by Figure 73, in which ΔC_M is plotted against E and hinge axis location. ΔC_M is an increment to be added to the basic wing C_M.

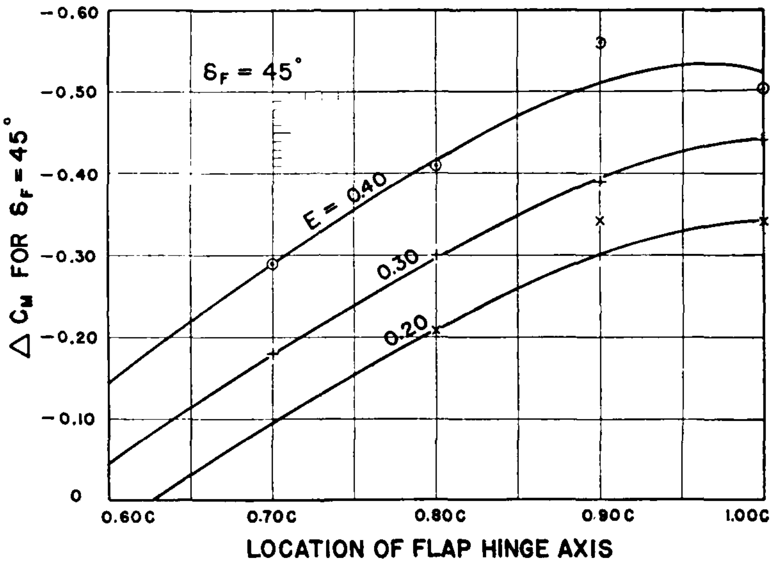

Figure 73. Effect of Full-Span Zap Flaps on Wing Moment Coefficient

Variable Area. A number of schemes have been proposed for varying the wing area in flight. In some of these schemes the area and span are to be changed simultaneously with a telescoping arrangement. In others the area change is achieved by a chordwise extension operating on tracks or levers. While variable-span wings have been constructed and flown, the advantages appear to be insufficient to justify the structural complications involved. On the other hand, the extending chord devices may be considered equivalent to a retracting flap that approximates the best aerodynamic arrangement for all conditions. In this connection it should be noted that in the extended position the best arrangement for a retracting flap type of variable-area wing is practically identical with the best arrangement for an external airfoil flap. This best location is very critical and appears to vary slightly with the basic sections of wing and flap. For a Clark Y flap with a Clark Y main wing, the center of the leading edge radius of the flap should be located about 2.5% of the main wing chord directly below the trailing edge.

---

[7] F. E. Weick and T. A. Harris, "The Aerodynamic Characteristics of a Model Wing having a Split Flap Deflected Downward and Moved to the Rear," N.A.C.A. T.N. No. 422 (1932).

The best known form of the retracting-flap type of variable-area wing is the Fowler flap investigated by N.A.C.A.[8] Like the external airfoil flap, this type obtains high values of C_L without excessive increase in C_{D_0}, so that a large increase in lift coefficient may be utilized efficiently in the take-off. The available test data indicate that the increase in profile drag for the Fowler flap is almost identical with that for a plain flap if compared at the same values of E and δ_F with a corresponding reduction in C_{D_0}. In this connection it should be noted that the comparisons are made on the basis of equivalent plan-forms in the extended position, since there is a change in induced drag due to the reduction in aspect ratio.

Figure 74 gives the variation of $C_{L_{max}}$ with the ratio E for a Clark Y Fowler flap on a Clark Y basic wing. In comparing these data with other flap data, it is advisable to use the values of C_L based on actual area since this is the design condition for stalling speed. A specific comparison should be made on the basis of the actual lift developed C_LS and not on C_L alone.

---

[8] F. E. Weick and R. C. Platt, "Wind-Tunnel Tests of the Fowler Variable-Area Wing," N.A.C.A. T.N. No. 419 (1932). See also T.R. No. 534 (1935).

This type of wing gives what appears to be excessive diving moments, but fortunately the downwash is directly proportional to C_L so that in an airplane having ample tail surface area there is a more or less complete counteraction of the diving moment by the increased download on the tail. The moment coefficient about the quarter-chord point of the actual total chord of the extended

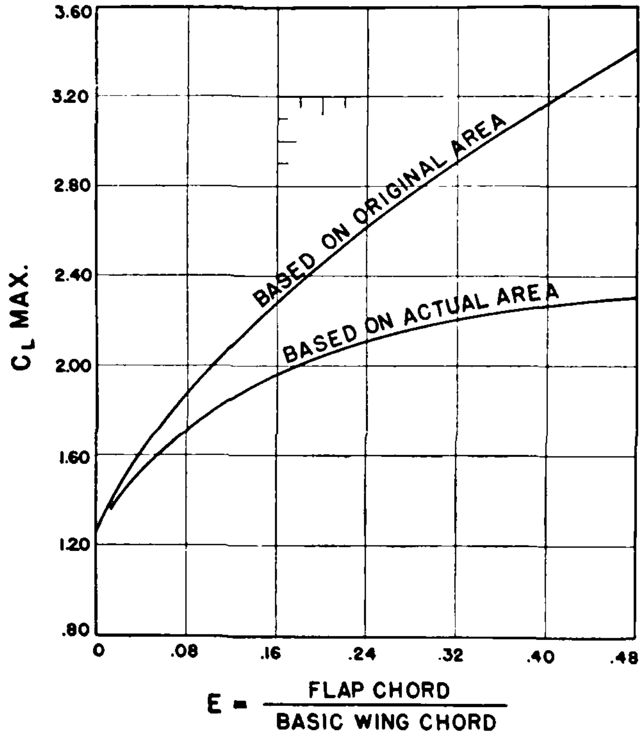

Figure 74. Maximum Lift Coefficient Obtained with Fowler Variable-Area Wing

Fowler wing is obtained to a close approximation in the normal flight range by

$$\Delta C_M = 0.55 \Delta C_L \qquad (101)$$

Due to the concentrated load on the Fowler flap, this increment in moment is about twice the increment for a plain flap.

The Slotted Wing. Two types of leading edge slots have been used. In the Leigh type, the auxiliary airfoil that forms the slot is fixed in the position giving the best compromise performance. In the second type (Lachmann-Handley Page) the auxiliary airfoil is movable on a track or linkage device so that the slot is open only at high angles of attack. The high negative pressures over the leading edge are sometimes employed to give automatic opening and closing of the slot. The load on the auxiliary airfoil is sufficient to operate the trailing edge flap that is required for utilization of the full slot effectiveness.

As a means of increasing lift and reducing stalling speed, the slot is very effective, although somewhat disappointing in that the full-scale net gain is much less than might be expected from wind-tunnel tests on airfoil models with a slot across the entire span. The loss may be ascribed to, two causes. In most practical applications, it is not feasible to extend the slot across the entire span or to keep the slot clear of obstructions, and any interruption to the slot, or to the flow through it, causes a very marked reduction in lift. The second cause for failure to obtain the full benefit of the slot is found in the very high angles of attack required for $C_{L\,max}$. The slot merely extends the lift curve against angle of attack without appreciably changing the slope and $C_{L\,max}$ is at an angle of attack between 23° and 29°. Maximum lift at these angles cannot be utilized in either take-off or landing unless the airplane is specially designed for this purpose.

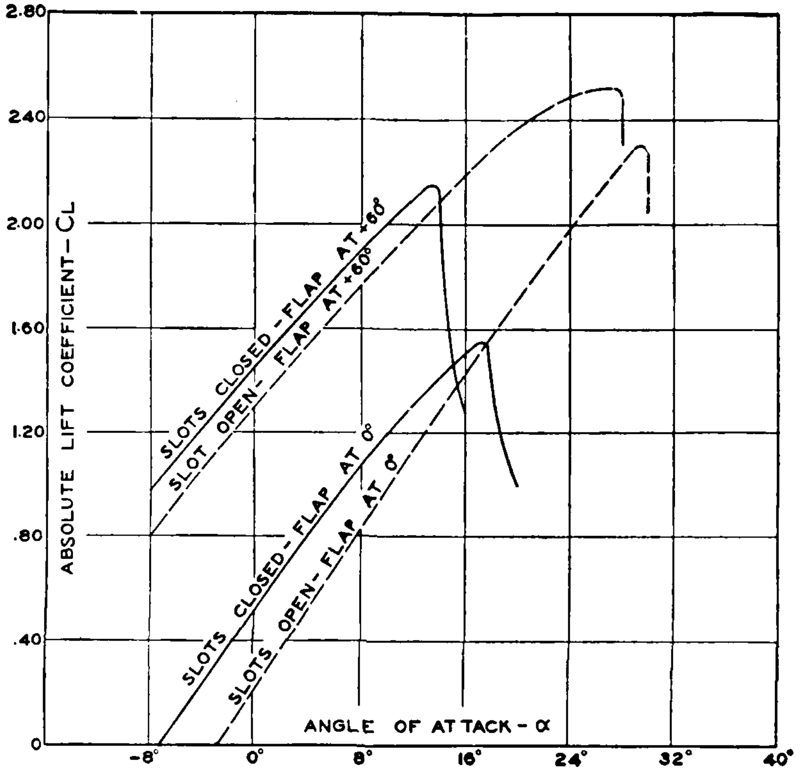

Figure 75. Effect of Slots and Flap on Lift Coefficient

Slots are most effective when used in conjunction with flaps as shown by Figure 75, which is based on wind-tunnel tests on a model wing fitted with two slots and a flap. If the slots alone were used at an angle of attack of 16°, there would actually be a decrease in lift coefficient from C_L = 1.50 to C_L = 1.40, but if a flap is used with the slots, the lift coefficient increases from 1.50 to 2.18.

The fixed slot or auxiliary leading-edge airfoil has the advantage of simplicity with the disadvantage of increased drag at high speed. Under favorable conditions, a value of $\Delta C_{L\,max}$ = 0.50 may be obtained with a fixed slot alone, but for such an arrangement, $C_{L\,max}$ will occur at an angle of attack of about 25°. Consequently, the use of the fixed leading-edge airfoil is restricted to extending the lift curve beyond the usual burble angle. The N.A.C.A. tests[9] show

Slot combination	$C_{L_{max}}$	$C_{D_{min}}$	$\frac{C_{L_{max}}}{C_{D_{min}}}$	$\alpha_{C_{L_{max}}}$
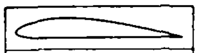	1.291	0.0152	85.0	15°
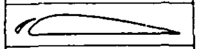	1.772	.0240	73.8	24
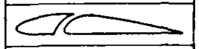	1.596	.0199	80.3	21
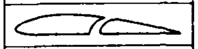	1.548	.0188	82.3	19
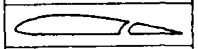	1.440	.0164	87.8	17
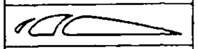	1.902	.0278	68.3	24
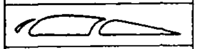	1.881	.0270	69.7	24
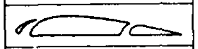	1.813	.0243	74.6	23
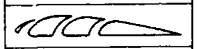	1.930	.0340	56.5	25
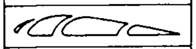	1.885	.0319	59.2	24
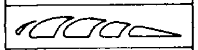	1.885	.0363	51.9	25
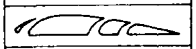	1.850	.0298	62.1	24
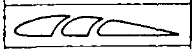	1.692	.0226	74.2	22
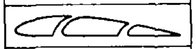	1.672	.0214	78.2	22
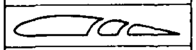	1.510	.0208	72.6	19
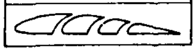	1.662	.0258	64.4	22

Figure 76. Aerodynamic Characteristics of a Clark Y Wing with Multiple Fixed Slots

that the ratio $C_{L\ max}/C_{D\ min}$ may be increased about 40% by the use of the fixed auxiliary airfoil. It is impracticable to reduce wing area to take advantage of this apparent improvement, owing to the high angles of attack involved.

---

[9] F. E. Weick and M. J. Bamber, "Wind-Tunnel Tests of a Clark Y Wing with a Narrow Auxiliary Airfoil in Different Positions," N.A.C.A. T.R. No. 428 (1932). F. E. Weick and R. Sanders, "Wind-Tunnel Tests on Combinations of a Wing with Fixed Auxiliary Airfoils having Various Chords and Profiles," N.A.C.A. T.R. No. 472 (1933).

In general, the efficient use of a slot always requires a flap, if for no other reason than to bring high lifts into a reasonable angular range. It is of interest to note that a staggered biplane has inherently some of the characteristics of a slotted wing, and slots are fully effective only on the upper wing in such arrangements.

Slot combination	$C_{L_{max}}$	$C_{D_{min}}$[1]	$\frac{C_{L_{max}}}{C_{D_{min}}}$	$\alpha_{C_{L_{max}}}$
				°
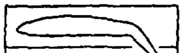	1.950	0.0152	128.2	12
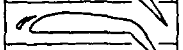	2.182	.0240	91.0	19
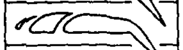	2.235	.0278	80.3	20
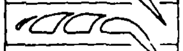	2.200	.0340	64.7	21
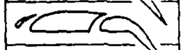	2.210	.0270	81.8	20
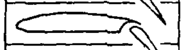	1.980	.0164	120.5	12
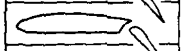	1.770	.0164	108.0	14
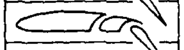	2.442	.0208	117.5	16
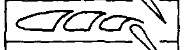	2.500	.0258	96.8	18
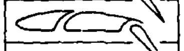	2.185	.0214	102.0	18
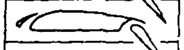	2.261	.0243	93.2	19
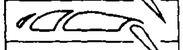	2.320	.0319	72.7	20
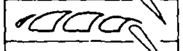	2.535	.0363	69.8	20
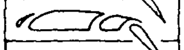	2.600	.0298	87.3	20
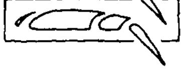	2.035	.0298	68.3	21

[1] $C_{D_{min}}$ with flap neutral.

Figure 77. Aerodynamic Characteristics of a Clark Y Wing with Multiple Fixed Slots and a Slotted Flap Down 45°

A most useful summary of slot and flap data is given by Weick and Shortal in Tables II and III of N.A.C.A. T.R. No. 427. These tables are reproduced in Figure 76 and Figure 77.

The External-Airfoil Flap. A small auxiliary wing mounted below the trailing edge of the main wing is very effective as a flap and shows considerable promise of providing a satisfactory lateral control device. N.A.C.A. tests[10] indicate that the location of the flap is highly critical and varies with the airfoil sections used. For a 23012 section, the center of the leading edge radius should be about 2% of the main wing chord below the trailing edge. For the 23021 section, the best location is 0.0125 *c* below the chord.

This type of flap has several marked advantages. In addition to the possibilities in lateral control, it shows up remarkably well in take-off and at high speed. A high-speed flap-setting of about -5° gives a low minimum drag coefficient. $C_{L\,max}$ is obtained with a moderate value of δ_F and a comparatively low value of C_D. With a cambered flap, it is possible to obtain a value of $C_{L\,max}$ greater than 2.4. By a suitable choice of hinge axis, the hinge moment coefficients may be reduced to any desired value. In this respect, the airfoil flap is probably superior to all other types.

The disadvantages are mostly structural. It is in a vulnerable position for damage in handling, either on a landplane or on a seaplane. When used as a lateral control device, the rolling moments are high, but the yawing moments are relatively higher. However, an external airfoil flap has been used very successfully for lift and lateral control on some of the Junker airplanes.[11]

In the high-lift position, the Junkers "Double-Wing," the Wragg flap, and the Fowler flap are almost identical from an aerodynamic viewpoint.

---

[10] R. W. Noyes, "Wind-Tunnel Tests of a Wing with a Trailing-Edge Auxiliary Airfoil Used as a Flap," N.A.C.A. T.N. No. 524 (1935). F. E. Weick and R. W. Noyes, "Wind-Tunnel Research Comparing Lateral Control Devices Particularly at High Angles of Attack. XIII Auxiliary Airfoils Used as Ailerons," N.A.C.A. T.R. No. 510 (1935). See also T R. No. 541 (1935).

[11] F. B. Fradfield and W. E. Wood, "Wind-Tunnel Tests on Junker Type Ailerons," Br.A.R.C. R. & M. No. 1583 (1933).

Rotor Wings. Considerable wind-tunnel research has been directed towards obtaining a practical application of the Magnus Effect employed in the Flettner Rotor.[12] In most of the investigations along these lines, a rotating cylinder formed the leading edge and its fairing formed the main body of the wing. It is possible to obtain values of C_L in excess of 2.0 with this arrangement, but the drag is very high and there appears to be little promise of sufficient improvement to make the scheme practicable.

Boundary Layer Control. There appear to be great possibilities of improving airfoil characteristics through control of the boundary layer. The preliminary N.A.C.A. tests[13] indicate that "suction" slots are more efficient than "pressure" slots and that the best location is on the upper surface at about 50% of the chord. The power required to maintain a suitable reduction in pressure at a suction slot is comparatively small. In the tests so far reported, however, very high lifts have been obtained only with very thick sections at angles of attack of the order of 40°. The showings made with thinner and more practicable sections have been somewhat disappointing.

Effect of Flaps on Performance. The major effects of flaps on performance are as follows:

1. Increase in maximum lift coefficient, giving a reduction in stalling speed and in take-off run.
2. Increase in drag coefficient, giving steeper gliding angles and reduced landing run, with a tendency to increase the take-off run.
3. Increase in lift coefficient at a given angle of attack. This effect is very important in take-off, particularly with seaplanes.

---

[12] E. G. Reid, "Tests of Rotating Cylinders," N.A.C.A. T.N. No. 209 (1924).

[13] M. J. Bamber, "Wind-Tunnel Tests on Airfoil Boundary Layer Control Using a Backward Opening Slot," N.A.C.A. T.R. No. 385 (1931).

Owing to the marked increase in drag due to flaps, the improvement in take-off run is a complex function of the power loading, wing loading, and flap setting. For all practical purposes, however, the theoretical reduction in distance required to take-off and climb 50 feet with the best flap setting, in a calm, is a function of wing loading

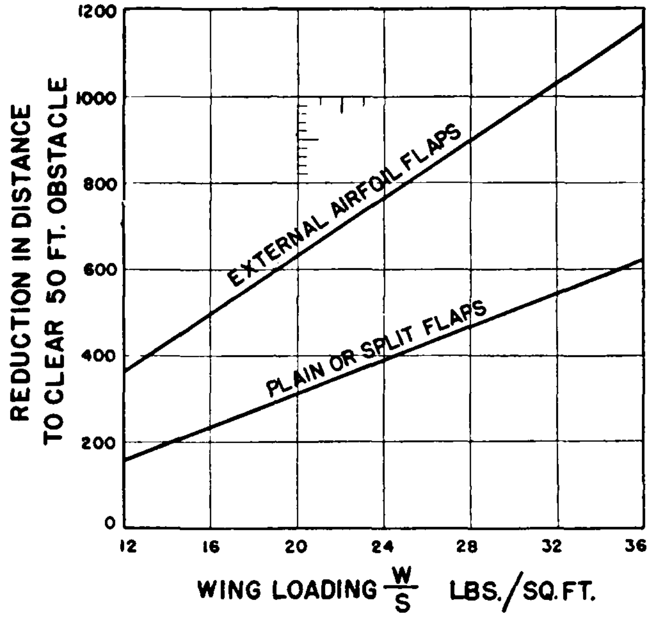

Figure 78. Effect of Flaps on Take-Off and Climb over an Obstacle

only as shown by Figure 78. This theoretical reduction is almost twice as much with the external airfoil types (Fowler, Wragg, etc.) as with the trailing edge types (plain, split, Zap, etc.). Flight tests seem to indicate less difference between the various types of flaps than would be expected from the theoretical analysis. This is perhaps due to the highly critical "best setting" that is found with the high-drag types.

Comparing the conditions of flaps neutral with flaps in best setting, there is a reduction in ground run between

20% and 40%. This, however, should not be considered the true effect of the flaps, since it is due almost entirely to the reduction in stalling speed, and an even greater reduction in ground run could be obtained with a plain wing increased in area to give the same reduction in stalling speed.

The exact increase in gliding angle is not ordinarily a matter of interest, but in some cases it is necessary to calculate the attitude of the airplane in a glide or in horizontal flight with flaps down. The attitude in horizontal flight may be obtained by subtracting from the total C_L the ΔC_L due to the flaps, thus finding the C_L of the basic wing. The absolute angle of attack corresponding to this basic C_L may then be found from the slope of the lift curve for the effective aspect ratio of the wing combination. In a glide, the inclination of the flight path below the horizontal is found from

$$\theta = \tan^{-1} (C_D / C_L) \tag{102}$$

where C_D is the total airplane drag coefficient. The attitude of the airplane with respect to the glide path may be assumed the same as in horizontal flight.

The reduction in distance required to land from a given elevation depends largely on the effect of flap drag in steepening the gliding angle. Hence, the high drag flaps give a greater reduction in distance than the low drag types. For a high speed transport, the external airfoil type of flaps will give about 30% to 35% reduction in distance and the high drag types about 50% reduction in the distance required to come to rest from an altitude of 200 feet.

In the case of a seaplane or flying boat, the efficient use of flaps is restricted during take-off by the requirement that the sum of the air drag plus water drag must be reduced. This means that the ratio of $\Delta C_L/\Delta C_D$ must be greater than the Δ/R of the hull. The maximum reduction in run is ordinarily obtained with a moderate initial setting that is rapidly increased to a full throw just as the take-off speed is attained. For this reason, the balanced or partially balanced types equipped for quick-acting mechanical operation appear most promising for use on flying boats.

Additional Comment on Flaps. The application of flaps to an airplane requires careful study of lateral stability and lateral control. Since the forces and moments vary as the square of the speed, a 5% reduction in speed means a 10% reduction in the available control. For this reason, the use of flap devices in airplanes of relatively short span has given unsatisfactory results. The designer must not confuse rolling moments and rolling-moment coefficients.

Another factor of considerable importance is the vertical location of the center of gravity. Owing to the inclination of the resultant force vector, a high-wing monoplane has a marked advantage over a low-wing monoplane in the matter of longitudinal balance change due to flap.

Another factor to be considered is the sudden stall that appears to be inherent with any of the high-lift devices. This is particularly noticeable with many low-wing monoplanes, where there is a marked tendency to drop the nose without previous warning of the approaching stall. An improvement can be obtained in this respect by use of washout and thinner sections at the wing tips. All airplanes with flaps should be provided with ample longitudinal control.

CHAPTER 7

STATIC STABILITY AND CONTROL

Stability. An airplane is statically stable if any displacement from a given attitude sets up forces and moments tending to restore the original attitude. It is dynamically stable if the resulting motion is stable, that is, if any oscillations due to static stability are quickly damped. Static stability may be easily measured by wind-tunnel tests on an airplane model; it is directly proportional to the slope of the moment curve. Dynamic stability, on the other hand, must be laboriously calculated from rather extensive wind-tunnel tests, using assumptions which are questionable. It is not surprising, therefore, to find that practically all aeronautical engineers have ignored dynamic stability as a design factor in the past.

In pitch, a fair degree of static stability with normal design proportions is usually accompanied by dynamic stability. Stability in pitch is called "longitudinal stability." Stability in roll and stability in yaw are not easily separated. They are always treated in combination as "lateral stability." Static stability in both roll and yaw does not insure dynamic lateral stability and, in fact, lateral instability may easily result from too much directional stability. In this connection, the use of moderate dihedral is probably desirable in all seaplanes and in most landplanes. The prejudice of many pilots against the use of dihedral in pursuit type airplanes is not substantiated by full-scale rolling and turning data.

The study of dynamic stability is of greater value to the aeronautical engineer than is generally realized. It is an excellent method of analyzing the effects of changes in design proportions and will be used more extensively for this purpose in the future when the demands for more refinement in design methods make it necessary. A brief treatment of dynamic stability is given in Chapter 8.

One of the most important problems in airplane design is to determine the sizes and proportions of the control surfaces so as to obtain a satisfactory degree of control and static stability under all conditions of flight. The remainder of this chapter is devoted to the general questions of control surface design.

Control Surface Design. Satisfactory control surface design requires:

1. A reasonable margin of static stability about the three axes in all flight attitudes and loading conditions.
2. Ample control over the attitude and motion of the airplane.
3. Moderate forces so that the controls can be operated without undue effort or fatigue by the average pilot.
4. Provision for control over trim. This is very important in types designed for extended flights or requiring divided attention on the part of the pilot.
5. Provisions to avoid flutter.

These requirements can usually be met by careful attention to certain general relations such as c.g. location, size and outline of the control surfaces, as will be indicated later.

Center-of-Gravity Location. The definite location of the center of gravity with respect to the wing or mean chord requires two coordinates. Consistent results cannot be obtained unless these coordinates are independent of wing section and wing incidence. The only satisfactory method by which the c.g. location can be definitely specified is with respect to its distance above or below the zero-lift line and its fore-and-aft location along the projection of the wing chord on this line.

For this purpose the zero-lift line should be drawn through the mean camber of the aerodynamic center or quarter chord point as in Figure 79. The coordinates of the c.g. are x (positive aft of the leading edge) and h (positive above the zero-lift line) as shown.

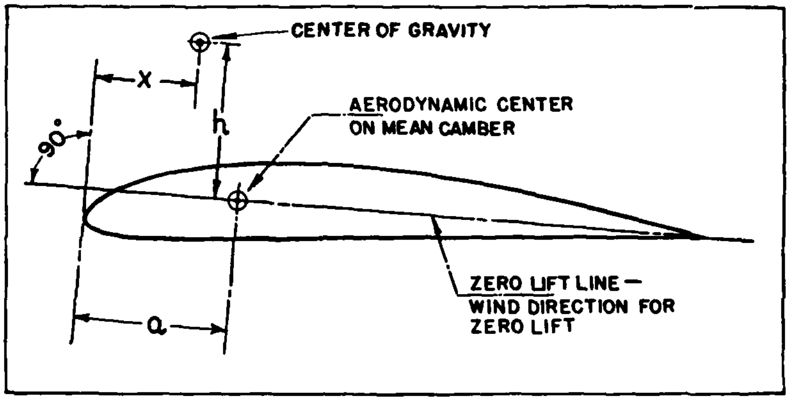
CENTER OF GRAVITY
X
h
90°
AERODYNAMIC CENTER ON MEAN CAMBER
ZERO LIFT LINE — WIND DIRECTION FOR ZERO LIFT
a

Figure 79. Coordinates for Center of Gravity

Effect of C.G. Location on Moment Curves. The different types of wing moment curves obtained with various c.g. locations with the N.A.C.A.–2412 section are shown on Figures 80, 81, and 82. Figure 80 corresponds to a high-wing monoplane. The low c.g. location increases stability at high-lift coefficients and decreases it at low-lift coefficients. When the c.g. is on the chord line, the moment curves are straight lines, as shown on Figure 81. When the c.g. is above the chord line as in a low-wing monoplane, the stability is better at high speeds than at low speeds, as shown on Figure 82. The effect of fore-and-aft c.g. location is shown for each vertical location.

With a low c.g., the stability is better at high angles of attack (low speed) than at small angles of attack. High c.g. gives better stability at small angles of attack than at high angles of attack. The effect of change in fore-and-aft location is independent of the vertical location.

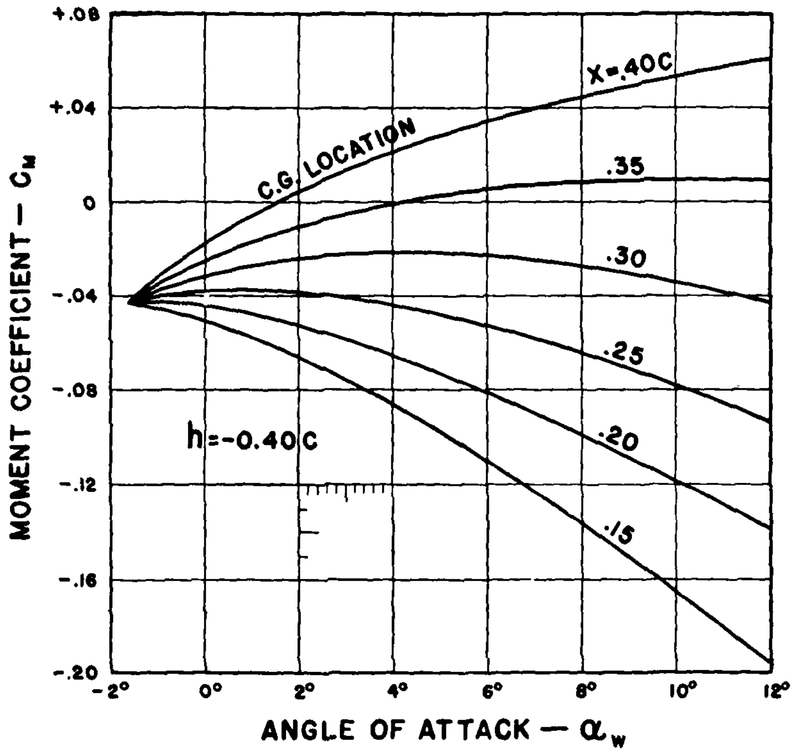

Figure 80. Moment Curves for c.g. Below Wing Chord

These effects may be summarized with mathematical symbols as follows:

c.g. location	Low	On chord	High
Stability at high speed..................	−	o	+
Stability at low speed..................	+	o	−

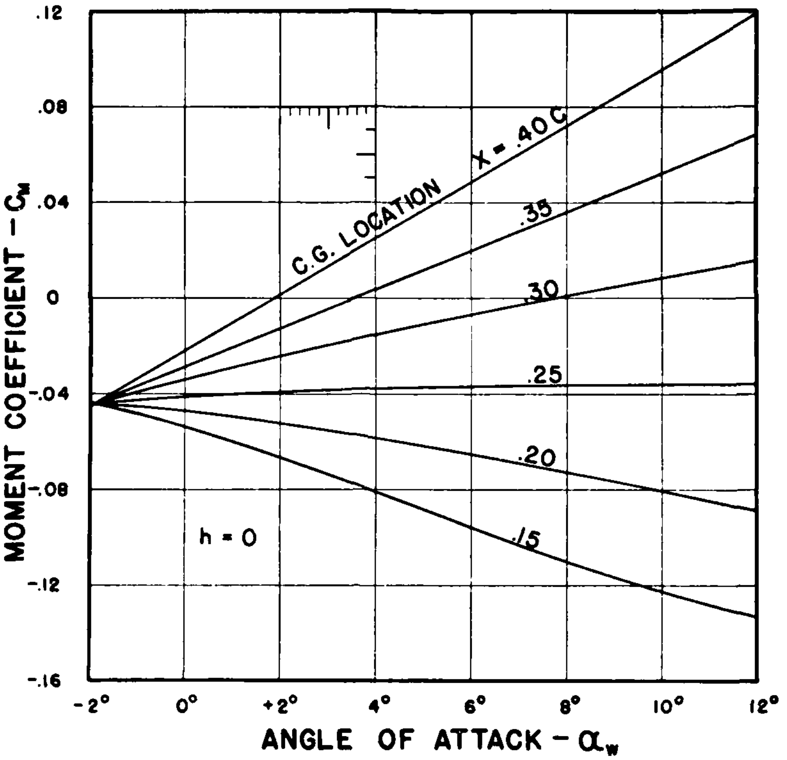

Figure 81. Moment Curves for c.g. on Wing Chord

A plus sign means an increase, a minus sign a decrease, and a zero means no change in the longitudinal stability.

Moment Coefficient About Any Point. The pitching moment coefficient about any point may be calculated by equation (49),

$$C_M = C_{M_0} - (a - x)\, C_L + 0.15\, h\, C_L^2 \qquad (49)$$

where a is the aerodynamic center, x is the fore-and-aft c.g. location, and h is the distance from the c.g. to the wing chord, as in Figure 79. h is positive when the c.g.

is above the chord. In the absence of exact data on the aerodynamic center, Figure 52 on page 123 may be used to determine *a*.

In the case of a biplane, the value of C_M is calculated by equations (56) and (57), using the method described on pages 70 to 72. This method is perhaps best illustrated by a simple example. The following arrangement has been tested by N.A.C.A.

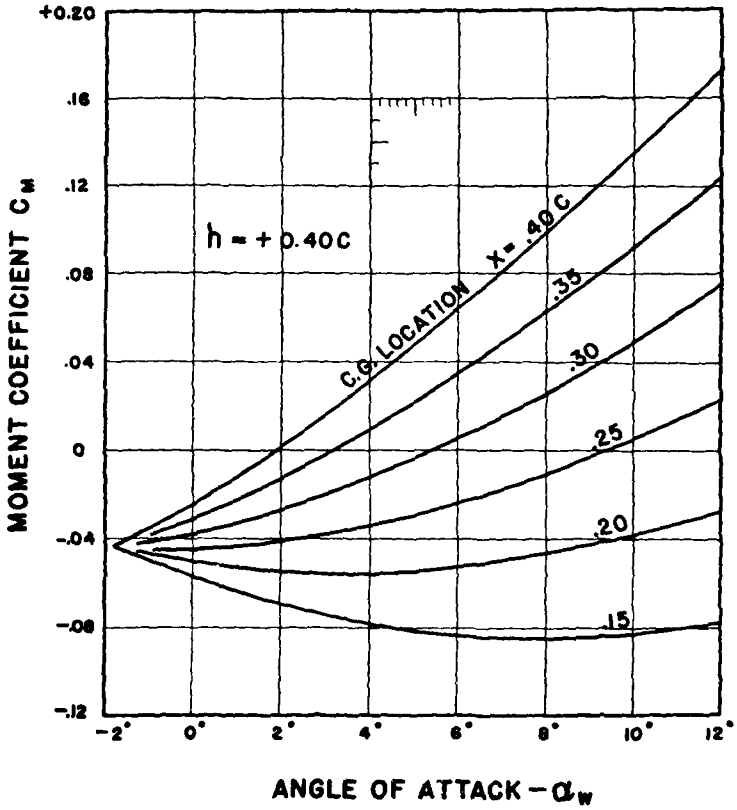

Figure 82. Moment Curves for c.g. Above Wing Chord

Section Clark Y $a = 0.25$ $C_{M_0} = -0.070$
Both wings 30″ x 5″, $S_U/S = S_L/S = 0.5$
Stagger 0.50 c
Gap = Chord

Moments will be taken about the mid-point of the line joining the leading edges. This point has the following coordinates:

$$x_U = 0.25 \qquad x_L = -0.25$$
$$(a - x_U) = 0 \qquad (a - x_L) = +0.50$$
$$h_U = -0.50 \qquad h_L = +0.50$$

Since the wings are of equal span and chord, equations (56) and (57) become

$$\Delta\, C_{MU} = \tfrac{1}{2}\,[-0.07 - 0.075\, C_{LU}^2]$$
$$\Delta\, C_{ML} = \tfrac{1}{2}\,[-0.07 - 0.50\, C_{LL} + 0.075\, C_{LL}^2]$$

TABLE 8. EXAMPLE OF CALCULATION FOR BIPLANE C_M

C_{LB} = Biplane C_L	.20	.60
C_{LU} = Upper wing C_L	.235	.690
C_{LL} = Lower wing C_L	.165	.510
C_{M_0} for Clark Y	−.070	−.070
$S_U c_U/Sc$	.5	.5
$S_L c_L/Sc$	.5	.5
$-(a-x_U)\ C_{LU}$	0	0
$-0.075\ C^2_{LU}$	−.004	−.036
C_{MU}	−.074	−.106
$\Delta C_{MB} = C_{MU}\ (S_U\ c_U/Sc)$	−.037	−.053
$-(a-x_L)\ C_{LL}$	−.082	−.255
$+0.075\ C_{LL}^2$	+.002	+.020
C_{ML}	−.150	−.305
$\Delta C_{MB} = C_{ML}\ (S_L c_L/Sc)$	−.075	−.152
C_{MB} Calculated	−.112	−.205
C_{MB} From tests	−.113	−.201

The calculations in Table 8 give $C_{MB} = -0.112$ at $C_L = 0.20$ and $C_{MB} = -0.205$ at $C_L = 0.60$. The corresponding experimental values (determined from the vector diagram in Figure 30 of T.R. No. 317) are -0.113 and -0.201.

Mean Chord of a Biplane. While the moment coefficient determined by equation (49) supplies sufficient information for tail surface design, the well-established use of the mean aerodynamic chord or "M.A.C." cannot be ignored.

The location of the mean aerodynamic chord is readily calculated from the three-term moment equation

$$C_{MB} = C_{M_0} - XC_L + YC_L^2 \tag{103}$$

obtained from equations (56) and (57). Let it first be assumed that it is desired to find the location of a monoplane wing having the same moment coefficient as the biplane arrangement with respect to the actual c.g. Second, let it be assumed that this monoplane chord has the weighted mean chord determined by

$$\text{W.M.C.} = \frac{c_U \cdot S_U + c_L \cdot S_L}{S_U + S_L} \tag{104}$$

If C_{MB} is calculated for two values of C_L, substitution in equation (103) gives two simultaneous equations in X and Y. On solution of these, the fore-and-aft location of the mean chord is found from

$$X = (a - x) \qquad \text{or } x = a - X$$

and the vertical location from

$$Y = 0.15\,h \qquad \text{or } h = Y/0.15$$

As an example, take the biplane considered in the preceding section, for which in Table 8 it was found that $C_M = -0.112$ for $C_L = 0.20$, and $C_M = -0.205$ for $C_L = 0.60$. These values give

$$-0.112 = -0.070 - 0.20X + 0.04Y$$

$$-0.205 = -0.070 - 0.60X + 0.36Y$$

from which $X = 0.202$ and $Y = -0.0375$. Since $a = 0.25$, the reference point at the middle of the line joining the leading edges is at

$$x = a - X = 0.25 - 0.202 = +0.048\,c$$

or 4.8% aft of the leading edge of the M.A.C. This reference point is at

$$h = -0.0375/0.15 = -0.25$$

or 25% of the chord below the M.A.C. Otherwise stated, the M.A.C. by calculation is located 25% c above the mid-line with its leading edge 20.2% c aft of the leading edge of the upper wing. The location determined experimentally by the method given later is $x = +0.05\,c$, $h = -0.30\,c$.

Virtual Mean Chord. The mean chord desired for design purposes is a "virtual" mean chord. Its location with respect to the wings of a biplane cellule may be determined from the vector diagram obtained in a wind-tunnel test by finding the position for monoplane and biplane vector coincidence. This position may be easily located by the use of a superimposed vector diagram drawn on transparent paper to represent the monoplane vectors for the geometrical mean chord (equation 104), which is moved to obtain vector coincidence.

The location of the virtual mean chord has been obtained by this method, using test data from N.A.C.A. Technical Report No. 317, and from unpublished Washington Navy Yard tests. The experimentally determined values have also been supplemented by values calculated from the lift distribution. The vertical location of the virtual mean chord is given on Figure 83 as a function of the ratio (stagger/geometrical mean chord); other ratios were tried but this gives reasonable agreement and is easier to use. The vertical location is given in terms of the geometrical mean chord. $(h_v - h_g)$ is the vertical distance between the virtual and the geometrical mean chords. The deviation from the mean curve is due to a combination of experimental error and extreme conditions. The average deviation may be expected to be less than 10%.

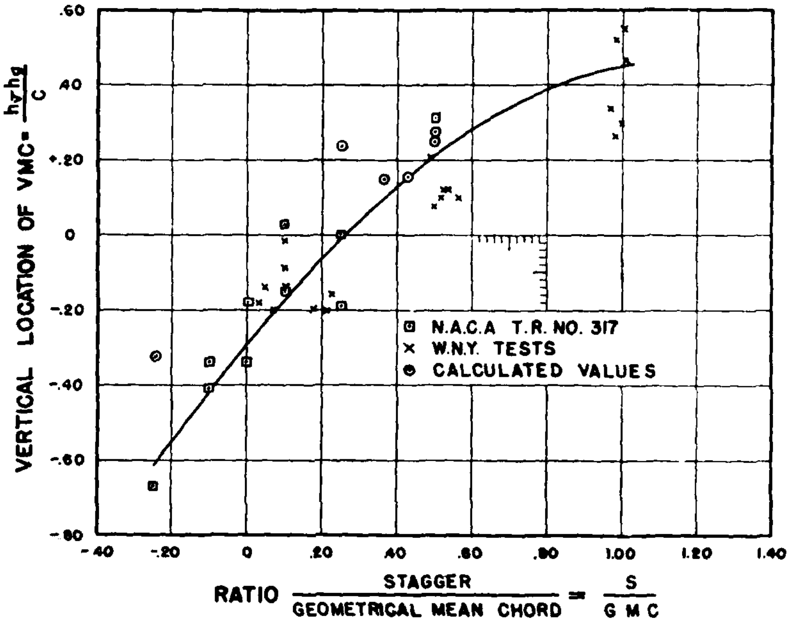

Figure 83. Vertical Location of Virtual Mean Chord with Respect to Geometrical Mean Chord

Further study will be required to improve the accuracy. In general, the virtual mean chord c_V lies ahead of the geometrical mean chord c_G. The fore-and-aft separation appears to depend on stagger and on the ratio of lower wing chord to upper wing chord, as shown on Figure 84.

According to the limited data in Technical Report No. 317, the vertical shift of the virtual mean chord due to decalage is

$$\frac{\Delta h}{\text{W.M.C.}} = +0.133\,\delta^\circ \qquad (105)$$

where δ is the angle of decalage measured positive when the chord lines intersect forward of the wings. Practical use may be made of this relation by introducing sufficient decalage to cause the virtual mean chord to pass through the c.g. In any event the vertical and fore-and-aft location of the virtual mean chord must be considered in locating the wings and the center of gravity to obtain a desired type of pitching moment curve.

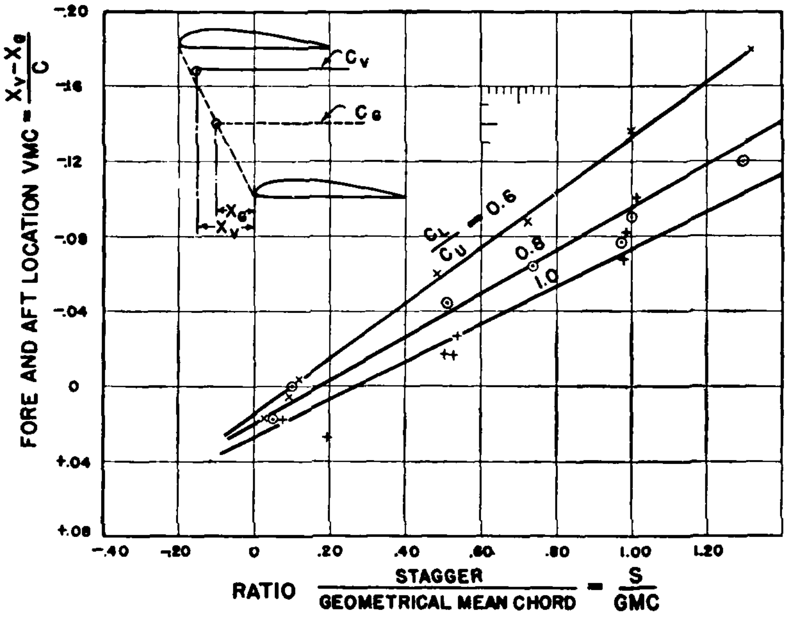

Figure 84. Horizontal Location of Virtual Mean Chord with Respect to Geometrical Mean Chord

Locus of C.G. for Constant Stability. A common design problem is to balance combined vertical and fore-and-aft shifts in c.g. to maintain constant stability. Obviously, as the c.g. moves aft, it should also move down or vice versa. The angle between the c.g. path and the normal to the chord depends on the value of C_L to be considered. The tangent of this angle is obtained equating the change in the last two terms on the right-hand side of equation (49), or

$$d\,(a - x)\,C_L = 0.15\,dh\,C_L^2$$

From which

$$dx/dh = -0.15\,C_L \tag{106}$$

Hence at $C_L = 1.0$, the stability will be unaffected by a shift of the c.g. along a line inclined upward and forward at an angle of about 8° 30′ to the normal to the zero-lift line.

Cases are on record where a vertical shift of a few inches in the c.g. was sufficient to change the stability characteristics. This condition can occur only with marginal stability.

Horizontal Tail Area. The horizontal tail area required to give static longitudinal stability may be obtained from the equation for the slope of the curve of pitching moment about the c.g. The basic equation in coefficient form is

$$\frac{dC_{MR}}{dC_L} = \frac{dC_{MW}}{dC_L} + \frac{dC_{MT}}{dC_L} \tag{107}$$

Where C_{MW} and C_{MT} are the pitching moments for the wing and the tail and C_{MR} is the resultant moment coefficient. It has been shown[1] that the desired slope of the resultant moment curve is of the form

$$dM_R/d\alpha = KqWc \tag{108}$$

Where W is the gross weight and K a constant proportional to the stability required. Equation (108) may be written in coefficient form as

$$\frac{dC_{MR}}{dC_L} = \frac{K \cdot w_s}{(dC_L/d\alpha)} \tag{109}$$

---

[1] Walter S. Diehl, "Two Practical Methods for the Calculation of the Horizontal Tail Area Necessary for a Statically Stable Airplane," N.A.C.A. T.R. No. 293 (1928).

The pitching moment due to the tail is

$$M_T = -C_{LT} \cdot qS_T l \tag{110}$$

where S_T is the tail area, l the distance between the c.g. and the point of application of the tail lift. For all practical purposes, l may be taken as the distance between the c.g. and the elevator hinge axis. From equation (110) in coefficient form

$$\frac{dC_{MT}}{dC_L} = -\frac{dC_{LT}}{dC_L}\left(\frac{S_T}{S_W}\frac{l}{c}\right) \tag{111}$$

Now

$$\frac{dC_{LT}}{dC_L} = \frac{d\alpha_T\,(dC_{LT}/d\alpha_T)}{d\alpha\,(dC_L/d\alpha)} = \frac{d\alpha_T}{d\alpha} \cdot \frac{F_1}{F_4} \cdot \eta_T \tag{112}$$

where F_1 and F_4 are the slopes of the lift curves for the tail and the wings, respectively. η_T is an efficiency factor that allows for the reduction in tail lift due to body interference and will be discussed later.

Since the angle of attack of the tail is $\alpha_T = \alpha_W + \beta - \epsilon$ where β is the tail setting and ϵ the downwash angle

$$(d\alpha_T/d\alpha) = 1 - (d\epsilon/d\alpha) \tag{113}$$

and from equation (41b)

$$\frac{d\epsilon}{d\alpha} = \frac{52\,F_4F_2}{n}$$

substituting these in equation (111) gives

$$\frac{dC_{MT}}{dC_L} = -\frac{F_1}{F_4}\left[1 - \frac{52\,F_4F_2}{n}\right]\left(\frac{S_T}{S_W} \cdot \frac{l}{c}\right)\eta_T \tag{114}$$

F_2 is a factor that gives the downwash correction for tail location.

The wing pitching moment about the c.g. is given by equation (49) from which by differentiation

$$(dC_{MW}/dC_L) = -(a - x) + 0.30hC_L \tag{115}$$

The complete slope equation is obtained by substitution of equations (109), (114), and (115) into equation (107)

$$\frac{K}{F_4}w_s = -(a - x) + 0.30hC_L - \frac{F_1}{F_4}\left[1 - \frac{52\,F_2F_4}{n}\right]\left(\frac{S_T}{S_W}\frac{l}{c}\right)\eta_T$$

and solving to obtain

$$\frac{S_T}{S_W}\frac{l}{c} = \frac{-(a - x) + 0.30hC_L - K \cdot w_s/F_4}{\dfrac{F_1}{F_4}\left[1 - \dfrac{52\,F_2 \cdot F_4}{n}\right]\eta_T} \tag{116}$$

in which for convenience the meanings of the symbols are as follows:

S_T = Tail area
S_W = Wing area
l = Tail length
c = Mean chord
a = Aerodynamic center in terms of c
x = c.g. location along chord in terms of c
h = c.g. location normal to chord in terms of c
K = Resultant slope coefficient
w_s = Wing loading
F_1 = Slope of tail lift curve
F_2 = Downwash correction factor
F_4 = Slope of wing lift curve
n = Effective aspect ratio of wings
η_T = Tail efficiency factor

K and η_T will be discussed below. All other factors are either known or readily determined from design data. The slopes of the lift curves F_1 and F_4 may be determined from Figure 85

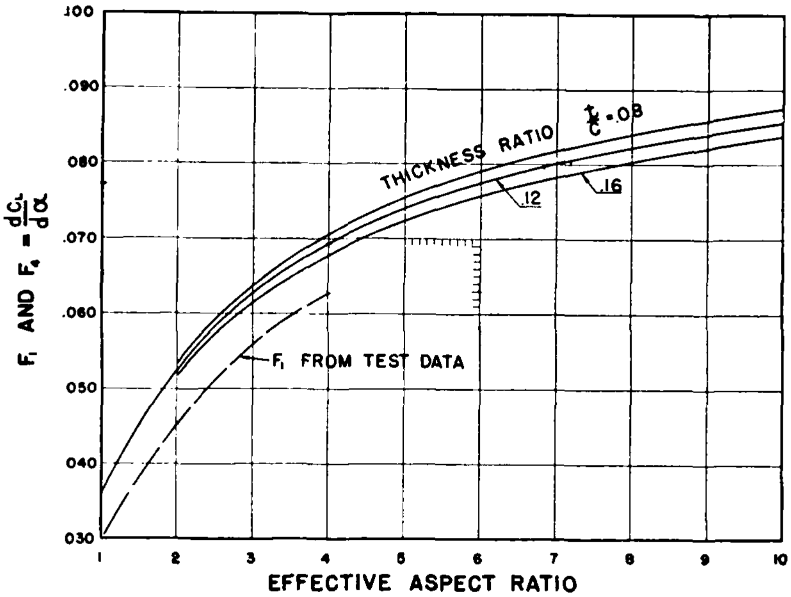

Figure 85. Slope of Lift Curve F_1 and F_4 for Tail Surface Equations

Longitudinal Stability Coefficient K. The shape of the curve of pitching moments against either lift coefficient or angle of attack depends on the h coordinate of the center of gravity. For c.g. locations above the chord (positive values of h), the stability is greater at low lift coefficients than at high lift coefficients. For c.g. locations below the chord, the stability is greatest at high lift coefficients and for c.g. location on the zero-lift chord, the stability is constant at all lift coefficients.

The desired degree of longitudinal stability depends primarily on the type of airplane, although a number of other factors must be considered. The basic conditions are that the stability must be positive at all lift coefficients, and that it must not be too great for satisfactory control. For $h = 0$ a single solution with the desired value of K

will be sufficient, but for positive or negative values of *h*, two or more solutions may be necessary, the first to determine the area coefficient at the critical condition, the second to determine whether or not the stability with this area is too great at the other extreme. For very large positive or negative values of *h*, it may be necessary to accept a low value of *K* at the critical condition, in order to avoid excessive stability at the other extreme. This is particularly true for negative values of *h*, as in high-wing monoplanes, where it is desired to employ a fixed stabilizer. The desired values of *K* in the normal flight range or at $C_L = 0.5$ are:

Type	K at $C_L = 0.5$
Highly maneuverable or with fixed stabilizer, *h* positive	$-.0003$ to $-.0005$
Moderate maneuverability normal stability, *h* small or zero	$-.0005$ to $-.0007$
Very stable, *h* negative	$-.0007$ to $-.0010$

It is probably undesirable to use a negative slope greater than -0.0010 at $C_L = 0.5$, unless a lower value produces instability at zero lift.

Tail Efficiency Factor η_T. Owing to the effect of interference from the wings, fuselage, and nacelles, the slope of the lift curve actually obtained on the horizontal tail surfaces is less than the theoretical value. The ratio of the actual to the theoretical slope is the tail efficiency factor η_T, which depends chiefly on the plan-form and vertical location of the horizontal tail. Average values from wind-tunnel tests are:

	η_T
Triangular plan-form:	
On fuselage center-line	.70
On top of fuselage	.75
Above fuselage (on fin)	.80
Elliptical plan-form:	
On fuselage center-line	.75
On top of fuselage	.85
Above fuselage (on fin)	.95
Rectangular or shaped-tip plan-form:	
On fuselage center-line	.80
On top of fuselage	.90
Above fuselage (on fin)	1.00

Any marked obstruction such as a nacelle ahead of the tail surfaces reduces the above values as much as 10% or even 20%, depending on the disturbance to the air flow.

The values of η_T are probably somewhat higher than indicated by most published data owing to the incorrect practice of calculating the aspect ratio of the tail from its actual area and span instead of using the effective area which includes the area intercepted by the fuselage. This partially explains the very low efficiency of a tail surface located on the fuselage center-line as reported by some observers. The low efficiency of the triangular shapes is due to the use of the actual span instead of the effective span. The effective span of a wing with sharply-raked tips is very close to the average span. Hence, the effective span of a triangular tail surface must be appreciably less than the actual extreme span.

In the absence of necessary information to estimate η_T from the data given above, it is advisable to assume $\eta_T = 0.80$.

A discussion of tail-plane efficiency with test data may be found in R. & M. No. 761 of the British Aeronautical Research Committee, "Experimental Determination of Tailplane Characteristics," by Glauert and Peatfield.

Downwash Factor F_2. With the exception of a narrow, highly turbulent wake, the downwash field behind a simple airfoil is fairly definite, but owing to the complex interference relations the local downwash at the tail surface of an airplane is subject to marked deviations and irregularities. It is easily seen how these disturbances are produced by the slipstream, center-section cut-outs, windshields, etc., but it is impracticable to calculate the exact downwash. Fortunately, the average downwash is of the same order of magnitude as the theoretical value so that there is no serious objection to the use of the theoretical variation in tail surface calculations.

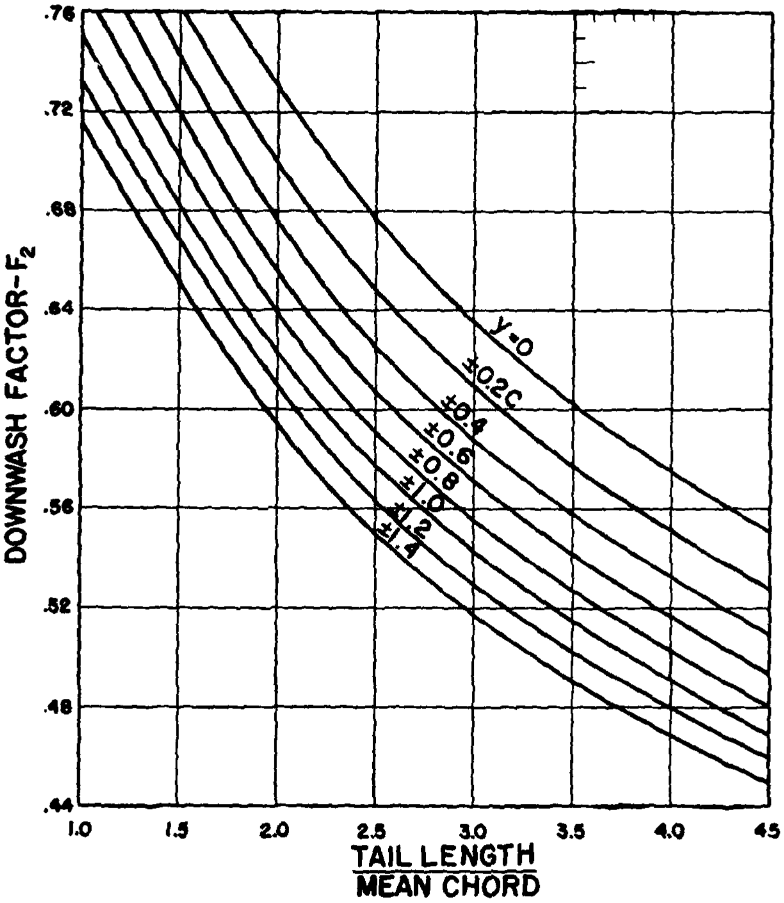

Figure 86. Downwash Correction Factor for Horizontal Tail Surface Equations

Figure 86 gives the downwash factor F_2 as a function of the coordinates of the tail surface. The coordinate y is the vertical distance of the tail above or below the zero-lift line drawn through the trailing edge of the wing. An average value of y may be used.

Relative Effect of Variables. The change in horizontal tail area due to change in any given variable is readily obtained from equation (116) by holding the remaining variables and coefficients constant. The results are best given in the forms of curves showing the relative tail area required for constant static stability.

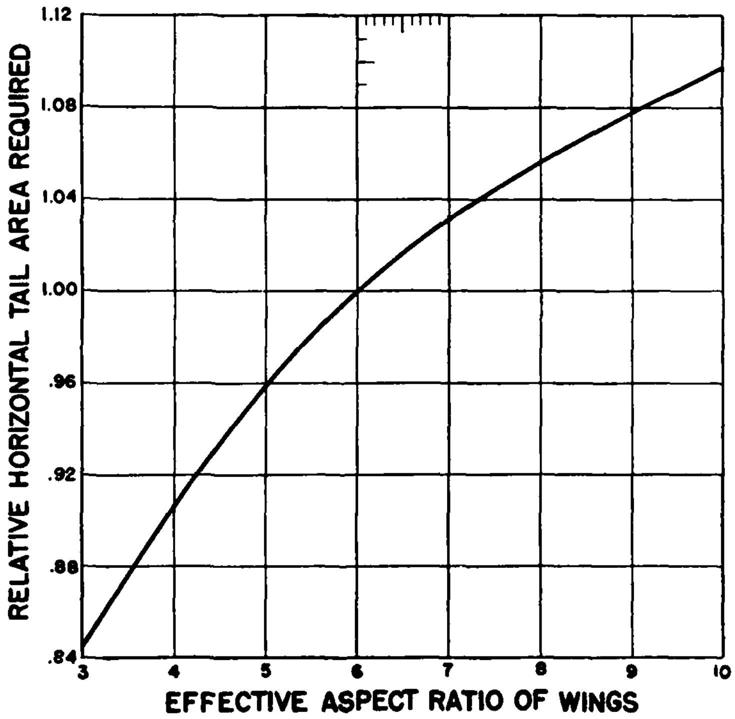

Figure 87. Effect of Wing Aspect Ratio on Horizontal Tail Area Required for Constant Static Stability

Figure 87 shows the effect of change in wing aspect ratio only. For aspect ratios in common use, this variable is of secondary importance. Figure 88 shows the effect of changing tail aspect ratio only. This effect is very marked if the tail aspect ratio is below 3.

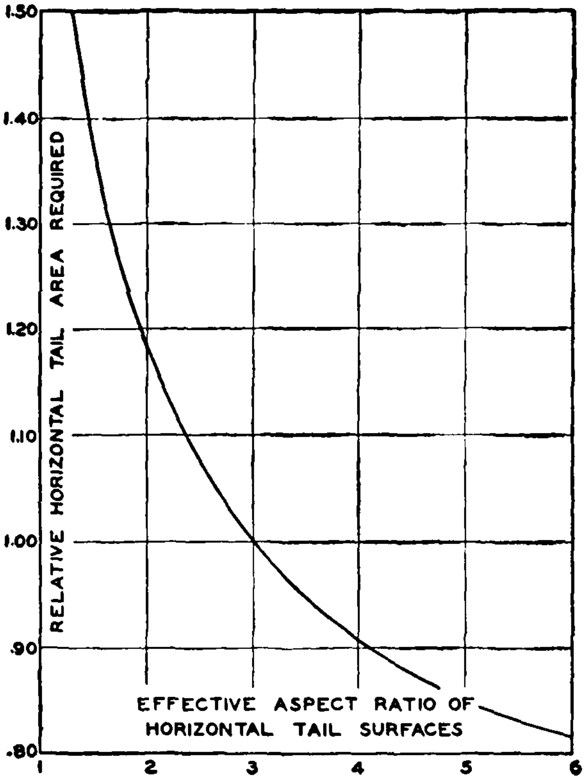

Figure 88. Effect of Tail Aspect Ratio on Tail Area Required for Constant Static Stability

Figure 89 shows the effect of changing tail length (l/c). Since the area varies inversely as (l/c), this accounts for most of the change shown. There is, however, an appreciable contribution from the downwash factor F_1 at low aspect ratios and low values of (l/c).

Figure 90 shows the effect of fore-and-aft c.g. location. For constant static stability, the area of the horizontal tail surfaces continues to decrease as the c.g. is moved forward, but in order to provide balance and maintain control, this decrease cannot be utilized. Experience indicates that control and stability requirements combine to give a minimum area for a c.g. location at about 30% of the mean chord. This effect would be approximated by the dotted line on Figure 90.

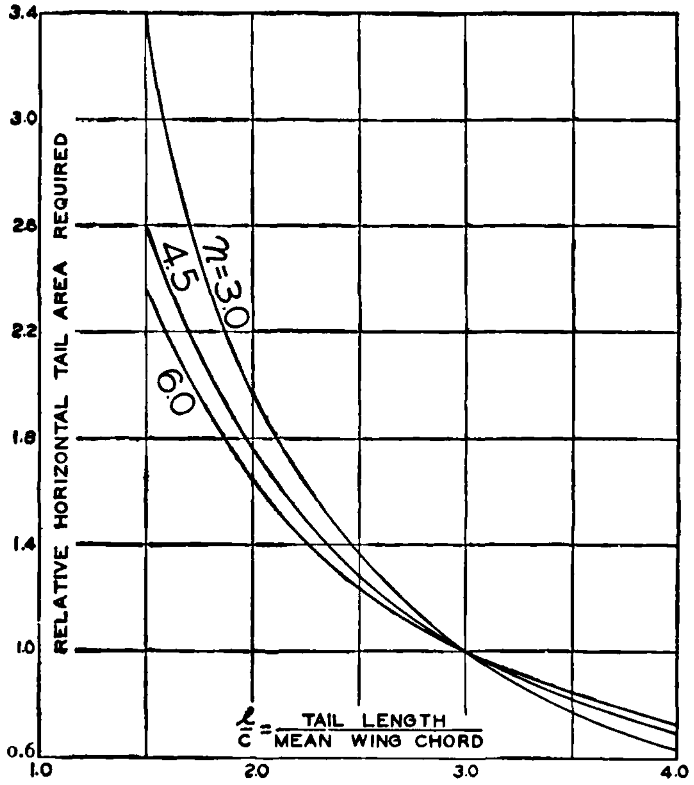

Figure 89. Effect of Tail Length on Tail Area Required for Constant Static Stability. n = Effective Aspect Ratio of Wings

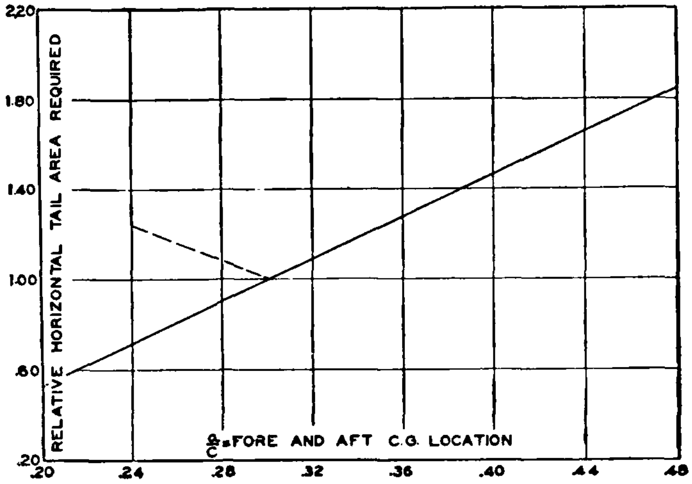

Figure 90. Effect of c.g. Location on Tail Area Required for Constant Static Stability

Turbulent Wake. In addition to the general downwash field behind a lifting wing, there is a narrow wake of highly turbulent flow and fairly low resultant velocity that persists many chord lengths down-stream. The effective velocity is reduced more than 10% for a thickness about equal to the wing depth in the region where a horizontal tail surface would be located. At the angles of attack where the horizontal tail surfaces lie within the wake, there will be an appreciable reduction in tail lift, usually apparent in the form of an inflection in the pitching-moment curves.

For all practical purposes, the center of the wake lies along a line drawn with the direction of the relative wind through the trailing edge of the wing. Consequently, if the tail surfaces are located below the wing chord line, the stability will be adversely affected at high speed, and if they are well above the chord line, the adverse effect will be at low speeds. Flight test data on monoplanes appear to favor the low tail location with a relative freedom from buffeting and with improved control at the stall.

Figure 91 shows the relative size and intensity of this wake according to N.A.C.A. tests.[2]

Stabilizer Setting for Trim. Trim at any speed requires that the pitching moment due to the tail surfaces be equal to the pitching moments due to the wings and the thrust. If the distance from the c.g. to the thrust axis is d and positive when the thrust axis is above the c.g., the thrust moment is $-Td$ and the thrust moment coefficient is

$$C_{ME} = -\, Td/qSc \tag{117}$$

Equating moments

$$C_{MT} = C_{MW} + C_{ME}$$

or

$$-\, C_{LT}\left(\frac{S_T}{S_W}\cdot\frac{l}{c}\right) = C_{M_0} - (a - x)\, C_L + 0.15h\, C_L{}^2 - C_{ME}$$

The tail lift coefficient is

$$C_{LT} = \alpha_T\,(dC_{LT}/d\alpha_T) = \alpha_T \cdot F_1 \cdot \eta_T$$

Hence, the angle of attack of the tail surface is

$$\alpha_T = -\left[\frac{C_{M_0} - (a - x)\, C_L + 0.15hC_L{}^2 - C_{ME}}{F_1\, \eta_T\left(\dfrac{S_T}{S_W}\cdot\dfrac{l}{c}\right)}\right] \tag{118}$$

Since $\alpha_T = \alpha_W + \beta - \epsilon$, where β is the absolute angle of attack of the stabilizer when the wing is at zero lift, it follows that

$$\beta = -\left[\frac{C_{M_0} - (a - x)\, C_L + 0.15hC_L{}^2 - C_{ME}}{F_1\, \eta_T\left(\dfrac{S_T}{S_W}\cdot\dfrac{l}{c}\right)}\right] - \frac{C_L}{F_1} + \frac{52C_LF_1}{n} \tag{119}$$

It is a matter of some interest and considerable importance that the change in stabilizer angle of attack, as repre-

---

[2] Rudolf Wallace, "Investigation of Full-Scale Split Trailing-Edge Wing Flaps with Various Chords and Hinge Locations," N.A.C.A. T.R. No. 539 (1935).

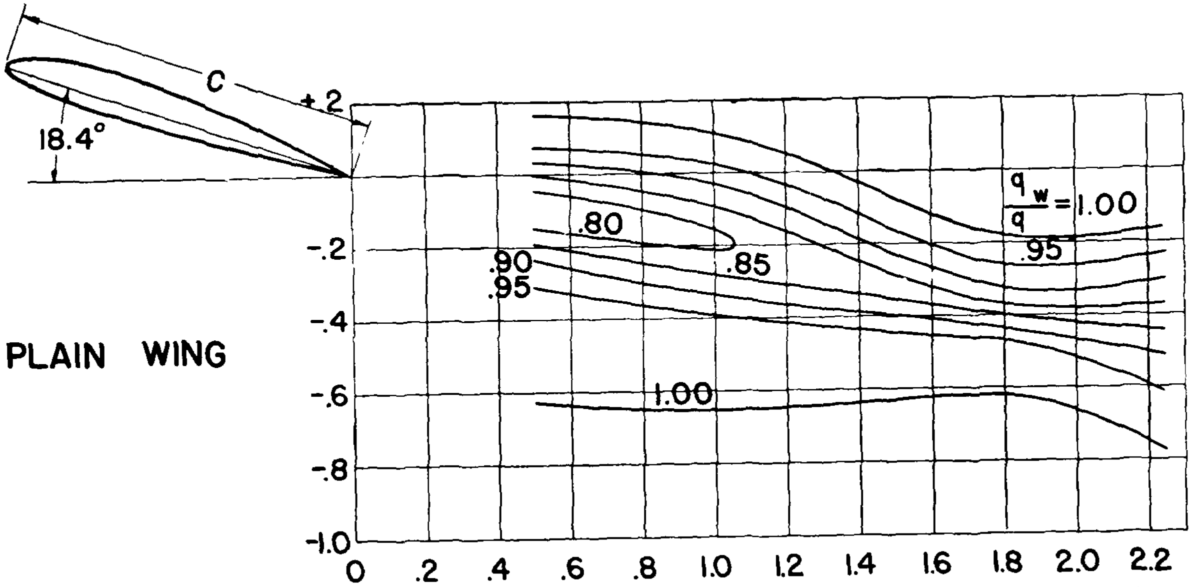

Figure 91a. Contours of Equal Resultant Velocity Around a Wing, Showing Turbulent Wake. Plain Wing

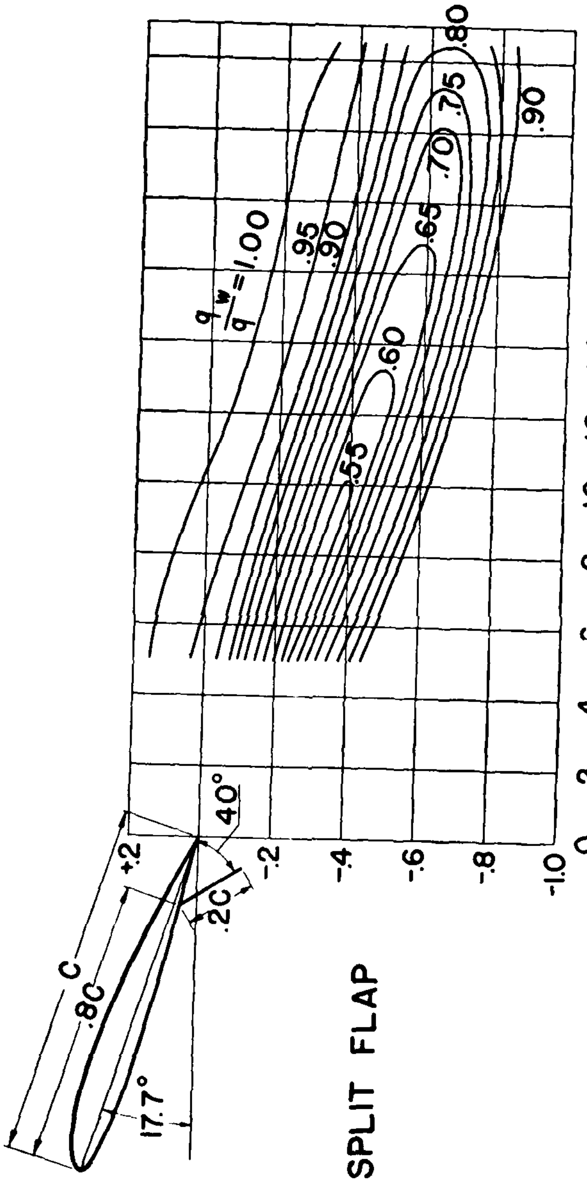

Figure 91b. Contours of Equal Resultant Velocity Around a Wing, Showing Turbulent Wake. Wing with Split Flap

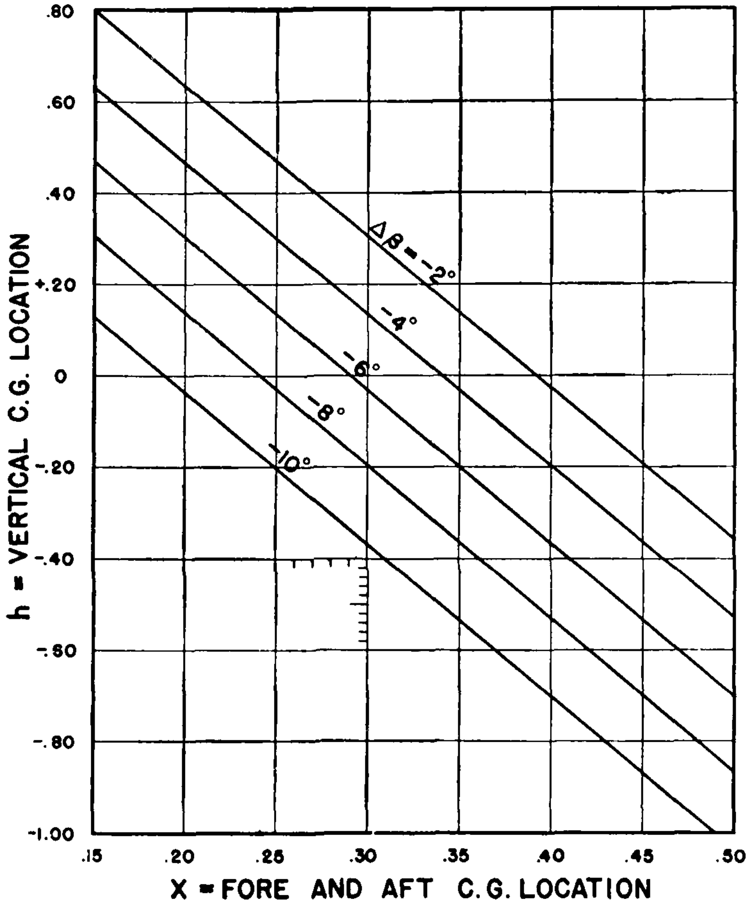

Figure 92. Effect of c.g. Location on Stabilizer Adjustment Required

sented by the last two terms on the right-hand side of equation (119), is practically independent of aspect ratio. The increased a_W required with low aspect ratio is compensated by increased downwash. $(a_W - \epsilon)$ at $C_L = 1.0$ varies from about 7° for $n = 4$ to 9° for $n = 15$. If the moment coefficient due to wings and thrust, as represented by the numerator of the term within brackets, is constant, the change of stabilizer setting between any two lift coefficients is $a_W - \epsilon$. A small range in required stabilizer setting is secured when the c.g. coordinates x and h are such that the term within the brackets becomes more positive with increasing C_L. If the stabilizer adjustment is to be satisfactorily replaced by servo-flap control on the elevators $d\beta/dC_L$ must be small. Since

$$\frac{d\beta}{dC_L} = \frac{-(a - x) + 0.30hC_L}{F_1\,\eta_T\left(\frac{S_T}{S_W}\cdot\frac{l}{c}\right)} - \frac{1}{F_4} + \frac{52\,F_2}{n} \qquad (120)$$

Substituting average values gives, at $C_L = 1.0$

$$d\beta/dC_L = -\,40\,(0.24 - x) + 0.30\,h - 8$$

Solution of this equation for assumed values of $d\beta/dC_L$ gives the average required range in stabilizer adjustment as plotted on Figure 92.

Servo-Controlled Elevators: Tabs. An inset adjustable portion of a movable control surface is known as a "tab." When deflected in one direction, the force due to the tab tends to move the main control in the opposite direction. Tabs are used for control of trim, for example, to replace an adjustable stabilizer, or as a balancing device. Five distinct types of tabs are in use. These are as follows:

1. *Fixed trimming tab:* Adjustable on ground only. Sometimes used on ailerons or rudder.
2. *Controllable trimming tab:* Adjustable in air. This is the usual type.

3. *Balancing tab:* In this type the tab is moved by fixed linkage in a direction opposite to control motion.
4. *Balancing and controllable trimming tab:* In this type an adjustment of the linkage of balancing tab provides a trim control.
5. *Servo-control tab:* In this type the control wires are attached to the tab only, and there is no direct connection with the main movable control.

If the stabilizer adjustment is to be satisfactorily replaced by a trim tab, certain conditions must be met as follows:

1. The required range in stabilizer adjustment must be small or moderate, preferably not more than 6°.
2. The fixed surface must be set at an angle that allows ample landing control.
3. In the larger sizes, the elevators should be provided with some form of aerodynamic balance.

Condition 1 can be met only by proper adjustment of the fore-and-aft and vertical c.g. location, as shown on Figure 92. Tabs are usually more effective on low-wing designs than on high-wing designs.

The curves of Figure 93 should be considered in tab design. These curves give the elevator angular movement which is equivalent to a given required stabilizer adjustment, as a function of the ratio of the elevator area to total horizontal area. It will be seen that there is little to be gained, in the form of additional control, from increasing the elevator area above about 45% of the total. Since the hinge moment of a movable surface increases more rapidly than its chord, it is probably undesirable to use elevators greater than about 50% of the total horizontal area, while experience indicates that the ratio should not be less than about 40%.

When tabs are used, it is very important that the stabilizer setting be correctly chosen. The limiting condition is obviously one in which full-up elevator just gives sufficient control for landing with forward c.g. In this connection the tab opposes the elevator control and reduces the control force by an amount roughly equivalent to about 6° to 10° elevator throw. Furthermore, the tab effectiveness falls off rapidly as the control is moved from its neutral position. Hence, it is necessary, not only to adopt a stabilizer setting that gives trim with neutral elevator at a fairly low speed, but also to provide the additional upthrow on the elevator required to compensate for the loss in effectiveness due to the tab. It is also desirable that the tab operating device be irreversible or self-locking at the elevator hinge axis to avoid any tendency for flutter.

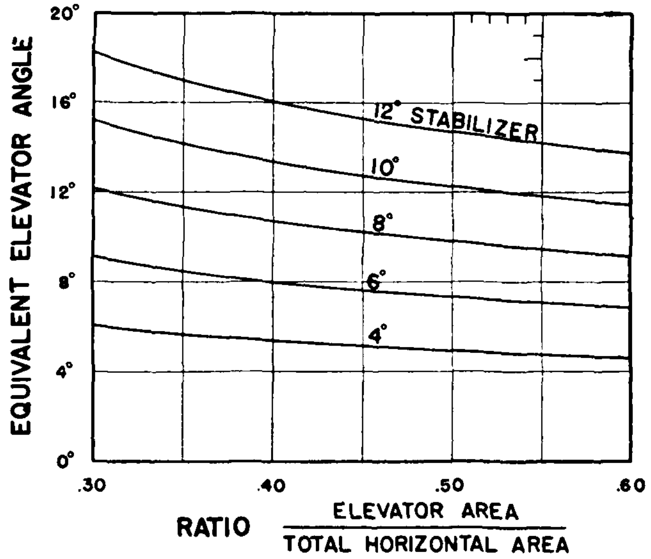

Figure 93. Effect of Elevator Area on Elevator Angle Equivalent to Given Stabilizer Angle

Very narrow tabs extending over a considerable length of the elevator trailing edge have been reported less desirable than a deeper, shorter-span tab. The short-span tab is less critical in its setting, and it is effective over a greater range in elevator angle. Very satisfactory control over trim has been obtained with a tab area between 5% and 8% of the elevator area, a tab chord between 20% and 25% of the elevator chord, and a tab span between 20% and 40% of the elevator span.

Plan-Form of Horizontal Tail Surfaces. Figure 94 gives the most frequently used plan-forms for horizontal tail surfaces. Form **A** is approximately rectangular with a modified elliptical tip. Form **B** has a circular or elliptical tip with raked, but straight, leading and trailing edges. Form **C** is elliptical, and Form **D** is approximately parabolical or triangular in shape. Form **D** is generally con-

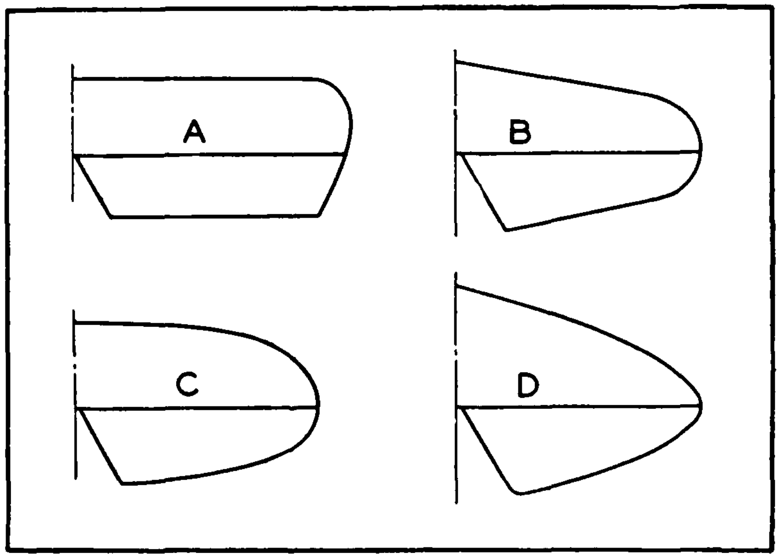

Figure 94. Tail Surface Plan-Forms

sidered undesirable. Hübner[3] states that, "Elevators excessively tapered in plan produced absolutely inadequate effects." Either form **B** or form **C** is satisfactory.

Tail Surface Sections. If the tail surfaces are to give maximum stabilizing and control effects, the section must be carefully chosen with regard to thickness and aerodynamic effects. For reasons not always fully understood, unsatisfactory results have been obtained in many airplanes where the thickness ratio of the tail surface section exceeded 10%. In one case reported by Carroll,[4] the objectionable action was eliminated by a thickening of the rudder with a plausible explanation that the original thin rudder had been shielded by the thick fin and that it was necessary to move the trailing edge to the outer boundary of the detached turbulent flow before any rudder action was evident. A similar thickening of the rudder has been beneficial in a number of cases, although wind-tunnel tests have failed to show any "dead center" effect in the normal force coefficient.

It is advisable to use a section with a thickness ratio not greater than 10%, but in some cantilever types this will be too thin. If it is necessary to exceed 10% thickness ratio, the area of the control surfaces, both fixed and movable, should be made larger than normal to counteract the loss in effectiveness.

The NACA–00 sections described in Technical Note No. 385 are considered especially desirable for tail surfaces. There is very little advantage in selecting a section on the basis of minimum drag coefficient since the differences are negligible for the normal condition with displaced controls. Also, a low value of C_L maximum on a basic section is of no particular significance owing to the pronounced change due to the introduction of effective camber with a displaced control.

---

[3] W. Hübner, "Erfahrungen bei Flugeigenschaftsprüfungen im Jahre 1927–1928," ZFM, April 29, 1929, pages 189–195.

[4] T. Carroll, "The Elimination of Dead Center in the Controls of Airplanes with Thick Sections," N.A.C.A. T.N. No. 119 (1922).

Effect of Flaps on Horizontal Tail Area. The horizontal tail-surface area required to balance and stabilize a wing fitted with a high-lift device must be checked against its ability to counteract the excessive diving moment. Assuming that the tail surface is developing full lift, the equation of equilibrium is

$$C_{LT} \cdot qS_T l = C_{MW}\, qS_W c$$

or

$$\frac{S_T}{S_W} \cdot \frac{l}{c} = \frac{C_{MW}}{C_{LT}}$$

where C_{MW} is the maximum negative wing moment with full-flap deflection. C_{MW} is referred to the airplane c.g. by the use of equation (49).

Various wind-tunnel tests on tail surfaces with full-up elevators[5] are in reasonable agreement and show a maximum value for C_{LT} of the order of -1.0. Hence, with flaps or other high-lift devices, the horizontal tail area must not be less than required by the relation

$$\frac{S_T}{S_W} \cdot \frac{l}{c} = -\,C_{MW} \tag{121}$$

It may require as much as 100% increase in horizontal tail area to satisfy this condition, which insures that the tail does not stall in the attempt to provide the necessary balancing moment.

The adverse effects of high-lift devices on static longitudinal stability appear to be confined chiefly to troubles arising from stalled tail surfaces.

---

[5] R. H. Smith, "Lift, Drag and Elevator Hinge Moments of Handley Page Control Surfaces," N.A.C.A. T.R. No. 278 (1927).

Vertical Tail Area. The area of the vertical tail surfaces required to insure adequate directional stability depends on the gross weight, the wing area, the span, the moment arm or tail length, and also on the projected side area of the major unstable components such as fuselage, hull, floats, nacelles, etc.

The unstable moment due to fuselages has been calculated from the test data on the series for which drag data are given in Chapter 9. As might be expected, there are large variations in cross-wind force and in the center of pressure, but these variations are found to give reasonably constant moment coefficients based on the side area and overall length. Various methods of presenting these data are available, but the most useful form appears to be that presented in Figure 95, in which the stabilizing area coefficient is plotted against fore-and-aft yawing axis location. The stabilizing area coefficient is

$$K_V = \frac{S_V}{S_B}\frac{l}{L}\left(\frac{dC_{LF}}{d\psi}\right)\eta_F \qquad (122)$$

where S_V is the vertical tail area necessary to stabilize the fuselage, S_B is the projected side area of the fuselage, l is the distance from the c.g. to the center of vertical tail area, or the "tail length," L is the total overall length of the fuselage, $dC_{LF}/d\psi$ is the slope of the lift curve for the vertical tail surface and η_F is the tail efficiency.

Figure 96 gives a plot of data on seaplane floats. The average slope is practically identical with that found for fuselages in Figure 95, but there is a marked vertical shift in the value of K_V. The explanation of this difference is to be found in the theoretical moment on a streamline body. According to Munk,[6] there should be a couple of the magnitude

$$N = q\ (\text{volume})\ (k_2 - k_1) \sin 2\psi \qquad (123)$$

---

[6] Max M. Munk, "Fundamentals of Fluid Dynamics for Aircraft Designers," Ronald Press Company (1929).

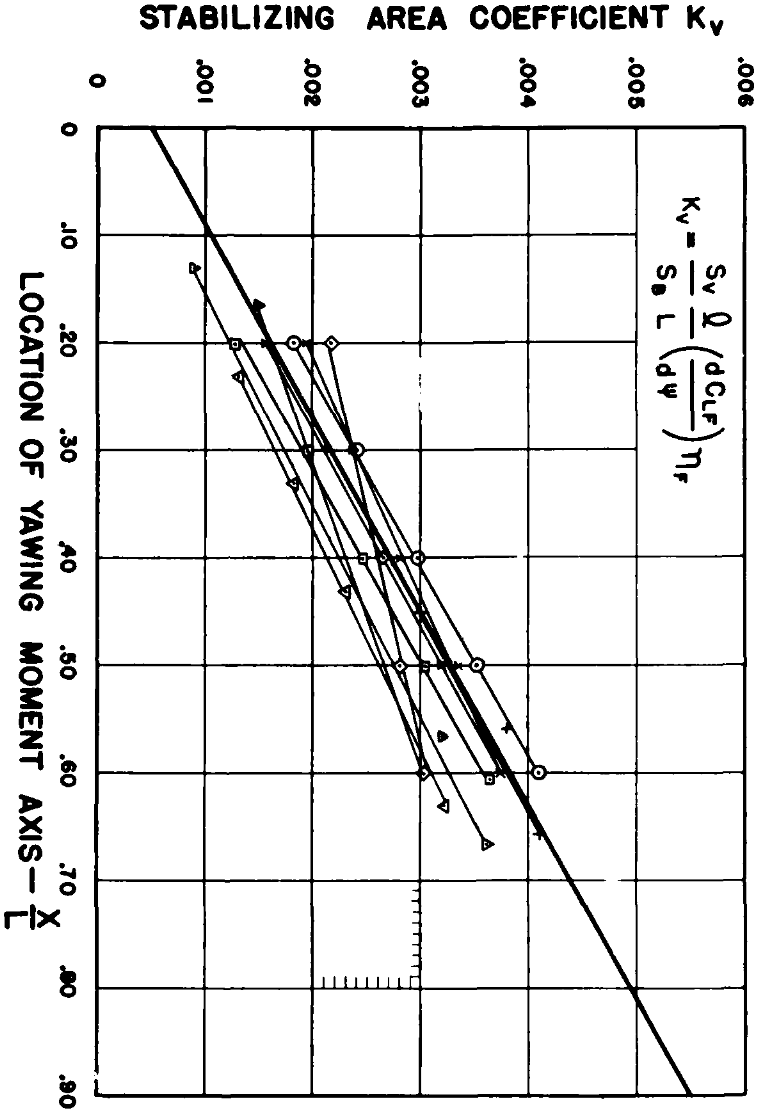

Figure 95. Stabilizing Area Coefficients for Fuselages

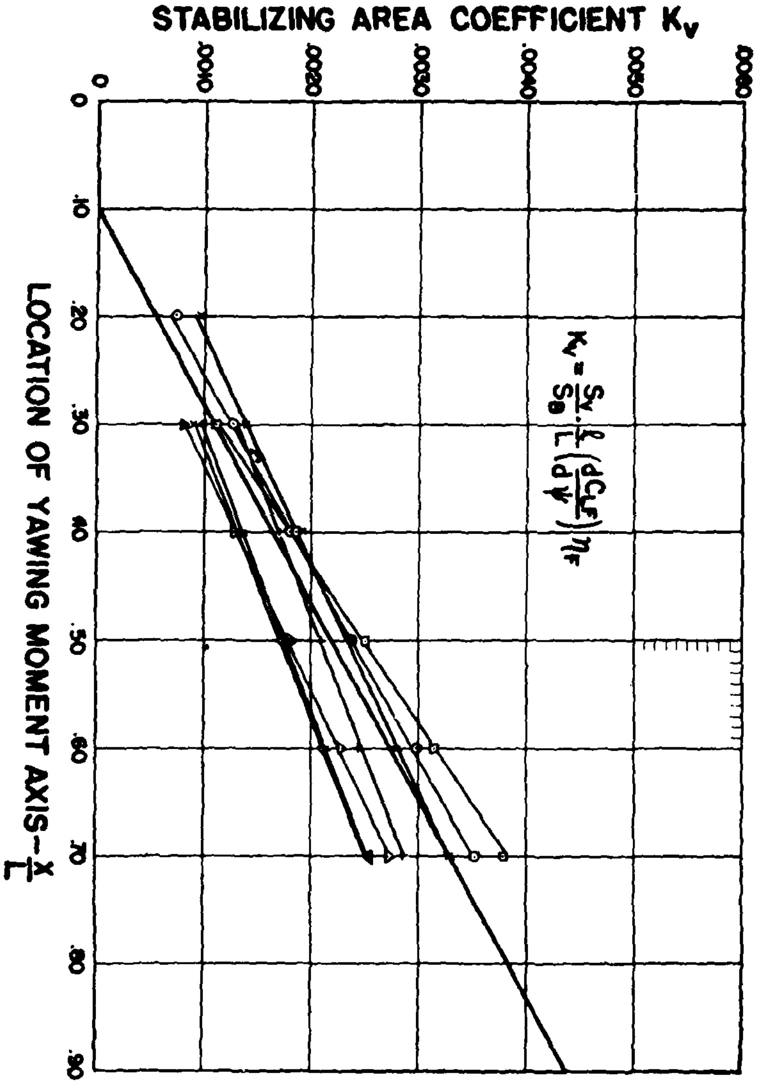

Figure 96. Stabilizing Area Coefficients for Seaplane Floats

Since the projected side area S_B varies as LD, and the volume varies as LD^2, the moment coefficient and hence the value of K_V should be given by

$$K_V \propto \frac{(k_2 - k_1)}{(L/D)} \qquad (124)$$

where $(k_2 - k_1)$ is the difference in the coefficients of additional mass. From this equation, it is obvious that the value of K_V decreases as the ratio of length to diameter increases. The relative values of K_V have been calculated from equation (124) and are plotted on Figure 97. For the fuselages in Figure 95 the average value of L/D was about 5.6. For the floats in Figure 96, the average value of L/D was about 10. If it be assumed that the theoretical variation in K_V is correct for an axis location at the center of volume (about 45% L) then the test data agree almost exactly with the theoretical ratio. While the theory calls for a couple and, hence, a moment independent of the axis location, the test data for definite angles of yaw show the variation indicated by Figures 95 and 96. It is logical therefore, in applying these data to use the slope indicated by the tests and to determine the moment about the center of volume from the theoretical variation in Figure 97. Such a plot is given in Figure 98 and it may be used for fuselages, floats, hulls, nacelles, and struts.

Analysis of numerous wind-tunnel tests for slopes of the curves of yawing moment indicates that the desirable slope is given by

$$dN/d\psi = -0.000050\ qWb$$

or

$$dN/d\psi = -0.000050(W/S)\ qSb \qquad (125)$$

where W is the gross weight in pounds, S the wing area in square feet, and b the span in feet.

The restoring moment due to the vertical fin surface is

$$dN_F/d\psi = -\ (dC_{LF}/d\psi)\ \eta_F\ qS_V l \qquad (126)$$

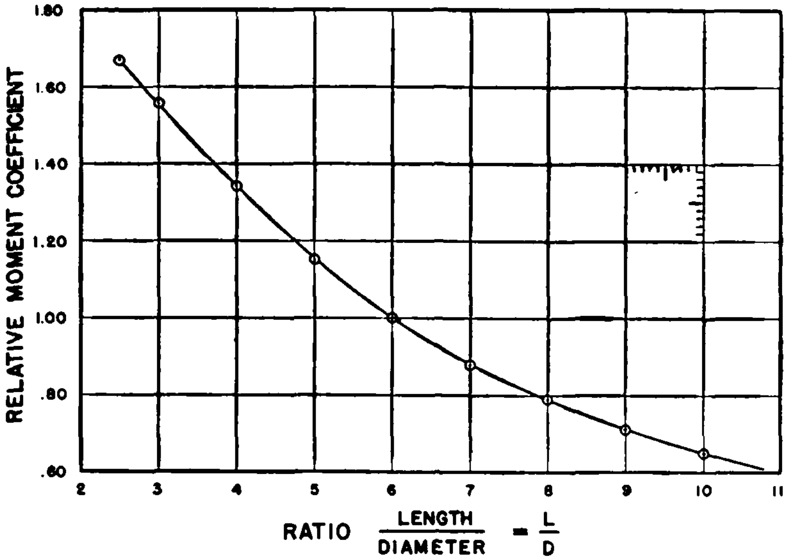

Figure 97. Effect of Fineness Ratio on Yawing Moment Coefficient

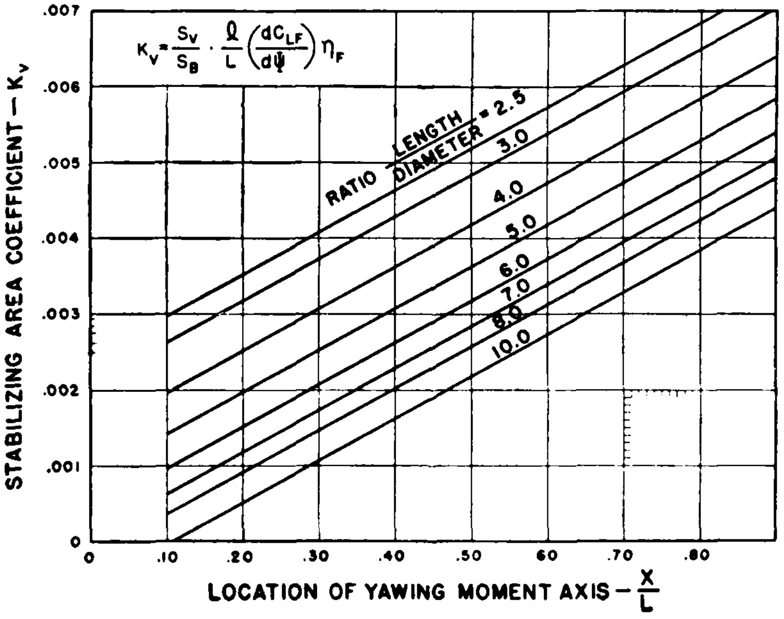

Figure 98. Stabilizing Area Coefficient

where $dC_{LF}/d\psi$ is the slope of the lift curve for the vertical tail, η_F is the efficiency of the vertical tail surface, S_V is the vertical tail area, and l is the tail length.

The desired directional stability is obtained when the vertical tail area is sufficient to counteract the unstable moment of fuselage, hull, floats, or nacelles, and to provide the additional stabilizing moment required by equation (125). The vertical area may be considered in two components: ΔS_{V_1} required to neutralize the unstable moments produced by fuselage, hull, or other parts of the airplane, and ΔS_{V_2} required to provide the desired directional stability. With this consideration, ΔS_{V_1} is obtained by summation of the ΔS_{V_1} values for each major unstable part. Each ΔS_{V_1} value is obtained by solution of equation (122),

$$\Delta S_{V_1} = K_V \frac{L}{l} \frac{S_B}{(dC_{LF}/d\psi)\ \eta_F} \tag{127}$$

The value of ΔS_{V_2} is obtained by solution of equations (125) and (126) giving

$$\Delta S_{V_2} = \frac{0.00005\ (W/S)\ Sb}{(dC_{LF}/d\psi)\eta_F \cdot l} \tag{128}$$

The required vertical fin area is

$$S_V = \Sigma\ (\Delta\ S_{V_1}) + \Delta\ S_{V_2} \tag{129}$$

The value of the slope of the fin lift curve depends on several indeterminate factors that affect the tail efficiency, but the average effective slope is given by Figure 99 which is based on tests of low aspect ratio airfoils and fin surfaces.

For preliminary layouts, the designer may desire to estimate the side area of a fuselage or float rather than go to the trouble of calculating the area. For all of the shapes likely to be used

$$S_B = K\ L\ D \tag{130}$$

in which L is the overall length and D the maximum depth.

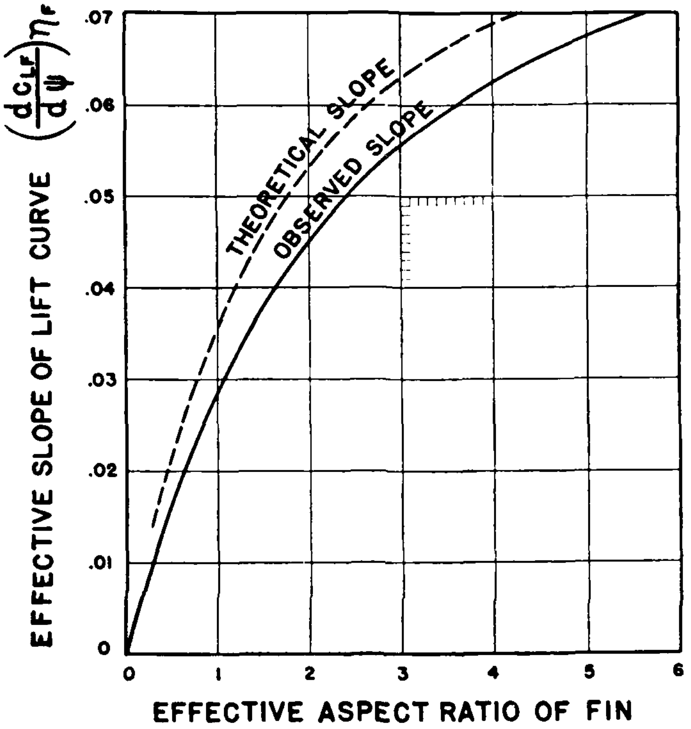

Figure 99. Slope of Lift Curve for Vertical Tail Surfaces

K varies from about 0.70 for a true streamline form with pointed stern to about 0.80 for a deep, full fuselage with a vertical stern post.

As an example of calculation of vertical fin area, consider an airplane having the following characteristics:

W = 2,660 lb S_W = 243 sq ft
W/S = 10.95 lb/sq ft
Span b = 30.1 ft
Tail length l = 15.4 ft
Fuselage length L = 21.0 ft
" depth D = 4.0 ft
" yawing axis, x = 5.8 ft aft of nose

Fuselage yawing axis, $x/L = 0.28$
" ratio $L/D = 5.2$
" $K_V = 0.0023$

Tail aspect ratio 1.4 $\left(\frac{dC_{LF}}{d\psi}\right)\eta_F = 0.037$

Fuselage side area $S_B = 0.775 \times 21 \times 4 = 65$ sq ft

$$\Delta S_{V_1} = 0.0023 \times 65 \times \frac{21.0}{15.4} \times \frac{1}{0.037} = 5.52 \text{ sq ft}$$

$$\Delta S_{V_2} = 0.00005 \times \frac{10.95 \times 243 \times 30.1}{0.037 \times 15.4} = \underline{7.02}$$

Total area $S_V = 12.54$ sq ft

Wind-tunnel tests on a model of this airplane with $S_V = 9.80$ sq ft gave a negative yawing moment slope of -0.0000327. Of the 9.8 sq ft on the model, 5.52 were required to counteract the fuselage moment. The difference, $9.80 - 5.52 = 4.28$ sq ft was available for stabilizing the airplane. Hence, the slope with 9.80 sq ft should have been

$$\frac{4.28}{7.02} \times (-0.000050) = -0.0000305$$

which checks with the observed value of -0.0000327.

Rudder Area. Experience has shown that satisfactory directional control is obtained when the rudder can neutralize the effect of a yaw angle approximately equal to the rudder throw. For example, a 10° rudder angle ($\delta_r = 10°$) should hold about 10° angle of yaw. This condition is obtained when the normal force on the vertical tail surfaces at +10° yaw and with −10° rudder angle is equal to the normal force at +10° yaw on that part of the fin area ΔS_{V_1} required to stabilize the fuselage and other unstable components. In general, this condition requires that the rudder area be somewhat less than ΔS_{V_2}. The ratio of rudder area to total vertical area as a function of the ratio of stabilizing fin area S_{V_1} to total fin area has been calculated from Munk's tests[7] and is given in Figure 100. Points are given on this figure as circles for four airplanes for which wind-tunnel and flight test data indicate normal rudder control.

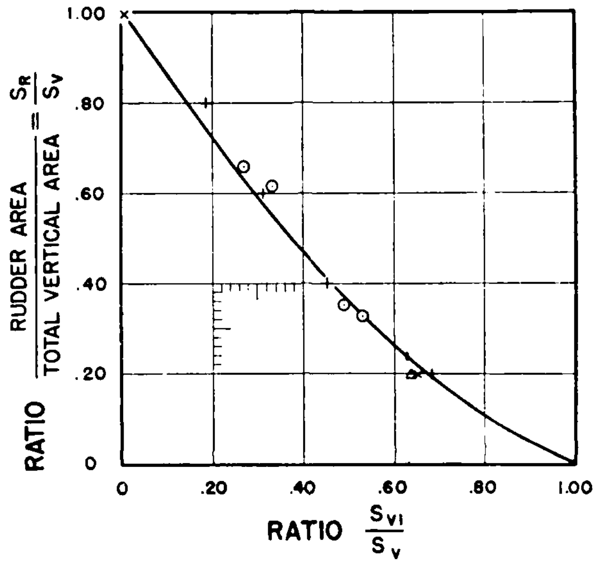

Figure 100. Ratio of Rudder Area to Total Vertical Fin Area

Effects of Dihedral. In a wing having dihedral, the tips are raised with respect to inboard sections to form a flat transverse "Vee." The effect of dihedral on lateral stability is very powerful. This effect is sometimes erroneously ascribed to the difference in the projected area of the two sides, but the change in projected area is obviously negligible for the angles actually used. The correct explanation of the effect of dihedral is found in the equal and opposite changes in angle of attack on the right and left wings. This change in angle of attack is shown in the sketch, Figure 101, to be in radians

$$\Delta\alpha = \psi \cdot \gamma \qquad (131)$$

---

[7] Max M. Munk, "Systematische Versuche an Leitwerkmodellen," Technische Berichte I-5, page 168.

where ψ is the angle of yaw and γ is the angle of dihedral. The corresponding change in lift coefficient is

$$\Delta C_L = \psi\gamma\,(dC_L/d\alpha) \tag{132}$$

The change in lift on each side of the center-line is $\Delta L = \Delta C_L\, q\, S/2$ and the average moment arm is $b/4$. Hence, the rolling moment due to dihedral is

$$L = \psi \cdot \gamma \left(\frac{dC_L}{d\alpha}\right) q\, S\, b/4 \tag{133}$$

Measured rolling moments for airfoils with dihedral show good agreement with the values calculated by this

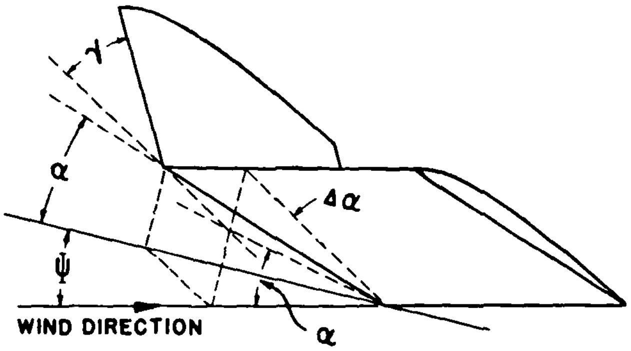

Figure 101. Effect of Dihedral in a Side Slip

equation. For airplane models, the agreement is less satisfactory owing to the disturbing effects of vertical fin surfaces. In many cases the dihedral is confined to the outboard portion of the wing. For such cases S should be the actual area in the portion having dihedral, and instead of $b/4$ the actual arm to the center of the area should be used. The angles and slopes in equation (133) are measured in radians.

The yawing moment due to dihedral may be calculated from the change in induced drag. Since the induced drag coefficient varies as C_L^2, or as $(C_L + \Delta C_L)^2$, the change in induced drag varies as $2\ C_L \cdot \Delta C_L$ or

$$\Delta C_{Di} = 2C_L \cdot \Delta C_L/\pi n$$

substituting the value of ΔC_L from equation (132) gives

$$\Delta C_{Di} = \frac{2C_L}{\pi n} \psi\gamma \frac{dC_L}{d\alpha} \tag{134}$$

on each side the change in drag is

$$\Delta D = \Delta C_{Di}\, qS/2$$

producing a yawing moment of

$$\begin{aligned} N &= 2 \cdot \Delta D \cdot b/4 \\ &= \frac{2C_L}{\pi n} \left(\frac{dC_L}{d\alpha}\right) \psi\gamma\, qS \frac{b}{4} \end{aligned} \tag{135}$$

Yawing moments calculated from this equation are in good agreement with test data except at small values of α and γ where other effects appear to predominate.

Dihedral Required. The proper amount of dihedral depends, in a complex relation, on various factors such as fin surface, rudder and aileron effectiveness, fuselage shape, wing location on the fuselage, wing span, and plan-form. It seems definitely proved that the best results were obtained with not less than 3° dihedral on a high-wing monoplane for which 6° appeared a little too much with the aileron control provided. There is considerable evidence to show that more dihedral should be used on low-wing than on high-wing monoplanes, more on tapered wings than on rectangular wings, more with seaplanes than with landplanes. 6° or more will not be too much for low-wing monoplanes with appreciable taper. Additional dihedral should be used when there is considerable fin area below the c.g.

The tremendous influence of dihedral can perhaps best be illustrated by quoting verbatim a section of the excellent report by Weick, Soulé, and Gough[8] on a series of tests on a high-wing monoplane.

"With 0° dihedral, the airplane was definitely unstable laterally. When deliberately caused to sideslip in either direction, it would turn in the direction of the initial slip and spiral indefinitely, whether the controls were freed or returned to neutral. By an increase of the dihedral to 3°, the stability characteristics were somewhat improved. In this condition, the airplane was unstable only with the controls freed. With the controls neutralized, the airplane would recover to straight flight after a few oscillations. With 6° dihedral, the airplane was stable, both with free controls and with the controls returned to neutral.

"The airplane exhibited instability of a different type with 9° dihedral and controls free. When sideslip was started to the right, for example, and the controls freed, the airplane would turn directly to the left away from the initial sideslip (whereas with 0° dihedral, it had turned *into* the sideslip) and would commence a left nose-down spiral accompanied by a rapidly increasing airspeed. When the controls were returned to neutral during a sideslip, the airplane returned to straight flight with no apparent oscillation.* * *

"With the wing set at 0° dihedral, the rudder gave almost independent directional control, the banking due to the yaw produced being very slight when the ailerons were held in neutral. Turns could be made without the ailerons, but they were characterized by skidding during entry and sideslipping during recovery, the amount depending on the abruptness with which the rudder was used.* * * The increased banking effect obtained with 3° dihedral eliminated all tendency of the forward wing to dig in and made sideslips easier to perform. The effect was noticeable also when rudder turns were made. Tight, or steeply banked, rudder turns, however, were difficult to enter as the airplane would nose down during the time taken to roll to the desired angle of bank. If an attempt was then made to bring up the nose with the rudder, the airplane would start sideslipping and would roll out of the bank. The airplane always banked in the direction of the turn set up by the rudder, whether the ailerons were set in neutral or freed. With 6° dihedral, the rudder had a powerful banking effect and it was difficult, with full aileron deflection, to hold the wings level for any but small amounts of sideslip. The roll that could be generated by the rudder at 9° dihedral was so great that the rudder had to be handled with discretion, and sideslipping was practically impossible. With 6° and 9° dihedral, the airplane showed a progressively greater tendency than at 3° to nose down and roll out of rudder turns."

---

[8] F. E. Weick, H. A. Soulé and M. N. Gough, "A Flight Investigation of the Latera Control Characteristics of Short Wide Ailerons and Various Spoilers with Different Amounts of Dihedral," N.A.C.A. T.R. No. 494 (1934).

Ailerons. An outstanding result of the National Advisory Committee for Aeronautics research on lateral control at low speeds appears to be a vindication of the aileron as a lateral control device. When the lateral control is unsatisfactory, the ailerons take the full blame although there may be a number of contributing factors. It is a highly significant fact that there are a few airplanes fitted with simple ailerons that show excellent control up to the stall.

Lateral control is inseparably coupled with directional control in normal flight and good lateral control, therefore, means good directional control also. The effect of dihedral on apparent lateral control is very powerful. An airplane having sufficient dihedral to insure lateral stability may appear to have very much better lateral control than it actually has. This has been discussed under dihedral.

Good lateral control requires that the rolling moment available from the ailerons be sufficient to give desired angular accelerations and to overcome adverse moments. The rolling moment coefficient is defined as

$$C'_l = \text{rolling moment}/qbS \tag{136}$$

where b is the wing span. Since it is a moment and not a moment coefficient that moves the airplane, the desirable value of C'_l will depend on both q and b. In other words, it is easy to get good lateral control when q and b are large, that is, for moderate or high stalling speeds with a comparatively large span. Conversely, it is difficult to get good lateral control with very low stalling speed and a comparatively short span. This reduction in lateral control is sometimes very marked where there is a large reduction in stalling speed with high-lift devices. The amount of aileron area required, therefore, varies in some inverse ratio of stalling speed and span.

The most effective aileron has a span about 60% of the wing semi-span and a chord about 20% of the wing chord. Very effective ailerons have been made with a chord ratio as low as 15% or as high as 25%, but these ratios should not be exceeded without good reason. Values of the chord ratio below 18% should be accompanied by provision for increased throw of the ailerons. This is particularly important on narrow, tapered ailerons. If possible, the aileron should extend to the tip of the wing. Thinning the tip of the wing and incorporating washout appear to give a definite improvement in lateral control.

On a biplane, it is desirable to use ailerons on both wings. The argument that the upper wing stalls first is probably correct, but ailerons on the lower wing only have not been entirely satisfactory. For one thing, the curvature they produce in the flow over the upper wing opposes the desired roll.

The mechanical details of the aileron control system are highly important in affecting the pilot's impressions of lateral control. Particular attention must be taken to avoid binding at the hinges due to aileron and wing flexure. Another source of trouble is found in short bellcrank arms that cause high loads on bearings with local structural distortion and high control forces.

Aileron Area Required. The effectiveness of an aileron, as measured by the rolling moment due to a given setting, varies with the aileron span and chord. It may be shown[9] from test data that the variation of efficiency with chord is given by

$$\eta_1/\eta_0 = 1.50 - 2.00\,(t/c) \tag{137}$$

where t is the aileron chord and c the total wing chord, including the aileron chord. In a similar manner the variation of efficiency with span is

$$\eta_2/\eta_0 = 1.20 - 0.60\,(l/b) \tag{137a}$$

where l is the aileron span and b the wing span.

Assuming that satisfactory control is given by an aileron of the proportions $t/c = 0.25$ and $l/b = 0.40$, it is possible to calculate the proportions of all other ailerons having the same effectiveness in producing rolling moments. The assumed aileron has $S_a/S_W = 0.10$, where S_a is the aileron area and S_W the wing area. The relative efficiencies are $\eta_1/\eta_0 = 1.00$ and $\eta_2/\eta_0 = 0.96$, and the "effective area" is the product of these efficiencies by the actual area, or

$$S_e = 0.10 \times 1.00 \times 0.96 = .096$$

The proportions of all ailerons having this effective area are given by

$$t\left[1.50 - 2.00\left(\frac{t}{c}\right)\right] \cdot l\left[1.20 - 0.60\left(\frac{l}{b}\right)\right] = 0.096\,bc \tag{138}$$

---

[9] W. S. Diehl, "Notes on the Design of Ailerons," N.A.C A. Technical Note No. 144 (1923).

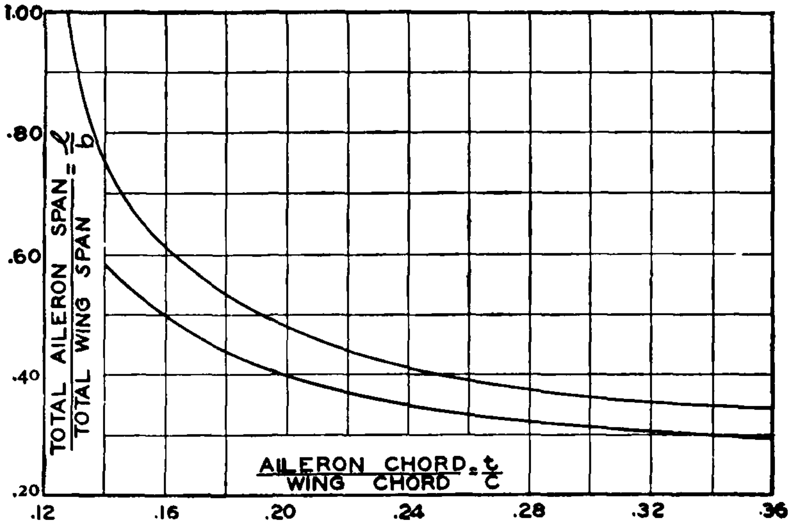

Figure 102. Aileron Proportions. Relative Span and Chord

If the satisfactory aileron proportions be assumed as $t/c = 0.20$ and $l/b = 0.40$, the proportions of equivalent ailerons are given by

$$t\left[1.50 - 2.00\left(\frac{t}{c}\right)\right] \cdot l\left[1.20 - 0.60\left(\frac{l}{b}\right)\right] = 0.0843\, bc \quad \textbf{(138a)}$$

Figure 102 is a plot of l/b against t/c and Figure 103 is a plot of S_a/S_W against t/c as calculated from the two equations. These are not the extreme limits for satisfactory ailerons, but the best results have been obtained from approximately the proportions given.*

An aileron when displaced from the neutral position affects the lift distribution over the whole wing, but chiefly over that part of which it forms the trailing edge. If the total wing area thus affected is S_e with the center of this area at a distance $d/2$ outboard from the fore-and-aft axis of the airplane, then a convenient measure of control effectiveness is given by

$$K_a = \frac{d}{b} \cdot \frac{S_e}{S_W} \tag{139}$$

where b is the span and S_W the total wing area. S_e is the total area, including the aileron area, in the way of the ailerons.

Figure 104 is a plot of K_a against $E = t/c$ showing the variation of K_a for constant control effectiveness corresponding to three ailerons as follows:

I. $l/b = .40$ $t/c = .25$
II. $l/b = .40$ $t/c = .20$
III. $l/b = .40$ $t/c = .15$

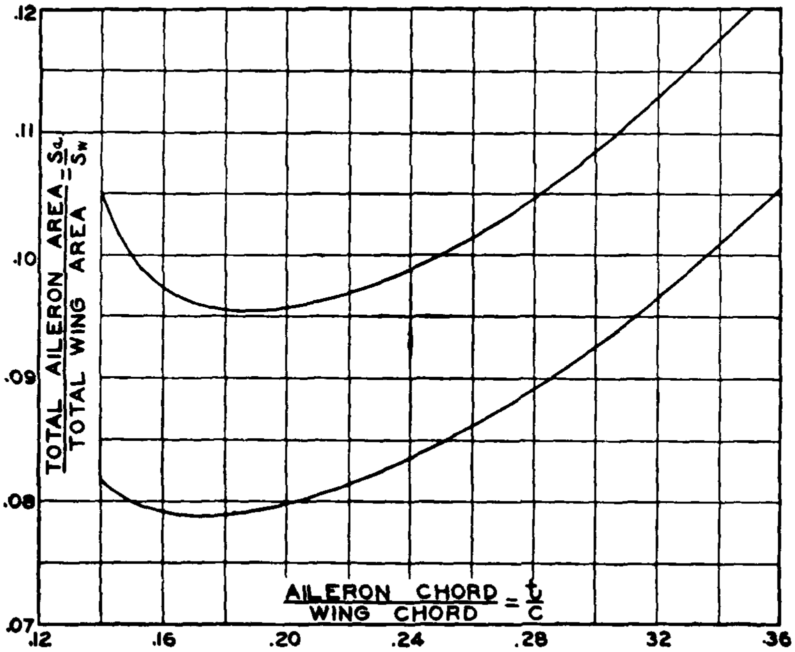

Figure 103 Aileron Proportions. Relative Area and Chord

Values of K_a for various airplanes are spotted on Figure 104 with a circle for normal control, a triangle for excellent control, and a square for unsatisfactory control. All airplanes having a value of K_a equal to or better than that required for Case II have been reported good or excellent.

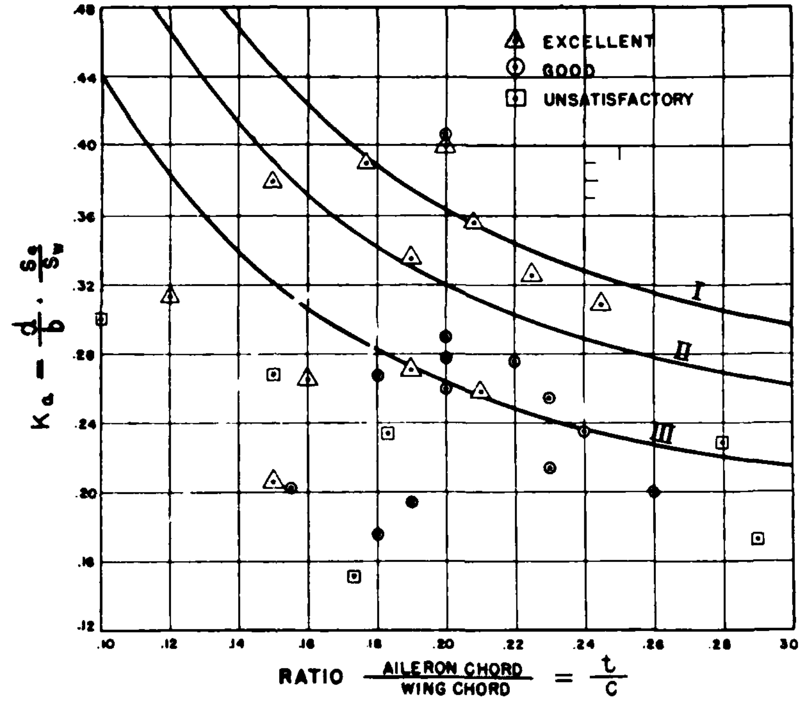

Figure 104. Aileron Coefficient K_a

It is significant that most of the unsatisfactory cases appear deficient in area.

Aileron Types. Figure 105 illustrates eight types of wing tips and ailerons. Types **A** and **B** are simple ailerons on elliptical tips. These are very satisfactory types and should be used whenever practicable on all high-speed airplanes. Types **C** and **D** are simple ailerons on modified elliptical tips. These forms are in extensive use and are entirely satisfactory. The inset type of aileron, formed from the inner portion of Type **D**, may be used with slow-speed airplanes having unusual flexibility in the wing tip. In such airplanes the aileron action may be opposed by the wing twist accompanying the use of an aileron extending to the tip.

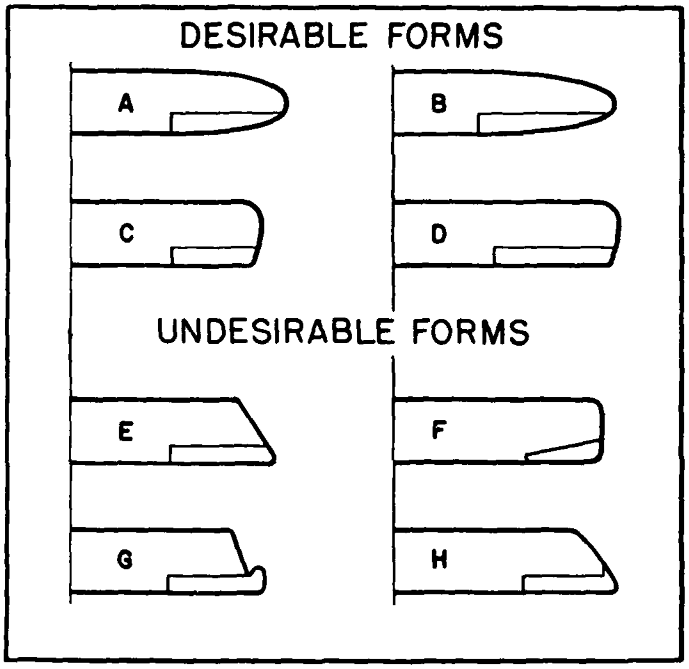

Figure 105. Aileron Types

Types **E**, **F**, **G**, and **H** are undesirable for various reasons. All of these tend to be heavy on control owing to the peak in loading at the tip. Types **G** and **H** should never be used on high-speed designs owing to probability of flutter.

Balanced Controls. Elevators, rudders, and ailerons are often "balanced" in order to reduce control forces. For small or moderate-sized airplanes the chief reason for balancing is to improve maneuverability, but for large airplanes it is necessary in order that the control forces do not exceed the pilot's strength. The most desirable type of balance varies with the use and size of the control surface. For example, what is probably the most satisfactory type of balance for a rudder is unsuited for an aileron on a high-speed airplane.

In general, no type of aileron balance should be considered satisfactory unless it allows the use of an efficient wing tip, and tends to bring the aileron c.g. near to the hinge axis. Likewise, no type of rudder balance can be considered satisfactory if it reduces the maximum rudder control, or in any way reduces the rudder control. Elevator balance requirements are similar to those for rudders.

Types of Balanced Controls. Figure 106 shows six types of balances. Types **A** and **B** were formerly used on all controls, but they are now employed only on rudders and elevators. There is little choice between them, but Type **B** is the more common at present. Neither **A** nor **B** should be used on ailerons owing to the poor wing tip and to the high peak loadings on the balanced portion. Type **C** is liable to overbalance and flutter. Type **D** has no advantages and is rarely used. Types **E** and **F** have been used to a limited extent, but have no outstanding advantage.

Figure 107 shows three widely used forms of balances. Type I is usually called the "Handley Page balance." It is satisfactory for control surfaces that need not be moved through large angles. With a normal airfoil section, the leading edge of the control emerges from the wake of the fixed surface at a control angle of about 15°. Above this critical angle no appreciable increase in control is obtained.

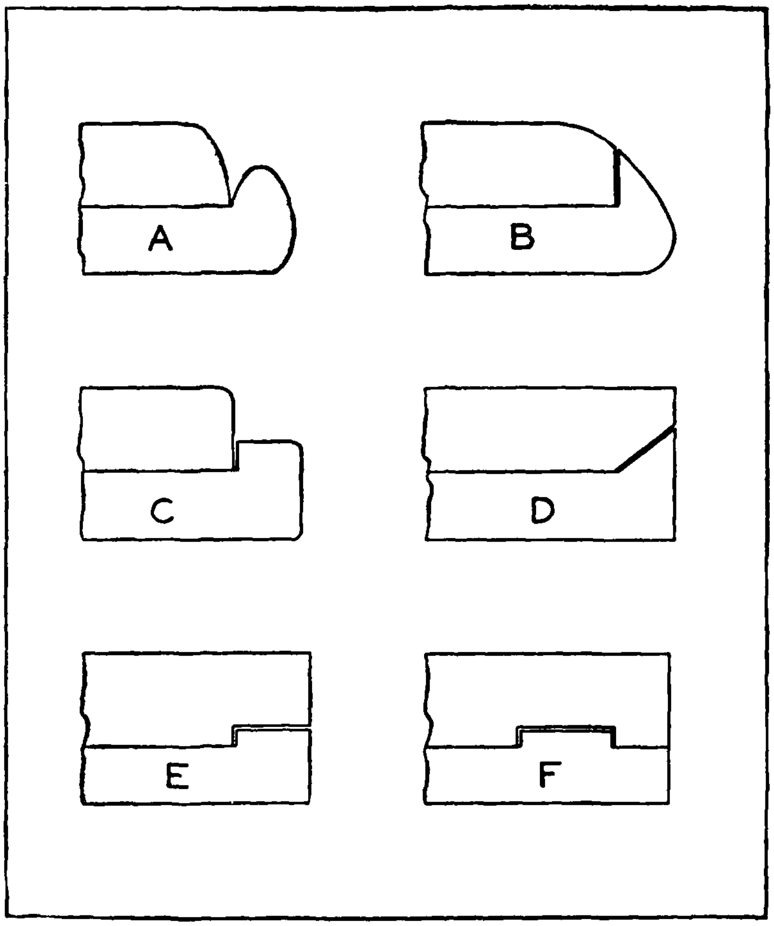

Figure 106. Balanced Controls

For best results, the hinge axis should be located at approximately 25% of control chord from its leading edge. Type H is the familiar "paddle" balance. Full balance cannot easily be secured with this type, but it has been fairly satisfactory on all surfaces. The auxiliary surface should be of large aspect ratio, and as far forward as practicable. The area should be generous for good balance. A symmetrical section is generally used, and on ailerons it is set at an angle of +3° to +5° to the wing chord. On rudders and elevators, the auxiliary surface would be set between 0° and 1° to the main surface axis. The amount of balance is readily calculated.

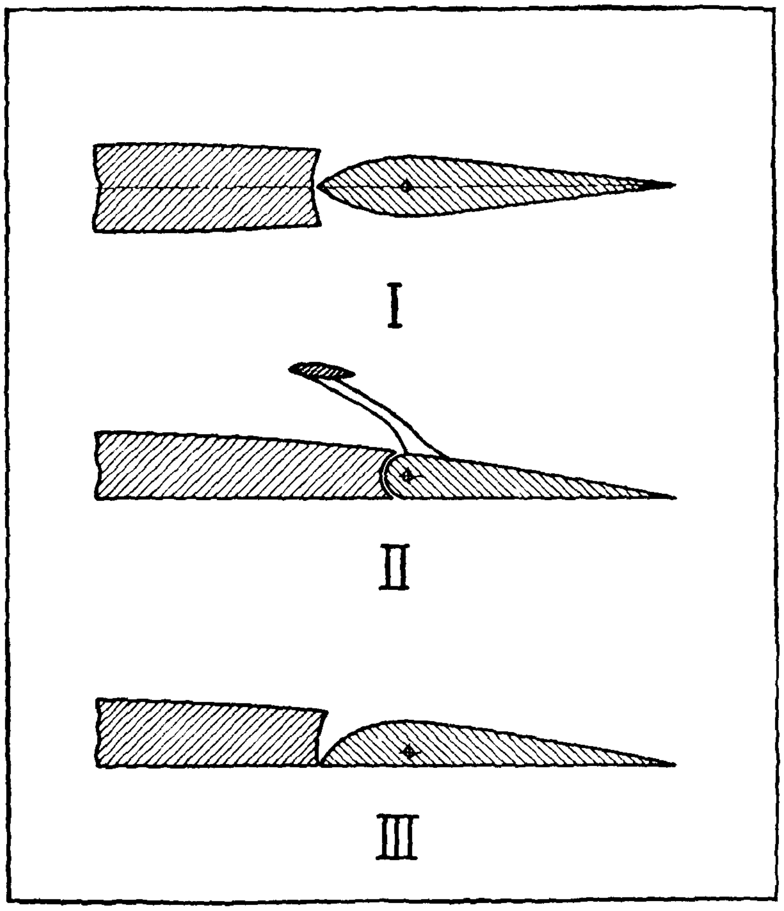

Figure 107. Balanced Controls

Type III is the Frise balance. This is the most satisfactory form of balance now available for ailerons. When the aileron is up, the leading edge projects below the wing and thus adds a drag which tends to counteract the yawing moment due to the drag of the down aileron. The hinge axis is preferably located below the aileron center-line and at about 20% to 22% of the aileron chord. The hinge axis should not be further aft than 25% of the aileron chord.

The effective area of a balanced-control surface of the Handley Page or the Frise type is measured between the hinge axis and the trailing edge. That part of the surface forward of the hinge axis does not contribute to the control effect.

Calculation for Simple Balances. For a long time naval architects have balanced rudders by assuming: (1) uniform loading, (2) that the center of pressure on a flat plate is at 0.20 c, (3) that the center of pressure on a movable surface of chord c_1 which trails a fixed surface is at 0.33 c_1. With these assumptions, the average center of pressure may be calculated and the axis placed forward of this point at a distance sufficient to avoid overbalance as determined by accumulated experience. This method is applicable to air as well as water, and it gives excellent results.

As applied to a rudder balance, for example, consider Figure 108. The rudder is divided into a number of strips **A**, **B**, **C**, **D**, etc., spaced as necessary in order to secure accuracy. The center of pressure of each strip is located as indicated by the circles, assuming C_p at 0.20 c for all of the overhanging strips and at 0.33 c_1 for all of the trailing strips. The area of each strip is then multiplied by the distance of its C_p from the axis, considering distances forward as negative. The algebraic sum of these moments divided by the total area is the average distance of the C_p from the axis. This distance should be between 4 and 6 inches for satisfactory balance, the distance decreasing slightly with the size of the airplane. Four and one-half inches to five inches is probably the best location for any airplane having a gross weight between 2500 and 10,000 lb. If the first calculation shows the center of pressure outside of the desired range, balance is added or subtracted as required, and additional calculations made until the desired location is obtained.

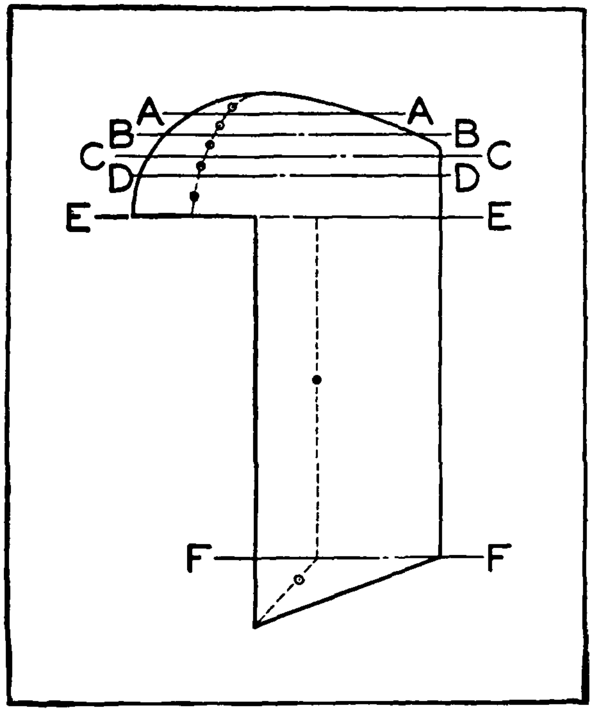

Figure 108. Illustrating Calculation for Rudder Balance

Leakage at Hinge Joints. Leakage between movable and fixed control surfaces is very detrimental to control effectiveness. Precautions should be taken by the designer to reduce the loss from this source.

In some airplanes the horizontal tail surfaces are attached to the fuselage with a fore-and-aft slot or gap between the stabilizer and the fuselage. This arrangement reduces the effective aspect ratio of the tail surface and may have a pronounced effect in reducing stability.

Effect of Balance Emergence. For small control deflections, the internal balance types, such as Handley Page or Frise, give values of ΔC_N and control effectiveness that are identical with those for a plain flap control having the same hinge axis location. At some control setting, depending on the hinge axis location and the thickness of the fixed surface, the leading edge emerges from its shielded position behind the fixed surface. This angle is normally about 20°. No additional increase in ΔC_N can be obtained with greater control displacements. In fact, the effect of leakage at the joint may begin to reduce the control effectiveness at values of δ_F well below the angle of emergence. The result may be a reduction of 50% or more in control effectiveness.

Figure 109 based on Smith's tests,[10] shows loss in effectiveness for a common type of balance. Some designers attempt to reduce this loss by using either a leading edge that is skewed to run diagonally from top to bottom, or by using a staggered Frise balance. With the skewed leading edge, the emergence begins at the initial deflection and is not complete until the throw is 30° or more. With the staggered Frise type, half of the leading edge is out for all control settings above a small range on either side of neutral.

In the event that an internal balance must be used on horizontal tail surfaces, it is desirable to make provision for the large download required in the landing condition.

---

[10] R. H. Smith, "Lift, Drag and Elevator Hinge Moments of Handley Page Control Surfaces," N.A.C.A. T.R. No. 278 (1927).

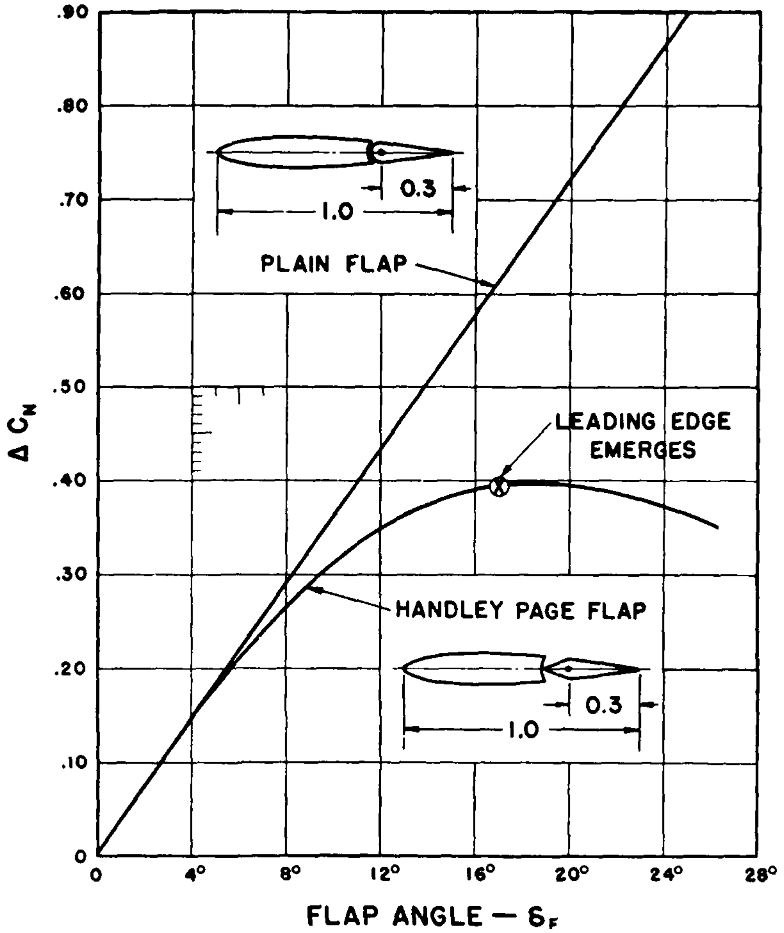

Figure 109. Loss of Control Effectiveness Due to Emergence of Leading Edge of Balanced Portion

One method is to raise the leading edge of the elevator balance so that it does not emerge with full-up elevator.

Static Balance. If the center of gravity of a control surface lies behind the hinge axis, any acceleration not in the plane of the surface will set up a hinge moment that tends to make the movable control surface lag behind the motion of the fixed surface. This lag has a tendency to increase the existing motion. The result is an instability leading to a dangerous type of oscillation known as "flutter" when the amplitude becomes appreciable.

Probably 90% of all tendency to flutter within the range of flight speeds can be eliminated by simple static balancing to bring the center of gravity of the movable surfaces up to the hinge line, but in addition to static balance, it is essential that the control mechanism have no appreciable play.

Static balance may be attained by adding weight ahead of the hinge axis. It is obviously desirable to limit the amount of weight that must be added. Careful design of the surface with concentrated weights near the hinge axis is indicated. In general, the use of metal-covered control surfaces makes it difficult to secure static balance. Metal-covered control surfaces should not be used on high-speed airplanes unless the designer is willing to add the necessary static-balance weight.

Complete static balance does not insure freedom from flutter unless the product of inertia about the longitudinal axis is also zero. This may be seen by study of Figure 110 showing an aileron. In pitch (or torsion) a simple static balance insures that the aileron acts in unison with the remainder of the wing. In roll or flexure, however, a particle *dw* is acted on by an accelerating force proportional to the distance from the longitudinal axis and this force has a moment arm x about the aileron hinge axis so that the effective moment is

$$dh = dw \cdot x \cdot y$$

the integral of this quantity over the whole surface is

$$h = \int dw \cdot x \cdot y$$

h is the product of inertia and unless it is zero or negative, there will be a tendency to flexural flutter. Static balance weights should be added to reduce the product of inertia. This means that they should be placed near the tip on ailerons and elevators and at the top of a rudder.

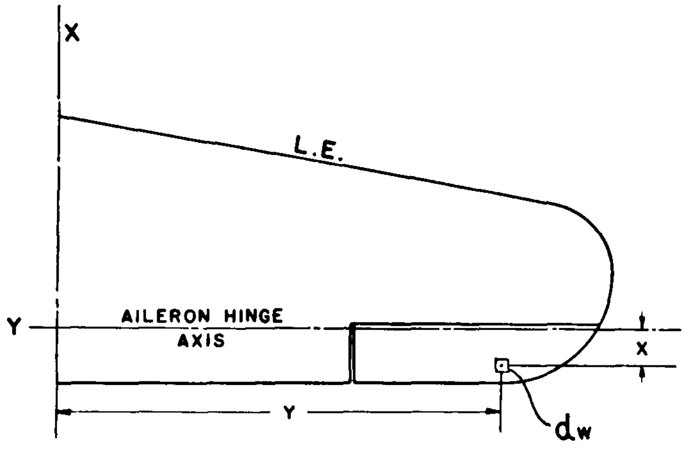

Figure 110. Mass Balance of an Aileron

Rudders and ailerons must be dynamically balanced to zero or negative products of inertia. With elevators, the direct-connected torque tube and small span are of some assistance in preventing flutter, but with large-span cantilever tail surfaces the elevators should also have zero or negative product of inertia. The current requirement of the Department of Commerce[11] is that

$$\frac{\Sigma\, dw \cdot xy}{W_c \cdot S_c} < 0.08 \qquad (139)$$

where $\Sigma\, dw \cdot xy$ is the product of inertia, W_c is the weight of the movable control surface and S_c is its area.

Flutter. Flutter is an oscillation of appreciable amplitude involving the wings or tail surfaces of an airplane.

---

[11] Bulletin 7-A, Section 30 (6).

It is usually, but not always, associated with aerodynamic and mass forces that form an unstable cycle of cause and effect in which a movable surface lags behind the motion of a fixed surface. Flutter usually begins suddenly at the critical speed and unless the speed is reduced immediately, there is great danger of the structure disintegrating. The tremendous kinetic energy in a high-speed airplane supplies what amounts to an inexhaustible source of power for continuing and increasing the amplitude of a destructive oscillation.

It is imperative that the designer of modern high-speed airplanes take every precaution to avoid all conditions known to lead to flutter at the speeds attainable in flight.

The theory of flutter has been treated by Frazer and Duncan,[12] and by Theodorsen.[13] Experimental data confirm the theoretical relations and enable a brief summary of the precautions necessary to avoid flutter depending on control surfaces.

Flutter Prevention. Design recommendations for the avoidance of flutter are listed and explained with great clarity by Frazer and Duncan[14] in a report that is by far the best available source of practical information. The recommendations for prevention of wing flutter are:

1. All elastic stiffnesses as large as possible.
2. Irreversibility of aileron control. If 2 is not provided then:
3. Center of gravity of aileron slightly ahead of hinge.
4. Moment of inertia of aileron small.
5. An appreciable part, preferably rather more than one-half of the aileron, should lie inboard of the

---

[12] R. A. Frazer and W. J. Duncan, "The Flutter of Airplane Wings," Br.A.R.C. R. & M. No. 1155 (1928).

[13] T. Theodorsen, "General Theory of Aerodynamic Instability and the Mechanism of Flutter," N.A.C.A. T.R. No. 496 (1935).

[14] R. A. Frazer and W. J. Duncan, "The Flutter of Monoplanes, Biplanes and Tail Units," Br.A.R.C. R. & M. No. 1255 (1931).

center-line of the attachments of the outermost inter-plane struts.

6. Aileron heavily damped, e.g., artificially.
7. Aileron definitely underbalanced aerodynamically.
8. Inter-aileron strut not outboard of the inter-plane struts. (Only of secondary importance if for any reason recommendation 3 is not adopted.)
9. Aileron controls to operate in the same section as the aileron strut.

The notes accompanying these recommendations are as follows:

Recommendation 1. A proportionate increase of all elastic stiffnesses raises the critical speeds. In the case of biplanes, the stiffness of the staying is naturally of great importance.

Recommendation 2. A properly designed irreversible control completely eliminates flutter involving the ailerons. All other recommendations relative to the ailerons can then be ignored.

Recommendation 3. This recommendation is of greatest importance, and should be interpreted strictly, since partial mass balance may be of no benefit. Allowance must be made for the mass of the inter-aileron strut and other appendages of the aileron. Interconnection of the ailerons by a wire instead of a strut may be of assistance here on account of the smaller mass of the wire.

Recommendation 4. All parts of the control system which move with the ailerons contribute effectively to the moment of inertia of the aileron. All such parts should, therefore, be as light as possible.

Recommendation 5. This measure assists to minimize some of the aileron couplings, but it must not be considered as an effective alternative to recommendation 3.

Recommendation 6. An artificial damping device, if employed, should be of the fluid friction or electrical type. The use of solid friction is viewed as objectionable.

Recommendation 7. Very close approach to the condition of aerodynamical balance is considered dangerous. However, experiments show that an aileron hinged at about 0.2 of the chord from its leading edge may be quite satisfactory.

Recommendation 8. This recommendation is of particular importance when one of the overhangs is long and the other short, and the ailerons are mass-balanced.

Recommendation 9. This measure results in the elimination of certain couplings, and is also clearly mechanically sound.

The design recommendations for preventing tail flutter are divided into four groups as follows:

I. *General:*
   (a) Tailplane and fin very stiff, both in flexure and torsion.
   (b) Rigidity of elevator planes and rudder.
   (c) Irreversibility of elevator and rudder controls.

II. *Elevators:*
   (d) Interconnection of elevators by tube very stiff in torsion.
   (e) Product of inertia of each elevator zero.
   (f) Moment of inertia of elevator about hinge axis small.
   (g) Elevators definitely underbalanced aerodynamically.
   (h) Elevators heavily damped.

III. *Rudder:*
   (i) Projection of part of rudder below fuselage. Optimum condition is rudder symmetrically bisected by center-line of fuselage.
   (j) Product of inertia of rudder zero.
   (k) Moment of inertia of rudder about hinge axis small.
   (l) Rudder definitely underbalanced aerodynamically.
   (m) Rudder heavily damped.

IV. *Tailplanes* [if (a) is not fulfilled]:
   (n) Balance of masses of each half of tailplane (including elevator), about its flexural axis.
   (o) Flexural axis close to axis of independence.

When the items of group I are *all* observed, the remaining groups can be ignored. When the requirements (a) and (b) are met but (c) is not met, a judicious observance of groups II and III is necessary. When only condition (b) is satisfied, group IV will also require attention. The condition of irreversibility is met if the control maintains a given setting until purposely moved by the pilot.

If the tailplane is extremely stiff, and if (d) is observed, then items (e) and (f) may be ignored.

Apparent Instability. Many symptoms of violent instability may be introduced by extraneous aerodynamic or mass forces. Most of these troubles are found in lateral or directional stability. A striking example is the Dichman effect, first explained by Mr. E. W. Dichman. This effect is found in biplanes having ailerons on upper and lower wings when the aileron connecting struts are attached behind the hinge axis and inclined upward and outward. In a side slip the lift on the inclined strut raises the trailing edge of the ailerons on the advancing wing and leads to an increasing slip, giving the pilot an impression of very definite instability. Since in the attainment of mass balance the struts will be attached forward of the hinge axis, they should then be inclined outward to avoid this effect.

An apparent instability has been very definitely obtained in several airplanes having the ailerons actuated by a single long tube within the wing. Unless the aileron connections are properly made to avoid it, the gravity or the acceleration effect on the tube is sufficient to operate the ailerons in the wrong direction.

A similar effect has been observed in pitch where, with balanced elevators, the weight of the control column or stick was sufficient to cause a dive or a stall.

Indications of lateral instability are sometimes found in airplanes having rudders well above the fuselage center-line. In such cases the rudder gives a rolling moment that is in the wrong direction for the yawing moment. Additional dihedral should be used when it is necessary to locate the rudder well above the fuselage.

The effect of thrust axis location with respect to the center of gravity is well known. When the thrust axis is below the c.g., the increase in thrust with reducing air speed tends to stall the airplane, or the decrease in thrust with increasing air speed tends to dive the airplane. This effect may be very pronounced if the stability is marginal.

Another type of instability is found with the thrust-line located well above the c.g. In this case the application of power gives an appreciable diving moment, and if the airplane is balanced power-on, it may stall when the throttle is closed. These effects can be neutralized by tilting the thrust axis to direct the slipstream on the horizontal tail surfaces, or by providing sufficient longitudinal stability to reduce the thrust effect to negligible proportions.

Apparent longitudinal instability may be produced by free liquid surface in fuel tanks. A free liquid surface acts as a pendulum of length

$$l = bm = i/v \tag{140}$$

where i is the moment of inertia of the free surface and v is the volume of the liquid. The effect is equivalent to a vertical shift in the c.g.

CHAPTER 8

DYNAMIC STABILITY

Dynamic Stability. The mathematical treatment of the motion of an airplane considered as a rigid body was first given in a complete form by Bryan,[1] who showed that the motion could be separated into two components, a "symmetrical" motion in pitch and an "unsymmetrical" motion in roll and yaw. Bryan's treatment is from the standpoint of the physicist and the resulting complexity is very confusing to the engineer.

The first practical application of Bryan's method to an actual airplane was made by Bairstow,[2] Jones, and Thompson who showed very clearly how the various derivatives were obtained and how it was possible to factor the stability biquadratic to obtain a very satisfactory approximate solution. Hunsaker[3] in two papers published about two years later gave additional information regarding the stability derivatives and drew definite practical conclusions from the study. Hunsaker's Smithsonian paper is perhaps the clearest presentation of the subject available at this time. Numerous papers were published subsequently by various authors, but very few designers had the mathematical training or the time to make the calculations as a part of routine design procedure, and it must be conceded that the formidable array of three moments of inertia, one product of inertia, and 18 derivatives was ample reason. Under these circumstances, the calculation of dynamic stability remained for many years an academic exercise involving a tremendous amount of drudgery. Several attempts were made to reduce the labor involved, mostly by providing graphical solutions for the biquadratic equations, but no appreciable progress was made until Glauert[4] developed a simplified form of the stability equation referred to wind axes and employing coefficient type. The adoption of wind axes results in a considerable saving in work since lift and drag data become directly applicable. Glauert also assumed that the products of inertia and certain minor derivatives are negligible. The simplified method, while frankly an approximation, has been shown by Gates[5] to give surprisingly good agreement with flight test data.

---

[1] G. H. Bryan, "Stability in Aviation," Macmillan & Co., Ltd., London (1911).

[2] L. Bairstow, B. M. Jones and A. W. H. Thompson, "Investigation into the Stability of an Aeroplane with an Examination into the Conditions Necessary in Order that the Symmetric and Asymmetric Oscillations can be Considered Independently," Br.A.C.A. R. & M. No. 77 (1913).

[3] J. C. Hunsaker, 'Experimental Analysis of Inherent Longitudinal Stability for a Typical *Biplane,*" N.A.C.A. *T.R.* No. 1, *Part I (1915), and Smithsonian* Miscellaneous Collections, Vol. 62, No. 5 (1916).

Zimmerman[6] has also prepared a set of charts covering a wide range of conditions for which longitudinal stability is of interest. In any practical investigation of stability these charts are adequate and indispensable.

Before giving the simplified stability equations, it appears desirable to indicate in a very brief manner the steps employed in deriving the classical forms. The only purpose in doing this is to provide the equivalent of a number of definitions that are otherwise very difficult. For a complete derivation, reference is made to the papers previously listed and to the following books:

W. L. Cowley, and H. Levy, "Aeronautics in Theory and Experiment," Longmans, Green & Co. (1918).
E. B. Wilson, "Aeronautics," John Wiley & Sons (1920).
L. Bairstow, "Applied Aerodynamics," Longmans, Green & Co., London (1920).

---

[4] H. Glauert, "A Non-Dimensional Form of the Stability Equations of an Aeroplane," Br.A.R.C. R. & M. No. 1093 (1927).

[5] S. B. Gates, "A Survey of Longitudinal Stability below the Stall with an Abstract for Designers' Use," Br.A.R.C. R. & M. No. 1118 (1927).

[6] C. H. Zimmerman, "An Analysis of Longitudinal Stability in Power-Off Flight with Charts for Use in Design," N.A.C.A. T.R. No. 521 (1935).

Stability Equation: General Considerations. For all practical purposes the airplane may be considered as a rigid body. Six equations are required to define its motion; one force equation and one moment equation for each of the three coordinate axes. These equations must include force and moment components due to both aerodynamic and mass reactions. By assuming that the deviations from the initial steady condition are restricted to comparatively small changes in angles or velocities, the second order products may be neglected and the equations simplified to a degree that permits a solution.

The general steps leading to the derivation of the stability biquadratic may be as follows: Let three mutually perpendicular axes be fixed in the airplane with the origin at the c.g. and the X axis in the direction of the relative wind. If the airplane is assumed to be in horizontal flight, the Z or normal axis is vertical and the Y or lateral axis is horizontal. The positive directions are OX forward, OY directed toward the right wing tip and OZ downward. Let the total aerodynamic force or the sum of the aerodynamic force components acting along these axes be X, Y, and Z. Let the total aerodynamic moment or the sum of the aerodynamic moment components about each of these axes be L, M, and N. Linear velocity increments along the axes are u, v, and w and the forward velocity of the airplane is $U_0 = V$. The angular velocities around these axes are p, q, and r. Then the X force, for example, is

$$X = f\,(V, u, v, w, p, q, r)$$

where the form of the function f is not known. However, for small oscillations, the function may be expanded by Maclaurin's theorem, neglecting second order terms, to obtain

$$X = X_0 + uX_u + vX_v + wX_w + pX_p + qX_q + rX_r \qquad (141)$$

X_u, X_v, etc., are partial derivatives of X with respect to u, v, etc. X_u is the rate of change of X with u, or

$$X_u = \partial X / \partial u$$

Exactly analogous expansions are made for Y, Z, L, M, and N. There are a total of 36 aerodynamic force derivatives, but fortunately the symmetry of the airplane about the XZ plane causes 18 of these to vanish; the changes being small, v, p, and r do not affect X, Z, or M, while u, w, and q do not affect Y, L, or N. The remaining derivatives are

$$(X, Z, M) \times (u, w, q)$$

$$(Y, L, N) \times (v, p, r)$$

The first group enters into the motion in the XZ plane and determines the longitudinal stability. The second group determines the rolling and yawing motion in lateral stability.

These aerodynamic stability derivatives may now be substituted with the mass forces into the six equations of motion for a rigid body having all degrees of freedom. The first group gives three simultaneous linear differential equations with constant coefficients in u, w, and θ. The second group gives a similar set of three equations in v, φ, and ψ (where φ is the angle of bank and ψ is the angle of yaw, $d\varphi/dt = p$, $d\psi/dt = r$). The motion can be assumed to be of the type where each variable is some function of $e^{\lambda t}$. Each group of three equations can then be combined into a biquadratic equation of the form

$$A\lambda^4 + B\lambda^3 + C\lambda^2 + D\lambda + E = 0 \tag{142}$$

where the coefficients A, B, C, D, and E are functions of the stability derivatives and λ is the "damping coefficient" in the exponent of the integrating factor $e^{\lambda t}$.

The solution of the biquadratic gives four roots, λ_1, λ_2, λ_3, and λ_4, and the longitudinal motion in θ, for example, would be

$$\theta = C_1 e^{\lambda_1 t} + C_2 e^{\lambda_2 t} + C_3 e^{\lambda_3 t} + C_4 e^{\lambda_4 t} \tag{143}$$

where the constants C_1, C_2, C_3, and C_4 depend on initial values of θ. There will be a corresponding solution for u with constants C_5 to C_8, depending on the initial conditions for u, and a corresponding solution for w with constants C_9 to C_{12}, depending on the initial conditions for w. The solutions for v, p, and r in the lateral motion are in the same form, but with four new values of λ and 12 new constants depending on the initial conditions in v, p, and r.

The four roots of the stability biquadratic may be all real, all complex, or two real and two complex. The type of motion involved will require at least one pair of complex roots of the form $\lambda = a \pm b\sqrt{-1}$, or $\lambda_1 = a + bi$ and $\lambda_2 = a - bi$. These two roots may be combined by means of the relation

$$e^{\pm i\theta} = \cos\theta \pm i\sin\theta$$

and substituted in equation (143) which becomes, for example,

$$\theta = e^{at}\,(C_1'\cos bt + C_2'\sin bt) + C_3e^{\lambda_3 t} + C_4e^{\lambda_4 t} \tag{144}$$

The term in the parenthesis is periodic and the motion will be damped, that is, it will decrease in amplitude if the exponent at is negative.

It has been necessary to indicate the physical significance of the stability biquadratic in some detail, but fortunately it is unnecessary to obtain the complete solution as outlined. The condition for longitudinal stability is simply that u, w, and θ diminish as t increases. Since this condition is met only when the exponent of e^{at} is negative, it follows that each of the four roots of equation (142) must be negative if the root is real, or must have negative real parts if the root is complex.

The condition of negative real roots or negative real parts of complex roots is obtained when each of the coefficients A, B, C, D, and E is positive in equation (142), and when Routh's Discriminant

$$R = BCD - AD^2 - B^2E \tag{145}$$

is also positive. There are occasional unimportant exceptions in lateral stability. The change from a motion originally stable to one that becomes unstable (by a gradual change in one or more of the stability derivatives) is first evident by a change in sign of E or R. When E becomes negative, the oscillations diverge instead of subsiding, and when R becomes negative, the damping is insufficient to prevent unstable oscillation.

The condition for lateral stability is that v, φ, and ψ diminish as t increases, and this requires that the lateral stability equation also have all negative roots, hence all positive coefficients and positive Routh's Discriminant. The general form of the longitudinal and lateral stability equations are identical, but the two sets of coefficients A, B, C, D, and E naturally depend on different sets of derivatives as will be indicated later.

"Wind" Axes. It is necessary to dwell at some length on the conventions regarding axes in order to avoid the confusion that has arisen in the literature on airplane stability owing to changes in the systems used.

In studying the motion of an airplane, there are several systems of axes that may be used. If the principal inertia axes are used, there is a considerable simplification in the exact mathematical analysis. If, on the other hand, we are chiefly concerned with a practical and a simple solution, and are willing to sacrifice some accuracy to obtain direct results, then "wind" axes are highly desirable.

In the discussion that follows, all forces and moments will be referred to orthogonal "wind" axes fixed-in and moving with the airplane, with the origin at the c.g. The positive directions will be forward for X, toward the right-wing tip for Y, and downward for Z. The X axis will lie in the direction of the relative wind for the initial undisturbed motion, and as the airplane pitches, rolls, or yaws, it carries these axes with it. Positive angles and moments are measured by rotation of positive X towards positive Y, positive Y towards positive Z, and positive Z towards positive X.

These axes are right-handed in that to an observer at the origin, the positive directions are simulated by the rotation and translation of a right-hand screw. It may be of assistance in visualizing the system to remember that positive pitch, roll, and yaw are obtained in a right-hand climbing turn.

The question is often asked, why use these axes which are diametrically opposed to the common left-hand wind-tunnel axes? The answer is that this is a consistent system, right-handed throughout and in well-established usage in Dynamics, and that with it, V and g are positive. As a matter of fact, it makes very little difference what system is used, provided there is no ambiguity.

Non-Dimensional Stability Derivatives. The non-dimensional force derivatives are obtained by dividing the total force derivatives by $\rho S V$. For example,

$$x_u = mX_u/\rho SV$$

where mX_u is the derivative of the total X force with respect to u. This distinction between x_u and mX_u is important to avoid confusion, since it has been customary to consider X_u as the derivative per unit mass.

The unit of time in the non-dimensional system is τ seconds where

$$\tau = m/\rho SV \tag{146}$$

and the unit of velocity is l/τ or V/μ where

$$\mu = m/\rho Sl \tag{147}$$

l is any convenient length in the airplane, but by general agreement, l is always taken as the distance from the c.g. to the elevator hinge axis. μ is the relative density of the airplane. It is physically the ratio of the mass of the airplane to the mass of air contained in the volume Sl.

The non-dimensional moment derivatives are formed by dividing each moment derivative by $k\rho SVl$ for linear velocity derivatives or by $k\rho SVl^2$ for angular velocity derivatives where k is ξ, η, or ζ depending on the axis involved. ξ, η, and ζ are defined by the equations:

$$A = mk^2{}_A = \xi\, ml^2$$

$$B = mk^2{}_B = \eta\, ml^2$$

$$C = mk^2{}_C = \zeta\, ml^2$$

The moment derivatives then take the forms

$$\begin{aligned}
l_v &= L_v/\rho SVl\,\xi \\
l_p &= L_p/\rho SVl^2\,\xi \\
l_r &= L_r/\rho S\,Vl^2\,\xi \\
m_u &= M_u/\rho SVl\,\eta \\
m_w &= M_w/\rho SVl\,\eta \\
m_q &= M_q/\rho SVl^2\,\eta \\
n_v &= N_v/\rho SVl\,\zeta \\
n_p &= N_p/\rho SVl^2\,\zeta \\
n_r &= N_r/\rho SVl^2\,\zeta
\end{aligned}$$

Glauert gives all of the non-dimensional coefficients negative signs on the grounds that practically all of the stability derivatives are inherently negative and that it is desirable to think in terms of positive factors. This argument is sound, but the result appears likely to be confusing, and there is already too much confusion. Having adopted the standard stability axes and conventions regarding signs, these will be used throughout.

Longitudinal Stability. Using non-dimensional stability derivatives with the stability wind axes, $w_0 = 0$ and $U_0 =$

V, and the second order derivatives x_q and z_q may be neglected to give the biquadratic

$$\lambda_1^4 + B_1\lambda_1^3 + C_1\lambda_1^2 + D_1\lambda_1 + E_1 = 0 \qquad (148)$$

where

$$\begin{aligned}
B_1 &= -m_q - (x_u + z_w)\\
C_1 &= m_q\,(x_u + z_w) - (x_w z_u - x_u z_w) - \mu m_w\\
D_1 &= m_q\,(x_w z_u - x_u z_w) + \mu m_u\,(\tfrac{1}{2}C_L - x_w)\\
&\quad + \mu m_w\,(\tfrac{1}{2}C_L \tan\theta_0 + x_u)\\
E_1 &= \mu\frac{C_L}{2}\,m_w\,(z_u - x_u\tan\theta_0) - \mu\frac{C_L}{2}\,m_u\,(z_w - x_w\tan\theta_0)
\end{aligned}$$

θ_0 is the angle of climb in the original undisturbed motion.

The longitudinal motion will be stable if each of the coefficients B_1, C_1, D_1, and E_1 and Routh's Discriminant $R = (B_1C_1D_1 - D_1^2 - B_1^2E_1)$ is positive.

Bairstow has shown that owing to the relative normal magnitudes[7] of the coefficients in equation (148) one pair of roots is given approximately by

$$\lambda_1^2 + B_1\lambda_1 + C_1 = 0 \qquad (149)$$

and hence the other pair by

$$\lambda_1^2 + \left(\frac{D_1}{C_1} - \frac{B_1E_1}{C_1^2}\right)\lambda_1 + \frac{E_1}{C_1} = 0 \qquad (150)$$

The motion represented by the first pair is a short-period heavily-damped oscillation that is of little interest. The motion represented by the second pair is the long-period, lightly-damped oscillation generally known as the "phugoid." The roots from this factorization are

$$\lambda_1 = -\tfrac{1}{2}\left[\frac{D_1C_1 - B_1E_1}{C_1^2}\right] \pm \sqrt{\left[\frac{D_1C_1 - B_1E_1}{2\,C_1^2}\right]^2 - \frac{E_1}{C_1}} \qquad (151)$$

and the period is approximately

$$t = 2\pi\,\tau\,\sqrt{C_1/E_1} = \frac{2\pi m}{\rho SV}\sqrt{C_1/E_1} \qquad (152)$$

---

[7] The approximation is sufficiently accurate if B_1 is less than C_1, E_1 is less than $C_1^2/20$, and if D_1 is less than $B_1C_1/20$.

The time for an oscillation to damp to one-half of its initial value is taken as a measure of the damping. The time in seconds to halve an amplitude is

$$T = -(\tau/a)\log_e 2 \tag{153}$$

where τ is the unit of time ($\tau = m/\rho SV$) and a is the "logarithmic decrement" or real part of λ_1 in equation (150). Hence

$$T = \frac{1.38}{\left[\dfrac{D_1}{C_1} - \dfrac{B_1E_1}{C_1^2}\right]} \times \frac{m}{\rho SV} \tag{153a}$$

Longitudinal Stability: Force Derivatives. The force derivatives entering into the longitudinal stability equation may be calculated from the following relations:

$$x_u = mX_u/\rho SV = -C_D$$

$$x_w = mX_w/\rho SV = -\tfrac{1}{2}\left[\frac{dC_D}{d\alpha} - C_L\right]$$

$$x_q = 0 \qquad z_q = 0$$

$$z_u = mZ_u/\rho SV = -C_L$$

$$z_w = mZ_w/\rho SV = -\tfrac{1}{2}\left[\frac{dC_L}{d\alpha} + C_D\right] = -\tfrac{1}{2}\frac{dC_L}{d\alpha}$$

In these relations C_L and C_D are the absolute lift and drag coefficients for the entire airplane at the initial angle of attack corresponding to θ_0. The slopes are absolute values based on radians instead of degrees.

x_w may be determined directly from the relation given above or by further calculation. Since

$$C_D = C_{DP} + C_{Di} = C_{DP} + (C_L^2/\pi n)$$

$$dC_D/d\alpha = 2C_L(dC_L/d\alpha)/\pi n$$

hence

$$x_w = C_L\Big(0.5 - [(dC_L/d\alpha)/\pi n]\Big) = KC_L \tag{154}$$

where K depends chiefly on aspect ratio, with values as follows:

Aspect ratio n =	4	5	6	8	10
K =	.15	.20	.24	.29	.33

These values may be used in the event that wind-tunnel test data are unavailable. It should be noted that x_w is the only positive *force* derivative.

z_w may be determined from the slope of the lift curve only, since analysis of wind-tunnel test data shows that although the value of $dC_L/d\alpha$ must be zero at maximum C_L, the C_D term is negligible below about 98% of C_L maximum. The average value of $dC_L/d\alpha$ is about 4.0. Hence, the average value of z_w is about 2.0.

Longitudinal Stability: Moment Derivatives. The moment derivatives entering into the longitudinal stability equation are

$$m_u = M_u/\rho S V l \eta$$
$$m_w = M_w/\rho S V l \eta$$
$$m_q = M_q/\rho S V l^2 \eta$$

where $\eta = B/ml^2$.

M_u is the change in pitching moment due to change in forward velocity and m_u has the value

$$m_u = C_M/\eta(l/c) \qquad (155)$$

m_u will be zero in gliding flight without power, since the pitching moment due to the wings is neutralized by the tail when there is no change in angle of attack.

m_u will not be zero in full power flight owing to thrust moment and to slipstream effects on the horizontal tail surfaces.

M_w is the change in pitching moment due to vertical velocity. A positive vertical velocity w compounds vectorially with the forward velocity V to produce a positive change in angle of attack of $\theta = w/V$, from which $d\theta/dw = 1/V$. The moment acting on the airplane is

$$M = C_M \frac{\rho}{2} S V^2 c$$

Hence

$$M_w = \frac{dM}{dw} = \frac{dM}{d\theta} \cdot \frac{d\theta}{dw} = \frac{dC_M}{d\theta} \frac{\rho}{2} S V c$$

and

$$m_w = \frac{M_w}{\rho S V l \eta} = \frac{1}{2\eta} \left(\frac{c}{l}\right) \left(\frac{dC_M}{d\theta}\right) \tag{156}$$

$(dC_M/d\theta)$ should be obtained from wind-tunnel test data. The slope is in radians. An approximate value of $dC_M/d\theta$ may be obtained from equations (107), (114), and (115).

M_q is the damping due to angular velocity in pitch. In general, about 80% of M_q is due to the tail and the remainder to the wings and other parts of the airplane. The value of m_q is usually taken as

$$m_q = -\frac{K}{2} \left(\frac{l}{k_B}\right)^2 \left(\frac{S_T}{S_W}\right) \left(\frac{dC_{LT}}{d\alpha_T}\right) \eta_T \tag{157}$$

where k_B is the radius of gyration in pitch, η_T is the tail efficiency factor, l the tail length, and K a factor allowing for wing damping and having a value of about 1.25.

The desirable range of $(dC_M/d\theta)$ in radians is between -0.20 and -0.40. $1/\eta$ varies between 5 and 20. Hence, m_w should be between -0.30 and -0.60. By similar reasoning, the value of m_q will probably be between -1.0 and -6.0.

Estimating Radii of Gyration. Analysis of N.A.C.A. data[8] on moments of inertia indicates that the radii of gyration can be estimated with fair accuracy from the span b and overall length L.

---

[8] H. A. Soulé and M. P. Miller, "The Experimental Determination of the Moments of Inertia of Airplanes," N.A.C.A. T.R. No. 467 (1933); also, by same authors, T.N. No. 375.

The radius of gyration in pitch, k_B, is required in longitudinal stability calculation. It may be obtained from

$$k_B = C_B \cdot L \tag{158}$$

where L is the overall length of the airplane "between perpendiculars." The coefficient C_B has an average value of 0.20. It is increased up to a maximum of about 0.22 for very short-coupled airplanes or for extreme fore-and-aft weight separation. It is reduced to a minimum value of about 0.18 for very long fuselages with compact weight grouping.

The radius of gyration in roll k_A is obtained from

$$k_A = C_A \cdot b \tag{159}$$

where b is the maximum wing span. The coefficient C_A has an average value of about 0.125 which may be increased to a maximum value of about 0.150 for airplanes with very heavy wings without taper. C_A may be decreased to a minimum value of about 0.100 for airplanes with very light wings with considerable taper.

The radius of gyration in yaw k_C is obtained from

$$k_C = C_C \cdot b \tag{160}$$

where b is the maximum span. The coefficient C_C has an average value of 0.18.

These empirical equations are based on all types except seaplanes and flying boats. There appear to be no consistent differences between monoplanes, sesquiplanes and biplanes, but the addition of any heavy weight well outboard requires an appropriate allowance in C_A and C_C.

The radii of gyration may be converted to the non-dimensional coefficients by the relations

$$A = mk_A^2 = mC_A^2b^2 = \xi\, ml^2$$

or

$$\xi = C_A^2\,(b/l)^2 \qquad (161)$$

$$B = mk_B^2 = mC_B^2L^2 = \eta\, ml^2$$

or

$$\eta = C_B^2\,(L/l)^2 \qquad (162)$$

$$C = mk_C^2 = mC_C^2\,b^2 = \zeta\, ml^2$$

or

$$\zeta = C_C^2\,(b/l)^2 \qquad (163)$$

l is the tail length, L the overall length, and b the span. It should be noted that $\xi l^2 = k_A^2$, $\eta l^2 = k_B^2$, and $\zeta l^2 = k_C^2$. Average values are: $\xi = 1/12$, $\eta = 1/10$, and $\zeta = 1/8$.

Notes on Longitudinal Stability. Hunsaker, in his Smithsonian paper, concludes that any airplane is likely to show mild dynamic instability at, and just above, stalling speeds and that dynamic stability is improved by decreasing wing loading, moment of inertia, and moment coefficient, and by increasing tail area, speed, and drag. Gates, in R. & M. No. 1118, lists a number of very practical conclusions substantially as follows:

1. Instability may arise as a divergence or as an increasing oscillation.
2. Static stability or negative $(dC_M/d\theta)$ and negative m_w is a rigid safeguard against divergence in the gliding condition. $(dC_M/d\theta)$ is made more negative by moving c.g. forward and by increasing tail area, but it is preferable to keep the tail area reasonably large. If a stable slope is obtained by a forward c.g. location in combination with a small tail, m_q is reduced and there is risk of increasing oscillations at low speeds.
3. The effect of slipstream on the tail is such that there is risk of divergence with engine on, even with static stability. This danger is characteristic of high speed, especially with wings having large C_{M_0}. On

the other hand, the slipstream effect tends to increase the danger of an undamped oscillation at low speeds when C_{M_0} is small.

4. A large angle of climb reduces damping.
5. The range of speeds for stability is less for power-on than for power-off, and it becomes less as the power is increased.
6. A large moment of inertia is undesirable.
7. At moderate and low speed, it is generally true that the damping coefficient decreases as wing loading and altitude are increased, all other parameters remaining constant.

The desirable condition in longitudinal stability is a heavily-damped long period. This is best obtained with large m_q and small or moderate m_w. The airplane must be statically stable, that is, m_w must be negative for dynamic stability.

Longitudinal Stability: Power-on. The effects of thrust and slipstream are so complex that the calculations for longitudinal stability with power-on are not very reliable. It is possible, however, to trace the effect of some of the variables. x_u will obviously be modified to

$$x_u = -C_D + (dT/dV)/\rho S V \tag{164}$$

but the negative (dT/dV) tends to balance the reduced propeller drag and the net change is probably negligible. z_u will be modified to the extent that the slipstream affects the lift. This may be considerable in multi-engine airplanes where the engines are mounted along the leading edge, where the result may be approximated by a fixed percentage increase based on the percentage of the wing area in the slipstream and assuming constant slipstream velocity. Hence

$$z_u = -(1 + S_S/S_W)C_L = -K_S C_L \tag{165}$$

x_w and z_w will be affected to substantially the same degree as z_u, or $x_w = K(1 + S_S/S_W)C_L$, and $z_w = -\frac{1}{2}(1 + S_S/S_W)\,(dC_L/d\alpha)$.

The greatest effect of power will be through m_u and the corresponding modification of the coefficient E_1. m_u is influenced directly by the thrust moment and indirectly by the slipstream on the tail. If h is the distance from the c.g. to the thrust line, positive if the c.g. is above, then the thrust moment is

$$M = +Th$$

Neglecting slipstream effects and assuming that the thrust horsepower is constant, $T = K \cdot \text{bhp}/V$ and $dT/dV = -K \cdot \text{bhp}/V^2$, where K will have an average value of 550 × 0.80 = 440. From this

$$M_u = \frac{dm}{du} \cdot \frac{du}{dV} = -\frac{440\,h\,\text{bhp}}{V^2}$$

and

$$m_u = -\frac{220\,h\,C_L}{(W/\text{bhp})\,V\eta} \tag{166}$$

This effect deserves more consideration than it has received in the past. If the c.g. is below the thrust line (h negative), the increasing thrust with decreasing speed has a stabilizing effect. If the c.g. is above the thrust line there is a definite destabilizing tendency. While the slipstream on wings and tail enters into the value of m_u, it does not appear practicable to calculate this effect, the major part of which is probably due to a varying velocity over the wings and a substantially constant slipstream velocity over the tail instead of the same velocity over both wings and tail.

Lateral Stability. The asymmetrical motion in side slip v, roll φ, and yaw ψ is treated under the heading of lateral stability. This motion is represented by a biquadratic, identical in form with the equation for motion in the XZ plane

$$\lambda_2^4 + B_2\,\lambda_2^3 + C_2\,\lambda_2^2 + D_2\,\lambda_2 + E_2 = 0 \qquad (167)$$

where, omitting the negligible derivatives y_p and y_r,

$$B_2 = -l_p - n_r - y_v$$

$$C_2 = (l_p n_r - l_r n_p) + y_v\,(l_p + n_r) + \mu\, n_v$$

$$D_2 = y_v\,(l_r\, n_p - l_p\, n_r) - \mu n_v \left(\frac{C_L}{2} \tan \theta_0 + l_p\right) + \mu l_v \left(n_p - \frac{C_L}{2}\right)$$

$$E_2 = \frac{\mu C_L}{2}\,[(l_v n_r - l_r n_v) + (l_p n_v - l_v n_p) \tan \theta_0]$$

The condition for stability is that v, φ, and ψ decrease with time. This condition is obtained when each of the coefficients B_2, C_2, D_2, and E_2 is positive and Routh's Discriminant,

$$R = B_2\, C_2\, D_2 - D_2^2 - B_2^2\, E_2$$

is also positive, since this insures that the real roots and the real part of complex roots are negative.

The approximate factorization used with equation (148) cannot be used on equation (167), but fortunately another type of approximation is available, since approximately two roots are given by

$$\lambda_2 = l_p \qquad (168)$$

and

$$\lambda_2 = -E_2/D_2 \qquad (169)$$

Extracting these two factors from equation (167) leaves an oscillatory quadratic that can be solved without difficulty. The rolling motion represented by equation (168) is strongly damped as long as l_p is negative. It is of little interest or importance below the stall. The motion represented by equation (169) is the "spiral" stability. In level flight this motion will be stable if

$$l_v\, n_r - l_r\, n_v > 0 \qquad (170)$$

This relation determines the vertical fin area that can be used with a given dihedral, but it is not highly critical since n_v and n_r are both affected by change in the vertical fin area.

In most cases the period and the damping of the lateral oscillatory motion are given to a reasonable approximation by

$$p = 2\pi\tau\sqrt{B_2/D_2} \tag{171}$$

and

$$T = 2\tau\log_e 2/(C_2/B_2) \tag{172}$$

but these approximations are not always valid, and it is advisable to obtain a solution of equation (167) using the approximations of equations (168) and (169).

Discussion of Lateral Stability. The condition for spiral stability is that

$$l_v n_r - l_r n_v > 0 \tag{170}$$

l_v is derived from the rolling moment due to *side slip*, which is due almost entirely to dihedral, although vertical fin surface above and below the c.g. may become important. n_r is due to the damping in yaw; it depends on the fin surface and on the square of the distance of this surface from the c.g. l_r is derived from the rolling moment due to yawing, and is due chiefly to the difference in linear velocity along the wing span in a turn. The only control over l_r is found in taper or reduced span. n_v is derived from the yawing moment due to side slip and is directly proportional to the slope of the usual yawing moment curve obtained in a wind-tunnel test. There is little that the designer can do to control n_r and l_r, but both l_v and n_v may be changed at will, the former by varying dihedral and the latter by varying the vertical tail surface. Since physically l_v and n_r are negative, and l_r and n_v are positive (with the present system of axes), it follows that the positive product $l_v\ n_r$ should be greater than the positive product $l_r\ n_v$. Hence, insufficient dihedral or too much vertical fin surface tend to cause spiral instability.

The requirements for stability in the lateral oscillation are dependent on the type of motion desired. A small value of n_v and a large value of n_r will tend to give a long period heavily damped. A large value of n_v and a small value of n_r will tend to give a short period oscillation. Ample fuselage length with considerable equivalent fin surface ahead of the center of gravity appears desirable.

In general, increasing l_v reduces the damping and shortens the period, increasing n_v increases the damping and shortens the period, and increasing n_r increases the damping without affecting the period.

Calculation of Lateral Stability Derivatives. The only force coefficient entering into lateral stability is $y_v = mY_v/\rho SV$. mY_v is the total side or cross-wind force due to yaw. It is determined from the slope of the curve of cross-wind force coefficient against yaw as obtained in a wind-tunnel test. The lateral velocity v compounds with the forward velocity V to produce an effective yaw angle $\psi = -v/V$, hence, $d\psi = -dv/V$ and since $mY_v = \dfrac{dY}{dv} = \dfrac{d}{dv}\,(C_c qS)$

$$mY_v = \frac{dY}{d\psi}\cdot\frac{d\psi}{dv} = -\left(\frac{dC_c}{d\psi}\right)\frac{\rho}{2}\,SV \tag{173}$$

Hence, $y_v = -\frac{1}{2}\,[dC_c/d\psi]$ (174)

where the slope is taken in radians. The total cross-wind force should be a function of the span b and the overall length L of the airplane, or

$$(dY/d\psi) = kqbL \tag{175}$$

From wind-tunnel tests, k has an average value of about 0.10 for landplanes and about 0.14 for seaplanes and flying boats. Hence, y_v can be approximated by

$$y_v = -0.06bL/S \tag{176}$$

l_v is best obtained from a wind-tunnel test for rolling moments at various angles of yaw. Since $l_v = L_v/\rho SVl\xi$ and $L = C_l \rho bSV^2/2$

$$L_v = \frac{dL}{d\psi} \cdot \frac{d\psi}{dv} = -\frac{dC_l}{d\psi}\frac{\rho}{2}bSV$$

and

$$l_v = -\frac{b}{2\xi l}\left(\frac{dC_l}{d\psi}\right) \tag{177}$$

where b is the span, l is the tail length, and $\xi = (k_A/l)^2$. The slope of the rolling moment coefficient $(dC_l/d\psi)$ is measured in radians.

In the average airplane, l_v is due chiefly to dihedral, although the vertical location of the fin surface or effective fin surface is important. The rolling moment due to dihedral may be calculated from equation (133) from which

$$\frac{dL}{d\psi} = k\gamma\left(\frac{dC_L}{d\alpha}\right) q\, S_d b$$

and

$$\left(\frac{dC_l}{d\psi}\right) = k\gamma\left(\frac{dC_L}{d\alpha}\right)\left(\frac{S_d}{S_W}\right)$$

where γ is the dihedral angle in radians, $dC_L/d\alpha$ is the slope of the wing lift curve in radians, S_d is that part of the wing having the dihedral, and k is a constant to allow for the moment arm (in terms of the span) of the area S_d having dihedral. If $S_d = S_W$ on a wing of rectangular plan-form, then $k = 0.25$. Hence, approximately

$$l_v = \frac{-kb\gamma}{2\xi l}\left(\frac{dC_L}{d\alpha}\right)\left(\frac{S_d}{S_W}\right) \tag{178}$$

An excessive area of equivalent fin surface well below the c.g., as in a flying boat, may reduce l_v. The approximate reduction is $\Delta l_v = + y_v(h/b)$ where h is the vertical distance between the c.g. of the airplane and the center of the effective area. h is negative when the area is below the c.g.

n_v is obtained from the slope of the common yawing moment curve of a wind-tunnel test, using the same method employed to determine l_v. Since $n_v = N_v/\rho S V l \zeta$ and $N = C_N \frac{\rho}{2} S b V^2$

$$N_v = \frac{dN}{d\psi} \cdot \frac{d\psi}{dv} = -\left(\frac{dC_N}{d\psi}\right)\frac{\rho}{2} SbV$$

and

$$n_v = -\frac{b}{2l\zeta}\left(\frac{dC_N}{d\psi}\right) \tag{179}$$

where $\zeta = (k_C/l)^2$, l is the tail length and b is the span. $(dC_N/d\psi)$ is the slope of the yawing moment coefficient in radians:

$$(dC_N/d\psi) = (dN/d\psi)/qSb$$

The only accurate method available for obtaining n_v is by use of wind-tunnel test data. A fair approximation is possible, however, by use of the vertical tail surface design data in Chapter 7. If the vertical surfaces are normal, then from the data used to determine equation (125)

$$-\frac{dC_N}{d\psi} = +\ 57.3 \times 0.00050 = +\ 0.030$$

Hence

$$n_v = +\frac{0.015\, b}{l\zeta} \tag{180}$$

l_p is obtained from the rolling moment due to rolling. This is the damping in roll. It may be measured in a wind-tunnel test with a continuous rotation balance, but it may also be calculated with reasonable accuracy from the change in lift due to the change in angle of attack along the span. The calculated value is

$$L_p = -\tfrac{1}{2}\rho S V \cdot \frac{dC_L}{d\alpha} \cdot \frac{b^2}{12} \qquad (181)$$

for a rectangular wing of span b and area S.

L_p will be slightly reduced by taper. The value of l_p is

$$l_p = L_p/\rho S V l^2 \xi = -\left(\frac{dC_L}{d\alpha}\right) b^2/24 l^2 \xi \qquad (182)$$

n_p is obtained from the yawing moment due to rolling. This effect is due almost entirely to the yawing moment resulting from the change in lift direction and induced drag along the span. N_p may be obtained from wind-tunnel tests or from calculations. This quantity is difficult to measure in wind-tunnel tests so that calculated values are preferable. An integration of the moment of the lift component and the induced drag change along the span gives

$$N_p = \frac{C_L \rho S V b^2}{12}\left[\frac{1}{\pi n}\left(\frac{dC_L}{d\alpha}\right) - \frac{1}{2}\right]$$

Hence,

$$n_p = \frac{C_L b^2}{12 l^2 \zeta}\left[\frac{1}{\pi n}\left(\frac{dC_L}{d\alpha}\right) - \frac{1}{2}\right] \qquad (183)$$

where n is the effective aspect ratio and $\zeta = (k_C/l)^2$.

l_r is easily calculated from the rolling moment due to yawing, since it depends almost entirely on the change in velocity along the span. Integration of the moment due to this change in velocity along the span gives

$$L_r = C_L \rho S V b^2/12$$

from which

$$l_r = b^2 C_L/12\,\xi\,l^2 \qquad (184)$$

l_r will be reduced somewhat by tapering the wings.

N_r is derived from the yawing moment due to yawing. This is the damping in yaw usually obtained with an oscillator device in a wind tunnel. It may be calculated with fair accuracy for the wings and for the tail surfaces For the wings, the integration along the span of the yawing moment due to change in drag from change in local velocity gives

$$N'_r = -\rho V C_D S b^2/12$$

or

$$n'_r = -C_D b^2/12\,l^2\zeta \qquad (185)$$

An angular velocity of r radians per second changes the angle of attack of the vertical tail surfaces by $\Delta\psi = +l_v\,v$, from which, it may be shown that

$$N''_r = -\left(\frac{dC_{LT}}{d\psi}\right)\frac{\rho}{2}\,S_v\,Vl^2$$

or

$$n''_r = \frac{-1}{2\zeta}\left(\frac{dC_{LT}}{d\psi}\right)\left(\frac{S_v}{S_W}\right) \qquad (186)$$

Hence, by addition, the total n_r is

$$n_r = n'_r + n''_r = \frac{-C_D b^2}{12 l^2\zeta} - \frac{1}{2\zeta}\,\frac{dC_{LT}}{d\psi}\cdot\frac{S_v}{S_W} \qquad (187)$$

Collected Lateral Stability Formulas. It is convenient to have in tabular form the approximation formulas for lateral stability derivatives. These are given in Table 9 with typical values, to serve as a check on calculated values.

The derivatives y_v, l_v, and l_p do not vary greatly with the attitude of the airplane, but the others do, and for these derivatives the typical values are simply average values.

TABLE 9. LATERAL STABILITY APPROXIMATION FORMULAS

Derivative	Approximation Formula	Typical Values
y_v	$-0.06bL/S$	-0.20
l_v	$-\left(\frac{b\gamma}{8\xi l}\right)\left(\frac{dC_L}{d\alpha}\right)\left(\frac{S_d}{S_W}\right)$	-1.0
n_v	$+\frac{0.015b}{l\zeta}$	$+0.2$
l_p	$-\frac{b^2}{24l^2\xi}\left(\frac{dC_L}{d\alpha}\right)$	-5.0
n_p	$\frac{C_L b^2}{12\zeta l^2}\left[\frac{1}{\pi u}\left(\frac{dC_L}{d\alpha}\right)-\frac{1}{2}\right]$	-0.5
l_r	$\frac{b^2 C_L}{12\xi l^2}$	$+3.0$
n_r	$\frac{-b^2 C_D}{12\zeta l^2}-\frac{1}{2\zeta}\left(\frac{dC_{LT}}{d\psi}\right)\left(\frac{S_v}{S_W}\right)$	-0.6

b = Span S_W = wing area S_d = area having dihedral
S_v = Vertical area l = tail length u = effective aspect ratio
γ = Dihedral angle $\xi = (k_A/l)^2$ $\zeta = (k_C/l)^2$

All angles and slopes in radians. C_L, C_D, $\frac{dC_L}{d\alpha}$ considered positive

CHAPTER 9

PARASITE DRAG DATA

Drag Coefficients. Drag data may be given in four forms:

1. Absolute drag coefficients defined by $C_D = D/qS$ where q is the dynamic pressure $\rho V^2/2$ and S is the total surface area.
2. Absolute drag coefficients defined by $C_{DA} = D/qA$ where A is the maximum cross-sectional area.
3. Engineering drag coefficients defined by $K = D/\sigma A V^2$, where σ is the relative air density, $\sigma = \rho/\rho_0$ and V is in mph.
4. As actual drag in lb/sq ft at 100 mph in air of standard density. Denoted by symbol D_{100}.

No one of these four forms is universally desirable. Where practicable, the absolute drag coefficient C_{DA} will be used, but it is frequently convenient to use K or D_{100}. It should be noted that K is the drag in lb/sq ft at 1 mph, and that $D_{100} = K \times 10^4 = 25.58\ C_D$.

Square Flat Plates. Eiffel[1] investigated the drag of square, flat plates over a limited range in Reynolds Number. These results were originally reported as the effect of area on the drag of square plates as shown on Figure 111. These data have been converted and for a test speed of 10 m/sec they are as follows:

Length of Side cm	C_D	K	Reynolds Number
10.0	1.040	.00266	68,000
15.0	1.055	.00270	102,000
25.0	1.072	.00274	170,000
37.5	1.140	.00292	255,000
50.0	1.193	.00305	340,000
70.7	1.234	.00316	482,000
100.0	1.263	.00323	680,000

---

[1] "The Resistance of the Air and Aviation," Ch. II.

Eiffel states that for a very large plate C_D approaches the value of 1.28, or $K = 0.00328$. This value is generally used in calculating the drag at very high Reynolds Number, and in calculating the equivalent flat-plate area of parasite drag.

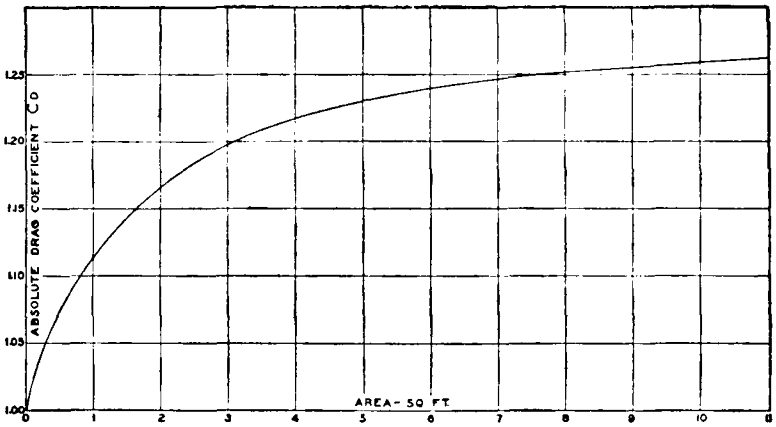

Figure 111. Effect of Area on Drag Coefficient for Square Flat Plates

Rectangular Flat Plates Normal to Wind. The drag coefficient of rectangular flat plates increases as the aspect ratio is increased. Eiffel's tests[2] are well known. Foppl made some similar tests at Göttingen.[3] Eiffel's and Foppl's data do not agree very well probably on account of the differences in Reynolds Numbers. Wieselsberger[4] has made some tests which appear more consistent; his data are plotted on Figure 112. He also tested a number of annular discs, the data for which are plotted on the same figure. It is interesting to note that the drag coefficient for infinite aspect ratio is $C_D = 2.00$, or $K = 0.00512$.

---

[2] Chapter II, "The Resistance of the Air and Aviation."

[3] Reported in the "Jahrbuch der Motorluftschiff-Studiengesellschaft," Julius Springer, Berlin (1910-1911).

[4] Göttingen Ergebnisse II, R. Oldenbourg, München (1923).

Tests at Langley Field reported in an appendix to T.R. No. 317 gives $C_D = 1.40$ for a flat plate of aspect ratio 6 at 90° angle of attack.

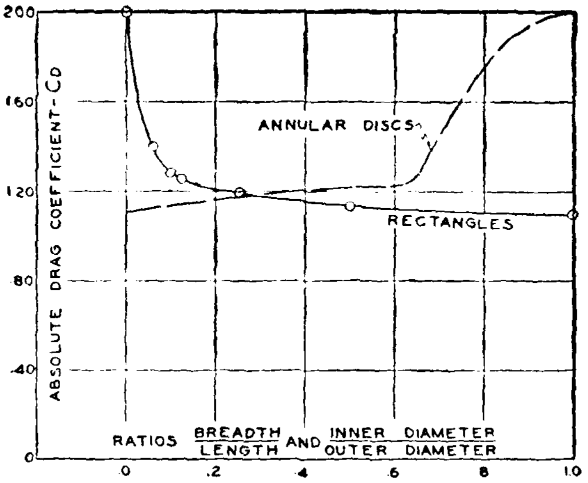

Figure 112. Drag Coefficients for Rectangles and Annular Discs

Circular Discs. The resistance of circular discs has been measured in various wind tunnels, and the results are in excellent agreement. Eiffel found $C_D = 1.055$ and 1.08 for 15 cm and 30 cm discs respectively, when tested at a speed of 10 m sec. Wieselsberger[5] tested four discs 3, 6, 15.1, and 40 cm in diameter over a wide range in Reynolds Number obtaining values of C_D varying from 1.07 to 1.13, with an average value of about 1.11.

A 15-cm disc tested in the N.A.C.A. variable-density wind tunnel[6] at Reynolds Numbers ranging from 210,000 to 4,440,000 gave values of C_D between 1.077 to 1.139 with an average value of about 1.11.

---

[5] See "Ergebnisse der Aerodynamischen Versuch-Anstalt Zu Göttingen," II, pp. 28 32, R. Oldenbourg, Munchen (1923).

[6] James M. Shoemaker, "Resistance of a Fifteen-Centimeter Disc," N.A.C.A. Technical Note No. 252 (1926).

In both the Göttingen and the N.A.C.A. tests there was no definite change of C_D with Reynolds Number, although there is a little evidence of the existence of the critical Reynolds Number which is found for cylinders and spheres. For any ordinary size of disc or wind speed, the average value $C_D = 1.11$ may be used. For Reynolds Numbers above 6,000,000, the coefficient is unknown.

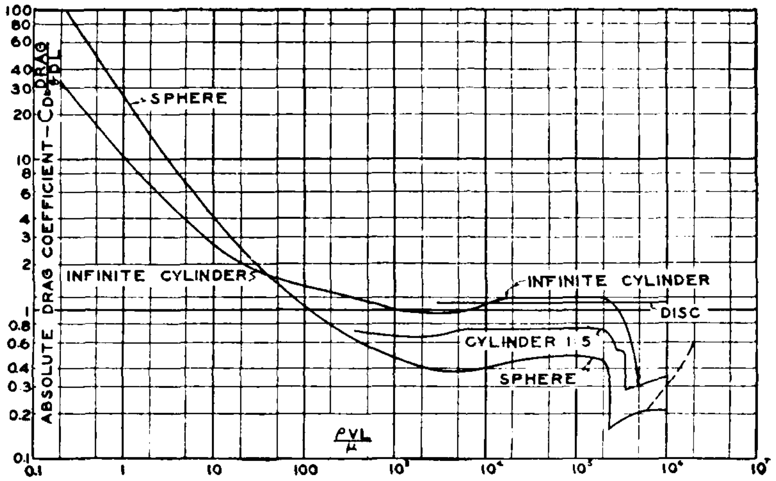

Figure 113. Variation of C_D with Reynolds Number—Cylinders and Spheres

Spheres. The drag of spheres has been measured over an extremely wide range in Reynolds Number. The variation of C_D with Reynolds Number given on Figure 113 is based on a compilation of test data from various sources made at the Washington Navy Yard by Dr. A. F. Zahm[7] and Mr. F. A. Louden. Additional data on sphere drag are given on page 87.

Spheroids and Ellipsoids. Drag coefficients of two ellipsoids are compared with those for a sphere[8] in Figure 114.

---

[7] A. F. Zahm, "Flow and Drag Formulas for Simple Quadrics," N.A.C.A. Technical Report No. 253 (1926).

[8] Based on data in "Göttingen Ergebnisse," II.

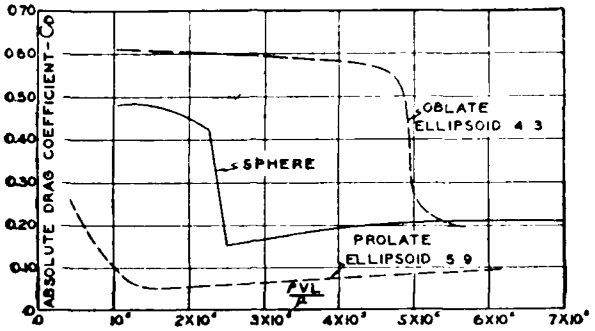

Figure 114. Drag Coefficients for Spheroids and Ellipsoids

Hemispheres; Parachutes. Eiffel tested a hemispherical cup and found $C_D = 0.33$ when the convex side was presented to the wind and $C_D = 1.33$ when the concave side was presented to the wind. Tests made by N.A.C.A.[9] in an extensive study of the Robinson-type cup anemometer indicate values of $C_D = 0.28$ and $C_D = 1.38$. These values do not appear to depend to any appreciable extent on the Reynolds Number or the form of the cup.

The value $C_D = 1.33$ is often used for parachutes on the basis of the projected area when inflated. The form of an inflated parachute is approximately that of the surface of an ellipsoid and the projected area is about 55% of the surface area. The limiting velocity of a parachute is therefore given by

$$V_L = \sqrt{\frac{2W}{1.33\,\rho\,(0.55S)}} \tag{188}$$

where W is the total weight of the parachute plus its load, S is the total surface area and ρ is the air density. For W in pounds, S in square feet, the value of V_L in ft/sec in air of standard density is

$$V_L = 34\sqrt{W/S} \tag{189}$$

---

[9] M. J. Brevoort and U. T. Joyner, "Experimental Investigation of the Robinson-Type Cup Anemometer," N.A.C.A. T.R. No. 513 (1935).

Cylinder with Axis Normal to Wind. The drag of cylinders normal to the wind has been thoroughly investigated. Figure 113 gives the variation of C_D with Reynolds Number, both for a section of an infinite cylinder and for a section 5 diameters in length. These curves are based on test data obtained at the Washington Navy Yard and other laboratories, as compiled by Dr. A. F. Zahm[10] and Mr. F. A. Louden.

Cylinder with Axis Parallel to Wind. Eiffel tested two series of cylinders with the axes parallel to the wind. In one series the diameter was 30 cm and in the other 15 cm. Lengths from a thin disc up to 7.0 diameters were tested at a wind speed of 10 m/sec. The ratio of the drag of the cylinders to the drag of the discs are plotted against length/diameter ratio in Figure 115.

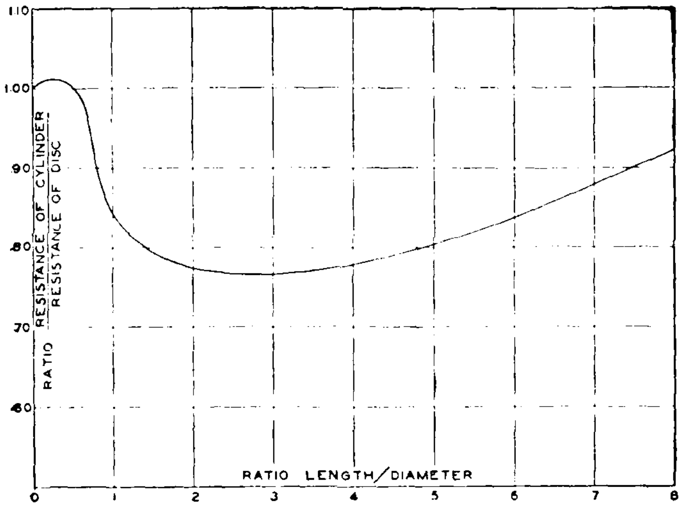

Figure 115. Drag Coefficients for Cylinders Parallel to the Wind

---

[10] See N.A.C.A. Technical Report No. 253.

Subsequent tests on the cylinder with length/diameter = 7.0 showed the value of C_D to be reduced from 0.94 to 0.19 by fitting hemispherical ends.

Skin Friction. The skin friction resistance of a very smooth surface such as glass, varnished wood, or doped fabric, is given by

$$D_F = C_{DF}\frac{\rho}{2}SV^2 \tag{190}$$

where ρ is the air density, S the total area or "wetted surface," V the air speed, and C_{DF} the frictional drag coefficient given on Figure 116. C_{DF} is also given by the relation

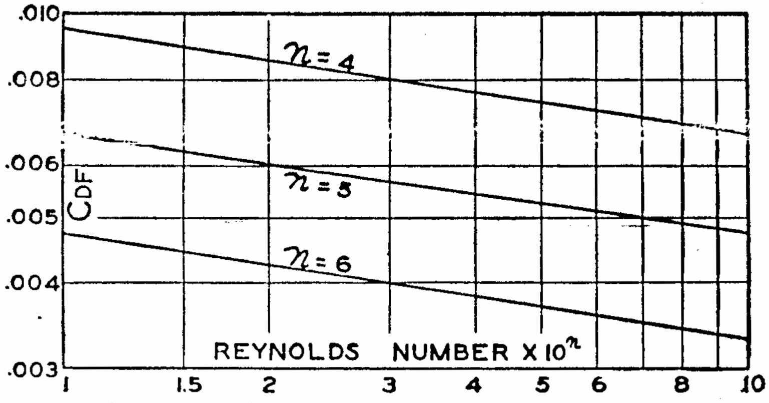

Figure 116. Skin Friction Drag Coefficient C_{DF}

$$C_{DF} = 0.0375\left(\frac{\rho VL}{\mu}\right)^{-0.15}$$

$$= 0.0375\,(\text{RN})^{-0.15} \tag{191}$$

hence

$$D_F = 0.0375\,(\text{RN})^{-0.15}\,qS \tag{192}$$

The frictional drag coefficient of a surface which is not very smooth, such as unvarnished wood, undoped cloth, etc., varies with the roughness of the surface between 0.005 and 0.010 and is substantially constant for all Reynolds Numbers over a wide range, including the common full-scale values.

Some doubt exists as to the correct form of equation (192) on the basis that breadth should enter directly, so that the frictional coefficient varies as a function of length and Reynolds Number. There is also some doubt as to the validity of the equation for short lengths, but this doubt probably arises from the difficulty which some experimenters have had in separating form resistance from frictional resistance. The total "profile drag" of a thin section may be less than the skin friction. Equation (192) is certainly sufficiently accurate for most engineering purposes.

For L = 10.0 ft and V = 100 mph at sea-level, RN = 9,350,000 and $C_{DF} = 0.0033$. Hence, the skin friction per unit area of wetted surface is $D/S = C_{DF} \cdot q = 0.084$ lb/sq ft.

Values of C_{DF} are as follows:

Reynolds Number	C_{DF}
100,000	.0067
500,000	.0052
1,000,000	.0047
2,000,000	.0042
5,000,000	.0037
10,000,000	.0033
20,000,000	.0030
50,000,000	.0026

Wing Profile Drag. The minimum wing profile drag is primarily a function of camber and thickness ratio, as indicated by Figure 45. It is also a function of surface finish and smoothness. For wings having a very smooth surface in good condition, the value of C_{D_0} minimum will be about 10% greater than the variable-density wind-tunnel values. Average values of D/S at 100 mph for 2% mean camber are given on Figure 117.

It is of considerable interest to note that the values of C_{D_0} minimum for the thinner sections are approximately equal to the skin friction coefficient doubled. Hence, in the better wing sections, the minimum profile drag is entirely frictional in its origin.

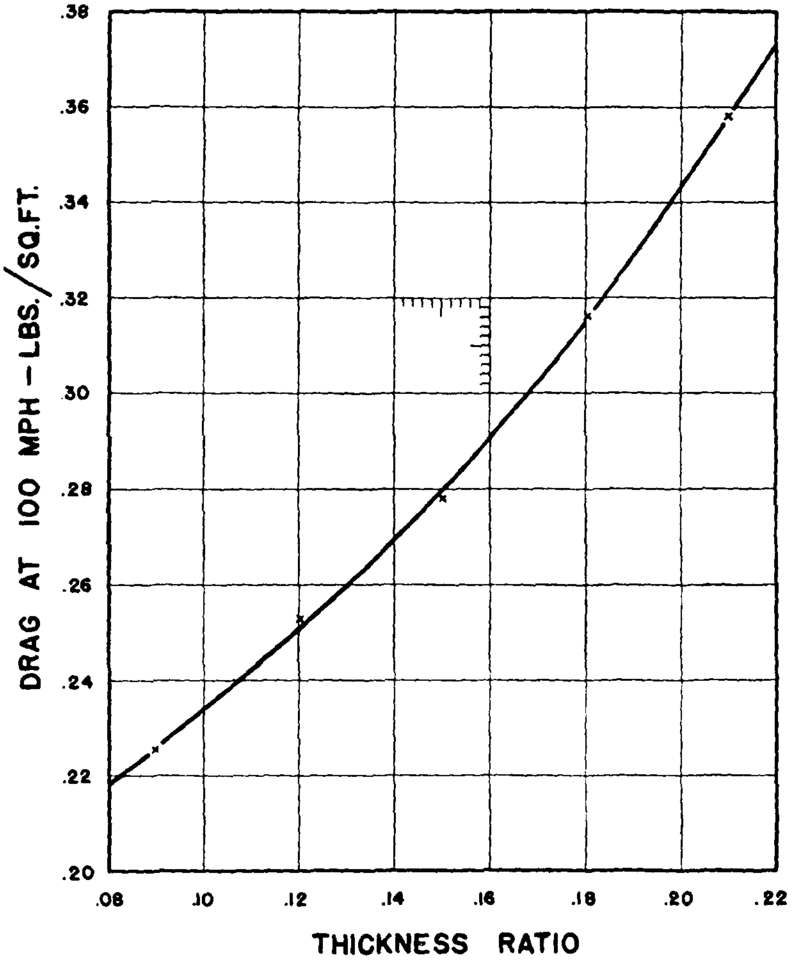

Figure 117. Airfoil Drag as a Function of Thickness Ratio

Wing Surface Finish. The wing surface finish is an important factor in determining the profile drag. Tests in the variable-density wind tunnel[11] show marked effects on lift and drag due to surface finish as follows:

---

[11] R. W. Hooker, "The Aerodynamic Characteristics of Airfoils as Affected by Surface Roughness," N.A.C.A. T.N. No. 457 (1933).

Metal airfoil, polished . . . . $C_L = 0.20$ . . . . $C_{D_0} = .0080$
Wooden airfoil, 2 coats shellac . . . . $C_{D_0} = .0095$
Wooden airfoil, highly polished . . . . $C_{D_0} = .0085$
Metal, 180 carborundum on upper surface . . . . $C_{D_0} = .0160$

The first three finishes are not greatly different. The last is, of course, noticeably rough and simulates a walkway. The effect of simulated lap-joints was small but not negligible.

Tests in the N.A.C.A. Full-Scale Wind Tunnel[12] show that the minimum C_D is reduced by 0.0010 when a wing surface with standard commercial finish is treated with 12 additional coats of clear lacquer and 3 coats of wax, thoroughly polished between each coat. This is about a 10% reduction in wing drag, but the required treatment is impracticable, and the chief value of the test is to show one reason why the variable-density tunnel drag data cannot be used without correction.

Rivets. The drag increase due to exposed rivet heads on an airplane wing has been measured in the full-scale wind tunnel at Langley Field.[13]

The rivet heads were simulated by lead stampings 5/16 inch in diameter by 1/16 inch in thickness, spaced 1 inch apart. The results are as follows:

	C_D at 55 mph	C_D at 120 mph	% Increase
Plain wing	.0094	.0090	0
1 Row on L. E.	.0096	.0092	2.0
1 Row at 5% C	.0112	.0102	13.0
1 Row at 15% C	.0109	.0100	11.0
1 Row at 30% C	.0103	.0096	7.0
9 Rows on top surface	.0114	.0103	14.0
9 Rows on each surface	.0120	.0106	18.0

Protuberances on Wing. Wing lift and profile drag may be profoundly affected by small protuberances,[14] especially if these are on the upper surface near the leading edge. The variation of effect with protuberance height, and location, is rather complex but as a general rule, the additional drag is obtained with reasonable accuracy by considering the frontal area as a flat plate. This holds for all reasonable heights and locations on the lower surface and for heights less than 0.001 *c* on the upper surface. For heights greater than 0.002 *c* and locations between 0.05 *c* and 0.65 *c*, the drag added will be approximately twice the flat-plate drag of the protuberance frontal area. This additional drag is very large in comparison with the airfoil drag, at $C_L = 0.2$ a protuberance 0.002 *c*, or 0.1 in. on a 50-in. chord increases the wing C_D from 0.0085 to about 0.0120. A protuberance of short span has more effect on lift than on drag.

---

[12] S. J. DeFrance, "Effect of the Surface Condition of a Wing on the Aerodynamic Characteristics of an Airplane," N.A.C.A. T.N. No. 495 (1934).

[13] C. H. Dearborn, "The Effect of Rivet Heads on the Characteristics of a 6 by 36-foot Clark Y Metal Airfoil," N.A.C.A. T.N. No. 461 (1933).

[14] E. N. Jacobs, "Airfoil Section Characteristics as Affected by Protuberances," N.A.C.A. T.R. No. 446 (1932), also E. N. Jacobs and A. Sherman, "Wing Characteristics as Affected by Protuberances of Short Span," N.A.C.A. T.R. No. 449.

The references listed should be given careful study by the designers, since it is shown that most of the bad effects can be eliminated by simple fairing.

Corrugated Metal Wings. Tests on 2 x 12-ft wing models[15] at a Reynolds Number of 2,000,000 gave minimum profile drag coefficients as follows:

	C_{D0}	% Increase
Plain Clark Y	.0086	0
Corrugated A	.0118	37.0
Corrugated B	.0104	21.0

The corrugations had a depth of 0.0052 *c* and a pitch of 0.0165 *c*. In corrugation A the bottom of the corrugations formed the Clark Y section, while in corrugation B, the top of the corrugations formed the Clark Y section.

An average increase of about 30% in C_{D0} should be allowed for corrugated metal wing covering.

Gas Tank on Wing. A local unsymmetrical increase in wing thickness to provide volume for a fuel tank has a marked effect on both lift and drag.[16] Doubling the thickness of the Clark Y section over 1/15th of the span at the center gives approximately

---

[15] D. H. Wood, "Tests of Large Airfoils in the Propeller Research Tunnel, Including Two with Corrugated Surfaces." N.A.C.A. T.R. No. 336 (1929).

	$C_{L\,max}$	C_{D_0}
Plain Clark Y	1.50	.0095
Increased above	1.41	.0120
Increased below	1.38	.0140

Any necessary local increase of the wing thickness should be symmetrical with respect to the mean camber line, which will not give any appreciable effect on either lift or drag.

Tail Surfaces. The normal drag of the tail surfaces is, in general, about twice the drag of the basic undistorted

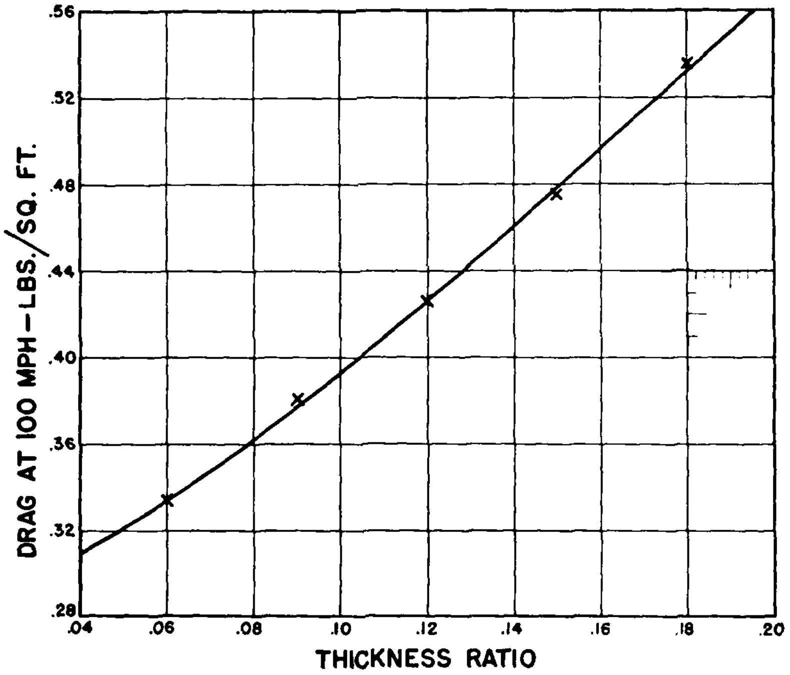

Figure 118. Tail Surface Drag as a Function of Thickness Ratio

section, or about 0.40 lb per sq ft at 100 mph. This figure may be increased to as much as 0.50 lb per sq ft for very thick sections, or reduced to 0.30 lb per sq ft for very thin sections. The curve of Figure 118 gives the variation of unit drag with thickness ratio.

---

[16] E. N. Jacobs, "Effect of Protruding Gasoline Tanks upon the Characteristics of an Airfoil," N.A.C.A. T.N. No. 249.

The drag of the tail surfaces is appreciably affected by the stabilizer setting and elevator angle for trim. Where speed is of prime importance, the best stabilizer setting must be carefully determined, since the profile drag coefficient may easily be doubled by a low tail lift obtained with a large elevator angle.

TABLE 10. OFFSETS FOR NAVY STRUT AND C-CLASS AIRSHIP

% *L*	% *D*		% *L*	% *D*	
	Navy No. 1 Strut	C-Class Air-ship		Navy No. 1 Strut	C-Class Air-ship
0	0	0			
1.25	26.0	20.0	35.00	100.0	99.9
2.50	37.1	33.5	40.00	99.5	99.0
5.00	52.5	52.6	50.00	95.0	95.0
7.50	63.6	65.8	60.00	86.1	88.5
10.00	72.0	75.8	70.00	73.2	79.0
12.50	78.5	83.5	80.00	56.2	66.5
15.00	83.6	88.7	90.00	33.8	49.3
20.00	91.1	94.7	95.00	19.0	36.2
25.00	95.9	98.2	98.00	7.8	22.5
30.00	98.8	99.8	100.00	0	0

Struts. Figure 119 shows the drag coefficients obtained on Navy No. 1 struts in tests at the Washington Navy Yard and at Langley Field. The Navy No. 1 appears to have the lowest drag yet recorded for a strut section. The offsets are given in Table 10.

In Figure 119, C_D is plotted against *VD* instead of Reynolds Number. *V* is the air speed in ft/sec and *D*

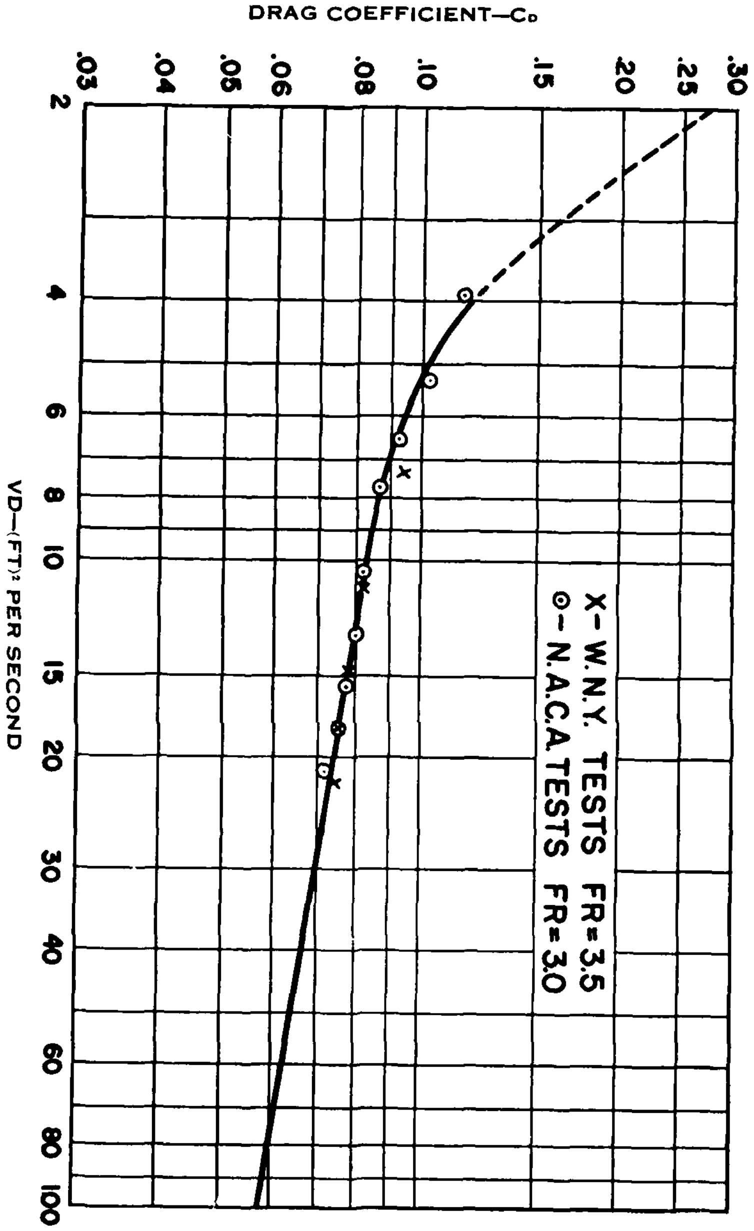

Figure 119. Drag Coefficients for Struts

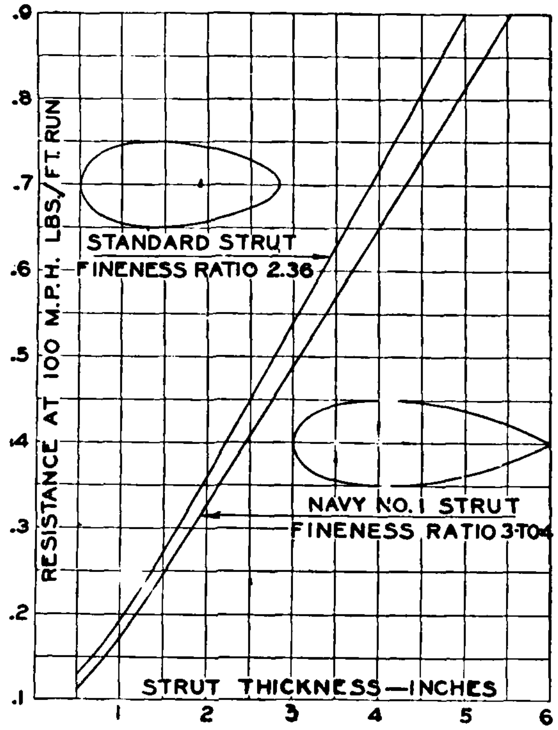

Figure 120. Drag per Foot at 100 mph. Navy Struts

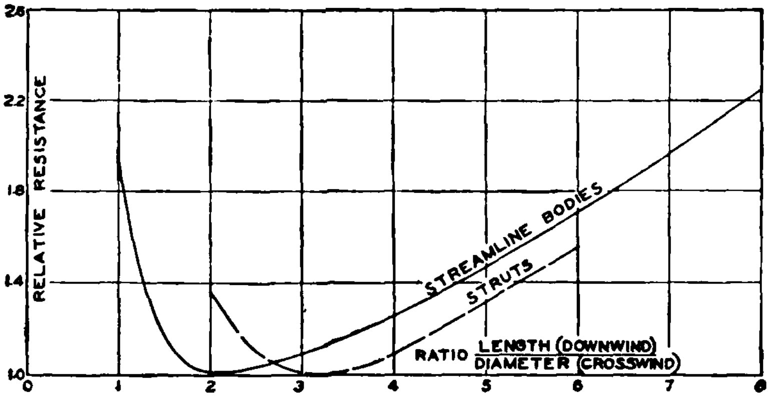

Figure 121. Variation of Drag Coefficient with Fineness Ratio for Struts and Streamline Bodies

is the width of the strut. Reynolds Number = $VD \times 6378$. For values of VD greater than 10, C_D is given by

$$C_D = 0.12\ (VD)^{-0.15} \tag{193}$$

Drag in lb per ft at 100 mph in standard air for a strut of fineness ratio 3, is plotted against strut thickness in Figure 120. Rounding the trailing edge does not appear likely to give large increase in drag, providing the radius is small. Cutting off about 15% from the rear of a strut does not affect the drag at all, according to Munk's tests reported in the Technische Berichte.

The change in drag with fineness ratio is shown on Figure 121. This is a composite curve based on British, German, and American tests, which differ very little.

Streamline Bodies. The drag of streamline bodies at 0° pitch and yaw is not only very difficult to measure accurately, but it is also greatly affected by surface irregularities, disturbance, or turbulence in the air flow, and by change in Reynolds Number. The form having the least drag per unit of cross-section area does not necessarily have the least drag per unit of volume, and the form which shows up best at one Reynolds Number may be comparatively poor at some other Reynolds Number.

The C-Class airship is a form which has a very low drag under all conditions. This shape has been thoroughly tested at the Washington Navy Yard for the effect of inserting parallel middle body[17] and for the effect of varying the spacing between stations. The drag may be written in the form

$$D = K\left(\frac{\rho}{\rho_0}\right)\left(\frac{Vd}{100}\right)^n \tag{194}$$

where D is the drag in lb, V the air speed in ft per sec, and d the diameter in ft. Both K and n vary with fineness

---

[17] A. F. Zahm, R. H. Smith, and G. C. Hill, "The Drag of the C-Class Airship Hull with Varying Lengths of Cylindric Midships," N.A.C.A. Technical Report No. 138 (1922).

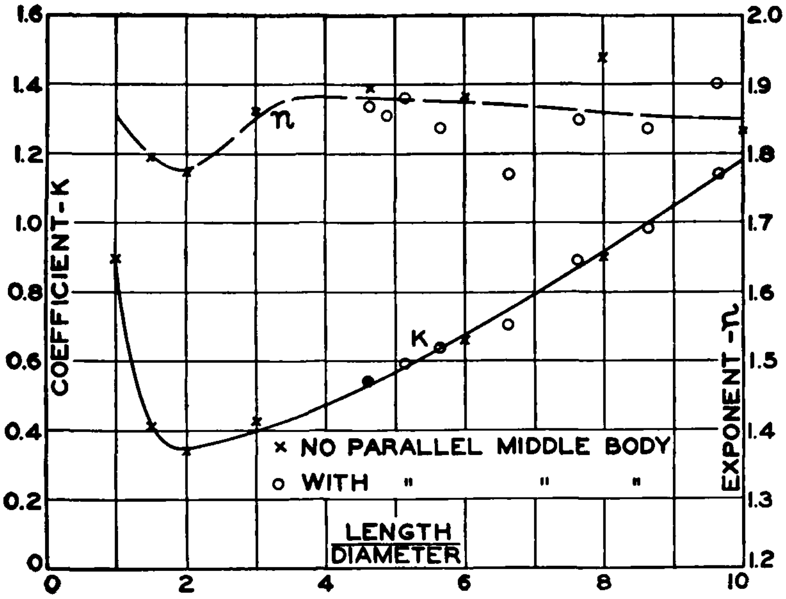

Figure 122. Effect of Fineness Ratio on K and n in Equation for Drag of C-Class Airship

ratio as shown on Figure 122. Allowing for the fact that the value of n is very difficult to determine, the test data are quite consistent.

Offsets for the C-Class are given in Table 10.

Aircraft Cable. The variation of C_D with Reynolds Number for round wire is given on Figure 123. The range in C_D actually encountered is not very large and it is customary to take $C_D = 1.20$ for all normal sizes and speeds. This applies only to full scale, and gives

$$D \text{ lb/ft} = 2.56\, d\, (V/100)^2 \tag{195}$$

where d is the diameter in inches and V the air speed in mph at standard density. The drag of various sizes of wires and turnbuckles may be found with other data in Table 11.

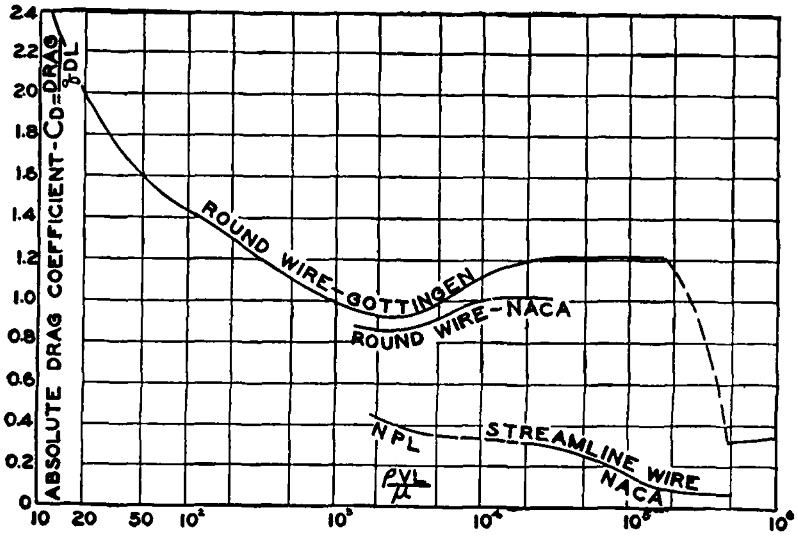

Figure 123. Variation of C_D with Reynolds Number for Wires

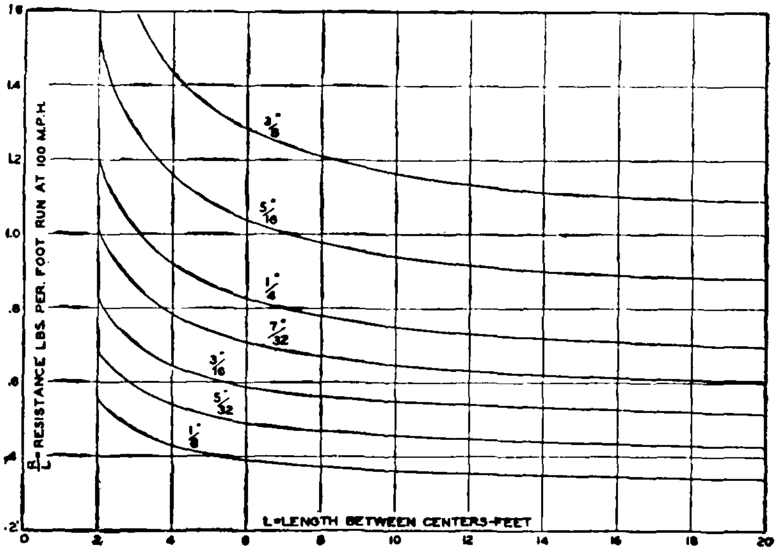

Figure 124. Drag per Foot at 100 mph for Cables with Turnbuckles and Eyes

Figure 124 is a plot of total drag divided by total length, that is, drag per foot, at 100 mph for various sizes and lengths of cable, complete with terminals.

The effect of fore-and-aft spacing is shown on Figure 125.

The effect of inclination is given on Figure 126. The curves marked *A* and *B* are two sets of test data for which the drag ratio refers to unit length. The curve marked *C* is the average drag ratio per unit of projected length.

Lift and drag coefficients as a function of angle of attack are given for both smooth wire and cable on Figure 127. These are the usual absolute coefficients, for example,

$$\text{Lift} = C_L \frac{\rho}{2} S V^2$$

S being the product of the wire length in feet by its diameter in feet.

TABLE 11. DATA ON AIRCRAFT CABLE

Diameter		Approximate Wt. per 100 ft. lbs.	Breaking Strength min. lbs.	Resistance at 100 mi. hr.		
Nominal in.	in.			Wire Alone per ft. run	Turnbuckles Plus Eyes Complete	Turnbuckles Plus One Eye Only
$\frac{1}{16}$	.062	.81	480	.16	.42	.25
$\frac{5}{64}$	.078	.95	550	.20	.48	.29
$\frac{3}{32}$	.094	1.45	920	.24	.52	.33
$\frac{1}{8}$	.125	2.45	1,350	.32	.65	.43
$\frac{5}{32}$	.156	4.67	2,600	.40	.82	.53
$\frac{3}{16}$	.187	5.80	3,200	.48	1.01	.63
$\frac{7}{32}$	.218	8.30	4,600	.56	1.24	.74
$\frac{1}{4}$	.250	10.50	5,800	.64	1.50	.86
$\frac{5}{16}$	.312	16.70	9,200	.80	2.05	1.08
$\frac{3}{8}$	.375	....	....	.96	2.60	1.33

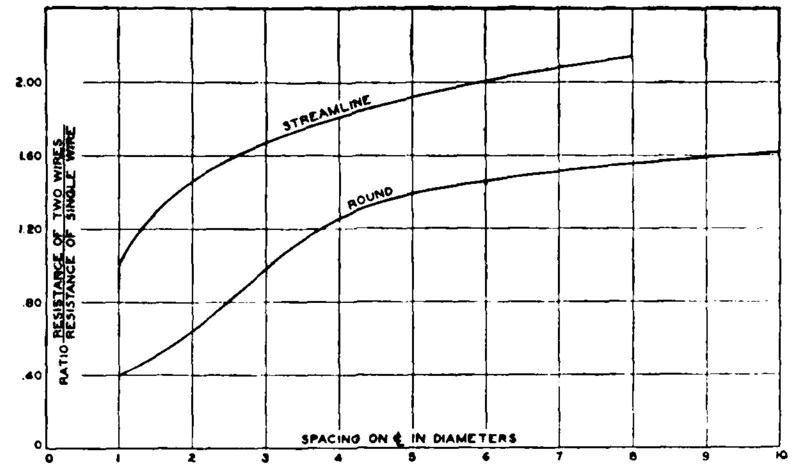

Figure 125. Effect of Fore-and-aft Spacing on the Drag of a Pair of Wires

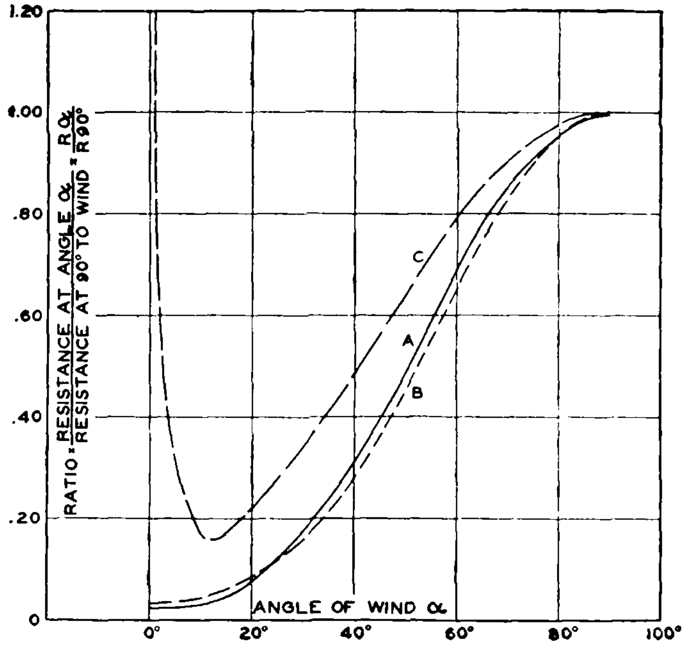

Figure 126. Effect of Inclination on the Drag of Wire and Cable. Curves *A* and *B* are based on Unit Length; Curve *C* on Projected Length

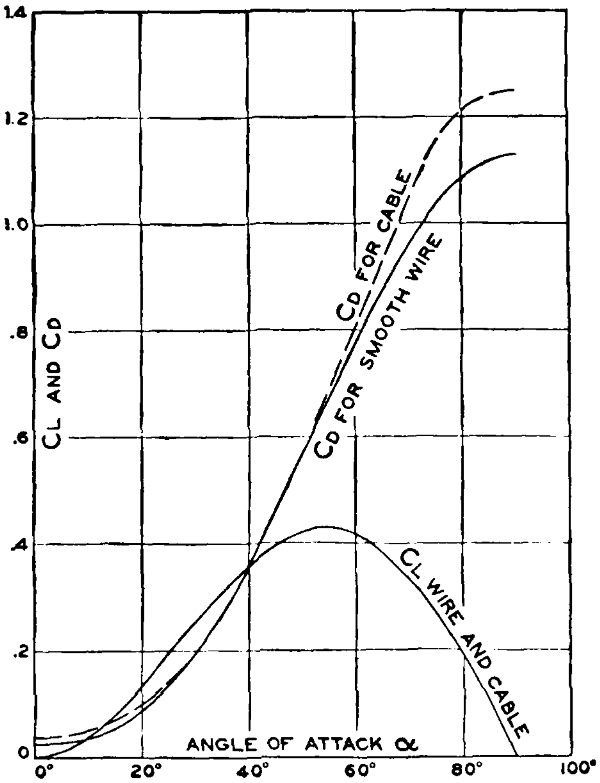

Figure 127. Lift and Drag Coefficients for Round Wire and Cable

Streamline Wire. The drag of streamline wire has been measured by N.P.L. and N.A.C.A. and the variation of C_D with Reynolds Number is given on Figure 123. The two sets of data fall on a single curve.

Figure 128 gives the drag in lb per ft at 100 mph; also the drag of two standard terminals at the same speed. It is customary to use the projected length of inclined streamline wire in calculating the drag. This is an approximation which is sufficiently exact if the angle is not less than about 40°.

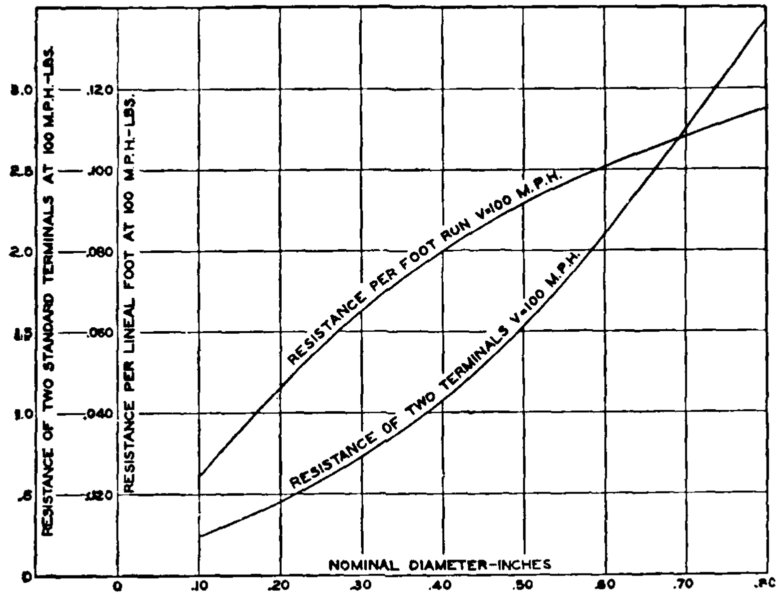

Figure 128. Drag of Streamline Wire and Standard Terminals

Figure 129 gives the total drag divided by total projected length for various sizes and lengths of streamline wires with standard terminals.

The effect of fore-and-aft spacing on double streamline wires is shown on Figure 125, and the effect of yaw on the drag of a single wire is shown on Figure 130.

Table 12 contains data on the standard sizes of streamline wire.

Tests have been made at Langley Field[18] to supply data for comparing drag of wires having the standard lenticular streamline section and wires having true streamline sections. The C_D values are as follows:

Reynolds Number	20,000	40,000	60,000	80,000
Standard Streamline	.20	.16	.11	.09
0025 64	.18	.11	.08	.07
0025 63	.10	.07	.06	.06

---

[18] E. N. Jacobs, "The Drag of Streamline Wires," N.A.C.A. T. N. No. 480 (1933).

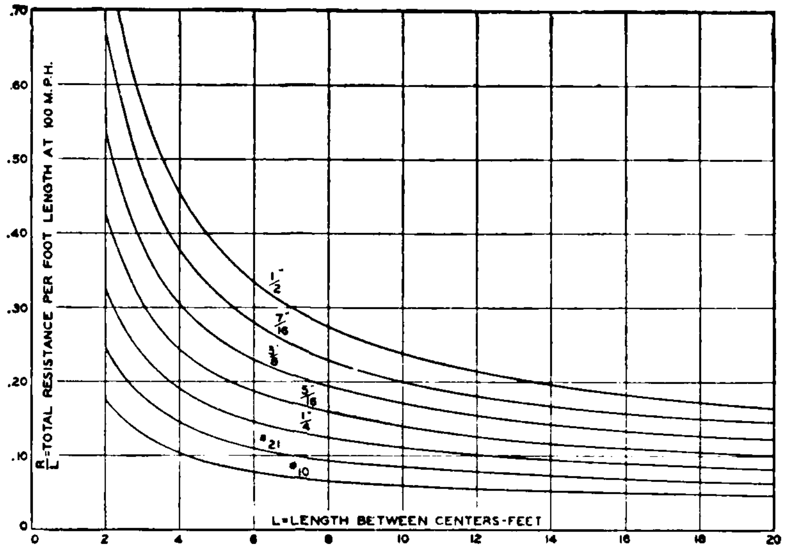

Figure 129. Drag per Foot at 100 mph for Streamline Wire with Standard Terminals

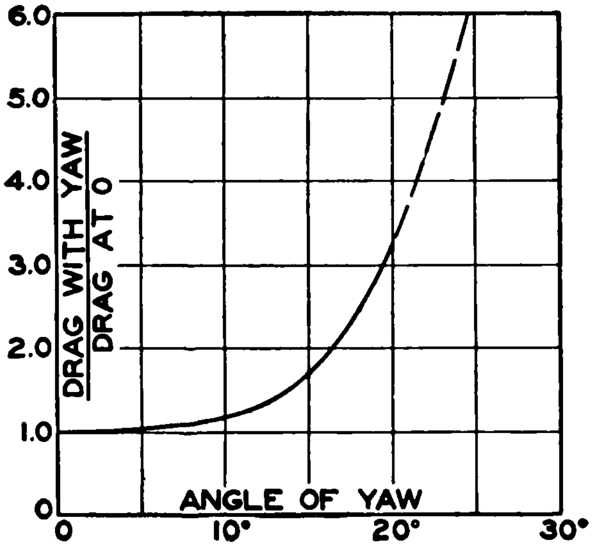

Figure 130. Effect of Yaw on Drag of Streamline Wire

In the above, RN = $V\lambda/\nu$ and $C_D = D/qL\lambda$, where λ is the square root of the cross-sectional area. Both true streamline sections appear to have a marked advantage over the standard section, but practical considerations favor the standard section.

TABLE 12. STREAMLINE WIRE DATA

AN No.	Size	Threads per Inch	Diam. at Ends Inches	Breaking Strength	Streamline Section Inches	Resistance per foot Projected Length at 100 mph lb	Resistance of Two End Fittings at 100 mph
671	6	40	.138	1,000	.048 x .192	.033	.30
673	10	32	.190	2,100	.064 x .256	.044	.43
674	$\frac{1}{4}$	28	.250	3,400	.087 x .348	.056	.58
675	$\frac{5}{16}$	24	.312	6,100	.110 x .440	.067	.76
676	$\frac{3}{8}$	24	.375	8,000	.135 x .540	.077	.97
677	$\frac{7}{16}$	20	.437	11,500	.159 x .636	.085	1.23
678	$\frac{1}{2}$	20	.500	15,500	.183 x .732	.092	1.53
679	$\frac{9}{16}$	18	.562	20,200	.209 x .836	.098	1.90
680	$\frac{5}{8}$	18	.625	24,700	.231 x .924	.104	2.30

Fuselage Drag: Model Data. Drag data on fuselages and similar airplane parts have been compiled by the Bureau of Aeronautics, Navy Department, and published as N.A.C.A. Technical Report No. 236.[19] Since the publication of this report, additional tests have been made at the Washington Navy Yard on the models illustrated in Figure 131. The data on these models are given in Table 13.

Models Nos. 3, 4, and 5 are practically pure streamlines, which were tested in order to supply a basis for comparison. Models 7 and 9 were tested in order to find some form of simple model construction that would have the same drag as an air-cooled engine; No. 9 gives a close approximation. Several additional models not shown

---

[19] W. S. Diehl, "Tests on Airplane Fuselages, Floats and Hulls," N.A.C.A. Technical Report No. 230 (1926).

TABLE 13. DATA ON AIRPLANE FUSELAGE MODELS SHOWN IN FIGURE 131

Model No.	Dimensions		Measured Drag at 40 mi./hr. lb.	K	Absolute Drag Coefficient
	Length ft.	Cross Section Area A sq. ft.			
1	1.670	.0457	.066	.00091	.353
2	1.668	.0459	.050	.00068	.266
3	1.669	.0472	.012	.00016	.062
4	1.668	.0548	.016	.00018	.071
5	1.673	.0621	.016	.00016	.063
6	1.673	.0463	.022	.00030	.116
7	1.673	.0708	.058	.00051	.200
8	1.663	.0550	.021	.00024	.094
9	1.662	.0662	.068	.00064	.251
10	1.667	.0862	.036	.00026	.102
11	1.667	.0481	.026	.00034	.132
12	1.667	.0397	.027	.00042	.166

were tested in this investigation; the conclusion was reached that the model cylinders should be solid to the outer edge of the fins and up to the top of the cylinder. The remaining models closely represent well-known airplane fuselages.

If all the engine, radiators, windshields, fittings, and other details are considered separately, the average value of K is approximately 0.00040. If all of the minor details are not considered, the average value of K will be about 0.00050. The latter figure takes care of the minor items only, such as fittings and irregularities of construction.

The drag coefficients for nacelles are not appreciably different from those for fuselages.

Effect of Pitch on Fuselage Drag. The drag of a fuselage with well-rounded section does not change greatly with angle of pitch while the drag of a fuselage with square or rectangular sections increases rapidly with increasing pitch. Consider models Nos. 2 and 3 in Figure 131.

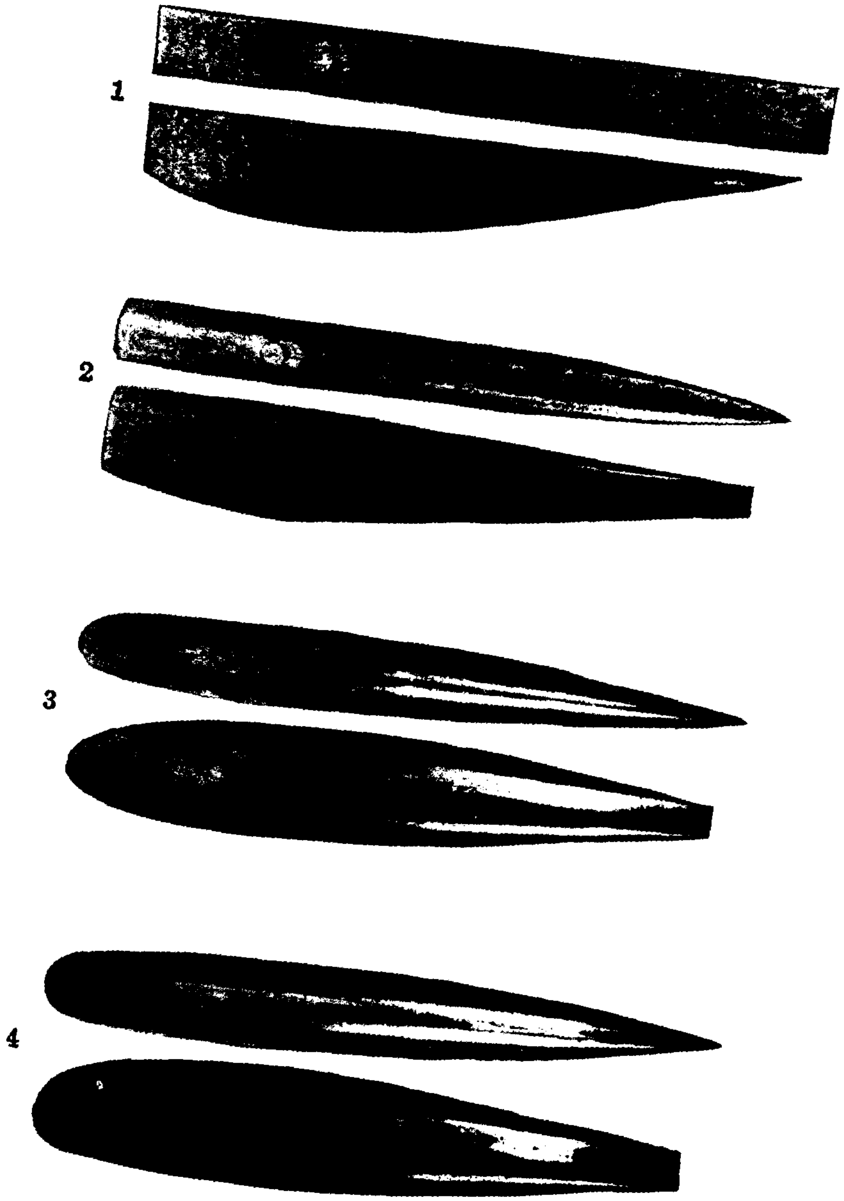

Figure 131a. Fuselage Models

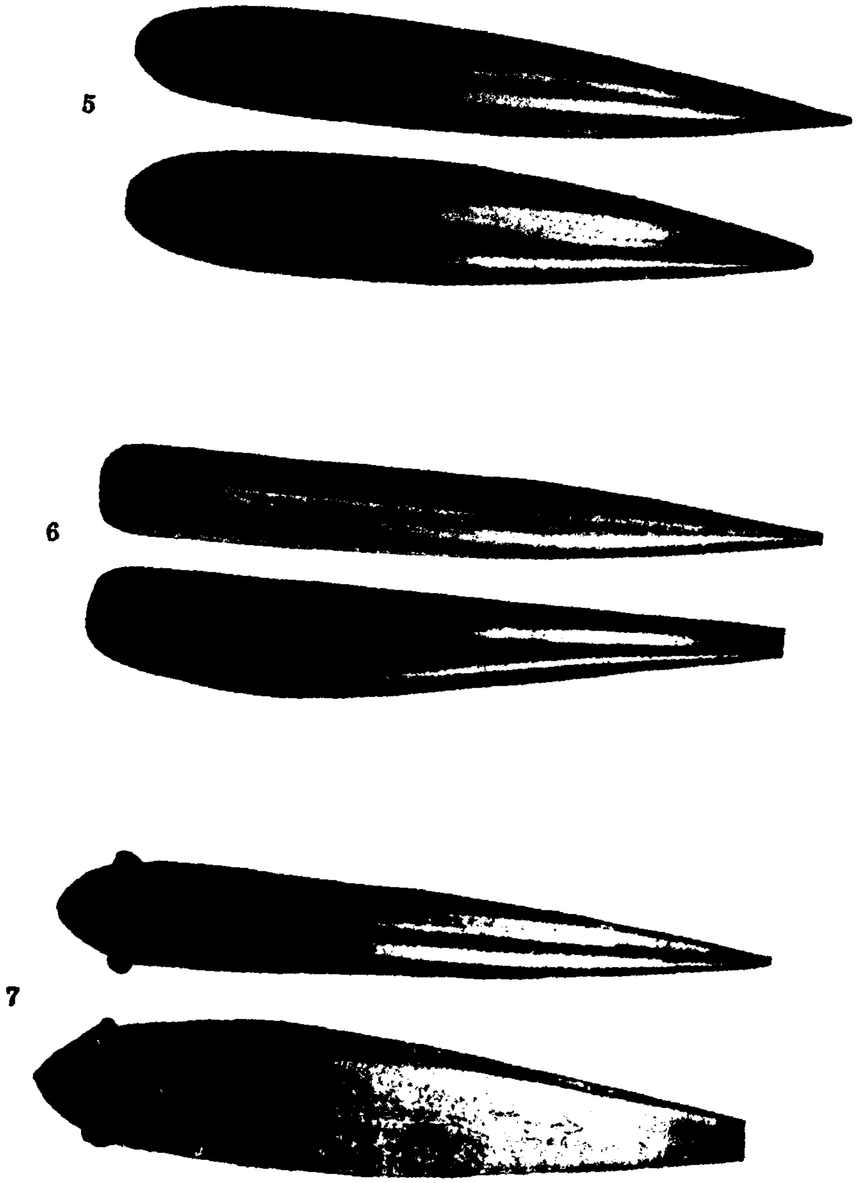

Figure 131b. Fuselage Models

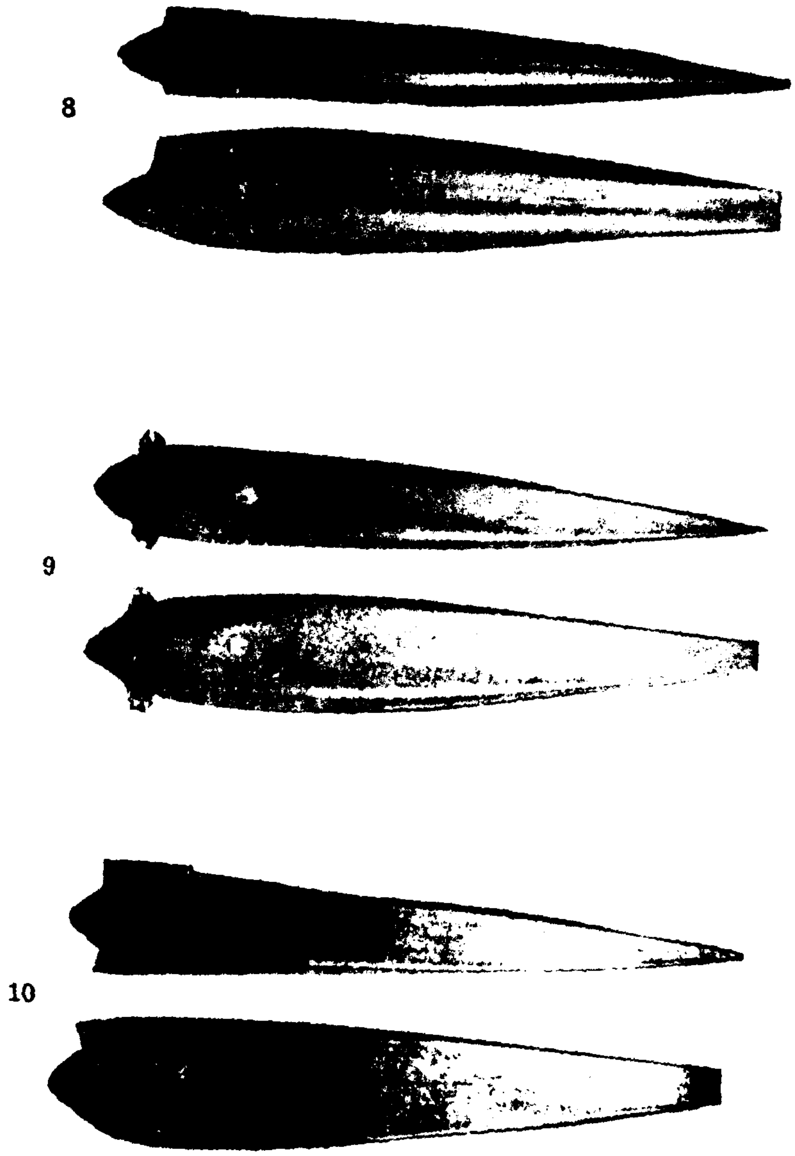

Figure 131c. Fuselage Models

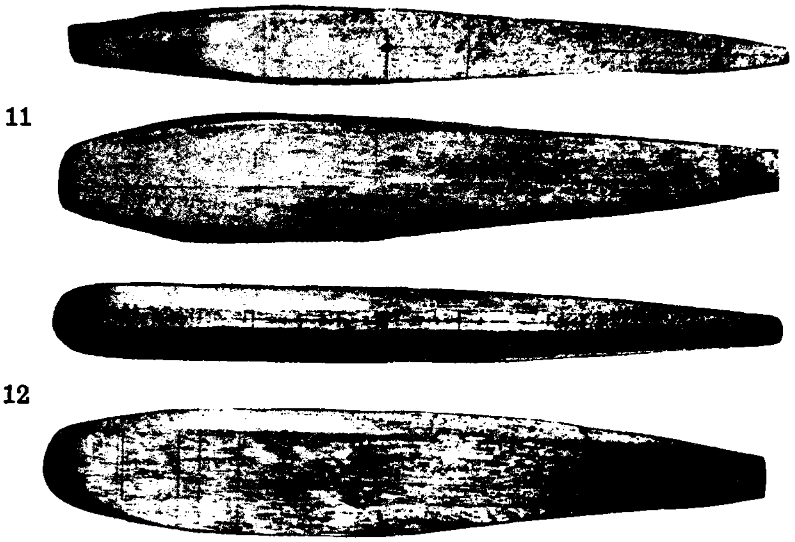

Figure 131d. Fuselage Models

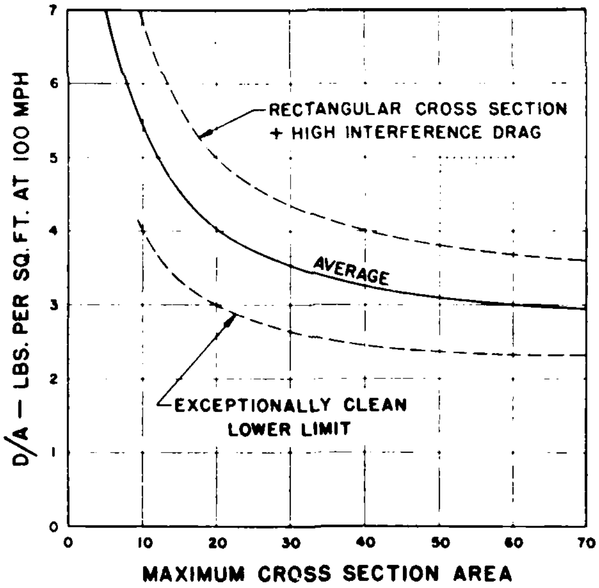

Figure 132. Fuselage Drag as a Function of Cross-Section Area

The measured model drag in pounds at 40 mph varies with pitch as follows:

Angle of Pitch:	0°	5°	10°	15°	20°
Model No. 2	.050	.057	.070	.083	.129
Model No. 3	.012	.012	.010	.014	.022

Rounding the sections of a fuselage reduces the drag at 0°, and gives an even greater improvement at cruising and climbing speeds.

Fuselage Drag: Full Scale. N.A.C.A. tests[20] on the Sperry Messenger gave a drag of 25.0 lb. at 100 mph for the fuselage having a maximum cross-section area of about 6.0 sq ft. The windshield and open cockpit each added 3.0 lb drag at 100 mph.

The idealized cabin fuselage used in the original cowling tests[21] had a drag of 40 lb at 100 mph, with a maximum cross-section area of 21.3 sq ft. Hence, $D/A = 1.88$ lb/sq ft. or $C_D = 0.0735$. This value cannot be attained in a practicable design.

The idealized open-cockpit fuselage used in the original cowling tests had a basic drag of 28 lb at 100 mph. This drag was increased to 42 lb by the addition of the windshield and cockpit opening. With a maximum cross-section area of 11.2 sq ft, the values of D/A are 2.50 lb/sq ft and 3.75 lb/sq ft. These must be considered minimum values not attainable in normal construction. The actual values attained will obviously depend on the type of construction and the size of the fuselage. The average value of D/A at 100 mph will be given approximately by a basic form drag of 2.50 lb per sq ft plus 1 sq ft of added flat-plate interference drag, or

$$D = 2.5A + 30 \text{ lb at 100 mph} \qquad (196)$$

---

[20] F. E. Weick, "Full-Scale Drag Tests on Various Parts of Sperry Messenger Airplane," N.A.C.A. T.N. No. 271 (1928).

[21] F. E. Weick, "Drag and Cooling with Various Forms of Cowling for a 'Whirlwind' Radial Air-Cooled Engine," I, N.A.C.A. T.R. No. 313 (1929). Also Part II, T.R. No. 314 (1929).

This gives

A sq ft.................	10	15	20	30	40	60
D/A lb/sq ft...........	5.5	4.5	4.0	3.5	3.2	3.0

These values of D/A should be increased by as much as 1.0 lb/sq ft for poor basic shapes of rectangular sections with numerous protuberances. The values of D/A should be decreased by not more than 1.0 lb/sq ft for very clean streamline types. The limits will be approximately as indicated on Figure 132. In using these curves, it should be remembered that the "average" curve really represents a clean fuselage with elliptical cross-sections and a very low interference drag. The curve marked "lower limit" cannot be attained without exceptional attention to details of design and construction.

Floats. Table 14 gives data for a number of seaplane floats shown on Figure 133. These models, representing about an equal number of actual floats and of design studies, were tested at the Washington Navy Yard. The actual floats represented by models Nos. 1–10, and No. 19, show fairly uniform drag coefficients. For the average float $K = 0.00050$.

Float No. 12 is practically a pure streamline form tested for comparison. Models Nos. 11, 12, 13, and 14 are included for comparison purposes only. They cannot be used as actual floats on account of undesirable water performance.

The drag of a float may be calculated from the "shape coefficient" C_S, the gross weight of the seaplane, and the excess buoyancy. Since the weight of sea water is 64 lb/cu ft, the cubic displacement for a weight W is $W/64$. Letting the ratio of submerged displacement to load displacement equal $(1 + e)$, the total volume of the float is $W(1 + e)/64$, and the drag

$$D = C_S \frac{\rho}{2} V^2 \left[\frac{W(1 + e)}{64} \right]^{\frac{2}{3}} \qquad (197)$$

TABLE 14. DATA ON SEAPLANE FLOAT MODELS SHOWN IN FIGURE 133

Model No.	Dimensions		Drag at 40 mi. hr. lb.	Model K	Absolute Coefficients	
	Length ft.	Cross Section Area A sq. ft.			C_D	C_S
1	1.670	.0272	.0252	.00058	.226	.060
2	1.664	.0258	.0253	.00061	.239	.063
3	1.667	.0276	.0236	.00053	.209	.058
4	1.671	.0304	.0268	.00055	.215	.061
5	1.670	.0274	.0239	.00055	.213	.059
6	1.667	.0269	.0228	.00053	.207	.056
7	1.667	.0340	.0286	.00053	.205	.063
8	1.667	.0300	.0339	.00071	.276	.076
9	1.659	.0292	.0243	.00052	.203	.054
10	1.655	.0305	.0178	.00036	.143	.041
11	1.665	.0365	.0139	.00024	.093	.029
12	1.667	.0369	.0085	.00014	.056	.020
13	1.666	.0368	.0118	.00020	.079	.026
14	1.662	.0370	0105	.00018	.070	.025
15	1.665	.0339	.0184	.00034	.132	.041
16	1.665	.0253	.0247	.00061	.238	.062
17	1.654	.0405	.0313	.00048	.189	.058
18	1.733	.0319	.0163	.00032	.124	.034
19	1.605	.0305	.0165	.00034	.132	.038

The factor e is the decimal value of the usual percentage excess displacement. For example, with 80% excess, the value of e is 0.80.

The use of a pronounced hollow bottom increases the drag 10% to 15% over that for the conventional "Vee" bottom.

Wing-Tip Floats. The basic drag coefficient of a wing-tip float varies between 0.08 and 0.30. These values should be increased about 50% for average fitting and strut interference. A well-streamlined wing-tip float will have a drag between 3.0 lb/sq ft and 6.0 lb sq ft at 100 mph. In the absence of specific data, a value D/A = 5.0 lb/sq ft may be used.

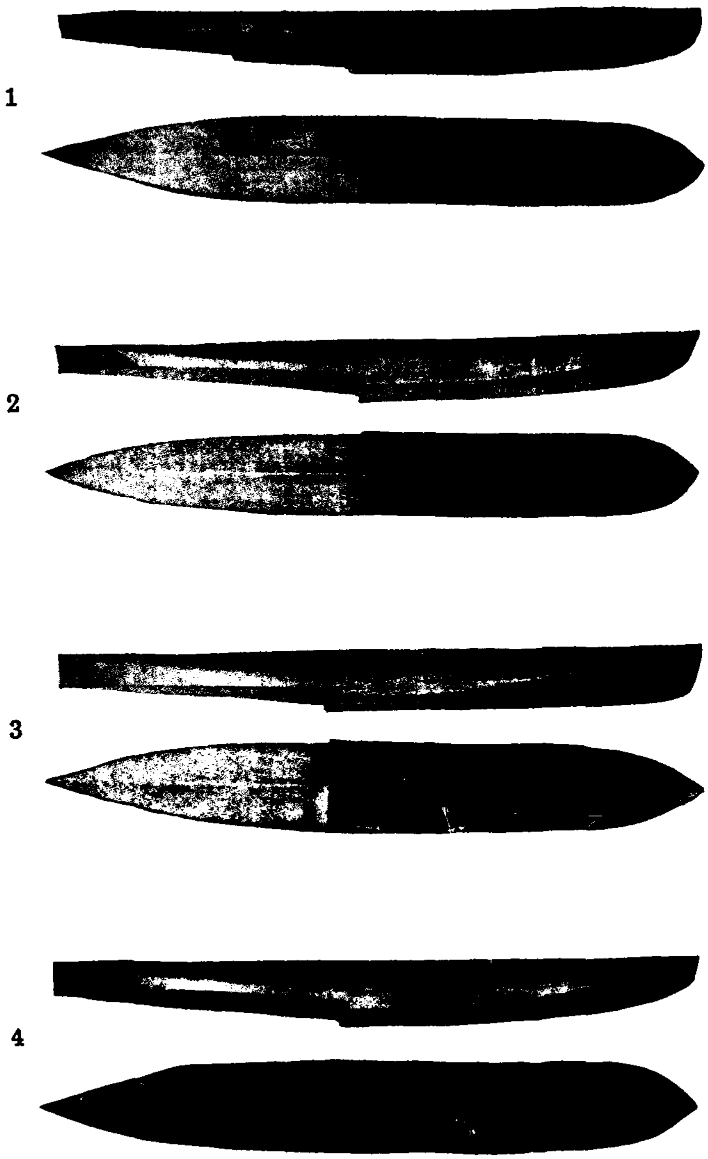

Figure 133a. Float Models

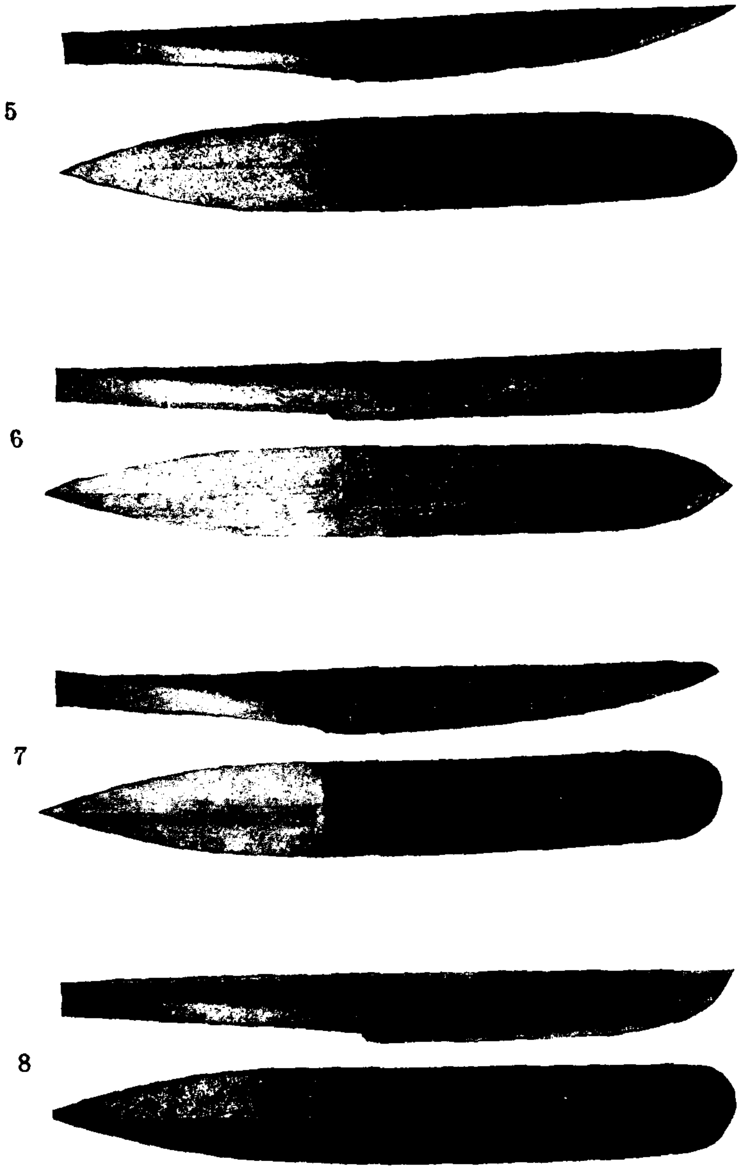

Figure 133b. Float Models

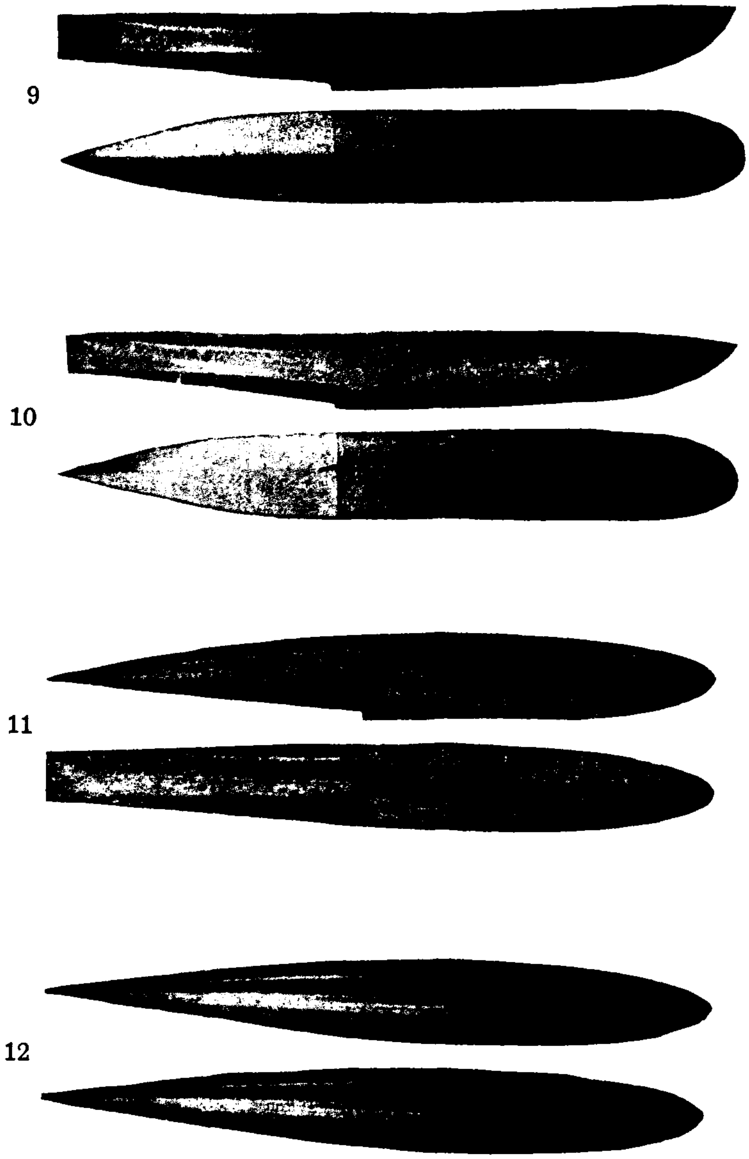

Figure 133c. Float Models

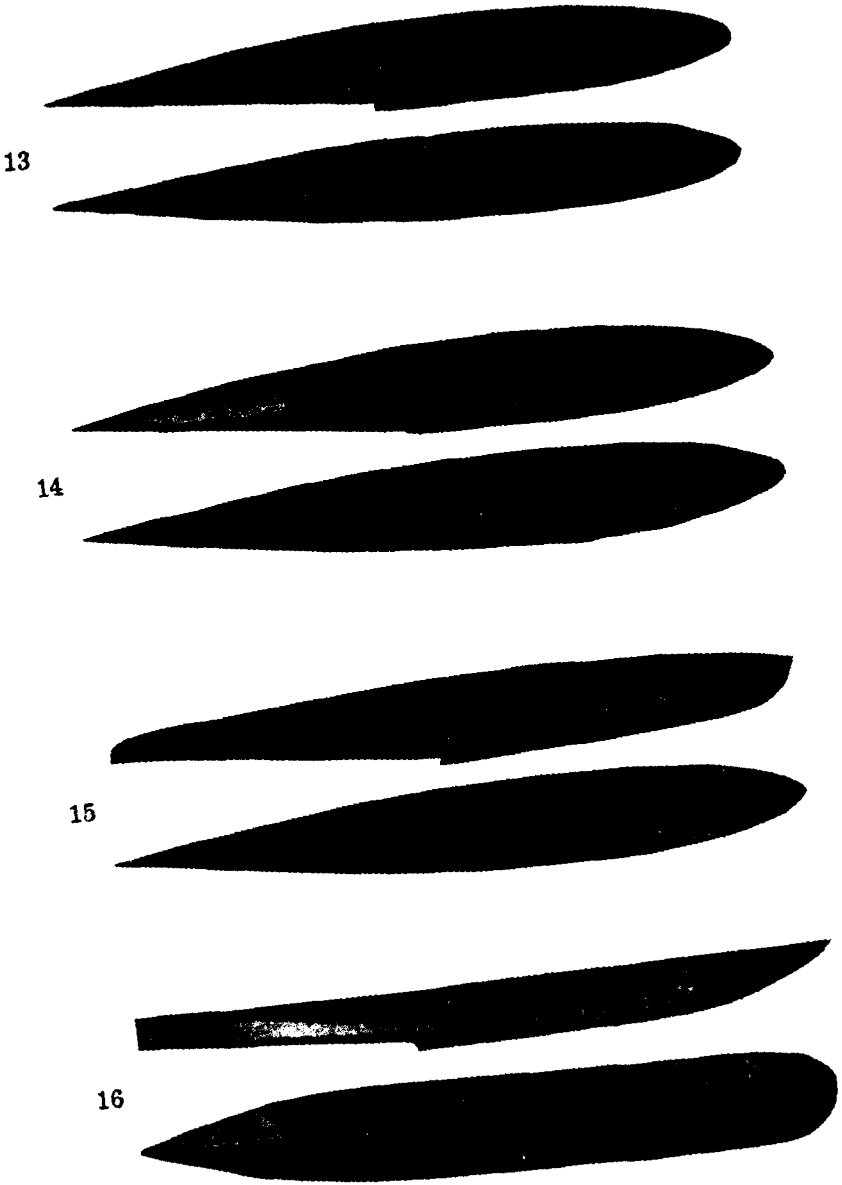

Figure 133d. Float Models

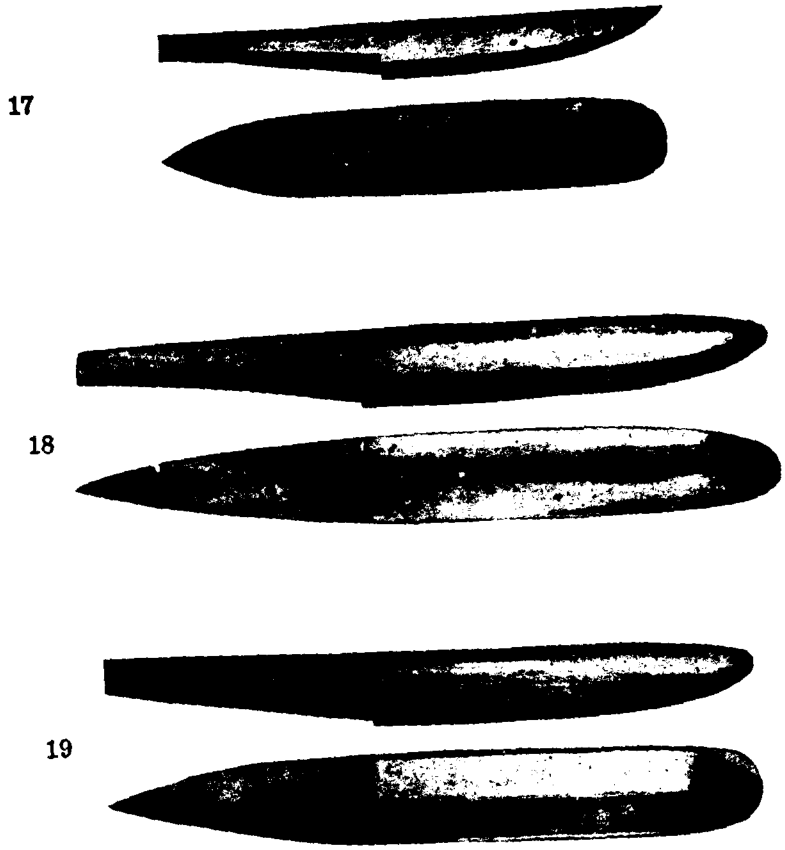

Figure 133e. Float Models

Flying Boat Hulls. A number of the large models originally constructed for tests in the seaplane tank have been given drag tests in the N.A.C.A. 20-ft wind tunnel.[22]

The results show comparatively little variation with form. C_D based on maximum cross-section area ranges from 0.092 to 0.130 for models with rounded decks and from 0.119 to 0.158 for models with flat decks. These values apply to a perfectly smooth hull, and represent a condition that cannot readily be attained in normal construction. The probable actual full-scale value for very clean designs as actually built are from 25% to 50% greater than the model values. This includes the numerous small items of parasite that are not ordinarily listed in a summation. The unit drag will also depend on the size of the hull, decreasing as the hull size increases. Average values of D/A are as follows:

A sq ft	20	40	60	80	100
D/A at 100 mph	5.0	4.5	4.3	4.1	4.0

These values should be increased by as much as 1.0 lb sq ft for flat deck or numerous corners and projections, and decreased by not more than 1.0 lb sq ft for very clean types with full elliptical cross-sections.

According to data in Technical Note No. 525, the hull drag is increased 5% by a plain faired-in windshield and 30% by an undercut windshield. The normal windshield has an effect somewhere between these two values depending on the type. The step appears to increase the basic hull drag about 10%.

Air-Cooled Engines: Uncowled. According to N.A.C.A. tests[23] the drag of the uncowled J-5 engine is 99 lb at

---

[22] E. P. Hartman, "The Aerodynamic Drag of Flying Boat Hull Models as Measured in the N.A.C.A. 20-foot Wind Tunnel," I, N.A.C.A. T. N. No. 525 (1935).

[23] F. E. Weick, "Drag and Cooling with Various Forms of Cowling for a 'Whirlwind' Radial Air-Cooled Engine," II, N.A.C.A. T.R. No. 314.

100 mph. Since the diameter of the J-5 is 45 inches, the unit drag is 9.0 lb/sq ft or

$$D = 0.049\, d^2 \text{ lb}$$

where d is the engine diameter in inches.

From flight tests, the drag of an uncowled two-row radial air-cooled engine appears slightly greater than the drag of an uncowled single-row engine of the same diameter, or approximately

$$D = 0.055\, d^2 \text{ lb}$$

Air-Cooled Engines: Cowled. The drag added by a cowled air-cooled engine depends on a number of factors including the fuselage shape and size, the engine diameter, type and number of cylinders and, of course, on the effectiveness of the cowl. Assuming that the cowl is of a type known to be highly efficient, the drag will depend almost entirely on engine diameter.

The marked superiority of the nacelle tested in N.A.C.A. Technical Report No. 314 is due to the low drag of the basic form. According to equation (194) and Figure 122, drag of nacelle No. 14 should be about 9.0 lb at 100 mph. The drag of the completely cowled nacelle was 43 lb at 100 mph. Hence, the cowled J-5 adds 34 lb drag at 100 mph. The cowled J-5 adds 31 lb drag to the fuselage and 35 lb drag to the cabin fuselage. Assuming (1) 33 lb drag at 100 mph for the J-5 with 45 in. diameter, (2) that the added drag varies as the square of the engine diameter, and (3) that the two-row radial engine has about 12% more drag than the single-row radial engine of the same diameter, the drag at 100 mph added by any cowled air-cooled engine is determined by

$$D = 0.0163\, d^2 \qquad (198)$$

for single-row engines or by

$$D = 0.0183\, d^2 \qquad (199)$$

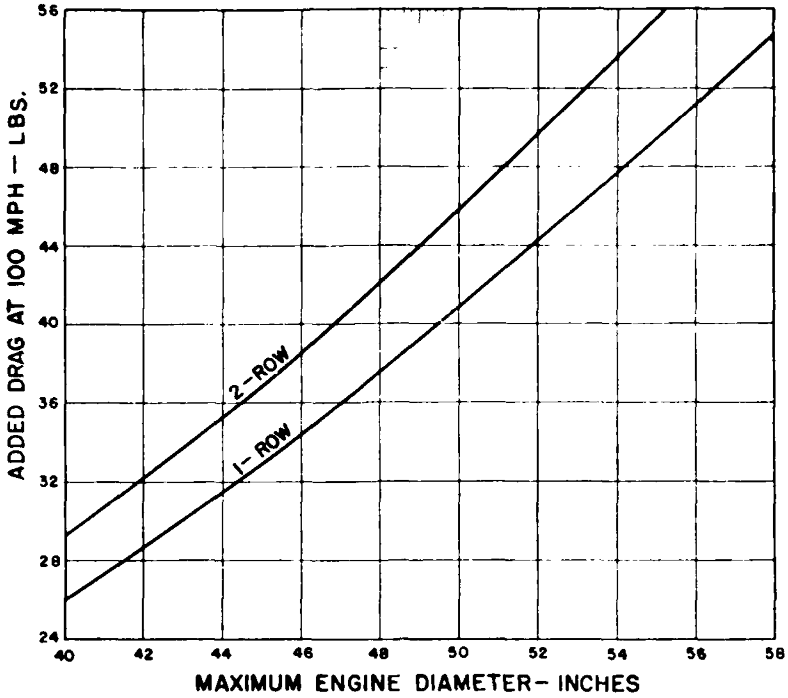

Figure 134. Drag Due to Cowled Air-Cooled Engine

for twin-row engines, *d* being the overall diameter in inches. Drag values from these equations are plotted on Figure 134.

Nacelles on Monoplane Wings. The drag of a nacelle on a monoplane wing has been investigated extensively in the Langley Field tests.[a] The data in Table XI of T.R. No. 415 are of greatest interest and value in the study of nacelle drag. These data may be plotted in a contour diagram as in Figure 135, giving the nacelle drag in terms

---

[a] D. H. Wood, "Tests of Nacelle-Propeller Combinations in Various Positions with Reference to Wings," Part I—"Thick Wing, N.A.C.A. Cowled Nacelle, Tractor Propeller," N.A.C.A. T.R. No. 415 (1932); Part II—"Thick Wing, Various Radial Engine Cowlings, Tractor Propeller," N.A.C.A. T.R. No. 436 (1932); Part III—"Clark Y Wing, Various Radial Engine Cowlings, Tractor Propeller," N.A.C.A. T.R. No. 462 (1933).

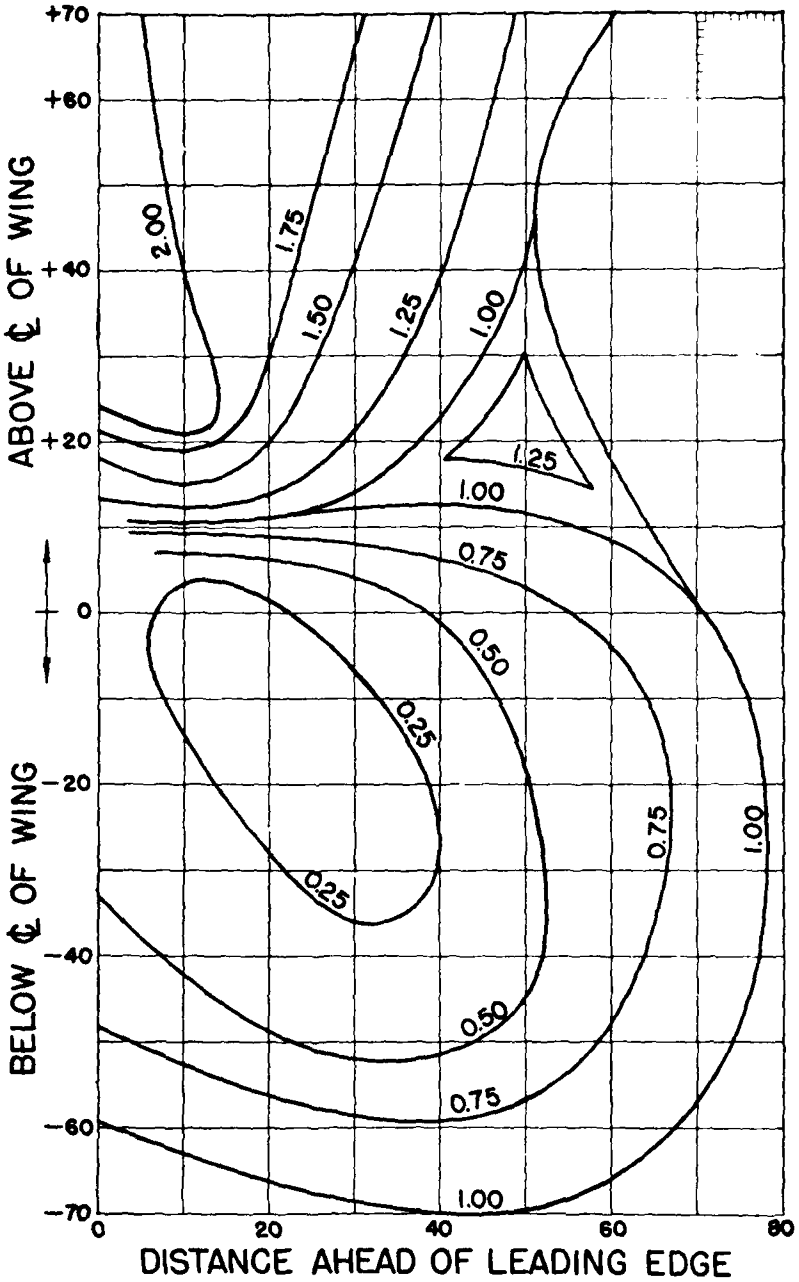

Figure 135. Relative Drag Contours of a Cowled Tractor Nacelle at 0°. Free-Air Drag = 1.00. Center of Propeller Hub is Reference Point

of its free-air drag at 0°, and as a function of its location in respect to the wing chord.

Nacelles on Biplane Wings. The drag of a nacelle on a biplane[25] does not vary greatly with location. The drag in terms of the free-air nacelle drag is given on Figure 136 which is taken from N.A.C.A. T.R. No. 506.

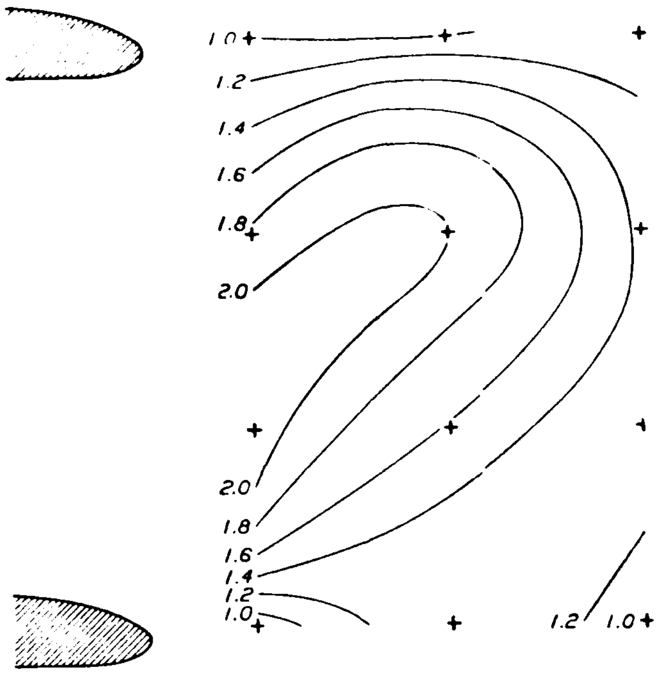

Figure 136. Relative Drag of a Cowled Tractor Nacelle on a Biplane

Pusher Nacelles. Pusher nacelles detached from the wing have a comparatively high drag per unit of engine disc area. The N.A.C.A. measured data[26] on a 4/9th scale model of the J-5 engine indicate that the full-scale drag at 100 mph will be

---

[25] E. F. Valentine, "Tests of Nacelle-Propeller Combinations in Various Positions with Reference to Wings," V, "Clark Y Biplane Cellule N.A.C.A. Cowled Nacelle Tractor Propeller," N.A.C.A. T.R. No. 506 (1934).

[26] D. H. Wood and C. Bioletti, "Tests of Nacelle-Propeller Combinations in Various Positions with Reference to Wings," VI, "Wings and Nacelles with Pusher Propeller," N.A.C.A. T.R. No. 507 (1934).

Condition	Location	D_{100}
Exposed cyl.	Nacelle alone	127
Ring at 5	Nacelle alone	94
Ring at 5	1 c above wing	116
Ring at 5	On wing center-line	76
Ring at 5	1 c below wing	96

Tandem Nacelles. From data given in N.A.C.A. T.R. No. 505,[27] the drag per unit engine disc area of a nacelle fitted with radial air-cooled engines is approximately:

Nacelle Location	Engine Cowlings	D/A, at 100 mph
0.5 c above wing	Cylinders exposed	19.4
" " " "	Hood and Ring	13.2
0.5 c below wing	Cylinders exposed	12.7
" " " "	Hood and Ring	7.3
On wing center line	Cylinders exposed	9.0
" " " "	Hood and Ring	6.0

These data are for a nacelle having the same maximum diameter as the engine; reducing the nacelle diameter increases the drag slightly.

Landing Gear. British tests[28] on wheels give at 100 mph for each wheel:

	D Alone	D With Joint Interference
26 x 5, high pressure disc	7.1	11.4
26 x 5, " " wire	7.1	11.3
26 x 5, " " faired	4.6	8.4
19½ x 7, intermediate	5.4	9.0
19½ x 9, low pressure	5.7	12.7
22 x 10, " "	8.2	13.5
30 x 13, " "	13.3	16.6

N.A.C.A. has published data[29] from an extensive research on landing gears in a series of three reports, to which reference should be made for more detailed information than can be given here. The basic wheel drags at 100 mph are, for each wheel and tire:

---

[27] J. G. McHugh, "Tests of Nacelle-Propeller Combinations in Various Positions with Reference to Wings," N.A.C.A. T.R. No. 505 (1934).

[28] F. B. Bradfield and G. F. Midwood, "Some Wind-Tunnel Tests on Wheels, Fairings and Mudguards," Br. A.R.C. R. & M. No. 1479 (1932).

[29] W. H. Herrenstein, Jr., and D. Biermann, "The Drag of Airplane Wheels, Wheel Fairings and Landing Gears," Part I, N.A.C.A. T.R. No. 485 (1934); Part II, N.A.C.A. T.R. No. 518 (1935); Part III, N.A.C.A. T.R. No. 522 (1935).

8.50 x 10, low pressure	9.5 lb.
25 x 11-4, extra low pressure	11.1
27-inch streamline	7.8
30 x 5, high pressure	9.2
32 x 6, high pressure	10.8

These values are increased approximately 50% by interference drag in any ordinary installation.

The 8.50 x 10 low-pressure wheel and tire was tested with a series of enclosing streamline fairings. The drag of one faired wheel at 100 mph is as follows:

1. 21″ diam. x 42″ length, streamline fairing with lower third of wheel exposed, $D = 8.3$ lb.
2. Similar to 1, except a "half-fairing" with inner side close to wheel, $D = 7.2$ lb.
3. Similar to 1 and 2 except a *half-fairing with vertical* inner side, removed entirely along wheel, $D = 12.0$ lb.
    - (a) When the front edge of rear portion of the inner face of fairing 3 is bent-in, $D = 8.6$ lb.
4. Fairing over fitting and rear of wheel only, inner portion bent-in as in 3*(a)*, $D = 10.0$ lb.
5. Streamline fairing with substantially vertical sides 12″ width x 42″ length, lower third of wheel exposed, $D = 5.5$ lb.
    - (a) Similar to 5 except that bottom fairing is lowered to cover about 80% of wheel diameter, $D = 4.5$ lb.
    - (b) Wheel completely enclosed in flat-sided symmetrical fairing, $D = 2.7$ lb.

The drag of complete landing gears incorporating these fairings are as shown in the table at the top of the following page.

Type	D at 100 mph
Unfaired	36.0 lb.
1	30.3
1 with filleted-strut ends	28.1
2	28.1
2 with filleted-strut ends	25.9
3	36.5
4	28.8
5	31.9
5 with circular-axle fairing	33.1
5 with streamline-axle fairing	28.1

Various forms of complete landing gears of the strut-and-wire type, with no streamlining on the wheels, have substantially the same drag—about 45 lb at 100 mph.

A single strut cantilever gear with 90° connection to the wheel has drag values, $D = 23.5$ lb with plain 8.50 x 10 wheels or $D = 17.5$ lb at 100 mph with fairing 5.

An 8.50 x 10 wheel with a vertical single strut from wing to top of fairing 5 gives $D = 20.0$ lb. This is reduced to 13.0 lb if the wheel fairing is extended up to the wing. Expanding fillets between this fairing and the lower surface of the wing are necessary if the low drag is to be secured.

Tests on a 42 x 15.00–16 low-pressure wheel with a strut-shaped fairing from wheel up to wing give $D = 60$ lb at 100 mph at $C_L = 0.3$ and at zero lift $D = 225$ lb without expanding fillet or 93 lb with expanding fillet. Either the 42 x 15.00–16 low-pressure wheel or the 45-inch streamline wheel has a drag of about 90 lb each when placed in contact with the lower wing at 0.50 c.

A 10 x 3–4 tail wheel gave $D = 4.0$ lb at 100 mph. Various types of tail skids ranged from $D = 1.0$ lb to $D = 4.0$ lb. In general, the drag of a tail skid would probably be not less than $D = 3.0$ lb.

Fittings. The average drag of a fitting mounted on a wing, fuselage, float, or tail surface is given approximately by considering the fitting as a flat plate of double its projected frontal area. This allowance is necessary in order to account for the "interference" drag due to the fitting.

The drag of a fitting is surprisingly high. The drag of an average strut end-fitting with wire attachments on a 4,000-lb airplane will probably be about 3.0 lb at 100 mph. Most of this is in the wire terminals and can be included in the wire drag where it belongs.

Miscellaneous projecting parts, not streamlined, should be treated as fittings, and considered as a flat plate of double the projected area if located on the upper surface of the wing, or as direct flat plate area if located elsewhere. This drag can be greatly reduced by proper streamlining.

The drag of external control horns varies from about 0.2 lb to about 2.0 lb each at 100 mph, depending on the size and nature of exposed parts.

Cellular Radiators. Tests at the Washington Navy Yard[30] on cellular radiators gave values of C_D between 0.57 and 0.78, with an average value of about 0.70. This coefficient is for the core alone and it decreases slightly as the core thickness is increased. The average C_D corresponds to about 18.0 lb/sq ft of core at 100 mph.

When a cellular radiator is covered by closed shutters, the drag coefficient is substantially that of a flat plate, i.e., $C_D = 1.10$ approximately. Allowance must be made for the additional resistance of the internal flow over engine, etc., when calculating the drag of nose radiators. The drag of headers on free-air radiators should be considered as that of a flat plate of the same area.

Full-scale wind-tunnel tests[31] on the YO-31A airplane gave radiator drags at 100 mph as follows:

Radiator	Frontal Area A sq ft	Drag D lb	D/A
Oil	0.61	9.5	15.6
Prestone	1.20	25.0	20.8

---

[30] R. H. Smith, "Resistance and Cooling Power of Various Radiators," N.A.C.A. T.R. No. 261 (1927).

[31] S. J. DeFrance, "Drag of Prestone and Oil Radiators on the YO-31A Airplane," N.A.C.A. T.N. No. 549 (1933).

Landing Lamps. A landing lamp 6$\frac{3}{4}$ inches diameter, mounted on an 8 x 48 ft Clark Y wing, has drag characteristics as follows:[32]

	ΔD at 100 mph
In leading edge, unfaired	2.8 lb
In leading edge, faired	1.4
On lower surface, unfaired	11.2
On lower surface, faired	4.2

Tests made at 5% and 10% c for the lower surface locations showed no appreciable difference.

Wire Mesh. The drag of wire mesh is sometimes required for model construction. From some unpublished data obtained by R. M. Bear in the Washington Navy Yard wind tunnel, the drag coefficient of wire mesh is a function of the percentage of the area blocked by the wire, as follows:

% A closed	100	80	60	50	40	30	20
% A open	0	20	40	50	60	70	86
% Flat plate C_D	100	92	77	60	43	26	10

Machine Guns. Flight tests indicate that the drag of the Lewis gun with fully exposed scarff-ring mount is about 20 lb with the gun aligned fore and aft and about 30 lb at 100 mph with the gun cross-wind. The later types of guns with faired mountings have very low drag, approximately 1.0 to 2.0 lb at 100 mph. The usual form of gun sight has a drag of approximately 3.0 lb at 100 mph.

Bombs and Torpedoes. The free-air drag of bombs or torpedoes is comparatively low considering the frontal area, but as installed, the drag of the racks plus interference may be large. The average drag at 100 mph is given by

$$D = D_o + 0.020\ W_B \qquad (200)$$

---

[32] C. H. Dearborn, "Full-Scale Drag Tests of Landing Lamps," N.A.C.A. T.N. No. 407 (1934).

where W_B is the weight of the bombs and D_0 is the drag added by the rack and interference. For a well-faired rack on the center-line of the fuselage or under the wing, D_0 is about 10.0 lb.

The drag of a torpedo is approximately

$$D = 0.015\ W_T \qquad (201)$$

where W_T is the weight of the torpedo.

Radio Antenna. The drag of a V type radio antenna including masts, insulators, lead-in wires, etc., is about 10.0 lb at 100 mph for the average installation on an airplane having a span of about 35 ft. This drag obviously depends on the size of the installation and may be as high as 30.0 lb at 100 mph for the W type used on large flying boats.

Interference. The "interference" effect between two objects varies greatly, sometimes decreasing the total resistance and sometimes increasing it. The reduction of drag when two wires are lined up fore and aft has been given. When two wires are side by side, the total resistance, for spacings less than about 6 diameters, is greater than twice that of a single wire, but very little actual test data are available. It is usually assumed that no interference exists for lateral spacings of 10 diameters or greater. This has been verified at the Washington Navy Yard, but no record was made of the tests.

The "upstream wake" of a cylinder, which is very aptly designated as an "air prow" by Dr. Zahm, extends to a distance of about 5 diameters and the lateral disturbance extends to a similar distance before the velocity is normal. The theoretical velocity distributions about a number of simple shapes are shown in N.A.C.A. Technical Report

No. 253.[33] From these, one may secure an idea of the extent of the disturbance created by a moving object.

The drag of two adjacent struts was partially investigated by Nayler and Jones.[34] Two 1-in. x 3-in. streamline struts were tested at several spacings and the average drags found to be as follows:

$\frac{\text{Spacing}}{\text{Thickness}}$	∞	4.90	3.970	2.890
Total Drag, lb	048	.050	.052	.053

These data indicate that two struts spaced laterally 3 "diameters" apart on their center lines have about 10% more drag than with normal spacing.

Interference drag has been obtained for a number of combinations tested by N.A.C.A.[35] The increase in drag of two adjacent 2½-in. struts was found to be as follows:

$\frac{\text{Spacing}}{\text{Thickness}}$	5	4	3	2	1.5	1.25
D/D_0	1.00	1.06	1.12	1.25	2.25	2.87

An even greater effect was obtained with smaller struts, but in all cases, the interference drag was negligible for spacings greater than 6 diameters.

Similar tests with cylinders gave rather erratic results. For a 2½-in. cylinder the effect was as follows:

$\frac{\text{Spacing}}{\text{Diameter}}$	5	3	2.5	2.0	1.75	1.50	1.25
D/D_0	1.00	1.10	1.13	.92	.84	1.04	1.06

For spacings between 1.70 and 2.10 diameters, the interference is negative and the drag of two cylinders is less than twice the drag of a single cylinder.

---

[33] A. F. Zahm, "Flow and Drag Formulas for Simple Quadrics" (1926).

[34] "The Determination of the Forces on Two Struts in Close Proximity to One Another," Br.A.C.A. R. & M. No. 204 (1915).

[35] D. Biermann and W. H. Herrenstein, Jr., "The Interference between Struts in Various Combinations," N.A.C.A. T.R. No. 408 (1933).

Two struts in tandem show interference drags approximately as follows:

$\frac{\text{Spacing}}{\text{Diameter}}$	12	9	6	5	4	3
D/D_0	1.10	1.13	1.16	1.22	1.28	1.07

The condition for spacing at 3 diameters has the two struts in contact. The drag of tandem struts separated less than 10 diameters is reduced by a flat-sided fairing.

The interference drag of a strut connecting a flat surface is approximated by the following:

θ	90°	70°	60°	50°	40°	30°	20°
ΔL	0	1.5	2.5	4.0	6.0	9.5	14.0

θ is the intersection angle and ΔL is the equivalent strut length, in diameters, of the interference drag. This interference drag is reduced by as much as 30% at values of θ between 20° and 30° by rounding off the feather edge of the strut and using a fillet with a radius of 30% to 50% of the strut diameter in the Vee.

A *simple strut intersection* has a large interference drag approximately as follows:

θ	90°	60°	45°	30°	21.5°
ΔL no fillet	12.3	19.0	24.9	27.5	24.2
ΔL with fillet	9.6	13.9	21.7	23.0	23.6

The fillet used gave a poor streamline for the intersection. A tail-fairing would probably give greater improvement.

The most important form of interference is that which occurs when anything is attached to an airplane wing, particularly on the upper surface. This may be illustrated by the results of some tests on a twin-engine airplane model at the Washington Navy Yard. The drag in the first test appeared high and the nacelles were removed and tested alone. At 40 mph the nacelle drag was found to be 0.078 lb in free air, and 0.120 lb on the model. A plasticine fairing with generous fillets between the nacelle and the wing reduced the interference drag from 0.042 lb to 0.002 lb. This model was a biplane with the nacelles mounted directly on the upper surface of the lower wing. A still greater effect would probably be found if the nacelles were located on the upper surface of the upper wing of a biplane or on the upper surface of a monoplane wing. When it is necessary to mount nacelles above a wing, wind-tunnel tests with and without nacelles in place are advisable, in order to determine whether or not the fairing is adequate, and to find the fairing that gives a minimum interference drag.

Any projection from the upper surface of an airplane wing such as strut-fittings, bolts, brackets, etc., will show interference drags ranging from 50% to 200% of the free air drag of the part in question. Any form of fairing between wings and fuselage that interferes with the natural flow of air over the wing may be expected to show a pronounced interference effect. Horizontal tail surfaces fitted just above the fuselage may also be expected to show interference drag effects if the gap is not filled.

The interference effects associated with wing location are being studied intensively in various laboratories and preliminary results indicate certain features to be avoided in design. An interference drag usually indicates a breakdown in a normal flow. When this breakdown is in the flow over a wing, the effects may be disastrous in so far as the efficiency of the design is concerned. It seems a general rule that the more efficient the wing section, the more likely are such adverse effects to occur. Particular care is required to provide adequate fillets and intersections with sections such as the 2212, 23012, etc. High-wing and mid-wing monoplanes are inherently less susceptible than low-wing monoplanes to the effects of poor wing-root fairing. If provided with proper wing-root fillets, the low-wing compares favorably with other types, but each low-wing design is a problem in itself because the state of the art does not justify either calculations or assumptions. The wind tunnel probably will remain the only source of reliable information on wing interference.

The best source of data on wing-fuselage interference available at this time is N.A.C.A. T.R. No. 540.[36] The information contained in this report is very valuable to the designer in that it indicates the arrangements most susceptible to interference and the extent to which improvement may be expected by proper fairing.

---

[36] E. N. Jacobs and K. E. Ward, "Interference of Wing and Fuselage from Tests of 209 Combinations in the N.A.C.A. Variable-Density Tunnel," N.A.C.A. T.R. No. 540 (1935).

CHAPTER 10

ENGINE AND PROPELLER CONSIDERATIONS

Engine and Propeller. The engine and the propeller characteristics are affected by so many variables that it is useless to attempt any extensive or exact analysis of test data. However, the importance of the power plant is so fundamental that certain definite general relations are required for intelligent design. Fortunately some of the more important of these relations can be obtained with fair accuracy, but other relations must be given to an average or approximate value that may at times be unreliable.

In assembling the data that comprise the remainder of this chapter, an attempt has been made to present in workable form those general relations required in preliminary design studies. These data should be supplemented by the engine manufacturers' power and fuel-consumption curves, and by actual propeller test data where available.

General Power Curves: Sea-Level Engines. Curves of bhp against rpm for various engines are similar in form and differ chiefly in the rate with which the power falls off as rpm decrease. The characteristic slope is determined partially by the engine design and partially by the rated rpm. The general type of the power curve can be specified very closely by a power-drop factor defined as the ratio of power to rated maximum when rpm is 80% of the rated rpm or PDF = bhp/bhp_0 for $N/N_0 = 0.80$. The choice of this point is purely arbitrary but it is selected to give reasonable differences in the normal working range.

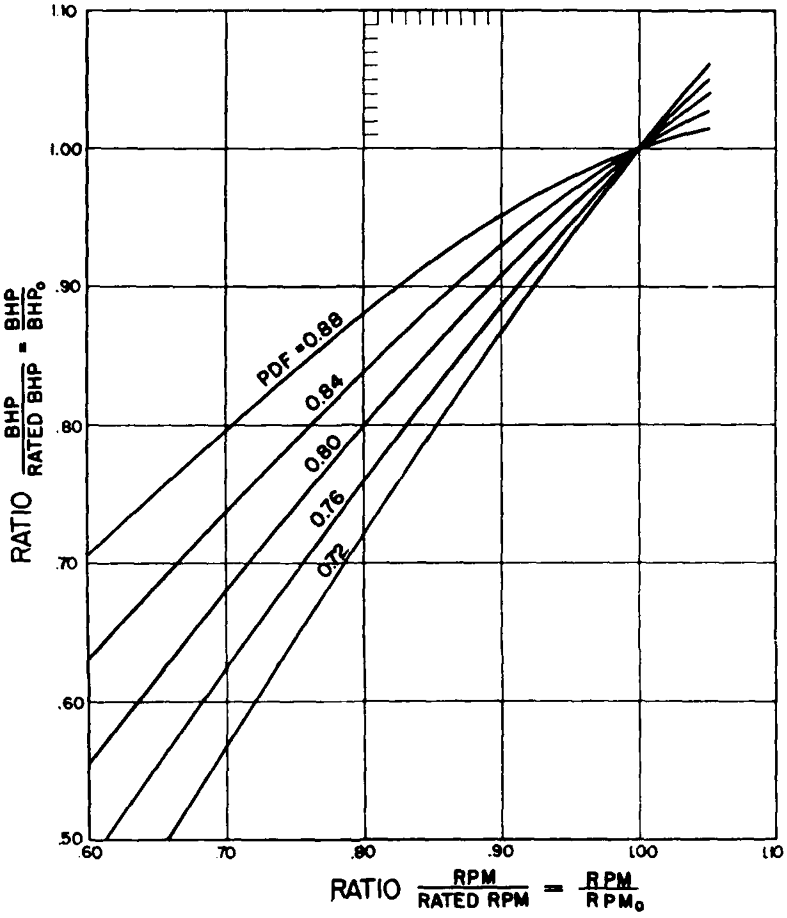

Figure 137. General bhp Curves

Typical general power curves are given on Figure 137 for power-drop factors from 0.72 to 0.88. Normal values of PDF range from 0.75 to 0.85.

General Power Curves: Supercharged Engines. The general curve for a supercharged engine is modified by a dual loss in power with decrease in rpm. The decrease in rpm

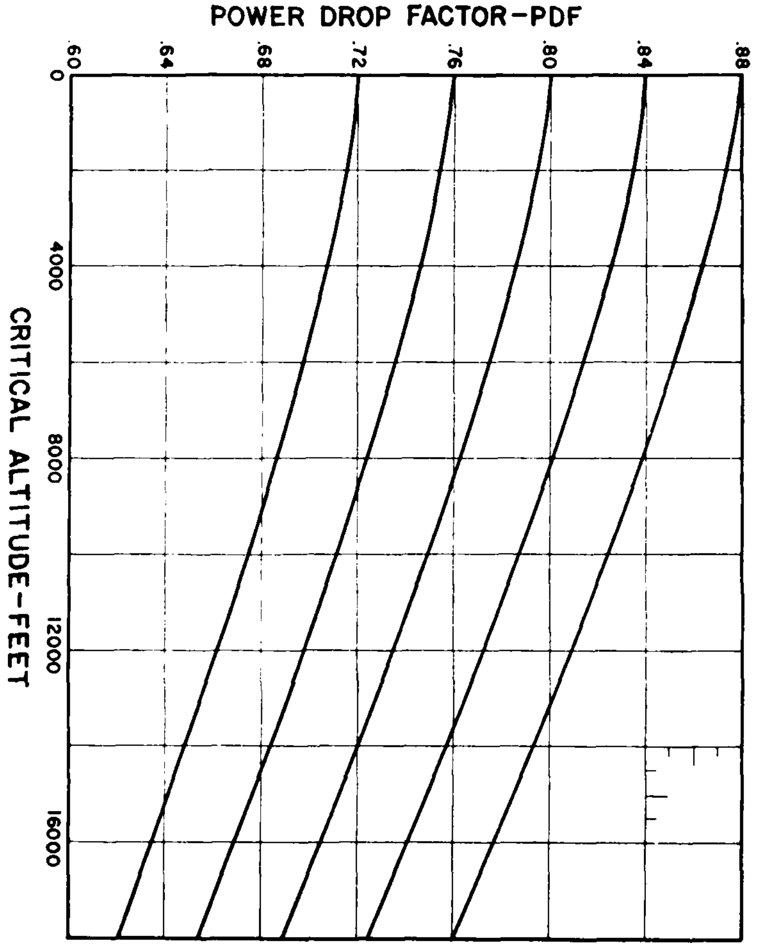

Figure 138. Effect of Supercharging on Power Drop Factor

gives a direct loss in power identical with the loss for an unsupercharged engine plus an additional loss due to the decreased supercharging effect. It is this rapid loss in power with decreasing rpm that makes a controllable-pitch propeller so important on supercharged engines.

The observed decrease in PDF with critical altitude for two engines has been used to construct the curves of

Figure 138, which is believed to be a close approximation for other engines.

Variation of bhp with Altitude. From altitude test-chamber data, the bhp at constant rpm varies as $(P/P_0)^{1.15}$ at constant temperature and as $(T_0/T)^{0.5}$ at constant pressure. In the standard atmosphere

$$T/T_0 = (P/P_0)^{0.19} \tag{202}$$

and

$$P/P_0 = (\rho/\rho_0)^{1.235} \tag{203}$$

Hence, in the standard atmosphere

$$(\text{bhp}/\text{bhp}_0) = (P/P_0)^{1.055} = (\rho/\rho_0)^{1.305} \tag{204}$$

This relation is in reasonable agreement with flight-test data. As a result of National Advisory Committee for Aeronautics flight tests on a DH-4 airplane fitted with a Bendemann dynamometer hub on a Liberty engine, Gove and Green[1] recommended the relation

$$(\text{bhp}/\text{bhp}_0) = 1.088\,(\rho/\rho_0) - 0.088 \tag{205}$$

This relation had been used extensively for many years.

Later tests with the same equipment[2] indicated that better results were obtained from the complete equation

$$\frac{\text{bhp}}{\text{bhp}_0} = \left(\frac{P}{P_0}\right)\left(\frac{T_0}{T}\right)^{\frac{1}{2}}\left(1 + \frac{\lambda - \lambda n}{n}\right) - \left(\frac{\lambda - \lambda n}{n}\right) \tag{206}$$

where n is the mechanical efficiency at sea-level and λ is the ratio of mechanical friction horsepower to total sea-level friction horsepower. The normal value of λ is about 0.5.

These various relations have been compared with other published data and the conclusion reached that the differences are probably less than the variation between individual engines of the same type. A composite curve showing the average variation of bhp with altitude is given on Figure 139. For convenience, the numerical values of the power ratio are given at 4,000-ft intervals.

---

[1] W. D. Gove and M. W. Green, "The Direct Measurement of Engine Power on an Airplane in Flight with a Hub Dynamometer," N.A.C.A. T. R. No. 252 (1926).

[2] W. D. Gove, "The Variation in Engine Power with Altitude Determined from Measurements in Flight with a Hub Dynamometer," N.A.C.A. T.R. No. 295 (1928).

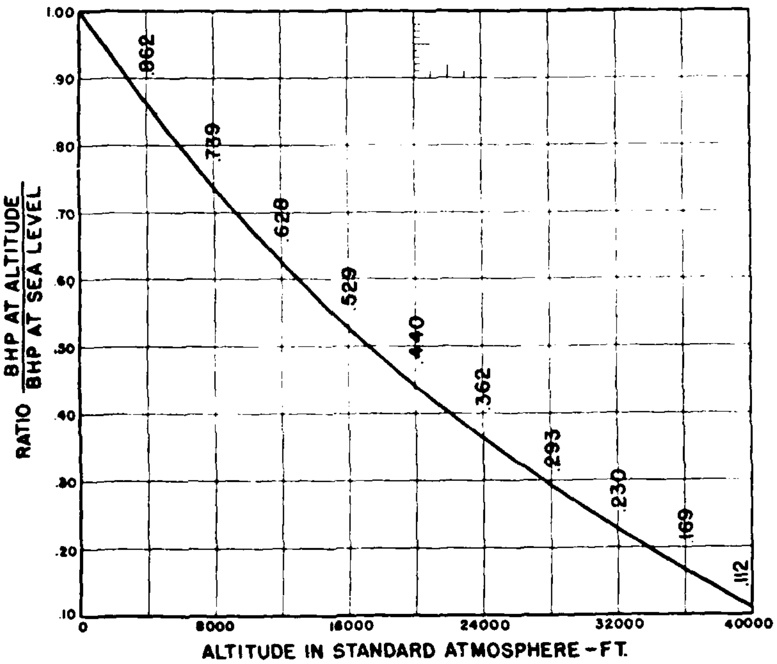

Figure 139. Variation of bhp with Altitude

Variation of bhp with Altitude: Supercharged Engine. At a given full-throttle rpm there is no real difference in the rate of variation of power with altitude for supercharged and unsupercharged engines. The difference is essentially in the restrictions imposed on the operation of supercharged engines at full-throttle below the "critical altitude." At the critical altitude, the supercharged engine develops the full sea-level power when operated at full

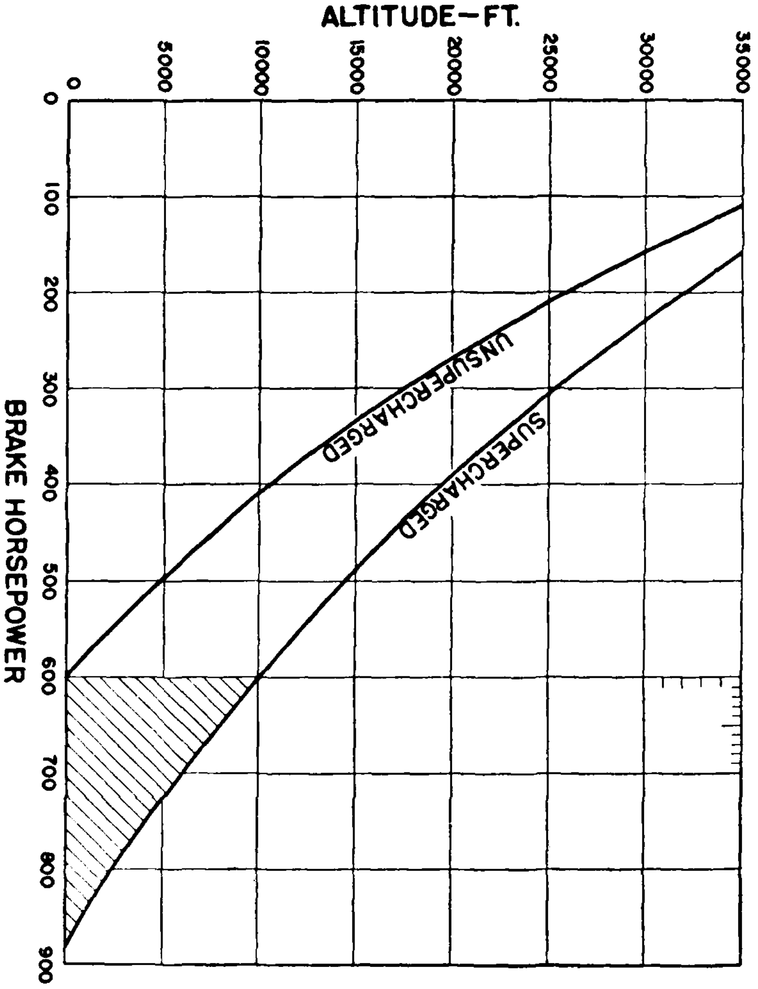

Figure 140. Effect of Supercharging on Power-Altitude Curve

throttle. Below the critical altitude, part-throttle must always be used if the full sea-level power is not to be exceeded. For example, an engine that is designed for 600 bhp at sea-level, may be supercharged to give 600 bhp at 10,000 ft. This supercharged engine if operated with wide-open throttle at sea-level will develop 880 bhp. If the 600 bhp rating is not to be exceeded, full throttle cannot be used below the critical altitude of 10,000 ft for this engine. These relations are indicated on Figure 140. The cross-hatched area represents power that cannot be used on account of structural limitations in the engine design.

While the rate of decrease of the two curves in Figure 140 is identical, the percentage decrease for a given altitude increment will not be the same for increments taken from sea-level and from the critical altitude. In other

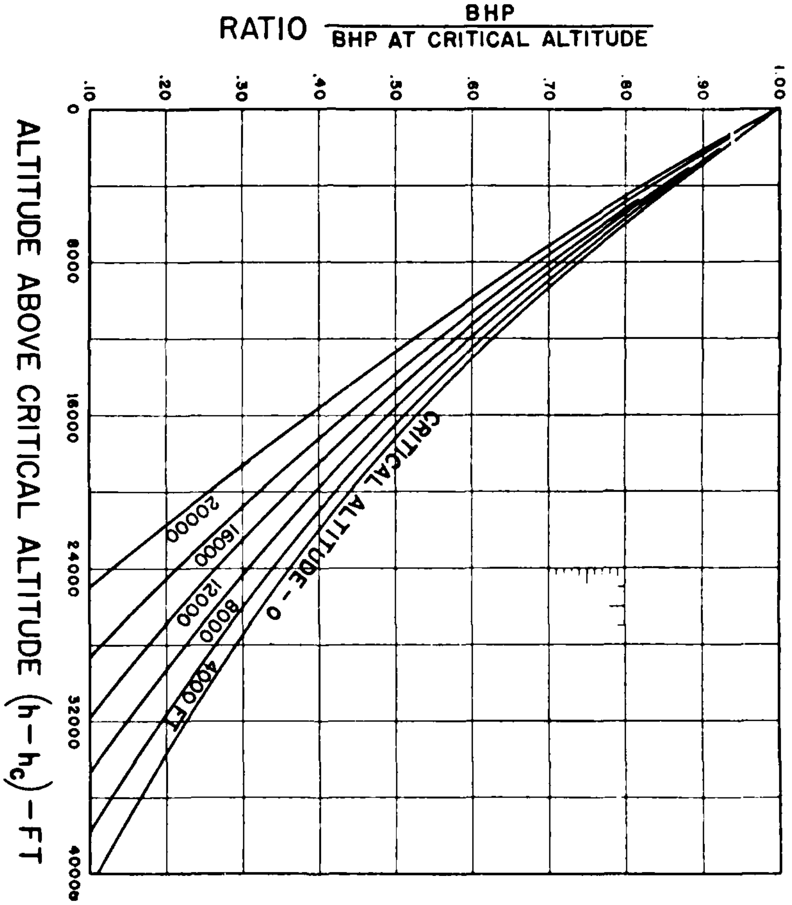

Figure 141. Variation of bhp with Altitude for Supercharged Engines

words, the relative power of the supercharged engine falls off faster from the critical altitude than does the relative power of the unsupercharged engine from sea-level. Taking a 10,000-ft increase in altitude, the comparative values are 387 bhp for the supercharged engine at 20,000 ft and 409 bhp for the unsupercharged engine at 10,000 ft. This effect depends on the critical altitude as shown on Figure 141.

Specific Fuel Consumption. The specific fuel consumption varies over a wide range depending on the condition of the engine and the carburetor adjustment, but the effects of throttling, mixture ratio and compression ratio are fairly definite.

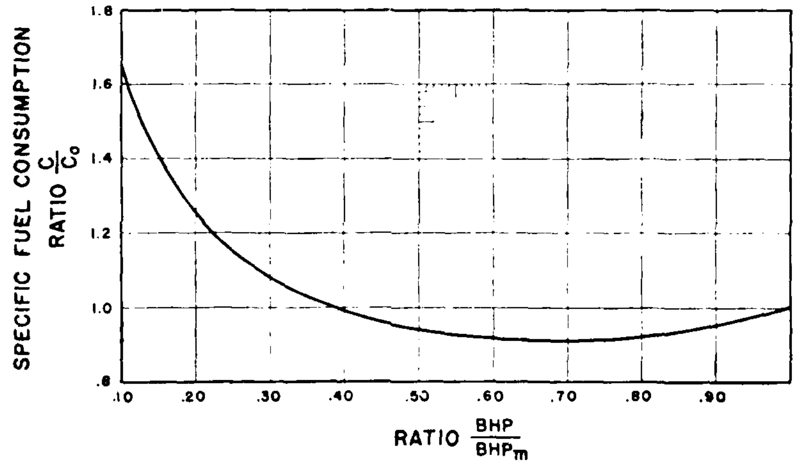

Figure 142. Average Specific Fuel Consumption at Part Throttle

The effect of throttling is shown on Figure 142. This curve is the average of a number of curves obtained from test-stand data and flight-test data. Individual tests on certain types of engines are from 10% to 20% below or above the average so that the curve must be considered only as an average. Actual engine data should be used when available.

The effect of compression ratio on the full throttle specific fuel consumption is shown on Figure 143. The curve labeled "normal mixture" corresponds to normal minimum values although with water-cooled engines and improved designs of air-cooled engines, it is possible to approach the curve marked "lean mixture." This curve is about the minimum that can be obtained in flight under ideal conditions.

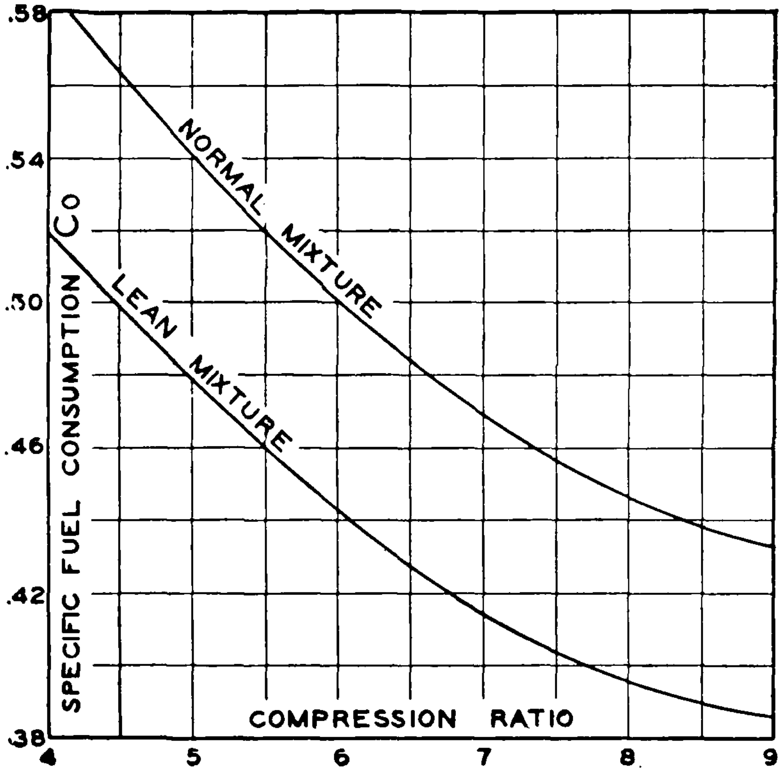

Figure 143. Variation of Specific Fuel Consumption with Compression Ratio and Mixture Control

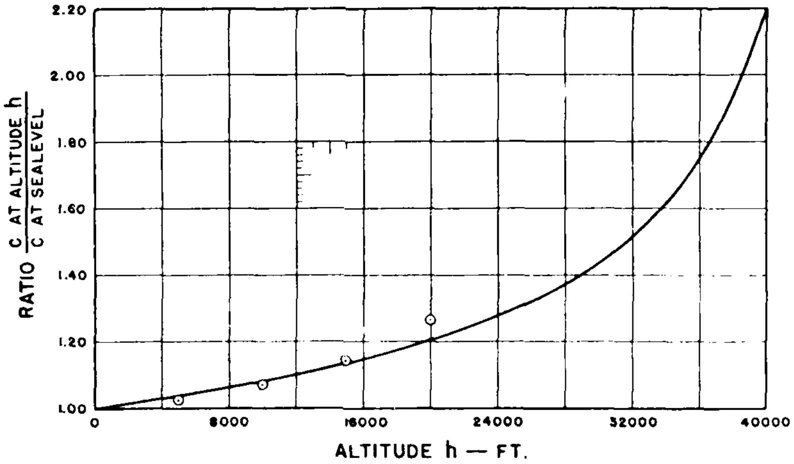

Figure 144. Variation of Specific Fuel Consumption with Altitude

The theoretical variation in specific fuel consumption with altitude is given by the curve on Figure 144. The points are from the Bureau of Standards altitude chamber tests.

Propeller Coefficients. Propeller characteristics are thrust, torque, and power absorbed. These are conveniently expressed as non-dimensional coefficients and given as functions of the non-dimensional ratio V/nD. These relations are analogous to those existing for wing coefficients C_L and C_D, and the ratio V/nD determines the angle of attack of a propeller-blade section. V, n, and D must either be in a consistent system of units such as ft/sec, rps and ft, or a conversion factor must be used. For V in mph, n in rpm and D in ft, this conversion factor is 88, or

$$\frac{V}{nD} = \frac{88\ V_{\text{mph}}}{(\text{rpm}) \times D_{\text{ft}}} \tag{207}$$

The absolute coefficient of thrust is

$$C_T = T/\rho n^2 D^4 \tag{208}$$

multiplying both sides of this equation by the non-dimensional term $(nD/V)^2$ gives

$$C_T' = C_T\,(nD/V)^2 = T/\rho V^2 D^2 \tag{209}$$

Multiplying both sides by $(nD/V)^4$ gives

$$C_T'' = C_T\,(nD/V)^4 = Tn^2/\rho V^4 \tag{210}$$

In a similar manner the torque coefficients are obtained as

$$C_Q = Q/\rho n^2 D^5 \tag{211}$$

$$C_Q' = Q/\rho V^2 D^3 \tag{212}$$

$$C_Q'' = Qn^3/\rho V^5 \tag{213}$$

and the power coefficients as:

$$C_P = P/\rho n^3 D^5 \tag{214}$$

$$C_P' = P/\rho V^3 D^2 \tag{215}$$

$$C_P'' = Pn^2/\rho V^5 \tag{216}$$

These coefficients may be formed into other coefficients employing the three variables V, n, and D or they may be used in exponential form. For example, as will be shown later, a propeller is conveniently selected by use of the coefficient C_s defined by

$$C_s = (1/C_P'')^{\frac{1}{5}} = (\rho V^5/Pn^2)^{\frac{1}{5}} \tag{217}$$

Propulsive Efficiency. The efficiency of a propeller is defined as the ratio of the energy output to the energy input or

$$\eta = TV/P \tag{218}$$

where T is the thrust, V is the air speed, and P is the input power. If T is in lb and V in ft/sec, then P must be in ft-lb/sec or $P = 550$ bhp.

The simple propeller efficiency is of greatest practical interest as a control, or reference value for determining "propulsive efficiency." A part of the propeller thrust must be used to overcome the increased drag of objects in the slipstream. This part does no useful work; it merely increases the load on the thrust bearing. The total propeller thrust T and the slipstream drag ΔD are difficult to measure separately, but the net thrust

$$T_e = T - \Delta D \tag{219}$$

is readily obtained. Denoting the net thrust force on the system with the propeller operating by R, and corresponding drag with the propeller removed by D, the net thrust is the sum or

$$T_e = D + R = T - \Delta D \tag{220}$$

The propulsive efficiency is

$$\eta = T_e \cdot V/P \tag{221}$$

Propulsive efficiency is used far more than the free-air propeller efficiency. Unless otherwise specified, propeller efficiency means propulsive efficiency.

Propeller Pitch. As a propeller rotates and moves forward, each section of the blade describes a helical path that may be developed into a right triangle with base = $2\pi r$ and altitude = p = distance travelled forward in one revolution. The helix angle of the element is

$$\theta = \tan^{-1}(p/2\pi r) \tag{222}$$

and the apparent slip is $s = p_G - p_a$, where p_G is the advance for a helix angle equal to the blade angle and p_a is the actual advance. p_G is the apparent geometrical pitch of the blade element. The actual or aerodynamic pitch must be measured from the zero-lift lines of the blade elements.

The distribution of pitch along the blade may be uniform or variable. Tests indicate that best results are obtained with a pitch increasing towards the tip. This is the common type found in adjustable and controllable-pitch propellers, for which the pitch distribution is uniform along the blade at some low pitch setting. Higher pitch settings are obtained by a uniform increase in blade angle along the radius.

Since pitch is second only to diameter in its effect on propeller characteristics, its specification must be definite. At present only two methods are employed. Test data give the blade angle at 0.75 *R*, and propellers are adjusted in service with a setting at the 42-in. radius. These two settings are definitely related, as shown on Figure 145.

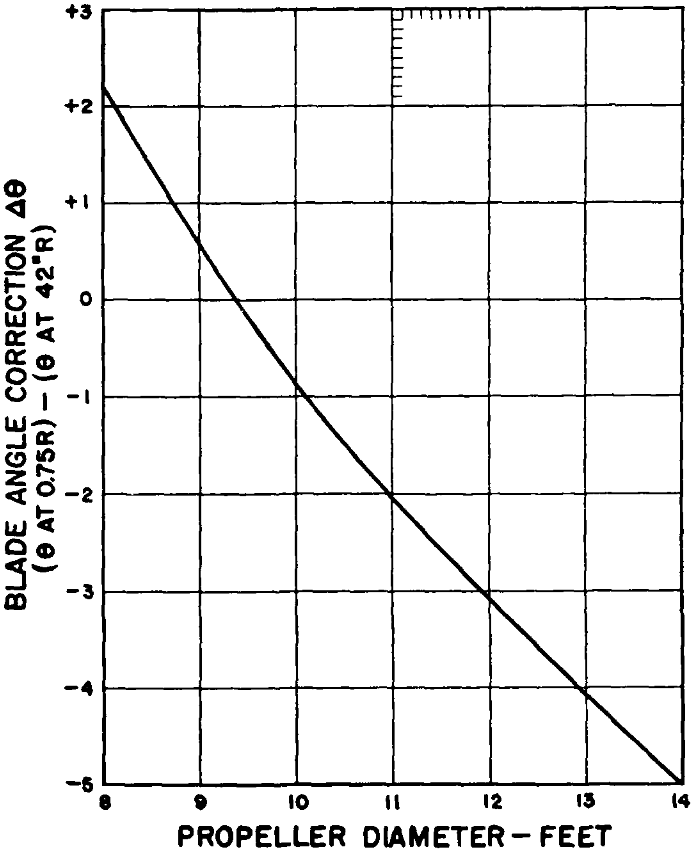

Figure 145. Difference between Blade Angle at 0.75 *R* and at 42-in. Radius

Owing to the effect of blade twist under load, there is an appreciable difference between the static setting and the operating setting. There is an increase in blade angle depending on the power absorbed. According to N.A.C.A. data,[3] the increase in blade angle is negligible below 100 bhp per blade, but for higher powers the increase is approximately 1° per 100 bhp per blade or

$$\Delta\theta^{\circ} = +K\left[\frac{\text{bhp}}{100N} - 1\right] \tag{223}$$

where N is the number of blades and K is the reduction-gear ratio or the ratio of propeller rpm to engine rpm.

Propeller test data are given for conditions involving negligible deflection; hence, the chart values of θ must be reduced by $\Delta\theta$ from equation (223) to obtain the static setting at 0.75 R. The static setting at 0.75 R is then converted to static setting at 42-in. radius for service settings.

Propeller Design Characteristics. Propeller diameters, blade settings, and maximum efficiencies are readily obtained from some plotting of the coefficient $C_P'' = Pn^2 \div \rho V^5$. The N.A.C.A. propeller reports employ a "speed-power" coefficient in the form

$$C_s = (1/C_P'')^{\frac{1}{5}} = V\sqrt[5]{\rho/Pn^2} \tag{217}$$

although the form

$$K_s = (1/C_P'')^{\frac{1}{2}} = (V/n)\sqrt{\rho V^3/P} \tag{224}$$

is more convenient to use. It will be noted that C_s or K_s is determined by the power absorbed at a given speed and rps. The value of C_s or K_s can, therefore, be calculated from design data and the best diameter determined from a curve of V/nD plotted against C_s or K_s, since

$$D = (V/n) \div (V/nD) \tag{225}$$

---

[3] F. E. Weick, "Working Charts for the Selection of Aluminum Alloy Propellers of a Standard Form to Operate with Various Aircraft Engines and Bodies," N.A.C.A. T.R. No. 350 (1930).

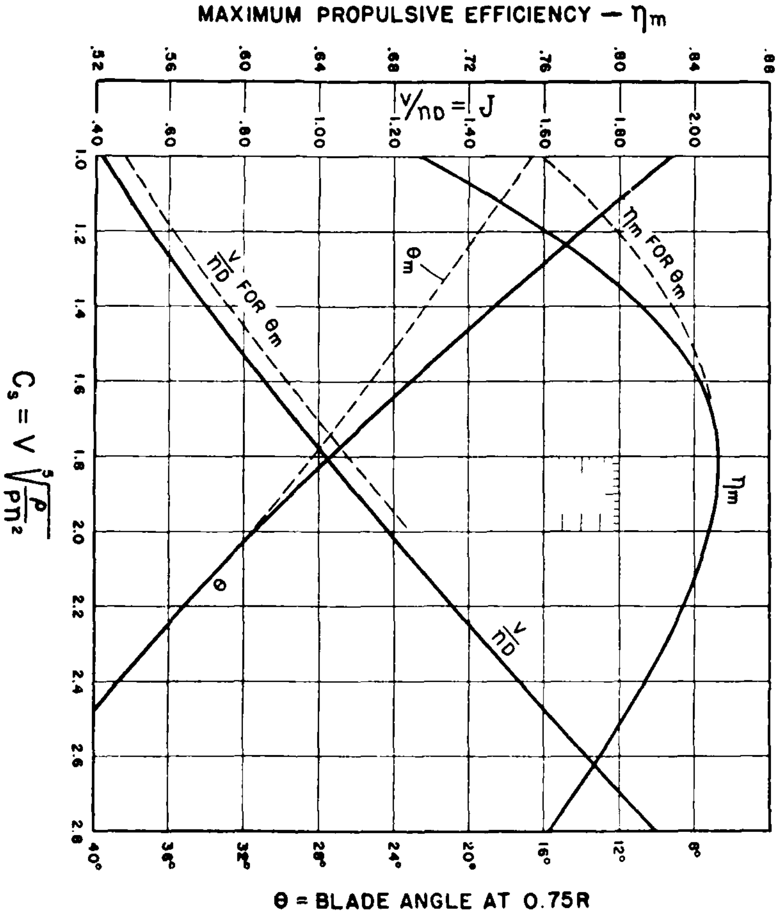

Figure 146. Propeller Design Chart Based on Speed-Power Coefficient C_s

Maximum propulsive efficiencies and blade angles can also be plotted against C_s as in Figure 146.

Using the engineering units mph, bhp, and rpm, the value of C_s is

$$C_s = \frac{0.638(\sigma)^{\frac{1}{5}}\,(\text{mph})}{(\text{bhp})^{\frac{1}{5}} \times (\text{rpm})^{\frac{2}{5}}} \tag{226}$$

The fifth root terms are not easily obtained without the assistance of the supplementary chart, see Figure 147.

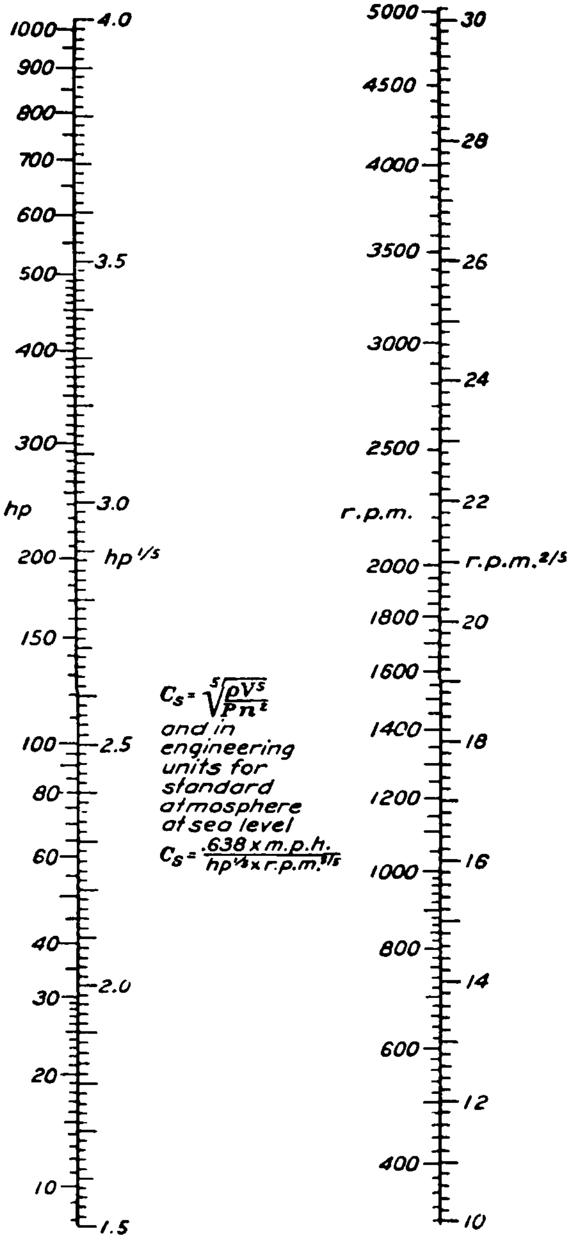

Figure 147. Fifth Roots for Calculating C_s

The fifth root of the density ratio σ is linear with altitude

$$(\sigma)^{\frac{1}{5}} = 1.000 - 0.0059\,(h/1{,}000) \qquad (227)$$

where h is the altitude in feet. The variation is as follows:

h	0	4,000	8,000	12,000	16,000	20,000
$\sigma^{\frac{1}{5}}$	1.000	.976	.953	.930	.906	.882

Propeller design is always a compromise to a certain extent. Even with the tremendous improvement due to the controllable-pitch propeller there remains a considerable range in diameter from which selection must be made to obtain the characteristics most desired. The solid lines of Figure 146 represent a series of propellers having maximum efficiency at each given value of C_s. For low values of C_s, an appreciably higher value of η can be obtained by using a slightly smaller diameter and a larger blade angle than required for the propeller having its maximum efficiency at the given value of C_s. The limits are indicated by broken lines on Figure 146. It should be understood, however, that improving the efficiency at high speed by this method results in a reduced performance in take-off and climb. The solid lines indicate the best compromise design.

The data from various N.A.C.A. Reports, chiefly T.R. No. 350, that were used in Figure 146 have been replotted against K_s on Figure 148. In mph, bhp, and rpm units

$$K_s = 0.00369\left(\frac{88\,V}{\text{rpm}}\right)\sqrt{\frac{\sigma V^3}{\text{bhp}}} \qquad (228)$$

Note that $88V/\text{rpm} = V/n$, a factor used in finding the diameter, equation (225).

The density ratio $\sigma = \rho/\rho_0$ may be obtained from Figure 263. For all practical purposes

$$\sqrt{\sigma} = 1.000 - 0.0140\,(h/1000) \qquad (229)$$

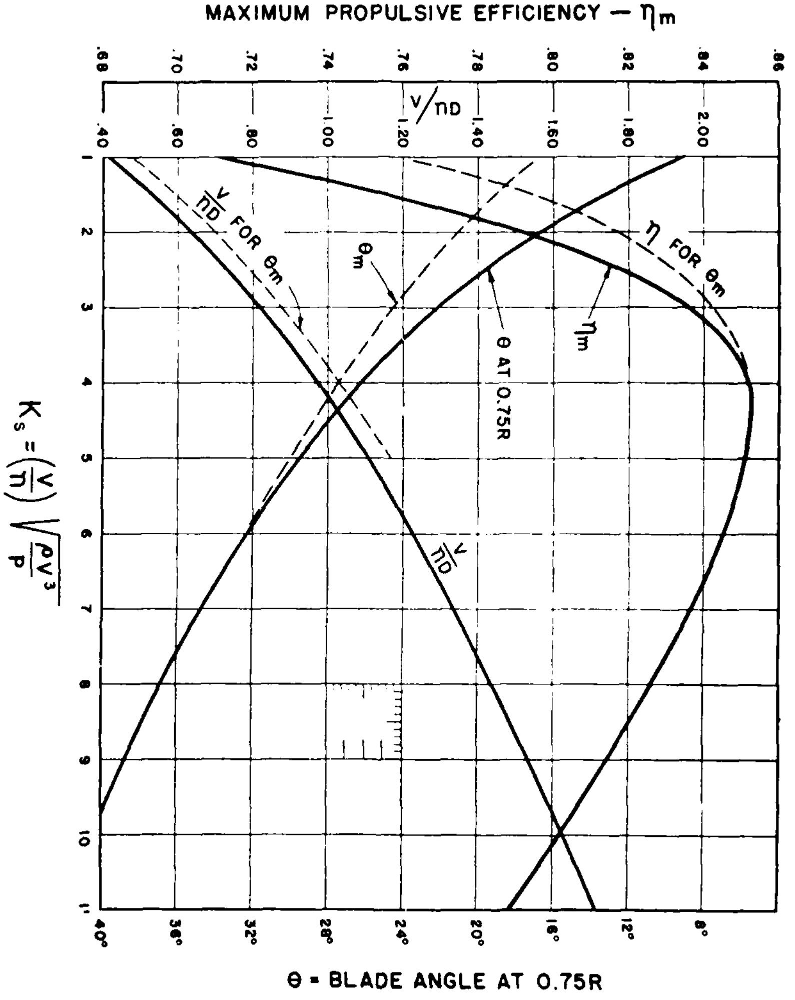

Figure 148. Propeller Design Chart Based on Speed-Power Coefficient K_s

The values of θ on Figures 146 and 148 are the actual angles under load. The approximate static angle may be estimated by equation (223).

The data on Figures 146 and 148 apply to two-bladed metal propellers having normal blade widths and thickness ratios. Weick[4] states that a two-bladed propeller will always absorb about 70% of the power absorbed by a *three*-bladed propeller having the same blades and blade angle. The maximum efficiency of the three-bladed propeller will be about 3% less than the maximum efficiency of the two-bladed propellers.

---

[4] F. E. Weick, "Aircraft Propeller Design," McGraw-Hill Book Co., Inc. (1930).

Tip-Speed. The resultant speed of a propeller tip is

$$V_R = [V^2 + (\pi D n)^2]^{\frac{1}{2}} \tag{230}$$

When the tip-speed approaches the velocity of sound, the propeller characteristics are adversely affected. These *adverse effects first* become apparent at a tip-speed between 950 and 1100 ft/sec, depending chiefly on the blade section and thickness.[5] The average effect on maximum efficiency is indicated on Figure 149. Above the critical tip-speed, η_{max} is decreased about 10% for each 10% increase in V_R.

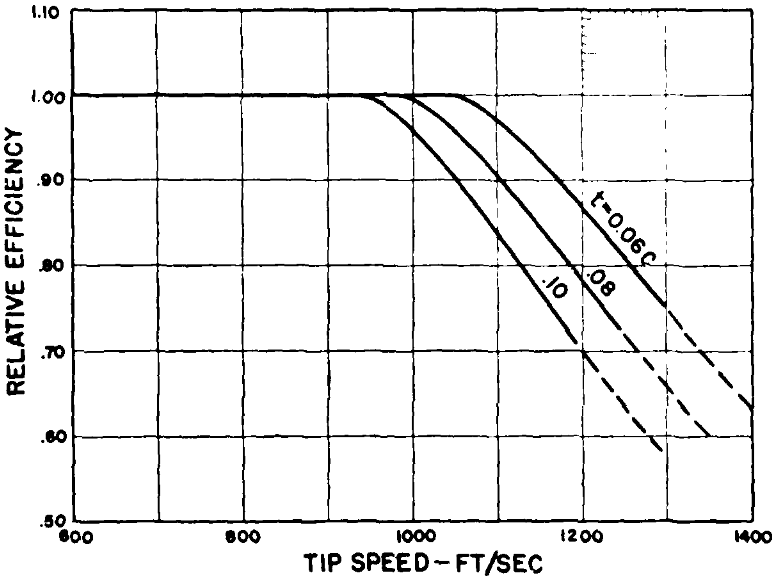

Figure 149. Characteristic Curves Showing Loss of Efficiency Due to Excessive Tip Speed

---

[5] D. H. Wood, "Full Scale Tests of Metal Propellers at High Tip Speeds," N.A.C.A. T.R. No. 375 (1931).

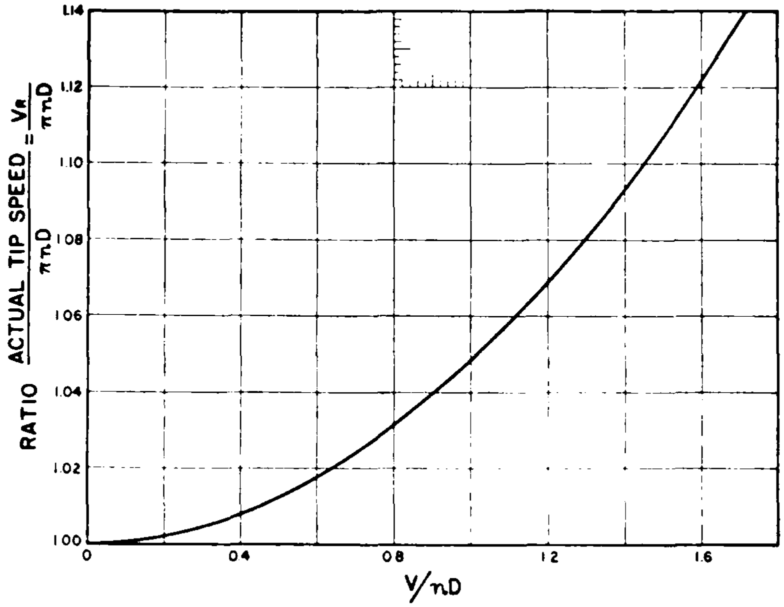

Figure 150 Relation Between Actual Tip Speed and Rotational Tip Speed

With low-pitch propellers, V_R may be taken equal to $\pi D n$, but for high values of V/nD, the forward component is not negligible. V_R may be conveniently calculated from

$$V_R = \frac{K \times \text{rpm} \times D}{19.10} \qquad (231)$$

where K is a function of V/nD as shown on Figure 150.

Velocity of Sound in Air. The velocity of sound in any gas is

$$a = \sqrt{kp/\rho} \qquad (232)$$

where p is the pressure, ρ the density, and k the ratio of specific heat at constant pressure to that at constant volume. The equation may be written in the form

$$a = \left[k\frac{p_0}{\rho_0}\frac{p}{p_0}\frac{\rho_0}{\rho}\right]^{\frac{1}{2}} = \left[k\frac{p_0}{\rho_0}\frac{T}{T_0}\right]^{\frac{1}{2}} \qquad (233)$$

for air $k = 1.41$, $p_0 = 2116$ lb/sq ft and $\rho_0 = 0.002378$ lb sec^2/ft^4. Substituting these values gives

$$a = \left[1.41 \times \frac{2116}{0.002378} \times \frac{T}{T_0}\right]^{\frac{1}{2}} = 1120\left(\frac{T}{T_0}\right)^{\frac{1}{2}} \qquad (234)$$

T being in °C absolute. The variation with temperature is as follows:

T, °C	−20	0	10	15	20	30
a, ft/sec	1,050	1,090	1,110	1,120	1,130	1,150

The variation with altitude in the standard atmosphere is:

h, ft	0	5,000	10,000	15,000	20,000	25,000	30,000
a	1,120	1,101	1,081	1,061	1,040	1,019	998

This variation is approximated by

$$a = 1120 - 0.0040\,h \qquad (235)$$

Cut-off Tips. It is customary to secure a desired diameter by cutting off the tips of a larger propeller. The resulting propeller has pitch and blade area distributions differing from standard and the characteristics are affected slightly. From N.A.C.A. tests[6] there is a linear loss in η_m as the diameter is reduced. This loss averages 2.3% for each 10% reduction in diameter or

$$\Delta\eta_m = 0.23\,(\Delta D/D) \qquad (236)$$

For the same blade settings at 0.75 R, the other characteristics are not greatly affected. Hence, to compensate for the reduced diameter, the blade setting at the 42-in radius must be increased about 0.7° for each 5% reduction in diameter or

$$\Delta\theta \text{ at } 42''R = 14\,(\Delta D/D)$$

These relations should not be used for diameter reductions greater than 20%.

---

[6] D. H. Wood, "Full-Scale Wind-Tunnel Tests of a Propeller with the Diameter Changed by Cutting Off the Blade Tips," N.A.C.A. T.R. No. 351 (1930).

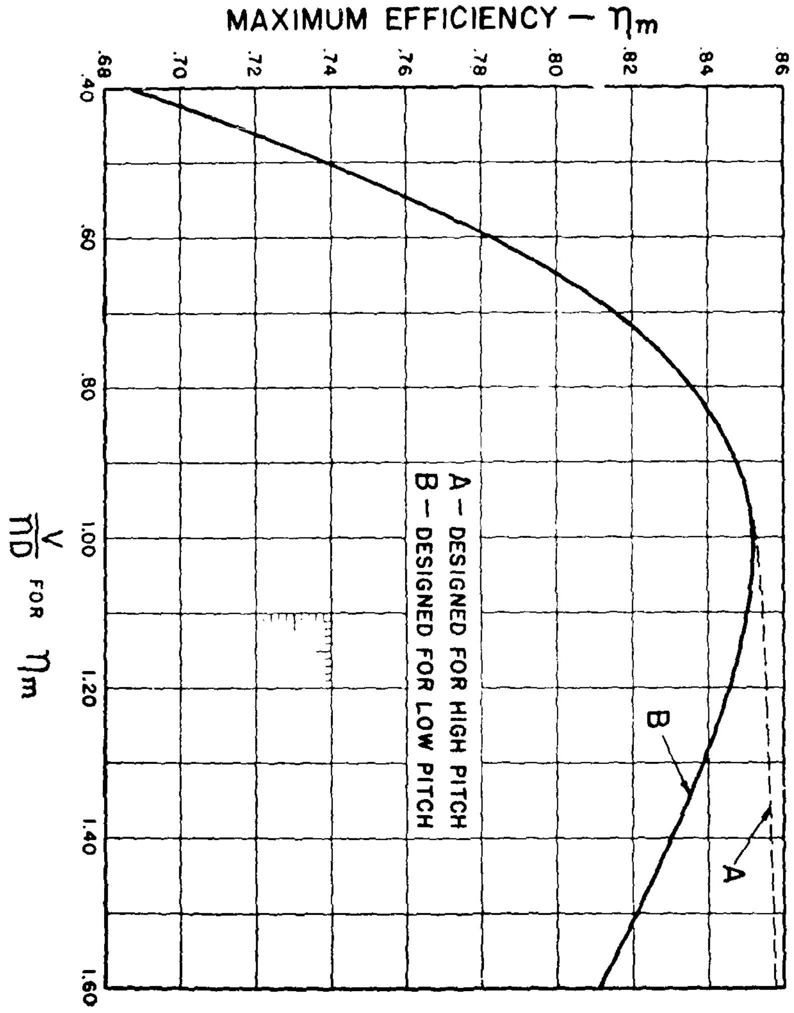

Figure 151. Maximum Efficiency as a Function of V/nD

Approximate Diameter Formula. An approximate value of propeller diameter may be quickly obtained from

$$D^4 = \left(\frac{K^2}{\text{rpm}}\right)^2 \left(\frac{\rho_0}{\rho}\right) \frac{\text{bhp}}{V} \qquad (237)$$

where V is the speed in mph. K varies with pitch angle, and for a two-bladed propeller

Design V/nD	0.6	0.8	1.0	1.2	1.4
K	325	317	311	306	302

The diameter of a 3-bladed propeller is about 7% less than the diameter of a 2-bladed propeller.

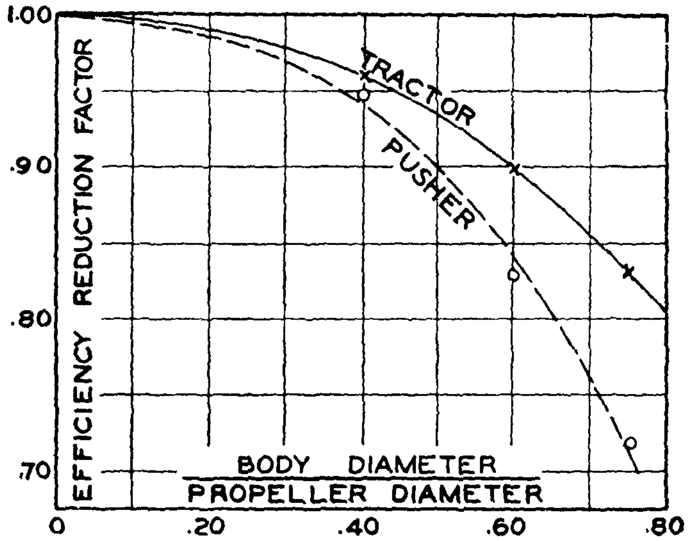

Figure 152. Effect of Body Interference on Propulsive Efficiency

Maximum Efficiency. The maximum propulsive efficiency for any propeller of a geometrically similar series depends on V/nD, slipstream obstruction and tip-speed. Figure 151 gives the values of η_m as a function of V/nD. These values are for two-bladed metal propellers with a minimum of slipstream obstruction, corresponding to a reduction of about 2% in the propeller efficiency. The approximate

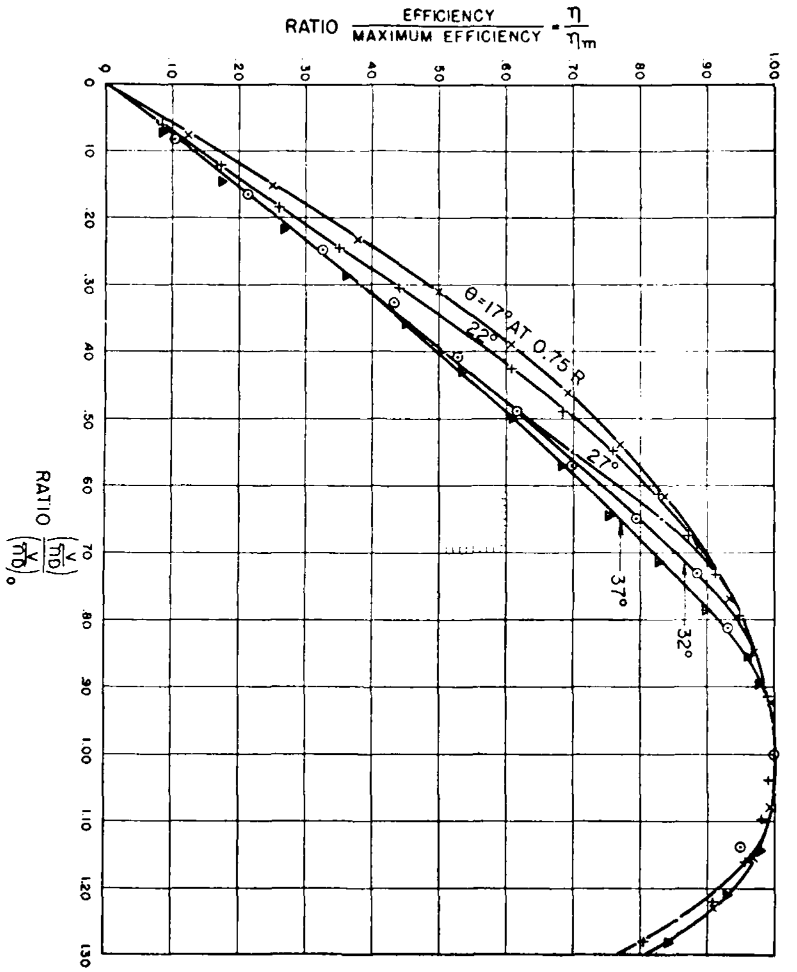

Figure 153. General Efficiency Curves as a Function of V/nD and θ

loss due to slipstream obstruction is given by Figure 152, which is based on British tests[7] and confirmed by the data in N.A.C.A. T.R. No. 339.[8] The body diameter should be taken at a point about one propeller diameter aft of the propeller.

General Efficiency Curves. The curves of efficiency against V/nD are similar for all conventional propellers operating at low and moderate blade angles. For blade angles above 20°, a portion of the blade is "stalled" at low values of V/nD. The effect is clearly shown in Figure 153, where the ratio of η/η_m is plotted against the ratio $(V/nD)/(V/nD)_0$. The maximum efficiency η_m occurs at $(V/nD)_0$. For blade settings below about 20°, the points lie on a single curve, marked 17°. The stall becomes progressively more complete as the blade angle is increased above 20.°

Figure 153 gives a close approximation to the efficiency curve of any propeller for which η_m, $(V/nD)_0$, and θ are known.

Controllable-Pitch Propellers. The controllable-pitch propeller introduces an indeterminate factor unless there is some limiting specification. The normal specification is that the rpm is to be constant and in some cases this is accomplished automatically. For constant rpm, the only unknown factor is propeller efficiency η. Since $C_P = P/\rho n^3 D^5$ is constant and $V/V_m = J/J_m$ where $J = V/nD$, the variation of blade angle θ with V may be determined from the usual plot of C_P against V/nD. This determines the efficiency also.

Using the method outlined above, the variation of η/η_m has been determined as a function of V/V_m for a number of initial settings with the N.A.C.A. full-scale propeller test data. The curve in Figure 154 may be used to calculate thp available with constant rpm propellers. For a two-position propeller, however, it is necessary to use the appropriate curve from Figures 165–169, corrected for the V and n corresponding to each blade angle.

---

[7] A. Fage, C. N. H. Lock, H. Bateman, and D. H. Williams, "Experiments with a Family of Airscrews Including Effect of Tractor and Pusher Bodies," Part II, Br. A.R.C. R. & M. No. 830 (1922).

[8] F. E. Weick, "Full-Scale Wind-Tunnel Tests with a Series of Propellers of Different Diameters on a Single Fuselage," N.A.C.A. T.R. No. 339 (1929).

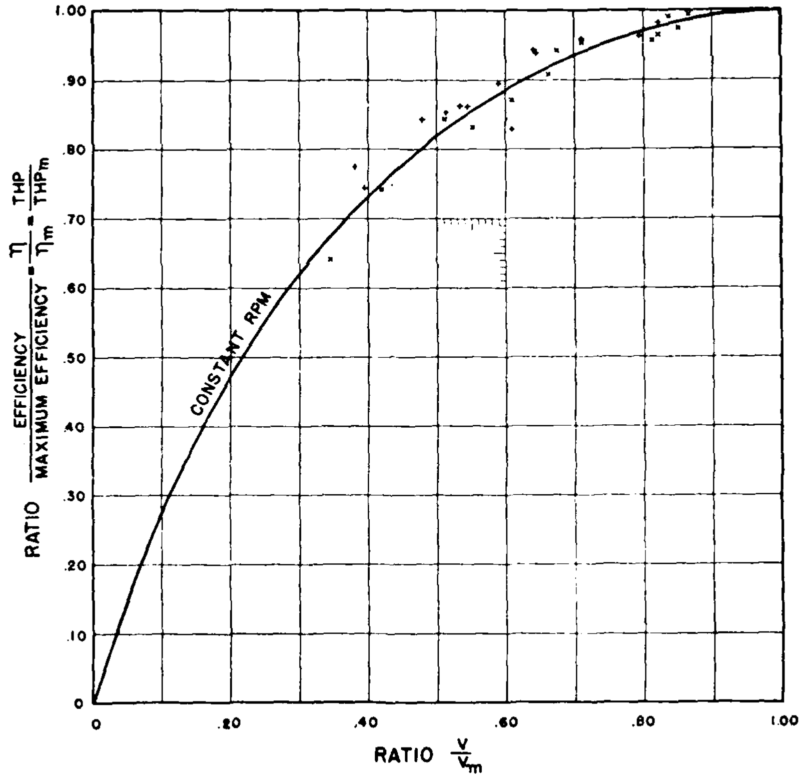

Figure 154. General Efficiency and thp Curve for Controllable-Pitch Propellers

The low-pitch or static setting of a controllable-pitch propeller may be obtained from the variation of C_P with blade angle. A plot of N.A.C.A. test data shows that

$$\frac{\theta_0}{\theta_v} = 0.82 \left[\frac{P_0}{P_v} \frac{\rho_v}{\rho_0} \left(\frac{n_v}{n_0} \right)^3 \right]^{0.60} \tag{238}$$

where the subscript *o* indicates static conditions and the subscript *v* indicates maximum speed conditions. This equation may be used to determine the blade angle for calculating static thrust when the engine has both altitude and take-off ratings.

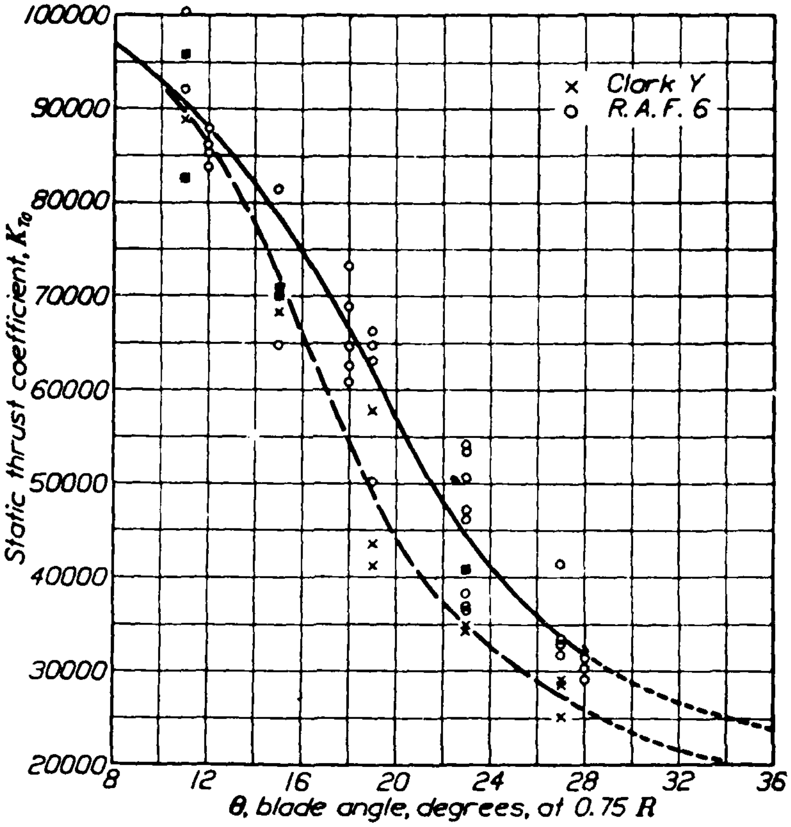

Figure 155. Static Thrust Coefficients for Adjustable-Blade Metal Propellers

Static Thrust. Static thrust may be calculated[9] by the equation

$$T_0 = \frac{K_{To} \times \text{bhp}}{\text{rpm} \times D} \tag{239}$$

---

[9] W. S. Diehl, "Static Thrust of Airplane Propellers," N.A.C.A. T.R. No. 447 (1932).

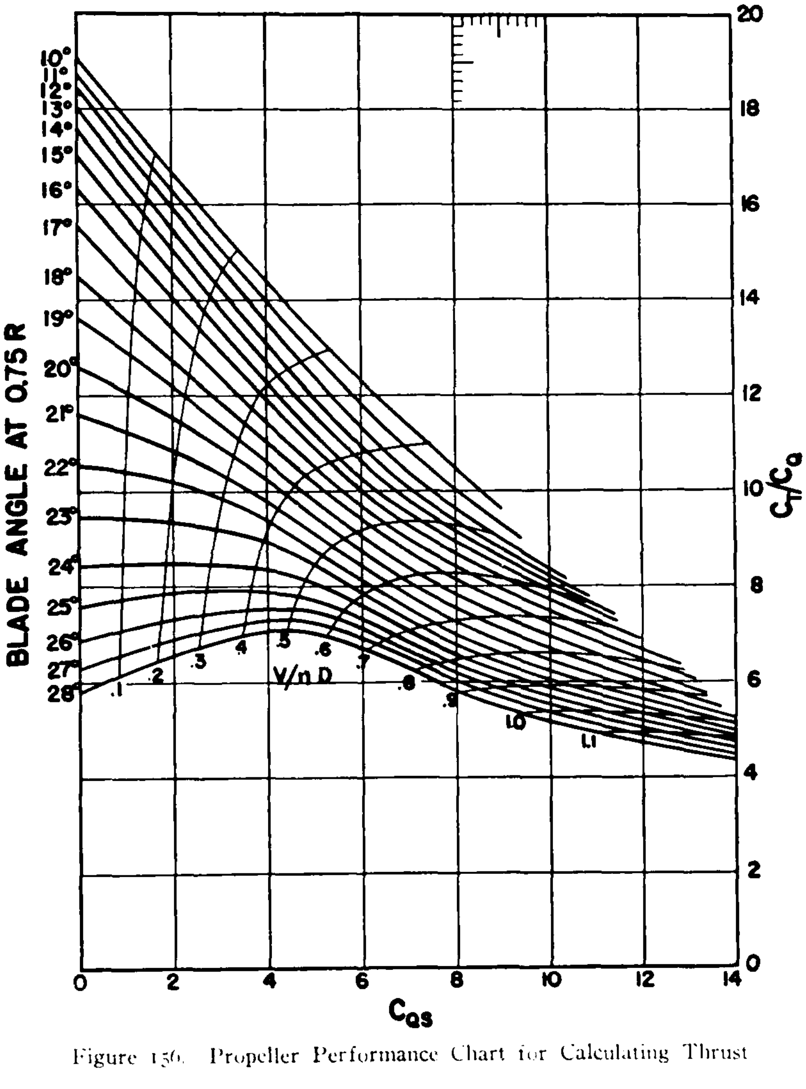

Figure 156. Propeller Performance Chart for Calculating Thrust

where the static thrust coefficient K_{T_0} is a function of blade setting and blade section as shown on Figure 155.

Propeller Thrust at Any Speed. The propeller thrust at any speed may be calculated by the method outlined in N.A.C.A. T.R. No. 481,[10] using Figure 156 which is taken from that report. In Figure 156, the ratio C_T/C_Q is plotted against C_{QS}. The thrust is found from the relation

$$
\begin{aligned}
C_T/C_Q &= TD/Q \\
T &= (C_T/C_Q) \times Q/D \\
&= (C_T/C_Q) \times \frac{5{,}250 \text{ bhp}}{\text{rpm} \times \text{diam}} \qquad (240)
\end{aligned}
$$

The coefficient C_{QS} is a torque coefficient directly proportional to V

$$C_{QS} = V\sqrt{\rho D^3/Q} \qquad (241)$$

where the torque $Q = 5{,}250$ bhp/rpm.

Calculated Thrust Power. It is possible to calculate the thrust power available by several methods, such as those outlined in N.A.C.A. Technical Note No. 446,[11] and Technical Report No. 481.[10] Figure 156 gives the necessary data for such calculation, using the coefficient

$$C_{QS} = \sqrt{2qD^3/Q} = K_{QS}\sqrt{2\pi} \qquad (241a)$$

where q is the dynamic pressure $\rho V^2/2$, and Q is the engine torque $Q = 5250$ bhp/rpm. If instead of C_T/C_Q, we plot ηC_P and V/nD against K_{QS} as in Figure 157, it is possible to read the values of V/nD and ηC_P directly. These determine n and thp which is obtained from

$$\text{thp} = \frac{(\eta C_P)\cdot\rho\, n^3 D^5}{550} \qquad (242)$$

---

[10] E. P. Hartman, "Working Charts for the Determination of Propeller Thrust at Various Air Speeds," N.A.C.A. T.R. No. 481 (1934).

[11] S. Ober, "Estimation of the Variation of Thrust Horsepower Available," N.A.C.A. T.N. No. 446 (1933).

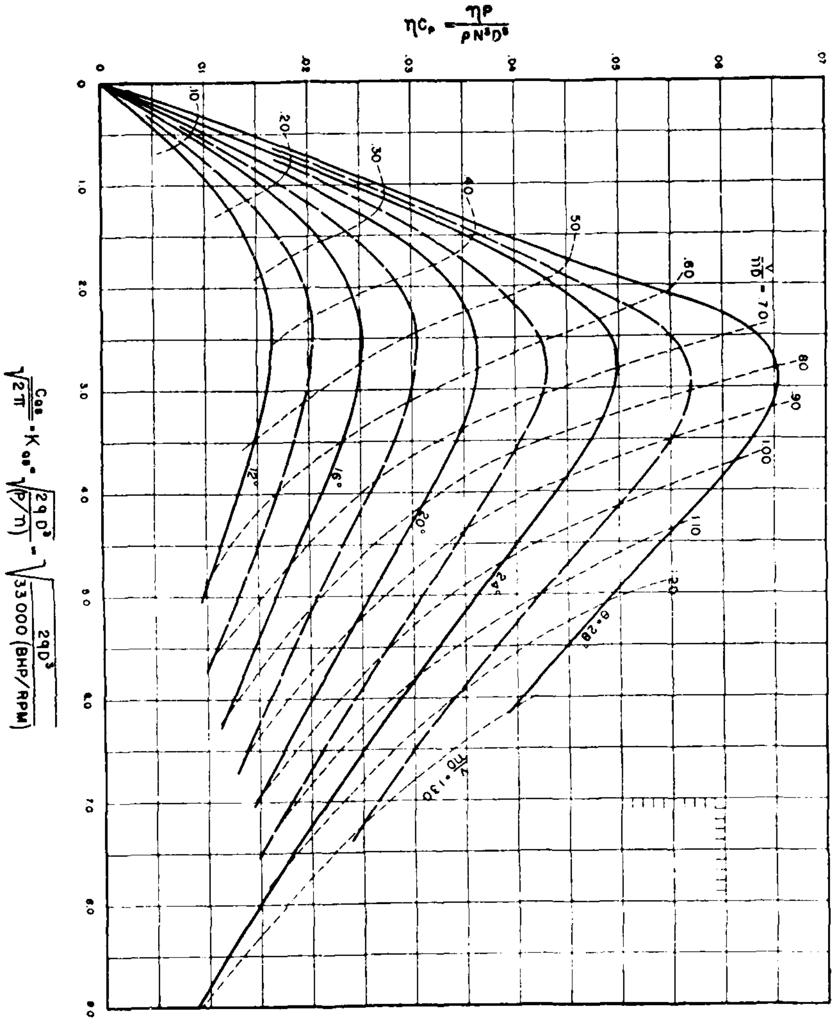

Figure 157. Effective Power Coefficient and V/nD as Functions of θ and K_{QS}

While this method is exact, it is no more accurate than the propeller data selected for the installation under consideration. Owing to the various factors affecting propeller performance, the net accuracy is probably not increased sufficiently to justify the additional labor involved. In general, it is better to select the proper curve of thp/thp_0 from Figures 165 to 169.

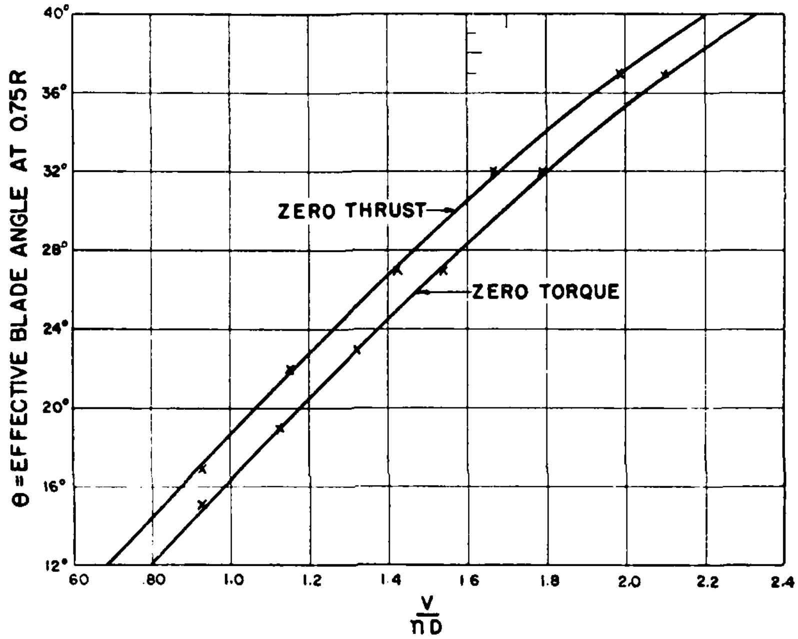

Figure 158. V/nD for Zero Thrust and Zero Torque

Zero Thrust: Zero Torque. The values of V/nD for zero thrust or zero torque depend on the blade angle as shown on Figure 158. For any speed V mph, the rpm for zero thrust is

$$\text{rpm}_{T_0} = \frac{88V}{(V/nD)_{T_0} \cdot D} \tag{243}$$

Negative Thrust and Torque. The negative thrust and torque of a propeller "wind-milling" are sometimes required. These may be obtained from Figure 159 which is taken from N.A.C.A. Technical Report No. 464.[12]

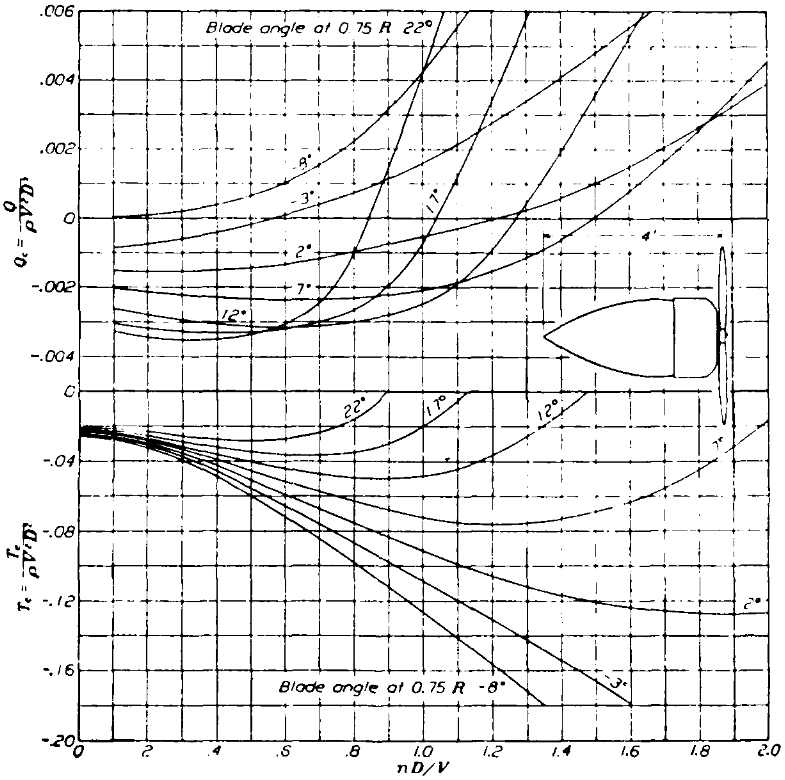

Figure 159. Negative Thrust and Torque Coefficients with a Nacelle

Drag of a Locked Propeller. The drag of a locked propeller may be determined from the curve of negative thrust coefficient against blade angle in Figure 160, which is taken from N.A.C.A. Technical Report No. 464.[12] It is of interest to note that a propeller set or "feathered" to

---

[12] E. P. Hartman, "Negative Thrust and Torque Characteristics of an Adjustable-Pitch Metal Propeller," N.A.C.A. T.R. No. 464, 1933.

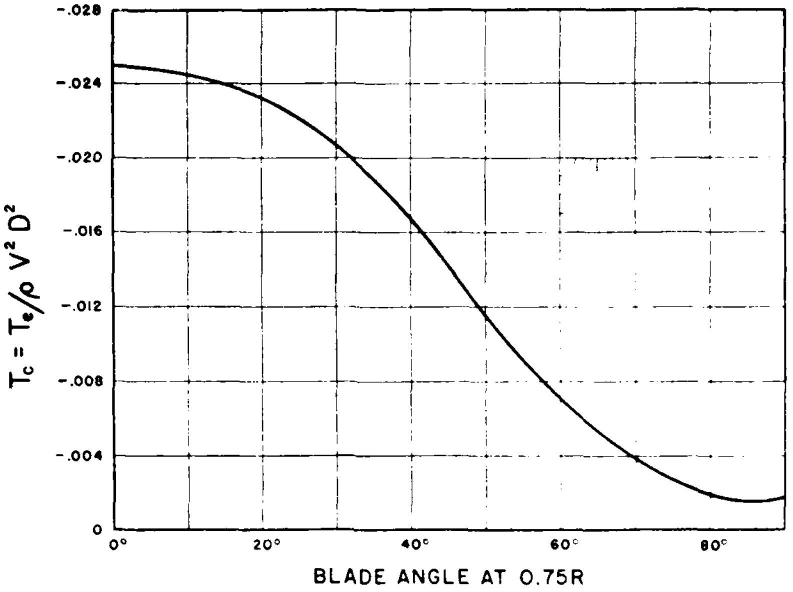

Figure 160. Variation of Negative Thrust Coefficient with Blade Angle for a Locked Propeller

about 90° has less than 10% of the drag of a stopped propeller with a normal blade angle. The coefficient on Figure 160 is $T_C = C_T' = T/\rho V^2D^2$. Hence,

$$\text{Drag} = T_C\rho V^2D^2 = 2T_C qD^2 \qquad (244)$$

General Power Coefficient Curves. Over the range in V/nD covered by extreme flight speeds, the variation of the power coefficient

$$C'_P = C_2 = P/\rho V^3D^2 \qquad (215)$$

is similar for all propellers. Taking $C'_P = C'_{P_0}$ for $(V/nD) = (V/nD)_0$ at maximum efficiency, the ratio of all values of the C'_P/C'_{P_0} plot as a single curve against the ratio $(V/nD)/(V/nD)_0$. Such a curve constitutes a general power coefficient curve that enables a general solution of many problems involving P, V, and n.

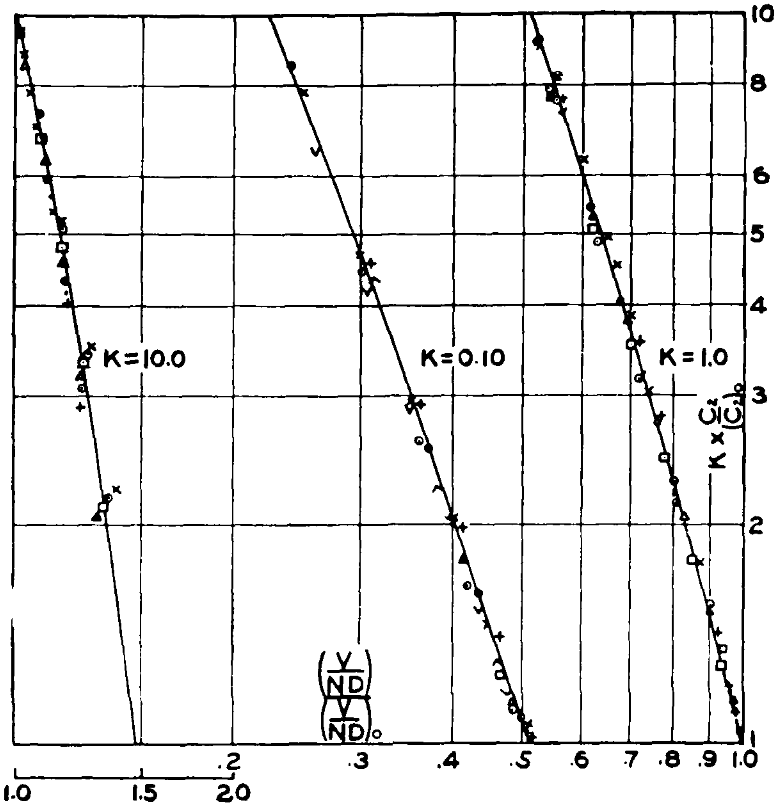

Figure 161. General Power Coefficient Curve

A folded logarithmic plot of the general power coefficient curve is given in Figure 161. This curve was originally derived from Durand's data on wooden propellers, but all available N.A.C.A. test data on metal propellers are in complete agreement. General thrust power coefficient curves may be obtained from Figures 153 and 161.

Applications of the general power coefficient curves follow.

Variation of bhp with *V*. Assuming a series of values of V/V_0 and n/n_0 determines $(V/nD)/(V/nD)_0$ from which

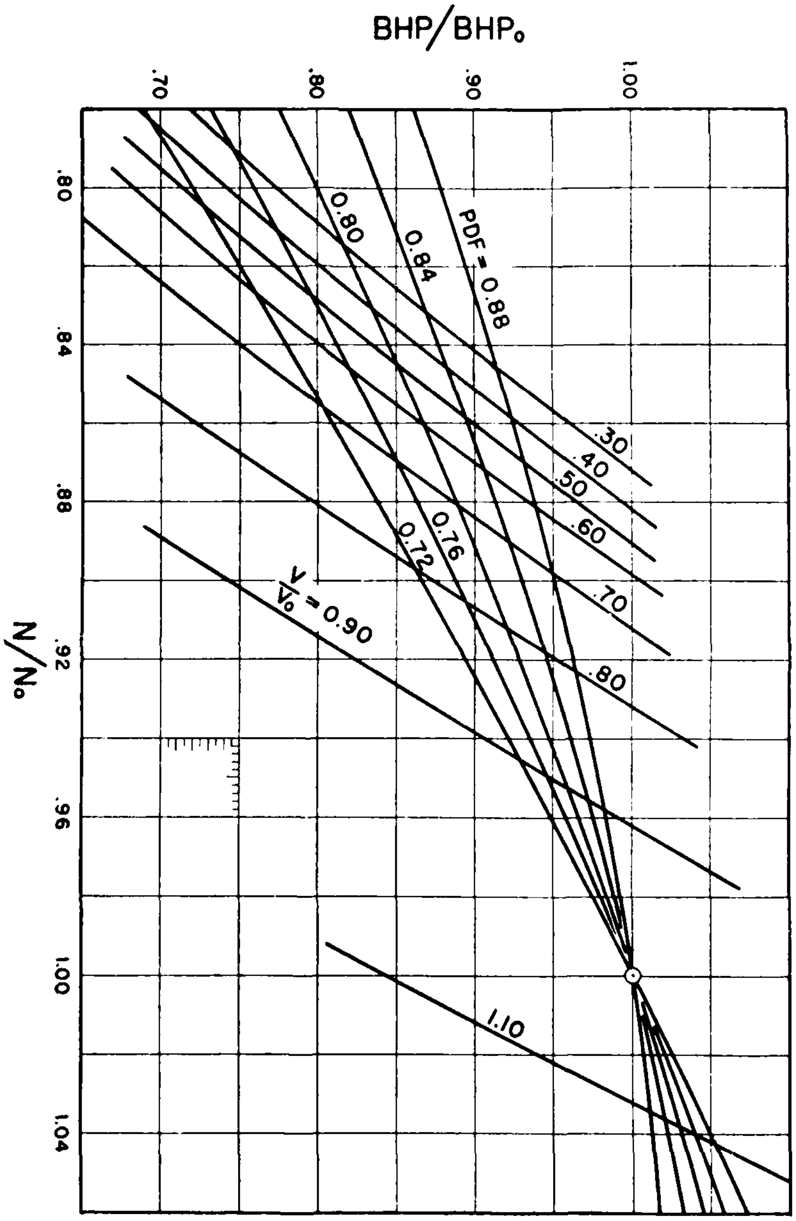

Figure 10.2 General Curves of Bhp, *V* and *N*

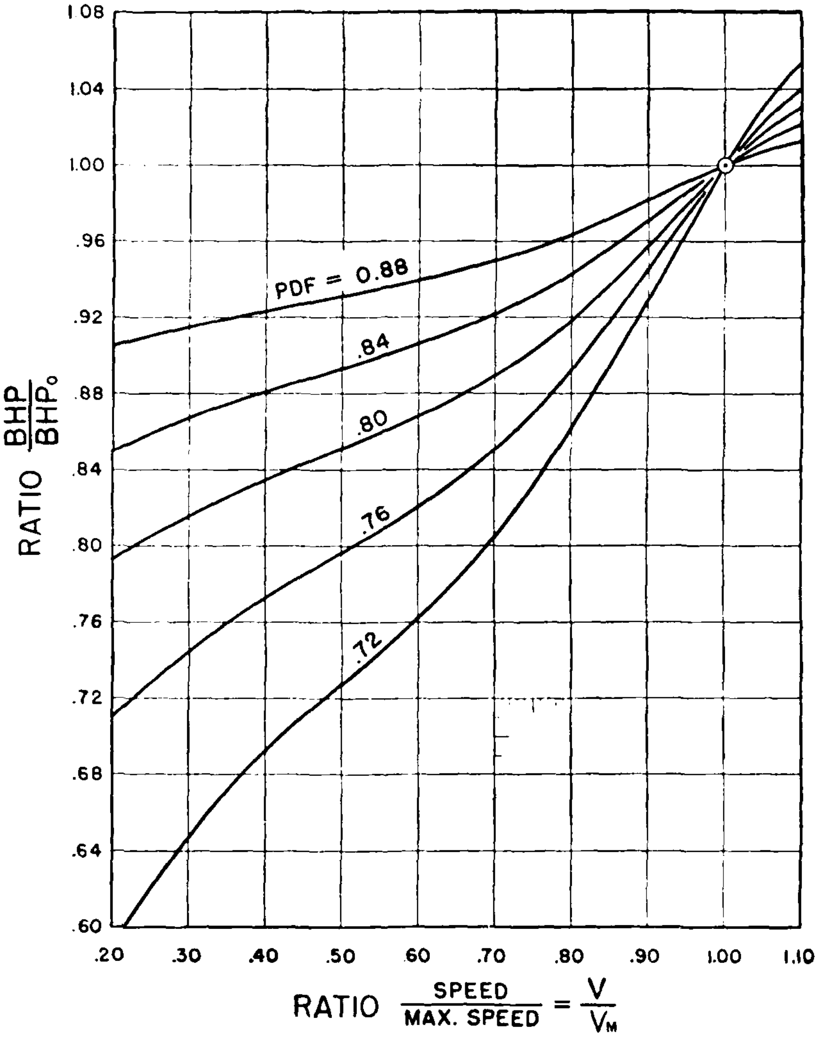

Figure 103. Variation of bhp with V—Fixed-Pitch Propeller

the corresponding values of C'_P/C'_{P_0} may be read from Figure 161.

Then since D is constant, the relative power required by the propeller is

$$\frac{\text{bhp}}{\text{bhp}_0} = \left(\frac{C'_P}{C'_{P_0}}\right) \times \left(\frac{V}{V_0}\right)^3 \tag{245}$$

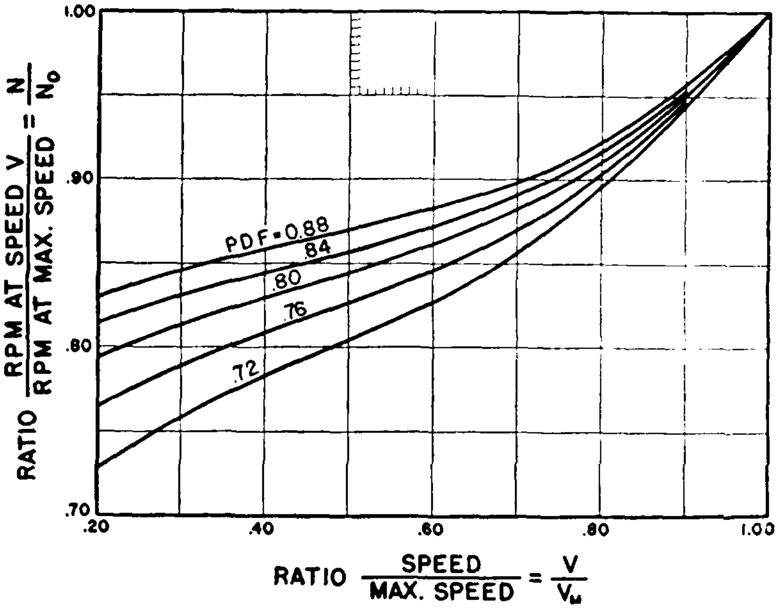

Figure 164. Variation of rpm with V—Fixed-Pitch Propeller

These values may be plotted for example as a family of curves of bhp/bhp₀ against n/n_0, one curve for each value of V/V_0. If the general bhp curves from Figure 137 (page 313) are superposed on this plot as in Figure 162 (page 346), the intersections give the variation in bhp and rpm with

V, as shown on Figure 163 (page 347) and Figure 164 above.

This method is exact but the actual flight values may be expected to differ by an amount depending on the twist in the propeller blade. This effect on rpm may be quite pronounced for certain propellers having a tendency to excessive twist.

General Thrust Horsepower Curves. The general curves of bhp/bhp_0, n/n_0 and η/η_0 may be combined to give general curves of thp/thp_0 as a function of V/V_m. These curves are so often required that they have been prepared to cover the entire range in power-drop factor PDF and blade angle θ.

To do this satisfactorily, five sets of curves are necessary. These are given in Figures 165 to 169, inclusive, which appear on the following pages.

The thrust power available at any speed may be determined from these curves when V_{max} and thp_m at V_{max} are known. The curves assume a fixed-pitch propeller set to give maximum efficiency at V_{max}.

For calculating thp with a controllable-pitch propeller, the curve which is illustrated in Figure 154 (page 337) should be used.

Variation of thp with Altitude: Fixed-Pitch Propeller. At constant air speed the power absorbed by a propeller varies directly as the density and substantially as the cube of the rpm. At constant rpm the power developed by the engine decreases more rapidly than the density. In a climb at constant air speed with a fixed-pitch propeller, the engine rpm must decrease to maintain equality of the engine and propeller torques. This decrease in rpm gives a slight increase in V/nD and η, but the decrease in engine power is predominant.

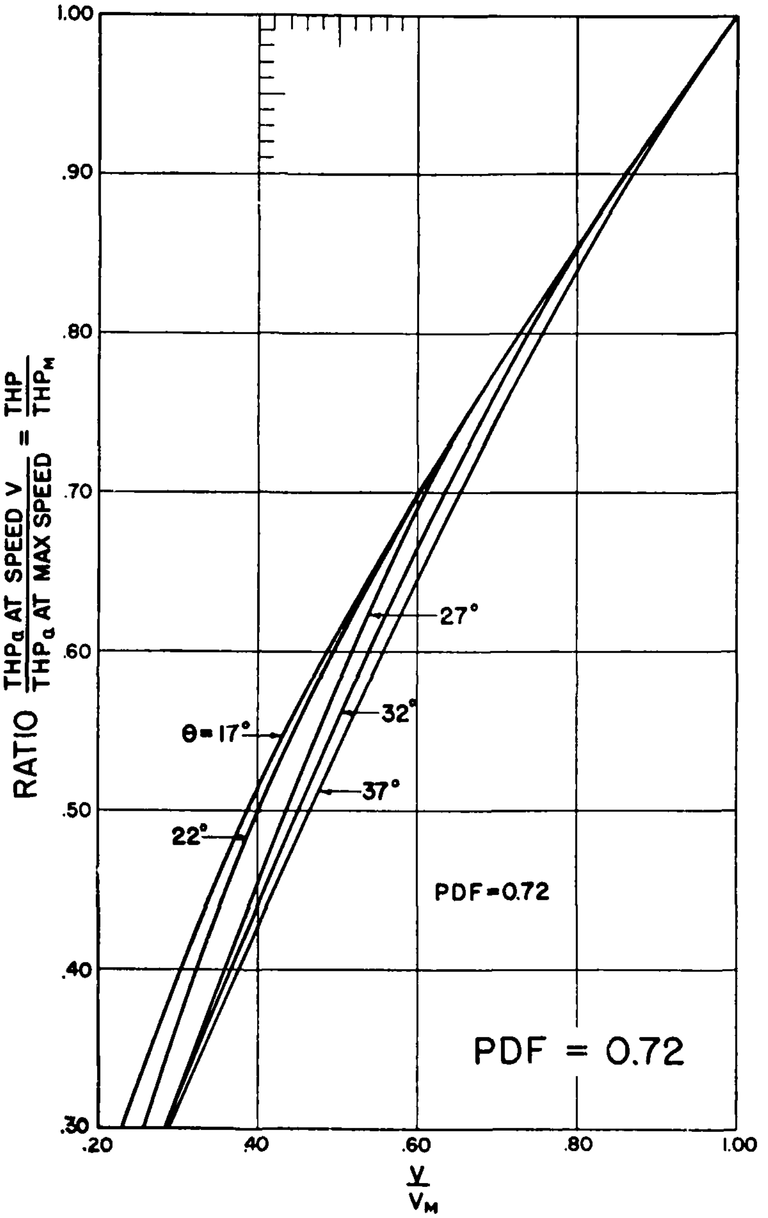

Figure 165. Variation of thp with V—Fixed-Pitch Propeller. PDF = 0.72

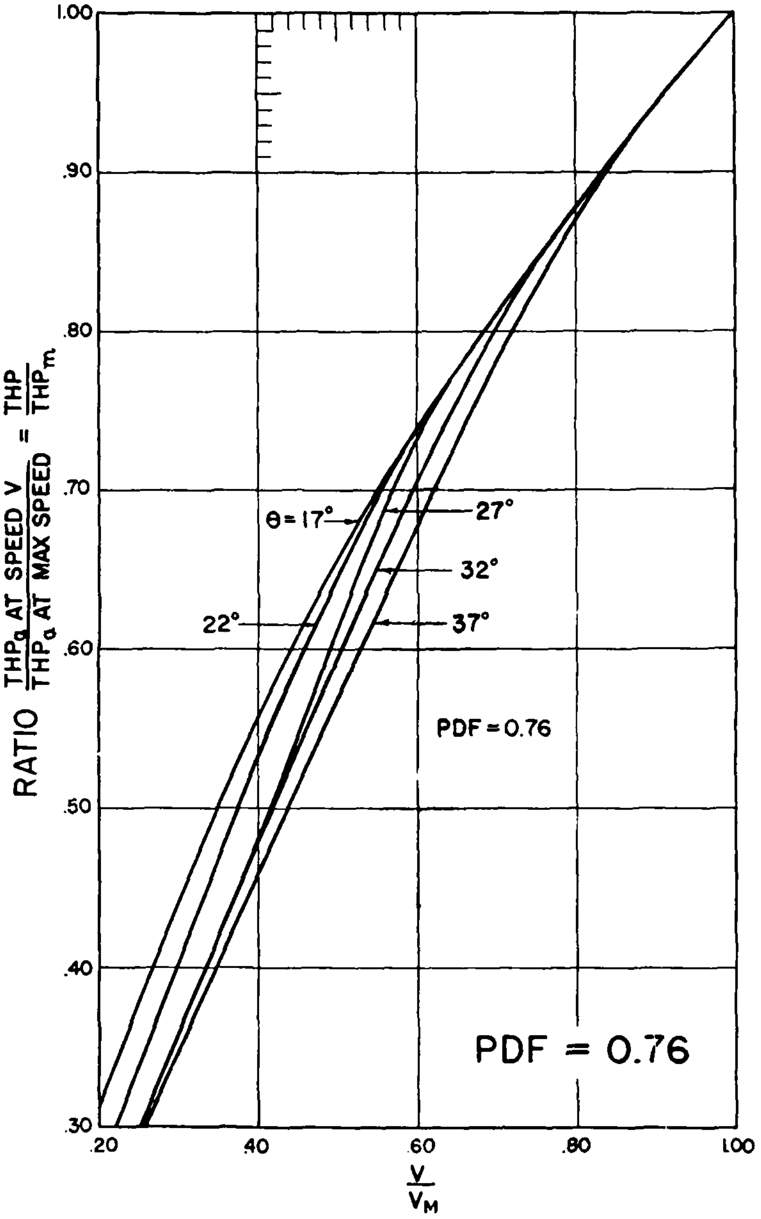

Figure 166. Variation of thp with V—Fixed-Pitch Propeller. PDF=0.76

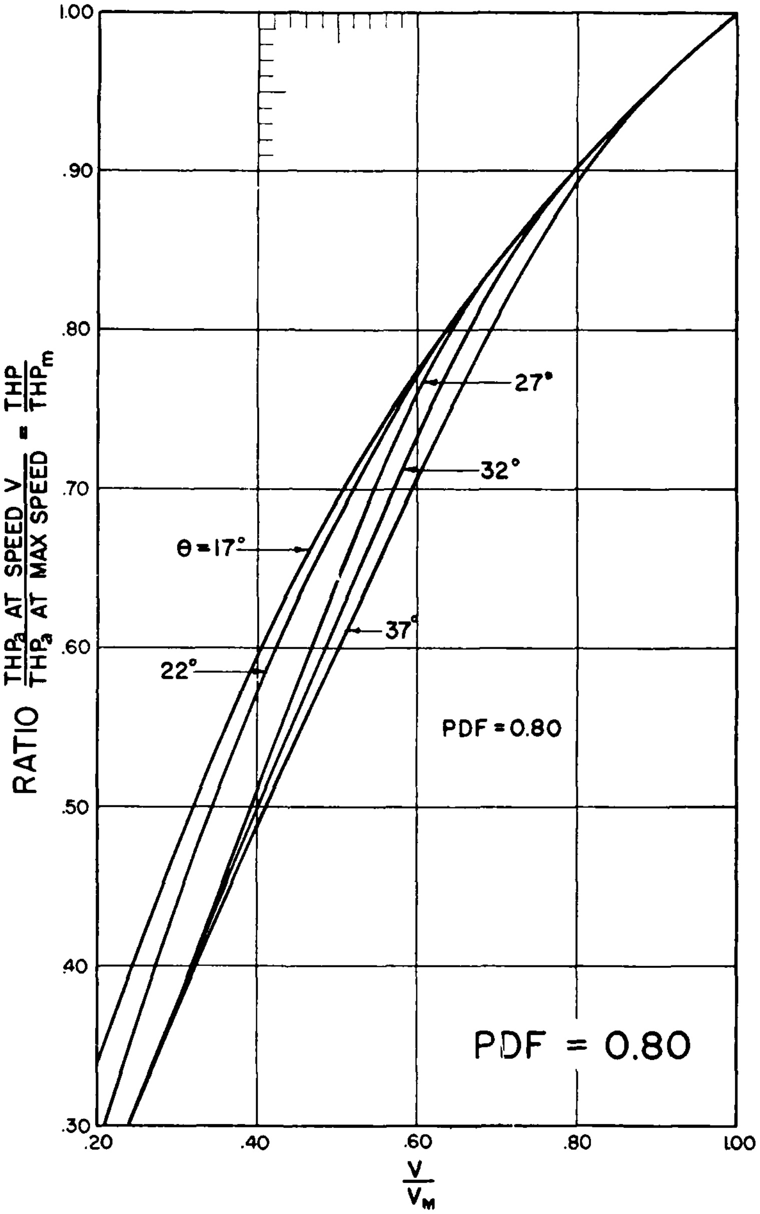

Figure 167. Variation of thp with V—Fixed-Pitch Propeller. PDF = 0.80

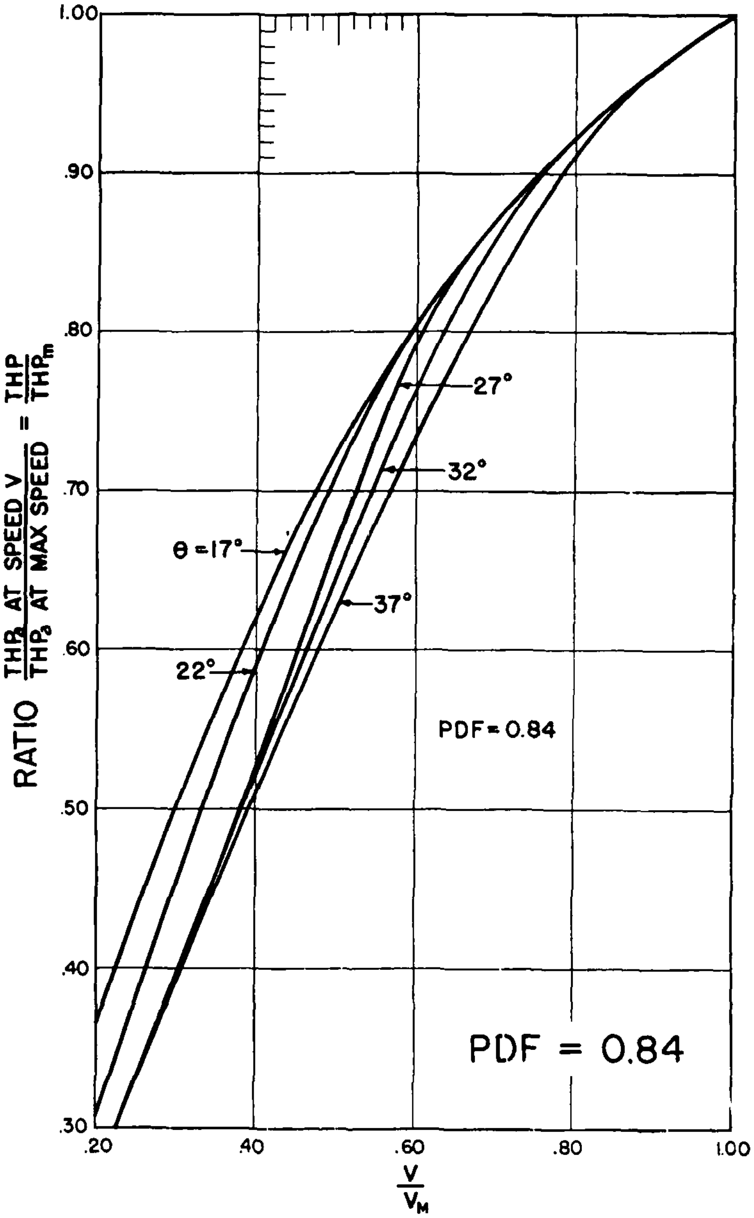

Figure 168. Variation of thp with V—Fixed-Pitch Propeller. PDF = 0.84

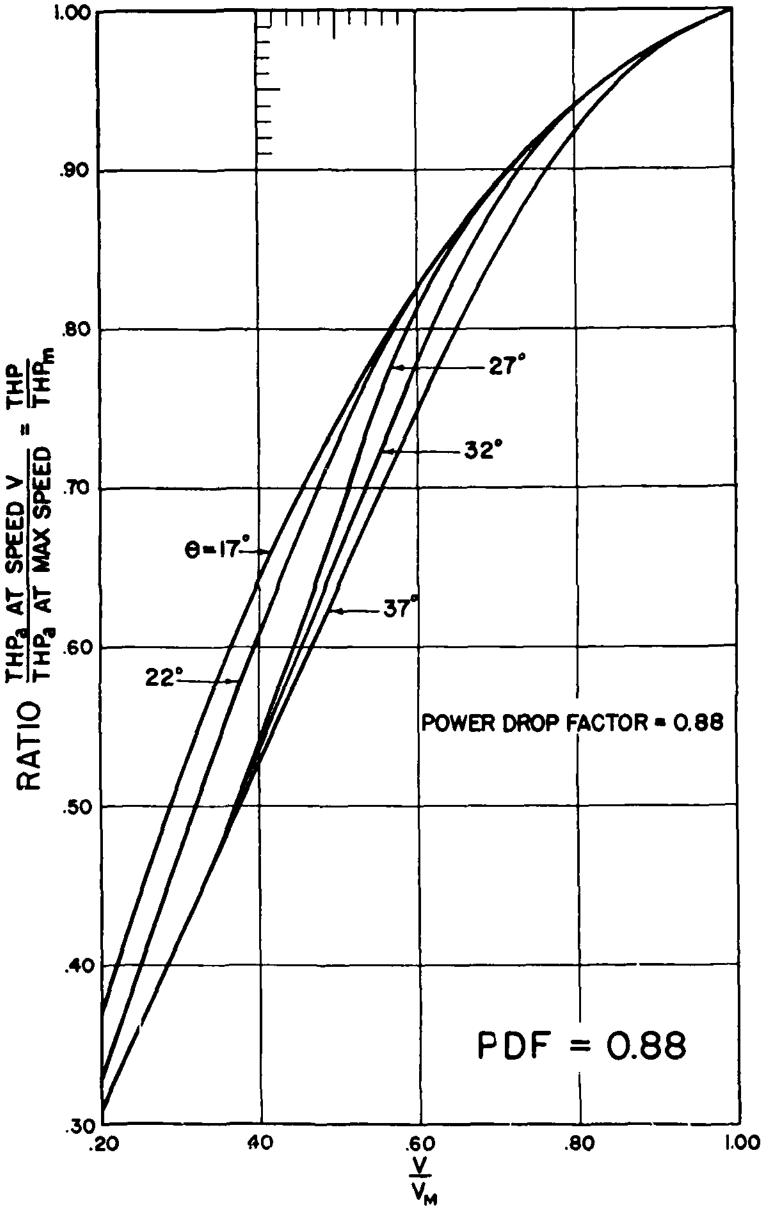

Figure 169. Variation of thp with V—Fixed-Pitch Propeller. PDF 0.88

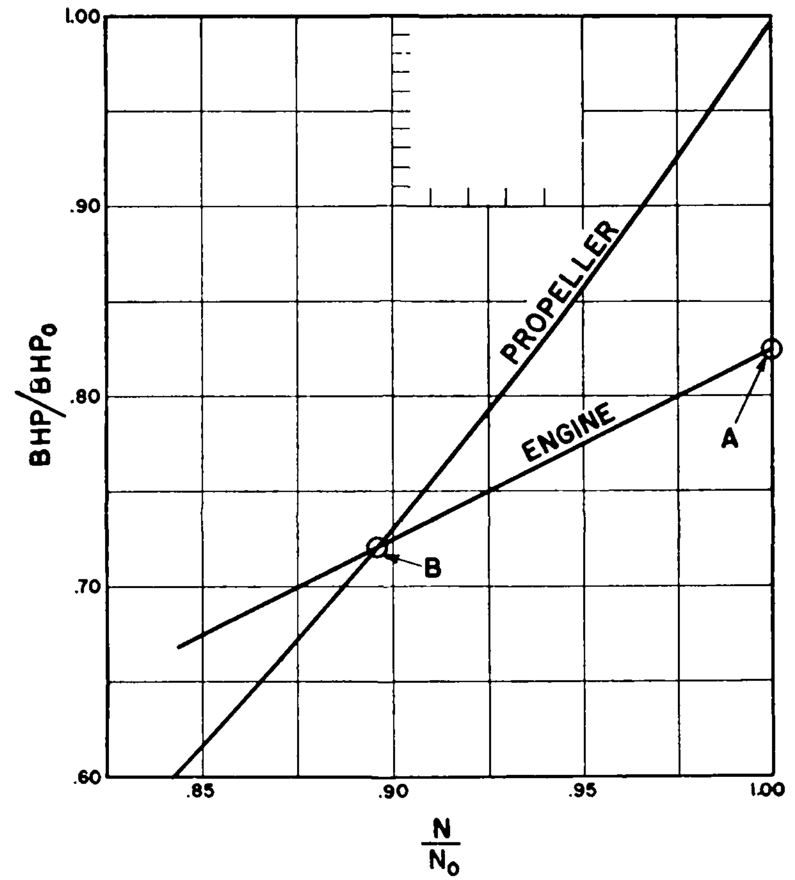

Figure 170. Effect of rpm on Propeller and Engine bhp

The decrease with altitude is more rapid for thrust horsepower at constant air speed than it is for bhp at constant rpm.

There are several methods available for calculating the variation of thp with altitude. If the decrease in rpm with altitude is obtained in a climb at constant true air speed, the power may be calculated from the general power coefficient curves of Figure 161. This method has been used in a number of cases, but a better method is based on general engine and propeller characteristics, as shown by Figure 170.

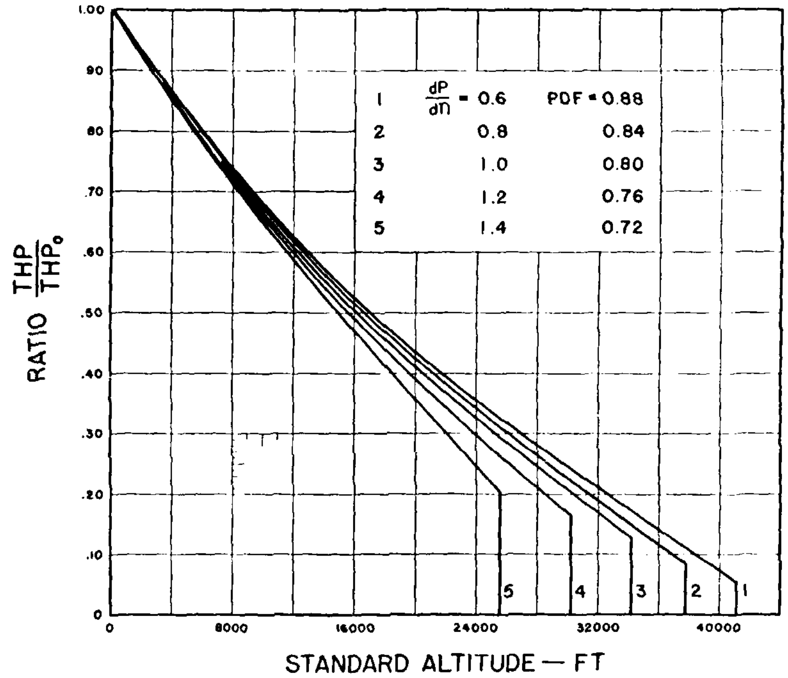

Figure 171. Variation of thp with Altitude Fixed-Pitch Propeller

Under this method a propeller power cubic is drawn on a non-dimensional plot of P against N. At 20,000 feet the propeller power is proportional to the density ratio $\rho/\rho_0 = 0.5327$ and the bhp of the engine is 0.440 of its sea-level value. At sea-level rpm, $N = N_0$, the ratio of engine power to propeller power is $0.440 \div 0.5327 = 0.826$. If from the point **A** at 0.826 a line is drawn on Figure 170 with the slope of the engine-power curve, the intersection with the propeller curve at the point **B** gives the bhp and rpm ratios for the altitude under consideration. The value of thp/thp$_0$ may then be calculated. Using this method, the variation of thp with altitude has been calculated for various slopes of engine-power curves corresponding to the power drop factors indicated on the resultant curves of Figure 171.

TABLE 15. VARIATION OF THRUST POWER WITH ALTITUDE: FIXED-PITCH PROPELLER

Standard Altitude ft	PDF = 0.88	0.84	0.80	0.76	0.72	$\sqrt{\frac{\rho_0}{\rho}}$
0	1.000	1.000	1.000	1.000	1.000	1.000
4,000	.868	.864	.860	.855	.850	1.061
5,000	.829	.825	.820	.816	.811	1.077
8,000	.738	.732	.725	.718	.711	1.128
10,000	.678	.672	.666	.656	.648	1.164
12,000	.625	.616	.608	.598	.588	1.201
15,000	.548	.540	.528	.514	.502	1.261
16,000	.523	.515	.505	.491	.472	1.282
20,000	.432	.422	.410	.392	.358	1.370
24,000	.355	.340	.325	.295	.245	1.468
25,000	.337	.322	.305	.275	.218	1.494
28,000	.280	.264	.245	.210	....	1.577
32,000	.210	.190	.165	....	....	1.697
36,000	.143	.114	....	....	....	1.837
40,000	.058	....	....	....	....	2.022

It should be noted that these curves are for propellers giving maximum efficiency at maximum speed. The climb and ceiling are, of course, greatly improved by using a lower pitch setting which is equivalent to increasing the slope of the engine power curve, since the reference point at full throttle will be nearer the peak of the power curve.

For convenience, the values of thp/thp$_0$ are given in tabular form in Table 15, which is shown on the preceding page.

It is of interest to note that for each engine PDF there will be a point of tangency, representing a limit to the power curve. For any further increase of altitude above this critical value, the propeller will stall the engine. The critical altitudes are as follows:

PDF	.88	.84	.80	.76	.72
dP/dN	.60	.80	1.00	1.20	1.40
Critical h	41,100	37,700	34,200	30,200	25,500

Variation of thp with Altitude: Controllable-Pitch Propeller. With a controllable-pitch propeller, the engine rpm can be maintained constant by decreasing pitch during the climb.

Since V, n, and D are constant, and $P = C_P \rho n^3 D^5$, it follows that

$$\frac{P}{P_0} = \left(\frac{C_P}{C_{P_0}}\right) \frac{\rho}{\rho_0}$$

where P/P_0 is the engine bhp relative to the sea-level value, as given in Figure 139. From this relation the variation in C_P, θ, η and thp may be calculated, with the results shown on Figure 172 and Table 16. The increase in thp ratio above the bhp ratio is partially fictitious, since the initial thp ratio is affected by the low propeller efficiencies for high blade angles (see Figure 146, page 326). Part of the gain shown is due to the step-up to a higher efficiency curve.

It is of interest to note the change in blade angle required to maintain constant rpm. In all cases investigated, the ratio of $\Delta\theta/\theta_0$ was a function of altitude only as shown by Figure 173.

Propeller rpm in Throttled Flight. It is possible to obtain the propeller rpm in throttled flight by plotting $\eta C_P = \eta P/\rho n^3 D^5$ against $\eta C'_P = \eta P/\rho V^3 D^2$ for various blade angles. On such a plot V/nD lines radiate from the origin. Since $\eta C'_P$ is known, the rpm may be obtained either from the value of V/nD or from the value of ηC_P.

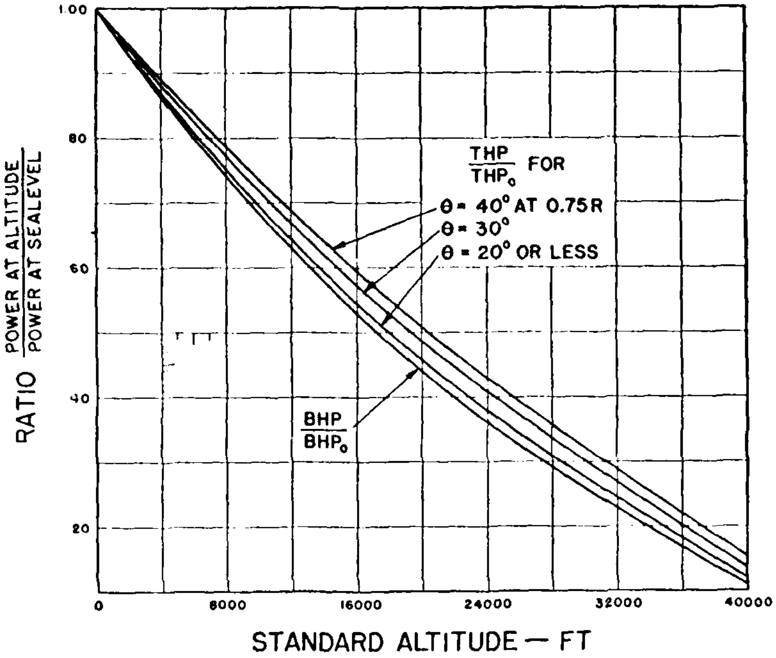

Figure 172. Variation of thp with Altitude Controllable-Pitch Propeller. (Constant rpm)

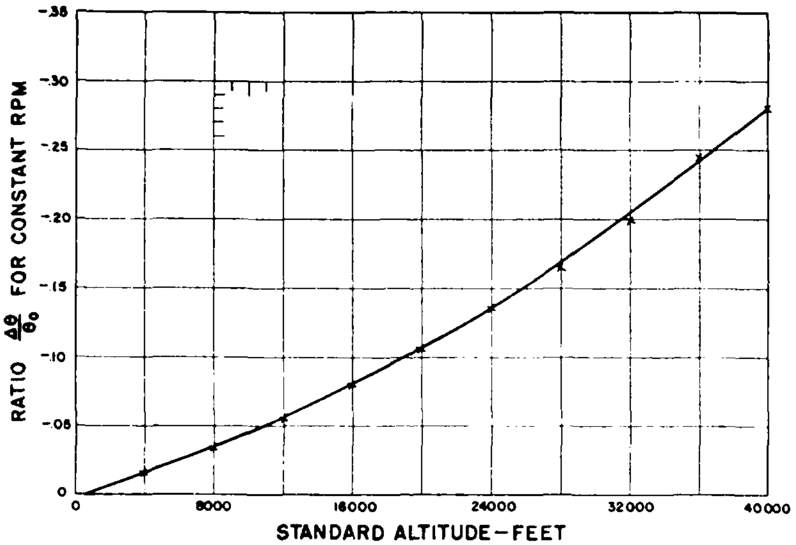

Figure 173. Effect of Altitude on Propeller Blade Angle (at 0.75 R) for Constant rpm

Table 16. Variation of Thrust Power with Altitude: Controllable-Pitch Propeller

Standard Altitude ft	$\theta = 20°$	$\theta = 30°$	$\theta = 40°$
0	1.000	1.000	1.000
4,000	.872	.880	.892
8,000	.752	.772	.788
12,000	.645	.668	.688
16,000	.546	.573	.596
20,000	.459	.487	.508
24,000	.376	.410	.430
28,000	.309	.338	.358
32,000	.245	.268	.288
36,000	.183	.201	.220
40,000	.121	.135	.152

θ = Blade angle at $0.75R$.

Analyses of flight test data for a number of airplanes show that the rpm in horizontal flight can be calculated accurately from the relation

$$\frac{n}{n_0} = K \sqrt[3]{\frac{\text{thp}}{\text{thp}_m}} \tag{246}$$

where K has an average value of 0.98.

CHAPTER 11

PERFORMANCE CALCULATION—POWER CURVES

Performance Calculation. The complete performance of an airplane comprises its maximum and minimum speeds, rate of climb at various altitudes, time to climb to various altitudes, and range and endurance at given speeds with specified fuel loads. While it is possible to calculate performance by purely analytical methods, a combination of the graphical and analytical will be found more simple and direct. The usual method is to calculate, for horizontal flight at various speeds and at a given altitude, the thrust power required for horizontal flight and the maximum thrust power available. If the curves of power required and power available are plotted against speed, their intersection obviously will determine the maximum speed at the altitude under consideration. The difference between power available and power required, at any given speed, is the excess power available for climb, and the maximum rate of climb occurs at that speed at which the excess power is a maximum.

Before going into a detailed explanation of the general methods for calculating performance, a brief statement of the basic assumptions will be given. In steady horizontal flight the forces acting on an airplane are: lift, drag, gravity, and propeller thrust. Since the motion is steady, the vector sum of the forces or their components in any direction, and the resultant moment about any axis must be zero. The equations of motion are easily obtained. Vertical and horizontal components give respectively

$$L + T \sin \theta - W = \frac{W}{g}\frac{dh}{dt} = 0 \qquad (247)$$

$$D - T \cos \theta = \frac{W}{g}\frac{dv}{dt} = 0 \qquad (248)$$

where θ is the angle of pitch of the thrust axis, L the lift, D the drag, and T the thrust. The thrust correction $T \sin \theta$ in equation (247) is negligible except at fairly large angles, and it is usually neglected, although the effect of a moderate throttle opening may be a reduction of the order of 5 mph in landing speed for an airplane having a low power loading. θ is ordinarily less than 20°, so that $\cos \theta = 1.0$ for all practical purposes. Therefore, unless extreme accuracy is required, it is always assumed that $L = W$ and $D = T$.

With the foregoing assumptions, the equation connecting weight and speed is

$$L = W = C_L q S = C_L \tfrac{1}{2} \rho S V^2 \qquad (249)$$

from which

$$V = \sqrt{2W/C_L \rho S} \qquad (250)$$

When W is in lb and S is in sq ft, equation (250) becomes

$$V = 29.00 \sqrt{\left(\frac{W}{S}\right)\Big/ C_L} \cdot \sqrt{\frac{1}{\sigma}} \qquad (250a)$$

for V in ft/sec, or

$$V = 19.77 \sqrt{\left(\frac{W}{S}\right)\Big/ C_L} \cdot \sqrt{\frac{1}{\sigma}} \qquad (250b)$$

for V in mph. The minimum or "stalling speed" is obviously determined by using the maximum value of C_L in equation (250). σ is the relative air density ρ/ρ_0.

Power Required for Horizontal Flight. The power required for horizontal flight is

$$\text{thp}_r = \frac{DV}{550} \; (V \text{ in ft/sec}) \qquad (251)$$

or,
$$\text{thp}_r = \frac{DV}{375}\ (V \text{ in mph}) \qquad (251a)$$

D being the total drag at the air speed V. The drag D can be divided into two parts, each with two subdivisions. The major components are wing drag and the residual, or parasite, drag. Wing drag is further divided into induced and profile (or section) drags. The coefficient of the former depends only on the lift coefficient and effective aspect ratio, while the coefficient of the latter varies with the wing section. Parasite drag must be divided into two parts, the first variable with angle of attack and designated here as P_1, the second independent of angle of attack and designated as P_2. P_1 includes such items as nacelles, floats, hulls, tail surfaces, wing-section drag, and fuselages having square or rectangular cross-sections. P_2 includes struts, wires, fittings, wheels, tail skids, ordnance equipment, air-cooled engines, radiators, and fuselages having circular or elliptical cross-sections. If there is any doubt as to the classification of the fuselage drag, it should be put in P_1.

P_1 and P_2 vary directly as V^2, while induced drag varies inversely as V^2.

Wing Drag, Induced. The induced drag is that part of the total wing drag which is due to a virtual inclination of the lift vector as a result of the downwash, the effect being the same as if the wing were operating along an upward slope. The induced drag is independent of wing section and varies only with lift coefficient C_L and effective aspect ratio n.

$$\text{Induced drag coefficient } C_{Di} = \frac{C_L^2 S}{\pi (kb)^2} = \frac{C_L^2}{\pi n} \qquad (252)$$

where S is the total wing area, b the maximum wing span, and k Munk's factor for equivalent monoplane span. For a monoplane k = 1.0. For a biplane k varies with the ratio of gap/maximum-span, and with the ratio of spans. Figures 12 and 13 (Chapter 3) give the values of k for any conventional biplane arrangement.

Equation (252) is most conveniently used in performance calculations if written in the form

$$D_i = \frac{2W^2}{\pi\rho\, V^2\, (kb)^2} \qquad (253)$$

W being the gross weight. This reduces to

$$D_i = \frac{267.7}{\sigma V^2}\left(\frac{W}{kb}\right)^2 \quad (V \text{ in ft/sec}) \qquad (254)$$

or

$$D_i = \frac{124.5}{\sigma V^2}\left(\frac{W}{kb}\right)^2 \quad (V \text{ in mph}) \qquad (255)$$

These equations reduce to the form $D_i = K/V^2$ for any particular case.

It is often desirable to calculate directly the induced power required. The equations are:

$$\text{thp}_i = \frac{D_i V}{550} = \frac{0.487}{\sigma V}\left(\frac{W}{kb}\right)^2 \quad (V \text{ in ft/sec}) \qquad (254a)$$

or

$$\text{thp}_i = \frac{D_i V}{375} = \frac{0.332}{\sigma V}\left(\frac{W}{kb}\right)^2 \quad (V \text{ in mph}) \qquad (255a)$$

In any particular case, these reduce to the form $\text{thp}_i = K/V$.

Parasite Drag P_1: Variation with Angle of Attack. A study of the drag of nacelles, floats, hulls, and fuselages, having square or rectangular cross-section, shows a very definite dependence on angle of attack. (See Figure 3, N.A.C.A. Technical Report No. 236.) (A study of the profile drag of a number of the most widely used wing sections shows that at any given value of V/V_S the ratio $C_{D_0}/(C_{D_0})_0$ is practically independent of section. If the relation previously found for variation with angle is converted to aver-

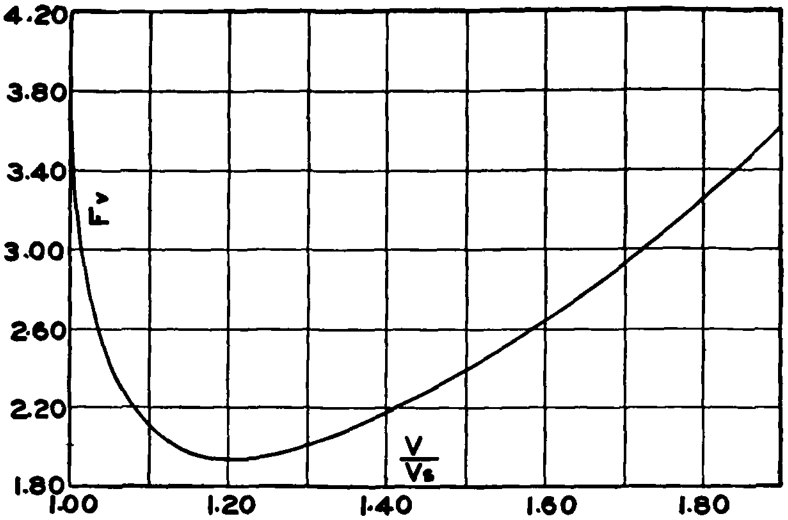

Figure 174. Factor F_v for Finding Value of Variable Parasite Drag P_1 at Any Speed

age speed range, the agreement will be found very close, so that a single curve of D/D_0 against V/V_S is sufficient, but in most cases it will be found more convenient to use $F_v = (D/D_0)\ (V/V_S)^2$ which is plotted in Figure 174. The values most frequently used are as follows:

$\left(\frac{V}{V_S}\right)$	$\left(\frac{D}{D_0}\right)$	$F_v = \left(\frac{D}{D_0}\right) \cdot \left(\frac{V}{V_S}\right)^2$
1.00	4.100	4.10
1.05	2.210	2.44
1.10	1.750	2.12
1.15	1.500	1.98
1.20	1.350	1.95
1.30	1.190	2.01
1.40	1.110	2.18
1.50	1.060	2.38
1.60	1.025	2.63
1.70	1.007	2.91
1.80	1.000	3.24
2.00	1.000	4.00
2.20	1.000	4.84
2.40	1.000	5.76

By the use of F_v, the accurate calculation of performance is considerably simplified since $P_1 = (P_1)_0 \cdot F_v$, where $(P_1)_0$ is the value of P_1 (without correction for angle) at stalling speed, V_S. P_1 is usually calculated for the condition of thrust line horizontal. An example of the calculation of power required for horizontal flight will follow.

Example of Calculation of Power Required. The steps required in the calculation of power required in horizontal flight at various speeds will be illustrated by means of a fictitious airplane assumed to be a tractor biplane with the following characteristics:

Gross weight .... $W = 4{,}500$
Wing area .... $S = 300$
Wing section NACA-2212
Wing span .... $b_1 = b_2 = 35$ ft
Gap $G = 5.25$ $G/b = 0.15$
Span factor $k = 1.13$
Effective aspect ratio = 5.20
Engine, direct-drive 450 bhp at 2,100 rpm at sea-level; N.A.C.A. cowl
Propeller 2-blade, metal

A summation of all of the items of parasite drag for an airplane of this type would be about as follows at 100 mph.

P_1	Wings	85.0 lb
	Tail surfaces	25.0
		110.0 lb
P_2	Fuselage plus cowled engine	85.0 lb
	Landing gear	45.0
	Structural details	50.0
		180.0 lb

From which $C_{DP_1} = 0.0143$, $C_{DP_2} = 0.0234$ and $C_{DP_0} = 0.0377$.

The maximum lift coefficient for the 2212 section in a biplane arrangement is $C_{L\,max} = 1.45$. Hence, the stalling speed is

$$V_S = 19.77\sqrt{\frac{4{,}500}{1.45 \times 300}} = 63.6 \text{ mph}$$

From equation (255) for V in mph, the induced drag is

$$D_i = \frac{124.5}{V^2}\left(\frac{W}{kb}\right)^2 = \frac{1{,}615{,}000}{V^2}$$

The basic value of P_1 at stalling speed is

$$(P_1)_0 = 110 \times (V_S/100)^2 = 44.6$$

The value of P_1 at any speed is

$$P_1 = (P_1)_0\ F_v = 44.6F_v$$

The basic value of P_2 is

$$(P_2)_0 = 180\ (V_S/100)^2 = 72.8$$

The value of P_2 at any speed is

$$P_2 = 72.8\ (V/V_S)^2$$

Calculations for thrust power required are given in Table 17. Note that the ratio $L/D = W/D$ has been tabulated along with thp_{r0} in Table 17. This is not necessary, except as a general check on the calculations, unless the power required is to be obtained for two or more weights. If the change in weight does not affect the parasite drag coefficients, as for example with a varying fuel load, the value of L/D at any given speed ratio V/V_S remains constant, so that it is unnecessary to carry out the full calculation to find the new values of thp_{r0}. At any value of V/V_S and at constant density, the following relations hold:

$$V_2/V_1 = \sqrt{W_2/W_1} \tag{256}$$

$$D_1 = W_1/(L/D) \qquad D_2/D_1 = W_2/W_1 \tag{257}$$

$$(\text{thp}_r)_2/(\text{thp}_r)_1 = (W_2/W_1)^{1.5} \tag{258}$$

Equations (256), (257), and (258) are often used in performance calculations.

TABLE 17. EXAMPLE OF CALCULATION FOR THRUST POWER REQUIRED AT SEA-LEVEL

Gross Weight = 4500 lb

Speed Ratio V/V_S	Air Speed V mph	F_v	Drag - lb			Total D	thp$_{ro}$	L/D
			Parasite		Induced D_i			
			P_1	P_2				
1.00	63.6	4.10	182	73	400	655	111.2	6.87
1.05	66.8	2.44	109	80	363	552	98.3	8.14
1.10	70.0	2.12	94	88	330	512	95.6	8.78
1.15	73.1	1.98	88	96	303	487	95.0	9.24
1.20	76.3	1.95	87	105	278	470	95.6	9.57
1.40	89.1	2.16	97	143	204	444	105.6	10.12
1.70	108.2	2.91	130	210	138	478	138.0	9.40
2.00	127.2	4.00	178	291	100	569	193.0	7.90
2.30	146.3	5.29	235	385	76	696	272	6.46
2.60	165.3	6.76	301	492	59	852	375	5.28

Maximum Thrust Power Available at Sea-Level. The next step is to calculate the maximum thrust power available at various air speeds. To do this the propeller characteristics are required. The propeller efficiency will be of the order of 80% so that 0.80 × 450 = 360 thp will be available for high speed. From Table 17, 360 hp will be required at about 160 mph. Hence, the propeller must absorb 450 bhp at 2100 rpm at 160 mph, from which $C_s = 1.41$. [See equation (226).] From Figure 146 this gives $V/nD = 0.73$, $\theta = 19.4°$ and $\eta_m = 0.82$. The diameter will be $D = (V/n) \div (V/nD) = 9.2$ ft. This propeller will have a tip-speed slightly greater than 1000 ft/sec, but it can be used if the tip sections are reasonably thin. The blade setting 19.4° is the effective setting. According to equation (223), the static setting would be about 1.2° less.

The thrust power available may be calculated from the data in Figure 157. Assuming that the engine has a power drop factor PDF = 0.80 and that the slope of bhp/rpm is constant over the range involved, the value of K_{QS} at 100 mph is, from equation (241a)

$$(K_{QS})_0 = \left[\frac{2 \times 25.6 \times (9.2)^3}{33{,}000 \times 0.214}\right]^{\frac{1}{2}} = 2.375$$

or

$$K_{QS} = 0.02375\ V$$

The calculations for thp_{ao} at sea-level are given in Table 18.

The accuracy obtained by the method used above is more apparent than real. In general, it will be more desirable to select the proper curve of thp/thp_0 from Figures 165 to 169, and thus obtain thp values directly. From the data derived in selecting the propeller, $\eta_m = 0.82$, hence $\text{thp}_0 = 0.82 \times 450 = 369$ at the design speed $V_0 = 160$ mph. These values are used with the 17° curve from Figure 167 in calculating thp by the short method, Table 19. The results are in close agreement with the calculations of Table 18. The agreement would be exact if ηC_P and V/nD could be read correctly from Figure 157.

TABLE 18. EXAMPLE OF CALCULATION OF THRUST POWER AVAILABLE AT VARIOUS SPEEDS

Airspeed V mph	Torque Coeff. K_{QS}	ηC_p	V/nD	n	rpm	thp_{ao}
60	1.43	.0255	.31	30.8	1,850	211
80	1.90	.0305	.41	31.1	1,870	260
100	2.37	.0325	.50+	31.6	1,900	291
120	2.85	.0335	.59	32.5	1,950	325
140	3.32	.0320	.66	33.8	2,030	350
160	3.80	.0300	.73	35.0	2,100	364
170	4.03	.0288	.76	35.7	2,140	371

$$K_{QS} = 0.0237\ V_{\text{mph}}$$

$$\text{thp}_{ao} = \frac{\eta\, C_P\, \rho\, n\, D^5}{550}$$

TABLE 19. CALCULATION OF MAXIMUM THRUST HORSEPOWER AVAILABLE USING GENERAL CURVES

Air Speed	V/V_a	thp/thp$_0$	thp
60	.375	.565	209
80	.500	.695	257
100	.625	.792	293
120	.750	.874	323
140	.875	.943	348
160	1.000	1.000	369
170	1.061	1.018	375

Rate of Climb. If the value of thp_r and thp_a from Tables 17 and 18 are plotted against air speed as in Figure 175, the sea-level performance is readily obtained by graphical solution. The intersection of the curves shows that the maximum speed is 164.6 mph. The difference between thp_a and thp_r at any speed is excess power ehp, available for climb. The maximum difference is at 95 mph where $\text{thp}_a - \text{thp}_r = 173$ ehp. The rate of climb in ft/min corresponding to any value of ehp is

$$\frac{dh}{dt} = \text{ehp} \times \frac{33{,}000}{W} \tag{259}$$

where W is the gross weight of the airplane. In this case ehp = 173 and W = 4500 lb so that

$$\frac{dh}{dt} = 173 \times \frac{33{,}000}{4500} = 1270 \text{ ft/min}$$

This is the rate of climb at sea-level, usually designated as "initial rate of climb."

Absolute Ceiling. The absolute ceiling or the altitude where the rate of climb is zero may now be determined accurately by a simple graphical construction. At the absolute ceiling the curves of thp_a and thp_r will be tangent and the airplane can fly at only one angle of attack. This angle will be approximately that for minimum power.

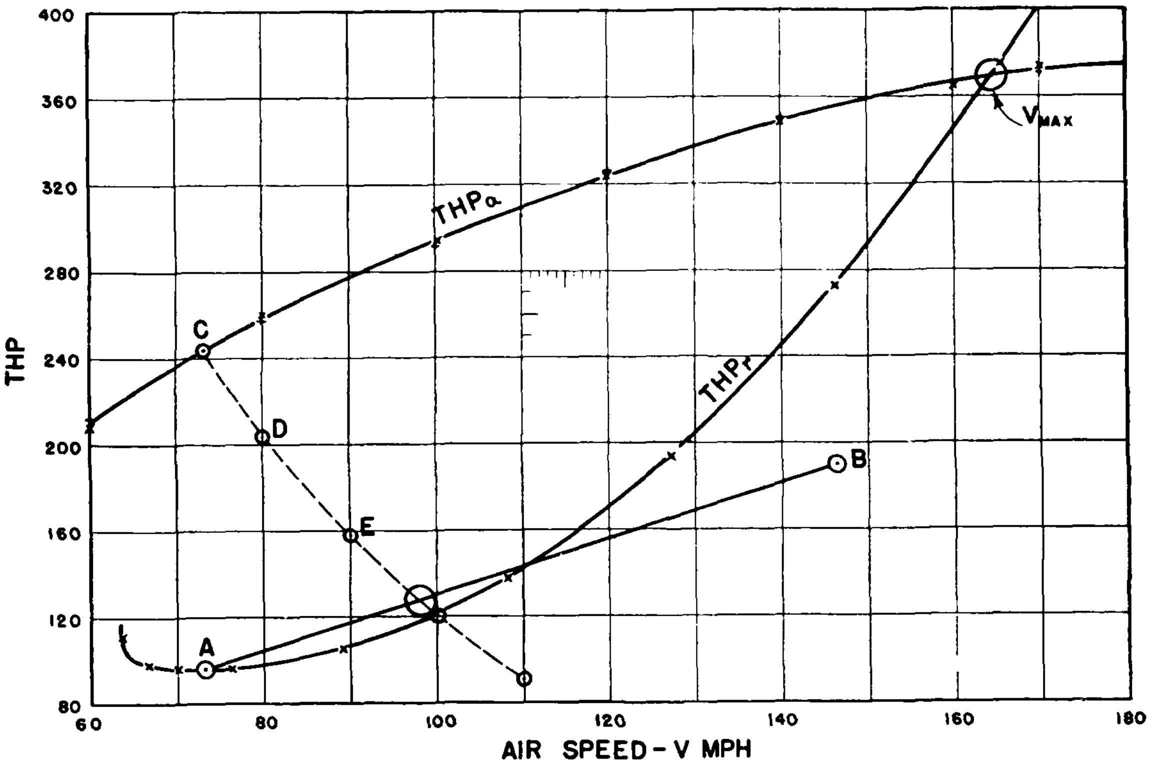

Figure 175. Curves of Power Available and Power Required, Illustrating Graphical Solution for Absolute Ceiling

If a climb was started at sea-level at this angle of attack and continued all the way up to the absolute ceiling without change, the maximum rate of climb would not be obtained at any altitude, but the absolute ceiling would be the same as that obtained if the correct air speeds for best climb had been used. In this climb at constant angle of attack, both the air speed and thp required will vary inversely as the square root of the density. That is

$$V = V_0 \sqrt{\rho_0/\rho}$$

and

$$\text{thp}_r = \text{thp}_{r0} \sqrt{\rho_0/\rho}$$

or when $V = KV_0$, $\text{thp}_r = K \times \text{thp}_{r0}$. Referring to Table 17 and Figure 175, it will be seen that the minimum value of thp_{r0} is 95 at $V_0 = 73.1$ mph. To maintain horizontal flight at the value of α and C_L corresponding to this sea-level speed would require, when $\sqrt{\rho_0/\rho} = 2.0$, that $V = 146.2$ mph and $\text{thp}_r = 190$. A straight line passing through this point **B** and the initial point ($V_0 = 73.1$ mph and $\text{thp}_{r0} = 95$) also passes through the origin $V_0 = 0$, $\text{thp}_r = 0$, and is *the locus of minimum power required* at all densities. Consider now the power available.

At $V_0 = 73.1$ mph, $\text{thp}_0 = 244$. This is the initial value **C**. At the altitude where $V = 80$ mph, $\sqrt{\rho_0/\rho} = 80/73.1 = 1.095$ from which $\rho/\rho_0 = 0.833$. The altitude and the corresponding ratio of thp/thp_0 for the engine used may thus be determined, using the data in Table 15. It is more convenient, however, to plot the ratio of thp/thp_0 against $\sqrt{\rho_0/\rho} = V/V_0$ as in Figure 176 and eliminate the intermediate step. In either case thp_a at 80 mph and at the altitude where $\sqrt{\rho_0/\rho} = 80/73.1$ is determined. Figure 176 gives $\text{thp}/\text{thp}_0 = 0.787$ at $V/V_0 = 1.095$ for the assumed engine having PDF = 0.80. Figure 175 shows that at 80 mph $\text{thp}_{a0} = 259$. Hence, $\text{thp}_a = 0.787 \times 259 = 204$, which is plotted at the point **D** on Figure 175. Repeating this process for various speeds gives

V	V/V_0	thp/thp$_0$	thp$_0$	thp
73.1	1.000	1.000	244	244
80.0	1.095	.787	259	204
90.0	1.231	.568	278	158
100.0	1.368	.407	294	120
110.0	1.505	.296	309	91

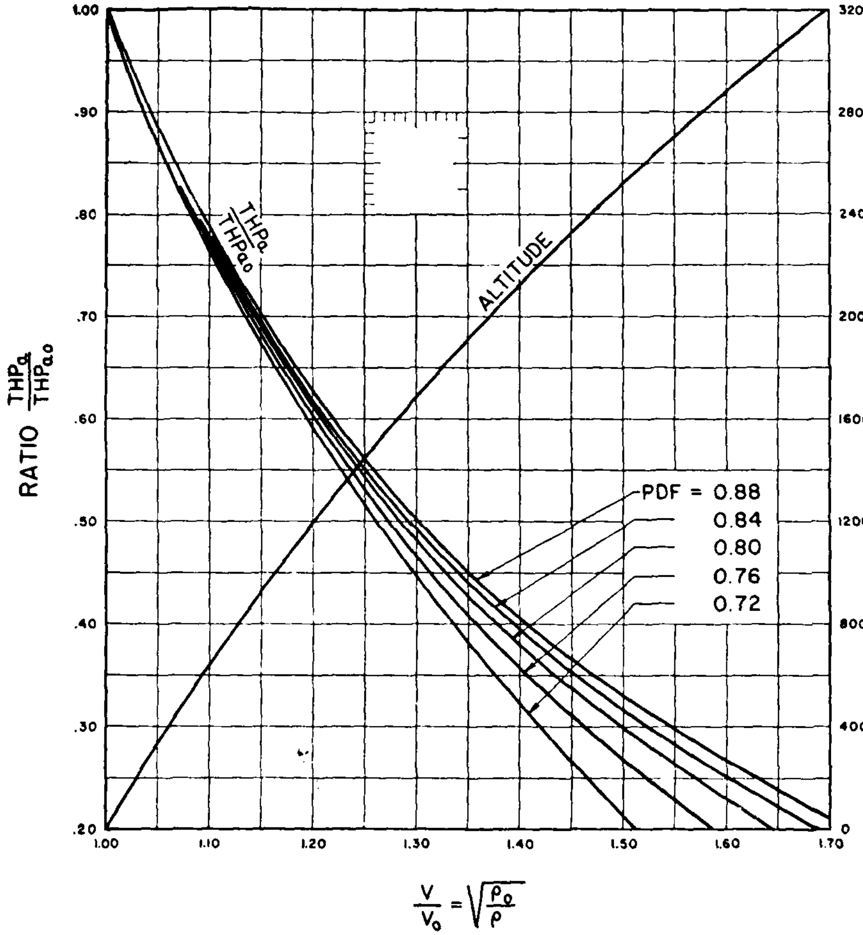

Figure 176. Absolute Ceiling Chart. Variation of thp and V with Altitude

Plotting these values of thp against V on Figure 175 and passing the curve **CDEO** through the points, it is found to intersect the line **AB** at $V = 98.2$ mph. This indicates that at the density where the air speed for minimum power is 98.2 mph, the curves of thp_a and thp_r are tangent. This is the condition for zero climb and the absolute ceiling. The density ratio may be found from $\sigma = (V_0/V)^2 = (73.1/98.2)^2 = 0.554$ and the corresponding altitude from standard atmosphere tables and charts or the altitude may be read directly from Figure 176 where it has been included for convenience. This altitude is 18,800 ft.

The points **C, D, E—O** just calculated are each a single point on a curve of thp_a for the altitude represented by the relation $\sqrt{\rho_0/\rho} = V/V_0$. In the example 5 points were used to determine the curve **C, D, E—O,** but 3 or 4 points usually are sufficient.

Service Ceiling. The service ceiling is the altitude at which the rate of climb is 100 ft/min. If the rate of climb be assumed linear with altitude, that is

$$\frac{dh}{dt} = C_0 - ah \tag{260}$$

then the service ceiling is given by

$$h_s = H\left[\frac{C_0 - 100}{C_0}\right] \tag{261}$$

where H is the absolute ceiling and C_0 is the initial rate of climb. For the case just calculated $H = 18{,}800$ ft and $C_0 = 1270$ ft/min. Hence,

$$h_s = 18{,}800\left[\frac{1270 - 100}{1270}\right] = 17{,}300 \text{ ft}$$

Time of Climb. *Time of Climb to Any Altitude.* On the assumption that $dh/dt = (C_0 - ah)$, the time of climb to any altitude h is

$$T = \frac{H}{C_0}\log_e\left[\frac{H}{H - h}\right] = 2.303\frac{H}{C_0}\log_{10}\left[\frac{H}{H - h}\right] \tag{262}$$

T will be in minutes if the absolute ceiling H is in feet and the initial rate of climb C_0 is in ft/min.

Altitude Climbed in a Given Time T. The preceding equation may be converted to the form

$$h = H\ (1 - e^{-aT}) \tag{263}$$

where $a = C_0/H$. In this form it may be used for calculating the altitude climbed in time T.

Calculation of Power Required at Altitude. In steady horizontal or climbing flight C_L and C_D will be constant at a given angle of attack provided that the slipstream effects are negligible and these effects usually are negligible. Hence, at any given angle of attack, C_L and V/V_S are constant and the following relations hold in passing from density ρ_1 to ρ_2:

$$V_2/V_1 = \sqrt{\rho_1/\rho_2} \tag{264}$$

$$D_2 = D_1 \tag{265}$$

$$(\text{thp}_r)_2/(\text{thp}_r)_1 = \sqrt{\rho_1/\rho_2} \tag{266}$$

These equations supplement equation (256), (257), and (258). They are often used in calculating performance at altitude. Table 20 contains the calculations for V and thp_r at 5000, 10,000, and 15,000 ft, using the sea-level data from Table 17.

TABLE 20. THRUST POWER REQUIRED AT ALTITUDE

Sea-Level		5000 feet $\sqrt{\rho_0/\rho} = 1.077$		10,000 feet $\sqrt{\rho_0/\rho} = 1.164$		15,000 feet $\sqrt{\rho_0/\rho} = 1.261$		V/V_S
V_0	thp_{r0}	V	thp_r	V	thp_r	V	thp_r	
63.6	111.2	68.5	119.8	74.1	129.4	80.2	140.2	1.00
66.8	98.3	71.9	105.8	77.8	114.4	84.2	124.0	1.05
70.0	95.6	75.4	103.0	81.4	111.3	88.3	120.6	1.10
76.3	95.6	82.2	103.0	88.8	111.3	96.2	120.6	1.20
89.1	105.6	95.9	113.7	103.7	122.9	112.4	133.3	1.40
108.2	138.0	116.2	148.6	125.8	160.6	136.5	174.0	1.70
127.2	193.0	137.0	208.	148.0	224.7	160.5	243.3	2.00
146.3	272.0	157.5	293.	170.5	317.0	....	....	2.30

Calculation of Power Available at Altitude. The decrease of thp with altitude depends on engine and propeller characteristics as explained in Chapter 10. The decrease shown on Figures 171 and 172 includes the effects of changes in bhp, rpm and propeller efficiency at constant true air speed. Hence, if thp_{a_0} is known for a given speed at sea-level, the corresponding value for the same speed at any other altitude is $\text{thp}_a = \text{thp}_{a_0} \times (\text{thp}/\text{thp}_0)$ where the value of thp/thp_0 for the altitude under consideration is read from the appropriate curve on Figure 171 or Figure 172.

Table 21 contains the calculation for thp_a at various altitudes, based on the data in Table 18 and the curve for fixed-pitch propeller with engine PDF = 0.80 (as previously assumed) on Figure 171. If desired, thp_a at altitude can be calculated from the propeller data as in Table 18, using K_{QS} and ηC_P.

TABLE 21. MAXIMUM THRUST HORSEPOWER AVAILABLE AT ALTITUDES

Air Speed V mph	thp_{a_0} at Sea-level	thp at Altitude		
		5,000 ft $F = 0.820$	10,000 ft $F = 0.666$	15,000 ft $F = 0.528$
60	211	173	140	111
80	260	213	173	137
100	291	238	194	154
120	325	266	216	172
140	350	287	233	185
160	364	298	242	192
170	371	304	247	196

Performance at Altitude. If the values of thp_r and thp_a for various altitudes are plotted against speed as in Figure 177, speeds and rates of climb are readily obtained.

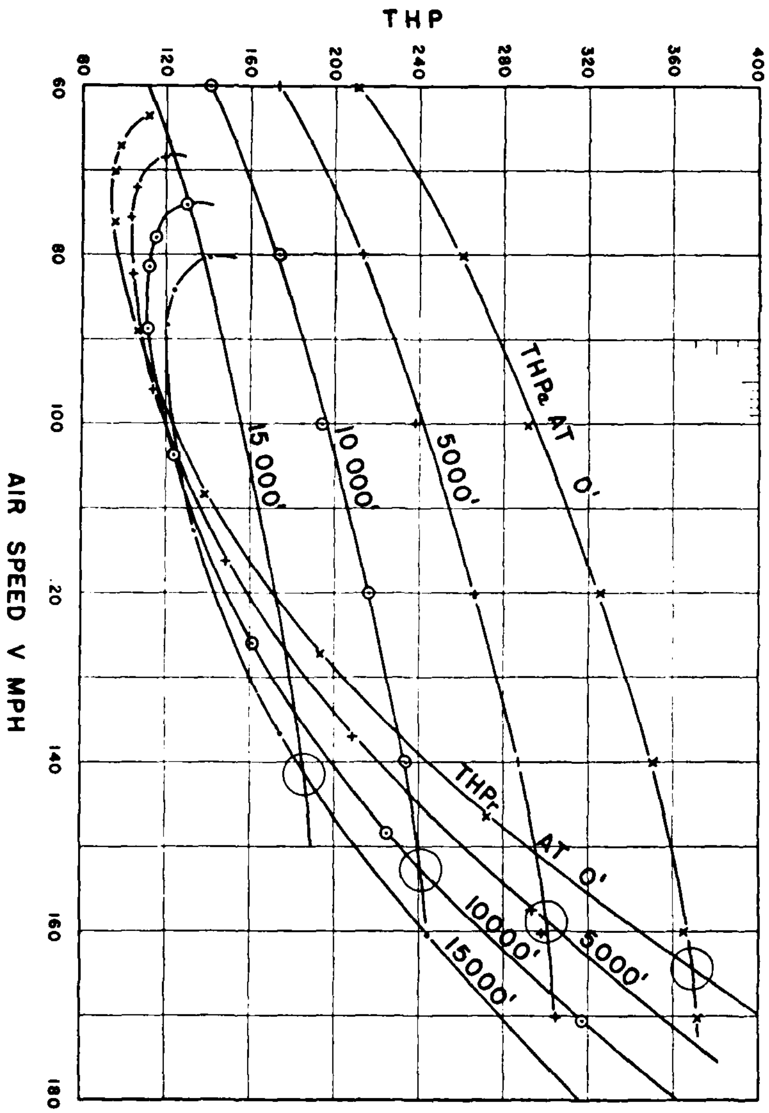

Figure 177. Curves of Power Available and Power Required at Various Altitudes

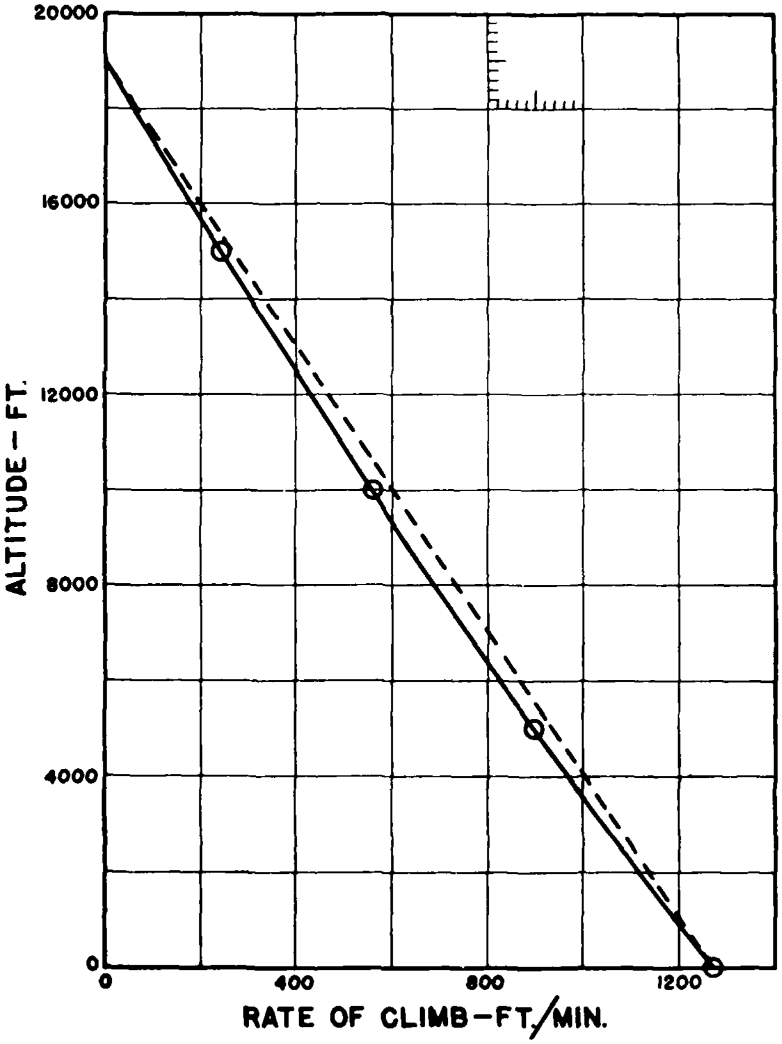

Figure 178. Variation of Rate of Climb with Altitude

Following the method previously used, one obtains:

Altitude	Maximum Speed	Maximum ehp	Air Speed for Climb V_c	Rate of Climb
0	164.6	173	95.0	1,270
5,000	158.8	122	98.0	895
10,000	152.8	76	102.0	557
15,000	141.2	33	106.0	242

The rates of climb in the fifth column are plotted against altitude in Figure 178 and a smooth curve is drawn through the points. This curve intersects the altitude axis (rate of climb = 0) at about 19,000 ft. The absolute ceiling obtained by plotting rates of climb therefore checks almost exactly with the 18,800 feet obtained by the short method illustrated on Figure 175. Figure 178 shows, however, that in general it is not permissible to assume a linear relation between rate of climb and altitude if strict accuracy is desired. This subject will be discussed later.

Figure 179 is a plot of maximum air speed and air speed for best climb against altitude. The variation of maximum speed with altitude is much the same for all airplanes, but there may be considerable differences in the form of the curve for best air speed in climb. Whether the best air speed remains constant or increases with altitude depends chiefly on the parasite resistance and only slightly on aspect ratio as will be shown in Chapter 18.

Performance with Supercharged Engines and Controllable-Pitch Propeller. The performance with a supercharged engine is readily calculated by the method just illustrated if the power curve is extrapolated to obtain a fictitious thp_0 value. For example, assume an engine developing 800 bhp at a critical altitude of 10,000 ft (below which full throttle cannot be used). If the propeller efficiency is 80%. the thp = 640 at 10,000 ft may be considered as a

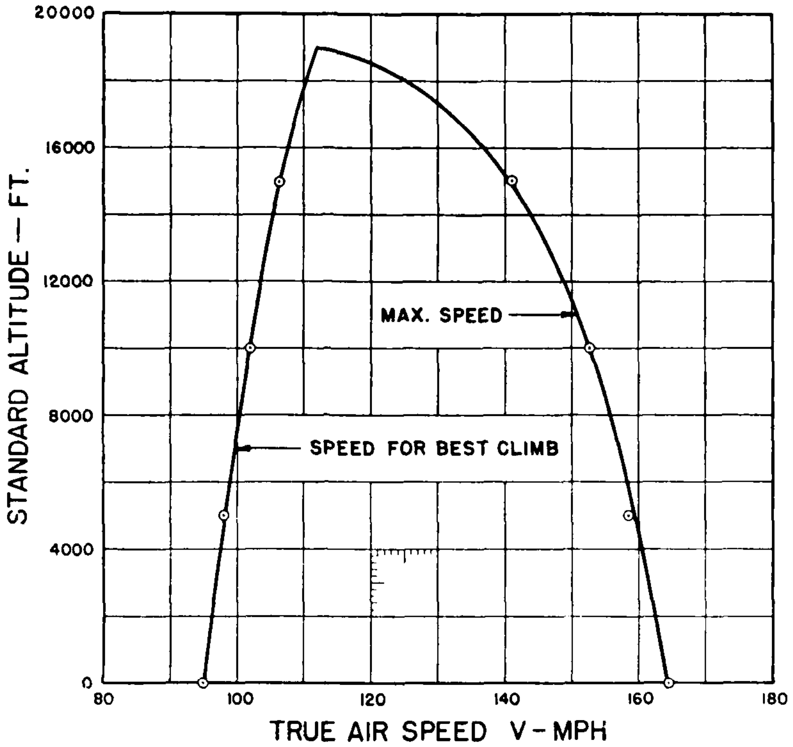

Figure 179. Variation of Maximum Speed and Best Climbing Speed with Altitude

point on a normal thp curve, which would have a sea-level value of

$$\text{thp}_0 = 640/PF$$

where $PF = \text{thp}/\text{thp}_0$ from the curve of Figure 171 corresponding to the particular engine-power curve. For a value PDF = 0.80, the fictitious sea-level power is $\text{thp}_0 = 640/0.666 = 961$ and the performance above 10,000 ft is obtained by assuming power curves corresponding to 961 thp at sea-level. Below the critical altitude 10,000 ft the performance will depend on the engine restrictions and the propeller characteristics.

When a controllable-pitch propeller is used, the ratio thp/thp_0 is taken from Figure 172.

Effect of Slipstream and Miscellaneous Corrections. It is usually unnecessary to apply any corrections other than those given. In particular, the effects of slipstream on drag are either negligible or they may be handled by an appropriate reduction in propeller efficiency. It should be noted that the factor k (the ratio of the span of the equivalent monoplane to the span of a biplane) includes the effects of the various factors formerly listed under biplane interference, gap/chord ratio, aspect ratio. The effect of stagger is considered negligible from a theoretical standpoint.

CHAPTER 12

PERFORMANCE ESTIMATION

Performance Estimation. It is frequently necessary to estimate the performance of an airplane without calculating the power curves. Where the parasite drag coefficient is known, this can be done quickly and accurately. The same methods may be applied to problems involving the change in performance due to changes in design, loading, or operating conditions. In any event, the parasite drag must either be known or estimated, and the accuracy of the results will depend on the accuracy with which the parasite drag is obtained.

Estimating Parasite Drag. For the purpose of performance estimation, it is unnecessary to separate the parasite drag into parts affected and unaffected by angle of attack. The principal items will be

Wings
Fuselage or hull
Engines and nacelles
Tail surfaces
Landing gear
Struts, wires, etc.
Interference
Miscellaneous items

Appropriate drag values may be obtained from the data in Chapter 9.

Stalling Speed. The stalling speed in miles per hour at sea-level is

$$V_S = 19.77 \sqrt{w_s/C_{L\,max}} \qquad (267)$$

where $w_s = W/S$, the wing loading in lb/sq ft, and C_L maximum is effective maximum lift coefficient. The accurate determination of C_L maximum from design characteristics is very tedious and unsatisfactory, particularly when part-span flaps or other high-lift devices are used. If accurate full-scale stalling speed data are available on a similar design, the value of the effective C_L maximum may be calculated from equation (267) in the form

$$C_{L\,max} = 391\, w_s/V_S^2 \qquad (268)$$

If accurate stalling-speed data are not available, it will be necessary to use wind-tunnel data on the basic wing section and apply corrections for scale effect, flap effect, etc.

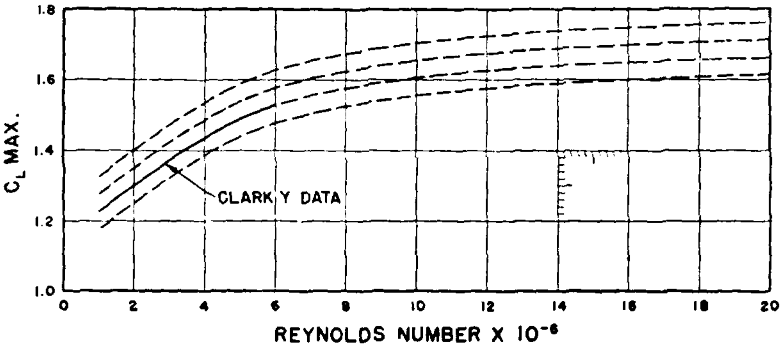

Figure 180. Variation of C_L Maximum with Reynolds Number

The basic airfoil data are preferably taken from the N.A.C.A. variable-density or full-scale wind-tunnel tests. The variation of C_L maximum with Reynolds Number is approximated by the contour curves on Figure 180. A test point may be extrapolated along a curve similar to the contour lines to obtain the value at the Reynolds Number corresponding to stalling speed. The Reynolds Number at stalling speed is approximately

$$RN = 9350\, c_a \cdot V_S \qquad (269)$$

where c_a is the average wing chord in feet (c_a = wing area ÷ maximum span) and V_S is the approximate stalling speed in mph.

The effect of flaps of various types and proportions are given in Chapter 6. In the case of a biplane, the maximum lift coefficients of each wing should be calculated separately and combined by the obvious relation

$$C_{L\ max} = \frac{S_U \cdot C_{LU\ max} + S_L \cdot C_{LL\ max}}{S} \qquad (270)$$

where the subscripts U and L refer to upper and lower wings respectively. Care must be taken, however, that the individual maximum values occur at or reasonably near to the same angle of attack. Allowance must also be made for mutual interference effects. Flaps on either wing alone adversely affect the flow on the other wing. If the flaps are on the lower wing only, the curvature of the streamline is equivalent to a reduction in camber of the upper wing. The downwash and reduced velocity over the lower wing, *due to flaps on the upper wing only*, prevents full utilization of the flap effect. The net effect will depend on the relative proportions and arrangement of the biplane wings, but in any event, the ΔC_L maximum due to flaps on both wings will be considerably greater than the sum of the ΔC_L maximum due to flaps on the upper wing only plus ΔC_L maximum due to flaps on the lower wing only.

In general, the wing loading w_s used in equation (267) should be based on the net wing area, not including any portion of the wing intercepted by the fuselage. At low and moderate angles of attack the lift of the wing-fuselage system is substantially equivalent to that of a wing extending through the fuselage, but at high angles of attack and at maximum lift the contribution of the fuselage may become negligible and the lift approaches that due to the net wing area, unless the wing arrangement is favorable.

This point may be checked by reference to the N.A.C.A. tests in Technical Report No. 540.[1] In any event the value of C_L maximum will depend on the wing arrangement and fairing and the adjustment must either be made in accordance with the data of Technical Report No. 540, or based on experience obtained in flight tests on similar designs.

Stalling speed at other than sea-level density may be obtained from

$$V_S = V_{S_0} \sqrt{\rho_0/\rho} \qquad (264a)$$

or from

$$V_S = 19.77 \sqrt{w_s/\sigma\, C_{L\,max}} \qquad (267a)$$

where $\sigma = \rho/\rho_0$.

Maximum Speed. The most direct method of obtaining maximum speed in horizontal flight at any altitude is to calculate V_M for the available thrust horsepower and parasite drag and then apply a correction for the induced drag. That is

$$V_M = V_P - \Delta V \qquad (271)$$

where V_P is the maximum speed for zero induced drag and ΔV is the reduction in speed due to induced drag. V_P is readily obtained from

$$V_P = 100 \left[\frac{\eta \text{ bhp}}{6.82\, \sigma\, C_{DP_0}\, S}\right]^{\frac{1}{3}} \qquad (272)$$

or

$$V_P = 100 \left[\frac{3.75\, \eta \text{ bhp}}{\sigma\, P_{100}}\right]^{\frac{1}{3}} \qquad (273)$$

where η is the propeller efficiency at V_{max}, σ is the relative density, C_{DP_0} is the parasite drag coefficient, S is the wing area on which C_{DP_0} is based, and P_{100} is the parasite drag at 100 mph at sea-level density, $P_{100} = 25.58\, C_{DP_0}\, S$.

---

[1] E. N. Jacobs and K. E. Ward, "Interference of Wing and Fuselage from Tests of 209 Combinations in the N.A.C.A. Variable-Density Tunnel," N.A.C.A. T.R. No. 540 (1935.)

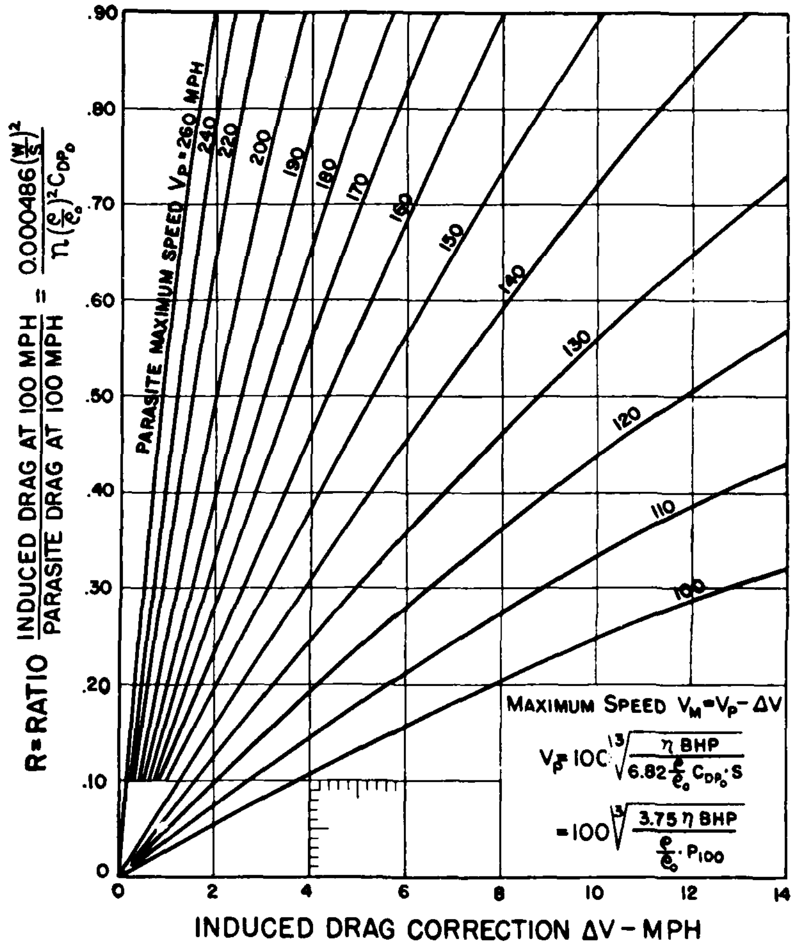

Figure 181. Effect of Induced Drag on Maximum Speed

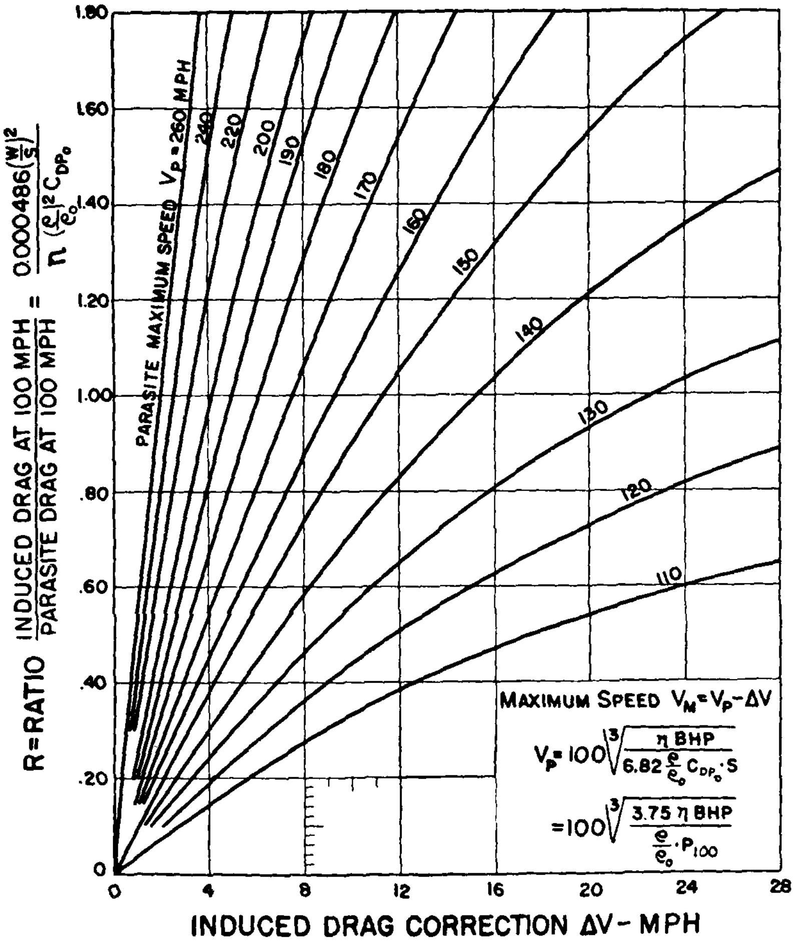

Figure 182. Effect of Induced Drag on Maximum Speed

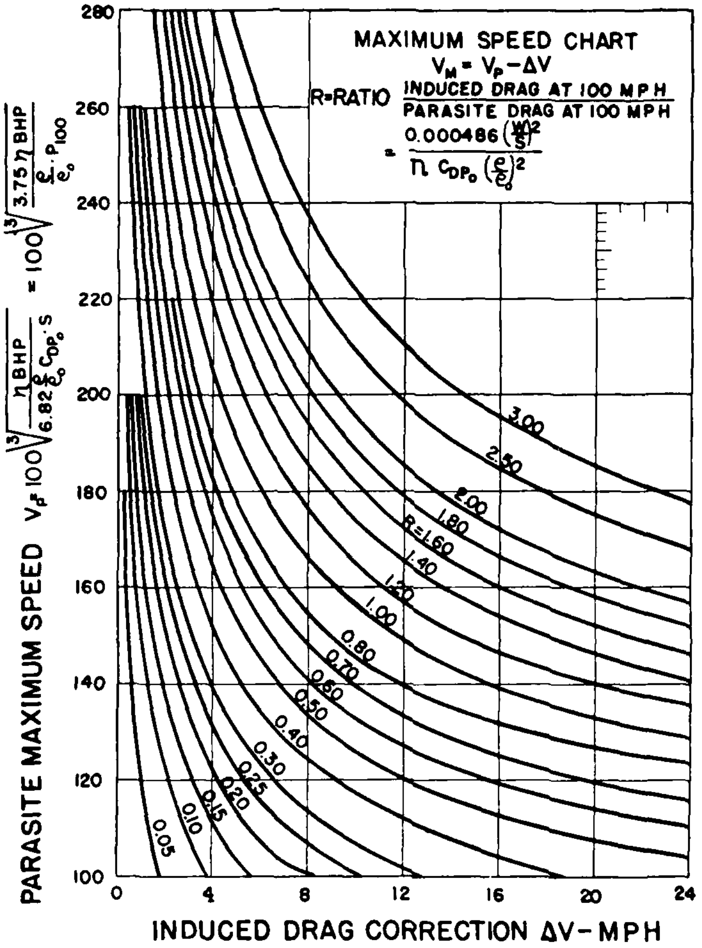

Figure 183. Effect of Induced Drag on Maximum Speed

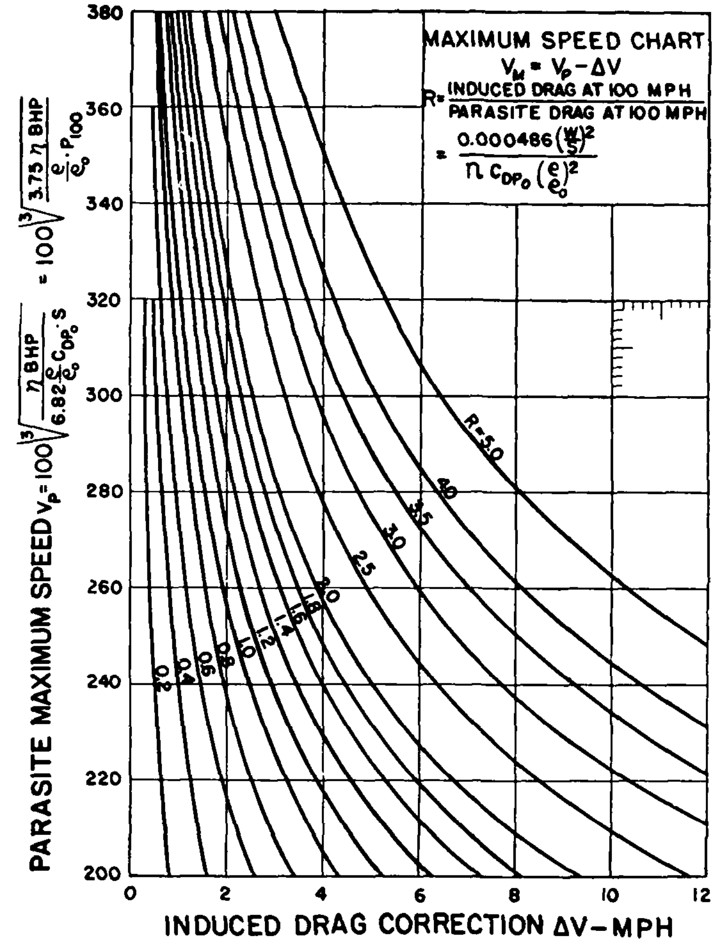

Figure 184. Effect of Induced Drag on Maximum Speed

The induced drag correction ΔV is obtained from Figures 181 and 182 or Figures 183 and 184. In each of these four figures the induced drag correction ΔV is plotted as abscissas with either V_P or R as ordinates. R is defined as the ratio, at 100 mph, of the induced drag to the parasite drag, or

$$R = \frac{\text{Induced drag at 100 mph}}{\text{Parasite drag at 100 mph}} \tag{274}$$

This ratio is either known from the induced drag, equation (253), and the summation of the parasite drag, or it may be obtained from

$$R = \frac{0.000486\ (w_s/\sigma)^2}{n\ C_{DP_0}} \tag{275}$$

where $w_s = W/S$ the wing loading, $\sigma = \rho/\rho_0$ the relative density, n is the effective aspect ratio, and C_{DP_0} is the parasite drag coefficient.

In Figures 181 and 182 the ordinate is R and the parameter of the curves is V_P. These charts are convenient to use with airplanes having $R < 1.0$ with a moderate value of V_P. When V_P is greater than 150 or 200 mph, either Figure 183 or Figure 184 will be found more convenient.

The method employed here is exact and the accuracy of the results depends entirely on the accuracy used in determining η, C_{DP_0}, and R.

Variation in V_{max} with Altitude. The decrease in V_{max} at high altitudes is readily obtained from equation (271), by calculating at each altitude the values of V_P and ΔV. Figure 185 will simplify these calculations by giving in ratio form the values of V_P and R at any desired altitude.

When great accuracy is not required, the curve of Figure 186 may be used. If the engine is supercharged, the value of V_M at the critical altitude should be considered as a point on this curve to obtain a fictitious sea-level value of V_M for use at other altitudes.

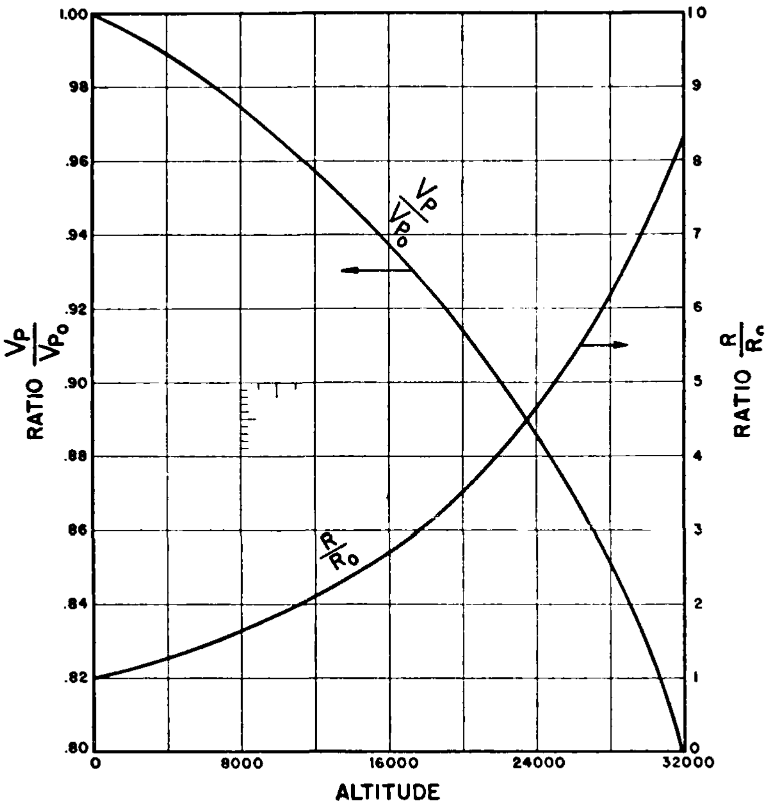

Figure 185. Effect of Altitude on V_P and R

Effect of Gross Weight on V_M. The effect of gross weight on maximum speed is readily obtained from the change in ΔV due to the change in R. From equation (275)

$$\frac{R_2}{R_1} = \left(\frac{W_2}{W_1}\right)^2 \tag{276}$$

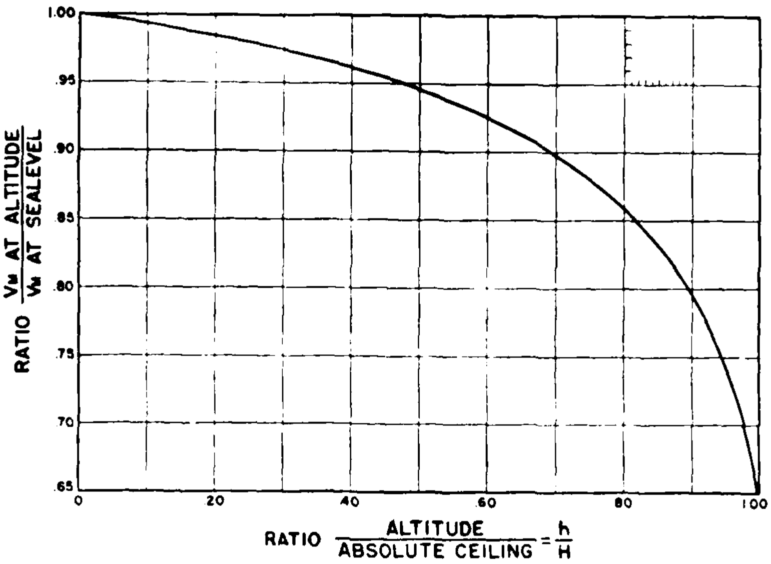

Figure 186 Effect of Altitude on Maximum Speed (Sea-Level Engine)

For example, assume an airplane having $V_p = 200$ mph with $R = 1.00$ giving $\Delta V = 4.3$ mph and $V_{max} = 195.7$. If the weight is increased 20%, R will be increased to 1.44 and ΔV to 6.4 and $V_{max} = 193.6$, or a reduction of 2.1 mph. If the weight is decreased 40%, R becomes 0.36 and $\Delta V = 1.5$, so that the maximum speed would be increased 2.8 mph.

General Power and Drag Relations. Letting A = induced power and B = parasite power required for horizontal flight at 100 mph,

$$R = \frac{P_i}{P_{100}} = \left(\frac{D_i}{D_p}\right)_{100} = \frac{A}{B} \tag{274}$$

At any speed the total power required will be

$$P = (100\, A/V) + B(V/100)^3 \tag{277}$$

The speed for minimum power is found by differentiating and equating to zero, or

$$\frac{dP}{dV} = -(100\,A/V^2) + 3BV^2 \times 10^{-6} = 0$$

from which

$$V_{MP} = \left[\frac{10^8 A}{3B}\right]^{\frac{1}{4}} = 75.98\ R^{\frac{1}{4}} \qquad \textbf{(278)}$$

The speed for maximum L/D is found by differentiating the total drag equation

$$D = (10^4\,A/V^2) + 10^{-4}\,BV^2 \qquad \textbf{(279)}$$

and equating to zero or

$$\frac{dD}{dV} = \frac{-2 \times 10^4 A}{V^3} + \frac{2BV}{10^4} = 0$$

from which

$$V_C = \left[\frac{10^8\,A}{B}\right]^{\frac{1}{4}} = 100R^{\frac{1}{4}} = 1.316\ V_{MP} \qquad \textbf{(280)}$$

Equations (278) and (280) may be used for determining the fundamental speed and power relations as follows:

Air speed for minimum drag V_C
Minimum drag D_{min}
Maximum ratio, Lift/Drag
Power required at V_C
Air speed for minimum power
Minimum power required

The fundamental relations are given in ratio form in Table 22. These ratios are based on the drag and power required at 100 mph, $D_0 = [D_i + D_p]$

$$P_0 = A + B = 100\,(D_i + D_p)/375$$

and

$$(L/D)_0 = W/D_0 = W/(D_i + D_p)$$

Hence, we have

$$\text{Minimum drag, } D_{min} = \left[\frac{D_{min}}{D_o}\right] \times D_o$$

$$\text{Maximum } (L/D) = K\,(W/D_o)$$

$$\text{Power at max } (L/D) = (P_C/P_o)\,P_o$$

$$\text{Minimum power } P_{min} = (P_{min}/P_o)\,P_o$$

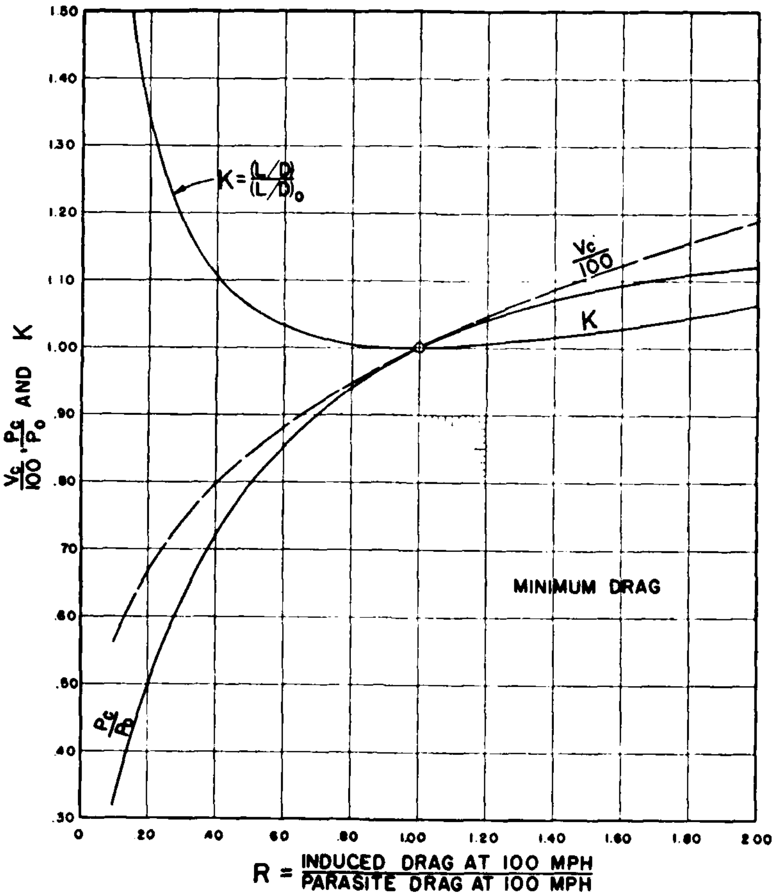

Figure 187. L/D, Power Required, and Speed for Minimum Drag

Figure 187 is a plot of $V_C/100$, P_C/P_o and K against the ratio R. These determine the conditions for flight at minimum drag or maximum L/D.

The conditions for minimum power are plotted on Figure 188.

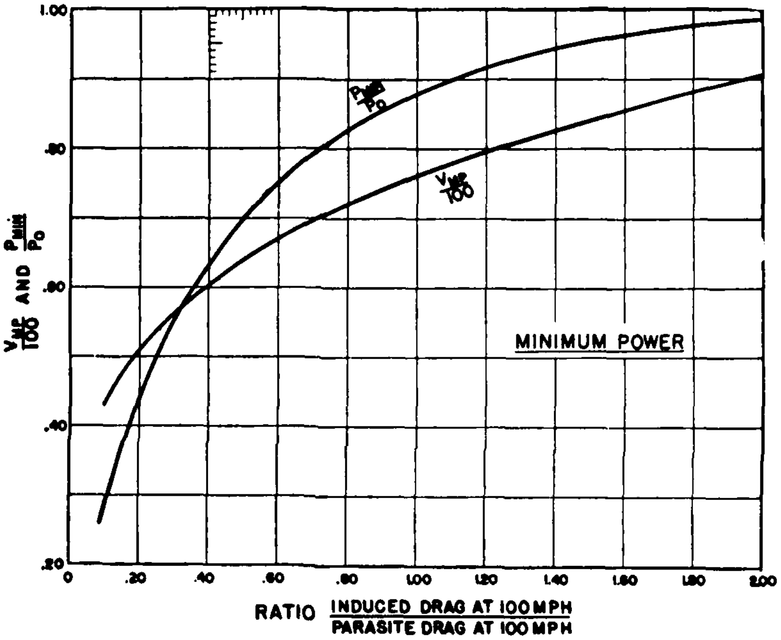

Figure 188. Minimum Power and Speed for Minimum Power

It may be shown that the drag for minimum power is 1.1549 times the minimum drag. Hence,

$$(L/D)_{\text{min. power}} = 0.8659\,(L/D)_{max} \tag{281}$$

In order to obtain accurate results with the relations at minimum power, it is necessary to employ the conception of virtual aspect ratio given later.

TABLE 22. GENERAL SPEED, DRAG AND POWER RELATIONS

	MINIMUM DRAG				MINIMUM POWER	
R	Speed for Minimum Drag V_C	Minimum Drag D_{min}/D_0	Relative Ratio L/D K	Relative Power P_C/P_0 K_P	Speed for Minimum Power V_{MP}	Relative Power at V_{MP} P_{min}/P_0
.10	56.2	.575	1.740	.323	42.7	.284
.20	66.9	.745	1.342	.498	50.8	.437
.30	74.0	.843	1.187	.624	56.2	.547
.40	79.5	.904	1.107	.719	60.4	.631
.50	84.1	.943	1.061	.793	63.9	.696
.60	88.0	.968	1.033	.852	66.9	.748
.70	91.5	.984	1.016	.900	69.5	.790
.80	94.6	.994	1.006	.940	71.9	.825
.90	97.4	.999	1.001	.973	74.0	.854
1.00	100.0	1.000	1.000	1.000	76.0	.878
1.20	104.7	.994	1.006	1.041	79.5	.916
1.40	108.8	.986	1.014	1.073	82.7	.941
1.60	112.5	.973	1.028	1.094	85.5	.961
1.80	115.8	.959	1.043	1.111	88.0	.974
2.00	118.9	.943	1.061	1.121	90.4	.984
3.00	131.6	.866	1.154	1.140	100.0	1.000
4.00	141.4	.800	1.250	1.131	107.5	.993
5.00	149.6	.746	1.340	1.110	113.7	.978

Maximum L/D. The maximum value of the ratio L/D may be determined from Table 22 or Figure 187. It may also be calculated from the aspect ratio n and parasite drag coefficient C_{DP_0}. The ratio

$$\left(\frac{L}{D}\right) = \frac{C_L}{C_{D_i} + C_{DP_0}} \tag{282}$$

will be a maximum when

$$C_{D_i} = C_{DP_0}$$

from which

$$C_L^2 = C_{DP_0} \cdot \pi n$$

Hence

$$\left(\frac{L}{D}\right)_{max} = \sqrt{\frac{\pi n}{4C_{DP_0}}} = 0.886\sqrt{\frac{n}{C_{DP_0}}} \tag{283}$$

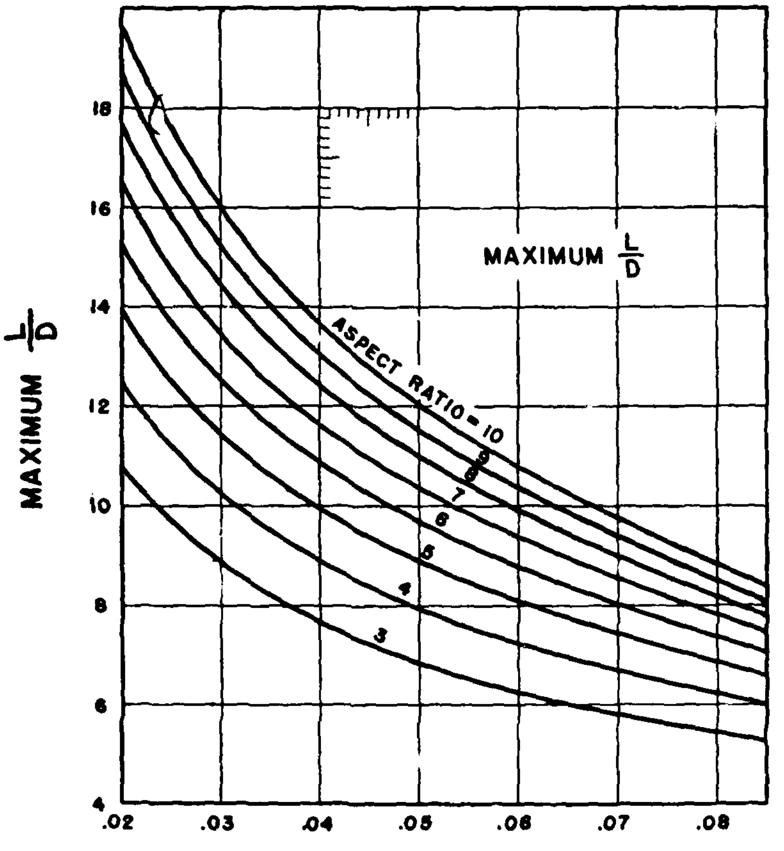

Figure 189 Maximum L/D as a Function of Aspect Ratio and Parasite Drag Coefficient

Values of L/D maximum are plotted against n and C_{DP_0} on Figure 189.

Virtual Aspect Ratio. For values of C_L greater than about 0.5 $C_{L\,max}$ the increase in the parasite drag C_{DP_1} (see page 365) may be approximated by considering the effect due to a decrease in geometrical aspect ratio. Oswald[2] uses the term "airplane efficiency" defined by

$$e = n_e/n \tag{284}$$

where n is the geometrical effective aspect ratio and n_e is the apparent or virtual aspect ratio. The airplane efficiency thus defined is dependent chiefly on the values of n and C_{DP_0}, although it may also be dependent to a large degree on interference drag due to improper fairings. Assuming that all of the increase in parasite drag is charged to an apparent decrease in aspect ratio and that the increase in parasite drag is $K \cdot C_{DP_0}$, it may be shown that

$$\begin{aligned} e &= \frac{C_{Di}}{C_{Di} + KC_{DP_0}} \\ &= \frac{C_L^2}{C_L^2 + K\pi\, n\, C_{DP_0}} \end{aligned} \tag{285}$$

Comparing this equation with observed airplane polars, it is found that the best agreement is obtained between $0.7\ C_{L\,max}$ and $C_{L\,max}$ when $K\pi = 2\ C_L^2$ or when

$$e = \frac{1}{1 + 2n\, C_{DP_0}} \tag{286}$$

The variation of e with n and C_{DP_0} is given on Figure 190. These values of e are somewhat lower than the accepted values. This is due to the fact that equation (286) adjusts the curves for agreement at a high lift coefficient corresponding to minimum power for the airplane, while it has been a common practice to favor the adjustment at a lower lift coefficient. Equation (286) will give values in good agreement at minimum power or for lift coefficients greater than that corresponding to $1.2\ V_S$. If the stalling speed is below 80 mph, the basic values of

---

[2] W. B. Oswald, "General Formulas and Charts for the Calculation of Airplane Performance," N.A.C.A. T.R. No. 408 (1932).

D_i and D_p at 100 mph should be used with the modified R to obtain minimum power.

For example, take the airplane considered in Chapter 11 for which at 100 mph $D_i = 161.5$ and $D_p = 290$. Hence, $D_{100} = 451.5$, $P_{100} = 120.5$, $(L/D)_0 = 9.96$, and $R = 0.557$. From Figure 187 the minimum drag will be at $V_C = 86.5$ mph and the maximum $L/D = K\ (L/D)_0 = 1.045 \times 9.96 = 10.40$. These values may be compared with the calculations in Table 17.

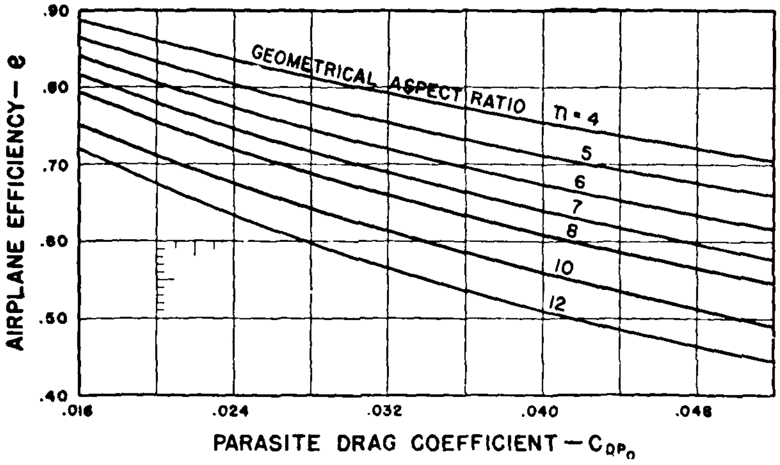

Figure 190. Airplane Efficiency as a Function of Aspect Ratio and Parasite Drag Coefficient

The aspect ratio of the airplane was $n = 5.2$ and the total parasite drag coefficient was $C_{DP_0} = 0.0377$. From Figure 190, $e = 0.71$. Hence, for calculating minimum power, the value of $R_e = R/e = 0.557/0.71 = 0.785$ must be used. From Figure 188 the minimum power for $R = 0.785$ will be at 71.5 mph with $P_{min}/P_0 = 0.82$. Hence, the minimum power is $P_{min} = 0.82 \times 120.5 = 98.7$. The calculations in Chapter 11 give 95 hp required at 73.1 mph.

Determination of Airplane Efficiency. The airplane efficiency e defined by equation (284) may readily be determined from wind-tunnel test data by the reverse of the usual process for finding total drag. Assuming that the parasite drag coefficient is constant, the virtual induced drag is

$$(C_{Di})_V = C_D - C_{DP_0} \tag{287}$$

If $(C_{Di})_V$ is plotted against C_L on log-paper and a line having the slope $\tan \theta = 2$ is drawn through the points at high values of C_L, the intercept at $C_L = 1.0$ gives

$$C_{Di} = k_1 \, C_L^2 / \pi k_2 n \tag{288}$$

where k_1 is the ratio of the observed induced drag to that expected for some arbitrary aspect ratio $k_2 n$. If $k_2 n$ is assumed as 3.18 so that $C_{Di} = 0.100$ at $C_L = 1.0$, then the intercept is $(k_1/10)$ and the efficiency is

$$e = 3.18/k_1 n \tag{289}$$

A typical wind-tunnel model test gives, for example:

$C_L =$	0	.2	.4	.6	.8	1.0	1.2
$C_D =$	.022	.025	.033	.045	.064	.089	.120
$(C_{Di})_V =$	0	.003	.011	.023	.042	.067	.098

These points plot on a straight line of slope 2 passing through 0.067 at $C_L = 1.0$. Hence, $k_1 = 0.67$. The geometrical aspect ratio of the model was 6.0, hence

$$e = 3.18/(0.67 \times 6) = 0.79$$

Figure 190 indicates $e = 0.79$ in exact agreement with the model data.

Initial Rate of Climb. The initial rate of climb in ft/min may be calculated from the formula

$$\left(\frac{dh}{dt}\right)_0 = C_0 = 33{,}000 \left[\frac{K_2 \eta_m}{w_p} - \frac{V_c}{375(L/D)}\right] \tag{290}$$

in which w_p is the power loading in lb/bhp, η_m is the maximum propulsive efficiency, V_c is the air speed in climb in mph, L/D is the overall ratio of lift to drag and K_2 is the ratio of power available at climbing speed V_c to power available at maximum speed V_M. $K_2 = (\text{thp}/\text{thp}_m)$ and is read at the value of $V/V_M = V_c/V_M$ from the appropriate curve for engine and propeller used, Figure 165 to Figure 169. The air speed for best climb may be obtained from Figure 191 from which an average value is

$$V_c = V_S + 0.3\,(V_M - V_S) \tag{291}$$

The value of L/D at V_c may be obtained from

$$D = D_i\left(\frac{100}{V_c}\right)^2 + D_p\left(\frac{V_c}{100}\right)^2 \tag{292}$$

The speed for best climb is somewhat greater than the speed for L/D maximum due to the effect of increasing

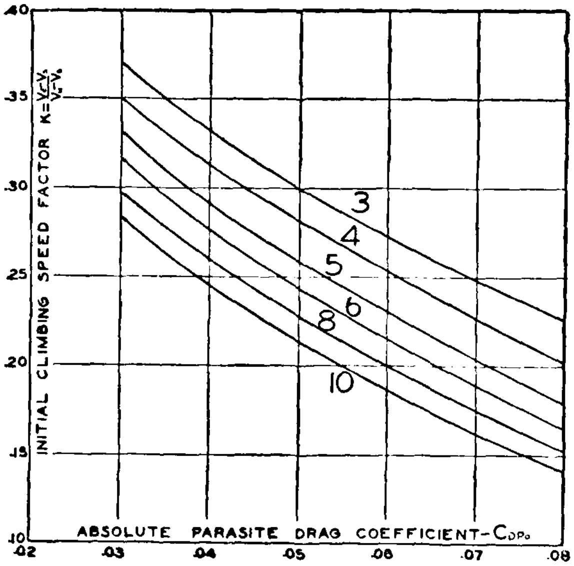

Figure 191. Effect of Aspect Ratio and Parasite on Air Speed for Best Climb at Sea-Level

propulsive efficiency. The difference between L/D at best climbing speed and $(L/D)_{max}$ is normally very small and much less than the uncertainty involved in determining η.

Equation (290) may be used to determine the rate of climb at the critical altitude for a supercharged engine if the proper values of K_2 and V_c are used. It will also determine the rate of climb at any altitude if the proper values of K_2, V_c, and w_p are used.

For the airplane considered in Chapter 11

$$\eta = 0.82 \quad R = 0.557$$
$$w_p = 4500/450 = 10.0$$
$$V_S = 63.6$$
$$V_M = 164.6$$
$$(L/D)_o = 9.96 \text{ at } 100 \text{ mph}$$

From Figure 191, $K = 0.29$, instead of the average value 0.30 used in equation (291). Hence,

$$V_c = 63.6 + 0.29\,(164.6 - 63.6) = 92.9 \text{ mph}$$

and at this speed

$$D = 161.5\,(100/92.9)^2 + 290\,(92.9/100)^2 = 437 \text{ lb}$$

and

$$L/D = 4500/437 = 10.30$$

From Figure 167 at the ratio $V_c/V_m = 92.9/164.6 = 0.564$, the value of K_2 is 0.748

Substituting these values in equation (290) gives

$$C_o = 33{,}000\left[\frac{0.748 \times 0.82}{10.0} - \frac{92.9}{375 \times 10.3}\right] = 1230 \text{ ft/min}$$

as compared with $C_o = 1270$ ft/min obtained by the calculations in Chapter 11.

Absolute Ceiling: Fixed-Pitch Propeller. The graphical method illustrated by Figure 175 may be modified to form a general chart for the estimation of absolute ceiling. Let the powers at sea-level at the speed for minimum power required be $A = \text{thp}_{ro} = P_{ro}$ and $C = \text{thp}_{ao} =$

P_{ao}. P_r varies with $\sqrt{\rho_0/\rho}$ while P_a depends on both (ρ/ρ_0) and V/V_M. The variation in P_a is readily determined from Figure 176 and Figures 165 to 169. If all powers are expressed in terms of the sea-level value of $P_{ao} = 1.000$, then it is possible to construct a chart giving a general solution for absolute ceiling as in Figure 192.

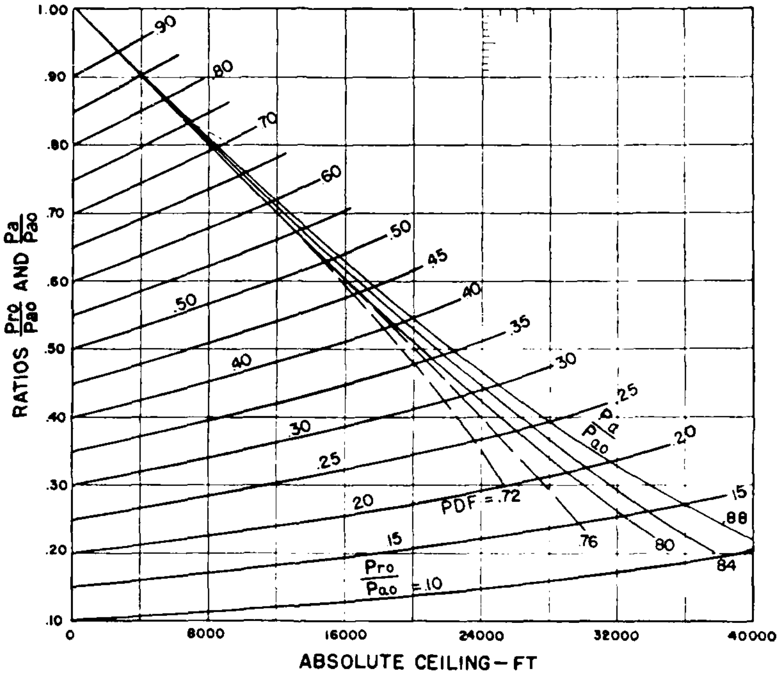

Figure 192. Absolute Ceiling Chart—Fixed-Pitch Propeller

The lines sloping downward from the top of the chart give the average decrease in the relative power available with altitude for each of the engine-power drop factors previously considered in Chapter 10. The family of curves sloping upward toward the right on Figure 192 give the increase in minimum power required with altitude. The absolute ceiling is determined by the intersection of the proper curve of P_{ro}/P_{ao} (interpolated if necessary) with the power-available curve that applies to the engine used.

The method may be illustrated by means of the data from Figure 175. The power curves on this figure give minimum power required $P_{ro} = 95$ at 73.1 mph at sea-level. At this speed the power available was $P_{ao} = 244$. Hence, $P_{ro}/P_{ao} = 0.39$. The 0.39 contour on Figure 192 intersects the P_a/P_{ao} curve for PDF = 0.80 at 19,400 ft. The extrapolation of the rate of climb curve Figure 178 gave 19,000 ft.

Normally, the ratio of P_{ro}/P_{ao} would be obtained by estimating both P_{ro} and P_{ao} at the speed for minimum power. According to the figures on page 400, $V_{MP} =$ 71.5 mph and $P_{ro} = 98.7$. Taking the ratio $V_{MP}/V_M =$ $71.5/164.6 = 0.434$ it is found from Figure 167 that $\text{thp}/\text{thp}_m = 0.650$. Since $\eta_m = 0.82$, $P_{ao} = 0.65 \times 0.82$ $\times 450 = 240$ and $P_{ro}/P_{ao} = 98.7/240 = 0.411$ which indicates an absolute ceiling of about 18,500 ft.

Values of the ratio P_a/P_{ao} for various altitudes are given in Table 23.

TABLE 23. POWER AVAILABLE IN A CLIMB AT CONSTANT ANGLE OF ATTACK

Altitude h ft	PDF = 0.88	PDF = 0.84	PDF = 0.80	PDF = 0.76	PDF = 0.72
0	1.000	1.000	1.000	1.000	1.000
4,000	.906	.902	.898	.898	.898
8,000	.812	.806	.797	.797	.797
12,000	.720	.710	.698	.698	.698
16,000	.630	.618	.603	.602	.593
20,000	.546	.530	.510	.500	.478
24,000	.467	.446	.422	.397	.350
28,000	.394	.367	.338	.292	....
32,000	.329	.293	.262	....	....
36,000	.270	.227	....	....	....
40,000	.217	....	....	....	....

This method may be applied to a supercharged engine by extrapolating the power available to obtain a fictitious sea-level value as explained on page 380. In practice this may be done by finding (1) the value of $P_{ro}/P_{ao} = A$ for the airplane at the critical altitude, (2) the value of $P_{ro}/P_{ao} = B$ that gives H = critical altitude and (3) the effective value of $P_{ro}/P_{ao} = A \times B$ which will give the absolute ceiling for the supercharged engine.

Absolute Ceiling: Controllable-Pitch Propeller. The absolute ceiling with a controllable-pitch propeller is given by the curve for PDF = 0.80 on Figure 192. The effect of the controllable-pitch propeller is to increase the initial value of P_{ao}, thus decreasing the ratio P_{ro}/P_{ao}. It is merely a coincidence that the power-available curve for a controllable-pitch propeller is almost identical with the curve for PDF = 0.80 on Figure 192.

Service Ceiling. If the rate of climb decreased linearly with altitude, the service ceiling (at which the rate of climb is 100 ft/min) should be given by

$$h_s = H\left[\frac{C_0 - 100}{C_0}\right] \tag{261}$$

Owing to the inflection in the rate-of-climb curve, the actual service ceiling will be slightly below the value given by equation (261). Figure 193 is a plot of Δh_s against absolute ceiling H, Δh_s being the difference between the straight line value and the exact value of h_s. Δh_s is closely approximated by the relation

$$\Delta h_s = 35\,(H/10{,}000)^3 \tag{293}$$

consequently the exact service ceiling is given by

$$h_s = H\left[\frac{C_0 - 100}{C_0}\right] - 35\left[\frac{H}{10{,}000}\right]^3 \tag{294}$$

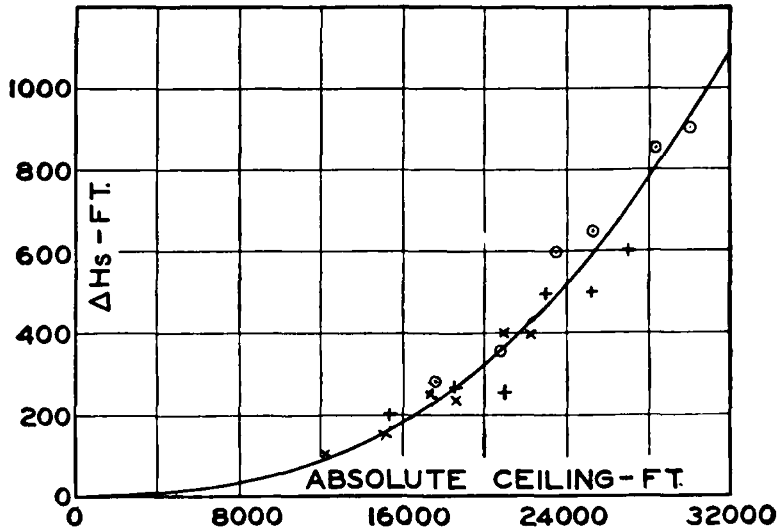

Figure 193. Difference Between Service Ceilings for Linear and for Non-Linear Rate-of-Climb Curves

For supercharged engines the service ceiling is given by

$$h_s = h_c + (H - h_c)\left[\frac{C_0' - 100}{C_0'}\right] \tag{295}$$

where h_c is the critical altitude and C_0' is the rate of climb at the critical altitude.

Time of Climb. With a linear relation between rate of climb and altitude, the altitude h climbed in T minutes is

$$h = H\left[1 - e^{-\frac{C_0 T}{H}}\right] \tag{263}$$

where H is the absolute ceiling (ft), and C_0 the initial rate of climb (ft/min). A simple relation may be found between the altitude given by equation (263) and the actual altitude for a non-linear rate of climb.

When the ratio of C/C_0 is plotted against h/H as in Figure 194, the various points (representing about 20 airplanes) lie very near a single curve, which indicates that all climb curves may be similar. Figure 194 may be used for drawing up estimated rate-of-climb curves when the initial rate of climb C_0 and the absolute ceiling H are known. It may also be used to determine some general relations.

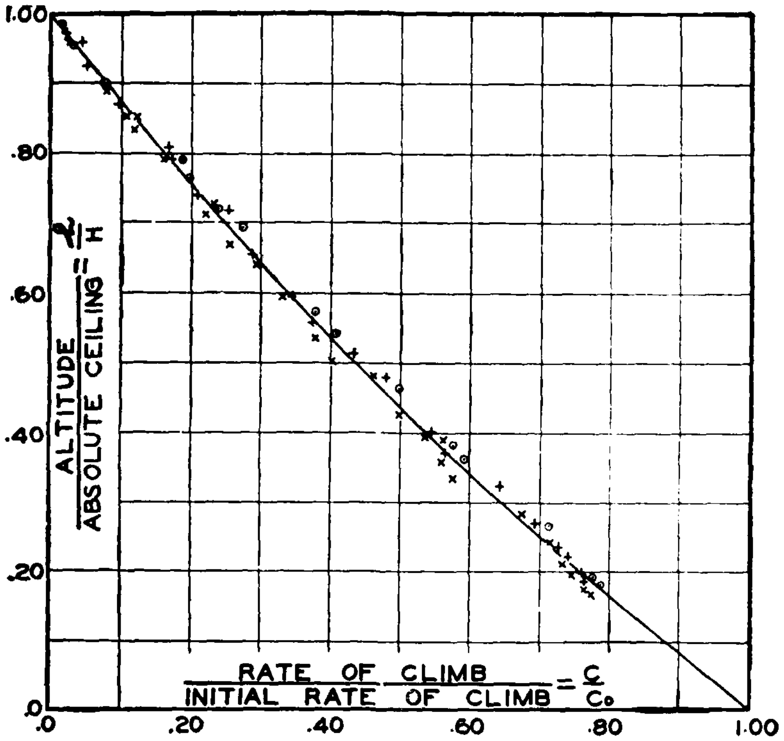

Figure 194. General Rate-of-Climb Curve

Plotting C_0/C from Figure 194 against h/H and integrating the area under the curve gives factors proportional to the times required to climb to any altitude h. A similar plot of C_0/C from equation (260) gives similar factors for linear rate of climb. The ratio of these factors gives the ratio between the times T_c/T_s to climb to a given percentage of the absolute ceiling, T_c being the time for non-linear and T_s the time for linear rate of climb against altitude. T_c/T_s is plotted against h/H in Figure 195. This

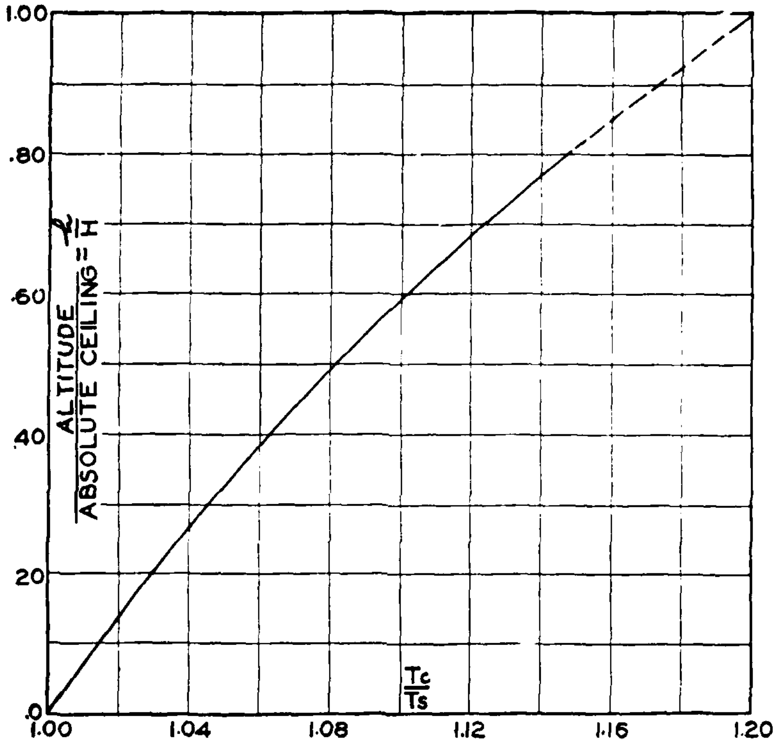

Figure 195. Relation Between the Times to Climb to a Given Altitude with Linear and Non-Linear Rate-of-Climb Curves

figure may be used to determine the value of T_c from a known or easily determined value of T_s.

Figure 196 is a plot of $T_s/(H/C_0)$ and $T_c/(H/C_0)$ against h/H, using the data in Table 24. This figure may be used to calculate either the time required to climb to a given altitude or the altitude climbed in a given time, for either a linear or non-linear rate of climb. For example, assume $H = 20{,}000$ ft, $C_0 = 1600$ ft/min, then $H/C_0 = 12.5$ min. The times to climb to 10,000 ft, $h/H = 0.5$,

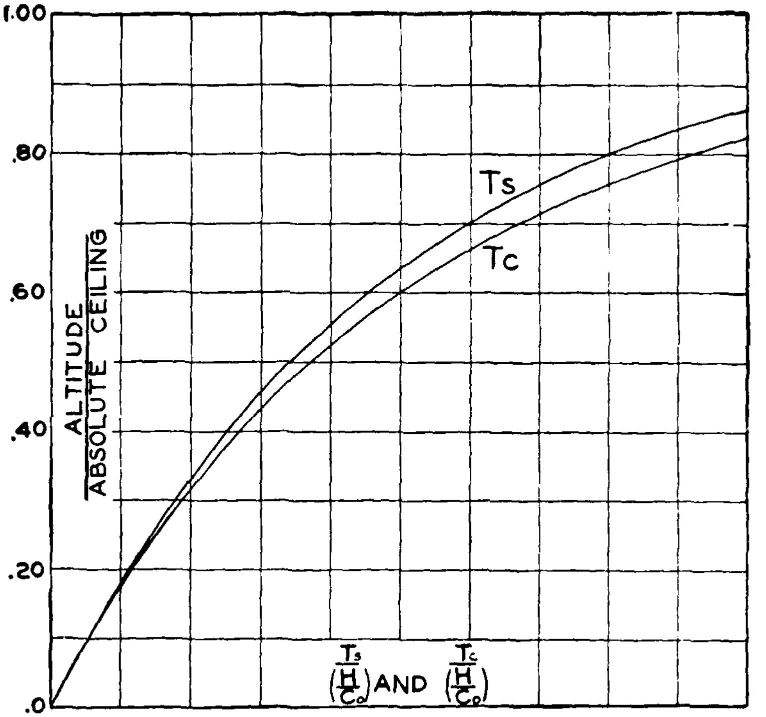

Figure 196. Time to Climb to a Given Altitude. T_s for Linear, T_c for Non-Linear Rate-of-Climb Curves

are $T_s = 0.69H/C_0 = 8.62$ min, and $T_c = 0.75H/C_0 = 9.37$ min. The altitudes climbed in 10 minutes are found from $T_s/(H/C_0) = T_c/(H/C_0) = 10/12.5 = 0.80$, giving $h_s/H = 0.55$ from which $h_s = 11{,}000$ ft, and $h_c/H = 0.52$ from which $h_c = 10{,}400$.

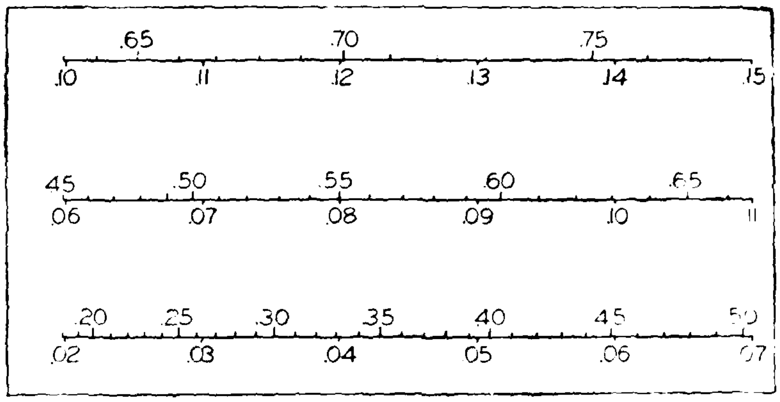

Figure 197. Climb in 10 Minutes, from Absolute Ceiling and Initial Rate of Climb (linear). Values of $\frac{h_{10}}{H}$ are Above and Values of $\frac{C}{H}$ are Below Base Lines

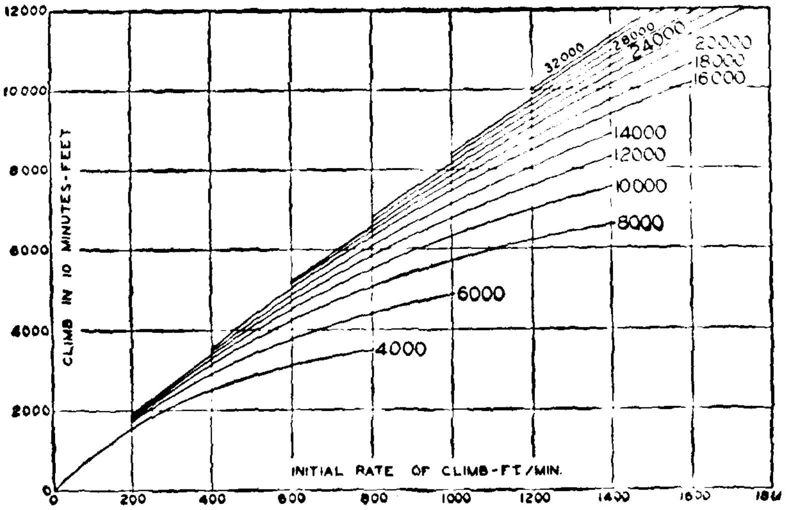

Figure 198. Climb in 10 Minutes from Absolute Ceiling and Initial Rate of Climb (Linear)

The climb in 10 minutes is used extensively as a measure of performance. Three charts based on the linear relation have been prepared for the solution of various problems involving this factor. Figure 197 is a plot of h_{10}/H against C_0/H from which h_{10} may be accurately determined.

TABLE 24. TIME OF CLIMB FACTORS

$\frac{h}{H}$	$\frac{T_S}{\left(\frac{H}{C_0}\right)}$	$\frac{T_C}{\left(\frac{H}{C_0}\right)}$	$\frac{T_C}{T_S}$
0	0	0	1.000
.10	.1053	.1068	1.014
.20	.2232	.2300	1.029
.25	.2875	.2982	1.037
.30	.3563	.3723	1.045
.35	.4305	.4540	1.054
.40	.511	.544	1.063
.45	.598	.642	1.072
.50	.693	.749	1.081
.55	.797	.870	1.091
.60	.916	1.009	1.102
.65	1.051	1.171	1.113
.70	1.203	1.352	1.124
.75	1.386	1.574	1.139
.80	1.609	1.849	1.148
.90	2.303	2.703	1.173

This value may then be corrected for the non-linear relation, if desired, using one of the preceding figures. Figure 198 is a plot of h_{10} against H and C_0, from which h_{10} may be read directly. Figure 199 is a similar plot with the service ceiling h_s instead of the absolute ceiling H. The latter figure may be used to determine initial rate of climb when only h_{10} and h_s are given.

The foregoing discussion has been based on the use of a sea-level engine. For a supercharged engine, the conditions above the critical altitude may be obtained by extrapolation of the engine curve to fictitious sea-level initial rate of climb, as explained in Chapter 11.

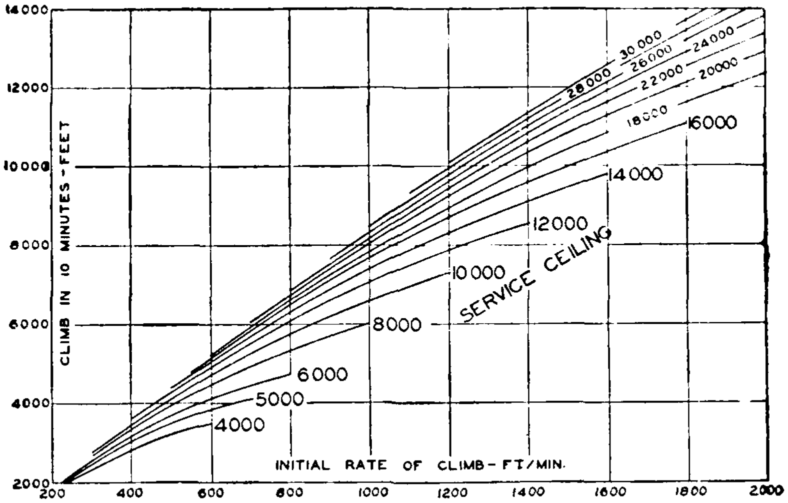

Figure 199. Climb in 10 Minutes from Service Ceiling and Initial Rate of Climb (Linear)

CHAPTER 13

RANGE AND ENDURANCE

Maximum Range. The maximum range for a given fuel load is obtained by continuously flying, until the fuel is exhausted, at the air speed giving the most miles per pound (or the minimum pounds per mile). For a given airplane this air speed, usually designated as the "most economical air speed," or "economical speed," varies almost linearly with gross weight. The fuel consumption in lb/mile also varies almost linearly with gross weight. It therefore follows that the most economical speed and corresponding fuel consumption need be calculated for only three gross weights in order to determine the maximum range. These weights should obviously be at, or near full load, half-fuel load, and no-fuel load.

Fuel consumption is obtained at a given speed and weight by calculating the rpm and bhp, using the data given in Chapter 10. The various steps in a typical calculation may be tabulated as follows:

1. Air speed V
2. Ratio V/V_{max}
3. thp required at speed V. This may be read from the curve of power required or calculated from the induced and parasite powers.
4. Ratio $\text{thp}_r/\text{thp}_m$. $\text{thp}_m = \text{thp}_r$ at V_{max}
5. n/n_0. Obtain from equation 246.

   $n/n_0 = 0.98 \sqrt[3]{\text{thp}/\text{thp}_m}$
6. $\text{rpm} = \text{rpm}_0 \times (n/n_0)$
7. $(V/nD)/(V/nD)_0 = (V/V_m)/(n/n_0)$
8. η/η_m from Figure 153 or Figure 154

9. $\eta = \eta_m \times (\eta/\eta_m)$. η_m is the maximum propulsive efficiency
10. bhp = thp/η
11. Specific fuel consumption, C. Obtain from engine data or Figure 142
12. Fuel consumption lb/hr = bhp $\times$ C
13. Fuel consumption lb/mile = bhp $\times$ C/V

The fuel consumption in lb/mile is plotted against speed in order to obtain the minimum consumption and the corresponding speed (most economical speed). This operation is repeated for the other gross loads. The minimum fuel consumption in lb/mile and the corresponding economical speeds are then plotted against gross weight. If there is a pronounced curvature in the line passed through the minimum fuel consumption points on this plot, the range must be determined either by a step-by-step integration, or by a planimeter. In the step-by-step method the average fuel consumptions are determined for convenient increments in weight, say 500 lb or 1000 lb. The distance flown for the ΔW under consideration is obviously $\Delta r = \Delta W/C_a$ where C_a is the average lb/mile for the increment ΔW. The endurance may be calculated along with the range from ΔE hr $= \Delta r/V_a$, where V_a is the average speed for the increment Δr.

If it is desired to use a planimeter, the reciprocal of the minimum fuel consumption, that is, the maximum miles per pound of fuel must be plotted against gross weight. The area under this curve has the dimensions of (mi/lb) $\times$ lb = miles, and the distance flown while using a given weight of fuel is proportional to the area under the curve and between the two corresponding gross weights. If the curve is plotted to the scales of 1″ = 1000 lb weight, and 1″ = 0.10 (mi/lb) each square inch under the curve will represent 100 miles. The endurance may be found in the same manner by plotting (hr endurance/lb fuel) against gross weight and measuring the area under the curve.

The range may be calculated very quickly by formula when the fuel consumption in lb/mile plots as a straight line against gross weight. If the slope of the fuel consumption curve, lb/mile, against weight is b, and the equation of fuel consumption $C = a + bW$, then

$$r = \int_{W_0}^{W_1} \frac{dW}{(a + bW)}$$

$$= \frac{2.303}{b} \log_{10} \left[\frac{a + bW_0}{a + bW_1}\right] \tag{296}$$

Since $(a + bW_0)$ = initial fuel consumption, C_0 (lb/mile), and $(a + bW_1)$ = final fuel consumption, C_1, this becomes

$$r = \frac{2.303}{b} \log_{10} \left[\frac{C_0 \text{ lb/mile}}{C_1 \text{ lb/mile}}\right] \tag{297}$$

The endurance is found directly from the fuel consumption in lb/hr, if C is of the form $(m + nW)$:

$$T = \int_{W_0}^{W_1} \frac{dW}{(m + nW)}$$

$$= \frac{2.303}{n} \log_{10} \left[\frac{m + nW_0}{m + nW_1}\right]$$

$$= \frac{2.303}{n} \log_{10} \left[\frac{C_0 \text{ lb/hr}}{C_1 \text{ lb/hr}}\right] \tag{298}$$

Theoretically, the specific fuel consumption should include both gas and oil consumption, and the final weight should be based on the amount of oil remaining when all of the gasoline is gone. Practically the oil consumption may be neglected when modern engines are used and the final weight W_1 taken as W_0 less the weight of gasoline W_g. That is, $W_1 = W_0 - W$

Calculation of Maximum Endurance. Maximum range is obtained by flying at a speed about 40% greater than the stalling speed, but maximum endurance is obtained at a considerably lower speed, 15% to 20% greater than the stalling speed. The calculation for maximum endurance is exactly like that for maximum range except that the factor now desired is the maximum (hr/lb fuel) at a given gross weight. Plotting (max hr/lb fuel) against gross weight, the area under the curve will be proportional to the maximum endurance in hours.

The maximum (hr/lb fuel) should be obtained by calculating (hr/lb) at a number of speeds from 1.05 V_S to 1.50 V_S and plotting against speed.

General thp Curves. In Chapter 12 the value of V_{max} is determined from an induced drag correction depending on the ratio

$$R = \frac{\text{Induced drag at 100 mph}}{\text{Parasite drag at 100 mph}} \qquad (274)$$

The selection of 100 mph for the basic speed was partially arbitrary and partially a matter of convenience, since D_p is normally calculated for a speed of 100 mph. R varies inversely as the fourth power of the speed. Hence, R_V taken at the speed V is

$$R_V = R \times (100/V)^4 \qquad (299)$$

or

$$R_M = \frac{\text{Induced drag at } V_{max}}{\text{Parasite drag at } V_{max}}$$

$$= R \times (100/V_{max})^4 \qquad (299a)$$

The parameter R_M is of great assistance in calculating range and endurance. Figure 200 is a family of curves of relative power against relative speed showing the influence of R_M. These curves include a normal increase in parasite drag based on Figure 174. This increase is confined to speeds below that at which $D_i = D_p$ uncorrected.

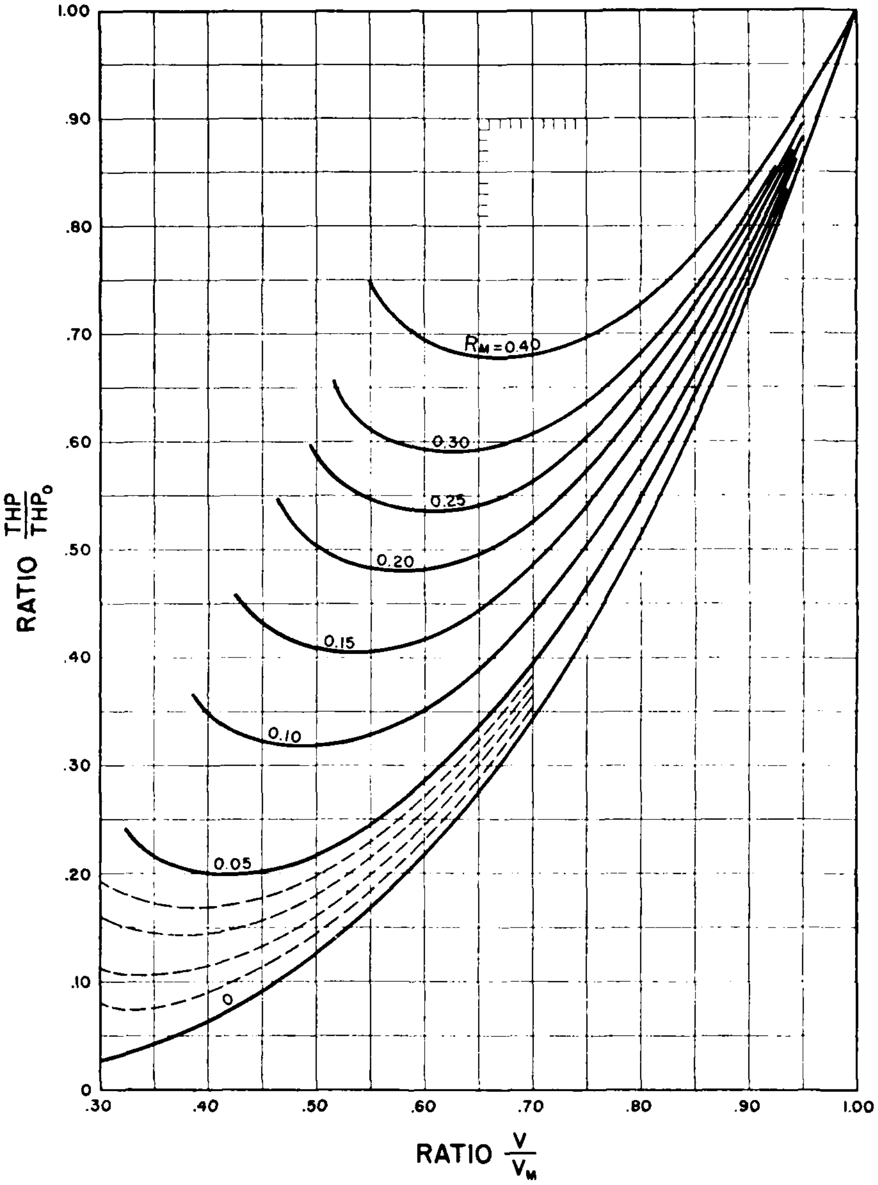

Figure 200. General thp Curves in Terms of V/V_M *and* R_M. R_M = $(D_i \text{ at } V_M)/(D_p \text{ at } V_M)$

Range and Endurance: Constant Angle of Attack. Breguet's formulas for range in miles and endurance in hours are:

$$\text{Range} = 863.5 \left(\frac{\eta}{C}\right)\left(\frac{L}{D}\right) \log_{10}\left(\frac{W_0}{W_1}\right) \qquad (300)$$

$$\text{Endurance} = 750 \frac{\sqrt{W}}{V_C}\left(\frac{\eta}{C}\right)\left(\frac{L}{D}\right)\left[\frac{1}{\sqrt{W_1}} - \frac{1}{\sqrt{W_0}}\right] \qquad (301)$$

where L/D is the ratio of lift to drag for the entire airplane, η is the average propulsive efficiency, C the average specific fuel consumption, W_0 the initial gross weight, W_1 the final gross weight, and V_C the cruising speed at the gross weight W. These formulas assume flight at constant angle of attack, hence the term $\sqrt{W}/V_C$ will be constant. They will give accurate results if the proper value of C can be obtained. Since there is always some uncertainty regarding the average value of C, the equations have been modified to use the initial value of C. It may be shown[1] that when the specific fuel consumption at low throttle settings is of the form

$$C = C_1\,(W_0/W)^n \qquad (302)$$

the equations for range and endurance become:

$$r = \frac{375}{n}\left(\frac{\eta}{C_1}\right)\left(\frac{L}{D}\right)\left[1 - \left(\frac{W_1}{W_0}\right)^n\right] \qquad (303)$$

$$T = \frac{375}{(n - 0.5)\,V_{C_0}}\left(\frac{\eta}{C_1}\right)\left(\frac{L}{D}\right)\left[1 - \left(\frac{W_1}{W_0}\right)^{n - 0.5}\right] \qquad (304)$$

where C_1 is the initial specific fuel consumption and V_{C_0} is the initial crusing speed, both at the weight W_0.

The original analysis of fuel consumption data indicated values of $n = 0.45$ for a normal mixture and $n = 0.42$ for a lean mixture. Subsequent analysis of published data indicates that there has been a considerable change in the general appearance of the fuel consumption curve, accompanied by an increase to $n = 0.60$. All data recently analyzed have been in close agreement at this value. The increase in n results from reduced consumption at intermediate power rather than from an increase at very low power.

---

[1] W. S. Diehl, "Three Methods of Calculating Range and Endurance of Airplanes," N.A.C.A. T.R. No. 234 (1926).

Using the value $n = 0.60$, equations (303) and (304) become:

$$r = 625\left(\frac{\eta}{C_1}\right)\left(\frac{L}{D}\right)\left[1 - \left(\frac{W_1}{W_0}\right)^{0.60}\right] \tag{305}$$

$$T = \frac{3750}{V_{C_0}}\left(\frac{\eta}{C_1}\right)\left(\frac{L}{D}\right)\left[1 - \left(\frac{W_1}{W_0}\right)^{0.30}\right] \tag{306}$$

Equations (300) and (301) reduce to

$$r = B_R\left(\frac{\eta}{C}\right)\left(\frac{L}{D}\right) \tag{307}$$

$$T = \frac{B_F}{V_{C_0}}\left(\frac{\eta}{C}\right)\left(\frac{L}{D}\right) \tag{308}$$

where B_R and B_E are functions of W_1/W_0 or W_F/W_0, W_F being the fuel load. In a similar manner equations (305) and (306) reduce to

$$r = K_R\left(\frac{\eta}{C_1}\right)\left(\frac{L}{D}\right) \tag{309}$$

$$T = \frac{K_E}{V_{C_0}}\left(\frac{\eta}{C_1}\right)\left(\frac{L}{D}\right) \tag{310}$$

Values of B_R, B_E, K_R, and K_E are given on Figure 201. The specific fuel consumption is obtained from data supplied by the engine manufacturer, or from Figure 142 and Figure 143. Figure 202 has been prepared to give the value of C_1/C_0 directly. The value of C_0 will depend on a number of factors, but an average value will be about 0.53, although it is possible to attain lower values under favorable conditions. The improved cooling of recent air-

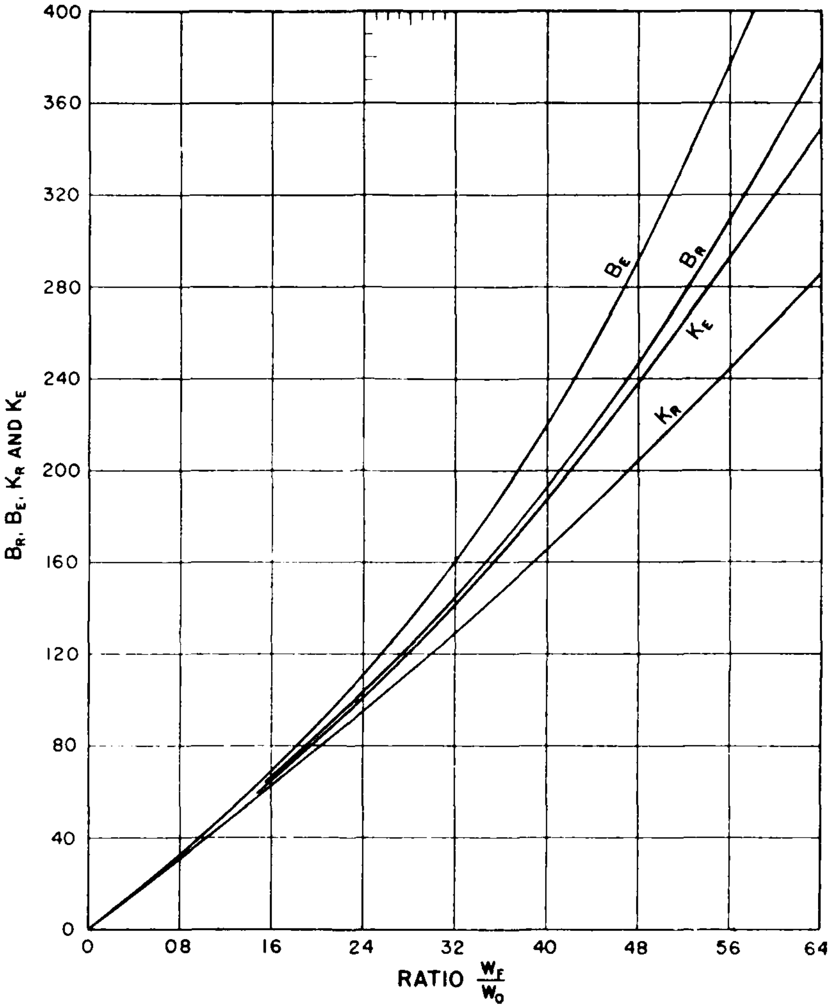

Figure 201. Range and Endurance Coefficients as a Function of Fuel-Load Ratio

cooled engines has resulted in a definite reduction in C_0. The automatic mixture control has given promise of a practically constant value $C = 0.48$ lb/bhp/hr. Values as low as $C = 0.42$ have been reported but until these values can be consistently duplicated, they should be used with caution in performance estimates.

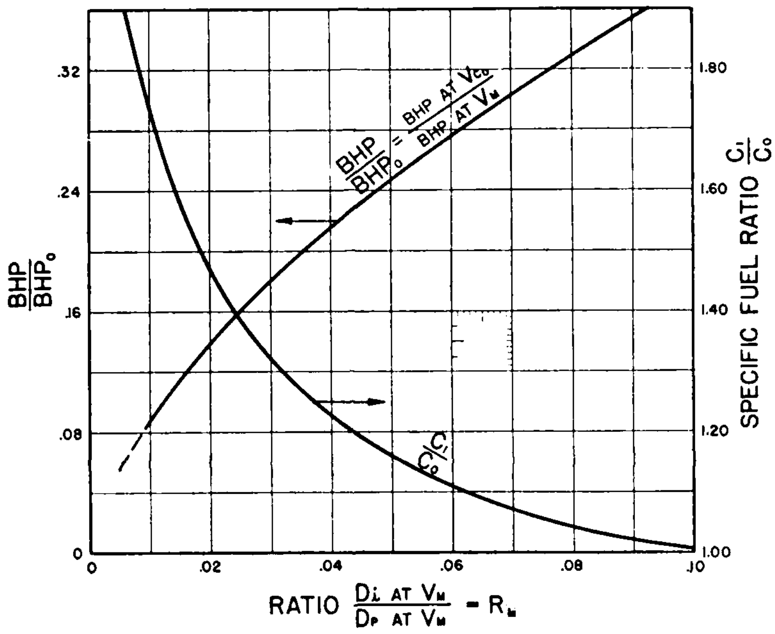

Figure 202. Initial Specific Fuel Consumption at Most Economical Speed

Range at Constant Air Speed. Equations (307) and (309) give the range for flight at constant angle of attack. In this case the air speed decreases as the weight is reduced by the fuel consumed. A common problem is to determine the range at constant air speed, which requires a change in angle of attack as the gross weight is reduced. The solution is as follows: Since,

$$C_{D_i} = C_L^2/\pi n = W^2/(qS)^2\pi n = W^2/K$$

where $K = (qS)^2\pi n$, and $dW/dt = -C \cdot \text{thp}/\eta$

$$\text{thp}_r = \frac{qSV}{375}\left[C_{DP} + (W^2/K)\right]$$

and

$$r = V\int_{W_0}^{W_1} dt = \frac{\eta}{C} \cdot \frac{375}{qS}\int_{W_0}^{W_1} \frac{dW}{[C_{DP} + (W^2/K)]}$$

from which

$$r = 375\,\frac{\eta}{C}\sqrt{\frac{\pi n}{C_{DP}}} \cdot \tan^{-1}\left[\frac{\sqrt{\dfrac{1}{C_{DP} \cdot K}}\,(W_0 - W_1)}{1 + \left(\dfrac{W_0 W_1}{C_{DP} \cdot K}\right)}\right] \qquad (311)$$

This equation is very much less complex than it appears. It is of particular interest in that the expression $\sqrt{\pi n / C_{DP}}$ is equivalent to $2(L/D)_{max}$ as shown by equation (283), and the expression $\sqrt{C_{DP} \cdot K}$ is equivalent to $2\ D_p \cdot (L/D)_{max}$. Introducing these equivalents and simplifying

$$r = 750\left(\frac{\eta}{C}\right)\left(\frac{L}{D}\right)_{max}\tan^{-1}\left[\frac{(W_0 - W_1)}{F + \dfrac{(W_0 W_1)}{F}}\right] \qquad (312)$$

where

$$F = 2\ D_{pm}\left(\frac{V}{V_M}\right)^2\left(\frac{L}{D}\right)_{max} \qquad (313)$$

In equation (312) W_0 is the initial gross weight and W_1 is the final gross weight. The difference $(W_0 - W_1)$ is the fuel consumed. In the simplifying factor F, equation (313), D_{pm} is the parasite drag at V_M.

Equation (312) should be compared with equation (300). The constant 863.5 in the latter contains the logarithmic conversion factor M ($M = \log_e 10$) and is 375 when natural logarithms are used. In view of the marked difference otherwise in the appearance of the two equations, a number of checks have been made on equation

(312) and excellent agreement has been obtained in comparison with the results from step-by-step calculations.

In applying equation (312) the specific fuel consumption C is to be taken at the speed V. The endurance is found from $T = r/V$.

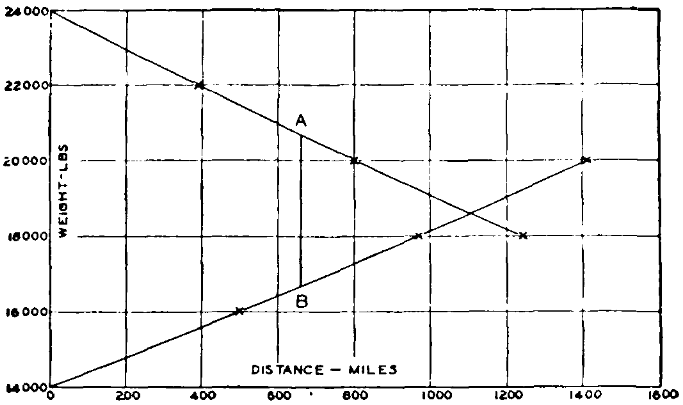

Figure 203. Graphical Solution for Bombing Range

Bombing Range. The distance that an airplane can fly with a given fuel load, drop a bomb, and return to the starting point, is easily obtained by a simple graphical solution. Let W_0 be the initial gross load including full bomb-and-fuel loads, and W_1 the final load without fuel or bombs. Calculate the range for two or three fuel loads assuming constant initial load = W_0. The largest fuel load should be somewhat more than $\frac{1}{2}(W_0 - W_1)$. Repeat the process assuming constant final load = W_1. Plot as two curves of range against weight, one starting from W_0 and showing increasing range with decreasing weight, the other starting from W_1 and showing increasing range with increasing weight. The intersection of these curves gives the maximum radius with all fuel and no bombs. Figure 203 illustrates how the range is found for any desired bomb load for an airplane weighing 24,000 lb and carrying 10,000 lb of fuel and bombs. For 10,000 lb of fuel and no bombs, the curves intersect at 1110 miles; hence the range is 2 × 1110 = 2220 miles. For a 4000-lb bomb load and 6000 lb of fuel, the airplane can fly out to the point **A** at 660 miles, drop the bomb load **AB** = 4000 lb, and return to the point of departure.

Calculations have been made on a systematic series of fictitious airplanes with bomb loads up to 50% of the initial gross weight. These calculations indicate that the effect on range due to dropping a bomb load is linear and dependent only on the ratio of the load dropped W_D to the initial gross load W_0. Letting r_0 = range with no drop and r_D = range with weight W_D dropped (at distance $r_D/2$) then

$$r_D/r_0 = 1.00 + 0.77\, W_D/W_0 \tag{314}$$

Hence, with the same initial load and the same fuel load, the radius is increased 7.7% by dropping a weight of 10% of the initial gross weight at the midway point. Equation (314) does not apply to the case of dropping a load at any point other than the midway point at distance $r_D/2$ from the starting point.

Effect of Wind on Range. The most economical speed is affected considerably by wind direction and force, being increased by head winds and decreased by following winds. The most economical speed is readily found for any wind velocity, by a simple graphical solution. If the fuel consumption in lb/hr is plotted against air speed in mph with both scales starting from zero, as in Figure 204, then a line drawn from any point on the speed axis is tangent to the curve at the most economical speed for the wind condition determined by the starting point. Since the ground speed is the difference between the air speed and the wind speed, the starting point or origin for ground speed is moved to the right or to the left for head winds and following winds respectively. That is, with a 40-mph head wind, the ground speeds will be 40 mph less than the air speeds, and the origin will be at 40 mph. A line drawn from this point in Figure 204 is tangent to the curve at 99 mph, which is the economical speed for a 40-mph head wind, at the gross weight represented by the fuel consumption curve. Similar tangents drawn for zero wind and 40 mph following wind indicate economical speeds of 86 mph and 81 mph respectively. It is obvious that this operation determines the minimum pounds of fuel per ground mile.

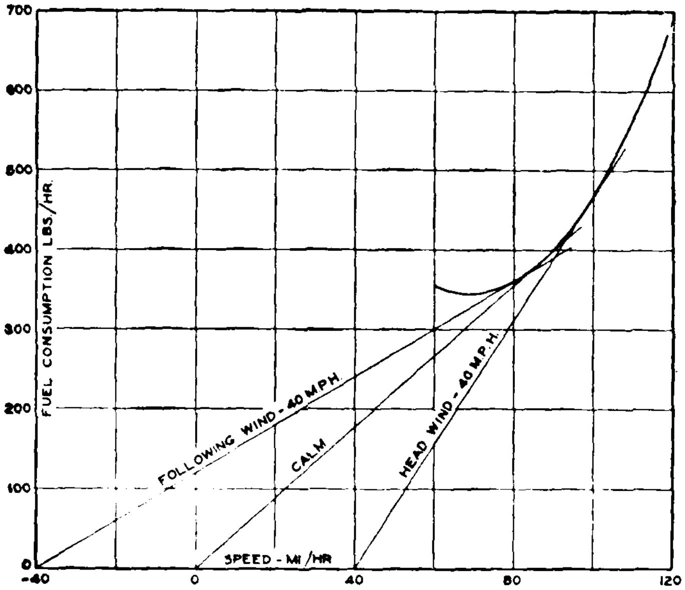

Figure 204. Effect of Wind on Most Economical Speed

It is somewhat longer, but perhaps more accurate, to calculate the pounds-fuel per ground-mile for various air speeds and wind speeds. If the pounds-fuel per ground-mile at a given wind speed be plotted against air speed, the most economical air speed is accurately determined.

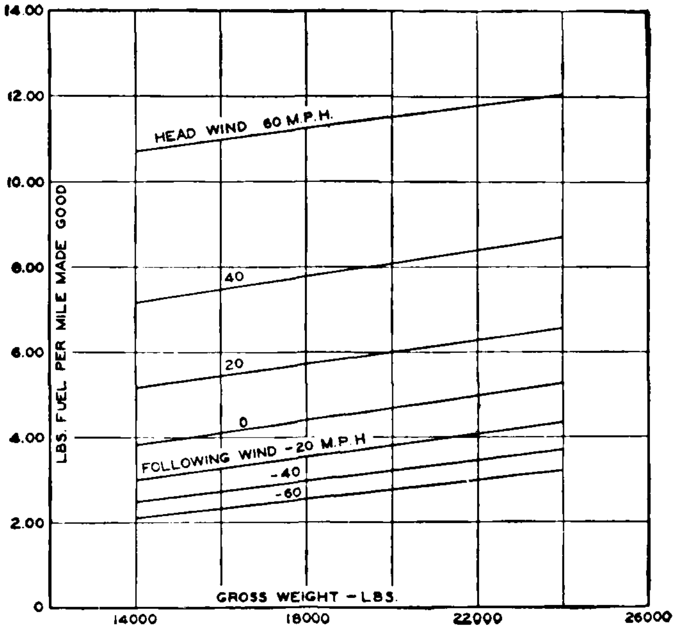

Figure 205. Effect of Wind on Fuel Consumption for a Typical Flying Boat

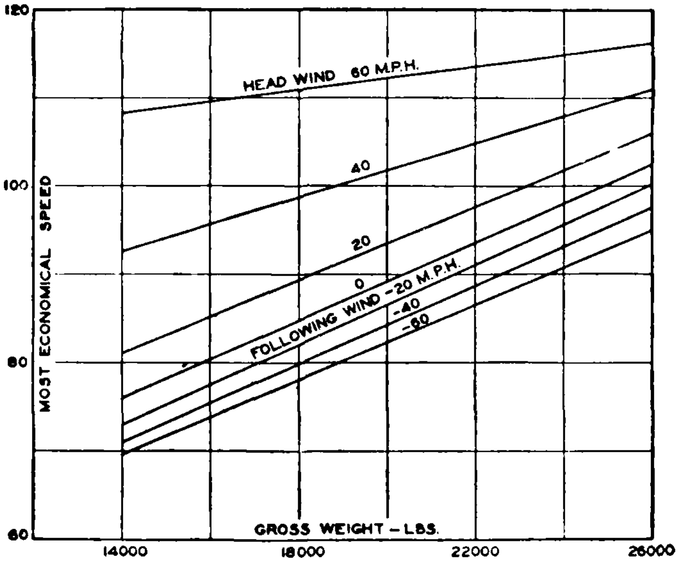

Figure 206. Effect of Wind on Most Economical Speed for a Typical Flying Boat

Figure 205 shows the variation in fuel consumption and Figure 206 shows the variation in the most economical speed for a typical large flying boat.

A head wind of a given velocity reduces range more than a following wind of the same velocity increases it. The maximum distance that can be flown out and return to starting point is less in a steady wind than in a calm, and decreases rapidly as the steady wind velocity increases.

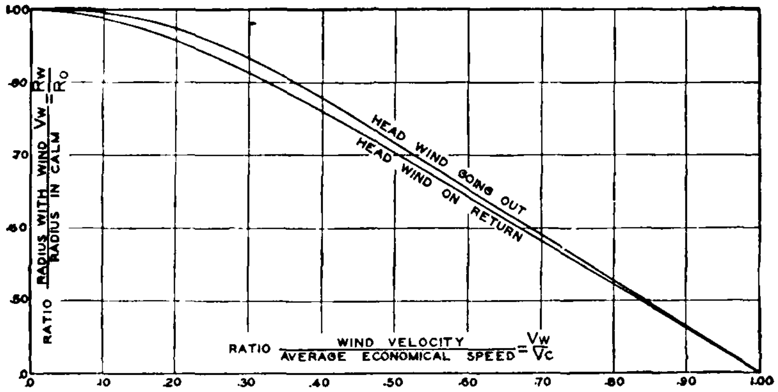

Figure 207. Reduction of Range in a Steady Wind

The radius is greater if the head wind is encountered going out with full load than if the head wind is met on the return flight. Figure 207 gives the average effect of a steady wind on radius of action.

Estimating Range and Endurance. The endurance at maximum speed E_0 is obtained by dividing the fuel load by the full-throttle specific fuel consumption and actual bhp if known, otherwise the rated or nominal bhp. If the specific fuel consumption for the engine is unknown, it must be estimated. C_0 may be anything between 0.42 and 0.65. The average values are probably between 0.50 and 0.58. These averages may be reduced by as much as

10% under favorable conditions. It should be noted that C_o is the full-throttle value, and not the minimum value. The minimum specific fuel consumption will be about 90% of the full-throttle value and it will occur at about 70% full power.

The range r_o at maximum speed is obviously

$$r_o = E_o \times V_M \tag{315}$$

The range and endurance at other speeds are readily found by the factor method based on the endurance factor F_E and the range factor F_R defined by

$$F_E = \frac{\text{Endurance at speed } V}{\text{Endurance at max speed}}$$

$$F_R = \frac{\text{Range at speed } V}{\text{Range at max speed}}$$

F_E and F_R vary with V/V_M and with the type of power required curve. The power required curve may be defined by the ratio of D_i to D_p taken at V_M, or

$$R_M = \frac{D_i \text{ at } V_M}{D_p \text{ at } V_M} \tag{316}$$

Values of F_E and F_R have been calculated for a series of R_M values. These are plotted on Figure 208 and Figure 209. Supplementary plots on Figures 210 and 211 give the same data in a form often used. When the fuel load is relatively large the average value of R_M must be used.

Analysis of these data for the maximum range condition yields several important relations as follows:

$$F_E \text{ for max range} = R_M^{-0.406} \tag{317}$$

$$F_R \text{ for max range} = R_M^{-0.206} \tag{318}$$

$$\frac{V_C}{V_M} \text{ for max range} = R_M^{0.206} \tag{319}$$

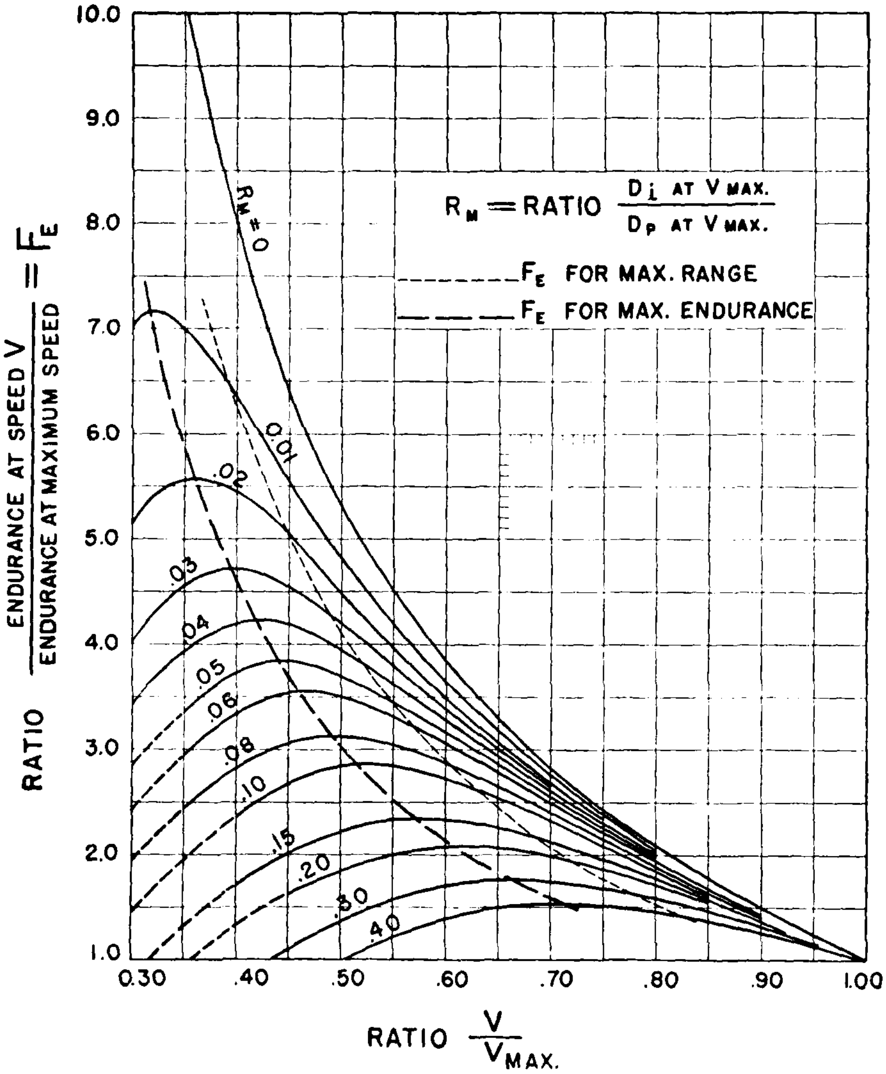

Figure 208. Endurance Factor F_E as a Function of V/V_M and R_M

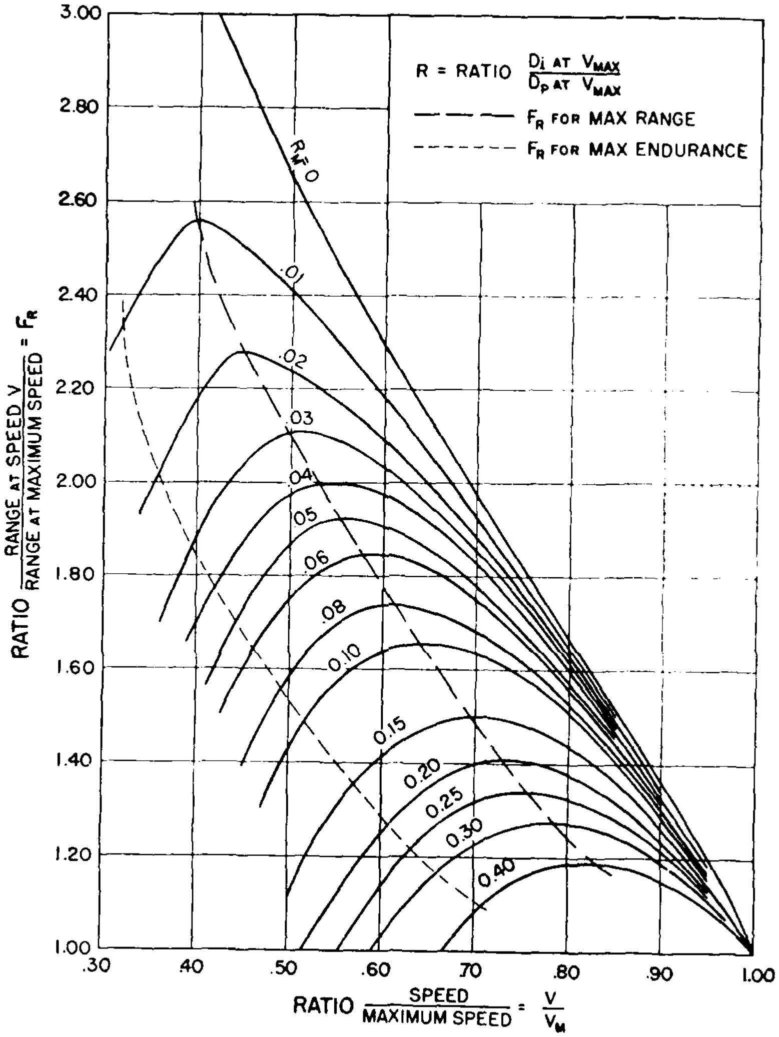

Figure 209. Range Factor F_R as a Function of V/V_M and R_M

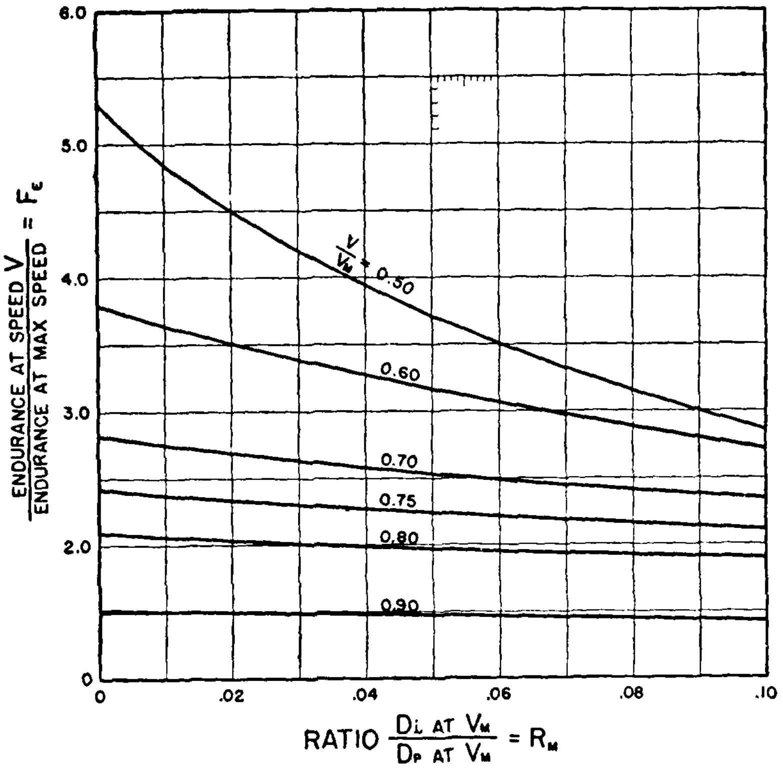

Figure 210. Endurance Factor F_E as a Function of R_M and V/V_M

These values are plotted on Figure 212. It also appears that the maximum endurance at a given value of R_M is about 13% greater than the endurance for maximum range or

$$\frac{E_{max}}{E_0} = 1.13\ R_M^{-0.406} \qquad (320)$$

where E_0 is the endurance at V_M. The speed for maximum endurance is about 82% of the speed for maximum range or

$$\frac{V_{CM}}{V_M} = 0.82\ R_M^{0.206} \qquad (321)$$

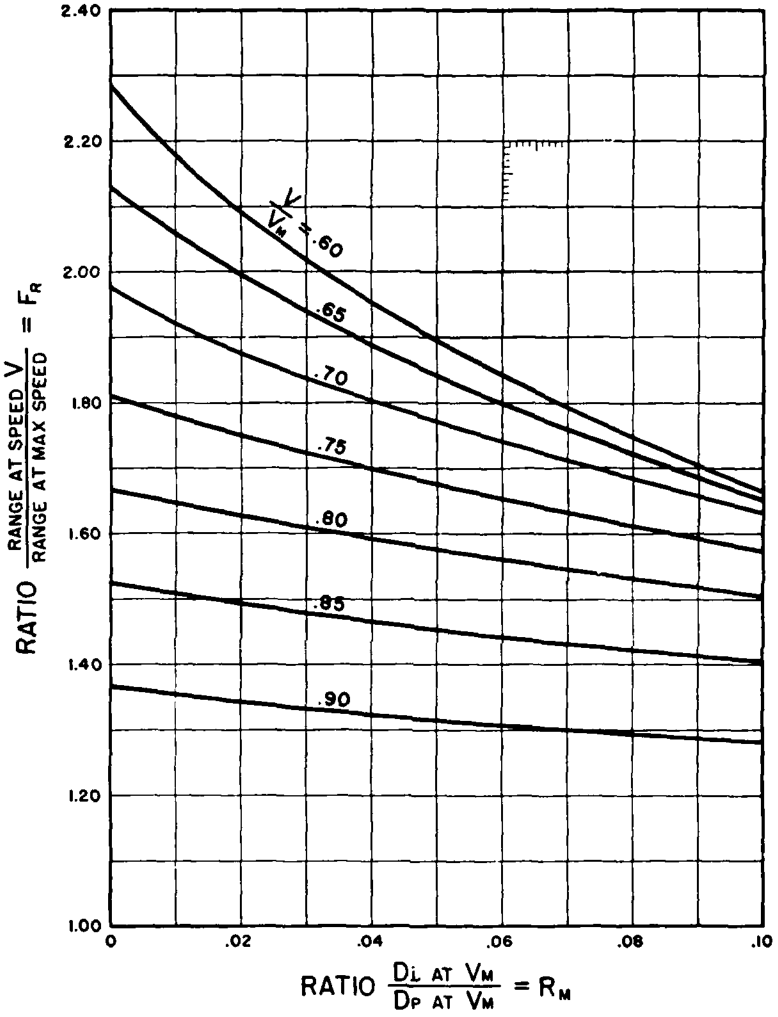

Figure 211. Range Factor F_R as a Function of R_M and V/V_M

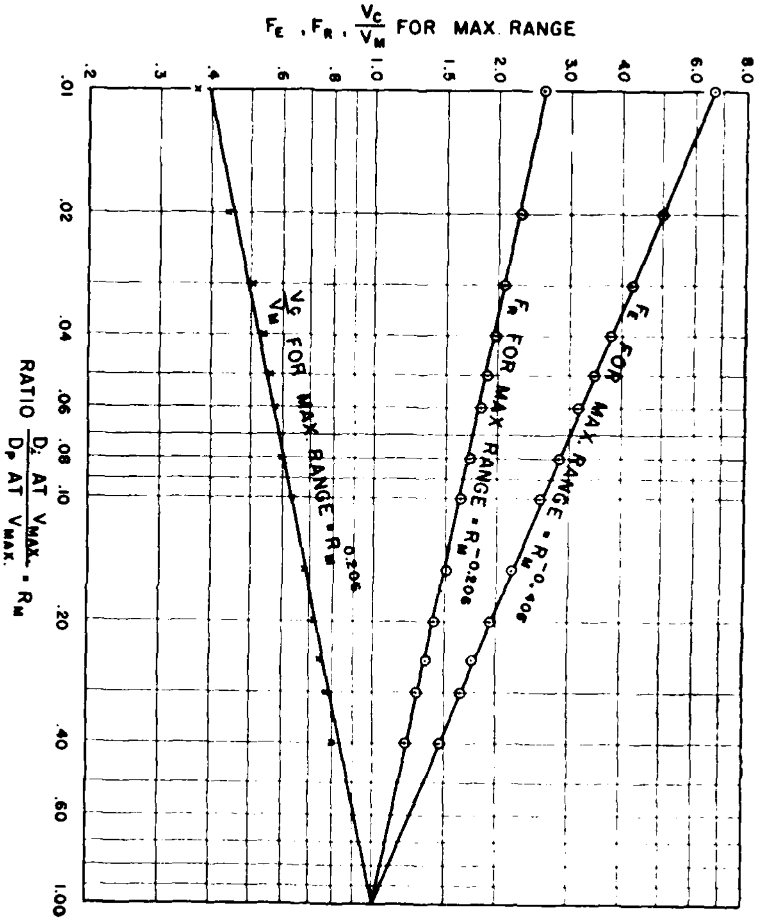

Figure 212. Effect of R_M on the Values of F_R and F_E for Maximum Range

CHAPTER 14

SPECIAL PERFORMANCE PROBLEMS

Take-off Run. The distance required for an airplane to accelerate from rest to a minimum flying speed is the take-off run. This distance is determined by the average accelerating force acting on the airplane during the run. The relations involved are such that an exact solution is impossible.

The net accelerating force F is the difference between the thrust T and the total resistance D. The total resistance includes the rolling friction and the air resistance. A graphical solution may be obtained by calculating $F = T - D$ at various speeds from zero to the minimum flying speed. Since $V = dS/dt$ and $a = gF/W = dV/dt$, the speed divided by the corresponding acceleration is

$$V/a = dS/dV \qquad (322)$$

Hence, if V/a is plotted against V, the area under the curve is proportional to the run S. For example, assume that the plotting is to a scale where one inch along the axis of X equals a ΔV of 10 ft/sec, and one inch along the axis of Y equals a $\Delta(V/a)$ of 2.0 sec, then each square inch under the curve will represent 2 sec × 10 ft/sec = 20 ft. The area under the curve may be obtained by the trapezoidal rule or by planimeter.

The approximate value of the take-off run may also be obtained by the use of a coefficient that allows for the type of thrust curve applying to the airplane in question. It may be shown[1] that the distance run in a calm to attain a speed V is

$$S_0 = K_s\, V^2/(T_1/W) \qquad (323)$$

---

[1] W. S. Diehl, "The Calculation of Take-Off Run," N.A.C.A. T.R. No. 450 (1932).

where K_s is the take-off coefficient depending on the ratio of the final net thrust T_r to the initial net thrust T_i as shown on Figure 213. W is the gross weight in pounds and V is the take-off speed in ft/sec.

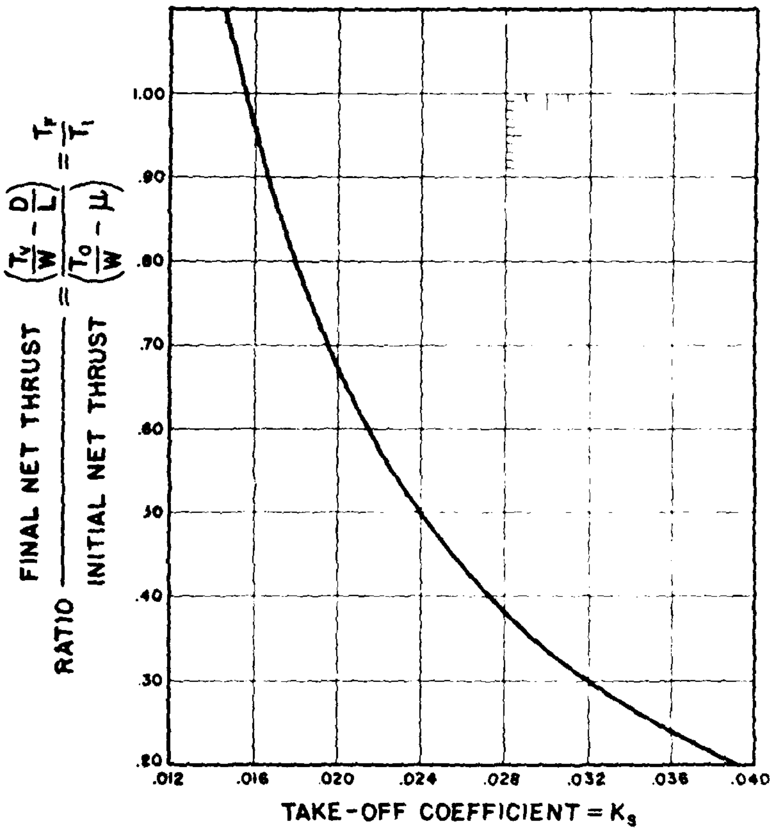

Figure 213. Take-off Coefficient K_s

The final net unit thrust is given by

$$T_F/W = T_v/W - (D/L) \tag{324}$$

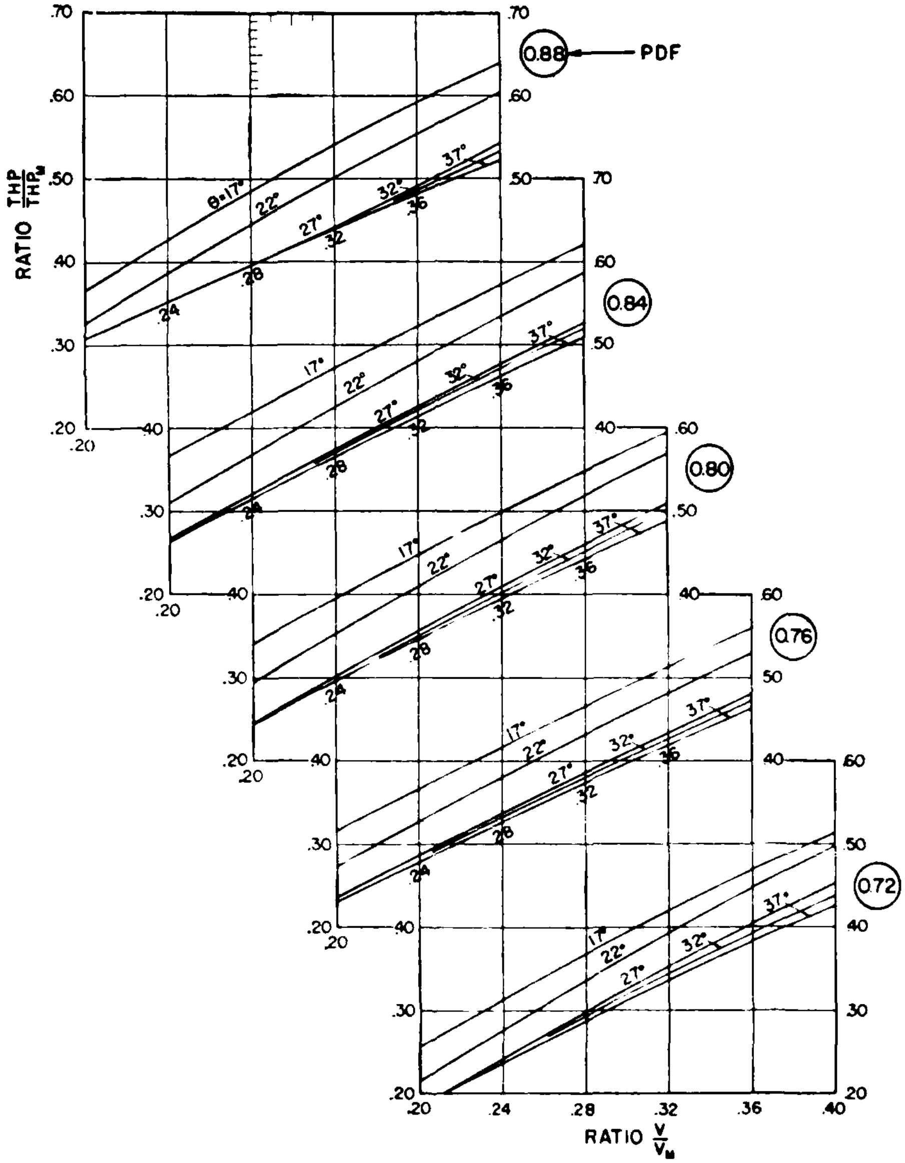

Figure 214. thp/thp$_M$ Curves for Use in Calculating Take-off Run. Fixed-Pitch Propeller

where T_v is the thrust at the speed V and D/L is the reciprocal of the L/D of the airplane at the average attitude held during the run. T_v may be found from

$$T_v = \frac{375\eta\ \text{bhp}_0}{V} \times \frac{\text{thp}}{\text{thp}_m} \tag{325}$$

where thp/thp_m is read from the appropriate curve on Figures 165 to 169. For convenience, the portions of these curves normally used in take-off are given on Figure 214.

The initial net unit thrust is

$$\frac{T_I}{W} = \frac{T_0}{W} - \mu \tag{326}$$

where μ is the coefficient of friction and T_0 is the static thrust. Values of μ are approximately:

Hard surface	$\mu = 0.02$
Good field, hard turf	0.04
Average field, short grass	0.05
Average field, long grass	0.10
Soft ground, gravel or sand	0.10 to 0.30

The static thrust T_0 is found from

$$T_0 = \frac{K_{T_0}\ \text{bhp}_0}{(\text{rpm})_0 \times (\text{diam})} \tag{239}$$

where the static thrust coefficient K_{T_0} is found from Figure 155. bhp_0 is the rated bhp at the rated rpm $= \text{rpm}_0$. K_{T_0} is a function of blade angle and blade setting. The static thrust may also be found from Figure 156.

Take-off Run with Controllable-Pitch Propeller. For a controllable-pitch propeller, the value of thp/thp_m for equation (325) is read from Figure 154. For convenience the portion of this curve normally used is given in Figure 215. The static thrust T_0 is based on the appropriate blade angle used in the low-pitch setting given by equation 238. Otherwise the procedure is exactly similar to that for a fixed-pitch propeller.

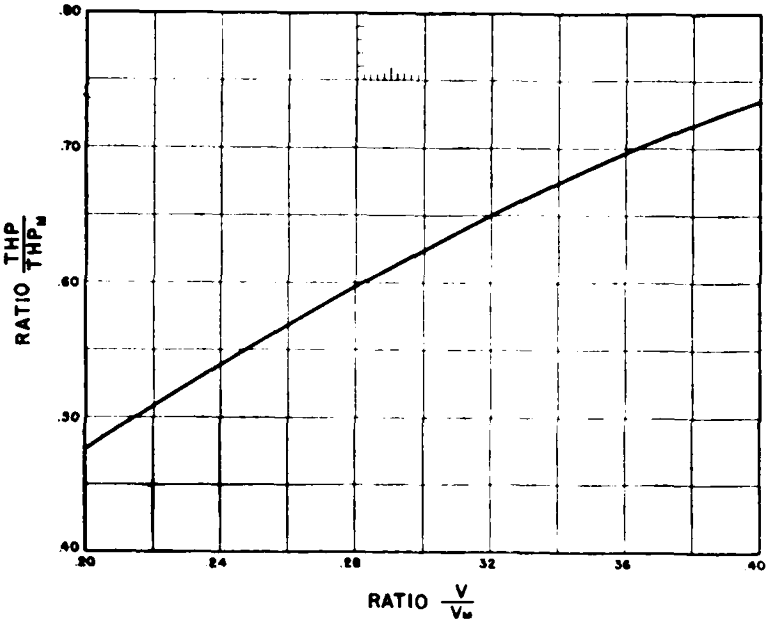

Figure 215. thp/thp$_m$ Curve for Use in Calculating Take-off Run. Controllable Pitch Propeller

For a two-position propeller, the maximum reduction in blade angle that can be used in take-off is a function of the maximum setting in flight. A plot of actual values of $\Delta\theta$ at 0.75 R gives

$$\Delta\theta \text{ at } 0.75\, R = -0.16\,\theta - 3 \tag{327}$$

Effect of Wind on Take-off Run. The effect of wind on the ground run appears to depend only on the ratio V_w/V_s as shown on Figure 216.

Effect of Gross Weight on Ground Run. The effect of a change in gross weight is given by

$$\frac{S_1}{S_2} = F\left(\frac{W_1}{W_2}\right)^2 \tag{328}$$

where F is a factor allowing for the change in K. The value of F depends on the ratios T_F/T_I and W_1/W_2 as

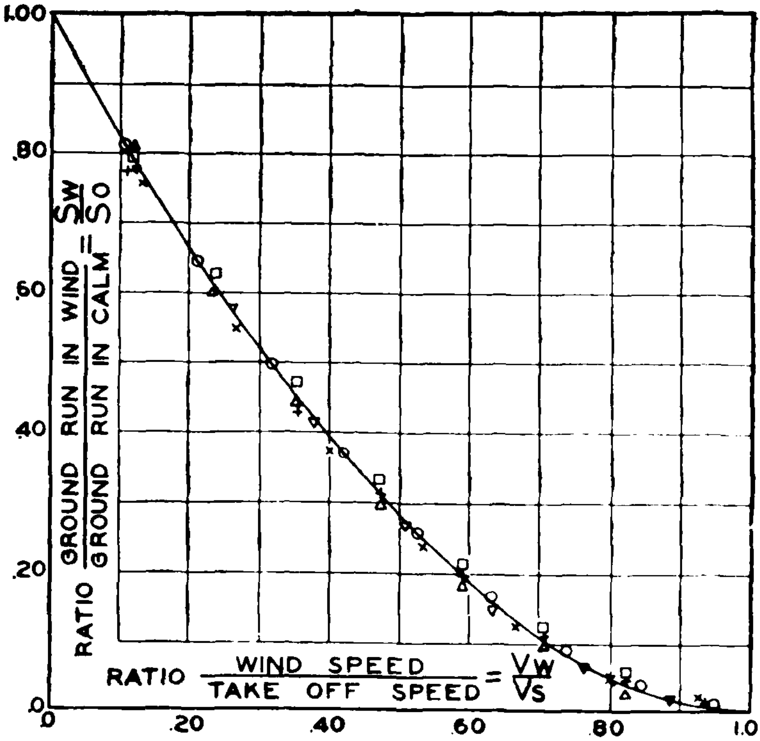

Figure 216. General Curve of Effect of Wind on Take-off Run

shown on Figure 217. For a small change in W and normal values of T_F/T_I, $F = 1.0$.

Effect of Change in Take-off Speed. The ground-run in a calm will vary substantially as the square of the take-off speed or

$$\frac{S_1}{S_2} = \left(\frac{V_1}{V_2}\right)^2 \qquad (329)$$

Effect of Altitude on Take-off Run. The increased stalling speed and decreased engine power at altitudes cause a rapid increase in take-off run with decrease in air density. The effect is approximately as indicated on the upper curve

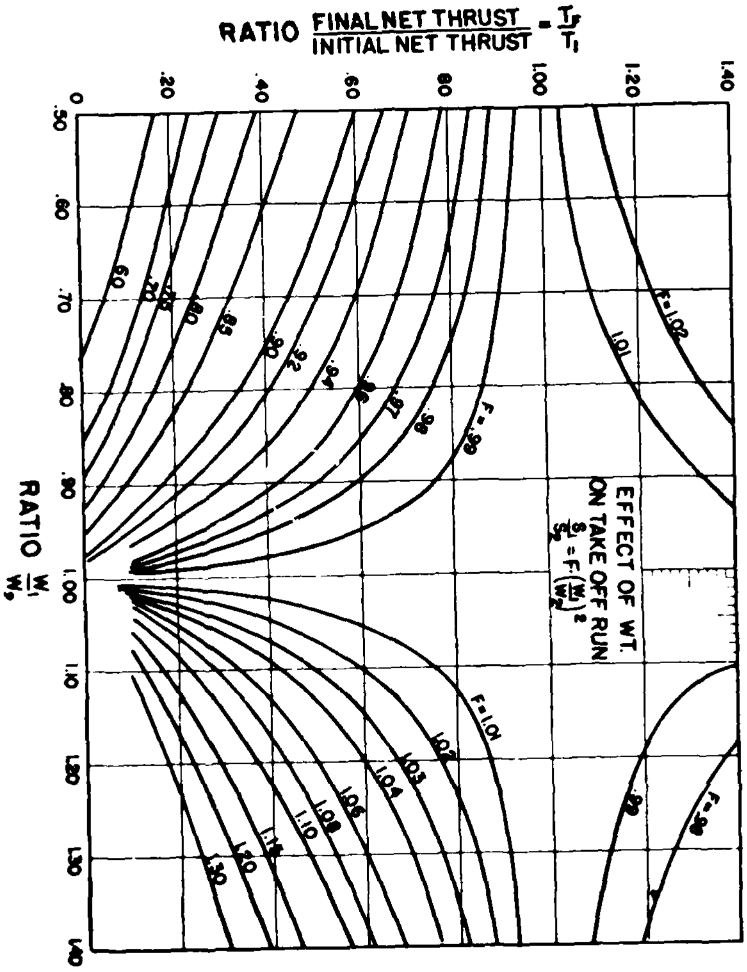

Figure 217. Change in Take-off Run Due to Change in Gross Weight

of Figure 218. The lower curve gives that part of the increase in run due to the increase in stalling speed and applies to a supercharged engine below its critical altitude. Above the critical altitude the variation will be in accordance with the upper curve.

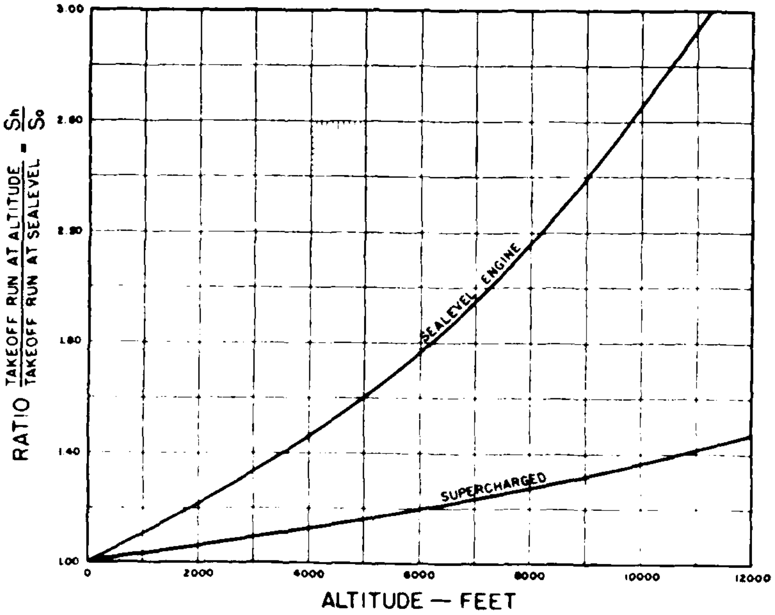

Figure 218. Effect of Altitude on Take-off Run

For example, the run for a sea-level engine is about 1.60 S_0 at 5000 ft and about 2.65 S_0 at 10,000 ft. The run for a supercharged engine with 5000 ft critical altitude is about 1.16 S_0 at 5000 ft and about

$$1.16 \times \frac{2.65}{1.60} S_0 = 1.92 S_0$$

at 10,000 ft.

Path Angle of Climb. The path angle of an airplane in a climb is given by

$$\theta = \sin^{-1} (V_c/V) \tag{330}$$

where V_c is the rate of climb and V is the speed along the flight path. V_c and V must be measured in the same units or a conversion factor will be required.

θ is normally less than 10° and very rarely greater than 15°. Hence, it is permissible to assume $\sin \theta = \tan \theta$ and obtain the maximum path angle by the graphical solution shown on Figure 219. In this figure the rates of climb in ft/min (based on Figure 175) are plotted against air speed in mph. The maximum path angle of climb is determined by the line from the origin tangent to the curve at the point

$$V_c = 1110 \text{ ft/min} = 18.5 \text{ ft/sec}$$

$$V = 74 \text{ mph} = 108.5 \text{ ft/sec}$$

from which

$$\sin \theta = 18.5/108.5 = 0.1705$$

or

$$\theta = 9° 49'$$

The maximum path angle of climb is obtained to a close approximation by using the rate of climb at the speed for minimum power.

Take-off Over an Obstacle. The distance required to take off and climb to a height h is obtained by addition of the take-off run and the distance required to climb to the height h. This distance required to climb to the height h must take into consideration the ground effect on induced power required, Figure 22.

The time of climb to a height h is greatly increased if the airplane is accelerating during the climb. The shortest distance for take-off run plus climb is obtained, in general, by take-off and steady climb at the speed for minimum power.

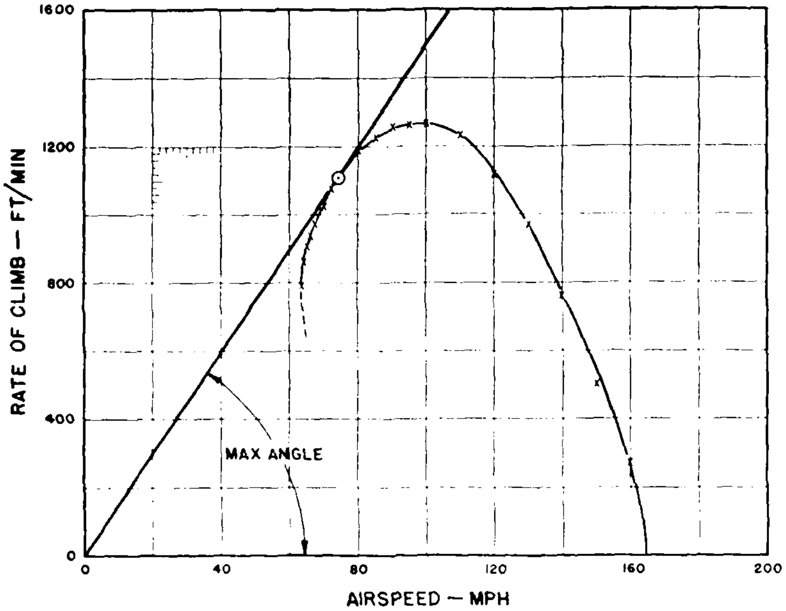

Figure 210. Graphical Solution of Maximum Path Angle of Climb

Gliding Angle. The gliding angle θ is obtained from the following:

$$\theta = \tan^{-1}\left(\frac{D}{L}\right) = \cot^{-1}\left(\frac{L}{D}\right) \qquad (331)$$

where D is the net drag and L is the lift. The minimum angle or glide for zero thrust corresponds to the maximum value of L/D.

Landing Over an Obstacle. The distance required for an airplane to come to a full stop, after clearing an obstacle h feet in height at the edge of a field, may be divided into three parts:

1. The glide, assumed at a constant speed and angle. x_1
2. Leveling off and losing speed at substantially constant height. x_2
3. Ground-run. x_3

The horizontal distance in the glide is simply

$$\begin{aligned} x_1 &= h \cot \theta \\ &= h \, (L/D) \end{aligned} \tag{332}$$

where θ is the glide angle and L/D is the overall value at the speed assumed. Normally this speed will be of the order $1.2\,V_S$. The value of L/D is greatly affected by flaps or other high-lift devices.

The second part of the landing can be obtained by a reasonably precise solution, but the assumptions necessary can hardly be justified. It appears more logical to admit an approximation that gives about the same accuracy with a direct solution. Such an approximation may be derived by assuming that the excess kinetic energy at the time of leveling off is being absorbed at an average rate. The speed during the glide and at the time of leveling off is $(V_S + \Delta V)$ and the kinetic energy to be absorbed is

$$\Delta(\text{KE}) = \frac{W}{g}\left(\frac{\Delta V}{V_S}\right) V_S^2 \tag{333}$$

The average speed will be $V_S + \frac{1}{2}\,\Delta V$ and energy will be absorbed at the average rate of $D\,(V_S + \frac{1}{2}\,\Delta V)$. Hence,

$$\begin{aligned} x_2 &= \frac{(W/g)\,(\Delta V/V_S)\,V_S^2\,(V_S + \frac{1}{2}\Delta V)}{D\,(V_S + \frac{1}{2}\Delta V)} \\ &= (1/g)\,(L/D)\,(\Delta V/V_S)\,V_S^2 \end{aligned} \tag{334}$$

where V_S is the stalling speed in ft/sec and L/D is the average value during the "floating" period, corrected for ground interference effect in accordance with the curves on Figure 220.

x_1 and x_2, as given by equations (332) and (334), are for zero wind. To find the effect of a given wind V_W, the time interval Δt must be obtained. For a head wind x_1 is reduced by the amount $V_W \cdot \Delta t_1$ and x_2 is reduced by the amount $V_W \cdot \Delta t_2$.

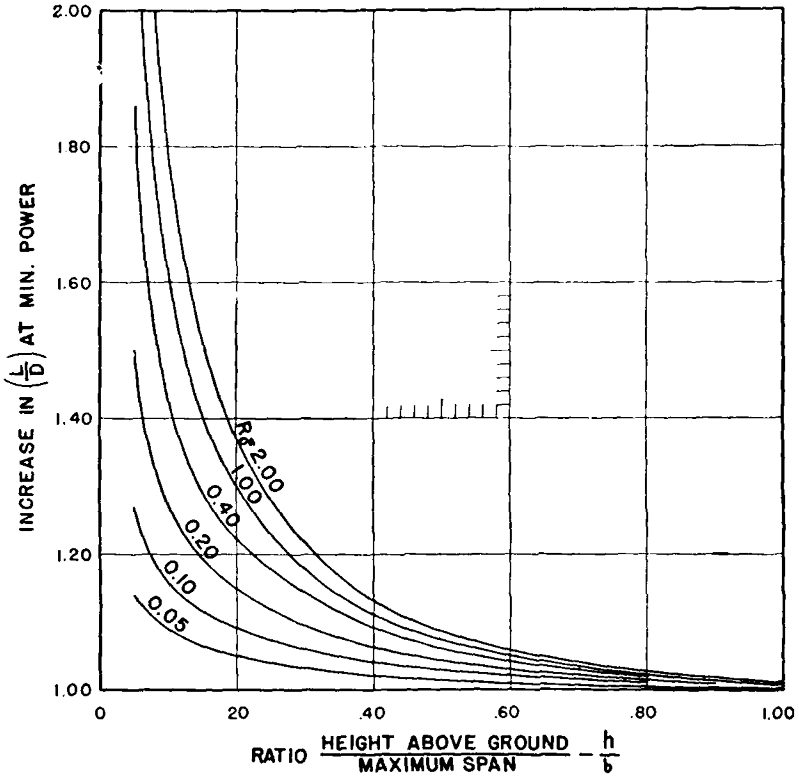

Figure 220. Ground Effect on L/D at Speed for Minimum Power

The ground-run x_3 is considered in the following section.

Landing Run. It may be shown[2] that the ground-run on landing is given by

$$S = \frac{V_L^2}{2g\left(\frac{D}{L} - \mu\right)} \log_e \left[\frac{D/L}{\mu}\right] \qquad (335)$$

where V_L is the landing speed in feet per second D/L the reciprocal of the L/D at the landing angle, and μ the coefficient of friction. The value of μ is higher than that in the take-off owing to the high value of the tail-skid drag. According to Glauert, the value of μ for the skid alone is 0.50, and the average effective value of μ for both skid and wheels is about 0.12. Obviously, this value is much affected by the shape of the skid and the load that it carries. Since there is considerable variation in landing speed according to the method of landing, a similar variation in run is to be expected.

The value of μ for a tail wheel is considered less than for a tail skid, but probably about twice that for the main wheels. The average effective value of μ for an airplane fitted with a tail wheel will be of the order of 0.06.

Figure 221 is a plot of S/V_L^2 against L/D and μ as calculated from equation (335). A study of this figure in connection with known landing runs leads to the conclusion that the average value of μ is probably between 0.06 and 0.10 and that the value of S/V_L^2 is normally between 0.10 and 0.20. The value of S/V_L^2 is considerably reduced by increasing the angle of attack of the wings when the skid or tail wheel is on the ground.

The landing run may be approximated by use of the average retardation during the run. For uniform retardation

$$S = V_L^2/2a \qquad (336)$$

where V_L is the landing speed in ft/sec, and a is the retardation in ft/sec/sec.

---

[2] H. Glauert, "The Landing of Airplanes," Br.A.C.A. R. & M. No. 666 (1920).

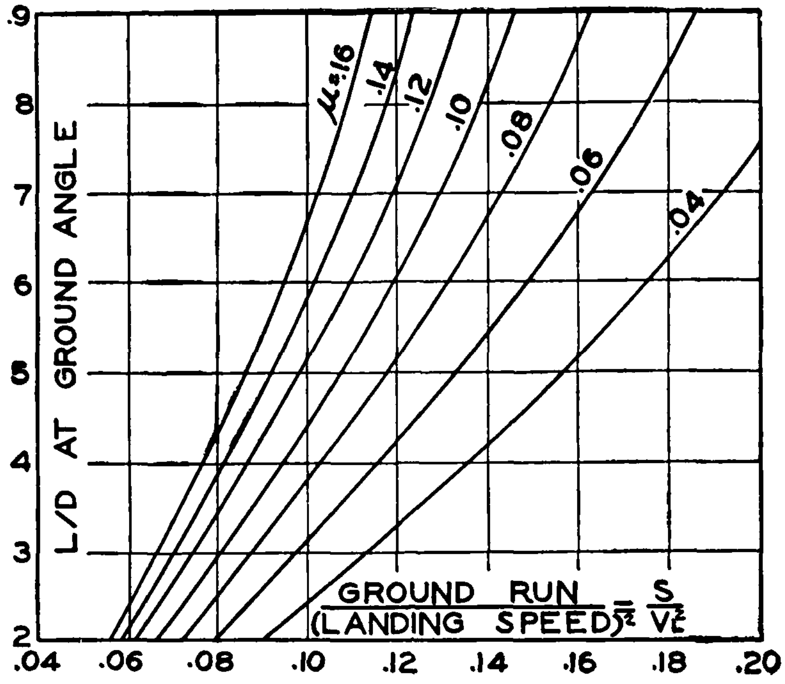

Figure 221. Relation Between Landing Run, Landing Speed, Coefficient of Friction, and L/D

The average values of a are approximately as follows:

	Tail Skid	Tail Wheel
Without brakes	3.5 – 4.7	2.7 – 3.7
With brakes	7.0 – 8.5	5.5 – 6.5

Sinking Speed. The conception of sinking speed is highly important in glider performance, although it is not often used in connection with airplane performance. It may be found approximately, either from the vertical component of the gliding velocity

$$V_z = V \tan \theta = V\,(D/L) \qquad (337)$$

or from the potential energy rate

$$V_z = \frac{550 \text{ thp}_r}{W} \text{ ft/sec} \tag{338}$$

where thp_r is the power required in horizontal flight and W is the gross weight. The exact value of V_z is obtained by equating the weight and the resultant air force

$$W = (L^2 + D^2)^{1/2} = C_R \rho S V^2/2$$

and substituting for V its equivalent

$$V = V_z (C_R/C_D)$$

to obtain

$$V_z = \left[\frac{2}{\rho} \frac{W}{S} \frac{C_D^2}{C_R^3}\right]^{\frac{1}{2}} \tag{339}$$

Terminal Velocity. The terminal velocity of any object in a free fall is reached when the air resistance is equal to the weight W. Assuming constant air density

$$V_T = \sqrt{W/K} \tag{340}$$

where K is a drag coefficient defined by $D = KV^2$. This equation applies when gravity and air resistance are the only forces. The motion that it represents is of interest in approximating the fall of any object except an airplane with rotating propeller. The effect of the propeller on a terminal velocity dive is given on page 450.

While the time required to attain the theoretical limiting velocity is infinite, the initial approach is very rapid. If the fall is from rest, the relation between velocity and time is

$$V = V_T \left[\frac{e^{at} - 1}{e^{at} + 1}\right] \tag{341}$$

where

$$a = 2g/V_T$$

The time required to attain any speed V is obtained by solving equation (341) for t, and is

$$t = \frac{V_T}{2g} \log_e \left[\frac{V_T + V}{V_T - V} \right] \tag{342}$$

The relation between velocity and altitude is

$$V = V_T \sqrt{1 - e^{-bh}} \tag{343}$$

where $b = 2g/V_T^2$ and h is the total altitude lost. If h is in feet and t is in seconds, V_T must be in ft/sec to determine a and b.

It is of interest to find how quickly speed is picked up in a fall. The relation between V, V_T, and h from equation (343) is:

V/V_T =	.2	4	.6	.8	.9	.95	.98
h/V_T^2 =	.00064	.0027	.00693	.0159	.0258	.0362	.0502

Terminal Velocity of an Airplane. The terminal velocity of an airplane depends on the gross weight W and the resultant drag coefficient C_{DR}. The value of C_{DR} depends on the propeller operating conditions in the dive.

Terminal velocity for any given engine rpm may be obtained graphically in a manner somewhat similar to the usual solution for maximum speed if, instead of curves of power required and power available, use is made of two types of drag coefficient curves plotted against speed as in Figure 222. The basic curve, which is analogous to the curve of power required, is simply a plot of C_D against V as obtained from the relation

$$W = D = C_{DR}\, q\, S$$

or

$$C_{DR} = W/qS \tag{344}$$

This curve gives the value of C_D that corresponds to any speed and since C_{DR} varies inversely with V^2, it is an hyperbola. It depends only on weight and wing area and not on any aerodynamic characteristics.

The second curve, whose intersection with the first gives the terminal velocity, must combine propeller and airplane characteristics. Such a curve, analogous to the usual power-available curve, is readily obtained. The actual C_{DA} for the airplane without propeller is known from

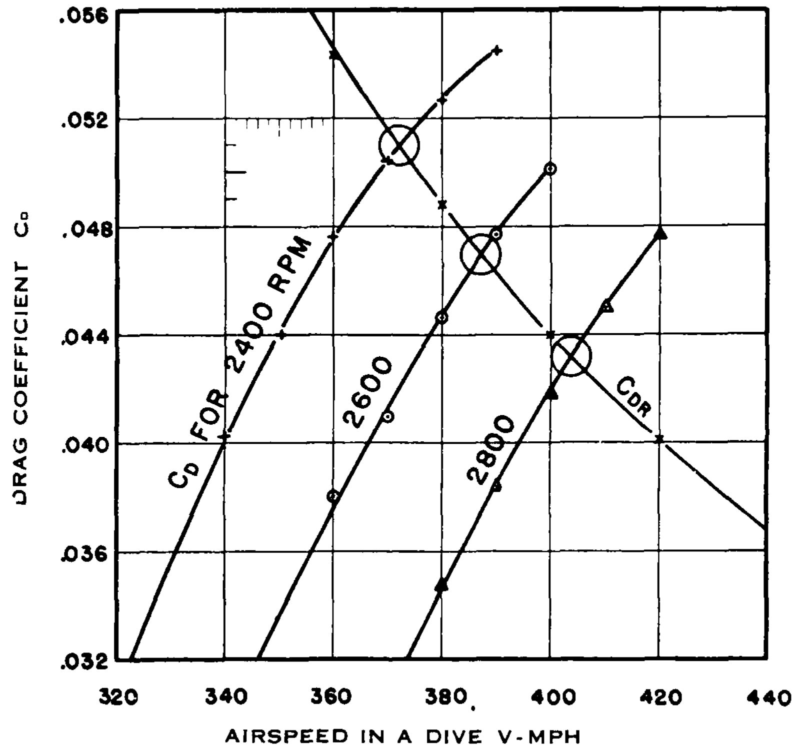

Figure 222. Graphical Solution for Terminal Velocity

a summary of the parasite drag, from wind-tunnel tests or to a fair approximation from flight tests. If the propeller thrust at a given rpm and at various speeds is converted to an equivalent drag coefficient, C_{D_r}, the addition of this equivalent drag coefficient and the airplane drag coefficient gives at each speed the total drag coefficient C_D or

$$C_D = C_{D_A} + C_{De} \qquad (345)$$

The intersection of the curves of C_D and C_{DR} give the terminal velocity at the assumed rpm. Similar curves of C_D may be calculated for other values of rpm as required.

The conversion of the effective thrust to an equivalent drag coefficient is based on the standard thrust equations

$$T = C_T \rho n^2 D^4 \qquad (208)$$

from which

$$C_{De} = \frac{T}{qS} = \frac{2C_T \rho n^2 D^4}{\rho S V^2} = \frac{2C_T D^2}{S(V/nD)^2} \qquad (346)$$

or

$$T = C_T' \rho V^2 D^2 = T_c \, \rho V^2 D^2 \qquad (209)$$

from which

$$C_{De} = \frac{2T_c \rho V^2 D^2}{\rho S V^2} = \frac{2T_c D^2}{S} \qquad (347)$$

The values of T_c are obtained from the propeller curves using the values of V/nD determined from assumed values of V and n.

The Terminal Velocity Dive. The motion of an airplane in a vertical dive may be studied by the use of a modified form of Wilson's equation,[3] incorporating a better approximation to the present standard atmosphere. If, instead of Wilson's equation 19, the change in pressure is taken as

$$\Delta P = 29.5 \log [1 + (h/26{,}900)] \qquad (348)$$

the equation of motion becomes

$$V^2 = \frac{1{,}730{,}960}{(n-1)}\left[1 + \frac{h_2}{26{,}900}\right]^n \times \left[\left(1 + \frac{h_2}{26{,}900}\right)^{1-n} - \left(1 + \frac{h_1}{26{,}900}\right)^{1-n}\right] \qquad (349)$$

---

[3] E. B. Wilson, "Aeronautics" (Ch. IV, Equation 20) John Wiley & Sons (1920).

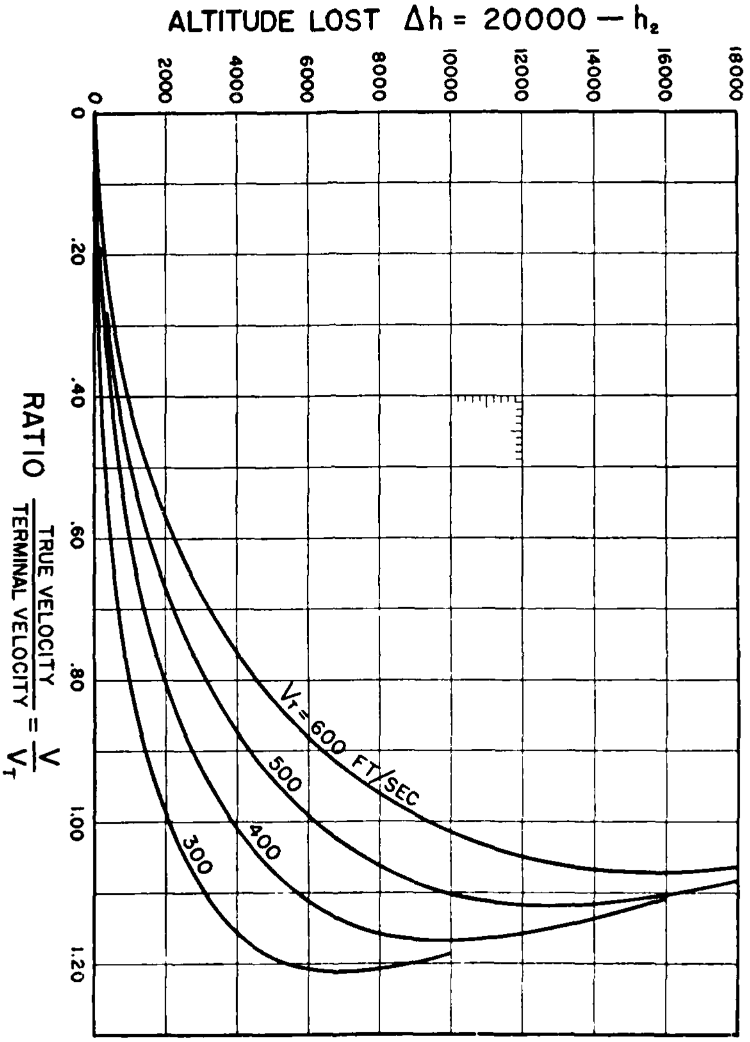

Figure 223. Relation Between True Velocity and Altitude for Terminal Velocity Dives Starting at 20,000 Feet

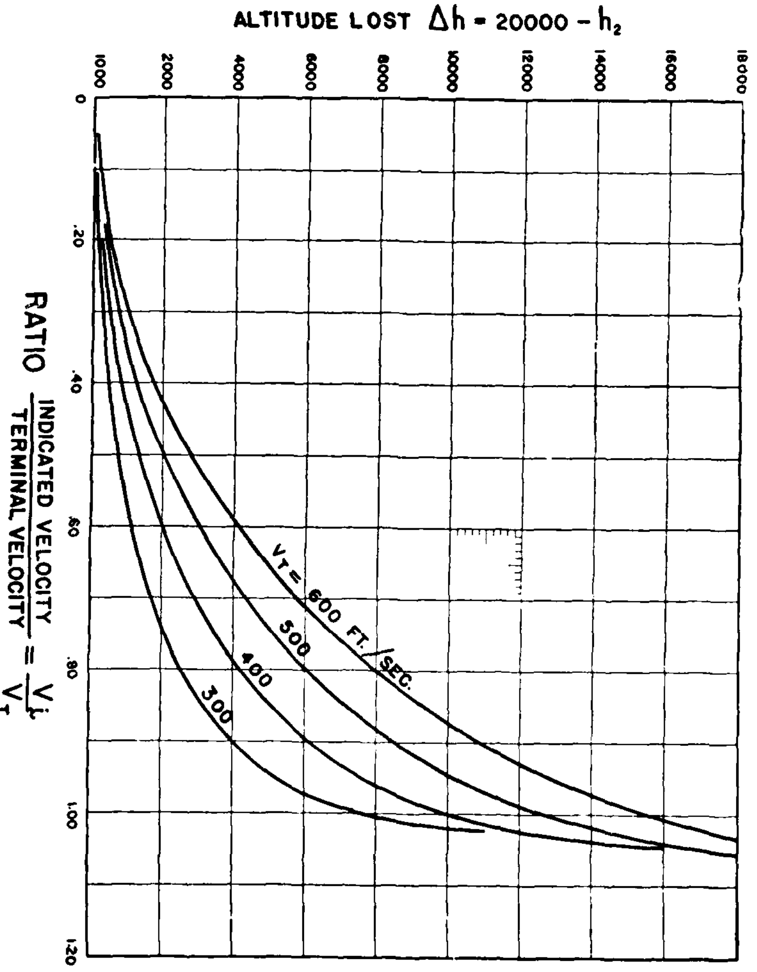

Figure 224. Relation Between Indicated Velocity and Altitude for Terminal Velocity Dives Starting at 20,000 Feet

where V is the air speed in ft/sec at the altitude h_2 in a dive started from V_0 at the altitude h_1. V_T is the terminal velocity in air of standard density. The value of the exponent n is

$$n = [1325/V_T]^2 \tag{350}$$

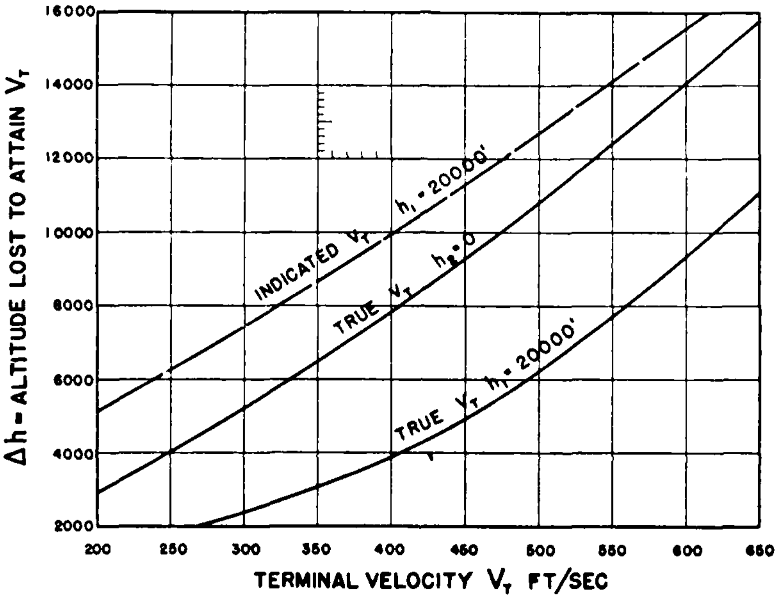

Figure 225. Altitude-Loss Required to Attain Terminal Velocity in a Vertical Dive

Equation (349) has been solved for a systematic series in values of h_1, h_2, and V_T. The variation in the ratio V/V_T with altitude lost in a dive from h_1 = 20,000 ft is given in Figure 223. This figure shows clearly how the true velocity reaches a maximum well in excess of the terminal value and then slows up due to the increasing air density. The ratio of indicated velocity to terminal velocity in a dive starting from h_1 = 20,000 ft is given on Figure 224. The length of dive necessary to attain a given indicated or true speed equal to the terminal velocity

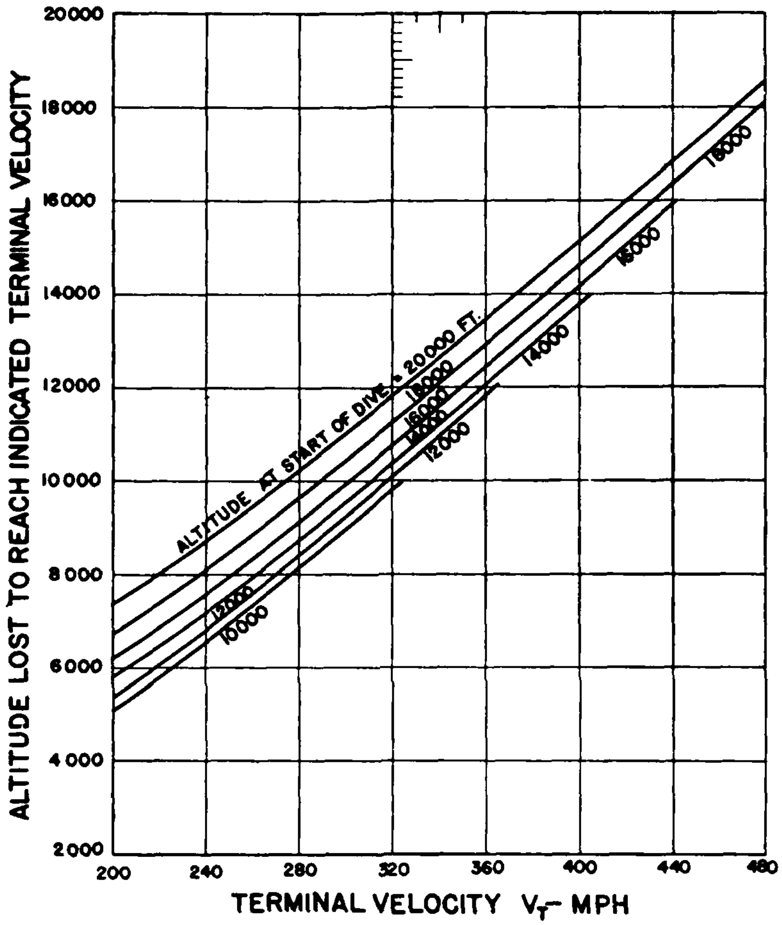

Figure 226. Altitude-Loss Required to Attain Indicated Terminal Velocity in a Vertical Dive

may be read from Figure 225. The upper curve on this figure gives the length of dive, starting at 20,000 ft, to attain the indicated terminal velocity. The lower curve gives the length of dive required from 20,000 ft to attain a true speed equal to the terminal velocity. The middle curve gives the elevation above which the dive must be started if terminal velocity is to be reached above sea-level.

Figure 226 gives the altitude lost to reach indicated terminal velocity in a dive starting from various altitudes.

An approximate value of the terminal velocity may be determined from a short dive by the use of Figure 227. For example, a velocity of 260 mph at 10,000 ft in a dive

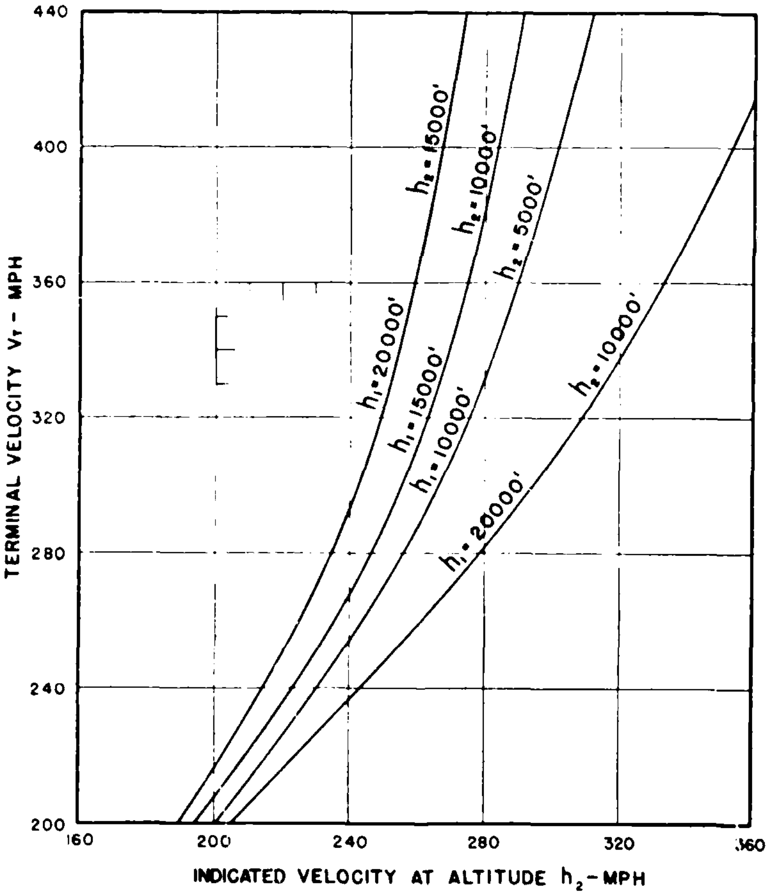

Figure 227. Determination of Approximate Terminal Velocity from a Short Vertical Dive

started at 15,000 ft indicates a terminal velocity of 312 mph.

Effect of Dive Angle on Terminal Velocity. The effect of flight path inclination[4] depends to a certain extent on the engine and propeller characteristics, but, in general, it is given closely by

$$\frac{V_T(\theta^\circ \text{ dive})}{V_T(90^\circ \text{ dive})} = \sqrt{\sin\theta} \tag{351}$$

---

[4] W. S. Diehl, "The Effect of Flight Path Inclination on Airplane Velocity." N.A.C.A. T.R. No. 238 (1926).

CHAPTER 15

SPECIAL FLIGHT PROBLEMS

There are a number of problems of considerable interest and some practical value connected with special flight conditions. For most solutions, extreme accuracy is not required, and reasonable simplifying assumptions are allowable. A few of the more important problems in this class will be outlined briefly.

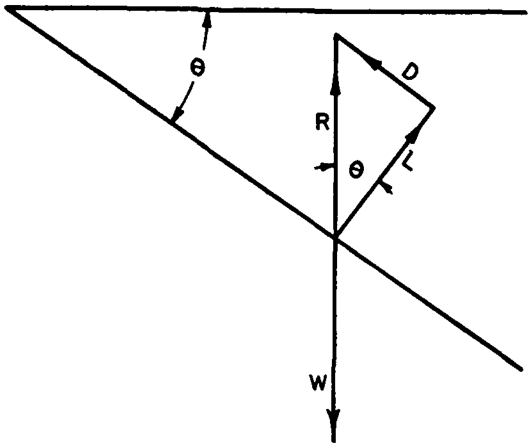

Figure 228. Equilibrium in a Glide Without Power

Gliding Flight Without Power. For equilibrium in a glide without power, at an angle θ to the horizontal, the forces are the lift L, the drag D, the resultant air force R, and the weight W, as shown in Figure 228. These forces are connected by the relations

$$\sqrt{L^2 + D^2} = R = W \tag{352}$$
$$W \sin \theta = D \tag{353}$$
$$W \cos \theta = L \tag{354}$$
$$L \cos \theta + D \sin \theta = W \tag{355}$$
$$L \sin \theta = D \cos \theta \tag{356}$$

Equation (356) is equivalent to

$$L/D = \cot \theta \tag{357}$$

Gliding Flight With Power. Assuming that the thrust T acts along the flight path and letting the angle θ between the flight path and the horizontal be positive upward, the equations of equilibrium are

$$T - W \sin \theta = D \tag{358}$$
$$L \cos \theta - (D - T) \sin \theta = W \tag{359}$$

and

$$L \sin \theta = (D - T) \cos \theta \tag{360}$$

The inclination of the thrust to the flight path may be allowed for, but little is to be gained in accuracy.

Assuming that the thrust varies inversely with velocity and that the drag is $D = KV^2$, it may be shown[1] that the velocity along the flight path is

$$V = V_M\left[-\tfrac{1}{2} + \sqrt{2.25 - (L/D)_0 \sin \theta}\right] \tag{361}$$

if the thrust at $V = 2V_M$ is zero. This condition applies to propellers of low pitch/diameter ratio. For propellers of high pitch/diameter ratio the thrust holds up better. Assuming that $T = T_0/2$ when $V = 2V_M$ (T_0 = thrust at $V = V_M$) the velocity along the flight path is

$$V = V_M\left[-\tfrac{1}{4} + \sqrt{1.5625 - (L/D)_0 \sin \theta}\right] \tag{362}$$

In these equations $(L/D)_0$ is the value of L/D for the airplane at the maximum horizontal speed V_M and has the value

$$\left(\frac{L}{D}\right)_0 = \frac{V_M}{375\eta} \cdot \frac{W}{\text{bhp}} \tag{363}$$

---

[1] W. S. Diehl, "The Effect of Flight Path Inclination on Airplane Velocity," N.A.C.A. Technical Report No. 238.

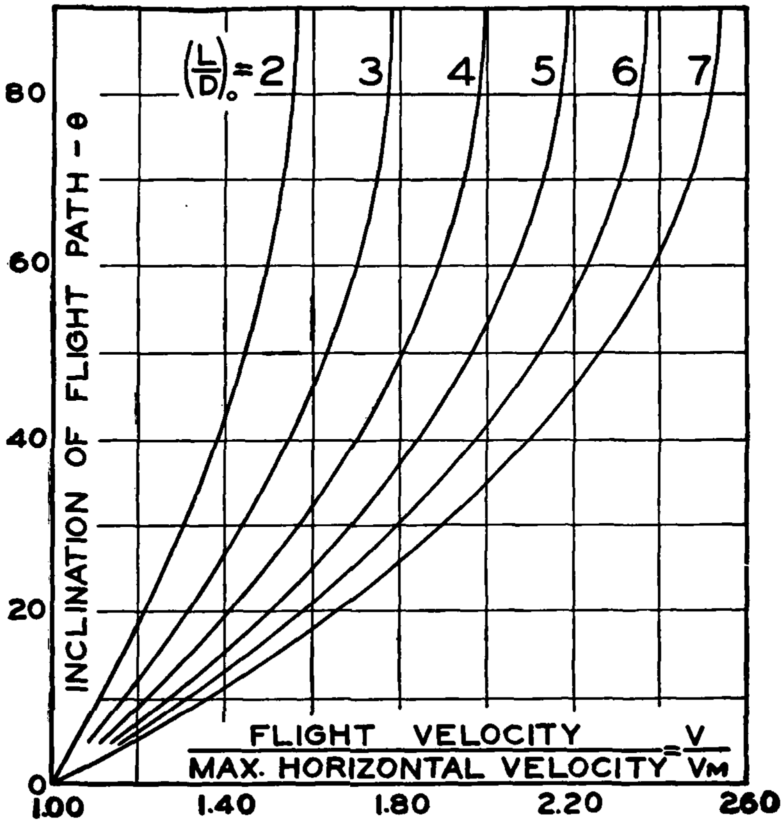

Figure 229. Air Speed in a Dive with Power On. Thrust Zero at $V = 2V_M$

$(L/D)_0$ has no direct relation to the maximum value of L/D. Figure 229 is a plot of V/V_M against θ for various values of $(L/D)_0$ according to equation (361), and Figure 230 is a similar plot according to equation (362). The effect of thrust on diving speed is comparatively small.

Circling Flight. For equilibrium in a horizontal turn, the weight must be balanced by the vertical component of the lift and the centrifugal force must be balanced by the horizontal component of the lift. If φ is the angle of bank, the equations for equilibrium are

$$W = L \cos \varphi \tag{364}$$

and

$$\text{centrifugal force} = \frac{WV_t^2}{gr} = L \sin \varphi \tag{365}$$

from which

$$\tan \varphi = \frac{V_t^2}{gr} \tag{366}$$

V_t and r must be consistent units, e.g., ft/sec and feet. Since W is constant, L must vary as secant φ and the acceleration in a turn is

$$a/g = L/W = \sec \varphi \tag{367}$$

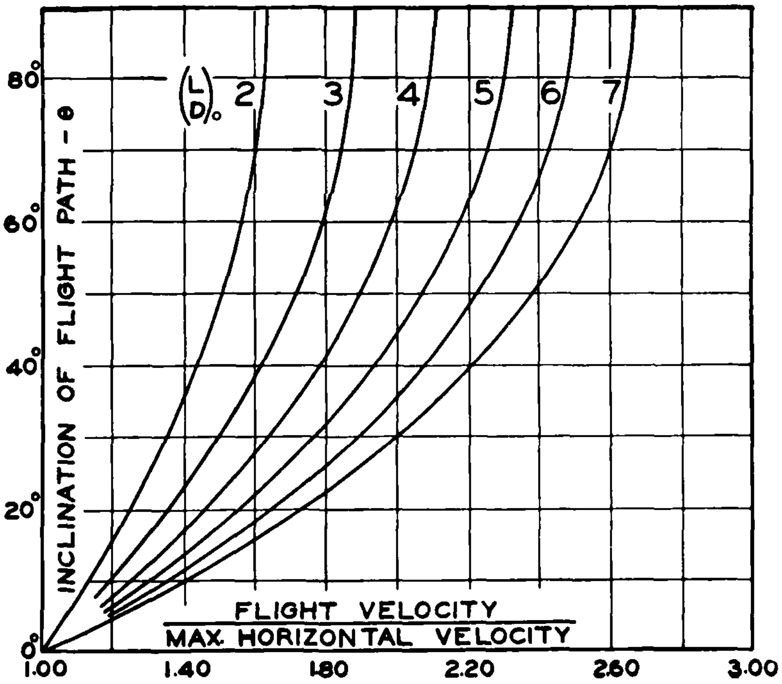

Figure 230. Air Speed in a Dive with Power On. $T = T_0/2$ at $V = 2V_M$

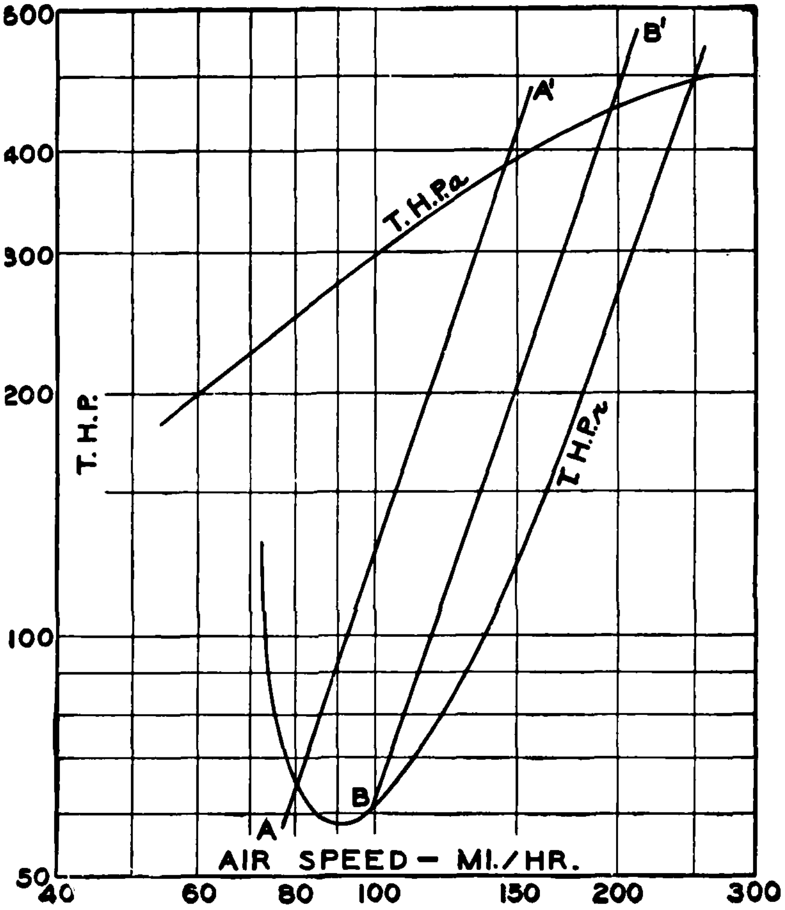

Figure 231. Graphical Solution for Speed in a Turn

Since L varies as V^2, the relation between the speed in straight horizontal flight and the speed in a turn at constant lift coefficient or angle of attack is

$$(V_t/V)^2 = \sec\varphi \tag{368}$$

At constant lift coefficient, or angle of attack, the drag will vary as V^2 and the thrust horsepower required as V^3. If curves of thp available and thp required are plotted against velocity on logarithmic scales as in Figure 231, the solution for minimum radius of turn at any given lift coefficient is made very simple. The power required varies as V^3, along straight lines **AA′** and **BB′**. The intersection of such a line with the curve thp_a gives the maximum air speed at which turning flight can be made with the initial lift coefficient. Consider the line **BB′**. **B** is at 100 mph and **B′** at 192 mph. Hence the angle of bank is

$$\sec\varphi = (V_t/V)^2 = (192/100)^2 = 3.68$$

or

$$\varphi = 74^\circ\, 13'$$

from equation (366) the radius of the turn is

$$r = \frac{V_t^2}{g}\cot\varphi = \frac{(192 \times 1.467)^2}{32.2} \times 0.282 = 695 \text{ ft}$$

This process may be repeated for as many points, lift coefficients, speeds, or angles of attack, as desired. The results may be listed as in Table 25.

If the time required to turn through a given angle is calculated, it is found that the minimum time corresponds with the maximum bank. The foregoing data are based on the wind-tunnel tests of a 1924 racing airplane.

"Squashing" in a turn is due to an attempt to fly under a condition requiring more power than is available. For example, any shorter radius of turn than 422 ft at $\alpha = 18^\circ$, in the case calculated above, will require more power than is available and the airplane will lose flying speed and

TABLE 25. CALCULATIONS FOR AIR SPEED IN A TURN

Angle of Attack Degrees	Air Speed in mph		Angle of Bank φ deg - min	Radius of Turn ft
	Horizontal Flight	In a Turn		
1	198.2	250.0	51 - 06	3,370
2	166.8	244.7	62 - 22	2,100
4	130.3	227.5	70 - 52	1,200
6	111.0	207.5	73 - 21	861
8	98.5	190.0	74 - 25	673
10	89.2	171.5	74 - 17	553
12	82.7	152.0	72 - 48	478
14	77.4	132.3	69 - 58	427
18	73.8	103.8	59 - 42	422
20	73.5	93.6	51 - 59	457

"squash" from centrifugal force since the centripetal force cannot be obtained from the reduced lift. The same condition exists in a pull-up from a dive. The lighter the load and wing loading and the greater the power, the more difficult to "squash" on a turn. High aspect ratio and low parasite resistance give low minimum power required and therefore reduce the tendency to "squash."

Spiral Gliding Flight. The spiral glide is a combination of gliding and circling, the path of the center of gravity being a true helix. If the angle of bank is φ and the helix angle is θ, then assuming that the radius r is large in comparison with the span, so that velocity over wings is substantially uniform, it follows that

$$L \cos \varphi \cos \theta + D \sin \theta = W \tag{369}$$

$$W \sin \theta = D \tag{370}$$

and

$$W \cos \theta = L \cos \varphi \tag{371}$$

from which

$$\frac{L}{D} = \frac{\cot \theta}{\cos \varphi} \tag{372}$$

which reduces to $L/D = \cot\theta$, equation (357), when the angle of bank $\varphi = 0$, that is, in a straight glide.

The proper angle of bank is determined as in simple circling flight by the balancing of the centrifugal force with the radial component of lift. That is

$$\text{centrifugal force} = \frac{WV_t^2 \cos^2\theta}{gr} = L \cos\theta \sin\varphi \qquad (373)$$

which reduces to equation (365) when $\theta = 0$.

Effect of a Diving Start on Speed over a Measured Course. If an airplane is dived at high speed and pulled out into level flight, it will have a speed in excess of that which can be maintained in horizontal flight. If a high-speed flight is made over a measured course after a diving start, the speed will asymptotically approach the normal maximum, and the average over the course will be greater than the normal maximum. This method was formerly used extensively in races, and sometimes by test pilots in order to get the maximum speed possible.

Assuming that the propeller thrust is constant and the flight over the course is at constant altitude, the effect of a diving start on the average speed may be calculated.[2] The speed at any time t is

$$V = \frac{C_1 e^{at} + C_2}{C_3 e^{at} + C_4} \qquad (374)$$

and the distance flown is

$$S = \frac{W}{gK} \log_e \left[\frac{C_3 e^{at} + C_4}{2\sqrt{TK}} \right] - V_0 t \qquad (375)$$

where V_0 is the speed (ft/sec) at the time of crossing the starting line ($t = t_0$), V the speed at time t, S the distance flown in t seconds, W the gross weight, T the thrust at normal maximum speed V_M, and K the drag coefficient, $K = T/V_M^2$. The other constants have the value:

---

[2] W. S. Diehl, "The Effect of a Diving Start on Airplane Speed," N.A.C.A. Technical Report No. 228 (1925).

$$C_1 = T + V_0\sqrt{TK}$$
$$C_2 = V_0\sqrt{TK} - T$$
$$C_3 = \sqrt{TK} + KV_0$$
$$C_4 = \sqrt{TK} - KV_0$$

and $$a = \frac{2g\sqrt{TK}}{W}$$

The persistence of excess velocity depends largely on the value of a which does not vary over as wide a range as might be expected. Representative values for various types of airplanes are:

Type	W lb	V_M mph	a
Racing	2,100	250	.050
Pursuit	2,800	160	.046
Observation	2,300	125	.076
Bomber	7,000	120	.101

A racing or pursuit airplane requires about two minutes to settle down to normal speed after a diving start and a 10% increase in velocity at the start of a one-mile course will give about 6% increase over the normal maximum speed.

The Zoom. A number of special problems involve the conversion of kinetic energy to potential energy or vice-versa. A simple problem of this class is to find the altitude that can be gained in a zoom from horizontal flight. In this case there is a loss of kinetic energy $\Delta K = (W/2g) \times (V_1^2 - V_2^2)$ and a gain in potential energy of $W \cdot h$. Neglecting the effect of the propeller during the zoom, the gain in altitude is

$$h = (V_1^2 - V_2^2)/2g \tag{376}$$

where V_1 is the initial velocity in horizontal flight and V_2 is the leveling off velocity. V_1 and V_2 should be in ft/sec.

CHAPTER 16

FUNDAMENTAL DESIGN CONSIDERATIONS

Fundamental Design Considerations. The fundamental design characteristics are aspect ratio *n*, parasite drag coefficient C_{DP_0}, stalling speed V_S (or wing loading w_s), and power loading w_p. These characteristics determine the performance of the airplane. It is desirable that the relative importance of these factors be known if the best compromise design is to be obtained.

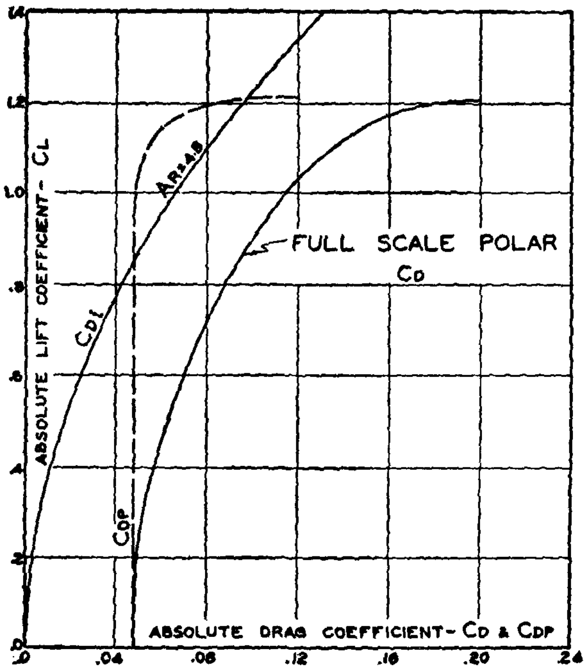

Figure 232. Full-Scale Polar for VE-7 Airplane

Owing to the excessive amount of calculating required, it has been found impracticable to cover more than a few points on this phase of airplane design. The data comprising the remainder of this chapter are presented simply as an indication of the approximate effects to be expected from basic design changes.

Some General Effects of Aspect Ratio and Parasite Drag. Aspect ratio and parasite drag are of fundamental importance in determining many items of airplane performance. While some of the theoretical relations involving these two parameters have been given in Chapter 12, the relative influence and importance may best be demon-

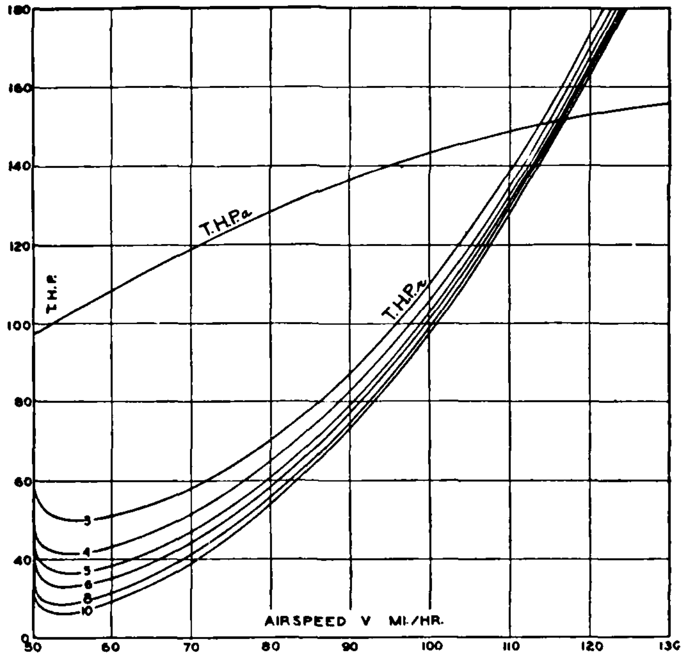

Figure 233. Curves of Power Required at Sea-Level for Various Aspect Ratios with Normal Parasite

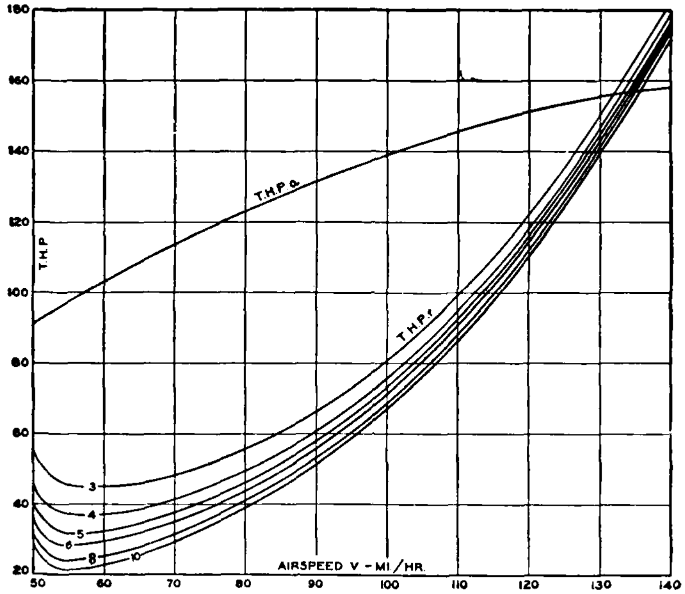

Figure 234. Curves of Power Required at Sea-Level for Various Aspect Ratios with Low Parasite

strated by comparative performance data on a series of fictitious airplanes in which no other variable is involved. A series of such calculations was made a number of years ago, using the VE-7 full-scale polar. Since the comparative results are independent of the airplane data supplying but one point of a network, there is no necessity for repeating the calculations using another polar.

The original VE-7 had a wing area of 290 sq ft of RAF-15 section. The aspect ratio was 4.8. With a gross load of 2230 lb the stalling speed was 50 mph. The full-scale polar from Durand and Lesley's tests[1] is given on Figure 232. Power curves have been calculated for aspect ratio values from 3 to 10 for $C_{DP_0} = 0.031$, 0.046 and 0.076 representing low, normal and high parasite. These power curves will be found on Figures 233, 234, and 235. The most striking characteristic shown by these curves is the small influence shown by aspect ratio at high speed. This is perhaps more clearly seen by the replotting of maximum speed against C_{DP_0} on Figure 236. The maximum speeds shown occur at $C_L = 0.2$ approximately. An even smaller effect would be obtained for a lower C_L at high speed and, of course, a much greater effect would be obtained for a high C_L at high speed corresponding to a very

---

[1] W. F. Durand and E. P. Lesley, "Comparison of Tests on Air Propellers in Flight with Wind-Tunnel Model Tests on Similar Forms," N.A.C.A. T.R. No. 220 (1925).

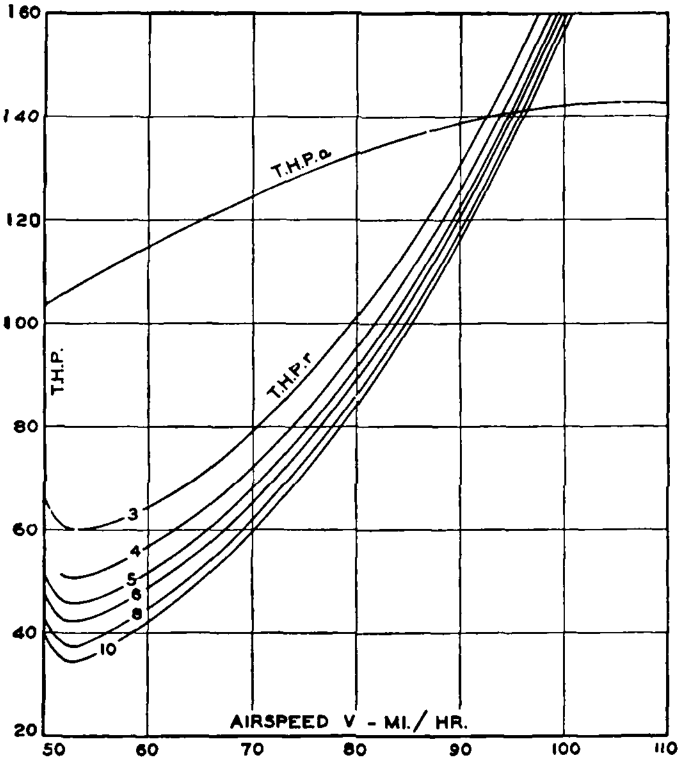

Figure 235. Curves of Power Required at Sea-Level for Various Aspect Ratios with High Parasite

heavily loaded airplane. This effect may be studied in more detail by reference to Figure 181.

The chief effect of aspect ratio is seen to be in the region of minimum power, where it has a profound influence on climb and ceiling, as shown by Figures 237 and 238.

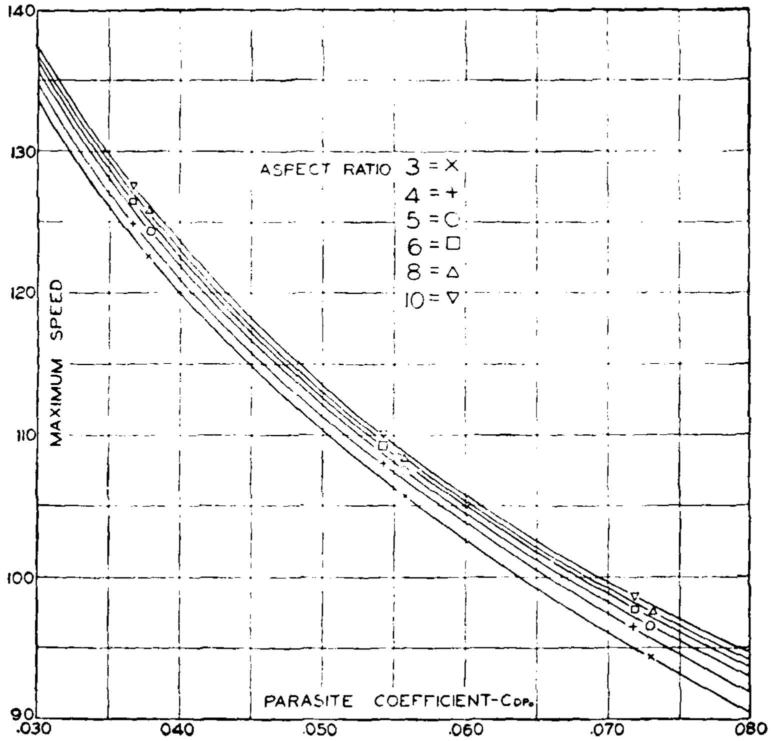

Figure 236. Comparative Effect of Aspect Ratio and Parasite on High Speed at Sea-Level

While the foregoing figures do not apply strictly except to the particular wing loading and power loading used, the type of variation shown will be very similar for any other set of values. Very high power or very low power loadings will reduce the spread between the curves of Figures 237 and 238. Very high power loadings magnify the effect and increase the spread. Hence, high aspect ratio is more important with high power loading than with low power loading. Low C_{DP_0} is always desired.

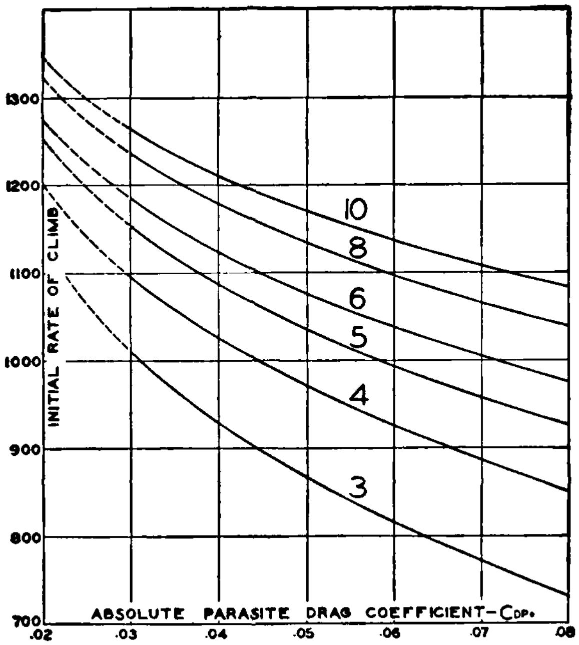

Figure 237. Comparative Effect of Aspect Ratio and Parasite on Initial Rate of Climb

Wing Area and Stalling Speed. Performance calculations have been made on a systematic series of fictitious airplanes in which wing area was the independent variable. Changing wing area, however, changes the tail area, the gross weight (with constant useful load), and the parasite drag coefficient. Starting with known performance data for an existing single-seater airplane, the aspect ratio was held constant at $n = 4.35$ and the necessary changes were made in gross weight and parasite drag to allow for the change in wing and tail area required at various stalling speeds. The series selected gave the performance indicated in Table 26.

The variation of climbing and maximum speeds with altitude is given on Figure 239. The variation of rate of climb with altitude is given on Figure 240. It is of particular interest to note that the advantages gained by reduced wing area are confined to low altitudes.

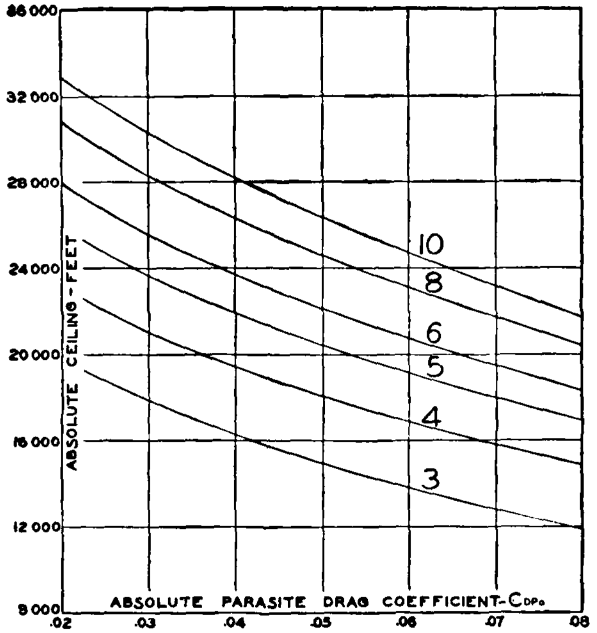

Figure 238. Comparative Effect of Aspect Ratio and Parasite on Absolute Ceiling

The variation in minimum radius of turn with altitude, Figure 241, leads to the curves shown on Figure 242, which appears to be a general relation holding for any unsupercharged engine, and by extrapolation from the critical altitude to sea-level it should also apply to a supercharged engine. Figure 241 shows the penalty that must be paid in loss of maneuverability at high altitude when the wings are clipped to increase the maximum speed of an airplane at low altitudes.

The maneuverability of an airplane is an indefinite characteristic depending on a number of factors such as absolute and relative control forces, angular accelerations, and angular velocities. It does not appear practicable to

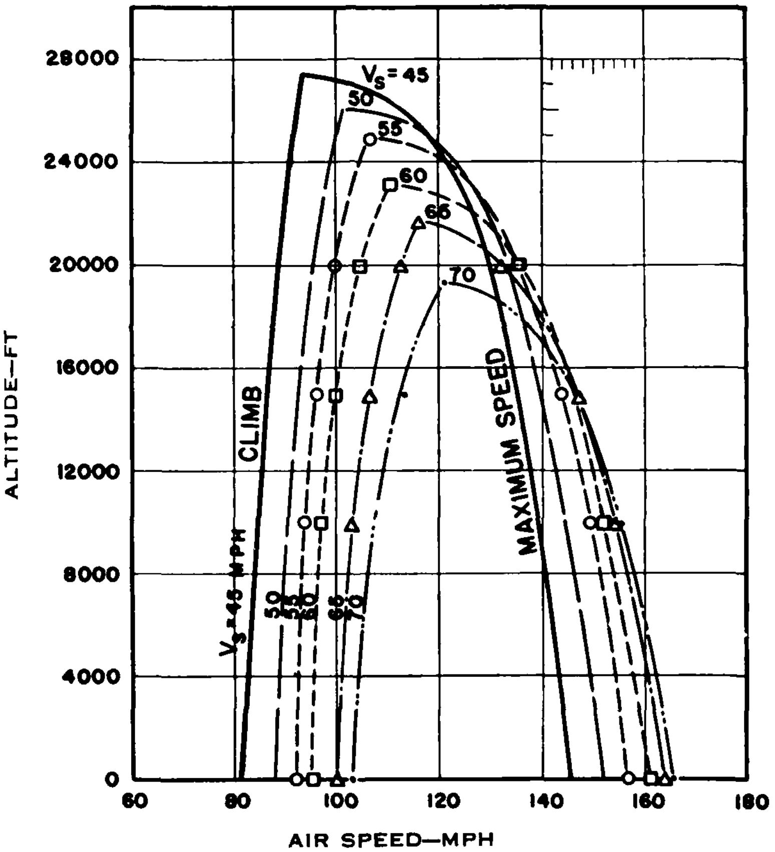

Figure 239. Effect of Wing Area on Speeds at Altitude

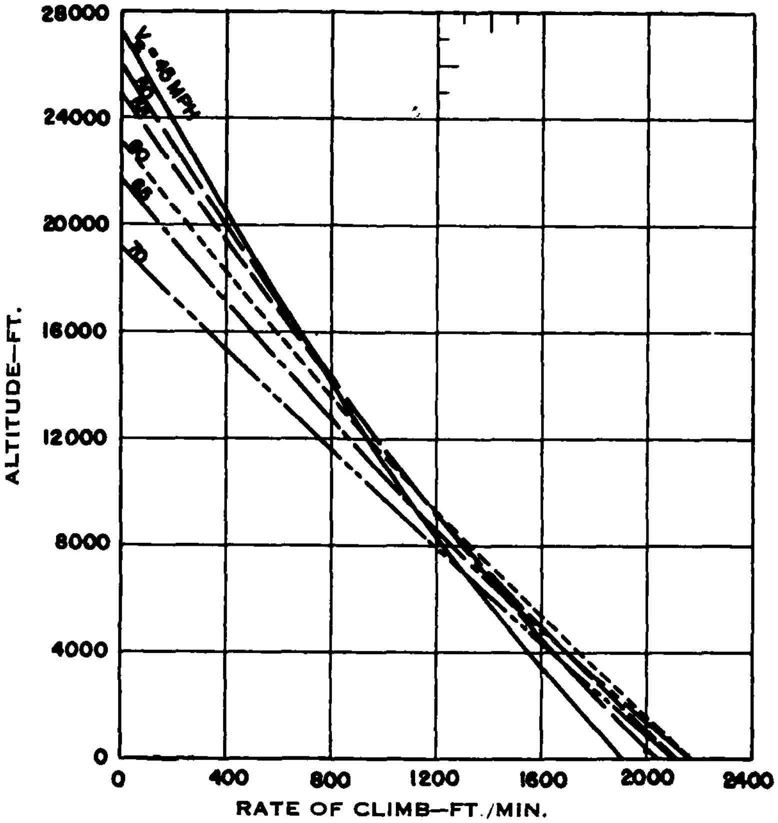

Figure 240. Effect of Wing Area on Rate of Climb at Altitude

give a definition of absolute maneuverability, but a measure of the inherent possibilities in a given airplane design might be taken as

$$M = \frac{C}{r}\left(\frac{V_M}{V_S}\right) \qquad (377)$$

where C is the rate of climb, r is the minimum radius of turn, V_M is the maximum speed and V_S is the stalling speed. M has the dimension of T^{-1} as required from general con-

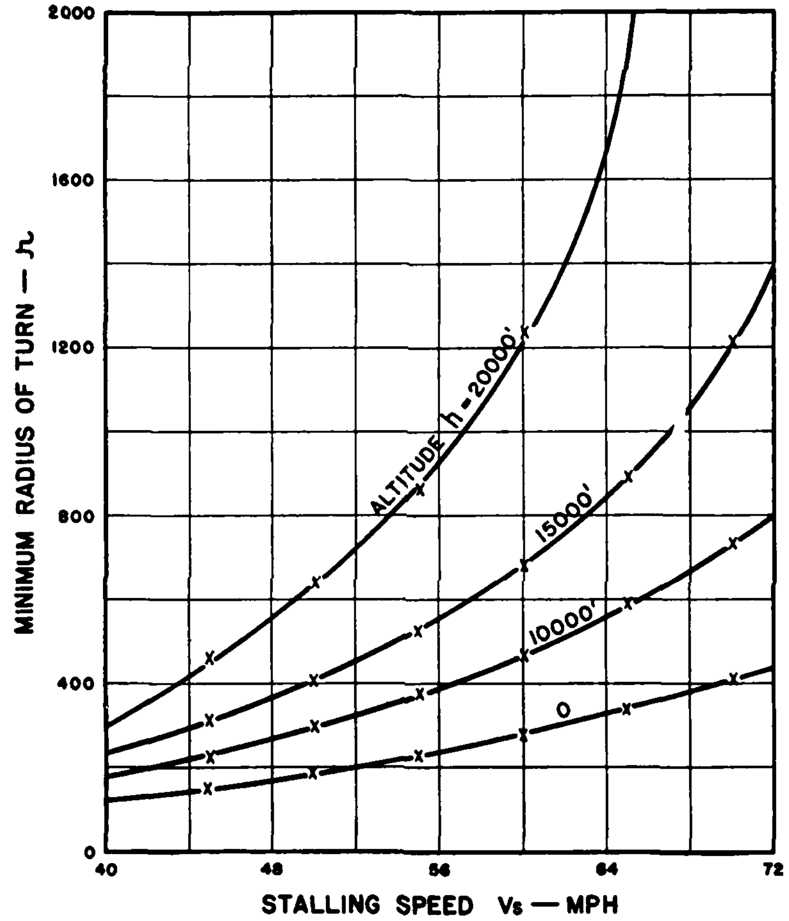

Figure 241. Effect of Wing Area on Minimum Radius of Turn at Various Altitudes

siderations. Values of *M* are plotted against altitude on Figure 243. These values plot on a single non-dimensional curve as in Figure 244, showing that the variation of *M* with relative altitude is the same for all of the airplanes in this series.

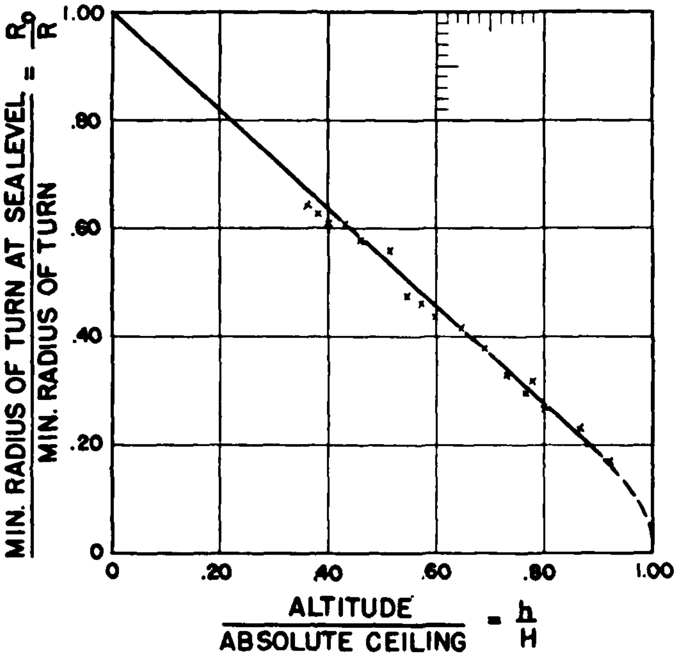

Figure 242. Variation of Minimum Radius of Turn with Altitude

If, instead of the arbitrary factor *M*, the measure of maneuverability is taken as the time required for a 360-degree turn, the comparison will be substantially unaltered, as may be seen by study of Figure 245.

All of the foregoing comparison has been on the basis of constant aspect ratio and constant power. It is obvious that if any advantage is to be obtained from reduced wing area, the reduction in area must not increase the span loading.

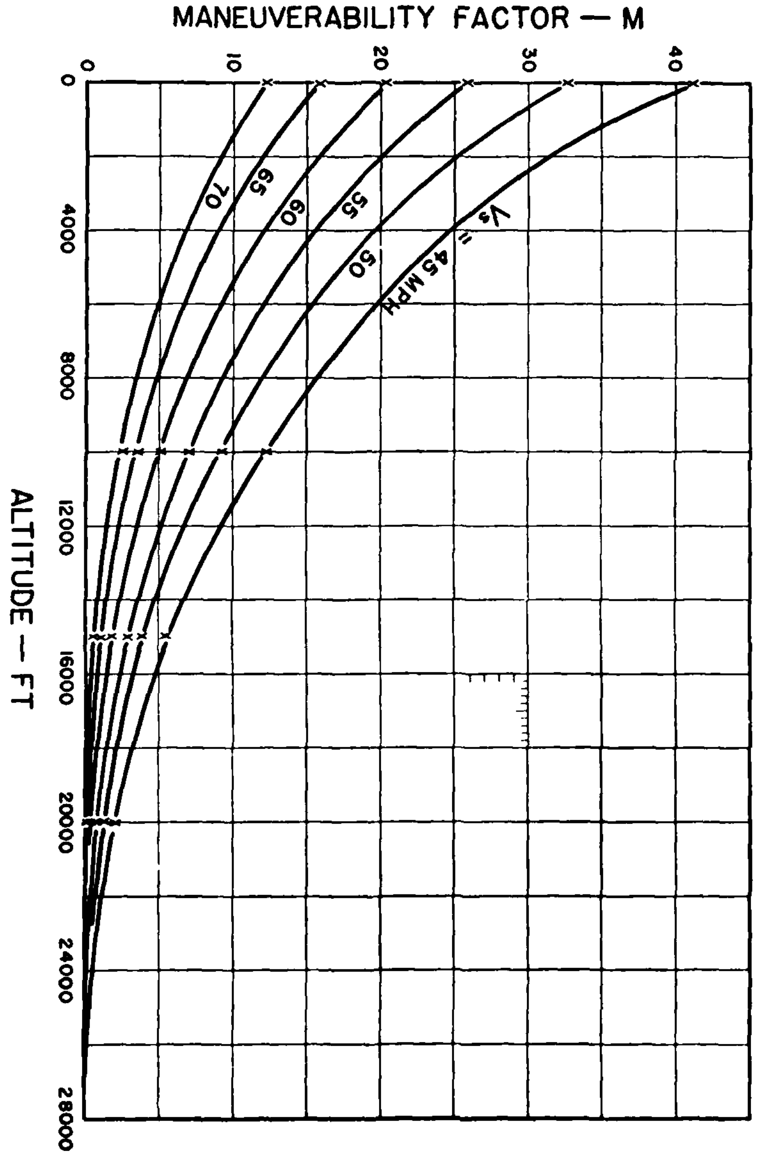

Figure 243. Effect of Stalling Speed and Altitude on Maneuverability Factor

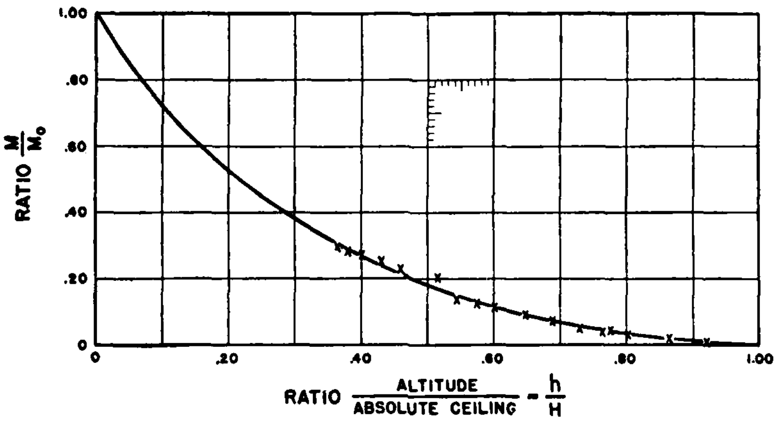

Figure 244. General Curve of Maneuverability Factor Against Altitude

TABLE 26. EFFECT OF STALLING SPEED ON PERFORMANCE

Stalling Speed, V_S mph	45	50	55	60	65	70
Wing Area, S sq ft	491	378	296	239	199	168
Gross Weight, W lb	3,440	3,216	3,054	2,941	2,861	2,799
Wing Loading, w_s lb/sq ft	7.00	8.50	10.30	12.30	14.40	16.70
Power Loading, w_p lb/bhp	7.64	7.15	6.79	6.53	6.36	6.22
Parasite Coefficient, C_{DP_0}	.0334	.0395	.0453	.0526	.0593	.0684
Maximum L/D	10.60	9.45	8.60	7.80	7.07	6.43
V_{max} at Sea-level, mph	145.5	151.6	156.5	161.0	163.5	165.0
Initial Rate of Climb, ft/min	1,910	2,030	2,120	2,170	2,165	2,135
Absolute Ceiling, ft	27,400	26,100	24,900	23,100	21,700	19,300
Service Ceiling, ft	25,700	24,500	23,500	21,900	20,500	18,300
Climb in 10 Minutes	13,000	13,400	13,600	13,500	13,300	12,500
Minimum Radius of Turn at Sea-level	150	189	233	286	342	412
Terminal Velocity in a Dive	282	290	299	304	307	309

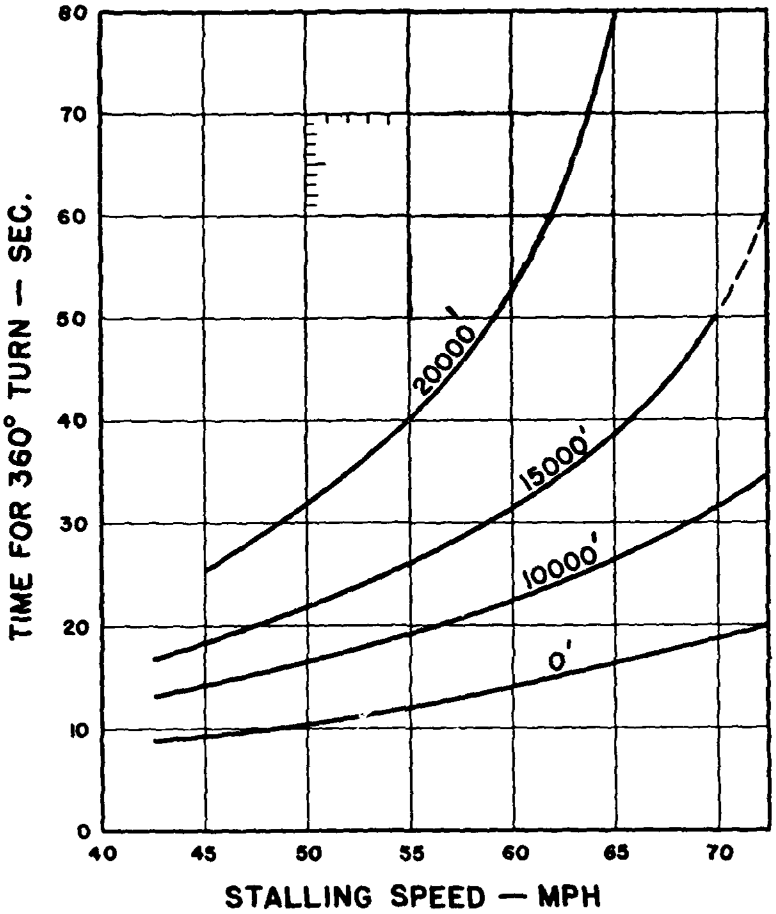

Figure 245. Effect of Stalling Speed and Altitude on Time for a 360° Turn

Limiting Performance. One of the general problems concerned with the weight-carrying ability of an airplane is the determination of the greatest possible load that can be carried with a given horsepower, or simply, the maximum power loading w_p. This problem has two solutions corresponding to the theoretical maximum and the practical maximum power loadings. The theoretical limit is the power loading at which horizontal flight is just possible, while the practical limit corresponds to the minimum safe initial rate of climb. Obviously, the minimum safe rate of climb depends to a certain extent on the type of airplane

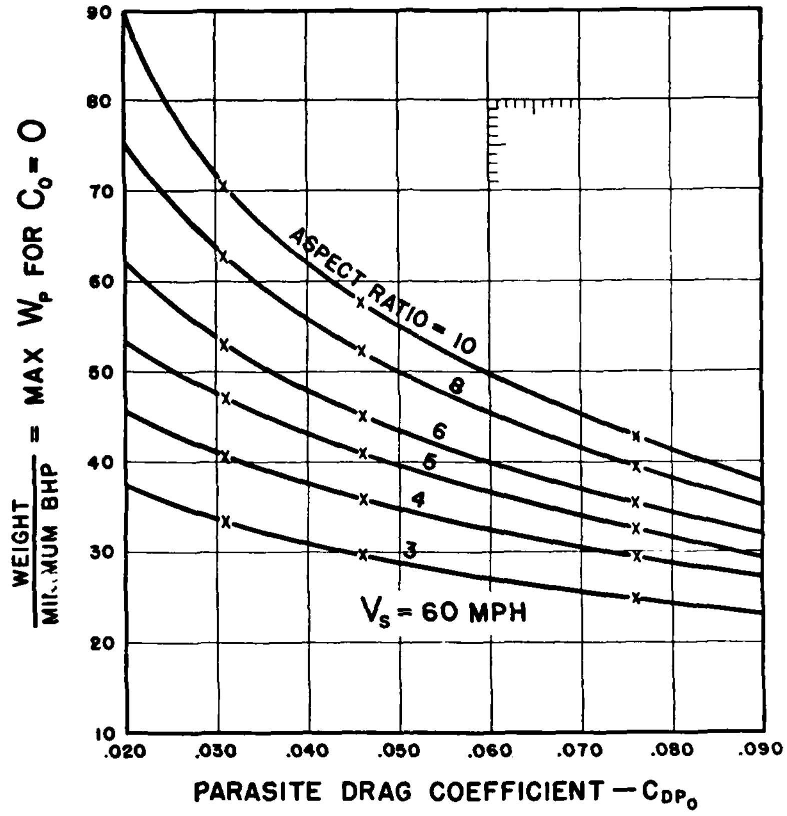

Figure 246. Effect of Aspect Ratio and Parasite on Maximum Possible Power Loading Corresponding to Zero Rate of Climb

and the use for which it is being considered, so that no definite value can be assigned, once and for all. However, there is a general agreement that the initial rate of climb should not be less than about 300 ft/min, which value has been arbitrarily adopted for this study.

Previous work on this problem appears to have been confined to the development of charts giving contour curves of rate of climb plotted against wing loading and power loading.[2] These charts are based on assumed average characteristics so that they apply to a single airplane. A complete study must consider the effects of wing loading (or stalling speed), aspect ratio, parasite

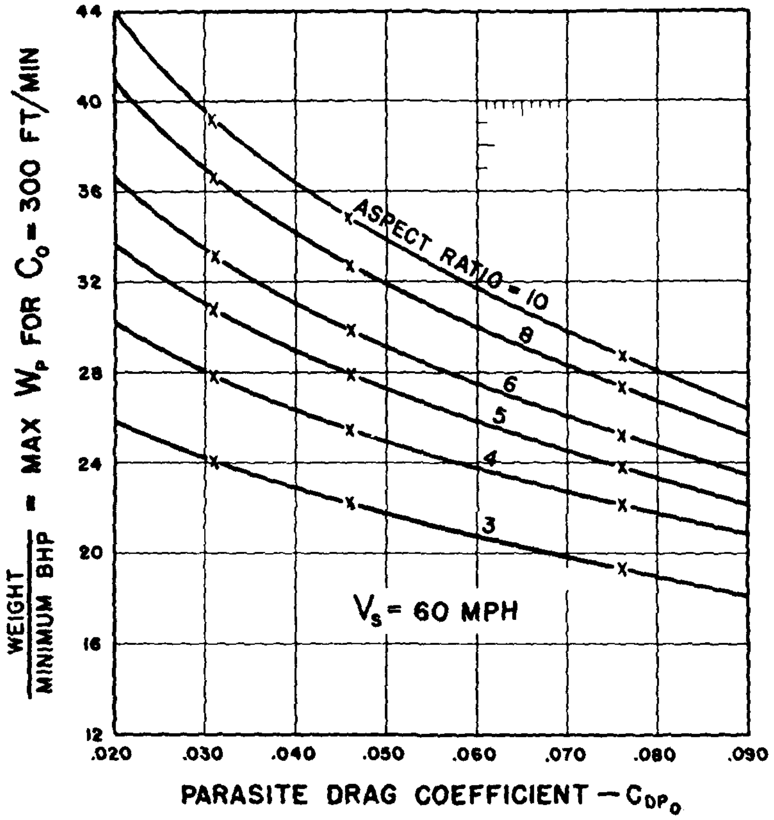

Figure 247. Effect of Aspect Ratio and Parasite on Maximum Practicable Power Loading Corresponding to 300 fpm Rate of Climb

drag, and propeller efficiency, and the amount of work required by the usual methods would be too great to justify the undertaking.

---

[2] E. P. Warner, "Airplane Design, Aerodynamics," p. 313, McGraw-Hill Book Co., Inc (1927).

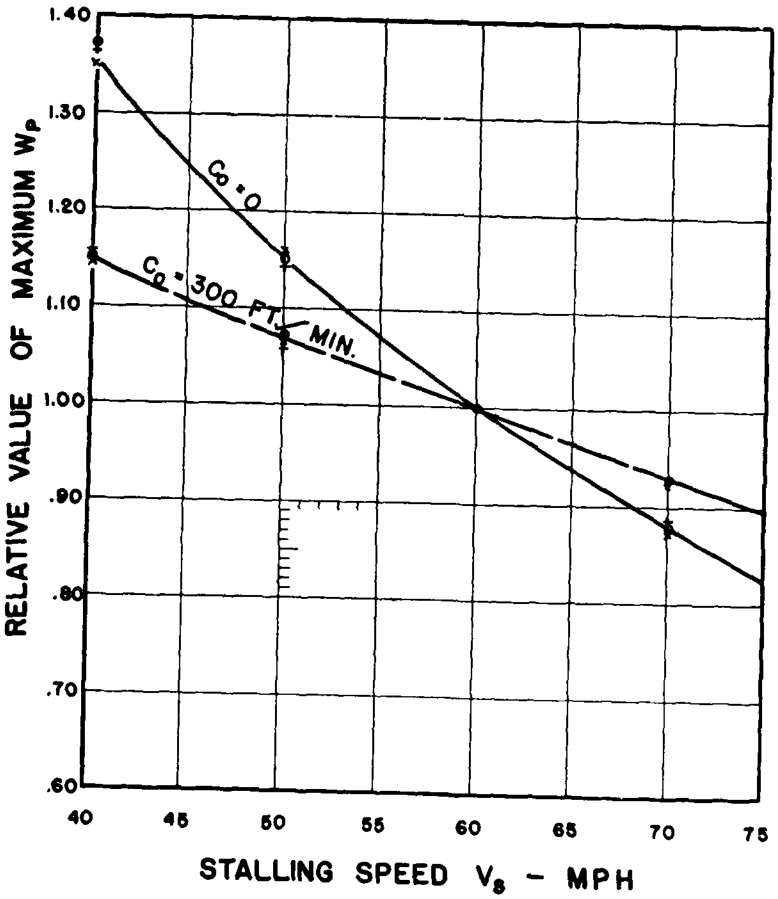

Figure 248. Effect of Stalling Speed on Maximum Power Loading

The present study was made with the help of several well known short-cuts which need not be described here, but without which the study would not have been practicable. Some idea of the ground covered can be obtained

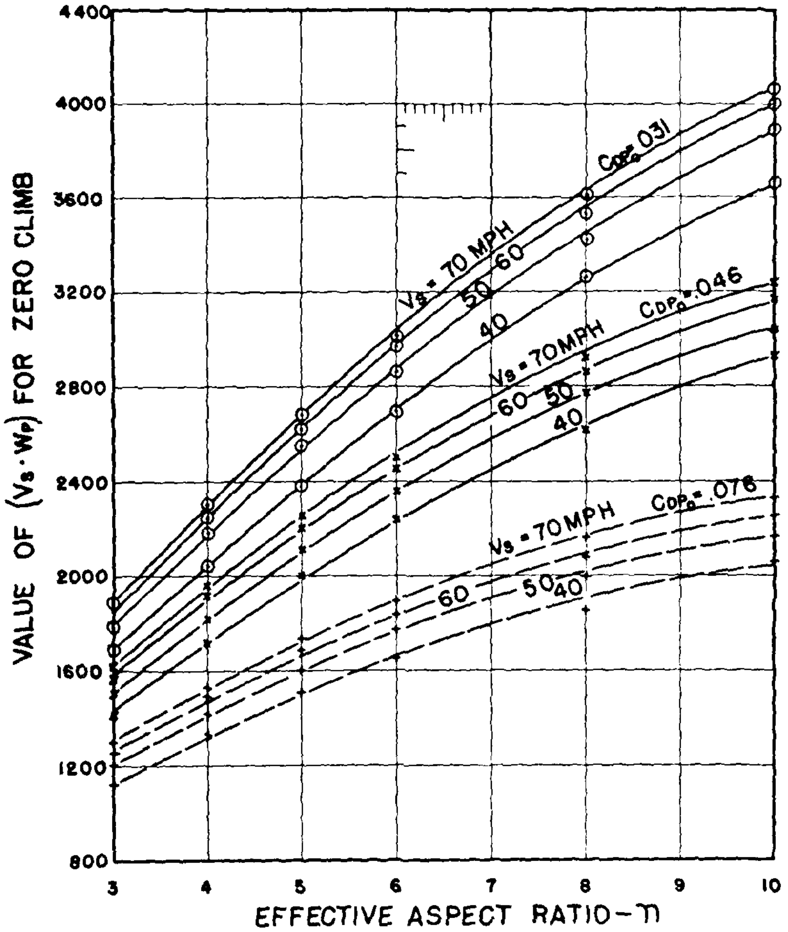

Figure 249. Effect of Stalling Speed, Aspect Ratio, and Parasite on the Product $V_S \cdot w_p$ for Zero Rate of Climb

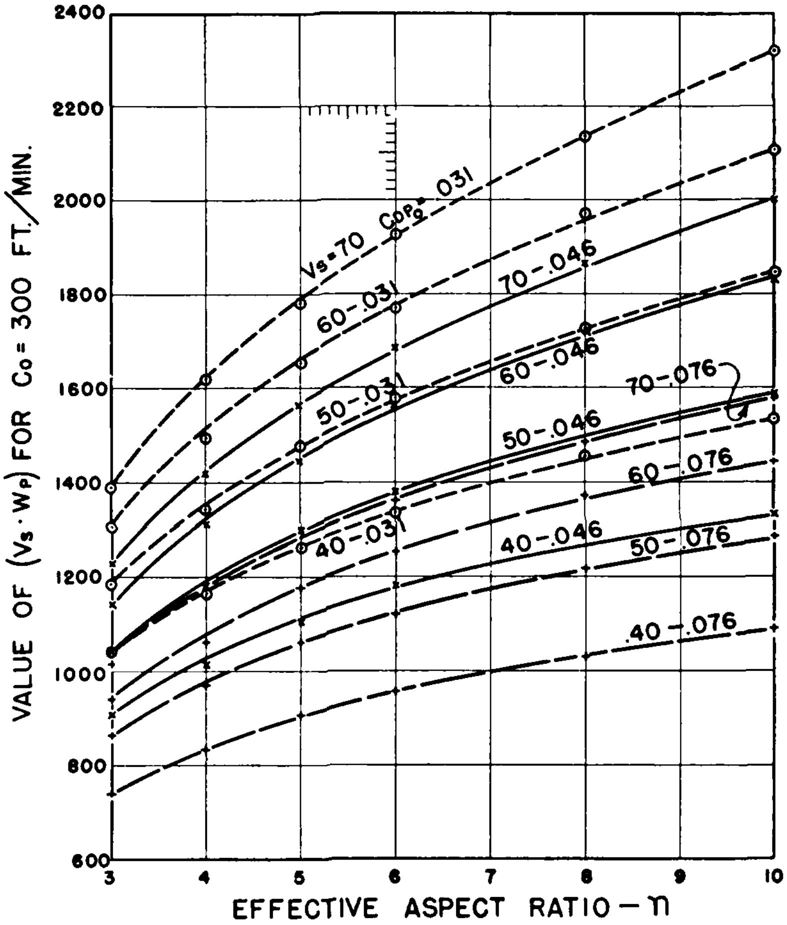

Figure 250. Effect of Stalling Speed, Aspect Ratio, and Parasite on the Product $V_S \cdot w_p$ for 300 fpm Rate of Climb

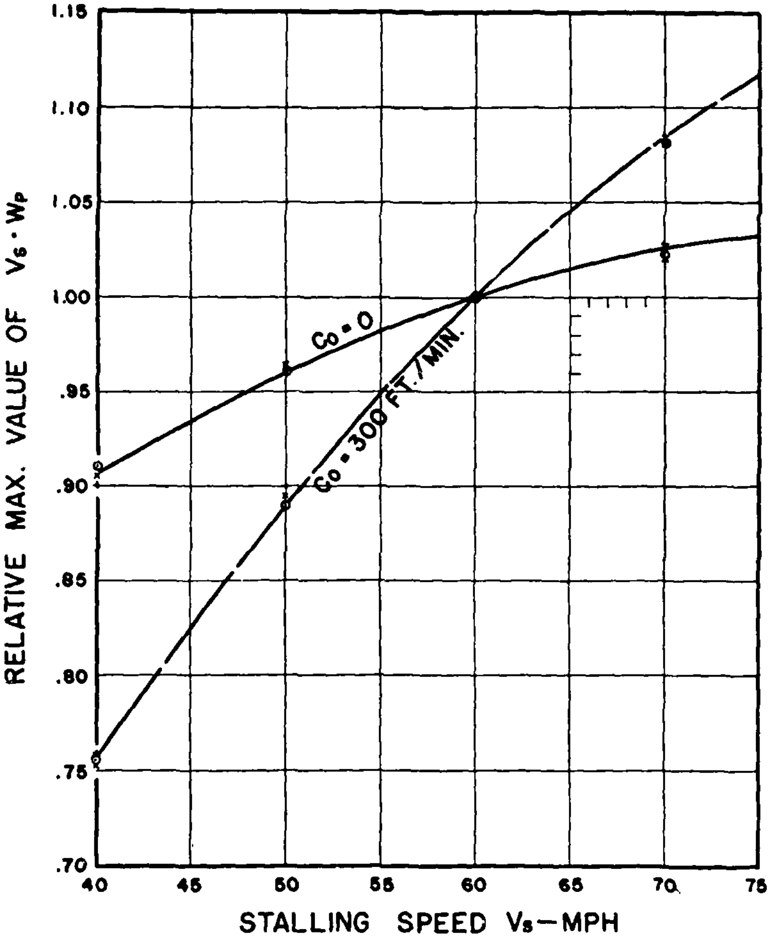

Figure 251. Effect of Stalling Speed of Maximum Value of $V_s \cdot w_p$

from the fact that the combination of six aspect ratios with three parasite drag coefficients at four stalling speeds gives the 72 basic thrust power-required curves which were studied for minimum brake horsepower under four con-

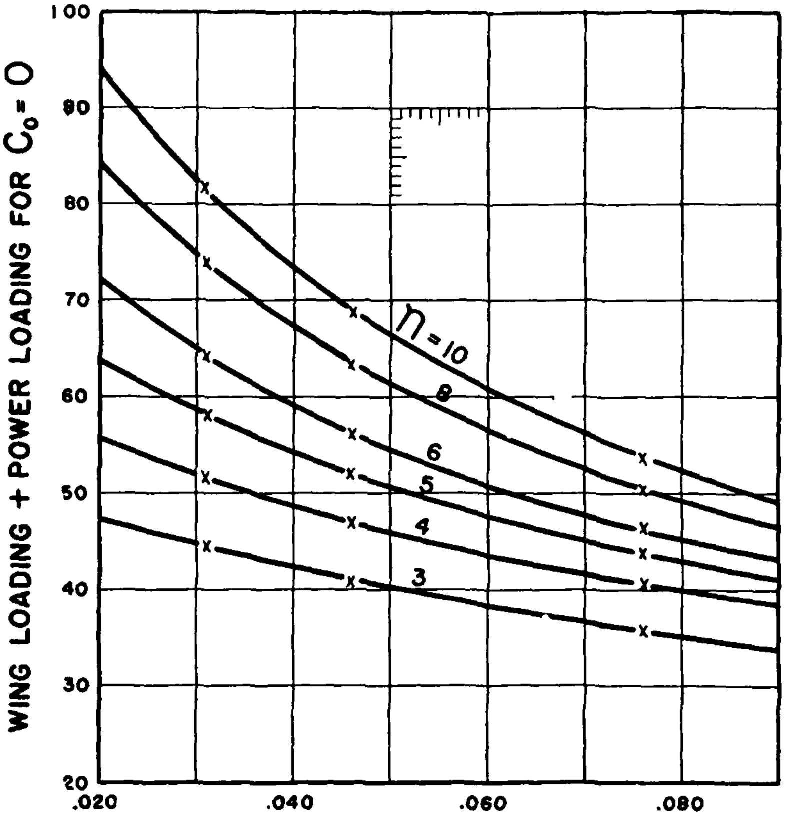

Figure 252. Effect of Aspect Ratio and Parasite on the Value of $w_s + w_p$ for Zero Rate of Climb

ditions of propeller operation and two rates of climb for a total of 576 cases.

The essential results of the study are given on Figures 246 to 253 inclusive. The differences due to propeller were found to be secondary and all of the figures given assume 80% efficiency at the point of tangency or climb. Actually, of course, the efficiency will probably be somewhat lower than this, but the actual calculated values do not affect the comparative results.

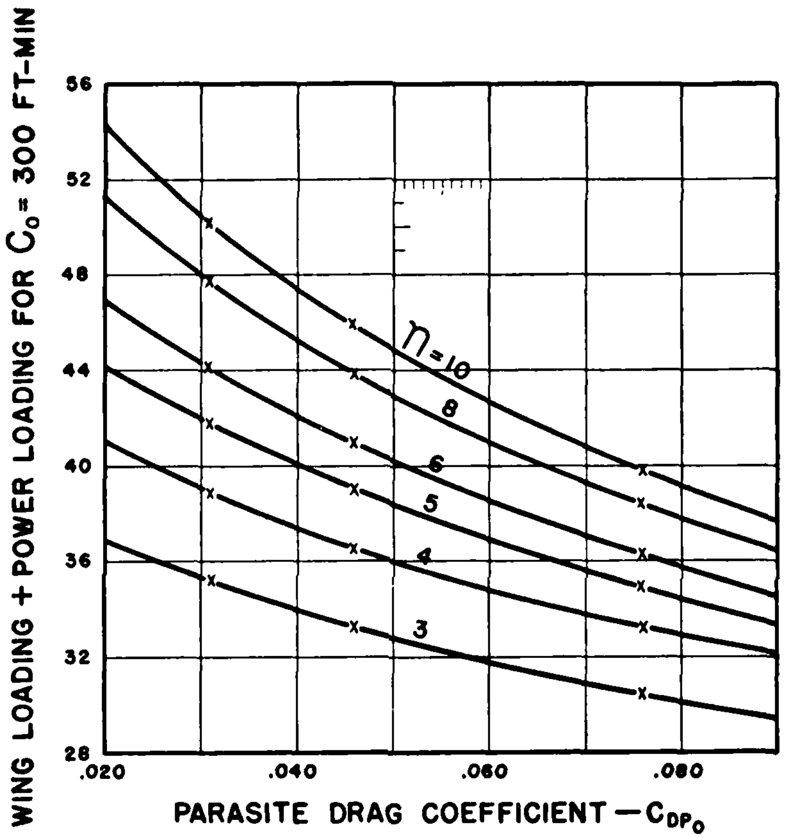

Figure 253. Effect of Aspect Ratio and Parasite on the Value of $w_s + w_p$ for 300 fpm Rate of Climb

Figure 246 gives the maximum power loading required for simple tangency of the power curves at sea-level with a stalling speed V_S = 60 mph. Figure 247 gives a similar set of curves for the value of w_p required for $C_o = 300$ ft/min. The effect of stalling speed is given on Figure 248. From the latter Figure it is seen that reducing the stalling speed from 60 mph to 50 mph increases the maximum value of w_p 15% for zero climb and about 7% for 300 ft/min initial climb.

These results are presented in another form in Figures 249, 250, and 251, where the product $V_S \cdot w_p$ is used instead of the maximum value of w_p. $V_S \cdot w_p$ is in lb-miles/hp-hr.

Figures 252 and 253 are a curious example of an unexpected relation that is devoid of dimensional justification. In spite of this defect, the variation of $(w_s + w_p)$ as shown on Figures 252 and 253 appears to represent a definite relation that checks closely with observed performance.

CHAPTER 17

SEAPLANES AND FLYING BOATS

Seaplanes and Flying Boats. The design of seaplane floats and flying boat hulls is a highly specialized application of the principles of Naval Architecture. While it is impracticable at this time to give more than a few of the basic principles involved, these few may be so selected as to give the seaplane designer most of the information ordinarily required.

Definitions. The naval architect describes seaplane floats with a number of technical words and phrases peculiar to his profession. For the benefit of the student and engineer who is unfamiliar with these terms, a short list of definitions has been prepared, limited to the most frequently used words and phrases.

AFTERBODY. That part of a float between the main step and the stern.

BOTTOM. The area included between chines and keel from bow to stern.

BOW. The extreme forward point, or portion of a float.

BUOYANCY. The displacement (in lb of sea water) to a given water line.

BUOYANCY, CENTER OF. The center of gravity of the displaced volume of water.

BUOYANCY, EXCESS. The difference between the total or submerged, and normal or load water-line displacements; usually expressed as a percentage of the normal displacement.

CHINE. The line of intersection of the bottom with the sides or deck.

DEAD RISE. The angle which each side of the bottom makes with the horizontal, as measured in a transverse plane.

DECK. The upper surface between the sides. If the sections are rounded without flat or vertical portion, then all of the upper surface between the chines is called the deck.

DECK LINE. The upper boundary of the float in a side elevation.

DISPLACEMENT. The weight of the sea water displaced to a given water line, or simply the load carried by a float under given conditions.

DISPLACEMENT SUBMERGED. The weight of the sea water displaced when the float is completely submerged.

DRAFT. Usually refers to the maximum depth below the water surface of any part of the float under given conditions.

FOREBODY. That part of the float between the main step and the bow.

KEEL. The main longitudinal and continuous strength member located along the bottom and on the center line.

KEEL, FALSE. A protective member attached along the bottom center line on the outside, to prevent damage from handling or grounding.

METACENTER. A point through which the resultant vertical buoyant force passes for all small displacements from the position of equilibrium.

METACENTRIC HEIGHT. The distance from the center of gravity to the metacenter.

PORPOISING. Any pronounced pitching oscillation in a moving float.

SPEED, GET-AWAY. The speed at which the entire weight of the seaplane is carried by the wings.

SPEED, HUMP. The speed or speeds at which the water resistance is a maximum.

SPONSONS. Lateral projections added to the sides of a float or hull to increase planing area or transverse stability.

SPRAY STRIPS. Thin longitudinal strips of triangular cross-section attached to the bottom along the chine to "beat down" the spray.

SQUATTING. A pronounced tendency to trim by the stern.

STEP. A line of discontinuity in a surface. In its usual form, a sudden change in transverse sections.

STERN. The extreme rear point, or portion of a float.

TRIM. The angle of pitch, usually measured between the deck line and the water surface.

TRIM BY BOW. An angle of trim produced by depressing the bow and raising the stern and measured in the same manner as trim by stern.

TRIM BY STERN. An angle of trim produced by raising the bow and depressing the stern; measured from a level position of some reference line, usually the deck line.

Metacentric Height. Metacentric height may be defined by considering a floating prism having its c. g. at a point G and its center of buoyancy at a point B. A line perpendicular to the water surface and passing through B will also pass through G. If the prism be inclined through a small angle θ while retaining the same volume of displacement, the center of buoyancy will shift to a point B'. A vertical through B' will intersect the original vertical BG at a point M, which is called the metacenter. The distance GM is called the metacentric height.

It is easily shown that the metacentric height is a measure of static stability. Considering a slight inclination θ and taking moments about the original center of buoyancy B, it is seen that the upsetting moment is $W \cdot BG \times \sin\theta$ and the righting moment is $W \cdot BM \cdot \sin\theta$. The total resultant moment is

$$\begin{aligned} M &= W \cdot (BM - BG) \cdot \sin\theta \\ &= W \cdot GM \cdot \sin\theta \end{aligned} \qquad (378)$$

and the slope of the resultant moment curve is

$$\frac{dM}{d\theta} = W \cdot GM \cdot \cos\theta$$

from which

$$GM = \frac{dM}{d\theta} \cdot \frac{1}{W \cdot \cos\theta} \text{ (for } \theta \text{ in radians)}$$

or

$$GM = \frac{57.3}{W} \frac{dM}{d\theta} \text{ (for } \theta \text{ in degrees)} \qquad (379)$$

This relation is used to determine metacentric heights from inclination tests on models.

The metacenter may be found by the use of the formula $BM = I/V$, where I is the moment of inertia of the waterplane about its center line and V is the total volume of displacement (see any book on Naval Architecture). I varies as L^4 and V varies as L^3, so that BM and the metacentric height vary directly as the length, or scale ratio.

Approximate metacentric heights for seaplane floats and hulls may be obtained from the empirical formulas given later.

Metacentric Height Required. Analysis of the performance of a number of seaplanes indicates that satisfactory static stability is obtained when the transverse metacentric height is given by

$$GM = K\Delta^{\frac{1}{3}} \tag{380}$$

where Δ is the gross load and K depends on the relative height of the c.g. above the c.b. For a small seaplane having a relatively high c.g. with relatively large upsetting moments, K should be about 1.4. For a large flying boat having a relatively low c.g., satisfactory stability may be obtained with a value of K as low as 0.75. It may be shown that the old righting factor is

$$\mathrm{RF} = BM/BG = 1 + (GM/h) \tag{381}$$

where h is the height of the c.g. above the c.b. Hence, in general, the value of K should be taken to give a value of GM that is between $2h$ and $5h$ depending on the span. This is discussed later under transverse stability.

For small seaplanes, the longitudinal GM should be investigated. It should not be smaller than the transverse GM.

Transverse Metacentric Height of Twin Floats. It has been shown[1] that with the design proportions in common use, the transverse metacentric height for twin floats is given closely by the empirical formula

$$GM = \frac{K_1 Ls^2 B}{\Delta} \tag{382}$$

where L is the overall length and B the beam of each float in ft, s the spacing on center lines in ft, Δ the gross weight of the seaplane, and K_1 a constant varying from 17.7 to 20.8 with an average value of 19.5. Equation (382) may be used to determine the spacing necessary for stability by substituting the average value of GM from equation (380). That is,

---

[1] W. S. Diehl, "Static Stability of Seaplane Floats and Hulls," N.A.C.A. Technical Note [illegible]

$$s = \left[\frac{1.4\,\Delta^{\frac{4}{3}}}{19.5\;LB}\right]^{\frac{1}{2}} = \frac{0.28\,\Delta^{\frac{2}{3}}}{\sqrt{LB}} \tag{383}$$

Longitudinal Metacentric Height. It has been shown in N.A.C.A. Technical Note No. 183 that the longitudinal metacentric height for either single or twin floats is given with sufficient accuracy by the empirical equation

$$GM = \frac{K_2\,nBL^3}{\Delta} \tag{384}$$

where n is the number of floats (i.e., one or two), B the beam of each float in ft, L the overall length in ft, Δ the gross weight of the seaplane, and K_2 a constant normally varying between 1.90 and 2.40 with an average value of 2.10.

Equation (384) may be used to determine the minimum length of a seaplane float for longitudinal stability by substituting the value of GM from equation (380)

$$L^3 = \frac{1.4\;\Delta^{\frac{4}{3}}}{2.10\;nB} = \frac{0.67\;\Delta^{\frac{4}{3}}}{nB} \tag{385}$$

Transverse Stability: Single-Float Seaplanes and Flying Boats. Single-float seaplanes and flying boats require the use of auxiliary flotation to secure static transverse stability. This auxiliary flotation may be in the form of (a) wing-tip floats, (b) inboard floats, or (c) sponsons. No one type is inherently superior to the others.

The functioning can be understood by reference to the sketch, Figure 254, showing the upsetting and righting moments for a seaplane with wing-tip floats. It is assumed that the float makes contact at 1° heel but as the curves are drawn, the condition of equilibrium will be at the intersection of the curves of righting moment and upsetting moment at the point **A** or 3° heel. This will be the static attitude of the seaplane at rest. An angle much greater than say 4° will be objectionable. As the angle of heel is increased, the tip float will be totally submerged at the point **B** which is usually about 8°. Further increase in heel gives a negligible increase in righting moment due to float bracing up to point **C** where the wing tip touches.

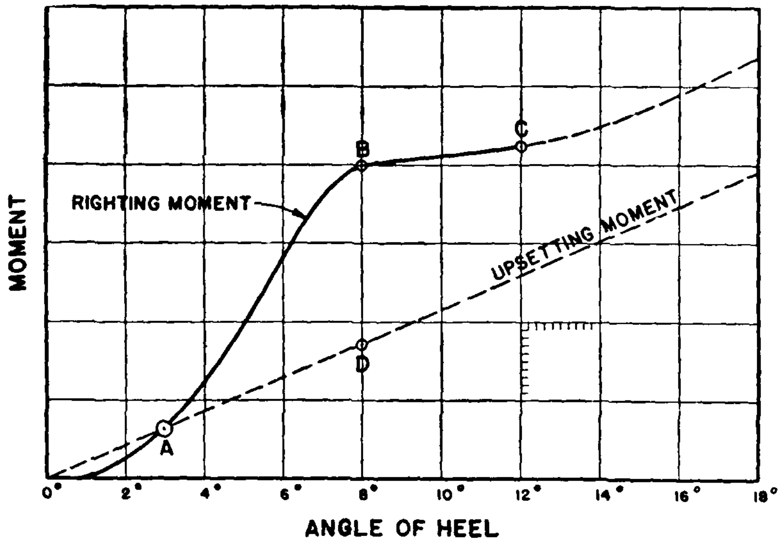

Figure 254. Variation of Moments with Angle of Heel for Seaplanes

The problem of design is to make the righting moment at the point **B** sufficiently greater than the upsetting moment **D**, at the same angle, to give a reasonable margin for additional upsetting moment due to wind or a member of the crew on the wing. There is a distinct difference between a margin that avoids trouble under favorable conditions and a margin that gives full protection. The latter is obtained when the displacement of each tip float is

$$\Delta_t = \frac{W}{l}\left(KW^{\frac{1}{3}} + h \sin \theta\right) \qquad (386)$$

where W is the gross weight in pounds, l is the distance between the c.g. of the tip float and the center-line of the airplane in feet, h is the height of the c.g. above the c.b. of the main hull in feet, θ is the angle of heel required to submerge a side float and K is a constant depending on the size and type of the seaplane. Values of K less than 0.060 have been unsatisfactory. For full protection against normal wind forces the value is

$$K = 0.060 + 0.0004b \tag{387}$$

where b is the span. For tapered wings with a relatively low h, and a low value of θ to submerge the wing tip, the span coefficient may perhaps be safely reduced to 0.0002.

It is of interest to note that the required righting factor or ratio of net restoring moment to upsetting moment increases for a given seaplane as $h \sin \theta$ decreases, since the net restoring moment depends only on the weight and span.

Vertical Location of Side Floats. A wing-tip float is most effective when located close to the water, but some clearance is required for rough water operation. The optimum clearance appears to be that requiring about 1° heel for contact, but this is a matter depending somewhat on the lines of the float. A smaller clearance might safely be used with a float having marked dead rise and set at a positive angle so that the initial contact is over a small portion of the stern. The cross-section and general shape should be selected to give rapid increase in submerged volume with angle of heel and the bottom should be designed to give a definite dynamic lift when underway.

Side floats are often located well inboard and given some initial displacement to form a 3-float system which rides at an even keel. The initial displacement also doubles the increase in moment with angle of heel but the total displacement of each float must be based on the maximum net restoring moment required by equation (386).

Float Performance. Float performance is too complex for a simple definition. In general, it is always a compromise, good performance in one respect usually being accompanied by poor performance in some other item. The ideal float would have ample stability at rest and underway. It would be entirely seaworthy for take-off or landing in any waves or swell normally encountered under anticipated operating conditions. It would be free from porpoising or other objectionable pitching motions during take-off and landing. It would throw a light or moderate spray. It would have low resistance and low or moderate trimming moments. All of these requirements can be reasonably met if no restrictions are placed on weight and air resistance. Otherwise stated, most of the troubles encountered in seaplane water performance are due to insufficient reserve buoyancy or to lines that are laid out primarily for low air resistance.

Float performance cannot be calculated, it must be determined experimentally on a scale model.

Corresponding Speeds: Froude's Law. The resistance of a ship or a seaplane float has two components, one due to skin friction, the other due to wave making. In equation form

$$R = R_f + R_w \tag{388}$$

where R_f is the frictional and R_w is the wave-making resistance.

The frictional resistance is assumed to be independent of the shape of the hull and to depend only on the wetted area, the speed and the relative smoothness of the surface that forms the wetted area. The wave-making resistance is some unknown function of the hull lines, the displacement, and the speed. A model test measures the total resistance. This is converted to a full-scale value by the use of Froude's Law of Comparison which states that at corresponding speeds the wave-making resistance varies as the cube of the length. The corresponding speed is determined by $V/\sqrt{gL}$ or usually by its equivalent $V/\sqrt{L}$. Denoting model values by lower case and full-scale values by capitals, the relations are

$$V/\sqrt{L} = v/\sqrt{l} \tag{389}$$

$$r = r_f + r_w \tag{390}$$

$$R = R_f + R_w \tag{391}$$

$$\lambda = \text{Scale Ratio} = L/l \tag{392}$$

The displacement and the wave-making resistance vary as λ^3. The moments vary as λ^4. Hence

$$\Delta = \Delta_m \lambda^3 \tag{393}$$

$$R_w = r_w \lambda^3 \tag{394}$$

$$M = m \lambda^4 \tag{395}$$

Dividing equation (393) by equation (394) gives

$$\Delta/R_w = \Delta_m/r_w \tag{396}$$

Since the frictional resistance is normally a small part of the total resistance, except at high planing speeds, it is customary to consider the resistance as all wave-making and write equation (396) as

$$\frac{\Delta}{R} = \frac{\Delta_m}{r_f + r_w} = \frac{\Delta}{R_f + R_w} \tag{397}$$

Equation (397) is an approximation, sufficiently accurate for most purposes, but it must always be considered as an approximation, particularly in the planing condition and for large values of λ.

Model Test Methods. Float models may be tested by the "specific" method, or the "general method." In the specific method the take-off run is assumed to be at a constant angle of attack *corresponding to the lift required* for take-off at the speed V_G. Since the wing lift varies as V^2, the displacement of the model is varied according to

$$\Delta_m = \Delta_{m0}\left[1 - \left(\frac{v}{v_g}\right)^2\right] \tag{398}$$

where v_g is the model get-away speed obtained from equation (389) in the form

$$v_g = V_G/\sqrt{\lambda} \tag{399}$$

Runs are normally made with the model "free-to-trim" and also at various fixed trims. The moments required to hold the fixed trims are usually obtained.

In the "general" method, readings of resistance and pitching moment are obtained at a series of speeds for various combinations of displacement and trim. The resultant data may then be plotted, for example, in the form of a group of curves of resistance against speed at constant trim, each individual curve representing a constant load or model displacement. A full description of the two methods of testing may be found in N.A.C.A. Technical Note No. 464[2] and Technical Report No. 470.[3]

Non-Dimensional Coefficients. The N.A.C.A. data are plotted in the form of non-dimensional coefficients defined as follows:

$$\text{Load Coefficient } C_\Delta = \Delta/wb^3 \tag{400}$$

$$\text{Resistance Coefficient } C_R = R/wb^3 \tag{401}$$

$$\text{Moment Coefficient } C_M = M/wb^4 \tag{402}$$

$$\text{Speed Coefficient } C_V = V/\sqrt{gb} \tag{403}$$

where Δ = load on water
R = resistance
w = weight (not mass) of water per unit volume
b = beam of hull
M = trimming moment
V = speed
g = acceleration of gravity

---

[2] J. M. Shoemaker and J. B. Parkinson, "A Complete Tank Test of a Model of a Flying Boat," N.A.C.A. T.N. No. 464 (1933)

[3] Starr Truscott, "The N.A.C.A. Tank—A High-Speed Towing Basin for Testing Models of Seaplane Floats," N.A.C.A. T.R. No. 470 (1933).

These must be in consistent units, for example, ft-lb-sec or kg-m-sec.

Calculation for Take-off. The method of calculating resistance curves for take-off depends on the type of data available and the accuracy desired. The most direct method, an approximation sufficiently accurate for all practical purposes, makes use of a curve of the ratio Δ/R (= displacement/resistance) as a function of the ratio V/V_G where V_G is the get-away speed. The get-away normally occurs at about 0.80 $C_{L\,max}$ or at about $1.10V_S$. Assuming that a curve of Δ/R is available for the loading condition desired, the procedure is as follows:

1. Calculate get-away speed V_G.
2. Assume a series of speeds V
3. Find the ratio V/V_G for each speed.
4. Read Δ/R at each V/V_G from the model basin data.
5. Calculate Δ at each speed
   $\Delta = W[1 - (V/V_G)^2]$.
6. Calculate R_W from $R_W = \Delta/(\Delta/R)$.
7. Calculate air resistance at each speed. Approximately, this is $R_a = W(V/V_G)^2/(L/D)$.
8. Total resistance $R = R_W + R_a$.

R may be plotted against V and a curve of propeller thrust added. It is customary to calculate the thrust at two points, $V = 0$ and $V = V_G$ and assume that the variation is linear between these. The difference between the two curves is $F = T - R$ available for acceleration $a = gF/W$. The value of V/a may be plotted against V to determine by the area under the curve the distance required for take-off. The area under the curve of $(1/a)$ plotted against V gives the time required for take-off.

The method of calculating the resistance from the complete test curves is fully explained by Shoemaker and Parkinson in N.A.C.A. Technical Note No. 464, previously referenced. Briefly, the method is as follows:

1. Assume V.
2. Calculate C_V. $C_V = V/\sqrt{gb}$
3. Assume approximate trim angle τ.
4. Angle of attack $\alpha_w = \alpha_0 + \tau$. α_0 is the angle of wing setting.
5. C_L corresponding to α_w.
6. Calculate lift $L = C_L\, q\, S$.
7. Calculate load on hull $\Delta = W - L$.
8. Calculate $C_\Delta = \Delta/wb^3$. If this value of C_Δ agrees with the value of C_V and the assumed τ then,
9. Read C_R from curves of C_Δ vs. C_V at best trim.
10. Calculate R from $R = C_R \cdot wb^3$.

If the first value of C_Δ in 8 is not at the assumed trim angle, it is necessary to assume another value of τ and repeat the calculations. The second approximation should be very close to the desired value.

Effect of Wind on Take-off. The effect of a wind on time and distance required for take-off may readily be determined by use of the complete method, if the value of the water speed is used to determine C_V and the value of the air speed is used to determine C_Δ.

Calculations have been made on a systematically varied series of seaplanes to determine the time required for take-off under various conditions. The results are given on Figure 255. The variation of t with V_W for any given seaplane will be along a curve similar to those given so that a single take-off time determines the entire curve.

The distance required for take-off in a wind is given closely by

$$\frac{S_W}{S_0} = \left(\frac{t_W}{t_0}\right)^2 \tag{404}$$

In an example given by Shoemaker and Dawson[4] the values were $t_0 = 39.6$ sec and $S_0 = 2570$ ft in a calm and

---

[4] J. M. Shoemaker and J. R. Dawson, "The Effect of Trim Angle on the Take-Off Performance of a Flying Boat." N.A.C.A. T.N. No. 486 (1934).

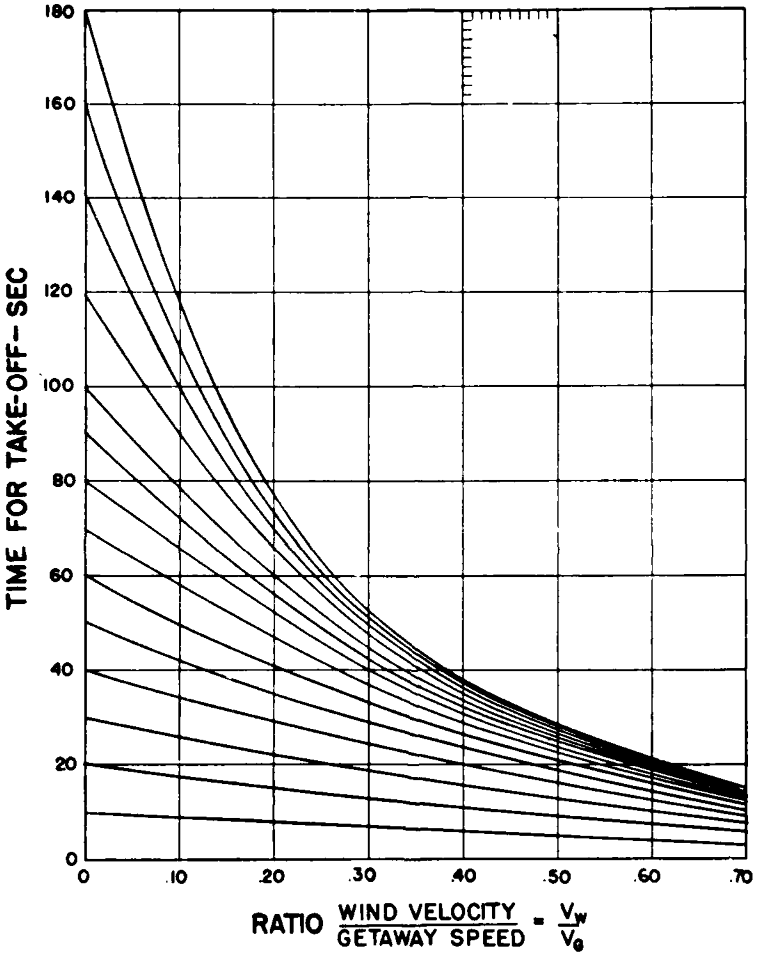

Figure 255. Effect of Wind on Time Required for Seaplane Take-off

$t_W = 26.3$ sec and $S_W = 1130$ ft in a wind $V_W = 25$ ft/sec with a value $V_G = 106$ ft/sec. The value of $V_W/V_G = 0.236$. Starting at $t_0 = 39.6$, it is seen that $t = 26.5$ at $V_W/V_G = 0.236$, which is in close agreement with the calculated value. Using the value from the curves

$$S_W = 2570\,(26.5/39.6)^2 = 1150 \text{ ft}$$

which checks with 1130 ft obtained by detailed calculation.

Maximum Load That Can Be Taken off. It may be shown[5] that the reciprocal of the take-off time plots as a straight line against power loading. The intersection of this line with the loading axis at $(1/t) = 0$ corresponds to the limiting condition requiring an infinite time for take-off. It may also be shown that the slopes of such lines are substantially the same for all seaplanes, and that the maximum load that can be taken off is given closely by

$$W_m = W + 140\,\frac{\text{bhp}}{t} \tag{405}$$

where t is the time in seconds required for take-off with the gross weight W pounds.

Equation (405) was derived from tests on flying boats, but subsequent checks show that it applies equally well to single-float and twin-float seaplanes.

The effect of change in W or bhp is readily obtained from equation (405) written in the form

$$\frac{W_1}{\text{bhp}_1} + \frac{140}{t_1} = \frac{W_2}{\text{bhp}_2} + \frac{140}{t_2} \tag{406}$$

Notes on Float and Hull Lines. Certain general considerations govern the proportions of float and hull lines required to give satisfactory performance. Some of these are based on model-basin tests, others on operating experience. The brief notes that follow will attempt to point out a few of the more important features that should either be incorporated or avoided as the case may be.

---

[5] W. S. Diehl, "The Estimation of the Maximum Load Capacity of Seaplanes and Flying Boats," N.A.C.A. T.R. No. 453 (1932).

Length. The length of a float or hull is usually determined by design conditions that have no bearing on the water performance. It is essential, however, that sufficient length be used to provide a safe longitudinal *GM*. It is also essential to have sufficient length and freeboard at the bow to prevent nosing over in take-off or alighting.

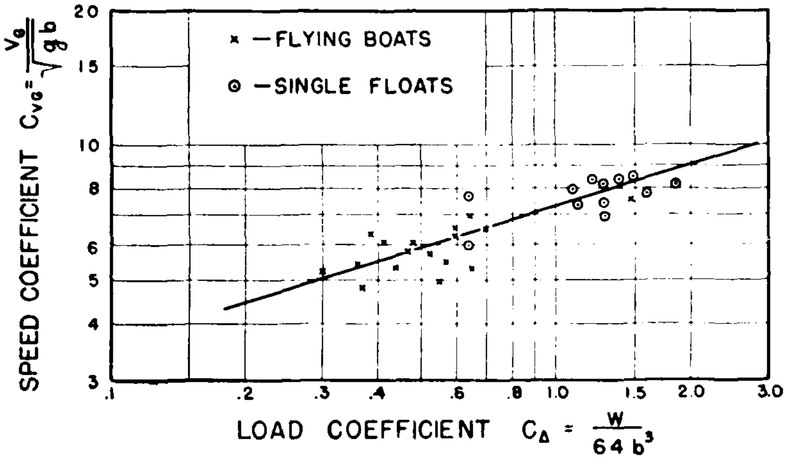

Figure 256. Variation of Load Coefficient with Speed Coefficient at Get-away Speed

Beam. The beam is probably the most important single factor in determining water performance. In general, a broad beam gives low resistance at the hump and high resistance at planing speeds. A narrow beam will have high resistance at the hump and low resistance at planing speeds. The best beam is a compromise, depending somewhat on the get-away speed, since the dynamic reaction may become excessive for a large *b* and high V_G. The connection between *b*, *W*, and V_G may be obtained approximately from a plot of C_Δ vs. C_V at get-away, as in Figure 256. The value of C_V at get-away may be designated C_{VG}. C_{VG} and C_Δ are connected by the relation

$$C_{VG} = 7.3\ C_\Delta^{\frac{1}{3}}$$

hence

$$\frac{V_G}{\sqrt{gb}} = 7.3\left(\frac{W}{64b^3}\right)^{\frac{1}{3}}$$

from which the beam in feet is

$$b = \frac{107.2\ W^{\frac{2}{3}}}{V_G^2} \tag{407}$$

where W is the gross weight in pounds and V_G is the get-away speed in ft/sec.

Owing to the effect of dead rise and other factors, the actual beam used may vary as much as 20% to 30% from the value indicated by equation (407). If the impact load on the float is to be constant, it follows that

$$W = K \cdot b^3\ V_G^2$$

where K is some function of the dead-rise angle α. Using von Kármán's formula for bottom pressure, equation (409), the average value of K for a number of seaplanes is found to be $K = 0.011 \cot \alpha$. Hence

$$b = \frac{9.5}{V_G}\sqrt{\frac{W}{\cot \alpha}} \tag{408}$$

where V_G is the get-away speed in ft/sec, W is the gross load in lb.

Depth. The depth of a float is usually determined by the reserve buoyancy to be provided and in the past this has been arbitrarily set at values ranging from 70% to 100%. There is some reason for believing that the ratio of the depth to the beam should be constant at about 0.70 and that the larger sizes should run at relatively lighter drafts. This is equivalent to increasing the reserve buoyancy as the size of the float increases.

Dead Rise. The proper amount of dead rise or transverse Vee in the float bottom depends on stalling speed and to a certain extent on power loading. A large dead rise is effective in reducing shock loads, but it increases the resistance and leads to undesirable spray formation. According to von Kármán[6] the maximum pressure developed is

$$p_m = \tfrac{1}{2} \rho V_0^2 \pi \cot \alpha \tag{409}$$

where V_0 is the vertical impact velocity, ρ is the water density, and α is the dead rise angle.

Model-basin tests on the effects of dead rise have been inconclusive, but the average design practice is to use an angle varying with get-away speed about as follows:

V_G mph =	40	50	60	70	80
α =	10°	15°	20°	25°	30°

The Step. The "step" is a transverse discontinuity in the bottom surface of a float. When properly located, the step gives a marked improvement in planing action and control over trim. The step should be so located aft of the c.g. that a line drawn from the c.g. to a point on the step midway between the keel and the chine makes an angle between 20° and 25° with the transverse plane containing the c.g. and c.b.

The depth of the step is not highly critical between 3% and 5% of the beam.[7] A shallow step improves conditions at and below hump speeds. A deep step improves planing. It is probable that a reasonably definite relation exists between the desirable depth of the step and the angle between the afterbody and forebody keels at the step. The plan-form of the step is relatively unimportant.[8]

---

[6] Th. von Kármán, "The Impact on Seaplane Floats During Landing," N.A.C.A. T.N. No. 321 (1929).

[7] J. W. Bell, "The Effect of Depth of Step on the Water Performance of a Flying Boat Hull Model, N.A.C.A. Model 11 C," N.A.C.A. T.N. No. 535 (1935).

[8] J. R. Dawson, "A General Tank Test of N.A.C.A. Model 11-C Flying Boat Hull, Including the Effect of Changing the Plan-Form of the Step," N.A.C.A. T.N. No. 538 (1935).

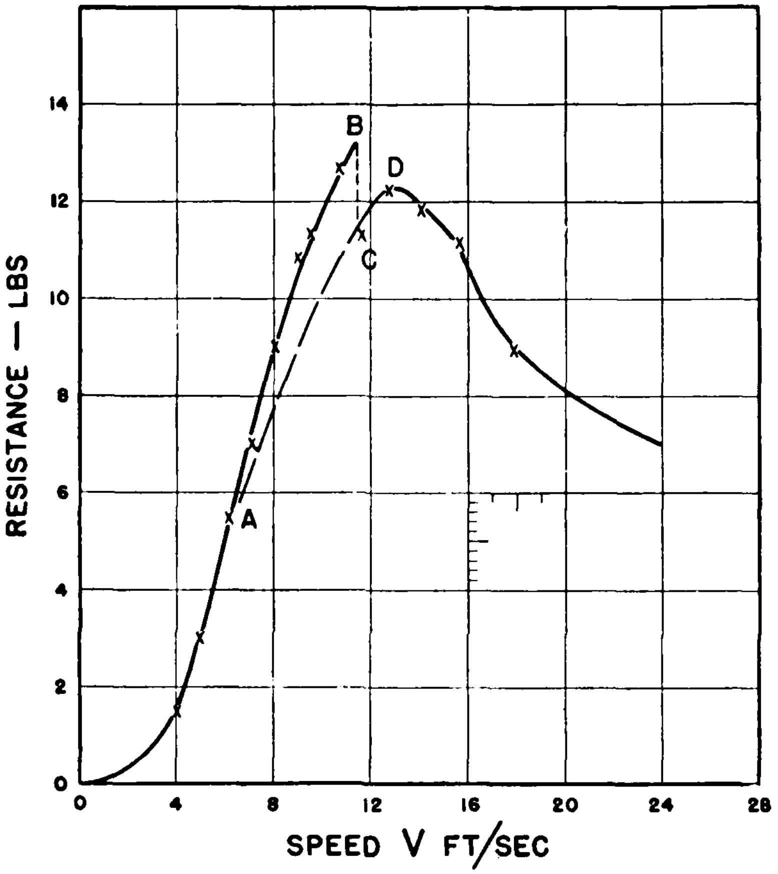

Figure 257. Effect of Step Ventilation at Hump Speed

Step ventilation is unnecessary except where the step and draft are deep. In such cases the resistance curve shows a sharp peak dropping abruptly to a much lower value as the outer edge of the step clears. This is shown on hydrovane runs only, for example, in Figure 257 which is based on Figure 10 of N.A.C.A. T.N. No. 482.[9] The observed resistance curve was **ABCD** - - - - . The break at **B** occurs as the step edge clears. Ventilating the step would give a resistance curve **ACD**.

---

[9] J. R. Dawson, "The Effect of Spray Strips on a Model of the P.M.-1 [illegible] N.A.C.A. T.N. No. 482 (19[illegible]).

Keel-Angle at Step. The angle between the forebody and the afterbody keels at the step is a major variable in its effect on float performance.[10] A small angle reduces trim angles and is better at hump speeds. A large angle is better at high speeds. In general, this angle should lie between 7° and 9°.

Spray Strips. Objectionable spray may be controlled by "spray strips" attached to the chine. According to N.A.C.A. tests,[11] strips having a width between 2% and 3% of the beam and set at angle between 30° and 45° below the horizontal were very effective in controlling the spray. The same or better results can usually be secured by the use of bottom sections incorporating a hook or tangent portion at the chine.

---

[10] J. M. Allison, "The Effect of the Angle of Afterbody Keel on the Water Performance of a Flying Boat Hull Model," N.A.C.A. T.N. No. 541 (1935).

[11] Starr Truscott, "The Effect of Spray Strips on the Take-Off Performance of a Model of a Flying-Boat Hull," N.A.C.A. T.R. No. 503 (1934).

CHAPTER 18

FLIGHT TESTING AND PERFORMANCE REDUCTION

The actual performance of the completed airplane is naturally the basis of comparison with other types. Steady improvement in minor details requires that the error in measuring performance be less than the effect of the part under consideration. Early investigators found a large variation in the apparent performance measured on different days or by different methods. Experience has shown that the apparent variation can be reduced to a low value if the performance tests are made with certain precautions and the observed data corrected for abnormal air temperatures. Some of the more important points will be discussed briefly.

Calibration of Air-Speed Indicators. In general, air-speed indicators must be calibrated by runs up and down wind over a measured course. Special methods, such as calibration against the reading of an instrument suspended well below the airplane[1] or against previously calibrated readings in a second airplane, are not available except at well-equipped flight-test organizations. Calibration runs should not be attempted when the cross-course component of the wind exceeds about 15% of the airplane speed, since this value reduces the measured speed more than 1%.

Assume that a series of runs in pairs has been made over a measured course, each pair consisting of a run up and down wind, during which the following data are recorded: time over course, air-speed indicator reading, rpm, air temperature, and pressure. The time over the course gives the ground speed. Averaging ground speeds (not the times over course) in each pair of runs gives the true air speed for the given rpm and indicator reading. The indicator reading is a function of $\rho V^2/2$ and V is the true air speed. The curve of readings plotted against $\rho V^2/2$ is the calibration curve. True speed may be obtained from the instrument reading and this curve when ρ is known. While the true speed is determined by the density, the speed itself must be plotted against pressure altitude.

---

[1] W. G. Brown, "Measuring an Airplane's True Speed in Flight Testing," N.A.C.A. T.N. No. 135 (1923).

Maximum Speed. In order to determine the actual maximum speed in horizontal flight, care must be taken to avoid errors due to following sources: (1) failure to maintain horizontal flight, (2) starting over a speed course before the airplane has settled down to steady flight, (3) variable winds, or cross-wind component too large. There are many other precautions to be observed, but those enumerated constitute the chief sources of error.

A change in altitude of 40 ft/mi will give 1% change in the measured high speed of an average airplane. For this reason high-speed runs are usually made at a very low altitude and, if available, a statoscope is carried in order that the flight path may be maintained horizontal. If the ratio of maximum to stalling speed is greater than 1.5, the error due to ground effect is negligible.

All high-speed runs should be started at a distance from the first marker on the course which will allow from 30 seconds to 60 seconds for settling down to steady conditions before crossing the line. This precaution is very important. The last two or three miles of high speed are attained by a comparatively slow acceleration, and any control movements or changes of altitude and direction will affect the high speed. In the first stages of the approach to the starting line of the course, the pilot should fix his altitude and direction. Under no conditions would a diving start be permissible.

High-speed runs should be made in a calm, if practicable, although good results can be obtained in any steady wind which does not have a cross-course component greater than 15% of the speed to be measured. Tests should never be made with gusty, variable, or unsteady winds, no matter how light.

Importance of Correct Air Speed in Climb. Figure 258 gives the calculated variation of rate of climb with true air speed

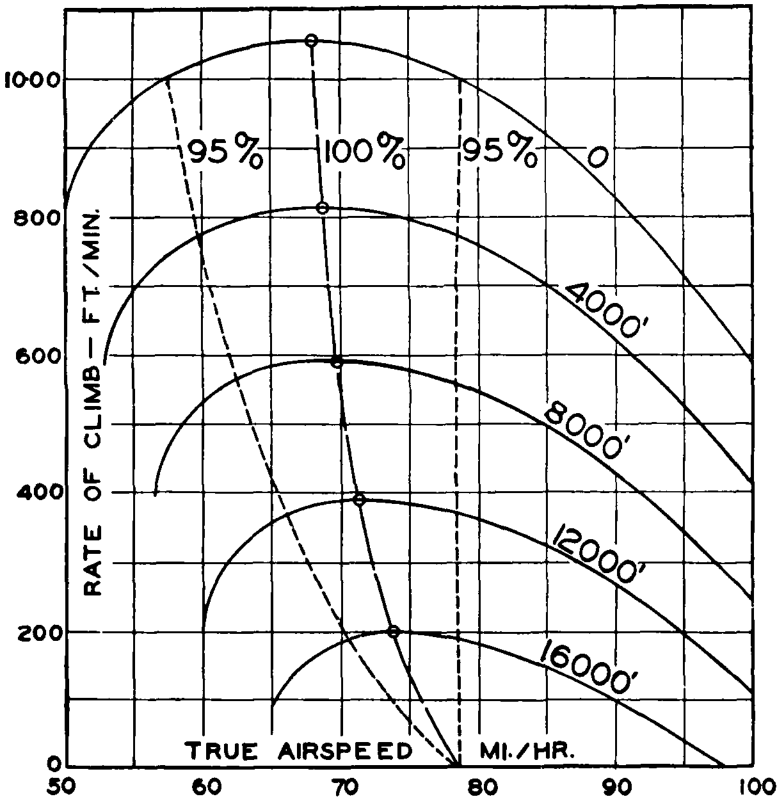

Figure 258. Variation of Climb with Air Speed and Altitude, Showing Necessity for Making Climb at Correct Air Speeds

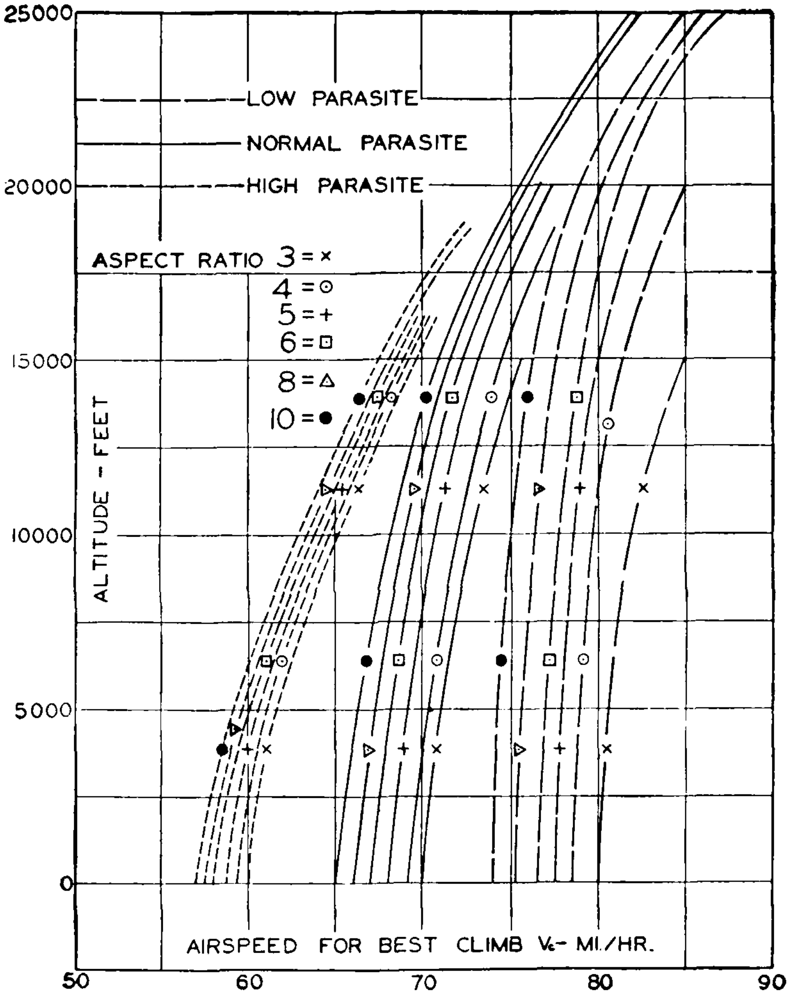

Figure 259. Effect of Aspect Ratio and Parasite on Air Speed for Best Climb at Altitudes

and altitude for a typical airplane. Each heavy curve gives the variation of rate of climb with air speed at constant standard altitude. The central cross curve (long dashes) passes through the maximum rate of climb at each altitude and, therefore, gives the variation of best climbing speed with altitude. The two outside cross curves (short dashes) are marked 95%, and pass through rates of climb 95% of maximum at all altitudes. These curves show very strikingly the importance of correct air speed in climb.

The general variation of true air speed for best climb is given on Figure 259.

Variation of Best Climbing Air Speed with Pressure and Temperature. In the study of performance reduction, the best climbing speeds for a typical airplane were determined at various pressure altitudes for temperatures 83.3%, 90.9%, 110%, and 120% normal. A large effect was found as follows:

Temperature, % Normal		83.3	90.9	100	110	120
Best climbing air speed at given pressure altitude, in feet.	4,000	66.0	67.5	70.0	70.5	71.0
	8,000	66.0	68.0	70.0	73.0	74.0
	10,000	65.0	68.0	70.0	72.0	74.0
	12,000	65.5	68.0	70.0	73.0	76.0
	16,000	67.0	70.0	72.0	76.0	79.0

Taking the ratio of these climbing speeds to the corresponding stalling speeds gives:

Temperature, % Normal		83.3	90.9	100	110	120
Ratio $\frac{\text{Best climbing speed}}{\text{Stalling speed}}$ at given pressure altitude, in feet	4,000	1.36	1.33	1.32	1.27	1.22
	8,000	1.28	1.26	1.24	1.23	1.20
	10,000	1.22	1.22	1.20	1.18	1.16
	12,000	1.19	1.19	1.17	1.16	1.16
	16,000	1.14	1.15	1.14	1.13	1.13

It is obvious that for all practical purposes the ratio of best climbing speed to stalling speed may be considered constant at any given pressure altitude. This means that the relation between angle of attack and pressure altitude is not affected by temperature variations. Consequently, the conditions for best climb at altitude must be specified as the relation between the readings of a sensitive angle-of-attack indicator and an aneroid. The common method of specifying the indicated air speeds at various indicated altitudes may give erroneous results. It will be found satisfactory, however, to use indicated air speeds and aneroid pressures.

Determination of Best Climbing Air Speeds. The procedure formerly followed was to make a series of "saw-tooth" climbs at various air speeds at a given altitude and thus determine the air speed giving the greatest rate of climb. This was repeated at various altitudes and a curve of climbing air speed plotted against altitude. Such a curve holds true only for the particular pressure and temperature conditions existing during the saw-tooth climbs. In order to obtain a general relation, it is necessary to specify either angles of attack or indicated air speeds in terms of aneroid pressure.

The recommended procedure is to determine the angle of attack, or indicated air speed, which gives the greatest rate of climb at each aneroid reading, and plot this against aneroid reading. For example, the angle of attack that gives the least time required to climb between aneroid readings of p = 510 mm and p = 490, would be taken as the best angle of attack for p = 500. The actual increment in pressure used to determine the best reading should be so varied according to the rate of climb as to give a minimum time interval of at least 30 seconds, and preferably more. Otherwise, experimental errors may affect the results. The desirable increment in pressure will vary with altitude (or pressure) but it is constant in all of the runs at a given pressure.

Climbing Tests. After the relation between angle of attack and pressure altitude has been determined, the actual climbs may be made. Under average conditions, the best method of starting a climb is to fly horizontally in a convenient direction and at a low altitude, long enough for the airplane to settle down to steady conditions at the proper angle of attack for the existing ground pressure. The time required is determined by the lag in the aneroid and air thermometer, and the climb should not be started until these instruments record ground conditions. At the proper time, the climb is started by opening the throttle while holding the angle of attack constant.

The climb should be made with a minimum number of turns, which should be rather wide for best results. It is advisable that a climb be repeated by one or more different pilots, if possible. The composite results of three climbs should be quite definite.

Variation of Rate of Climb with Aititude. The curve of rate of climb against altitude on Figure 260 is concave upward, as indicated by the dotted straight line connecting initial and zero rates of climb. Analysis of a number of climbs indicates that if strict accuracy is required, this curvature must be considered.

The equation for the actual climb curve is of the form

$$\frac{dh}{dt} = C_0 - ah + bh^2$$

Letting

$$K = \frac{1}{\sqrt{a^2 - 4bC_0}}$$

$$C_1 = (-a + \sqrt{a^2 - 4b\,C_0})$$

and

$$C_2 = (-a - \sqrt{a^2 - 4b\,C_0})$$

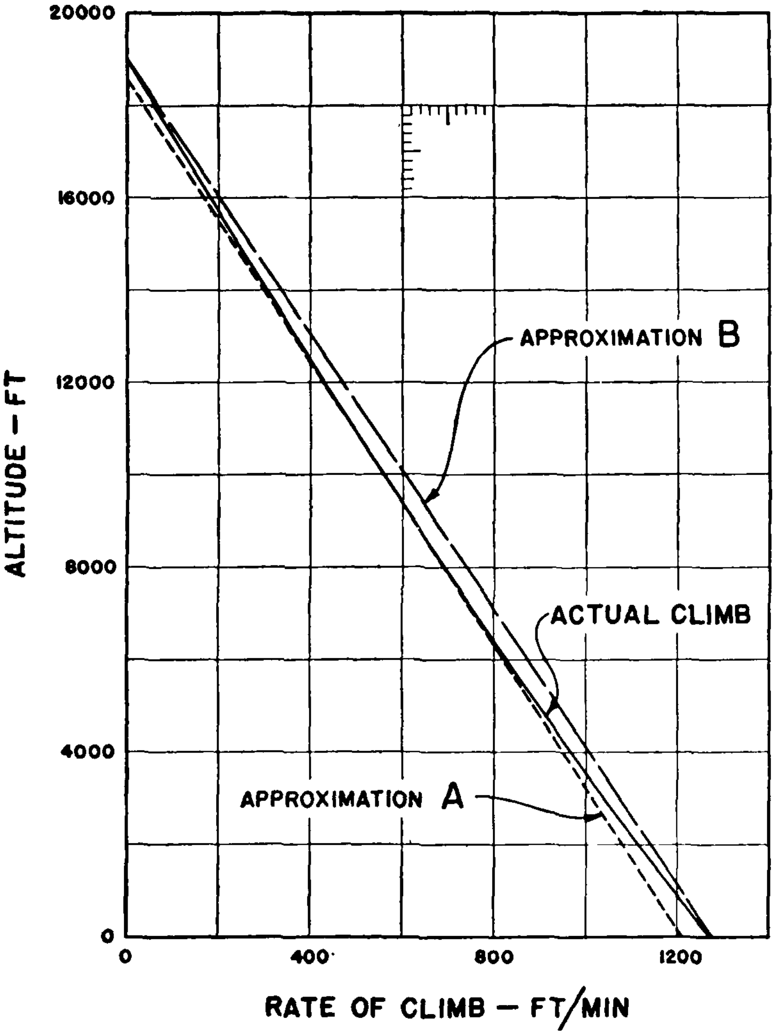

Figure 260. Variation of Rate of Climb with Altitude

The performance equations for climb are:

1. *Time of Climb to Altitude h:*

$$T = K \log_e \left[\frac{C_1 h + 2C_0}{C_2 h + 2C_0} \right] \tag{410}$$

2. *Absolute Ceiling:*

$$H = \frac{+a - \sqrt{a^2 - 4bC_0}}{2b} \tag{411}$$

3. *Service Ceiling:*

$$h_s = \frac{+a - \sqrt{a^2 - 4b\,(C_0 - 100)}}{2b} \tag{412}$$

4. *Altitude climbed in time T:*

$$h = \frac{2C_0\,(e^n - 1)}{C_1 - C_2\,e^n} \tag{413}$$

where

$$n = T/K$$

The constants a and b for any given rate-of-climb curve may be obtained by taking tangents to the rate-of-climb curve and plotting the slopes against altitude. The slope is

$$\frac{d}{dh}\left(\frac{dh}{dt}\right) = -a + 2bh \tag{414}$$

Values read from Figure 260 are plotted on Figure 261. The intersection with the axis at $h = 0$ gives $a = +0.075$. The slope of the line gives $b = +5.0 \times 10^{-7}$.

The practical significance of the curvature in the rate-of-climb curve may be illustrated by some definite values based on the climb of Figure 260. The usual practice is to draw a straight line through the points representing rates of climb at moderate altitudes. If this is done as with the line **A** in Figure 260, there will be a reduction in the indicated values of C_o, H, and h_s, compared with the true values about as follows:

	C_o	H	h_s
Actual curve	1270	19,000	17,300
Straight line A	1210	18,600	17,000

The approximation **B** is simply a straight line connecting the initial rate of climb and the absolute ceiling. It is optimistic on rates of climb at moderate altitudes.

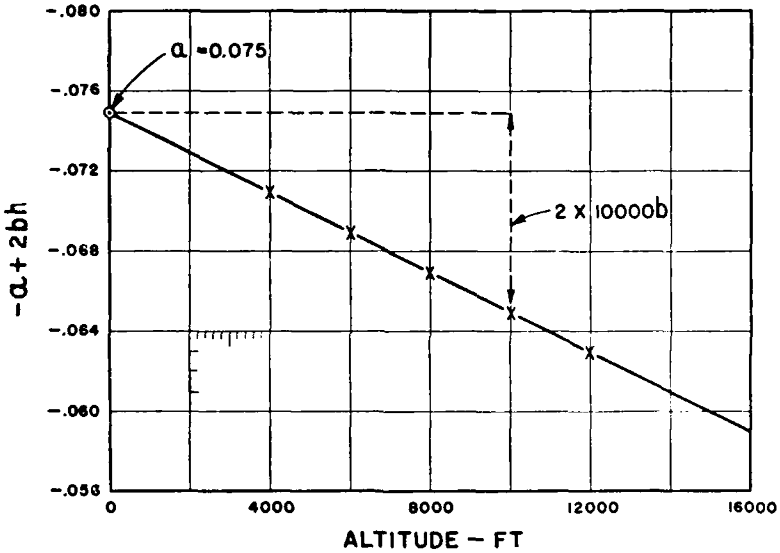

Figure 261. Graphical Solution for a and b

Reduction of Observed Performance to Standard Conditions. Since the power required for horizontal flight at a constant angle of attack varies as $\sqrt{\rho_0/\rho}$ regardless of the actual pressure and temperature while the thrust power available varies approximately as $p^{1.15}$ and $T^{-0.5}$, it follows that the performance obtained at any given pressure varies with the temperature at that pressure. "Reduction to standard conditions" is descriptive of the corrections that must be applied to observed performance in order to bring into agreement test data obtained under different temperature-pressure relations. The standard condition generally agreed on is an arbitrary specified variation of pressure and free-air temperature with altitude, designated as the "standard atmosphere." If the method of reduction is correct, the reduced performance in standard atmosphere will be identical, regardless of the temperature-pressure conditions during the flights, providing necessarily that the temperatures are within reasonable limits imposed by the engine-cooling system.

Two general methods have been widely used in performance reduction. In the older of the two, the "density" method, an observed rate of climb or an observed air speed is plotted at the altitude in standard atmosphere at which the density is that determined by the observed pressure and temperature. In the other, the "pressure" method, the altitude is determined by the pressure only. Neither method is satisfactory, but *in general, the pressure method is the better of the two.* If the temperatures do not depart more than a few degrees from standard, both methods give very nearly identical results, but as the temperatures diverge from standard, the reduced data become unreliable. Consider two climbs, one made with temperature 10° C above normal, the other with temperature 10° C below normal at all altitudes. On the density basis, the reduction gives two approximately parallel climb curves, one starting at +1170 ft and the other at −1230 ft. On the pressure basis, the reduction gives two diverging curves, both starting at the same point. It can, therefore, be definitely stated that the density method will not give consistent results, and that the pressure method is the better, but not entirely satisfactory.

Several modifications to each method have been used at one time or another. A method proposed and investigated in England is[2] based on the use of an engine power-factor varying as $p^n \rho^{1-n}$ and according to recent reports[3] the best agreement is obtained when $n = 0.5$. It is of interest to note that the relation $p^{1.15} T^{-0.5}$ used here is equivalent to $p^{0.65} \rho^{0.5}$ so that the two systems are in substantial agreement.

Instead of trying to fit various theoretical or empirical methods to observed performance, it appears more logical to determine the variation of performance with temperature and pressure and thus determine an accurate method of performance reduction. An extensive series of systematic performance calculations have been made for this purpose and very definite results obtained.[4] Owing to the great number of calculations and curves involved, it will be possible to give only a brief outline of the methods followed and the final results.

In the first series of calculations, use was made of the performance data for aspect ratio 4.8 and normal parasite. Powers required and available were calculated for absolute temperatures 83.3%, 90.9%, 110%, and 120% normal at constant pressures corresponding to altitudes of 4000, 8000, 10,000, 12,000, and 16,000 ft. The particular low temperatures used were selected on account of the simplification in slide-rule calculations. Powers available were assumed to vary as $p^{1.15} T^{-0.5}$. The data were plotted on a fairly large scale so that maximum speeds, climbing speeds, and actual rates of climb could be determined accurately.

In the second series of calculations, the data on the six aspect ratios and three parasite coefficients were used. This investigation was limited to temperatures 83.3% and 120% normal at 10,000 ft only, the first series having shown the effects to be linear with temperature and independent of altitude. The results of this investigation are outlined in the following paragraphs.

---

[2] H. Glauert, "A Discussion of the Law of Variation of Engine Power with Height," Br.A.R.C. R. & M. No. 1099 (1927).

[3] J. L. Hutchinson and E. Finn, "Determination of the Best Basis of Aircraft Performance Reduction from Flight Tests," Br.A.R.C. R. & M. No. 1532 (1932). R. S. Capon, "The Reduction of Performance Tests to the Standard Atmosphere," Br.A.R.C. R. & M. No. 1080 (1927).

[4] W. S. Diehl, "The Reduction of Observed Airplane Performance to Standard Conditions," N.A.C.A. T.R. No. 297 (1928).

The Reduction of Climb to Standard. It was immediately apparent from an inspection of the preliminary data that a definite relation existed between the pressure altitude h_p, the density altitude h_d, and what may be called the "equivalent altitude" in standard atmosphere h. (At an "equivalent altitude" under standard conditions, the rate of climb is the same as that obtained under a given non-standard condition.) The final relation was found to be

$$h = h_p - K\,(h_p - h_d) \tag{415}$$

The values of K found at various altitudes are as follows:

T/T_s	.833	.909	1.10	1.20
Values of K at 4,000 ft............	.349	.326	.351	.362
8,000 ft............	.349	.352	.363	.356
10,000 ft............	.355	.358	.368	.378
12,000 ft............	.368	.382	.356	.373
16,000 ft............	.371	.391	.384	.377

The variation in K found in the second series is so slight that the value 0.36 may be used without appreciable error for any normal airplane.

Two methods of plotting are available. A curve of equivalent altitude $h = h_p - 0.36\,(h_p - h_d)$ against time may be drawn and the rates of climb at various altitudes determined from the slope of the curve, or the geometrical rate of climb may be calculated and plotted against h.

The Reduction of Maximum Speed to Standard Conditions. The maximum speed at 12,000 ft pressure altitude is decreased 1.4 mph by temperatures 83.3% normal and increased 1.0 mph by temperatures 120% normal. These two conditions correspond to density altitudes of 6150 ft and 17,620 ft respectively. It is therefore obvious that speeds should not be plotted on the density basis.

Maximum speeds have been calculated for six different aspect ratios and three parasite coefficients at temperatures 83.3% and 120% normal at 10,000 ft pressure altitude. These two temperatures correspond to density altitudes of 4040 ft and 15,670 ft, respectively. A study of the speed data shows that the effect of a temperature change at a given pressure increases very slightly with increase in aspect ratio and with decrease in parasite coefficient. Low temperatures decrease the maximum speed, high temperatures increase it, at a given pressure altitude. Up to 70% of the absolute ceiling, the change in high speed for normal temperatures is less than the experimental error, so that actual measured true air speed may be plotted, without correction, against the pressure altitude. A considerable error might easily be possible at altitudes about 70% of the absolute ceiling, if the measured speeds are followed too closely. The relations are such in this region that in all probability no satisfactory method of exact reduction can be found. It is recommended that this part of the data be obtained by extrapolation, to the absolute ceiling, of the curves of maximum speed and climbing speed plotted against altitude.

Assuming that the power available remains constant and the power required varies as the cube of the speed, the effect of temperature on V_M is given by

$$\frac{\Delta V_M}{V_M} = +\frac{1}{3}\left(1 - \sqrt{\frac{T_s}{T_a}}\right) \qquad (416)$$

where T_s is the standard (absolute) temperature and T_a is the actual (absolute) temperature at the observed pressure. There will be an additional ΔV due to change in power with temperature. These two effects may be calculated separately and combined to find the correct speed under specified conditions, for example, at the critical altitude with a supercharged engine.

Example of Climb Reduction to Standard. Tables 27 and 28 contain the observed data and calculated altitudes for two climbs on a typical airplane. In climb No. 1, the ground temperature was 26.5° C and at all altitudes the

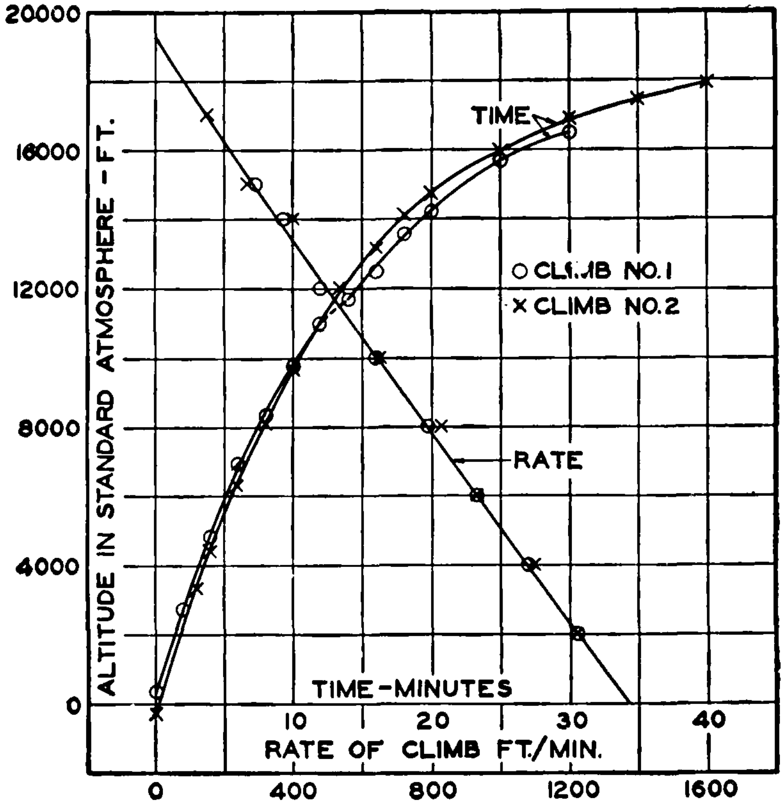

Figure 262. Comparison of Reduced Performance from Two Climbs by Different Pilots

TABLE 27. REDUCTION OF CLIMB TO STANDARD, CLIMB NO. 1

OBSERVED DATA			ALTITUDES (ft.)				
Time Min.	Pressure Mm. Hg.	Air Temp. °C.	Pressure h_p	Density h_d	$h_p - h_d$	Δh	h
0	762	26.5	−70	1,170	−1,240	−446	+376
2	697	18.5	2,370	3,330	−960	−345	2,715
4	642	12.0	4,590	5,290	−700	−252	4,842
6	594	8.0	6,660	7,430	−770	−277	6,937
8	563	5.0	8,070	8,780	−710	−255	8,325
10	533	3.0	9,490	10,270	−780	−280	9,770
12	509	0.5	10,680	11,460	−780	−280	10,960
14	493	−3.0	11,490	12,050	−560	−202	11,692
16	477	−6.0	12,330	12,730	−400	−144	12,474
18	458	−7.0	13,350	13,890	−540	−194	13,544
20	446	−8.5	14,020	14,470	−450	−162	14,182
25	421	−10.0	15,450	16,140	−690	−248	15,698
30	408	−11.0	16,230	16,950	−720	−259	16,489

$\Delta h = 0.36\,(h_p - h_d)$ $h = h_p - \Delta h$

TABLE 28. REDUCTION OF CLIMB TO STANDARD, CLIMB NO. 2

OBSERVED DATA			ALTITUDES (ft.)				
Time Min.	Pressure Mm. Hg.	Air Temp. °C.	Pressure h_p	Density h_d	$h_p - h_d$	Δh	h
0	764	12.0	−140	−520	+380	+137	−277
3	670	6.0	3,440	3,180	+260	+93	3,347
4	645	5.0	4,470	4,340	+130	+47	4,423
6	605	5.0	6,170	6,470	−300	−108	6,278
8	565	1.0	7,970	8,160	−190	−68	8,038
10	531	−3.0	9,580	9,700	−120	−43	9,623
12	507	−3.0	10,780	11,150	−370	−133	10,913
16	464	−6.5	13,030	13,330	−300	−108	13,138
18	447	−9.5	13,960	14,330	−370	−133	14,093
20	435	−10.5	14,640	14,950	−310	−111	14,751
25	414	−15.5	15,870	15,980	−110	−40	15,910
30	398	−17.5	16,830	16,950	−120	−43	16,873
35	388	−19.5	17,460	17,460	0	0	17,460
40	381	−20.5	17,900	17,880	20	+7	17,907

$\Delta h = 0.36\,(h_p - h_d)$ $h = h_p - \Delta h$

temperature was higher than normal. In climb No. 2, the ground temperature was 12° C and the temperature at altitudes was sometimes below, sometimes above normal.

The altitudes *h*, calculated from equation (415), are plotted on Figure 262 and the rates of climb determined by the slopes of the curves. In spite of the considerable difference in initial conditions, the rates of climb are in excellent agreement when reduced by this method. On either a density or a pressure basis alone, the results diverge to a marked degree.

APPENDIX I

STANDARD ATMOSPHERE

The "standard atmosphere" is an arbitrary variation of temperature, pressure, and density with altitude, which is used for numerous aeronautical purposes, but chiefly as a basis for comparing performance. The standard atmosphere recommended by the National Advisory Committee for Aeronautics[1] and adopted in 1925 by all interested government departments for official use in the United States is based on the following assumptions:

Ground temperature, $t_0 = 15° \text{ C} = 59° \text{ F}$
Isothermal temperature, $t = -55° \text{ C} = -67° \text{ F}$
Temperature gradient, $a = 0.0065° \text{ C/m} = 0.003566° \text{ F/ft}$
The air is a dry, perfect gas.

The resulting equations are:

$$T = T_0 - ah \tag{417}$$

$$p = Rg\rho T, \text{ or } \frac{p}{p_0} = \left(\frac{\rho}{\rho_0}\right)\left(\frac{T}{T_0}\right) \tag{418}$$

$$h = \frac{p_0}{g\rho_0}\frac{T_m}{T_0}\log_e\left(\frac{p_0}{p}\right) \tag{419}$$

$$T_m = \text{Harmonic mean temperature}$$

$$= \frac{ah}{\log_e\left(\dfrac{T_0}{T_0 - ah}\right)} \tag{420}$$

---

[1] See "Standard Atmosphere—Tables and Data," N.A.C.A. Technical Report No. 218 (1925).

TABLE 29. STANDARD ATMOSPHERE

h ft	$\frac{p}{p_0}$	$\frac{\rho}{\rho_0}$	$\sqrt{\frac{\rho}{\rho_0}}$	$\frac{\rho_0}{\rho}$	$\left(\frac{\rho_0}{\rho}\right)^2$	$\sqrt{\frac{\rho_0}{\rho}}$
−4,000	1.1533	1.1225	1.0595	.8909	.7937	.9438
−3,000	1.1134	1.0909	1.0445	.9167	.8403	.9574
−2,000	1.0745	1.0599	1.0295	.9435	.8902	.9713
−1,000	1.0367	1.0296	1.0148	.9713	.9433	.9855
0	1.0000	1.0000	1.0000	1.0000	1.0000	1.0000
1,000	.9644	.9710	.9854	1.0299	1.0607	1.0148
2,000	.9298	.9428	.9710	1.0607	1.1250	1.0299
3,000	.8962	.9151	.9566	1.0928	1.1941	1.0454
4,000	.8636	.8881	.9424	1.1260	1.2679	1.0611
5,000	.8320	.8616	.9282	1.1606	1.3470	1.0773
6,000	.8013	.8358	.9142	1.1965	1.4316	1.0939
7,000	.7716	.8106	.9003	1.2336	1.5218	1.1107
8,000	.7427	.7859	.8865	1.2724	1.6190	1.1280
9,000	.7147	.7619	.8729	1.3125	1.7227	1.1456
10,000	.6876	.7384	.8593	1.3542	1.8338	1.1637
11,000	.6614	.7154	.8458	1.3978	1.9538	1.1823
12,000	.6359	.6931	.8325	1.4427	2.0814	1.2012
13,000	.6112	.6712	.8193	1.4899	2.2198	1.2206
14,000	.5873	.6499	.8062	1.5386	2.3673	1.2404
15,000	.5642	.6291	.7932	1.5896	2.5268	1.2608
16,000	.5418	.6088	.7803	1.6425	2.6977	1.2816
17,000	.5202	.5891	.7675	1.6975	2.8815	1.3029
18,000	.4992	.5698	.7549	1.7550	3.0800	1.3248
19,000	.4790	.5509	.7422	1.8152	3.2950	1.3473
20,000	.4594	.5327	.7299	1.8772	3.5239	1.3701
21,000	.4405	.5148	.7175	1.9425	3.7733	1.3937
22,000	.4222	.4974	.7053	2.0104	4.0417	1.4179
23,000	.4045	.4805	.6932	2.0812	4.3313	1.4426
24,000	.3874	.4640	.6812	2.1551	4.6444	1.4681
25,000	.3709	.4480	.6693	2.2321	4.9823	1.4940
26,000	.3550	.4323	.6575	2.3132	5.3509	1.5209
27,000	.3397	.4171	.6458	2.3975	5.7480	1.5484
28,000	.3248	.4023	.6343	2.4857	6.1786	1.5766
29,000	.3106	.3879	.6228	2.5780	6.6460	1.6056
30,000	.2968	.3740	.6116	2.6737	7.1486	1.6352
31,000	.2834	.3603	.6002	2.7755	7.7034	1.6660
32,000	.2707	.3472	.5892	2.8801	8.2950	1.6971
33,000	.2583	.3343	.5782	2.9913	8.9478	1.7295
34,000	.2465	.3218	.5673	3.1075	9.6565	1.7628
35,000	.2352	.3098	.5566	3.2279	10.4192	1.7966
36,000	.2242	.2962	.5442	3.3761	11.3980	1.8374
37,000	.2137	.2824	.5314	3.5411	12.5394	1.8818
38,000	.2037	.2692	.5188	3.7147	13.7990	1.9274
39,000	.1943	.2566	.5066	3.8971	15.1874	1.9741
40,000	.1852	.2447	.4947	4.0866	16.7003	2.0215

Below the isothermal level (10,769 m or 35,332 ft) the following relations exist:

$$\frac{T}{T_0} = \left(\frac{p}{p_0}\right)^{0.19} = \left(\frac{\rho}{\rho_0}\right)^{0.235} \tag{421}$$

$$\left(\frac{p}{p_0}\right) = \left(\frac{T}{T_0}\right)^{5.256} = \left(\frac{\rho}{\rho_0}\right)^{1.235} \tag{422}$$

$$\left(\frac{\rho}{\rho_0}\right) = \left(\frac{T}{T_0}\right)^{4.256} = \left(\frac{p}{p_0}\right)^{0.81} \tag{423}$$

$$\left(\frac{p}{p_0}\right)^{0.19} = \left(1 - \frac{a}{T_0}h\right) \tag{424}$$

$$\left(\frac{p}{p_0}\right) = \left(1 - \frac{a}{T_0}h\right)^{5.256} \tag{425}$$

$$\left(\frac{\rho}{\rho_0}\right)^{0.235} = \left(1 - \frac{a}{T_0}h\right) \tag{426}$$

$$\left(\frac{\rho}{\rho_0}\right) = \left(1 - \frac{a}{T_0}h\right)^{4.256} \tag{427}$$

In the foregoing equations, the subscript 0 refers to the standard conditions at sea-level. h is the altitude and R the gas constant for air.

The commonly used standard atmosphere ratios are given in Table 29.

Approximate Equations for the Standard Atmosphere. Approximate relations are frequently desired for the standard atmosphere ratios. A study[2] has been made to develop a series of equations that are suitable for various purposes. The most useful or most accurate approximations obtained for density ratio are as follows:

$$\frac{\rho}{\rho_0} = 1 - \frac{h}{40,000} \tag{428}$$

$$= e^{\frac{-h}{34,100 - 0.12h}} \tag{429}$$

$$= \frac{33,600 - 0.53h}{33,600 + 0.47h} \tag{430}$$

---

[2] W. S. Diehl, "Some Approximate Equations for the Standard Atmosphere," N.A.C.A. T.R. No. 376 (1931).

Equation (428) is within 2% for values of h less than 16,000 ft, equation (429) is within 0.13% below 30,000 ft, and equation (430) is within 0.75% below 30,000 ft.

The approximate equations for $\sqrt{\rho_0/\rho}$ are

$$\sqrt{\frac{\rho_0}{\rho}} = 1 + \frac{h}{60{,}000} \tag{431}$$

$$= e^{\frac{-h}{68{,}320 - 0.707\,h}} \tag{432}$$

$$= \frac{68{,}320 + 0.293\,h}{68{,}320 - 0.707\,h} \tag{433}$$

Equation (431) is within 1% below 16,000 ft, equation (432) is within 0.10% below 30,000 ft, and equation (433) is within 0.02% below 30,000 ft.

The approximate equations for pressure ratio are

$$\frac{p}{p_0} = e^{\frac{-h}{27{,}000 - 0.097\,h}} \tag{434}$$

$$= \frac{27{,}000 - 0.48\,h}{27{,}000 + 0.52\,h} \tag{435}$$

Equation (434) is within 1% below 20,000 ft and equation (435) is within 1.3% below 30,000 ft.

Standard Atmospheric Relations Used in Performance Reduction. The relation between pressure, temperature, and density ratio, at any altitude is

$$\frac{\rho}{\rho_0} = 0.3789\,\frac{p \text{ mm Hg}}{(t\,^\circ\text{C} + 273^\circ)} \tag{436}$$

$$= 9.624\,\frac{p \text{ in Hg}}{(t\,^\circ\text{C} + 273^\circ)} \tag{437}$$

$$= 17.32\,\frac{p \text{ in Hg}}{(t\,^\circ\text{F} + 459.4^\circ)} \tag{438}$$

The relation between an increment of pressure $\Delta p = (p_1 - p_2)$, the average density ρ_m between p_1 and p_2, and the increment of altitude Δh is, in metric units:

$$\Delta h = \frac{-13.59\ \Delta p \text{ mm Hg}}{g\rho_m} \qquad (439)$$

and in English units

$$\Delta h = \frac{-70.67\ \Delta p \text{ in. Hg}}{g\rho_m} \qquad (440)$$

Figures 263, 264, and 265 are plots of ρ/ρ_0, p/p_0, and p against altitude in standard atmosphere. Density ratios may be calculated by equation (436), and the corresponding density altitudes found from Figure 263. Pressure altitudes may be read directly from Figure 265.

Figure 266 is a plot of $\sqrt{\rho_0/\rho}$ against altitude.

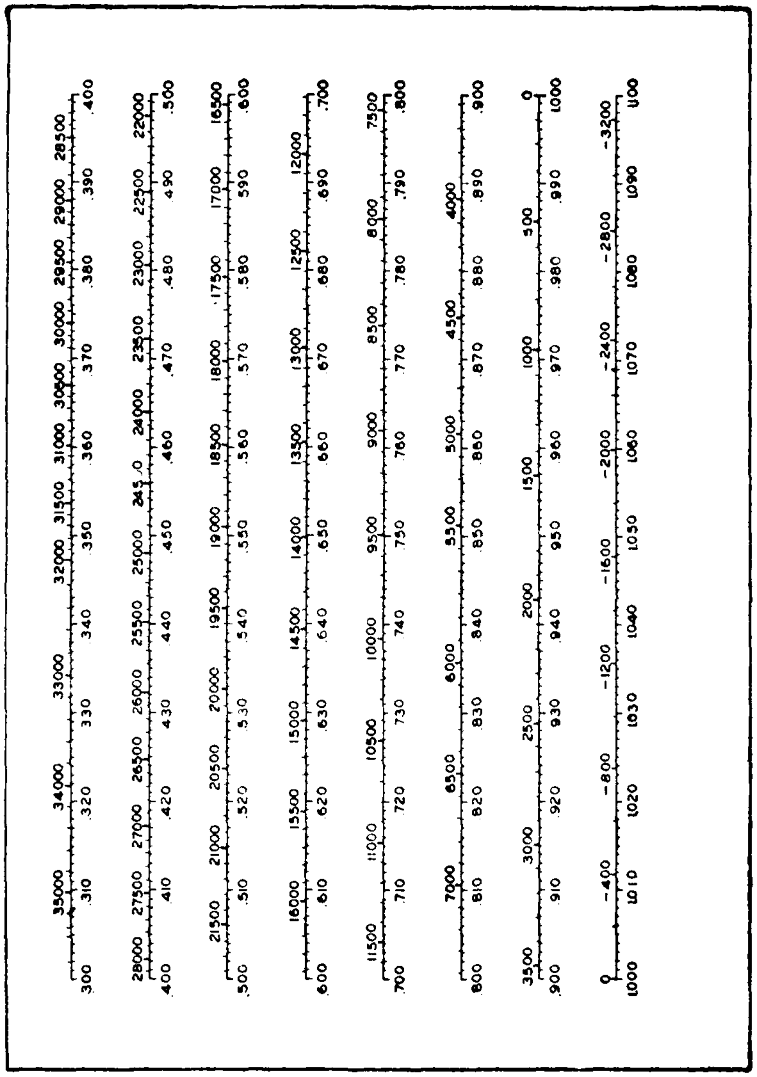

Figure 293. Density Ratio ρ/ρ_0 at Any Altitude in Standard Atmosphere. Density ratios are below and altitudes are above the base lines

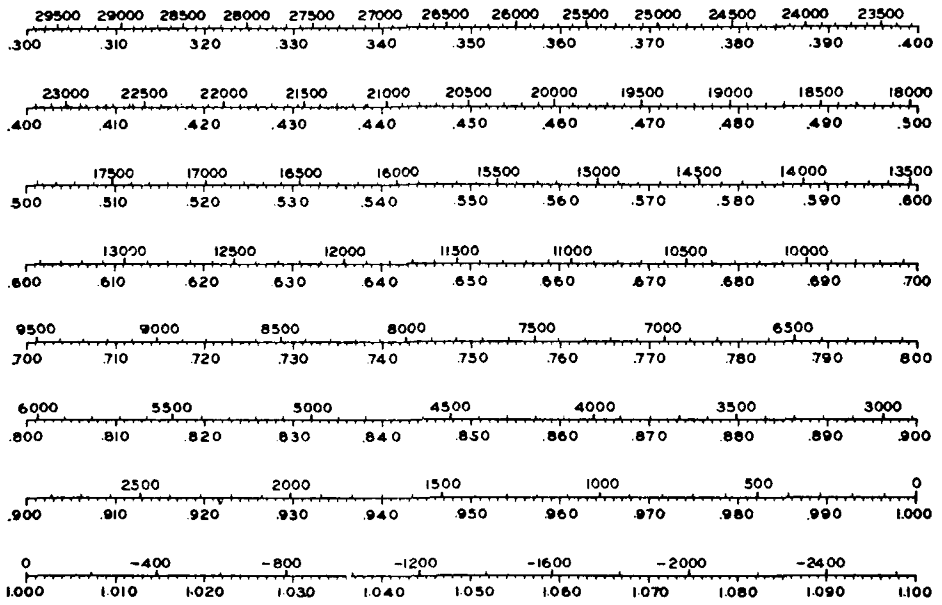

Figure 264. Pressure Ratio p/p_0 at Any Altitude in Standard Atmosphere. Pressure ratios are below and altitudes are above the base lines

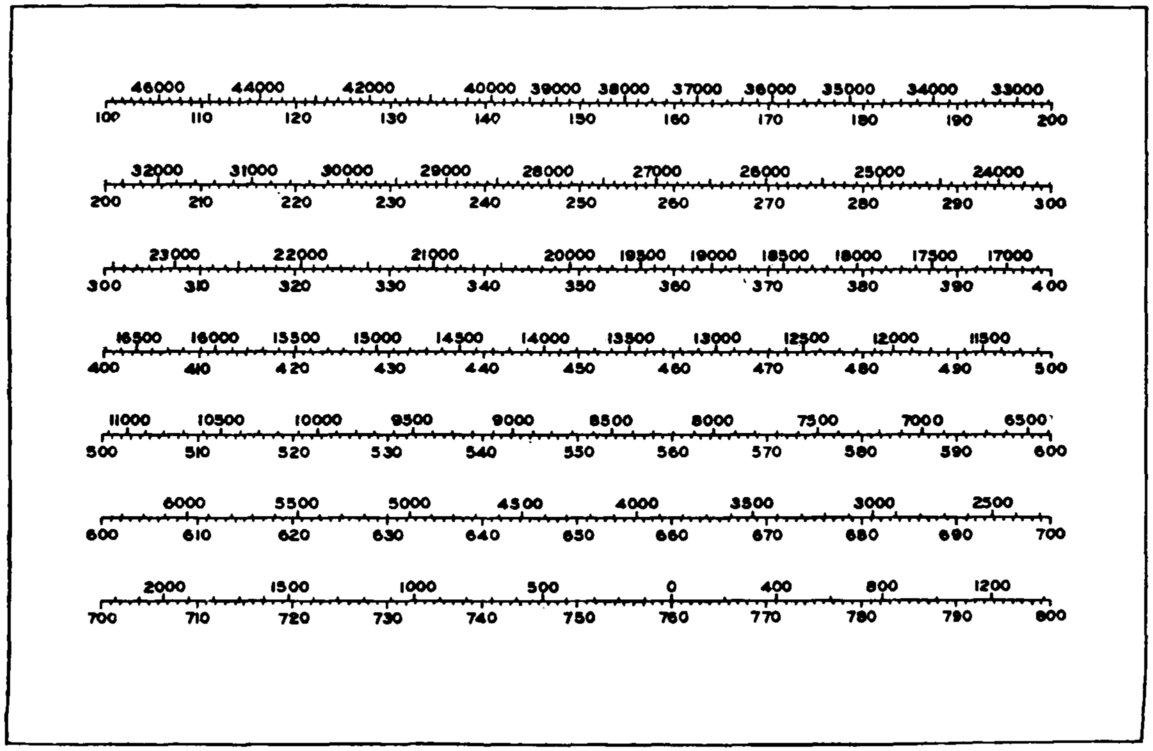

Figure 265. Pressure in mm. Hg at Any Altitude in Standard Atmosphere. Pressures are below and altitudes are above the base lines

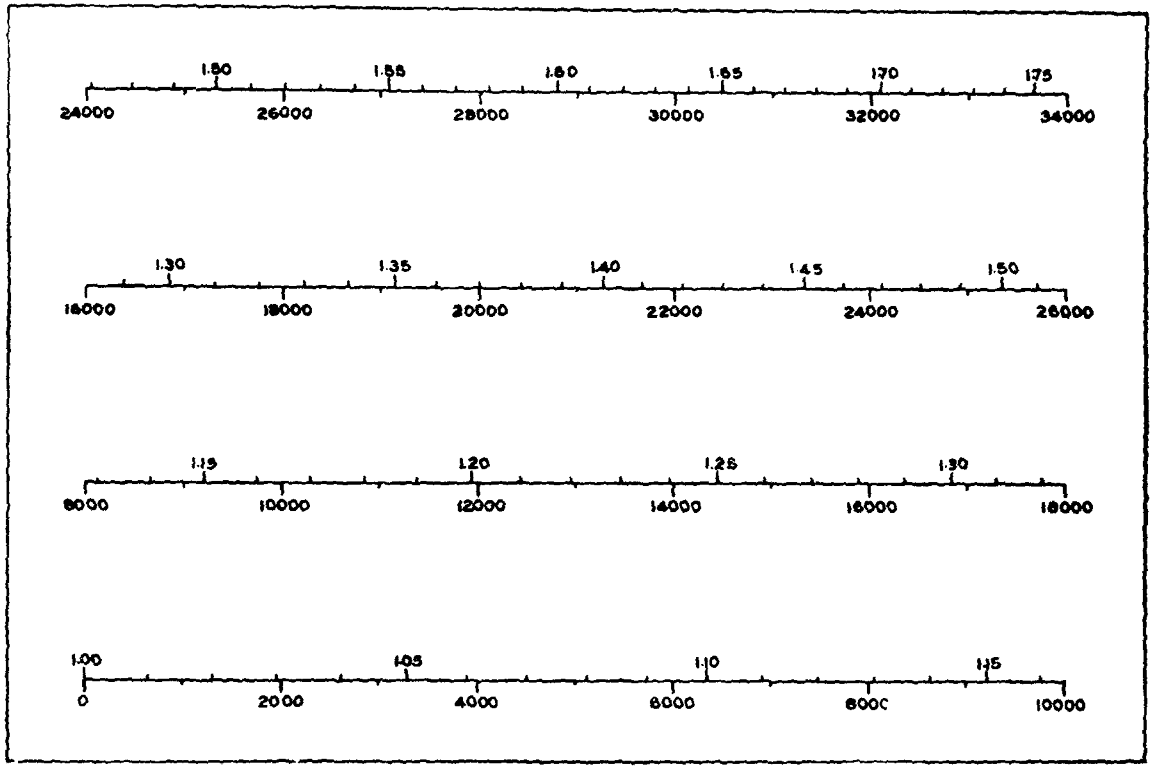

Figure 206. $\sqrt{\rho_0/\rho}$ at Any Altitude in Standard Atmosphere. Values of $\sqrt{\rho_0/\rho}$ are above and altitudes are below the base lines

APPENDIX II

GENERAL CONVERSION FACTORS

The following table of conversion factors departs from the conventional form in that the factors are given to as many significant figures as possible. While in most cases four or five significant figures are sufficient, it has been the author's experience that greater accuracy is often required. It is not intended that the factors be used as given, unless such accuracy is required. For example, the exact conversion factor from cubic inches to cubic centimeters is 16.3871624, but 16.39 or even 16.4 is often close enough.

Fundamental conversion factors.

1 meter = 39.37 inches (Act of U. S. Congress, 28 July, 1866)
= 3.2808333 feet

1 pound = 453.5924277 grams (International Bureau of Weights and Measures, July 1893)

Specific weight of dry air with normal CO_2 content at 760 mm. Hg. and 0° C. = .0012930 gr./cm.

Specific weight of mercury at 0°C. . . . . = 13,595.1 $kg./m^3$

Standard gravity (International) g . . . . = 980.665 $cm./sec.^2$
= 32.174 $ft./sec.^2$

MULTIPLY	BY	TO OBTAIN
Atmospheres	76.0	cm. mercury
"	29.9212	inches mercury
"	33.8985	feet of water
"	10,332.276	kilograms per sq. meter
"	14.69601	pounds per sq. in.
"	2,116.225	pounds per sq. ft.
"	1,013,250.	bars
Bars	1.0	dynes per sq. cm.
B. t. u. (mean)	777.98	foot-pounds
"	1,054.8	joules
"	.25198	kilogram-calories
"	107.560	kilogram-meters
Centimeters (cm.)	.393700	inches
"	.0328083	feet
cm. of mercury	5.352391	inches of water
"	.4460326	feet of water
"	.193368	pounds per sq. in.
"	27.84507	pounds per sq. ft.
"	135.9510	kilograms per sq. meter
cm. per sec.	.0328083	feet per sec.
cubic centimeters	.000999973	liters
"	.06102338	cubic inches
cubic feet	1,728.0	cubic inches
"	1/9	cubic yards
"	7.480519	gallons
"	28,317.017	cubic centimeters
"	28.31625	liters
"	.028317017	cubic meters
cubic feet per min.	.471704	liters per sec.
" "	.028317	cubic meters per min.
cubic feet of water	62.42833	pounds
cubic inches	16.3871624	cubic centimeters
"	.0163876	liters
"	1/231	gallons
cubic meters	10^6	cubic centimeters
"	61,023.3753	cubic inches
"	35.3144548	cubic feet
"	1.307943	cubic yards
"	264.170	gallons
cubic yards	27.	cubic feet
"	.76455945	cubic meters
Degrees (arc)	.017453292	radians
dynes	.00101972	grams
dynes per sq. cm.	1.0	bars
Ergs	1.0	dyne-centimeters

MULTIPLY	BY	TO OBTAIN
Fathoms	6.0	feet
"	1.82880	meters
feet	12.0	inches
"	1/3	yards
"	30.4800613	centimeters.
"	.3048006	meters
feet of water	.029500	atmospheres
"	.433530	pounds per sq. in.
"	62.428327	pounds per sq. ft.
"	304.8006	kilograms per sq. meter
"	.882671	inches of mercury
"	.224199	centimeters of mercury
feet per min.	.0113636	miles per hr.
"	.018288	kilometers per hr.
"	.508001	centimeters per sec.
feet per sec.	.681818	miles per hr.
"	1.09728220	kilometers per hr.
"	30.48006	centimeters per sec.
"	.3048006	meters per sec.
"	.5920858	knots
foot-pounds	.138255	meter-kilograms
foot-pounds per min.	1/33,000	horsepower
foot-pounds per sec.	1/550	horsepower
Gallons	231.0	cubic inches
"	.133680	cubic feet
"	3.785332	liters
"	.832680	imperial gallons
gallons-Imperial	1.20094	gallons
" "	277.4176	cubic inches
" "	4.5459631	liters
grains	.0647988	grams
grams	15.43236	grains
"	.0352739	ounces
"	.0022046223	pounds
"	1,000.0	milligrams
"	.001	kilograms
"	980.665	dynes
gram-calories	.0039685	B. t. u.
gram-centimeters	980.665	ergs
grams per cm.	0.1	kilograms per meter
"	.06719702	pounds per foot
"	.0055914	pounds per inch
grams per cu. cm.	1,000.0	kilograms per cu. m.
"	62.42833	pounds per cu. ft.
Horsepower	33,000.0	foot-pounds per min.
"	550.0	foot-pounds per sec.
"	76.04039	kilogram-meters per sec.
"	1.013872	metric horsepower

MULTIPLY	BY	TO OBTAIN
horsepower, metric	75.0	kilogram-meters per sec.
"	.986318	horsepower
horsepower-hours	2,545.06	B. t. u.
"	1,980,000.	foot-pounds
"	273,745.4	kilogram-meters
Inches	2.54000508	centimeters
inches of mercury	.0334211	atmospheres
"	13.5951	inches of water
"	1.132925	feet of water
"	.4911570	pounds per sq. in.
"	70.72661	pounds per sq. ft.
"	345.3162	kilograms per sq. meter
inches of water	.0735559	inches of mercury
"	.1868324	centimeters of mercury
"	.0361275	pounds per sq. in.
"	5.202360	pounds per sq. ft.
"	25.400051	kilograms per sq. meter
Joules	10^7	ergs
"	.7375606	foot-pounds
"	.1019716	kilogram-meters
Kilograms	2.20462234	pounds
"	35.273957	ounces
"	1,000.0	grams
kilogram-calories	3.9685	B. t. u.
"	3,087.4	foot-pounds
"	426.85	kilogram-meters
kilogram-meters	7.2329983	foot-pounds
"	9.80665×10^7	ergs
kilograms per cu. meter	.06242833	pounds per cu. ft.
" "	.001	grams per cu. cm.
kilograms per meter	.6719702	pounds per ft.
kilograms per sq. meter	.00142234	pounds per sq. in.
" "	.2048169	pounds per sq. ft.
" "	.00289590	inches of mercury
" "	.003280833	feet of water
" "	0.1	grams per sq. cm.
kilometers	3,280.833	feet
"	.6213700	miles
"	.539593	nautical miles
kilometers per hr.	.9113426	feet per sec.
" "	.6213700	miles per hr.
" "	.2777	meters per sec.
" "	.539593	knots
knots	1.0	nautical miles per hr.
"	1.688944	feet per sec.
"	1.151553	miles per hr.
"	1.853249	kilometers per hr.
"	.514791	meters per sec.

MULTIPLY	BY	TO OBTAIN
Liters	1,000.027	cubic centimeters
"	61.02503	cubic inches
"	.035315411	cubic feet
"	.264178	gallons
"	.219975	imperial gallons
Meters	39.37	inches
"	3.280833	feet
"	1.093611	yards
meters per sec.	3.280833	feet per sec.
"	2.2369317	miles per hr.
"	3.600	kilometers per hr.
microns	.0001	centimeters
miles	5,280.0	feet
"	1.609347	kilometers
"	.8683925	nautical miles
miles per hr.	1.46666	feet per sec.
"	.4470409	meters per sec.
"	1.609347	kilometers per hr.
"	.8683925	knots
miles per hr. squared	2.151111	feet per sec. squared
mills	.001	inches
"	.025400	millimeters
Nautical miles	6,080.20	feet
"	1.1515530	miles
"	1,853.2486	meters
Ounces	1/16	pounds
"	28.349527	grams
ounces per sq. yd.	33.906096	grams per sq. meter
Poundals	.0310810	pounds
"	13,825.561	dynes
pounds	453.5924277	grams
"	.45359243	kilograms
"	16	ounces
"	32.174	poundals
pounds-feet	.1382552	kilogram-meters
pounds per ft.	1.4881612	kilograms per meter
pounds per cu. ft.	16.018369	kilograms per cu. meter
" "	.016018369	grams per cu. cm.
pounds per cu. in.	1,728	pounds per cu. ft.
" "	27.6797424	grams per cu. cm.
pounds per sq. ft.	.192220	inches of water
" "	4.8824088	kilograms per sq. meter
pounds per sq. in.	2.036009	inches of mercury
" "	2.306645	feet of water
" "	.0680457	atmospheres
" "	703.06687	kilograms per sq. meter

MULTIPLY	BY	TO OBTAIN
Quarts (dry)	67.20	cubic inches
" (liquid)	57.75	cubic inches
Radians	57.29578	degrees (arc)
radians per sec.	57.29578	degrees per sec.
"	.159155	revolutions per sec.
"	9.54930	revolutions per min.
revolutions	6.283185	radians
revolutions per min.	.104720	radians per sec.
Slugs	32.174	pounds
square centimeters	.1549997	square inch
"	.00107639	square feet
square feet	929.03412	square centimeters
"	.092903412	square meters
square inches	645.162581	square millimeters
"	6.4516258I	square centimeters
square kilometers	.3861006	square miles
square meters	10.76386736	square feet
"	1.1959853	square yards
square miles	2.59000	square kilometers
square yards	.8361307	square meters
Tons, long	2,240.	pounds
"	1,016.047	kilograms
tons, short	2,000.	pounds
"	907.1849	kilograms
tons, metric	1,000.	kilograms
"	2,204.622	pounds
Yards	91.44018	centimeters
"	.9144018	meters

APPENDIX III

USEFUL FORMULAS

Powers and Roots.

$$a^{-n} = \frac{1}{a^n} \qquad a^m \cdot a^n = a^{(m+n)}$$

$$\frac{a^m}{a^n} = a^{(m-n)} \qquad (a^m)^n = (a^n)^m = a^{mn}$$

$$a^{\frac{1}{n}} = \sqrt[n]{a} \qquad a^{\frac{m}{n}} = \sqrt[n]{a^m}$$

$$(a^{\frac{1}{m}})^{\frac{1}{n}} = a^{\frac{1}{m \cdot n}}$$

$$(ab)^n = a^n b^n \qquad \left(\frac{a}{b}\right)^n = \frac{a^n}{b^n} = a^n b^{-n}$$

$$(ab)^{\frac{1}{n}} = a^{\frac{1}{n}} b^{\frac{1}{n}} = \sqrt[n]{ab}$$

Logarithms.

Let $b^x = N \qquad (b > 1.0)$

Then: $\log_b N = x \qquad \log_b b = 1.0$

$$\log_b 1 = 0 \qquad \log_b 0 = -\infty$$

$$\log_b MN = \log_b M + \log_b N$$

$$\log_b \frac{M}{N} = \log_b M - \log_b N$$

$$\log_b N^r = r \cdot \log_b N$$

$$\log_b \sqrt[s]{N^r} = \frac{r}{s} \cdot \log_b N$$

$$\log_b N = \frac{\log_a N}{\log_a b}$$

$$e = 2.71828183 \qquad \log_e 10 = 2.30258509$$

$$\log_e 2 = 0.69314718 \qquad \log_{10} e = 0.43429448$$

$$\log_e N = \log_e 10 \cdot \log_{10} N$$

Derivatives.

FUNCTION	DERIVATIVE
x	1
c	0
$\pm u \pm v$	$\pm \frac{du}{dx} \pm \frac{dv}{dx}$
$c \cdot u$	$c \cdot \frac{du}{dx}$
$u \cdot v$	$u\frac{dv}{dx} + v\frac{du}{dx}$
$\frac{u}{v}$	$\frac{v\frac{du}{dx} - u\frac{dv}{dx}}{v^2}$
u^n	$nu^{n-1}\frac{du}{dx}$
$\log_{10} u$	$\frac{\log_{10} e}{u} \cdot \frac{du}{dx}$
$\log_e u$	$\frac{1}{u} \cdot \frac{du}{dx}$
a^u	$a^u \cdot \log_e a \cdot \frac{du}{dx}$
e^u	$e^u \cdot \frac{du}{dx}$
u^v	$vu^{v-1} \cdot \frac{du}{dx} + u^v \log_e u \frac{du}{dx}$
$\sin u$	$\cos u \cdot \frac{du}{dx}$
$\cos u$	$-\sin u \cdot \frac{du}{dx}$
$\tan u$	$\sec^2 u \cdot \frac{du}{dx}$
$\cot u$	$-\csc^2 u \cdot \frac{du}{dx}$

c is any constant. u and v are any functions of x.

Integrals.

FUNCTION	INTEGRAL
$a \cdot u^n \cdot du$	$\frac{a \cdot u^{n+1}}{n+1} + c \quad (n \neq -1)$
$\frac{du}{u}$	$\log_e u + c$
$a^u \cdot du$	$\frac{a^u}{\log_e a} + c$
$e^{au} \cdot du$	$\frac{e^{au}}{a} + c$
$u \cdot dv$	$uv - \int v \cdot du$

u and v are any functions of x.

INDEX

Abbreviations, 18
Aerodynamics, definition, 3-5
Ailerons, 215-221
  balanced, 220-225, 228-233
  efficiency, 217-220
  moments, 100-102
  types, 220-222
  wind-tunnel tests, 100-102
Airfoil(s),
  center section cut-outs, 134-135
  data, 110-111, 115
  drag, 114-117
  efficiency, 119-120
  leading edge radius, 114
  lift, 112-114, 117
  N. A. C. A. related, 111-113
  ordinates, 130-131
  reflexed trailing edge, 96, 114
  selection of an, 128-130
  slotted, 162-165
  symbolic equivalents, 130-131
  tail surface, 201-202
  tapered, 133-134
  tests, 89-90
  with flaps, 141-170
  zero lift, 120-122
Airplane,
  axes, 9-12, 238, 241-242
  cross-wind force, 254-255
  design, 3, 141-142, 171-172, 468-490
  efficiency factor, 399-401
  equations of motion, 362-363, 450-452
  flight tests, 510-526
  forces acting on, 362-363
  model construction, 89, 92-93
  model tests, 90-108
  parts, drag of, 260-311
  performance, 362-382, 383-413, 428-434
  terminal velocity, 450-452
Airship, C-class offsets, 272
Air speed,
  determination of, 510-512
  economical, 414
  for best climb, 402-403, 512-515
  indicator calibration, 510-511, 515
  most economical, 414
  true, 356
  wind effect, 425-426
Altitude,
  bhp variation, 315-319
  climbed in a given time, 375-376, 407-412, 518
  critical, 314, 316-319, 358, 380-381, 406, 412, 442-443
    engine and propeller, 355-359
    extrapolation of curve, 380-381, 412
    supercharged engine, 314-319, 380-381, 406-407, 442-443
  effect on,
    maneuverability, 474-481
    specific fuel consumption, 321
    take-off run, 440, 442-443
  equivalent, 522
  loss in a vertical dive, 452-458
  variation of,
    bhp with, 315-319
    maximum speed, 391-393
    thp with, 355-360, 376-378
Aneroid, 515
Angle between keels at step, 507, 509
Angle of
  attack,
    for zero lift, 62-64, 120-121
    in a climb, 515
    induced, 34-35, 54
  bank, 461-462, 464-466
  blade setting, 324-325
  climb, 443-444
  dead rise, 506, 507
  dihedral, 211-215
  dive, 458, 460-462
  glide, 169, 459-460, 444-445
  tail setting, 193-197
Area,
  ailerons, 215-221
  balanced controls, measurement of, 225
  elevators, 197-201
  fin and rudder, 203-215
  measurement of, 187, 225, 385-386
  parasite flat plate, 261
  rudder, 210-211
  side, formula, 208-209
  stabilizer and elevator, 182-202
  variable, 159-162
  wing, 385-386

Aspect ratio, 33-34, 60-61, 91, 189-191
  corrections for, 130
  effect on,
    absolute ceiling, 472-474
    air speed for best climb, 402-403, 513-514
    downwash, 31-33, 57-58
    horizontal tail area, 189-191
    initial rate of climb, 472-473, 482-490
    maximum speed, 383-396, 469-473
    power required, 393-397, 417-418, 469-471, 482-490
    slope of lift curve, 51-55, 95-96, 126-128
    speed for minimum power, 393-398
  equivalent monoplane, 34-35
  low, 51
  virtual, 398-401
Atmosphere, standard, 520-535 (See also "Standard atmosphere")
Attack, angle of (See "Angle of attack")
Axes,
  airplane, 9-12
  reference, 9-12, 238, 241-242
  wind, 9-12, 101, 241-242

Balance,
  dynamic, 228-230
  effect of flaps on, 202
  longitudinal, 99-100, 202
  tail setting for, 99-100, 193-197
Balances, wind-tunnel, 74-75, 89-90
Bank, angle of, 461-462, 464-466
Beam, seaplane floats, 505-506
Bernoulli's theorem, 25-26
Biplane,
  drag of, 38-39
  flaps on, 385
  lift-curve slope, 55
  lift distribution, 66-72
  lift, maximum, 132-133
  mean chord, 178-181
  moment coefficient, 70-72, 175-178
  most efficient, 39, 47
  nacelle drag, 301
  virtual mean chord, 179-181
Biquadratic, stability, 236, 239-240, 244, 252
Blade,
  angle for constant rpm, 358, 360
  setting, 324-325, 329-330, 332, 337, 358, 360, 369
  twist, 325
Body-propeller interference, 334, 336
Bomb, drag of, 306-307
Bombing range, 424-425
Boundary layer control, 167
Brake horsepower,
  general curves for, 313, 345-347, 349
  in range calculation, 414-415
  variation with
    altitude, 315-319, 521
    pressure and temperature, 315
    speed, 346-347
Brakes, landing use, 448
Breguet's formulas, 419-422
Buffeting, tail, 192-193
Buoyancy,
  excess, 290, 506
  horizontal, 86, 90
Burble,
  compressibility, 140
  interference, 95-96

Cable, drag of, 276-280
Calculations,
  ceiling, absolute, 371-375
  performance, 361-382
  rate of climb, 371
Calibration of airspeed indicators, 510-511
Camber,
  effect on
    airfoil lift, 112-114
    profile drag, 114-117
  mean, 111-116
C-class airship,
  drag, 275-276
  offsets, 272
Ceiling,
  absolute, 324, 371-375, 380, 403-406, 518-519
  service, 375, 406-407
  supercharged engine, 406-407
Cellular radiator, drag of, 305
Center, aerodynamic, 61-62, 122-123, 178-181
Center of gravity, location, 170, 172-176, 181-182, 191-192, 251
Center of pressure, 62
  lateral, 101
Centrifugal force, 461-462, 465-466
Characteristics, wing-section, 110-111, 115
Chart, absolute ceiling, 374, 404
Chord,
  mean, 72, 178-181
  virtual, 179-181
Circling flight, 461-466

Circulation, 23-24
Climb,
  accurate curve for rate, 516-519
  air speed in, 371-375, 402-403, 512-515
  effect of temperature, 514-515, 520-522
  equation for rate, 401
  general curve for rate, 407-408
  graphical solution for rate, 367, 371
  initial rate, 371, 401-403, 473, 482-490
  in ten minutes, 411-413
  linear rate, 407-413, 518-519
  maximum path angle, 443-444
  minimum safe rate, 481-484, 486-487, 489-490
  path angle, 443-444
  rate of,
    general curve, 407-408
    initial, 367-371, 401-403, 472-473, 482-490
    linear, 406-413, 518-519
  reduction to standard, 520-522, 524-526
  sawtooth, 515
  tests, 515-516
  time of, 375-376, 407-413
  variation with altitude, 380-381, 516-519
  zero rate of, 482, 484-485, 487-488, 489
Coefficient(s), 13, 14, 260, 321, 322
  absolute, 13-14
  additional mass, 206
  damping, 239-240
  mass, additional, 203, 206
  non-dimensional, 13, 14, 321, 322, 500-501
  normal force, 62
  propeller drag, 450-452
  speed-power, 325-328
  traction in take-off, 438
Combined loading, 488-490
Compressibility, 77-78, 91-92, 139-140
  burble, 140
Compression ratio and fuel consumption, 319-320
Constant(s),
  angle of attack, range at, 419-422
  rate-of-climb curve, 516-519
  rpm, 336-338, 358-360
  speed, range at, 422-424
Control(s), 97-104, 171-235
  aerodynamic balance, 222-228
    calculations for, 225-226
Control(s)—*Continued*
  boundary layer, 167
  directional, 102-104, 203-215
  hinges, binding, 217
  horns, drag, 305
  lateral, 100-102, 170, 215-221
  longitudinal, 97-100, 182-202
  mass balance, 228-234
  surface,
    dead-center effect, 201
    design, 172-235
    sections, 201-202
  tabs, 197-200
Conversion factors, 14, 536-541
Coordinates of c.g., 173
Corrugations, drag, 270
Couple, 5, 203
Cup anemometer, 264
Curvature in rate of climb, 516-519
Curves, general, for,
  bhp, 312-315, 345-347, 349
  endurance, 430, 432, 434
  power coefficient, 344-345
  propeller efficiency, 333-335, 336-337
  range, 431, 433-434
  rate of climb, 408
  rpm, 348
  thp, 349-354, 417-418, 437, 439
  time of climb, 409-413
Cut-outs, center section, 134-135, 187
Cylinders, drag of, 263, 265-266

Damping,
  coefficient, 239-240
  in pitch, 247
  in roll, 101, 256-257
  in yaw, 258
  oscillation, 244-245
  to half-amplitude, 245, 253
Dead-center, control effect, 201
Dead rise, 506, 507
Decalage, 66-69, 180
Decrement, logarithmic, 245
Definitions, naval architecture, 491-492
Density,
  altitude, 522, 525
  effect on,
    bhp, 315
    speed in a climb, 371-375, 514-515
    speed in a dive, 450-458
    take-off run, 440, 442-443
  forces due to, 79
  method of performance reduction, 520

- Density—*Continued*
  - ratio, 527-532, 535
    - charts for, 532, 533, 535
  - standard, 12, 527
- Derivatives,
  - lateral stability, 254-259
  - longitudinal stability, 245-247
  - stability, 238-239, 242-247, 252-259
  - table of, 543
- Design,
  - airplane, 3, 141-142, 171-172, 468-490
  - propeller, 325-330
- Diagram,
  - Lilienthal, 90
  - vector, 98
- Diameter, propeller, 325-330, 332, 334
- Dihedral, 211-215, 255
- Discs, drag of, 262-263
- Displacement, wing-tip floats, 495-497
- Dive,
  - speed in, 458, 460-467
  - terminal velocity, 450-458
  - vertical, 449-458
- Diving start, effect on measured speed, 466-467, 511-512
- Downwash, 31-32, 57-58, 85, 142, 183, 187-189, 192-197, 364, 385
  - charts, 57, 188, 194-195
- Drag,
  - aircraft cable, 276-280
  - biplane, 38-39
  - bombs and torpedoes, 306-307
  - cable, aircraft, 276-280
  - circular discs, 262-263
  - coefficient, propeller, 450-452
  - corrections in model tests, 92-95
  - curves, general airplane,. 393-398
  - cylinders, 263, 265-266
  - engine, 297-302
  - fittings, 136, 304-305, 310
  - flat plates, 260-263
  - floats, 290-296, 498-499
  - frictional, 88, 135-136, 266-267, 498-499
  - fuselage, 283-290, 364
  - gas tank on wing, 270-271
  - general equation, 77-78, 91-92
  - hulls, 297, 498-499
  - induced, 31-39, 48-51, 54, 60-61, 364-365, 386-391, 395-401, 469-474, 482-489
    - biplane, 38-39
    - ground effect, 58-60
    - power curves, 417-418
    - span loading, 60-61
- Drag—*Continued*
  - induced—*Continued*
    - tandem wings, 48-51
    - triplane, 48-49
  - interference, 307-311
  - landing
    - gear, 302-304
    - light, 306
  - locked propeller, 343-344
  - machine gun, 306
  - nacelle, 298-302, 309-310
  - parasite, 260-309, 364, 365-367, 383-401, 469-474, 482-486
    - best climb, 513-514
    - estimation, 383
    - independent of angle of attack, 364
    - performance calculation, 364-367, 383
    - summation of, 364, 367, 383
    - varying with angle of attack, 364-367, 397-400
  - power relations, 393-398
  - profile, 33, 114-117, 155, 267-272, 364-365
    - coefficient,
      - flaps, 148, 150-151, 155
      - minimum, 116-117, 267
      - wing, 33, 114-117, 364, 365-367
    - scale effect, 80-81, 92-95, 117-119
    - thickness effect, 114-117, 268, 271
    - wing, 33, 114-117, 267-272, 364, 365-367
  - radiator, 305
  - radio antenna, 307
  - rivets, 136-137, 269
  - skin friction, 266-267, 498-499
  - sphere, 263
  - streamline form, 275-276, 283-286, 290-291
  - strut, 272-275
  - tail surface, 271-272
  - wheels, 302-304
  - wing, 267-271, 364-365
  - wing-tip float, 291
  - wire,
    - mesh, 306
    - round, 276-280
    - spacing effect, 278-279
    - streamline, 280-283

- Edge, reflexed trailing, 96, 114
- Efficiency,
  - airfoil, 120
  - airplane, 399-401
  - mechanical, of engine, 315

Efficiency—*Continued*
- propeller, 322-323, 325, 329
  - effect of body on, 334, 336
  - effect of tip speed, 330-331
  - general curves for, 333, 335-337
  - maximum, 334-336
- propulsive, 322-323
- tail, 183, 186-187

Elevator(s),
- angle, equivalent stabilizer, 199
- area, 197-201
- balanced, 197-198, 222-234
- plan-form of, 200
- tabs on, 197-200
- tests, 98-99

Ellipsoids, drag of, 263-264

Emergence, leading edge, 227-228

Endurance,
- Breguet's formula, 419-422
- calculation, 417
- estimation, 428-434
- factors, 420-421, 429-430, 432, 434
- formulas, 416, 419, 423, 429
- general curves, 430, 432, 434
- maximum, 417, 425-432, 434

Energy,
- conservation of, 6
- kinetic, 231, 445, 467
- potential, 440, 467

Engines,
- critical altitude, 314, 316-319, 380-381, 406-407, 442-443
- drag of air-cooled, 297-302
- general power curves, 312-315, 345-347, 349
- mechanical efficiency, 315
- power drop factor, 312-314, 349-354, 356, 357-358
- sea-level power, 380-381
- specific fuel consumption, 319-321
- stalling by propeller, 355-359
- supercharged, 313-319, 380-382, 391-392, 403, 407, 412, 440, 442-443, 524
- variation of bhp with altitude, 315-319, 521

Factors,
- conversion, 14, 536-541
- endurance, 420-421, 429-430, 432, 434
- range, 420-421, 429, 431, 433-444

Fairings, 95-97, 136-137, 303, 309-310

Fillet, expanding, 137

Fin area, vertical, 203-215

Fineness ratio, 274-276

Finish, surface, 135-136, 269

Fittings, drag of, 136, 304-305, 310

Fixed-trim runs in float tests, 500

Flaps, 141-170, 384-385
- effect on downwash, 142
  - horizontal tail area, 202
  - landing, 169
  - performance, 167-170
  - stalling speed, 141, 169-170, 385
  - take-off run, 167-170
- external airfoil, 166
- Fowler, 160-162
- hinge moment, 148-149
- leakage at hinge joint, 152-153
- moment due to, 142, 146-147
- on biplanes, 385
- on slotted wings, 162-165
- partial span, 157-158, 385
- plain, 144-152
- profile drag, 148, 150-151, 155
- retracting, 159-162
- slotted, 153, 162-165
- split, 153-158
- theory, 144-148
- types, 142-144
- Wragg, 166
- Zap, 143, 158-159

Flight,
- circling, 461-466
- gliding,
  - descent rate, 448-449
  - sinking speed, 448-449
  - without power, 459-460
  - with power, 460-462
- horizontal, 348-349, 361, 363-364
- problems, 459-467
- spiral, 465-466
- testing, 510-526
- throttled, rpm, 361

Floating, in a landing, 445

Floats,
- air drag, 290-296
- beam, 505-506
- dead rise, 291, 506, 507
- definitions, 491-492
- depth, 506
- excess buoyancy, 290, 506
- keel angle at step, 507, 509
- length, 495, 505
- metacentric heights, 492-495, 505
- model basin tests, 498-501
- non-dimensional coefficients, 500-501
- seaplane, 491-509
- speeds, corresponding, 498-499
- spray strips, 509
- stability, 492-497, 505
- step, 297, 507-509

Floats—*Continued*
  take-off calculations, 501-504
  Vee-bottom, 291, 506, 507
  wing-tip, 291, 495-497
  yawing moments, 203-206
Flow,
  fluid, 20-28, 78, 86-89
    laminar, 78
    turbulent, 78, 86-89
  superposed, 21
  three-dimensional, 22
  two-dimensional, 21-22, 28
Fluid, irrotational motion, 24-25
Flutter, 229-234
Flying boat,
  air drag of hull, 297
  effect of wind on take-off, 502-504
  maximum load for take-off, 504
Force,
  cross-wind, 254-255
  derivatives, 242, 245-246, 254
  general, 8-9
Fowler flaps, 143, 160-162
Friction (See "Skin friction")
Frise ailerons, 224-225, 227-228
Froude's law of comparison, 498-499
Fuel consumption,
  effect of compression ratio, 319-320
  in range calculations, 414-417, 419-420, 422, 428, 429
  part throttle, 319-320, 419-422, 428
  specific, 319-321, 414-429
  variation with altitude, 321
Fuselage,
  drag, 283-290, 364
    full-scale, 288-290
    model, 283-289
  interference,
    propeller, 334, 336
    wing, 95-96, 137-138, 309-310
  yawing moment, 203-207

Gap/chord ratio, 66, 132-133
Gas tank on wing, 270-271
Get-away speed, 501-507
Glauert, flap theory, 144-148
Glide, angle of, 169, 444-445
Glider, sinking speed, 448-449
Gravity, 8-9
Ground,
  effect, 58-60, 445-446
  friction coefficients, 438
  run,
    in landing, 447-448
    in take-off, 435-443
    effect of wind, 439-440
  speed, 425-426, 511-512

Guns, drag of, 306
Gyration, radius of, 247-249

Handley Page,
  balance, 222-225, 227-228
  slots, 143, 162-165
Height, metacentric, 492-495
Hemispheres, drag of, 264
Horns, drag of, 305
Horsepower (See "Power")
Horseshoe vortex, 30
Hulls,
  air drag, 297
  beam, 505-506
  flying boat (See "Floats, seaplane")
Hydrodynamics, 4, 20-30

Inclination,
  effect on wire drag, 278-280
  of flight path, 458
Induction, 33
Inertia,
  moment of, 247-249
  product of, 229-230
Instability, apparent, 234-235
Integrals, 544
Interference,
  body-propeller, 334, 336
  burble, 95-96
  factor,
    Munk's, 35-36
    Prandtl's, 36-39
  general, 83-85, 95-97, 307-311
  model supports, 90
  struts, 308-309
  wall, 83-85
  wing, 309-310
  wing-fuselage, 95-96, 137-138
  wing-nacelle, 309-310
  wire, 307
Intersection, drag of strut, 309

Joukowsky,
  airfoils, 109
  lift equation, 24
Junkers double-wing, 166

Keel angle at step, 507, 509
Kinematics, 4
  viscosity, 81-83
Kinetics, 4
Kutta-Joukowsky equation, 24

Laminar flow, 78
Landing,
  gear, drag of, 302-304

Landing—*Continued*
  light, drag of, 306
  over an obstacle, 444-446
  run, 447-449
  use of brakes, 448
Lap joints, drag of, 135
Leakage at,
  flap hinge, 152-153, 226-227
  wing-panel joint, 55
L/D ratio,
  airfoil, 128-129
  airplane, 304-398
  in performance calculation, 105-106
  maximum, 393-398
    formula for, 397
    speed for, 394-395
  near ground, 446
Lift coefficient,
  biplane, 132-133, 384-385
  definitions, 12-14
  flaps, 141-142, 151-166, 385
  maximum,
    general, 80-81, 112-114, 117-119, 132-133, 384-385
    negative, 125-126, 343
    tail surface, 202
    with flaps, 151-166, 384-385
  optimum, 124-125
  scale effect, 76, 117-119, 384-385
Lift-curve, slope, 51-55, 95-96, 126-128, 184-185
Lift distribution, biplane, 66-72
Lift, equation for, 24
Lifting-line in wing theory, 29-30
Lilienthal diagram, 90
Loading,
  biplane, relative, 66-72, 179-181
  combined, 488-490
  power, 403, 468, 480-490
  wing, 184, 383, 384, 386, 391, 468, 480-490
Load, maximum for take-off, 504
Location,
  center of gravity, 170, 172-176, 181-182, 507
  step, 507
  wing-tip floats, 494-497
Locus of c.g. for constant stability, 181-182
Logarithms, relations for, 542

Machine gun, drag of, 306
Maneuverability,
  altitude effect on, 478-480
  effect of stalling speed on, 474-481
  factor, 475-476, 478-480
Mass,
  additional, coefficient, 203, 206
  balance of control surfaces, 228-230
  definition, 6-9
  distribution, 228-235, 247-249
  units, 6-9
Measurement of area,
  balanced control surfaces, 225
  tail surfaces, 187
  wing, 385
Mechanics, fundamental, 5-9
Mesh, drag of wire, 306
Metacenter, 492, 493
Metacentric height,
  definition, 492-493
  longitudinal, 495
  required, 494
  transverse, 494-495
Metric system, 6-9
Mixture control, 319-320
Model
  alignment, 93
  basin tests, 499-500
  construction, 89, 92-93
  tests,
    airfoil, 89-90
    airplane, 90-108
    conversion to full scale, 105-106
    free-to-trim floats, 500
    performance, 104-108
Moment(s),
  about quarter-chord point, 61-62
  coefficient,
    about any point, 63-65, 175-178
    about c.g., 173-176
    at zero lift, 121-122
    biplane, 70-72, 175-178
    general, 14, 61-62
  curves, slope of
    pitching, 97-99, 173-176, 185-186
    yawing, 102-104, 206
  derivatives, 243, 246-247, 255-258
  due to dihedral, 211-213
  of inertia, airplane, 247-249
  pitching, 97-99, 173-176, 185-186
    about quarter-chord point, 61-62
    any point, 63-65, 175-178
    effect on maximum lift, 142
  righting, 493-497
  rolling, 100-102, 212, 216, 255-257
  upsetting, 493-497
  yawing, 102-104, 203-208, 212-213, 256-258
Monoplane,
  high-wing, 170, 173
  low-wing, 137, 170, 173

Munk's
  interference factor, 35-36
  moment equation, 203
  M sections, 109-110
  span factor, 34-35, 40-46

N. A. C. A. airfoil series, 110-112
Nacelles,
  drag of, 208 302, 309-310
  tandem, 302
Navy No. 1 strut, 272-275
Newton's laws, 5-6

Obstacle,
  landing over, 444-448
  take-off over, 443
Offsets,
  C-class airship, 272
  Navy No. 1 strut, 272
Oil consumption, effect on range, 416
Ordinates,
  airfoil, 131
  C-class airship, 272
  Navy No. 1 strut, 272
Oscillation,
  damped, 244-245
  phugoid, 244
  unstable, 241
Overhang in a biplane, 66-71

Paddle-balance for control surface, 222-225
Parachutes, drag of, 264
PDF, definition of, 312
Performance,
  at altitude, 377-381, 521-522
  calculation, 362-382
  definition, 362
  effect of,
    aspect ratio, 468-490
    parasite drag coefficient, 468-490
    pressure and temperature, 521-522
    stalling speed, 473-481
  estimation,
    absolute ceiling, 403-406
    climb, 401-403
    drag, parasite, 383
    endurance, 428-434
    general, 383-413, 428-434
    initial rate of climb, 401-403
    landing run, 445-448
    maximum endurance, 429-430, 432, 434
    maximum *L/D*, 393-398
    maximum load for take-off, 504
Performance—*Continued*
  estimation—*Continued*
    maximum range, 429, 431, 433-444
    maximum speed, 386-393
    parasite drag, 383
    range and endurance, 428-434
    service ceiling, 406-407, 516-518
    stalling speed, 383-386
    take-off run, 435-443, 444, 502-503
    time of climb, 407-413
  flight tests, 510-526
  limiting, 481-490
  reduction to standard, 519-526
  solution, graphic, 361
  wind-tunnel tests, 104-108
  with supercharged engine, 380-382, 403
Phugoid oscillation, 244
Pitch,
  controllable, 314, 336-338, 358-360, 406
  distribution, 323-324
  propeller, 323-325, 336-338, 358-360
Plan-form,
  ailerons, 221
  balanced controls, 223
  tail surfaces, 200-201
Plates, flat, drag, 260-263
Porpoising, seaplane floats, 492, 498
Potential, velocity, 26-27
Power,
  altitude, 376, 377, 380-381, 521
  available, 330-342, 349-354, 362, 366-371, 377
  calculation, 104-108, 339-342, 367-371
  coefficients, 321-322, 344-345
  curves,
    bhp, 312-315, 345-347, 349
    extrapolation, critical altitude, 380-381
    thp, 349-354, 393-398, 417-418
  drag relations, 393-398
  drop factor, 312-315, 349-354, 356
  excess, 362, 371
  horizontal flight, 363-364, 417-418
  in a turn, 463-465
  induced, 365
  loading, 403, 468, 480, 481-490
  minimum, 393-397, 481-490
  near ground, 58-60, 246
  pressure effect, 315
  stability effect, 250-251
Powers and roots, 542
Prandtl's interference factors, 36-39

Pressure,
  altitude, 511, 514
  dynamic, 12-13
  method of performance reduction, 520
Propeller,
  blade setting, 324-325, 329-330, 332, 337, 358, 360
  coefficients, 321-322, 450-452
  constant rpm, 336-338
  controllable pitch, 314, 336-338, 358-360, 380-382, 406, 438-439
  cut-off tips, 332
  design, 325-330
  diameter, 325-329, 334
  drag, 343-344, 450-452
  efficiency, 322-323, 332, 333, 334-337
  feathered blades, 343-344
  fuselage interference, 334, 336
  general curves, 333, 335-337, 344-345
  helix, angle, 323
  idling, 343
  in terminal velocity dive, 450-452
  maximum efficiency, 334-336
  negative thrust, 343
  pitch, 323-325
  propulsive efficiency, 322-323, 325-337
  rpm, 336-338, 348, 361
  stalled, 336
  static thrust, 337-340
  stopped, 344
  three-bladed, 329-330
  tip speed, 330-331
  twist in blade, 325, 329-330
  two-position, 337-338, 439
  wind-milling, 343
Protuberances, 136-137, 269-271

Quarter-chord point, 61-62, 122

Radial air-cooled engine, drag of, 297-302
Radiators, drag of, 305, 307
Radii of gyration, 247-249
Radio antenna, drag of, 307
Radius of turn, 404-405, 476-481
Range,
  at constant angle of attack, 419-422
  at constant speed, 422-424
  bombing, 424-425
  Breguet's formula, 419-422
  calculation of, 414-417, 419-428
  effect of wind, 425-428
Range—*Continued*
  estimation of, 428-434
  factors, 420-421, 429, 431, 433-434
  general curves for, 431, 433-444
  graphical solution, 415, 424-425
  maximum, 414-416, 419-422, 428-434
  oil consumption effect, 416
  with a bomb load, 424-425
Rate of climb,
  air speed for best, 402-403, 512-515
  at critical altitude, 407
  at equivalent altitude, 522
  by graphical methods, 367, 371
  curve, 377, 379-380, 406-413
  effect of assumed linear, 518-519
  effect of pressure and temperature, 520-522
  equation for, 401, 516
  estimation of, 401-403
  general curve, 408
  linear, 407-413, 518-519
  method of obtaining constants, 518-519
  minimum safe, 481-490
  non-linear, 406-413, 516-519
  reduction to standard, 520-522, 524-526
  slope of curve, 406, 516-519
  zero, 482, 484-485, 487-488, 489
Ratio, aspect (See "Aspect ratio")
  gap-chord, 66, 132-133
  induced to parasite drag, 387-397, 417-418, 420-434
Resistance,
  air (See "Drag")
  wave-making, 77, 91, 498-499
Retardation in landing run, 447-448
Reynolds Number,
  definition, 78-79
  determination, 81-83
  effective, 118
  effect on
    maximum lift, 80-81, 117-119, 384-385
    minimum drag, 118
  general, 76-83, 91-92, 110, 260, 263, 266-267, 384-385
Rivets, effect on drag, 136-137, 269
Rolling moment due to
  dihedral, 212, 255
  roll, 256-257
  yaw, 255-256
  yawing, 257
Rotation in a fluid, 24-25
Routh's Discriminant, 241, 244, 252

Rpm,
  constant, 336-338, 358-360
  engine, 355-358
  propeller, 355-358, 360-361
  throttled flight, 361
  variation with speed, 348, 361
Rudder(s),
  area, 210-211
  balanced, 225-226
  fin area, 203-215
  tests on, 102-104
Run,
  landing, 447-449
  take-off, 142, 167-170, 435-444, 501-504

Scale-effect, 76-81, 92-95, 117-119, 384-385
Sea-level,
  engine, 312
  fictitious speed, 391-392
  power, 380-381
  power available, 369-371
  power required, 367-369
Seaplanes (See "Floats" and "Take-off")
Service ceiling,
  calculation, 375
  definition, 375
  effect of curvature in climb, 406-407, 516-518
  estimation, 406-407
  with supercharged engine, 407
Servo-controls, 197-199
Side-slip, 212, 214-215
Similitude, 91-95
Skin friction, 79, 88, 118-119, 135-136, 266-267, 498-499
Slipstream, 322-323, 382
  obstruction, 334, 336
Slope of
  lift curve,
    airfoil, 51-55, 95-96, 126-128, 184-185
    approximate equation, 126-128
    biplane, 55
    effect of thickness, 126
  moment curves,
    in pitch, 99, 173-176, 185-186
    in yaw, 102-104, 206
Slot,
  fore-and-aft, 55-56
  Handley Page, 143, 162-165
  Leigh, 162
Slug, definition, 8
Sound, velocity, 77, 139-140, 330-332
Sources and sinks, 27-28
Spacing, effect on wire drag, 279
Span,
  equivalent monoplane, 34-35
  factor, Munk's, 34-46
  loading, 60-61
Speed(s),
  corresponding, 498-499
  cruising, 419
  for maximum *L/D*, 394-397
  for minimum powet, 394-397
  get-away, 501-507
  maximum,
    effect of aspect ratio on, 386-393
    effect of diving start on, 466-467
    effect of gross weight, 392-393
    effect of induced drag on, 386-393
    effect of parasite, 386-393
    effect of pressure and temperature on, 522-524
    estimation, 386-393
    flight tests, 511-512, 522-524
    reduction to standard, 522-524
    variation with altitude, 391-393
  propeller tip, 330-331
  relations between power and, 393-397
  sinking, 448-449
  stalling, 363, 383-386
Sphere,
  drag, 87-88, 263-264
  effect of turbulence, 87-88
Spheroid, drag of, 263-264
Spiral flight, 465-466
Spray-strips, 509
Squashing in a turn, 464-465
Stability,
  apparent lack of, 234-235
  axes, 238, 241-242
  critical, 186
  derivatives, 238-239, 242-243, 252-259
  directional, 102-104, 203-211, 256
  dynamic, 171, 236-259
  free liquid surface, 235
  lateral, 99-102, 211-221, 251-259
  longitudinal, 97-99, 170, 172-202, 237-251
    location of c.g. for constant, 181-182
  seaplane, 492-497, 505
  static, 97-104, 172-202
Stabilizer,
  angle, equivalent elevator, 199
  area, 182-202
    measurement of, 187
  down-load in landing, 202, 227

- Stabilizer—*Continued*
  - location, 192-195
  - section, 201-202
  - setting, 85, 98-100, 193-199
  - stalled, 202
- Stagger, 66-69, 132-133, 179-181
  - measurement of, 69
- Stall, 170
- Stalling,
  - engine by propeller, 355, 357-359
  - propeller blades, 336
  - speed, 105, 169, 363, 383-386
    - effect on
      - directional control, 103-104
      - lateral control, 216
      - performance, 473-490
- Standard atmosphere,
  - approximate equations, 529-530
  - charts, 532-535
  - definition, 527
  - exact equations, 527, 529-530
  - reduction of performance, 519-526
  - relations in reduction, 530
  - tabular values, 528
- Static,
  - balance, 228-230
  - pressure gradient, 85-86, 90
  - stability,
    - directional, 102-104, 203-211, 256
    - lateral, 99-102, 211-221
    - longitudinal, 97-99, 172-202
  - thrust, 337-340
- Statics, 4-5
- Step, seaplane floats, 297, 507-509
- Stream function, 22-23
- Streamline,
  - body, yawing moment, 203-207
  - definition, 23
  - forms, 275-276, 283-284, 290-291
  - wire, 280-283
- Strut(s),
  - drag of, 272-275
  - interference, 308-309
  - offsets for Navy No. 1, 272
- Surface,
  - effect, 77-78, 91-92, 110, 135-136, 268-270
  - free liquid, 235
  - plan-form, 200-201
  - tail area, 182-202
    - aspect ratio, 189-191
    - c.g. location, 191-192
    - equation for, 184
    - flaps, 202
    - length, 191
  - waxed on wing, 135, 269
- Symbols, table of, 14-18
- Tabs, 197-200
- Tail,
  - area,
    - horizontal, 182-202
    - measurement, 187
    - vertical, 203-215
  - aspect ratio, 189-191
  - efficiency, 183, 186-187
  - length, 190-191
  - lift with full-deflected elevator, 202
  - plan-form, 200
  - section, 201-202
  - setting, 193-197
  - surfaces,
    - drag of, 271-272
    - stalled, 202
- Take-off coefficient, 435-436
- Take-off over obstacle, 443-444
- Take-off rating of engine, 338
- Take-off run,
  - calculation, 435-444, 501-504
  - coefficient of friction, 438
  - controllable-pitch propeller, 438-439
  - effect of
    - altitude on, 440, 442-443
    - flaps on, 142, 167-170
    - gross weight, 328, 441
    - take-off speed on, 440
    - wind velocity on, 439-440, 502-504
  - graphic solution, 435
  - seaplane, 169-170, 501-504
  - supercharged engine, 440, 442-443
- Temperature, effect on
  - bhp, 315
  - maximum speed, 523-524
  - rate of climb, 514-515
  - speed for best climb, 514-515
  - velocity of sound, 331-332
- Terminal velocity,
  - altitude loss, 455-457
  - dives, 452-458
  - effect of dive-angle, 458
  - from short dive, 457
  - of airplane, 450-452
  - of parachute, 264
  - with rotating propeller, 450-452
- Tests,
  - airfoil, 89-90
  - airplane, 90-108
  - flight, 510-526
  - seaplane floats, 498-500
  - wind-tunnel, 73-108
- Thickness of airfoil, effect on
  - airfoil lift, 112-114, 126-128
  - control action, 201

Thickness of airfoil—*Continued*
  profile drag, 114-117, 268, 271
  slope of lift curve, 126-128
Throttling, effect on fuel consumption, 319-320, 419-422, 428-429
Thrust, calculation of, 337-340
  coefficients, 321-322
  horsepower,
    calculation of, 340-342, 367-369
    general curves, 349, 417, 437, 439
    maximum available, 369-371, 377
    required, 363-364, 367-369, 376
    variation with altitude, 355, 376
      rpm and *V*, 336-337, 349-354
  negative, 343
  static, 337-340
  zero, 342
Time for 360° turn, 478, 481
Time of climb, 375-376, 518
Tip speed, 330-331
Tips, propellers with cut-off, 332
Torque, 339-343
  coefficients, 321-322
Trim, definition, 193
  longitudinal, 99-100, 193-197
  stabilizer setting, 85, 98, 193, 196
Triplanes, induced drag, 48-49
Turbulence, 86, 91, 110, 118, 275
Turn, 461-465, 476-481
Turnbuckles, drag of, 276-283
Twist of propeller blades, 325, 329

Vector diagram, 98
Vee-bottom floats, 291
Velocity, limiting airplane, 450-452
  of sound, 77, 139-140, 330-332
  potential, 26-27
  terminal, 264, 450-458
Ventilation, step, 508-509
Viscosity, 77-83
Vortex motion, 28-30
Vortices, 28-30

Wake, turbulent, 57-58, 187, 192-195
Walkway, effect on wing, 135
Washout in wing tip, 216
Waxed surface on wing, 135, 269
Weight, effect on
  speed, 105-107, 392-393
  take-off run, 439-440, 441, 504
Wheels, drag of, 302-304
Wind axes, 9-12, 101, 241-242
Wind, effect on
  economical speed, 425-426
  flight tests, 510-512
  range, 425-428
  take-off run, 439-440, 502-504
Wind tunnel, balances, 74-75, 89-90
  full-scale, 118, 135
  static pressure gradient, 85-86
  tests, 89-108
  turbulence, 86-89, 91-92
  types, 73-74
  variable-density, 74, 110-111, 118, 128, 135
  wall interference, 83-85
Wing(s),
  area, 385, 473-481
  cut-outs, 134-135, 187
  drag,
    effect surface finish, 135, 268-270
    induced, 31-39, 48-51, 54, 60-61, 364-365, 386-403, 417-418
    in performance calculation, 267-271, 364-365
    interference effects, 95-96, 137-138, 309-310
    profile, 33, 114-117, 134-138, 267-271, 364-365
    scale effect, 118
  loading, 184, 383-386, 391, 468, 480-490
  net area, 385
  rotor, 167
  section, characteristics, 110-111, 115
    data, 109-140
    drag, 115
    selection of, 128-130
  slots, fore-and-aft, 55-56
    Handley Page, 143, 162-165
  tandem, 48-51
  theory, 31-72
  tips, 53-54, 127-128
    floats, 291, 495-497
Wire(s), drag,
  cable, 276-280
  interference, 278-279, 307
  mesh, 306
  streamline, 280-283
Wragg flap, 166

Yaw, effect on drag, streamline wire, 281-282
Yawing moment, 203-207, 212, 256

Zap flaps, 143, 158-159
Zero,
  lift, 62-64, 120-122, 172-173, 180, 193
  lift-line, 62, 172, 182, 185, 323
  moment, 62-64
  thrust, 342, 444
  torque, 342
Zoom, 467

☆ U.S. GOVERNMENT PRINTING OFFICE : 1987 O - 174-805 : QL 2